

**CARBON CYCLING IN ARCTIC LAKES: SEDIMENTARY
BIOMARKER RECONSTRUCTIONS FROM DISKO
ISLAND, WEST GREENLAND**

Mark A. Stevenson, BSc., MSc

Thesis submitted to the University of Nottingham
for the degree of Doctor of Philosophy

September 2017

Abstract

A palaeolimnological study of three lakes on Disko Island, West Greenland was conducted across a hydrogeomorphic landscape gradient, to reconstruct principally changes in algal pigments, lipid biomarkers and carbon isotopes ($\delta^{13}\text{C}$) to investigate carbon cycling at multiple scales and resolutions. All three records reconstructed recent change on Disko, with records from lake Disko 2 additionally spanning since ~7640 cal. yr BP and lake Disko 4 since ~1260 cal. yr BP. Changes in sedimentary proxies were broadly consistent with the spatially and temporally heterogeneous environmental change known to have occurred across the Arctic over these periods, including recent warming (RW), the Little Ice Age (LIA) and the Medieval Climate Anomaly (MCA). However, the individual lake responses to these changes were highly landscape specific. Changes in algal pigments were linked to variations in the inputs of nutrients and DOC from soil microbial activity, variations in permafrost melt regime and glacier melt.

Evidence of disturbance from catchment freeze-thaw processes, glacier inputs and the effects of permafrost melt on algal communities varied between lakes. At the highest position in the landscape gradient, lake Disko 2 had poorly developed soils and lower glacier coverage, with simple algal communities, but pigment and $\delta^{13}\text{C}_{\text{TOC}}$ changes since ~7640 cal. yr BP reflected individualistic responses to overarching drivers, consistent with the current understanding of heterogeneous pan-Arctic environmental change. Replicate cores with proximity to talus and debris flow had differing signatures, highlighting the role of geomorphology. In lake Disko 2 there was some similarity between Greenland Ice Sheet surface area and pigment biomarkers of cryptophytes (alloxanthin), which suggests if locally similar, catchment ice variation may regulate nutrient and DOC release from catchments, stimulating algae.

At a mid-elevation position in the catchment, lake Disko 1 meltwater inputs from an upstream retreating glacier (since the end of the LIA) may be stimulating algae through increased nutrients and DOC supply, although soil nutrient cycling and permafrost release present in the catchment U-shaped valley may also be contributing to these increases. At the lowest position in the landscape, lake Disko 4 has a complex and variable pigment response likely influenced by multiple glacier inputs, thicker permafrost, greater vegetation and more developed wetland areas, together regulating the cycling of nutrients and DOC. Higher maximum pigment concentration during the MCA, compared with the LIA reflect the spatially and temporally heterogeneous expression of these events across the Arctic.

Despite individuality in catchment filtering, all three lakes on Disko Island were found to have recent increases in algal production, which when combined with recent increases in

carbon burial suggests these lakes are becoming increased carbon sinks. Although this increased carbon burial reflects a minor store in lakes compared with release to downstream waterbodies, if upscaled across the Arctic this change could be globally significant and should be integrated in future models. With future warming, catchment processes are likely to play a pronounced role in mediating algal community structure in lakes across the Arctic.

Acknowledgements

I am particularly thankful to my supervisors Suzanne McGowan and George Swann for encouraging me to embark on this journey and supporting me at every stage of the endeavour. Suzanne you have always been a realist and have helped me see through the noise of complex environmental data to explore the sometimes ambiguous biological patterns in palaeolimnology with enthusiasm. George your door has always been open to discuss the next phase of the project with endless positive encouragement to help iron out solutions to many challenges and support me through numerous last minute grant application deadlines. I would also like to thank the supervisory input from Emma Pearson who kindly introduced me to the procedures involved in the preparation, interpretation and analysis of lipid biomarkers and warmly welcomed me when I visited Newcastle. The guidance from Melanie Leng concerning isotope analysis and interpretation while at the BGS is also gratefully acknowledged which helped give the project an additional dimension.

Numerous laboratories have welcomed me to conduct analysis, without their support and guidance this project would not have been possible. In the University of Nottingham, School of Geography I would particularly like to thank Teresa Needham who always met my laboratory requests with a smile and to Ian Conway for building and designing so many core boxes to transport samples back to the UK. I would like to thank Graham Morris and Julie Swales for assisting me with support, supplies and consumables and to Elaine Watts for cartographic advice. I would also like to thank Stephen Hall for GC-MS related advice and method development in the Faculty of Engineering.

In Newcastle I am indebted to Louise Foster and Emma Pearson who so kindly trained me in the complexities of lipid biomarker sample preparation and microwave digestion. I would also like to thank Ben Petrick, Simon Drew and Bunmi Eniola who assisted with technical matters and Paul Donohue and Bernie Bowler who ran the GC-MS.

At China University of Geoscience, Wuhan where I analysed lipid samples for $\delta^{13}\text{C}$ on FAMES I would like to thank Xianyu Huang who so kindly invited me to work in his laboratory and answered numerous questions concerning the analyses of these compounds. I am also extremely grateful to Qingwei Song and Jiantao Xue who taught me the analytical procedure and how to use the GC-MS. Their dedication was unquestionable, often working long into the night to ensure the machine never stopped

Acknowledgements

running. Thanks also go to Xu Chen who guided me while in Wuhan and his students Chunling and Linghan who so kindly gave me so many tours of the university and vibrant local area.

I would like to thank Maria Cisneros-Dozal at the NERC radiocarbon laboratory in East Kilbride and everyone who introduced me to the sample procedures for ^{14}C dating. Thanks also goes to Xiaomei Xu of the Keck Carbon Cycle AMS facility of the University of California who ran the smaller macrofossil samples. The support of Paula Reimer and Stephen Hoper for radiocarbon dating of samples at Queens University, Belfast is also acknowledged.

Thanks goes to Viv Jones and Ali Young at UCL for supplying me with diatom and XRF data for the Disko 2 short core. These data have proved invaluable for comparison with biomarker trends. The expert dating of this core by Handong Yang has helped add to the robustness of the conclusions. Also a great thanks goes to George Shaw and Thawatchai Ithipoonthanakorn for the recent dating of the Disko 4 short core using the new setup at Sutton Bonnington. Discussions with Matthew Jones and Charles Gowing on radiocarbon modelling are also gratefully acknowledged. Thanks also to Bo Elberling for provision of climate data related to Disko Island. The enthusiastic support of both Christopher Kendrick, Melanie Leng and Jonathan Dean while at the BGS is also gratefully acknowledged.

The fieldwork on Disko Island would not have been possible without the generous support, advice and hospitality received from Arktisk Station of the University of Copenhagen throughout our stay. Ole Stecher welcomed our research teams with enthusiasm and Kjeld Mølgaard (Akaaraq) and Erik were both excellent and skilled snowmobile drivers in challenging conditions. Erika Whiteford taught me on this trip how to be prepared for the fast-paced core recovery and was so enthusiastic and kind to participate in the trip along with Emma Pearson and Suzanne McGowan. The dedication and organisation of Joe Bailey during the summer expedition to Disko is gratefully acknowledged. Joe, you carried a lot of gear and encouraged me when the hiking was tough. For that I am forever grateful. It was fate that Kathryn Adamson and Timothy Lane were also present during both April and August field seasons to Arktisk Station. We had great discussions and during the summer visit sailed to Lakesebugt (Salmon Bay) with Akaaraq at the helm, the highlight of the trip!

A large number of institutions and organisations have generously funded this research. First, thanks to the NERC/ESRC studentship which supported me generously during this work (ES/J500100/1). The April 2013 fieldwork to Disko Island received support

from the INTERACT transnational access scheme (grant agreement No 262693) under the European Community's Seventh Framework Programme and NERC grant Lakes and the Arctic Carbon Cycle NE/K000276/1. This project has also received support from the NERC Radiocarbon Facility NRCF010001 (grants 1843.1014 and 1757.1013) and the NERC Isotope Geosciences Facilities Steering Committee (IP-1516-1114 and IP-1393-1113). I am also very thankful to the generous funding supplied from the Freshwater Biological Association through the 2015 Gilson Le Cren Memorial Award for the analysis of lipid biomarkers at Newcastle and to the ESRC DTC for funding the visits to China University of Geoscience, Wuhan through the Overseas Institutional Visits (OIV) scheme. The Quaternary Research Association (QRA) is also thanked for radiocarbon dating support and funding conference attendance to INQUA 2015.

A special thanks must go to Heather and Sarah for all the interesting pigment related debates and discussions we have had over the years. To Nick for preparing me for the cold Arctic weather with the provisioning of your equipment taken to Disko and to Jim for help and guidance with computer related issues. The years would have been very different without the comradery of Jeremy, Felix and Liam and everyone else in the School of Geography who were on a similar path, including all in the office past and present.

Finally the thesis is dedicated to my Mum, Dawn Stevenson who was always there for me and who I know would have thoroughly enjoyed reading this, and be pleased I have used these years to contribute to science.

Table of Contents

Abstract.....	ii
Acknowledgements	iv
Table of Contents.....	vii
List of Figures.....	xiv
List of Tables	xx
List of Equations.....	xxi
Abbreviations used in the thesis	xxii
Chapter 1: Introduction and Literature review.....	1
1.1 Carbon cycling.....	1
1.1.1 The global carbon cycle.....	1
1.1.2 Why is carbon cycling important in the Arctic?	2
1.1.3 Arctic lakes as integrators and regulators of carbon.....	3
1.1.4 Carbon cycling in Arctic lakes.....	4
1.1.5 The role of DOC and DOM in Arctic lakes.....	5
1.1.6 Heterotrophic and mixotrophic strategies in Arctic lakes.....	8
1.1.7 The importance of the lake ecosystem in Arctic lakes	9
1.2 Arctic landscape processes and impact on carbon cycling	11
1.2.1 Permafrost.....	11
1.2.2 Arctic soils and vegetation.....	12
1.2.3 Glaciers and snow cover	14
1.3 Study aims	15
1.4 Study area	17
1.5 Arctic Holocene environmental change in Greenland and the North Atlantic ..	21
1.5.1 Holocene palaeoclimatology	21
1.5.2 Hemispheric scale climate change over the Holocene.....	22

Table of Contents

1.5.3 Palaeoenvironmental change in the Disko Bugt region.....	25
1.5.4 Existing palaeolimnological studies on Disko Island.....	29
1.5.5 West Greenland palaeolimnological studies outside the Disko region	30
1.6 Holocene deglaciation of Disko Island and the Disko Bugt region	31
1.6.1 Holocene ice dynamics of Disko Island	31
1.6.2 Deglaciation of the Disko Bugt region.....	34
1.7 Thesis outline	35
Chapter 2: Literature review of key methods used in this thesis	36
2.1 Sedimentary pigment analysis.....	36
2.1.1 Pigment preservation and stability	38
2.1.2 Application of pigment analysis in palaeolimnological investigations of carbon cycling	40
2.2 Lipid biomarkers	42
2.2.1 Review of biomarker compounds, lipid ratios and equations in lakes	42
2.2.2 Selecting appropriate lipid biomarkers for the Disko 2 reconstruction.....	46
2.2.3 Palaeolimnological studies using lipid biomarkers for carbon cycling.....	47
2.3 Organic carbon stable isotope ratios ($\delta^{13}\text{C}_{\text{TOC}}$) and C/N ratios	48
2.3.1 Preservation and diagenesis of $\delta^{13}\text{C}_{\text{TOC}}$	51
2.3.2 C/N ratios	52
2.3.3 Example palaeolimnological studies using $\delta^{13}\text{C}$ and C/N to interpret carbon cycling	54
2.4 Compound specific carbon isotope analysis.....	55
2.4.1 Carbon isotopes on terrestrial leaf wax lipids	55
2.4.2 Carbon isotopes on short chain algal and mid chain macrophyte lipids.....	56
2.5 Summary – methods literature review.....	57
Chapter 3: Methods	59
3.1 Site selection.....	59

Table of Contents

3.2 Sediment coring	59
3.3 Sediment lithology, sectioning and LOI	60
3.4 Hydro-geomorphological survey and catchment sampling	61
3.5 Water chemistry analysis	62
3.6 Pigment analysis	63
3.7 Carbon isotope and elemental C/N analysis	65
3.8 Lipid biomarker analysis	66
3.9 Compound specific $\delta^{13}\text{C}$ analysis of FAMES	68
3.10 Sedimentary dating techniques	69
3.10.1 Radiocarbon dating	69
3.10.2 Recent dating (^{210}Pb , ^{137}Cs , ^{241}Am)	70
3.10.3 Age-depth modelling	71
3.11 Graphical and numerical	72
3.12 Additional analyses provided by UCL for core Disko 2 K1	72
3.12.1 Diatom analysis	72
3.12.2 XRF analysis	73
3.13 Overall methods summary	73
Chapter 4: Hydro-geomorphic vegetation catchment survey and site information ...	74
4.1 Location and local setting of the study lakes	74
4.1.1 Lake Disko 2	76
4.1.2 Lake Disko 1	80
4.1.3 Lake Disko 4	85
4.2 Land cover characteristics	89
4.3 Vegetation composition surveys of the study lakes local catchments	91
4.4 Water chemistry analyses	94
4.5 Water chlorophyll and carotenoid pigment analysis	97
4.6 Catchment sample survey	99
4.6.1 Disko 2	99

Table of Contents

4.6.2	Disko 1	102
4.6.3	Disko 4	106
4.6.4	Comparative trends in catchment samples	108
4.7	Lipid biomarker characterisation of selected samples from Disko 2	110
4.7.1	Carbon chain length distributions.....	110
4.7.2	Selected lipid ratios and equations for Disko 2 catchment samples.....	116
4.7.3	Compound specific $\delta^{13}\text{C}_{\text{FAMES}}$ on Disko 2 catchment samples	120
4.8	Discussion	122
4.8.1	Hydro-geomorphic position of the study catchments.....	122
4.8.2	Catchment samples ($\delta^{13}\text{C}_{\text{TOC}}$, $\delta^{13}\text{C}_{\text{FAMES}}$ and C/N)	126
4.8.3	Lipid biomarker characterisation of Disko 2 catchment samples.....	128
4.8.4	Key interpretations from selected Disko 2 biomarker catchment samples	131
4.9	Summary – hydro-geomorphic catchment survey	134
Chapter 5:	Disko 2 – Results and discussion.....	136
5.1	Results – Disko 2 Sequence 1	137
5.1.1	Core correlations	137
5.1.2	Stratigraphic descriptions	137
5.1.3	Radiometric dating and removal of instantaneous events	140
5.1.4	Disko 2 Sequence 1– pigment results.....	148
5.1.5	Exploratory statistics – Disko 2 Sequence 1	151
5.1.6	Disko 2 Sequence 1 – geochemical data, pigment ratios and PCA scores	152
5.1.7	Disko 2 S1 compound-specific fatty acid (FAMES) $\delta^{13}\text{C}$ results.....	155
5.1.8	Disko 2 S1 lipid biomarker ratios – <i>n</i> -alkanes	157
5.1.9	Disko 2 S1 lipid biomarker ratios – <i>n</i> -fatty acids (FAMES).....	159
5.1.10	Disko 2 S1 lipid biomarker ratios – <i>n</i> -alkanols, sterols and ketones.....	161
5.1.11	Disko 2 S1 diatom results.....	163
5.1.12	Disko 2 S1 XRF data.....	165
5.1.13	Disko 2 S1 Synthesis.....	167

Table of Contents

5.2 Results – Disko 2 – Sequence 2.....	170
5.2.1 Core correlations – Disko 2	170
5.2.2 Stratigraphic descriptions	170
5.2.3 Radiocarbon dating – Sequence 2.....	172
5.2.4 Disko 2 R2-1 Russian core – bulk organics & pigment concentrations ...	174
5.2.5 Disko 2 R2-2 Russian core – bulk organics & pigment concentrations ...	176
5.3 Disko 2 Discussion	178
5.3.1 Stratigraphy, core correlations and bulk measures	178
5.3.2 Radiometric dating.....	180
5.3.3 Disko 2 S1 Combined Sequence – Proxy interpretation.....	182
5.3.4 Disko 2 – Sequence 2 – Proxy Interpretation	195
5.4 Disko 2 summary.....	197
Chapter 6: Disko 1 Results and Discussion	199
6.1 Results – Disko 1	199
6.1.1 Core correlations – master stratigraphy	199
6.1.3 Radiometric dating.....	203
6.1.4 Bulk measures.....	207
6.1.5 Disko 1 sequence – Pigment results	209
6.1.6 Exploratory statistics – Disko 1 sequence	212
6.1.7 Pigment ratios and PCA scores – Disko 1 sequence.....	213
6.2 Discussion of sedimentary sequence from Disko 1	216
6.2.1 Stratigraphy.....	216
6.2.2 Bulk measures.....	217
6.2.3 Radiocarbon dating.....	217
6.2.4 Disko 1 geochemical interpretation	220
6.3 Summary – Disko 1	226
Chapter 7: Disko 4 – Results and discussion	227

Table of Contents

7.1 Results – Disko 4.....	227
7.1.1 Core correlations – master stratigraphy.....	227
7.1.2 Stratigraphic descriptions.....	228
7.1.3 Bulk measures.....	231
7.1.4 Radiometric dating.....	234
7.1.5 Disko 4 combined master sequence – pigment results.....	241
7.1.6 Exploratory statistics – Disko 4 combined sequence.....	244
7.1.7 Disko 4 combined master sequence – geochemical data, pigment ratios and PCA scores.....	245
7.2 Discussion Disko 4.....	249
7.2.1 Stratigraphy, core correlations and bulk measures.....	249
7.2.2 Radiometric dating.....	251
7.2.3 Disko 4 geochemical interpretation.....	253
7.2.4 Summary – Disko 4.....	260
Chapter 8: Synthesis and discussion – Carbon cycling in Arctic lakes on Disko Island	261
8.1 Project aims revisited.....	261
8.1.1 Primary aim.....	261
8.1.2 Focused aims.....	261
8.2 Critical review and proxy synthesis selection.....	262
8.1.1 Catchment study.....	262
8.1.2 Lake Disko 2.....	263
8.1.3 Lake Disko 1.....	264
8.1.4 Lake Disko 4.....	265
8.3 Thesis synthesis.....	266
8.3.1 Ecology.....	266
8.3.2 Geomorphology.....	268
8.3.3 Pan-Arctic synthesis.....	273

Table of Contents

8.3.4 Greenland scale synthesis	276
8.3.5 Regional scale synthesis	279
8.3.6 Lower elevation lake synthesis	281
8.3.7 Recent change synthesis	284
8.3.8 Implications for carbon cycling	287
8.4 Project challenges and future directions	290
References	295
Appendix A – Detailed review of lipid biomarker ratios and equations suitable for palaeolimnological studies.....	324
A1. Ratios and equations	324
A2. Chemical structure of example lipid biomarkers	328
Appendix B – Supplementary tables from hydro-geomorphic vegetation catchment survey and site information	329
Appendix C – Supplementary figures from lake Disko 2.....	333
Appendix D – Supplementary figures from lake Disko 1	338
Appendix E – Supplementary figures from lake Disko 4.....	341

List of Figures

Figure 1.1: Conceptual diagram representing how temperature and precipitation mediates DOC fluxes in lakes across broad regions in the mid-high latitudes.	7
Figure 1.2: Flux of dissolved organic carbon (DOC) through the landscape and into lakes.	8
Figure 1.3: Maps showing the location of Disko Island study area.	18
Figure 1.4: Air temperatures separated into winter (blue), spring (yellow), summer (green) and autumn (red) for Arktisk Station, Disko Island (1991-2011), Ilulissat historical data (1873-1992) and future metrological predictions (shaded) from the Danish Meteorological Institute’s HIRAM4 model.	20
Figure 1.5: Alkenone lake water temperature reconstruction (Kanger Stack) for west Greenland (Kangerlussuaq) derived from lakes Braya Sø and Lake E representing temperature fluctuations associated with transitions in populations (Thule, Norse, Dorset and Saqqaq).	24
Figure 1.6: Map of the Disko region and insert Greenland map with the location of existing proxy studies from lake, ocean and ice cores indicated.	26
Figure 1.7: Deglaciation of Greenland from the last glacial maximum (LGM).	32
Figure 1.8: The extent of glacial advance and retreat in the study region of Disko Island.	33
Figure 1.9: Age-altitude diagram showing ¹⁴ C (uncalibrated) dates from the south of Disko Island and Kitsissut.	34
Figure 2.1: Chemical structure of chlorophyll <i>a</i> (indicator of total algal production).	36
Figure 2.2: Pathways of pigment production, transformation and degradation in lakes.	39
Figure 2.3: Plot of $\delta^{13}\text{C}$ against C/N values to highlight expected zones for organic matter sourced from lacustrine algae, C ₃ land plants and C ₄ land plants.	52
Figure 3.1: Flowchart of the analytical procedure for pigment analysis using HPLC.	65
Figure 3.2: Flowchart of the analytical procedure for lipid analysis using GC/GC-MS or GC-C-IRMS.	67
Figure 3.3: Comparisons of Newcastle University Geography and Geoscience GC-MS relative abundance results for <i>n</i> -alkanes, showing the similar distributions when using different machines.	68
Figure 4.1: Location map of the area of Disko Island selected for this study.	75

Figure 4.2: Map of Disko 2 cirque lake study area (~575 m a.s.l; 69°23.342'N, 53°24.085' W) set above the Blæsedalen (Itinneq Kanglilleq) and Kuussuaq valleys.	77
Figure 4.3: Image in an easterly direction of the Disko 2 cirque lake.....	78
Figure 4.4: Multi-panel figure for the Disko 2 cirque lake.....	79
Figure 4.5: Map of Disko 1 lake (elevation ~299 m a.s.l; 69°21.204'N, 53°29.421'W) study catchment in the Blæsedalen (Itinneq Kanglilleq) U-shaped valley.	81
Figure 4.6: Panoramic image in a southerly direction of Lake Disko 1 in the Blæsedalen (Itinneq Kanglilleq) U-shaped valley.	82
Figure 4.7: Panoramic image in a westerly direction of the Blæsedalen (Itinneq Kanglilleq) U-shaped valley from the hiking shelter (left foreground).	83
.....	83
Figure 4.8: Image in a south-westerly direction of lake Disko 1 in the Blæsedalen (Itinneq Kanglilleq) U-shaped valley.	84
Figure 4.9: Map of Disko 4 study site adjacent to the Ipraatsi valley (214 m a.s.l; 69°17.841'N, 53°48.548'W).	86
Figure 4.10: Panoramic image of the Disko 4 study lake facing south.	87
Figure 4.11: Multi-panel figure for the Disko 4 lake.....	88
Figure 4.12: Example contrasting quadrats from the catchment of Disko 1 (A) and Disko 2 (B).	93
Figure 4.13: C/N vs $\delta^{13}\text{C}_{\text{TOC}}$ for catchment end-member samples from Disko 2.	102
Figure 4.14: C/N vs $\delta^{13}\text{C}_{\text{TOC}}$ for catchment end-member samples from Disko 1.	105
Figure 4.15: C/N vs $\delta^{13}\text{C}_{\text{TOC}}$ for catchment end-member samples from Disko 4.	108
Figure 4.16: C/N vs $\delta^{13}\text{C}_{\text{TOC}}$ for catchment end-member samples from all three Disko catchment study areas.	109
Figure 4.17: Part 1 of lipid distribution histograms for saturated (a) <i>n</i> -alkanoic acids, (b) <i>n</i> -alkanes and (c) <i>n</i> -alkanols for selected catchment plants analysed using GC-MS. Plotted as a percentage of total straight chain abundance.	114
Figure 4.18: Part 2 of lipid distribution histograms for saturated (a) <i>n</i> -alkanoic acids, (b) <i>n</i> -alkanes and (c) <i>n</i> -alkanols for selected catchment plants and soils analysed using GC-MS. Plotted as a percentage of total straight chain abundance.	115
Figure 4.19: Part 3 of lipid distribution histograms for saturated (a) <i>n</i> -alkanoic acids, (b) <i>n</i> -alkanes and (c) <i>n</i> -alkanols for selected catchment soils analysed using GC-MS. Plotted as a percentage of total straight chain abundance.	116
Figure 5.1: Stratigraphy for sequence 1 (S1) comprising lake Disko 2 R1-1 & R1-2 overlapping Russian and K1 HON-Kajak core drives with proposed depth matching sequence.....	139

Figure 5.2: Corrected and calibrated ^{14}C dates (cal. yr BP) with top and bottom date from $^{210}\text{Pb}/^{137}\text{Cs}$ CRS recent model plotted against master sequence depth (K1 & R1-1).	143
Figure 5.3: ^{210}Pb supported and unsupported activity plotted against depth for the Disko 2 K1 short core.	145
Figure 5.4: ^{137}Cs and ^{241}Am activity plotted against depth for the Disko 2 K1 short core.	145
Figure 5.5: Age depth models and sedimentation rates for the Disko 2 K1 short core.	146
Figure 5.6: Age-depth model for Disko 2 S1 combined HON-Kajak (K1) and Russian (R1-1) adjusted master sequence.	147
Figure 5.7: Stratigraphic plot for Disko 2 S1 pigment concentrations expressed against TOC.	150
Figure 5.8: PCA ordination biplot for Disko 2 S1. Complete with pigments (as species) plotted against samples. Sample zone origins are listed in the figure key....	151
Figure 5.9: Stratigraphic sequence 1 (S1) geochemical data (TOC, N, C/N, $\delta^{13}\text{C}_{\text{TOC}}$), carbon mass accumulation rate (CMAR) pigment PCA 1 ($\lambda = 0.46$) and PCA 2 ($\lambda = 0.20$) scores and key pigment ratios.	154
Figure 5.10: Stratigraphic sequence 1 (S1) Disko 2 compound specific fatty acid (FAMES) $\delta^{13}\text{C}$ data plotted against $\delta^{13}\text{C}_{\text{TOC}}$.	156
Figure 5.11: Stratigraphic Disko 2 sequence 1 (S1) <i>n</i> -alkane lipid biomarker data.	158
Figure 5.12: Stratigraphic Disko 2 sequence 1 (S1) <i>n</i> -fatty acid (FAMES) lipid biomarker data.	160
Figure 5.13: Sequence 1 (S1) Disko 2 R1-1 <i>n</i> -alkanol, sterol, ketone and phytol lipid biomarker data.	162
Figure 5.14: Disko 2 S1 key diatom concentration data supplied by A.Young and V.Jones, plotted against both date and depth from zone A and the upper parts of zone B.	164
Figure 5.15: Disko 2 S1 XRF data supplied by A.Young and V.Jones (UCL) presented as percentage (%) (Ti, Fe, Ca, Al, Si, P) and in $\mu\text{g/g}$ (Sr, Pb, Br, Cd).	166
Figure 5.16: Summary diagram for multi-proxy study of Disko 2 Sequence 1 presented against age (cal. yr BP).	169
Figure 5.17: Stratigraphy for sequence 2 (S2) comprising lake Disko 2 R2-1 and R2-2 Russian core drives presented separately.	171
Figure 5.18: Stratigraphic plot for Disko 2 R2-1 Russian core of selected pigment concentrations expressed against OM (LOI 550 °C).	175

Figure 5.19: Stratigraphic plot for Disko 2 R2-2 Russian core of selected pigment concentrations expressed against OM (LOI 550 °C).....	177
Figure 5.20: Disko 2 S1 sequence key proxies plotted against year (AD).	190
Figure 6.1: Stratigraphy for Disko 1 R2-1 and R2-2 overlapping Russian and K1 HON-Kajak core drives and proposed depth matching sequence.	202
Figure 6.2: Radiocarbon dating results plotted against depth.....	206
Figure 6.3: Stratigraphic diagram for Russian (R2-1 & R2-2) and HON-Kajak (R1-1) overlapping sequences from lake Disko 1.	208
Figure 6.4: Stratigraphic pigment diagram for final combined core sequence from lake Disko 1.	211
Figure 6.5: PCA ordination biplot for Disko 1 combined stratigraphy. Complete with pigments (as species) plotted against samples.	212
Figure 6.6: Disko 1 final combined core sequence pigment PCA 1 & 2 scores on log ¹⁰ transformed data (centred and standardised) and key pigment ratios.....	215
Figure 6.7: Disko 1 summary diagram combining OM, selected pigments (diatoxanthin, alloxanthin, lutein-zeaxanthin & chlorophyll <i>a</i>), pigment PCA axes (1 & 2) and the ratio of alloxanthin: diatoxanthin for clear comparison.....	222
Figure 7.1: Stratigraphy for Disko 4 R2-1 and R2-2 overlapping Russian and K2 HON-Kajak core drives and proposed depth matching sequence.	230
Figure 7.2: Stratigraphic diagram for Russian (R2-1 and R2-2) overlapping sequences and HON-Kajak (K2) core appended above.....	232
Figure 7.3: Stratigraphic diagram for adjusted values from Disko 4 for OM, TOC and DW which is used in subsequent graphs and expressed relative to pigment concentration.	233
Figure 7.4: ²¹⁰ Pb activity plotted against depth for the Disko 4 K2 short core.....	237
Figure 7.5: ²¹⁰ Pb age and ¹³⁷ Cs activity plotted against depth for the Disko 4 K2 short core.	237
Figure 7.6: ²¹⁰ Pb age and ²⁴¹ Am activity plotted against depth (cm) for the Disko 4 K2 short core.	238
Figure 7.7: Sedimentation rate plotted against ²¹⁰ Pb age for the Disko 4 K2 short core.	238
Figure 7.8: Age-depth model for Disko 4 combined HON-Kajak (K2) and Russian (R2-1 & R2-2) master sequence.	240
Figure 7.9: Stratigraphic plot for final combined HON-Kajak and Russian sequence (K2, R2-1 & R2-2) from Disko 4 of pigment concentrations expressed against TOC.	243

Figure 7.10: PCA ordination biplot for Disko 4 combined stratigraphy (R2-1, R2-2, K2).....	244
Figure 7.11: Stratigraphic Disko 4 geochemical data (% TOC, % N, C/N, $\delta^{13}\text{C}_{\text{TOC}}$), carbon accumulation rate (CMAR), pigment PCA 1 ($\lambda = 0.76$) and PCA 2 ($\lambda = 0.12$) scores and key pigment ratios.	248
Figure 7.12: Disko 4 summary diagram of key changes combining C/N ratio, selected pigments (fucoxanthin, diatoxanthin, alloxanthin, pheophytin <i>b</i>), pigment PCA axis 1 and the ratio of fucoxanthin: diatoxanthin for clear comparison.....	254
Figure 7.13: Disko 4 recent summary diagram of key changes combining %TOC, %N, C/N ratio and selected pigments (fucoxanthin, diatoxanthin, alloxanthin, canthaxanthin, pheophytin <i>a</i> & β -carotene) for clear comparison.	259
Figure 8.1: Schematic diagram of lake Disko 2 (cirque lake) positioned above Kaussuaq incised valley, extending to the north of the Blæsedalen (Itinneq Kanglilleq) valley.....	270
Figure 8.2: Schematic diagram of lake Disko 1 and its position in the Blæsedalen (Itinneq Kanglilleq) U-shaped valley.	271
Figure 8.3: Schematic diagram of lake Disko 4 (valley end lake) positioned above the Ipraatsi valley and feeding into Laksebugt bay.....	272
Figure 8.4: Pan-Arctic and hemispheric scale synthesis – comparing selected lake Disko 2 reconstructions with existing pan-Arctic and northern hemisphere proxies.	275
Figure 8.5: Greenland synthesis – comparing selected lake Disko 2 reconstructions with existing pan-Greenland proxies.....	278
Figure 8.6: Regional synthesis - comparing selected lake Disko 2 reconstructions with existing regional proxies.	280
Figure 8.7: Disko 4 combined sequence summary diagram of pigments canthaxanthin, diatoxanthin, alloxanthin, ratio of alloxanthin: diatoxanthin and C/N ratio.....	283
Figure 8.8: Recent change summary diagram for Disko 2 and 4 short cores.....	286
Figure 8.9: Comparing organic carbon mass accumulation rate (CMAR) for dated lake Disko 2 and 4 records.	289
Figure A.1: Chemical hydrocarbon structure of C_{17} <i>n</i> -alkane ($\text{C}_{17}\text{H}_{36}$, heptadecane).	328
Figure A.2: Chemical structure of C_{16} <i>n</i> -alcohol ($\text{C}_{16}\text{H}_{34}\text{O}$, hexadecan-1-ol).....	328
Figure A.3: Chemical structure of phytol ($\text{C}_{20}\text{H}_{40}\text{O}$, 3,7,11,15-tetramethyl-2-hexadecen-1-ol).....	328
Figure A.4: Chemical structure of C_{16} <i>n</i> -fatty acid ($\text{C}_{16}\text{H}_{32}\text{O}_2$, hexadecanoic acid).	328
Figure A.5: Chemical structure of cholesterol ($\text{C}_{27}\text{H}_{46}\text{O}$, cholest-5-en-3 β -ol).....	328

Figure C.1: Stratigraphic diagram of bulk measures for sequence 1 (S1) from lake Disko 2 including K1 (orange circles), R1-1(blue triangles) and R1-2 (green squares).
 333

Figure C.2: Stratigraphic diagram of geochemical variables for overlapping sequence 1 (S1) from lake Disko 2 including K1 (orange circles) and R1-1(green triangles).. 334

Figure C.3: Stratigraphic pigment diagram for HON-Kajak K1 (orange circles) and Russian R1-1 (green triangles) overlapping S1 sequence from lake Disko 2..... 335

Figure C.4: Stratigraphic pigment diagram for HON-Kajak K1 (orange circles) and Russian R1-1 (green triangles) overlapping S1 sequence from lake Disko 2..... 336

Figure C.5: Stratigraphic pigment diagram for HON-Kajak K1 (orange circles) and Russian R1-1 (green triangles) overlapping S1 sequence from lake Disko 2..... 337

Figure D.1: Stratigraphic pigment diagram corrected by OM for overlapping K1 (orange triangles), R2-1 (blue circles) and R2-2 (green squares) sequences from lake Disko 1..... 338

Figure D.2: Stratigraphic pigment diagram corrected by DW for overlapping K1 (orange triangles), R2-1 (blue circles) and R2-2 (green squares) sequences from lake Disko 1..... 339

Figure D.3: Stratigraphic diagram to compare the HON-Kajak short core (K1) with the top of the upper Russian core (R2-1) for Disko..... 340

Figure E.1: Stratigraphic pigment diagram corrected by OM for HON-Kajak K2 (orange circles), Russian overlapping sequences R2-1 (blue triangles) and R2-2 (green squares) cores from lake Disko 4..... 341

Figure E.2: Stratigraphic pigment diagram corrected by TOC for HON-Kajak K2 (orange circles), Russian overlapping sequences R2-1 (blue triangles) and R2-2 (green squares) cores from lake Disko 4..... 342

Figure E.3: Stratigraphic pigment diagram corrected by DW for HON-Kajak K2 (orange circles), Russian overlapping sequences R2-1 (blue triangles) and R2-2 (green squares) cores from lake Disko 4..... 343

List of Tables

Table 2.1: The stability of pigments typically detected in the water column and sediments of lakes.	38
Table 2.2: Lipid <i>n</i> -alkane (hydrocarbon) compounds typically detected in the sediments of lakes and catchment plant/soil samples.....	43
Table 2.3: Lipid <i>n</i> -fatty acid compounds typically detected in the sediments of lakes and catchment plant/soil samples.....	44
Table 2.4: Lipid <i>n</i> -alkanol and some sterol compounds detected in the sediments of lakes and catchment plant/soil samples.....	45
Table 2.5: Summary of the potential controls on bulk $\delta^{13}\text{C}_{\text{TOC}}$ in lakes collated by the author.....	50
Table 3.1: HPLC solvent programme for pigment analysis based on a modified version of Chen et al. (2001).....	64
Table 4.1: Study lake characteristics derived from in-field and imagery based land cover classification.....	90
Table 4.2: Vegetation composition surveys of the three study lakes local catchments.....	92
Table 4.3: Water chemistry spot samples from Disko Island lakes in April and August 2013.....	96
Table 4.4: HPLC pigment analysis of filtered water samples from Disko Island study lakes in August 2013.....	98
Table 4.5: End-member $\delta^{13}\text{C}_{\text{TOC}}$, TOC (%), N (%) and C/N results from the Disko 2 catchment.....	101
Table 4.6: End-member $\delta^{13}\text{C}_{\text{TOC}}$, %TOC, %N and C/N results from the Disko 1 catchment.....	104
Table 4.7: End-member $\delta^{13}\text{C}_{\text{TOC}}$, TOC (%), N (%) and C/N results from the Disko 4 catchment.....	107
Table 4.8: Selected lipid ratios for catchment samples from Disko 2 analysed using GC-MS.....	119
Table 4.9: Selected compound-specific catchment samples from Disko 2 analysed for $\delta^{13}\text{C}_{\text{FAMES}}$ compared with $\delta^{13}\text{C}_{\text{TOC}}$	121
Table 5.1: Radiocarbon dating results from Disko 2 (S1) sediment sequences (K1 & R1-1).....	141
Table 5.2: Corrected radiocarbon dating results from Disko 2 sediment sequences and selection decision for retention or exclusion from age-depth model.....	142
Table 5.3: Radiocarbon dating results from Disko 2 S2 sediment sequence.....	173

Table 6.1: Radiocarbon dating results from Disko 1 Russian sediment sequences R2-2 and R2-1.	205
Table 7.1: Radiocarbon dating results from Disko 4 Russian sediment sequences R2-2 and R2-1.	235

List of Equations

Equation 3.1: Calculation of sediment % dry weight (DW).	60
Equation 3.2: Calculation of %LOI 550 °C (OM).	60
Equation 3.3: Calculation of carbonate content (CaCO ₃).	61
Equation 3.4: Calculation of chl <i>a</i> concentration in lake waters.	63
Equation 3.5: Calculation of carbon isotope ratios.	66
Equation A.1: The Carbon Preference Index (CPI) (Bray and Evans, 1961; Cooper and Bray, 1963).	324
Equation A.2: The modified Carbon Preference Index 2 (Marzi et al., 1993).	324
Equation A.3: Carbon Preference Index for low molecular weight compounds (CPI _L) (Matsuda and Koyama, 1977).	325
Equation A.4: Carbon Preference Index for high molecular weight compounds (CPI _H) (Matsuda and Koyama, 1977).	325
Equation A.5: Carbon Preference Index for the entire range of saturated fatty acids detected (CPI _T) (Matsuda and Koyama, 1977).	325
Equation A.6: The Average Chain Length (ACL) index of Poynter et al. (1989). Where $\Sigma[C_i]$ is the concentration of the <i>n</i> -alkanes with carbon number <i>C_i</i> , over C ₂₇ -C ₃₃	326
Equation A.7: Terrigenous to aquatic hydrocarbon ratio (TAR _{HC}) of Bourbonniere and Meyers (1996).	326
Equation A.8: Terrigenous to aquatic fatty acid ratio (TAR _{FA}) of (Meyers, 1997). ...	326
Equation A.9: Aquatic macrophyte ratio (<i>P_{aq}</i>) of Ficken et al. (2000).	326
Equation A.10: The <i>P_{WAX}</i> index of waxy <i>n</i> -alkanes to total hydrocarbons.	327
Equation A.11: The autochthonous to allochthonous ratio for acid compounds (Aut/All ratio acid) as presented by Pearson et al. (2007).	327
Equation A.12: The autochthonous to allochthonous ratio for alkanol compounds (Aut/All ratio alkanol) as presented by Pearson et al. (2007).	327

Abbreviations used in the thesis

Accelerated solvent extraction (ASE)
Accelerator mass spectrometry (AMS)
Ammonium (NH_4^+)
Aquatic macrophyte ratio (P_{aq})
Average Chain Length (ACL)
Below detection limits (BDL)
Bicarbonate, (HCO_3^-)
Bis(trimethylsilyl)trifluoroacetamide (BSTFA)
Carbon (C)
Carbon dioxide (CO_2)
Carbon mass accumulation rate (CMAR)
Carbon Preference Index (CPI)
Carbonate content (CaCO_3)
Coloured dissolved organic matter (CDOM)
Compositional diversity index (CDI)
Compound specific isotope analysis (CSIA)
Constant initial concentration (CIC)
Constant rate of ^{210}Pb supply (CRS)
Detrended correspondence analysis (DCA)
Dissolved inorganic carbon (DIC)
Dissolved inorganic nitrogen (DIN)
Dissolved organic carbon (DOC)
Dissolved organic matter (DOM)
Dissolved organic nitrogen (DON)
Dissolved oxygen (DO)
East Greenland Current (EGC)
Elemental analyser (EA)
Fatty acid methyl esters (FAMES)
Gas chromatography – combustion – isotope ratio mass spectrometry (GC-C-IRMS)
Gas chromatography – mass spectrometry (GC-MS)
Greenland Ice Sheet (GIS)
High-performance liquid chromatography (HPLC)
Holocene Thermal Maximum (HTM)
Hydrochloric acid (HCl)
Intertropical convergence zone (ITCZ)
Irminger Current (IC)
Last Glacial Maximum (LGM)
Little Ice Age (LIA)
Long chain alkenones (LCAs)

Loss on ignition 550 °C (LOI 550 °C)
Marine isotope stage (MIS)
Medieval Climate Anomaly (MCA)
Methane (CH₄)
NERC Isotope Geosciences laboratory (NIGL)
NERC Radiocarbon Facility (NERC RCF)
Nitrogen (N)
Organic matter (OM)
Particulate organic carbon (POC)
Percentage dry weight (DW)
Phosphorus (P)
Photodiode Array Detector (PDA)
Photo-synthetically active radiation (PAR)
Principal components analysis (PCA)
Recent Warming (RW)
Relative abundance (RA)
Soluble reactive phosphorus (SRP)
Standard deviation (SD)
Terrigenous to aquatic fatty acid ratio (TAR_{FA})
Terrigenous to aquatic hydrocarbon ratio (TAR_{HC})
Total lipid extract (TLE)
Total lipid extract (TLE)
Total organic carbon (TOC)
Total Phosphorus (TP)
Ultraviolet radiation (UVR)
Ultra-violet radiation (UVR)
Unresolved complex mixture UCM
Vienna Pee Dee Belemnite (VPDB)
West Greenland Current (WGC)
X-ray fluorescence (XRF)
Younger Dryas (YD)

Chapter 1: Introduction and Literature review

This chapter provides the background on carbon cycling as an environmental issue, its relevance to the Arctic and to freshwater lakes, together with a review of key landscape processes. The study aims, objectives and research questions are then set, followed by a description of the study area, a review of regional Holocene environmental change and a summary of the regions deglacial history.

1.1 Carbon cycling

1.1.1 The global carbon cycle

The amount of carbon globally is fixed, but this carbon has many stores as it is transformed through the atmosphere, marine, terrestrial, land and freshwater sinks. Carbon is the key building block of life as all organisms contain carbon compounds which subsequently become sedimented. Globally, the combustion of fossil fuels and changes in land use have substantially increased CO₂ (carbon dioxide) emissions to the atmosphere (Keeling and Whorf, 2005), which as a greenhouse gas is contributing to spatially heterogeneous warming and the modification of global climate cycles. But the relationship between increased CO₂ and global carbon sinks is complex and non-linear, in part because the Holocene (since ~11,700 years BP) has generally seen stability in atmospheric CO₂ variations (<20 ppm), compared with more dramatic alterations during the past 200 years (increase of >100 ppm) (Sabine, 2004).

Feedbacks are known to be associated with increasing CO₂ and temperature. As photosynthesis can be greater at higher temperatures modelling has shown that up to 30% of current emissions may be absorbed by increased terrestrial carbon cycling (Schimel et al., 2015), but that beyond debated levels the biosphere is likely to switch from being a 'source' to a 'sink' (Cox et al., 2000). Oceans are also a 'sink' for anthropogenic carbon as increased atmospheric CO₂ dissolves to form carbonic acid (Sabine et al., 2004) but has deleterious effects on vulnerable carbonate ecosystems (Hoegh-Guldberg et al., 2007). Stores such as permafrost are known to be potentially vulnerable to warming, which is a large current store of both CO₂ and methane (CH₄). There is evidence that increased microbial activity may be transforming permafrost regions from greenhouse gas 'sinks' to 'sources', although the rate of future change is debated (Schuur et al., 2015). As climate becomes more extreme with more frequent storms and droughts due to global warming, the resilience of key carbon sinks may

decline, resulting in enhanced feedback and higher temperatures (Reichstein et al., 2013). Inland freshwater ecosystems are a key 'source' or 'sink' in the global carbon cycle but are often neglected (Cole et al., 2007), with this thesis focused on reconstructing the carbon cycle within Arctic lakes.

1.1.2 Why is carbon cycling important in the Arctic?

Arctic ecosystems have been influenced by multiple changes over the past century (Hinzman et al., 2013), including climate warming, but also other stressors such as nitrogen deposition, long-range contamination, changes in the length of the growing season and variations in precipitation (Anderson et al., 2017). The Arctic has large stores of carbon contained in permafrost, soils and in the sediments of lakes, wetlands and the high-latitude oceans (McGuire et al., 2009), but the sensitivity of these stores to anthropogenic perturbation needs to be understood to estimate the magnitude and consequences of future change. Despite the lower primary productivity of the Arctic compared with the lower latitudes, the Arctic is a sink of up to 0.8 Pg C/yr which is up to 25% of the global net land/ocean flux of carbon during the 1990s (McGuire et al., 2009), highlighting the importance of this region for global carbon budgets. Evidence is emerging that a system-wide shift across the Arctic to the altered climatic state is occurring as permafrost is warming, hydrological processes change, sea ice melts earlier, soils destabilise and biological systems evolve, resulting in a more unpredictable system (Hinzman et al., 2005). The changing Arctic should not be understood as isolated, but connected to lower latitudes through its impact on CO₂ and CH₄ cycling, connectivity through river runoff, links to thermohaline circulation of the oceans and moderating effects on atmospheric circulation (Overpeck et al., 1997).

Changes in temperature, precipitation and indirect effects between plants, microbes and their environment have modified soils, influencing the carbon cycle at multiple scales (Bardgett et al., 2008). Modelling suggests that the majority of warming-induced soil carbon loss may be concentrated in the Arctic and subarctic regions, leading to further amplification and vulnerability (Crowther et al., 2016). Although increased precipitation to permafrost (wetting) has been linked to increased primary production and more carbon storage in some settings (Lupascu et al., 2014), recent change is generally associated with Arctic permafrost instability, the microbial breakdown of organic carbon and release of CO₂ and CH₄ (Schuur et al., 2015). Arctic tundra is a key source of global CH₄ emissions (Zona et al., 2016) which is likely to increase with warming (Schuur et al., 2008). Arctic sea ice thickness and extent has

declined substantially since the 1950s (Stroeve et al., 2007; Kwok and Rothrock, 2009), affecting ecological dynamics, structure and function (Post et al., 2013) with further impacts on Arctic atmospheric circulation (Overland and Wang, 2010). Similarly, Arctic glaciers are generally in retreat, responding to changes in temperature, precipitation, and the ice-free season (Carr et al., 2014; Sharp et al., 2014; Solomina et al., 2016). The inland aquatic environment including lakes, rivers and wetlands is also modified by these marked changes (Overpeck et al., 1997; Smol and Douglas, 2007; McGuire et al., 2009; Anderson et al., 2017), although these impacts on carbon cycling are not always included in global budgets (Cole et al., 2007).

1.1.3 Arctic lakes as integrators and regulators of carbon

Lakes are increasingly recognised as active sources and sinks of carbon, mineralizing and processing carbon from a range of autochthonous and allochthonous origins (Klug, 2002; Cole et al., 2007; Clow et al., 2015; McGowan et al., 2016). High latitude Arctic lakes are understood to be particularly sensitive to environmental change as the biological communities present are often close to their northerly tolerances (Vincent and Hobbie, 2000; Smol and Douglas, 2007). Exploring shifts between lake net-autotrophy and carbon sequestration, or CO₂ release and net-heterotrophy is a key challenge in palaeolimnology (Jonsson et al., 2003; Algesten et al., 2004; Kortelainen et al., 2004; Jansson et al., 2012), particularly over Holocene timescales as this may help understand how lakes respond to present and future stressors. Existing studies that include measurements of lake net heterotrophy (Cole et al., 2000; Sand-Jensen and Staehr, 2009; Staehr et al., 2010) rarely also consider carbon sequestration through the analysis of organic geochemical proxies and so it is not usually possible to speculatively identify lakes that are simultaneously net-heterotrophic and sequesters of carbon. As lakes are sentinels, integrators and regulators of past environmental change (Williamson et al., 2009), they provide excellent archives of both the quantity and quality of carbon deposited (Tranvik et al., 2009).

1.1.4 Carbon cycling in Arctic lakes

Our understanding of how lakes process autochthonous and allochthonous carbon remains limited (Cole et al., 2007), particularly in Arctic lake catchments with multiple diverse catchment sources. Lakes integrate and process carbon from terrestrial and in-lake sources, but the response to environmental change may be non-linear with biotic couplings and feedbacks between plant functional types (PFTs) (Wookey et al., 2009), glaciers (Slemmons et al., 2013), permafrost (Schuur et al., 2008; Schuur et al., 2009) and climate (Smol and Douglas, 2007). Lakes can be conceptualised as net-heterotrophic, releasing CO₂ to the atmosphere or net-autotrophic and sequestering carbon (Jansson et al., 2000; Ask et al., 2009). Understanding the dynamic links between landscape processes, climate variability and lake carbon cycling is important as Arctic lakes are known to process large volumes of carbon per unit area and so have the potential to influence both regional and global carbon budgets (Kortelainen et al., 2004; Anderson et al., 2009; Sobek et al., 2009; Kastowski et al., 2011) and biogeochemical cycles (Tranvik et al., 2009). This subsection briefly outlines the relevance of carbon cycling studies to investigations of Arctic lakes, reviews the role of dissolved organic matter (DOM)/DOC and explains the relevance of heterotrophic and mixotrophic strategies as alternative mechanisms for biological production.

Recent warming since the end of the Little Ice Age (LIA) in the Arctic has been linked with the expansion of vegetation and ‘greening’ (Sturm et al., 2001), which can potentially modify the terrestrial cycling of carbon into lakes. Vegetation changes over Holocene timescales have probably influenced the quantity and quality of carbon mineralized in arctic lakes (Rosén and Hammarlund, 2007; Reuss et al., 2010a). Such changes in tree-line can be mediated both by climate and succession. Arctic wetlands are key areas of waterlogging, degradation and decomposition of terrestrial organic matter (Hobbie et al., 2000). However, the coupling between Arctic wetlands and lakes across highly heterogeneous landscapes is poorly understood. With warming, permafrost degradation is expected to increase causing uncertain impacts on Arctic hydrology, ecology, gas flux and the release of organic matter (Frey and McClelland, 2009). For example, thermokarst lakes may have contributed to climate warming in the early Holocene as there was a large release of methane (CH₄) (Walter et al., 2007).

Present warming may induce similar feedbacks releasing carbon from soils, peatlands and permafrost into lakes. Additionally, many high latitude and Arctic environments are significantly glaciated which can modify nutrient fluxes and the supply of organic,

inorganic and microbially modified material into catchment lakes (Anesio et al., 2009; Slemmons et al., 2013; Slemmons et al., 2015). Lake carbon cycling can also be driven by climate directly through length of the ice free season, for example in recent diatom, chironomid and chrysophyte communities of some Arctic lakes, influencing the time available for biological production and species composition (Smol et al., 2005). However, climate can also function as a secondary driver, with catchment and in-lake processes mediating carbon cycling (Anderson et al., 2008; McGowan et al., 2008; Law et al., 2015; Anderson et al., 2017).

Arctic lake sediments can store considerable amounts of organic carbon, comparable with other potential stores (e.g. soils). For example, in Kangerlussuaq, south-west Greenland the carbon accumulation rate ($\sim 4.9 \times 10^{13}$ g C) in small lakes (<100 ha) from the coast to the ice sheet margin of has been calculated to be half of the total soil pool despite lakes covering only 5% of the land surface (Anderson et al., 2009). However, studies that extrapolate a small number of dated sequences to cartographic lake area measurements in a specific region can only be estimations, are location specific and are unable to separate terrestrial from in-lake drivers of carbon cycling. At Flakkerhuk on Disko Island a 1,800 ha study site has been classified using supervised remote sensing and used to estimate the total soil carbon stored to be ~ 6.7 kg m⁻², with the greatest stocks in waterlogged fen areas (Jensen et al., 2006). It has also been demonstrated that lakes in northern regions can be supersaturated with CO₂, and so are more likely to be net-heterotrophic (Jonsson et al., 2003).

1.1.5 The role of DOC and DOM in Arctic lakes

Dissolved organic matter (DOM) is sourced from both external and in-lake sources. Allochthonous DOM is typically brown-coloured (CDOM) and is sourced from decomposing terrestrial organic matter and includes high levels of humic and fulvic acids. In contrast, autochthonous DOC or DOM is typically colourless and has a lower molecular weight due to the algal and microbial sources (McGowan et al., 2016). DOC is defined as any organic compound in water that can pass a 0.45- μ m filter, and is a key part of lake metabolism (Roulet and Moore, 2006). Lake response to environmental change is complicated by DOC as it functions as a photo-protectant, inhibiting harmful UV radiation (UVR) (Sommaruga, 2001). With low levels of DOC, for example in catchments that are not significantly vegetated the lack of DOC may mean high levels of UVR limit autotrophic production (Bothwell et al., 1994).

During periods of developed catchment vegetation, DOC flux may stimulate autotrophic production due to photo-protection of aquatic organisms indicated by changes in algal abundance (Leavitt et al., 2003). Aquatic organisms, particularly cyanobacteria may produce UVR-absorbing pigments (with spectra similar to scytonemin) which for these pigments in response to UV exposure as a form of photo-protection (Leavitt et al., 1997; McGowan, 2013). However, an alternative mechanism of algal production is the stimulation of facultative mixotrophic or heterotrophic organisms due to the input of DOC providing an energy supplement (Findlay et al., 2001). Increases in light-limiting DOC may also suppress autotrophic production, with the lake switching to a primarily net-heterotrophic state (Jansson et al., 2000).

With terrestrial plant succession, changes in plant functional types (PFTs) may lead to changes in litter fall, its microbial processing and the delivery of allochthonous DOM and DOC into lakes (Tranvik et al., 2009). The character and quality of aquatic carbon has been shown to influence biogeochemical cycles in lakes. Williamson et al. (1999) demonstrated that in addition to considering lakes in terms of their trophic status (from hyper-eutrophic to oligotrophic) an axis of CDOM, should be considered. The intensity of CDOM can regulate many processes, for example by providing a substrate for mixotrophy or by regulating light limitation, thus determining a lakes relative in-lake versus terrestrially derived production (Williamson et al., 1999). McGowan et al. (2016) characterise how differences in temperature and precipitation regulate DOC fluxes in lakes across broad mid-high latitude landscapes, highlighting the heterogeneity of lake response to carbon in diverse regions (Figure 1.1). Taking a more localised approach, Roulet and Moore (2006) have conceptualised how DOC exported to lakes in each catchment is closely coupled with catchment processes (Figure 1.2).

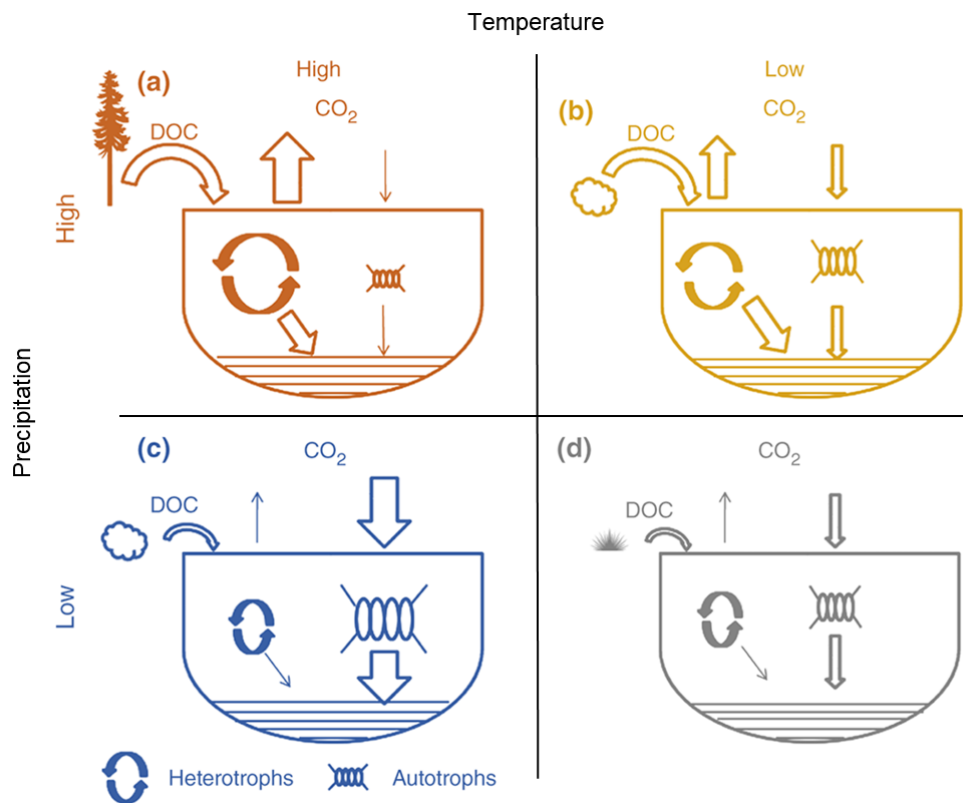


Figure 1.1: Conceptual diagram representing how temperature and precipitation mediates DOC fluxes in lakes across broad regions in the mid-high latitudes. The size of each arrow indicates the relative contribution from the relevant process. (a) Represents lakes with dominant allochthonous DOC, resulting in high levels of water colour, limiting light penetration but providing a source for heterotrophic organisms e.g. ‘humid/warm’ boreal regions (orange). (b) Represents zones where permafrost limits DOC transport and low temperatures prevent terrestrial vegetation decomposing. E.g. shrub/heath tundra, in cooler regions with high-moderate precipitation above treeline (yellow). (c) Represents areas where terrestrial vegetation and transport of DOC is limited by colourless DOC, and so a dominance of autotrophic production persists e.g. continental interiors, prairie, steppe or savannah in low precipitation regions, but with a warmer growing season (blue). (d) Represents areas of minimal vegetation development where allochthonous DOC is scarce and nutrient limitation restricts autotrophic production. E.g. the cold High Arctic, polar deserts and Montane (grey). Modified from McGowan et al. (2016).

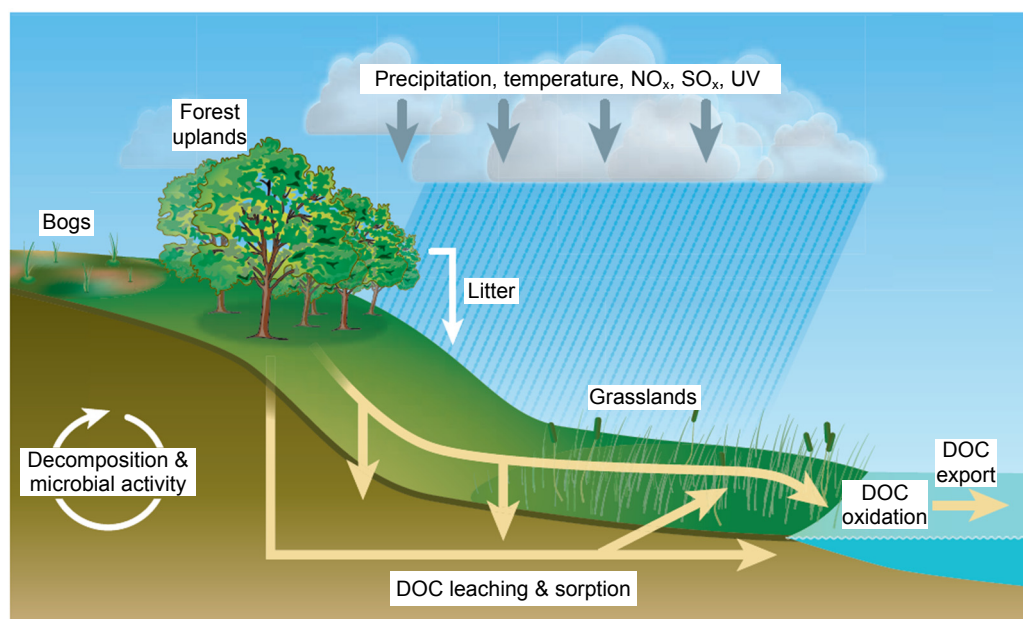


Figure 1.2: Flux of dissolved organic carbon (DOC) through the landscape and into lakes. DOC export into lakes is closely coupled to the landscapes rate of production, decomposition/microbial activity, mineral sorption by soils and hydrology. Modified from Roulet and Moore (2006).

1.1.6 Heterotrophic and mixotrophic strategies in Arctic lakes

When light is limiting or temperatures low, microbial protozoa may resort to mixotrophic or heterotrophic strategies for survival to supplement their carbon budget, or to source aquatic nutrients (Laybourn-Parry, 2002). Bacterioplankton may therefore dominate the food web of many light-limited humic lakes where allochthonous carbon compounds are readily available (Jansson et al., 2000). Flocculation, the cleaving of allochthonous humic molecules into fragments is particularly beneficial for allochthonous production as it has been found to promote attached bacteria which can be readily grazed by phagotrophic flagellates (Tranvik and Sieburth, 1989). Pålsson et al. (2005) demonstrated net-heterotrophy in Faroe Island clear water lakes was probably aided by the ability for mixotrophic phytoplankton (*Cryptomonas* spp., *Dinobryon* spp. and flagellates cf. *Ochromonas* spp.) to consume bacteria for nutrient acquisition, confirming that mixotrophy may aid in the survival of such species. Mixotrophy has been suggested to be an important survival mechanism in the cold polar lakes of the McMurdo Dry Valleys in Antarctica and may be similarly linked to limitations in the ability to fix carbon from photosynthetically active radiation (PAR) due to short ice-free periods (Roberts and Laybourn-Parry, 1999). Cryptophytes and cryptomonad-like microflagellate

populations are known to peak intermittently, following 'bloom' species and are known to function in light limiting conditions (Stewart and Wetzel, 1986). Solar radiation may help to oxidise DOM into dissolved inorganic carbon (DIC), carbon monoxide and other low-light compounds, which can either result in the complete photo-oxidation of DOC, or improve its bioavailability (Bertilsson and Tranvik, 2000).

1.1.7 The importance of the lake ecosystem in Arctic lakes

Nutrients, lake depth, basin morphometry and the balance between benthic and pelagic production, together with the extent of in-lake biotic cascades are all important controls on the lake ecosystem in Arctic lakes. Nutrients including N and P can be limiting factors restricting algal production, but the presence of nutrient limitation can be highly dependent on specific location and catchment (Hogan et al., 2014). Arctic lakes are typically nutrient poor (oligotrophic) and so slight changes in production can cause algal community shifts. Nutrient poor ecosystems are often reliant on mixotrophic algae and the microbial web for increasing the bioavailability of carbon (Brutemark et al., 2006). Variation in ice phenology can also be a key control, with lakes in the southwest region of Greenland switching from nitrate to phosphorus controlled production between ice-cover and ice-free conditions (Whiteford et al., 2016).

Climate is known not to be the only control on ecological trajectories in Arctic lakes, with catchment change and biotic relationships important controls on the source of carbon deposited (Anderson et al., 2008). Community trends were found to be more important for explaining variance than Holocene climate in a low Arctic lake on southwest Greenland, highlighting the importance of in-lake processes (Anderson et al., 2008). Benthic production is a particularly important component in Arctic lakes, due to their often oligotrophic status which can limit pelagic production (Sierszen et al., 2003). For example, periphyton can be responsible for high levels of primary production (80-98%) in nutrient poor Arctic lakes, in stark contrast to nutrient rich temperate lakes (nearly 100% pelagic) (Vadeboncoeur et al., 2003). Changes between clear water and turbid lake status can have beneficial or deleterious effects on habitat, benthic algae and macrophytes, sometimes with subsequent changes in pelagic algae (McGowan et al., 2005). Lake depth can also control basing morphometry and influence the benthic macrophyte contribution to primary production in lakes (Jeppesen et al., 2003). Clearly benthic habitats should not just be regarded as a source or sink of nutrients and energy, but as a key connected component of the lake

ecosystem (Vadeboncoeur et al., 2002) responsible for a large proportion of production in Arctic lakes (Vadeboncoeur et al., 2003).

1.2 Arctic landscape processes and impact on carbon cycling

Arctic lakes are closely coupled to the quantity and quality of carbon received from the catchment, which can be highly heterogeneous due to the diversity of Arctic geomorphology (Prairie, 2008). Permafrost, soils, vegetation succession and glaciers all have the potential to influence the inputs of nutrients and carbon (DOC and POC) into lakes. This section reviews the principal landscape processes present in Arctic lake catchments and how these processes regulate and mediate inputs of allochthonous carbon, or promote autochthonous production in lakes.

1.2.1 Permafrost

Permafrost is regarded as any subsurface material that is less than 0 °C for at least two consecutive years (Zhang et al., 1999) and makes up around 80% of the Arctic drainage basin (Frey and McClelland, 2009). It is split into categories of continuous, discontinuous, sporadic or isolated patches depending on the ice thickness. Permafrost always has a seasonally ‘active layer’ at the surface which melts during warm air temperatures (Hinkel and Nelson, 2003). The seasonally active layer can vary depending on local hydrology and temperature which can modify the delivery of organic matter, inorganic nutrients and major ions to Arctic lakes during and after precipitation events, or linked to groundwater flows (Frey and McClelland, 2009).

The effect of thawing is an active research area as recent warming has degraded permafrost in areas sensitive to changes in temperature and precipitation. Permafrost thawing has been linked to increased hydrological activity, enhanced nutrient flux, decomposition and carbon loss from soils (Lee et al., 2011). Such permafrost thawing can release old carbon from tundra (Schuur et al., 2009) and stimulate microbial decomposition (Jansson and Tas, 2014), increasing DOC in receiving waters such as lakes. Changes in permafrost active layer dynamics may also influence CO₂ emissions when coupled with wetting (Lupascu et al., 2014) and methane (CH₄) sinks (Jørgensen et al., 2015). Globally, permafrost represents a key store of carbon, but with warming most studies suggest the net effect of thawing will be to release GHGs and therefore provide a positive feedback to climate warming, despite the potential increases in carbon burial from increased growing season length and plant growth rates (Schuur et al., 2008). Thermokarst development results in significant slumping of the ground due to surface thawing which can dramatically disturb stored carbon, leading to increases in the export of DOM (Frey and McClelland, 2009). Although, the relationship is not

always linear as in the Yukon Territory of Alaska and Central Siberia, DOM released to watersheds may actually decline with permafrost degradation, as exposure to mineral soils facilitate adsorption of DOM (Carey, 2003; Prokushkin et al., 2007), albeit after an initial pulse of DOM rich meltwater from permafrost (Striegl et al., 2007). In contrast, other studies suggest that when permafrost transitions to peatland DOC concentrations rise substantially (Frey and Smith, 2005).

Past studies on the effect of permafrost thaw on aquatic ecosystems have demonstrated that the response can be complex. For example, in sediments of a lake in the Canadian Northwest Territories, degrading permafrost and linked collapsed peat scars was found in one lake to change nutrient and DOC dynamics, causing shifts in diatom species composition as small *Fragilaria* taxa are capable of thriving in low light conditions (Coleman et al., 2015). In thermokarst thaw lakes in subarctic Québec, Canada impacted lakes had higher phytoplankton (Chl *a*), TP and enhanced stratification compared with reference lakes (Przytulska et al., 2016). Both sub-sets of lakes contained diverse pigments and evidence of heterotrophy among ciliates and flagellates (Przytulska et al., 2016). Permafrost thawing has also been demonstrated in the Yukon River basin to increase groundwater discharge, potentially adjusting the overall ratio of DOC:DIC and DON:DIN in some catchments (Walvoord and Striegl, 2007). In northern Sweden, lakes in permafrost have been linked to expansion of wet minerotrophic areas, with changes in moisture balance (increased surface moisture) linked to increased TOC, rather than temperature (Kokfelt et al., 2009). This suggests the impact of changing permafrost on lakes can be complex and highly dependent on landscape position and geomorphology.

1.2.2 Arctic soils and vegetation

Arctic soils can be thin compared with temperate regions, are regulated by the thickness of the permafrost active layer and may be subject to the erosive activity of many periglacial processes such as solifluction (mass-wasting) and freeze-thaw. However, where geomorphology permits such as at the base of scoured valleys or in depressions in the landscape, significant peat deposits can build up over time. Arctic lowland soils include those on bogs, mires, fens and wet meadows, while uplands include forests, heath, tussock and shrub tundra (Hobbie et al., 2000). Although soil processes are more active during the summer growing season, biological activity may continue throughout the cold season (Elberling, 2007). Since the active layer reaches its maximum thickness during the cold season there may be many months where parts

of the active layer remain around 0 °C, with soil microbial activity still able to take place (Welker et al., 2000).

Snowpacks can insulate the active layer, enabling microbial activity to persist in soils. Leaf litter decomposition can take place from -5°C to $+25^{\circ}\text{C}$, especially when moist conditions are present (Hobbie et al., 2000). Plants with greater lignin proportions tend to resist decomposition (Hobbie, 1996), while deciduous leaf litter decomposes faster than coniferous litter, mosses and lichens. Decomposition can still take place over the winter (Grogan and Chapin, 1999) and is responsible for $\sim 20\%$ of annual soil respiration (Hobbie et al., 2000). Topographic position is a particularly important factor because much carbon stored in Arctic soils and subsequently hydrologically cycled as DOC and POC is formed in wetland areas. For example, in tundra environments soil carbon stocks form at higher levels in wet meadow or tussock tundra which have shallower thaw depths (Waddington and Roulet, 1996; Hobbie et al., 2000).

The influence of soil and vegetation on Arctic lakes is most effectively demonstrated by the process of succession on deglaciated terrain. Succession is the process by which vegetation colonises, leading to thicker soils and more microbial activity, gradually accommodating higher plant species and more complex plant communities (Chapin et al., 1994). As glaciers retreat they leave behind freshly exposed soils that are colonised firstly by microbial activity, then moss and lichen communities, followed by grasses, higher plants and shrubs, which subsequently increase soil organic content. In Glacier Bay, Alaska, lakes were investigated along a gradient of deglaciation, with each lake catchment subject to a different level of plant succession (Engstrom et al., 2000; Fritz et al., 2004). These studies demonstrated that contrary to expectations the lakes became more dilute and acidic over time, while they accumulated dissolved organic carbon and increased in nitrogen concentration. The results demonstrated changes in hydrological pathways as soil development provides the potential for a greater proportion of surface runoff and alder development leads to enhanced N cycling (Fritz and Anderson, 2013).

Similar trends have been observed in lakes in western Greenland where time-dependent ontogeny processes indicate lake development is closely coupled to the mediating effects of a deglaciated catchment (Law et al., 2015). N-fixing cyanobacteria are particularly important in environments that are nitrogen-limited such as recently deglaciated catchments, as they increase soil N-cycling and permit growth of dependent plant communities (Chapin et al., 1994; Schmidt et al., 2008).

Microbial biofilms are pioneer colonisers of barren deglacial deposits and have been demonstrated in cold plant-free soils of the high latitudes (Kaštovská et al., 2005; Aislabie et al., 2006) and high elevations, and are even able to function at sub-zero temperatures and high diurnal fluctuations in surface temperature following deglaciation (Schmidt et al., 2008; Schmidt et al., 2009). Additionally, seasonal temperature changes can be an important driver for increased shrub growth (e.g. *Betula nana*), increasing growing-degree days, for example coincident with recent warming (Hollesen et al., 2015).

1.2.3 Glaciers and snow cover

Glaciers are important ‘hot spots’ in the cycling of carbon with glacial melt regimes regulating biological production in downstream lakes (Slemmons et al., 2013). Glacial meltwater release varies at daily, seasonal and multi-decadal timescales linked to the mass balance of the ice mass. Cold meltwater can reduce lake temperature (Edmundson and Mazumder, 2002), and influence the depth of the epilimnion (Edmundson et al., 1997). Glacier basal scour may release glacial flour (often rich in inorganic carbon), altering water clarity, changing in-lake UVR regimes (Slemmons et al., 2013). Glaciers can be biologically active during seasonal melt with microbial communities in glacier cryoconite holes (mini lake ‘mesocosms’) building up sediments overtime and providing habitat for cyanobacteria, enabling C, N and P to be stored and released during peak meltwater (Telling et al., 2012; Bagshaw et al., 2013). DOC release from glaciers can be highly bioavailable to downstream organisms (Lawson et al., 2014b) and can be nitrogen rich (Lawson et al., 2014a), releasing ancient and labile organic matter downstream (Hood et al., 2015). In one study, nitrate concentrations in glacier fed lakes have been demonstrated to be higher than in snowpack fed lakes, linked to primary productivity (Slemmons and Saros, 2012).

Snow on glaciers and frozen lake ice may also subsidise lake carbon budgets as they can provide a habitat for microbial activity and algae (Felip et al., 1995; Anesio and Laybourn-Parry, 2012). Slush layers can be enriched in nutrients, particularly during the spring partial melting of snow (Catalan, 1989). Rock glaciers are flow features of frozen material and debris in high relief environments and are a common feature on Disko Island (Humlum, 1997) and can harbour active microbial communities (Williams et al., 1997). Nitrification processes may modify N making it biologically active (Enders et al., 2008), which can be released into downstream aquatic environments, particularly during warming (Thies et al., 2007).

1.3 Study aims

This thesis uses geochemical palaeolimnological methods to reconstruct changes in carbon flux in Arctic lakes on Disko Island (Qeqertarsuaq), West Greenland to investigate carbon is cycled in response to catchment landscape processes, landscape heterogeneity and biological interactions at multiple timescales since ~7640 cal, yr BP (in Disko 2) together with recent sub-centennial scale changes (in all lakes). Disko Island is a geomorphically diverse landscape and so this study considers lakes at multiple positions in the catchment to assess how direct and indirect drivers of autochthonous and allochthonous carbon cycling might have been mediated by catchment processes and environmental change.

Arctic lakes biologically metabolise, process and integrate carbon at the landscape scale, but there remains a lack of understanding of how carbon is cycled in diverse catchments, with multiple and varied inputs across key transitions. The study area of Disko Island, West Greenland is a highly heterogeneous landscape punctuated by glacial and periglacial features and so is ideally suited to a palaeolimnological study that both seeks to characterise response to environmental change influenced catchment processes in multiple proxies, while also develop our understanding of how lakes in sensitive regions biologically respond to change.

The regions proximal maritime location to the moderating influence of the West Greenland current and the less than 100 km distance from the Greenland Ice Sheet (GIS) provide further controls on climate change, which is known to have actively changed in this region, enabling local, regional and wider pan-Arctic (hemispheric) comparisons. This study is a palaeolimnological investigation of three lakes on Disko Island and their catchments, each with a diverse geomorphology and potentially varying proportions of allochthonous and autochthonous carbon from multiple sources.

1.3.1 Primary aim

- Investigate the effect of catchment position on carbon cycling in lakes at different positions along a hydro-geomorphic landscape gradient on Disko Island, West Greenland.

1.3.2 Focused aims

- Understand how lake geomorphology, position and ecology regulate and mediate palaeolimnological trends in carbon cycling.

- Elucidate how differences between catchments (presence of glaciers, permafrost and varying vegetation inputs) might influence the quality and quantity of autochthonous versus allochthonous carbon buried in Arctic lakes.
- Use a detailed hydrogeomorphic survey to provide catchment information and calibration samples to help interpret down-core reconstructions.
- Link changes in catchment coupled carbon cycling in palaeolimnological sequences to known environmental change for:
 - Recent change – lakes Disko 2, 1 & 4
 - Change since ~1260 cal. yr BP – lake Disko 4
 - Change since ~7640 cal. yr BP – Lake Disko 2
- Compare the most effective proxies of carbon cycling in lakes on Disko Island with known local, regional and pan-Arctic reconstructions and syntheses.
- Use palaeolimnological records to interpret lake metabolic status as a source or sink of carbon, linked to key periods of environmental change including recent warming.

1.4 Study area

Disko Island (Qeqertarsuaq) (Figure 1.3) is located within Disko Bugt, a large marine embayment between 69°15'N - 70°20'N and 51°50'W - 55°00'W. Across the Vaigat channel (Figure 1.3 – A) the distance to mainland Greenland is approximately 10 km, but between 70 and 80 km separates Disko from the mainland to the east and south (Ingólfsson et al., 1990). Disko is the largest island to the west of Greenland (approximately 8,575 km²) and is 19% glaciated with the main Sermersuaq (Storbræe) and Bræpasset ice caps covering the central plateaus (Humlum, 1987). Geologically, Disko Island is composed of Tertiary basalts, part of the Disko-Nussuaq surge cluster (Chalmers et al., 1999) dating to more than 60 Ma (Larsen et al., 1992), with a thickness estimated to be around 5,000m (Humlum, 1996).

U-shaped valleys and fjords stem from carved lava plateaus at high elevations. At low elevations from Qeqertarsuaq northwards Precambrian gneiss is exposed and to the east is a band of Cretaceous sandstone, deposited as fluvial and deltaic sediments (Rasch et al., 2003). Contemporary vegetation at a low altitude includes verdant dwarf shrub heaths (in well drained sites) and small mires (in wet or snowpack-fed localities) (Bennike, 1995). The dominant shrub present is *Salix glauca*, with interspersed fell field vegetation on upland expanse (Callaghan et al., 2011). At the bottom of glacial valleys (typically below 200m a.s.l), braided river systems are typical with extensive marine deltas (Rasch et al., 2003).

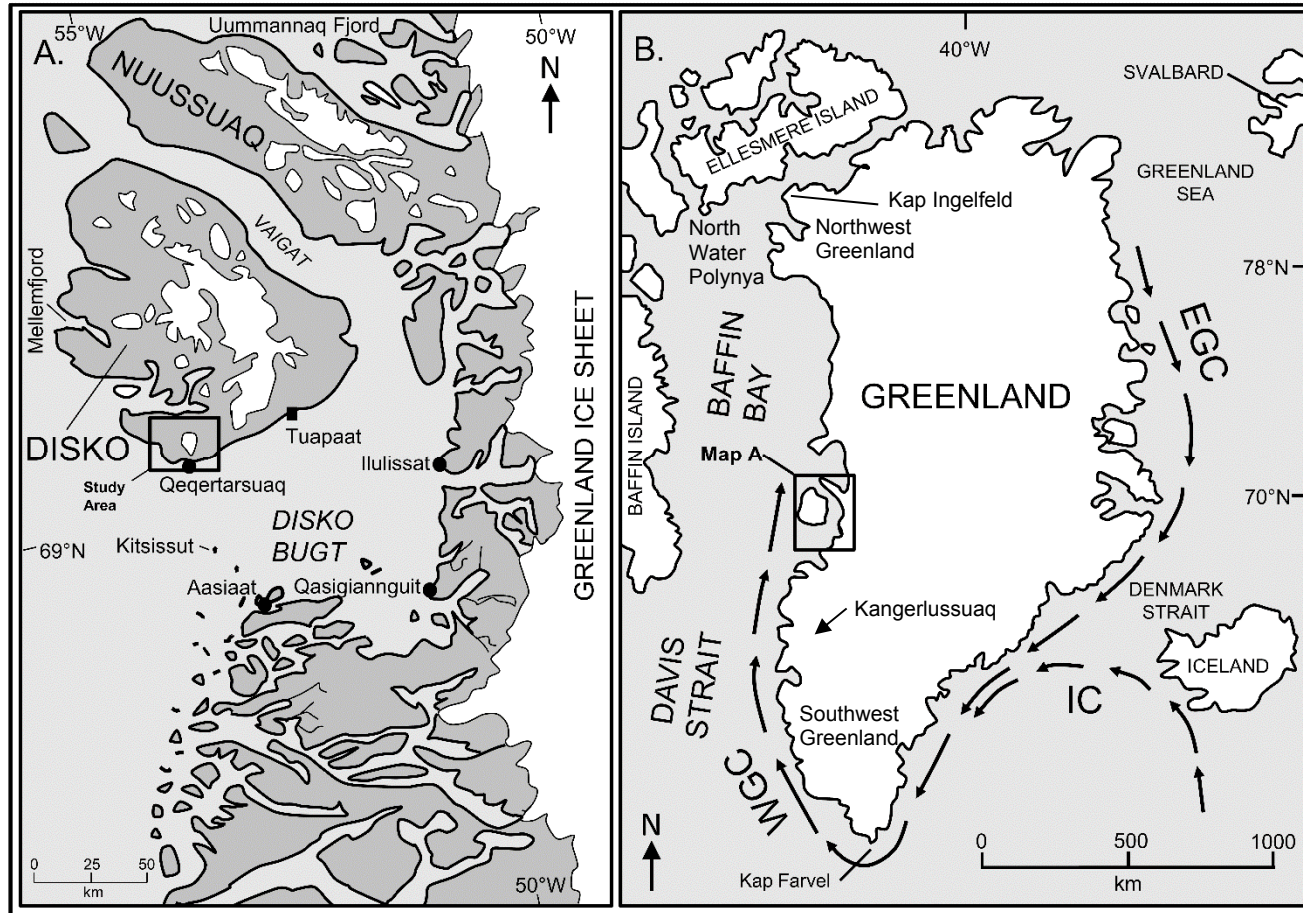


Figure 1.3: Maps showing the location of Disko Island study area. A - position of Disko Island in *Disko Bugt* (Disko Bay); B – position of Disko Island in west Greenland.

Disko has a polar maritime climate with a mean annual temperature of -4.5°C (1993-1997) and an overall mean precipitation of 400 mm, reported at Qeqertarsuaq in the south (Humlum, 1998), although precipitation can be as low as 100 mm y^{-1} in more continental locations to the north and east. Seasonal temperatures from Arktisk station (in Study Area, Figure 1.3 - A) for Disko Island are reported by Hollesen et al. (2015) between 1991 and 2011. To consider past regional recorded and future predicted regional temperature these data are reported with historical data from Ilulissat (1873-1992) and set with future modelling predictions (2012-2080) (Figure 1.4). Temperature measurements on the west coast near Mellemfjord report a colder mean annual temperature of -7.5°C (Rasch et al., 2003). Seasonally, moist air masses pass from the south and southwest via the Davis Strait during summer causing upward direction fjord winds in the day, which is reversed at night (Rasch et al., 2003). During winter more continental polar air masses dominate, bringing cooler temperatures from the Greenland Ice Sheet (Ingólfsson et al., 1990). At 70°N , Disko has a summer period of continuous midnight sun from 17th May to 28th July.

Regional climatology is complicated by the Disko Bugt (Figure 1.3), a large marine embayment which draws in a branch of the WGC, bringing warm water from the Atlantic into the bay (Ingólfsson et al., 1990). The strength of the WGC is related to momentum provided by the East Greenland Current (EGC) which is cold and has low salinity and merges with the North Atlantic Drift, turning around Kap Farvel (Greenland's most southern point) (Figure 1.3 - B). Disko Island's position between the Davis Strait and Baffin Bay make the Disko Bugt region particularly sensitive to sea current changes, influencing temperature fluctuations over the Quaternary (Funder, 1989). The islands orographic position means that glaciers respond more rapidly to climate variations, in comparison to the Greenland Ice Sheet (GIS) (Ingólfsson et al., 1990). Permafrost is discontinuous in the coastal areas, although continuous throughout most of the island, evidenced by the presence of numerous open-system pingos (Weidick, 1968). Thickness of permafrost in the Mellemfjord area has been found to be approximately 200 m, with the active layer between 175 and 180 cm in late September (Humlum, 1998). The marine limit, the result of isostatic uplift from glacial retreat since the Last Glacial Maximum (LGM) has been reported to rise on a transect from northwest to southeast Disko, from its minimum at 60 m a.s.l to a maximum at 90 m (Ingólfsson et al., 1990).

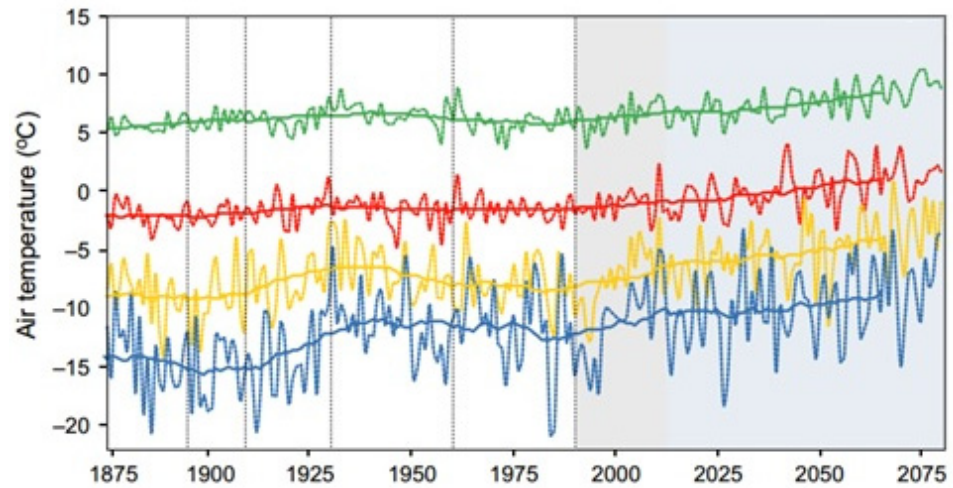


Figure 1.4: Air temperatures separated into winter (blue), spring (yellow), summer (green) and autumn (red) for Arktisk Station, Disko Island (1991-2011), Ilulissat historical data (1873-1992) and future metrological predictions (shaded) from the Danish Meteorological Institute’s HIRAM4 model. Each temperature trend is separated for comparison. Modified from Hollesen et al. (2015).

1.5 Arctic Holocene environmental change in Greenland and the North Atlantic

Environmental change in the Arctic over the Holocene is complex and is coupled closely to global environmental forcings, regional variations in meteorology, oceanography, sea-ice and local differences in climate, land-cover and catchment. This section provides a review of the palaeoenvironmental changes in the Arctic over the Holocene, with particular focus on the Disko region of west Greenland. The section explains the global processes responsible for climate forcing and then outlines the key periods of Holocene palaeoenvironmental change relevant to this thesis.

1.5.1 Holocene palaeoclimatology

The Holocene (~11,500 BP) is generally regarded as a relatively stable interglacial, in comparison to the Younger Dryas (~12,900 to ~11,500 BP) stadial period at the end of the Pleistocene which preceded it, according to multiple lines of evidence including for example (Muschitiello and Wohlfarth, 2015), ice cores (Dansgaard et al., 1993; Taylor et al., 1997), lake sediments (Lane et al., 2013), peatland sequences and ocean sediments (Mathewes, 1993). However, climate variations have still been regionally significant over the Holocene and are linked to solar variability, changes in the Earth's orbital axis (Mayewski et al., 2004), and interactions with meteorological, oceanographic and ice sheet dynamics (Rohling and Pälike, 2005). Holocene climate change has been detected in Greenland ice core records (Dahl-Jensen et al., 1998; Vinther et al., 2009), but the precise signal varies between records, highlighting the regional differences in Holocene climate on Greenland (O'Brien et al., 1995; Johnsen et al., 2001). Palaeoclimate records from regions across the globe also show varied responses to climate over the Holocene (Mayewski et al., 2004).

For example, Holocene climate variability has also been detected in numerous deep sea cores globally which has helped confirm climate fluctuations have occurred independently of glacial-interglacial cycles (Bond et al., 1997). Shifts in climate have been suggested from ice rafted debris events which altered North Atlantic thermohaline circulation, advecting cool waters further south (Bond et al., 1997). These abrupt events were found to operate on a ca. 1500-year cycle and have been controversially linked to variations in solar activity throughout the Holocene and which could be linked potentially to Dansgaard/Oeschger periodicity (Bond et al.,

2001). Such events remain highly controversial and it is unlikely one single mechanism is responsible for all Holocene cooling events (Wanner and Bütikofer, 2008).

1.5.2 Hemispheric scale climate change over the Holocene

The Younger Dryas (YD) abrupt cooling during the Pleistocene was followed by a return to the warmer interglacial climate of the Holocene, with the boundary dated in the NGRIP ice cores to ~11.7 ka BP (before AD 2000) (Walker et al., 2009). During the period from the YD to the Preboreal interval, snow accumulation increased on the Greenland Ice Sheet (GIS), suggesting a climate threshold or trigger was released, potentially a meltwater release (Alley et al., 1993). A sudden cold event at 8.2 ka BP has also been identified in the Greenland ice records and one dating to 9.3 ka BP in Ontario lake records (Yu et al., 2010). These abrupt events, can be explained by the curtailment of the North Atlantic Deep Water (NADW) formation due to a significant meltwater release into the North Atlantic, associated with Holocene ice-rafted debris (Rohling and Pälike, 2005). These events have also been detected more widely for example in Hawes Water, UK (Marshall et al., 2007) and in proxy records worldwide (Fleitmann et al., 2008).

Synthesis studies of northern hemispheric regions combining multiple proxy evidence (ice cores, glacier geomorphology, peat sequences, lake sediments, coastal and marine cores) now suggest that climate change during the Holocene was spatio-temporally complex (Briner et al., 2016; Kaufman et al., 2016; Sejrup et al., 2016). The simplicity of warming being delayed by the presence of the Laurentide Ice Sheet, with a later HTM in western Greenland (Kaufman et al., 2004), although correct for some proxies does not fully account for the heterogeneity in regional and spatial response when all reconstructions are considered (Briner et al., 2016; Kaufman et al., 2016; Sejrup et al., 2016). In eastern Beringia (NW North America) when all proxies were considered there was not found to be a prominent HTM, with temperatures interpreted to be both above and below the 20th century average at multiple times during the Holocene (Kaufman et al., 2016). Despite this individuality, average temperatures were highest between 7 and 5 ka (HTM), with declining temperatures between 4 and 3 ka (neoglacial) (Kaufman et al., 2016).

In the North Atlantic and Fennoscandia region statistical analysis of multiple proxy sequences found that although there is an insolation led signal, there is also a further

more heterogeneous non-uniform pattern (Sejrup et al., 2016). This analysis highlights the importance of the Laurentide Ice Sheet retreat, not only in terms of its meltwater supplies to the North Atlantic and Arctic Oceans, but also its topographic and albedo effects on regional climate (Sejrup et al., 2016). In Arctic Canada and Greenland the expression of the HTM was earlier in the north and east, but more diffuse in the south and west (Briner et al., 2016). Declining summer insolation was a key control, but the influence of early Holocene ice sheet retreat and variable influence of Atlantic currents to the region were also key mediating factors, exerting spatio-temporal variability (Briner et al., 2016).

For example, proxy evidence in West Greenland provides a range of dates for the HTM. Near Kangerlussuaq, the presence of the ostracod species *Ilyocypris bradyi* suggests a period of warmer lake water between 7 and 6.5 ka and enhanced lake water conductivity in lakes Braya Sø and SS6 between 8 and 5 ka also suggest warming (McGowan et al., 2003; Kaufman et al., 2004; Anderson et al., 2012). The presence of subarctic molluscs along the west coast of Greenland combined with glacial evidence suggest the HTM lasted between 8.0 and 3.5 ka (Kelly, 1980), although boreal taxa indicate warmest temperatures between 10.5 and 6 ka (Funder and Weidick, 1991; Kaufman et al., 2004; D'Andrea et al., 2011). Additionally, palynological studies in western Greenland have helped identify the HTM (Fredskild, 1973; Kelly, 1980) and in southwestern Greenland near Kangerlussuaq, this area is strongly influenced by inland continentality and so has some deviations from the more coastal records (Anderson et al., 2008). Stemming from the initial detection of the 8.2 ka BP event, up to six periods of rapid climate variability have been detected over the Holocene (Mayewski et al., 2004). Although the complexity of global hemispheric scale climate feedbacks and synchronicity mean these events were rarely globally ubiquitous, in western Greenland complex lake records of abrupt events have been associated with cultural migration (D'Andrea et al., 2011) (Figure 1.5). Current multiproxy synthesis studies place less emphasis on locally specific abrupt events, noting the high degree of spatial heterogeneity across the Arctic during the Holocene (Briner et al., 2016), although this continues to be debated.

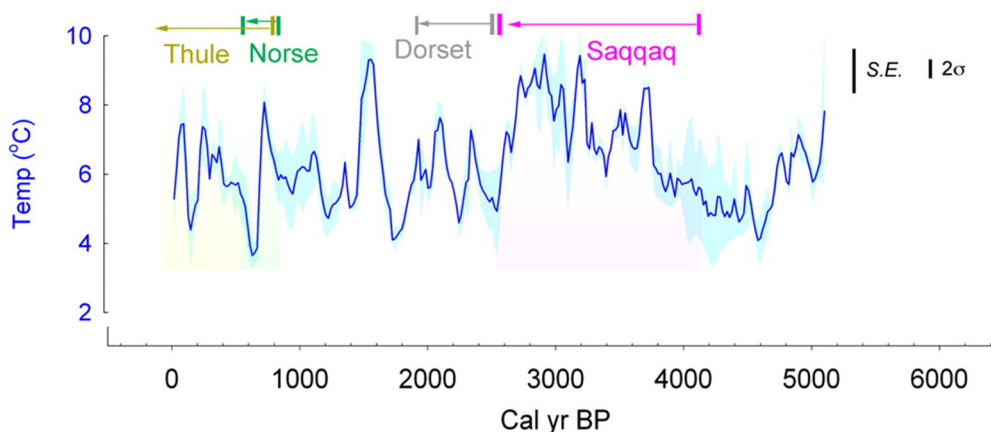


Figure 1.5: Alkenone lake water temperature reconstruction (Kanger Stack) for west Greenland (Kangerlussuaq) derived from lakes Braya Sø and Lake E representing temperature fluctuations associated with transitions in populations (Thule, Norse, Dorset and Saqqaq). Alkenones in Arctic environments reflect temperatures during the summer ice-free season (variable but generally May – October). See Figure 1.3 – B for location of Kangerlussuaq. Modified from (D’Andrea et al., 2011).

A general Neoglacial cooling trend mid-way through the Holocene is evident in many palaeoenvironmental records from the region (see Figure 1.5), although the exact timing is varied. The Camp Century $\delta^{18}\text{O}$ record from North West Greenland indicated neoglacial cooling between 3,000 – 3,500 BP and 2,400 – 2,800 BP (Johnsen et al., 1972; Vinther et al., 2009), with strong similarities in the Dye-3, GRIP, GISP 2 and NorthGRIP ice-core Holocene records (Dansgaard et al., 1982; Dansgaard et al., 1993; Grootes et al., 1993; Johnsen et al., 2001). However, in terrestrial records from west Greenland the precise nature of the Neoglacial is varied (Briner et al., 2016), with for example five lake records near Ilulissat displaying decreases in organic matter between 4.3 and 3.2 ka, potentially reflecting links to the contentious ‘4.2 ka event’ (Axford et al., 2013).

A period of increased temperature known as the Medieval Climate Anomaly (MCA) has been widely documented around AD 950 – AD 1250 (Mann et al., 2009), associated with changes in the frequency and persistence of circulation regimes such as the La Niña or El Niño southern oscillations, and periods of volcanic activity, although the precise drivers remain uncertain (Lamb, 1965; Bradley et al., 2003; Mann et al., 2009). The MCA has been linked with globally influencing causal mechanisms such as the 1500 periodicity ‘Bond’ cycles, although climate variability in this period was not globally synchronous (Denton and Broecker, 2008). This was followed by a cooling termed the Little Ice Age (LIA) between ~ AD 1350 and 1850, in the Northern Hemisphere which occurred during a minimum in solar activity that may have coincided with a number of tropical volcanic eruptions (Wanner et al., 2008). Most

Holocene reconstructions show a general cooling between ~ AD 1580 and 1880, but with cooler conditions earlier in the Arctic, Europe and Asia, in contrast with later in North America and the Southern Hemisphere (Pages 2K Consortium, 2013).

1.5.3 Palaeoenvironmental change in the Disko Bugt region

Records of palaeoenvironmental change regionally proximal to Disko Island over the Holocene have been primarily oceanographic (Moros et al., 2006; Lloyd et al., 2007; Andresen et al., 2010; Perner et al., 2011; Krawczyk et al., 2013; Moros et al., 2016). Additionally, they include a palaeolimnological study of multiple lakes close to the Greenland Ice Sheet (near Ilulissat, Figure 1.6 - A) which includes a chironomid temperature reconstruction (Axford et al., 2013), an investigation of macrofossil and pollen records from the island of Qeqertarsuatsiaq (Figure 1.6 - B) directly to the south of Disko Island, across Disko Bugt (Fredskild, 2000) and a macrofossil study of Nuussuaq Lake (Figure 1.6 - C), directly to the north of Disko Island across the Vaigat strait (Bennike, 2000). In this section the most recent regional time periods and evidence presented by Moros et al. (2016) are used as a framework for discussing regional palaeoclimatological change in the Disko Bugt region. Figure 1.6 presents the location of key sites mentioned in the text.

8.3 – 7.5 ka BP – early Holocene

In the early Holocene, Disko Bugt benthic foraminifera and diatom assemblages (Figure 1.6 - H) were found to reflect primarily cold surface and sub-surface water conditions (Moros et al., 2016). This was mirrored by cold surface air temperatures interpreted from Camp Century ice core $\delta^{18}\text{O}$ records (Figure 1.6 - J) (Johnsen et al., 1972; Vinther et al., 2009). The presence of *N. labradorica*, a benthic foraminifera in Disko Bugt ocean sediments suggested at this time Arctic sea ice met the Disko Bugt (Figure 1.6) shoreline (Moros et al., 2016). In Qeqertarsuatsiaq (Figure 1.6 - B) to the south of Disko Bugt the oldest Holocene lake sediments were found to reflect an early pioneer vegetation community including *Oxyria digyna*, *Saxifraga oppositifolia* and *Carex bigelowii* (Fredskild, 2000). A basal date of > 10,000 cal. yr BP on sediments from Nuussuaq lake (Figure 1.6 - C) imply the mainland north of Disko Island had early deglaciation (Bennike, 2000).

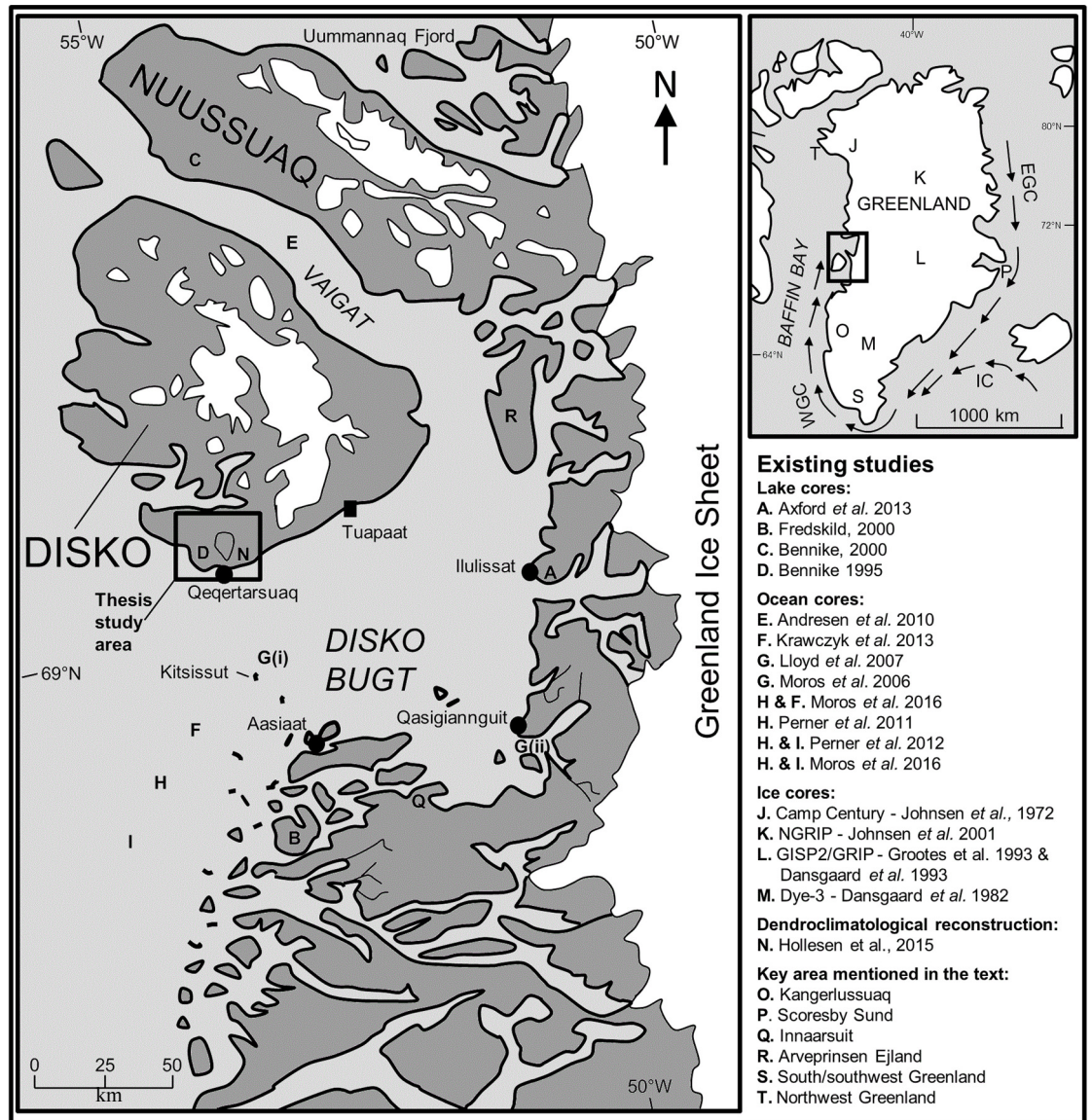


Figure 1.6: Map of the Disko region and insert Greenland map with the location of existing proxy studies from lake, ocean and ice cores indicated. Figure redrawn and based on Desloges *et al.* (2002) and Lloyd *et al.* (2005). Abbreviations: West Greenland Current (WGC), East Greenland Current (EGC), Irminger Current (IC).

7.5 – 6.2 ka BP – early to middle Holocene transition

In Disko Bugt (Figure 1.6), ocean sediment proxies indicated warm surface and sub-surface temperatures, with warm but variable benthic foraminifera assemblages (Moros *et al.*, 2016). These changes were linked to warming temperatures over north-western Greenland influencing ocean currents. Sea ice diatoms were low due to reduced spring sea ice, suggesting warmer conditions linked to the delayed Holocene Thermal Maximum (HTM). A delayed HTM has also been detected in the Canadian Arctic, Greenland Ice cores and lake sediments (Dahl-Jensen *et al.*, 1998; Kaplan and Wolfe, 2006; Vinther *et al.*, 2009; Moros *et al.*, 2016). Lake sediment records from

Qeqertarsuatsiaq (Figure 1.6 - B) indicated *Betula nana* pollen during this time period, although it may not have arrived locally until 6,000 BP (Fredskild, 2000). At Nuussuaq Lake (Figure 1.6 - C) this period marks maximum production, with the highest concentrations of Chironomidae, *Daphnia pulex* sp. ephippia, Rhabdocoela and *Plumatella repens* and the presence of early *Betula nana* and *Salix herbacea* remains (Bennike, 2000).

6.2 – 5.5 ka BP – middle Holocene (i)

Marine sediments from Disko Bugt (Figure 1.6 – H) marked this period as having abrupt sub-surface cooling, indicated by the reduction of the warmer benthic foraminifera *I.norcrossi* (Perner et al., 2013a; Moros et al., 2016). Increases in sea ice and planktonic foraminifera may also indicate enhanced meltwater during this time, which is confirmed by increases in % C_{37:4} values, although this proxy should be treated with caution (Moros et al., 2016). During this period (5.8-5.6 ka BP) the Camp Century (Figure 1.6 - J) ice core record marked a cold period (Johnsen et al., 1972; Vinther et al., 2009). Towards the end of this period LOI values in five lakes at the western Greenland ice sheet margin near Ilulissat (Figure 1.6 - A) demonstrated a rise in OM, suggesting increased summer production due to rising temperatures or increased length of the ice free season (Axford et al., 2013). The lake in Qeqertarsuatsiaq (Figure 1.6 - B) to the south of Disko Bugt was found to gradually become more oligotrophic, possibly due to ontogenetic lake processes (Fredskild, 2000).

5.5 – 3.5 ka BP – middle Holocene (ii)

Disko Bugt sediment proxies implied a return to warm sub-surface conditions (Moros et al., 2016). Although, diatom and dinocyst assemblages were complicated by the retreat of the frontal ice edge zone moving further north, and the opening up of the ice which previously blocked the Vaigat Strait to the north, changing meltwater flow (Perner et al., 2013b). Warm temperatures during this period are reflected in the Camp Century ice core records (Johnsen et al., 1972; Vinther et al., 2009) and the chironomid temperature reconstruction from North Lake near Ilulissat (Figure 1.6 – A), as at this time the ice margin was at its most retracted (Axford et al., 2013). Between 4.3 and 3.2 ka BP there were major decreases in organic matter content, suggesting cooling possibly linked to the “4.2 ka event” (Axford et al., 2013; Briner et al., 2016). At Qeqertarsuatsiaq (Figure 1.6 – B) *Betula* pollen reached its peak, while there was a slight increase in ericaceous shrub species like *Empetrum* (Fredskild, 2000). Peak warmth here in the Disko Bugt region was almost 1,000 years later than ~250 km

south in the Kangerlussuaq region where it was reached ~7.2-5.6 ka BP, (Anderson and Leng, 2004; Bennike et al., 2010) potentially due to local modulation of insulation, the climatic effect of local glaciers and the warming effect of the WGC but also the delayed immigration of taxa as Disko is further north. In Nuussuaq lake (Figure 1.6 – C) *Betula nana* remains were present until 4,000 cal. yr BP and so most of this period represents the local HTM.

3.5-2.6 ka BP – middle to late Holocene transition

Cooler conditions marked a transition to the Neoglacial. For example, in Disko Bugt ocean sediments (Figure 1.5 – H) the species *I. norcrossi* in benthic foraminifera assemblages abruptly declined at 3.5 ka BP (Perner et al., 2013a; Moros et al., 2016). Temperature reductions can be interpreted from the Camp Century (Figure 1.6 – J) ice core record (Johnsen et al., 1972; Vinther et al., 2009) and the widespread cooling of linked ocean currents, likely due to a weakening of the Irminger Current (IC) or a stronger East Greenland Current (EGC) (Andersen et al., 2004). At the ice margin near Ilulissat LOI values (Figure 1.6 – A) were lower suggesting reduced production (Axford et al., 2013), while at Qeqertarsuaq (Figure 1.6 – B) there was a marked decrease in the fruits and leaves of *Betula nana* and a fall in pollen percentage by half, implying cooling temperatures (Fredskild, 2000).

2.6 – 0.7 ka BP – late Holocene (i)

In Disko Bugt ocean sediments (Figure 1.6 – F) diatom and % C_{37:4} values were highly variable, representing a switch from warm water to cool water taxa (Moros et al., 2006; Ouellet-Bernier et al., 2014). A general cooling trend of sub-surface waters ended in cold conditions around the Little Ice Age (LIA). The initial warming may have corresponded to the Roman Warm Period (RWP), with further fluctuations linked to the Dark Ages cool period (DA) and Medieval Climate Anomaly (MCA). From ca 2.0 ka BP meltwater was at a maximum in the Disko Bugt region and terrestrial conditions were cool (Moros et al., 2016). Lakes near Ilulissat and the Jakobshavn ice margins had low accumulations in %LOI OM (Figure 1.6 – A), representing year-round frozen conditions (Axford et al., 2013). Slight warming in the Disko Bugt sub-surface after 2 ka BP may have mirrored increases in the Greenland Camp Century (Figure 1.6 – J) temperature record (Johnsen et al., 1972; Vinther et al., 2009; Moros et al., 2016).

0.7 - 0.2 ka BP late Holocene (ii)

Complex oceanographic changes occurred in the Disko region during this period. Disko Bugt sediments together marked a cooling of sub-surface waters, which links

closely to the declining temperature record at Camp Century (Johnsen et al., 1972; Vinther et al., 2009; Moros et al., 2016). But surface water conditions interpreted from dyncyst assemblages implied initial warming, but then cooling from *c.* 0.5-0.1 ka BP (Ribeiro et al., 2012). In lake sediments on Qeqertarsuatsiaq (Figure 1.6 – B), *Betula* reached its minimum since colonisation and *Daphnia* and *Simocephalus* also declined (Fredskild, 2000). Macrofossil concentrations were found to be reduced in the top ~40 cm (~1,100 cal. yr BP) of Nuussuaq Lake (Figure 1.6 – C), corroborating the regional cooling trend on land (Bennike, 2000).

20th Century and recent change

Over the past 100 years Disko Bugt sub-surface ocean temperatures have remained cold compared with the HTM (Moros et al., 2016). However, the Jakobshavn Isbræ has been in retreat since the end of the LIA (Motyka et al., 2011), with warm currents known to have entered Disko Bugt during ice calving retreat between AD 1920 – 1950 and again since 1998 (Lloyd et al., 2011). Temperature observations at Ilulissat and Qeqertarsuaq (see Figure 1.4) show recent warming trends since the end of the LIA increasing in rate since the 1990s (Box, 2002; Hansen et al., 2006). Additionally, *Salix* tree ring reconstructions (Figure 1.6 - N) provide evidence of local recent warming on Disko since the end of the LIA (Hollesen et al., 2015). The switch to recent Arctic warming marks the reversal of the long term cooling trend that has been observed across the Arctic (Kaufman et al., 2009).

1.5.4 Existing palaeolimnological studies on Disko Island

Palaeoecological studies using lake sediments directly on Disko Island are limited to one published study (Figure 1.6 – D) investigating two lakes for macrofossil and lithological analyses (Bennike, 1995). At Qivittut Lake, a transition between marine, brackish and limnic sediments was evident in the macrofossil fauna, indicating uplift as glaciers retreated (an isolation basin), whereas in Fortune Bay Lake all sediments were found to be limnic and reflected relatively stable conditions over approximately the last 3,900 years, but with relatively high accumulation rates for the Arctic position (Bennike, 1995).

1.5.5 West Greenland palaeolimnological studies outside the Disko region

Holocene climate variability to the south and north of Disko is reviewed by Briner et al. (2016). In South and Southwest Greenland (Figure 1.3 – B) warmest summer air temperatures interpreted from pollen reconstructions were from 7.5 to 7.0 ka, with cooling after 5.5 to 5 ka BP (Fréchette and de Vernal, 2009), but only after 3 ka BP did organic matter and silica abundance decrease (Kaplan et al., 2002), with similar warming at the southern Greenland tip from ~8 to 5 ka (Andresen et al., 2004). Pollen temperature reconstructions had contrasting warming trends with July temperatures peaking after 4 ka (Gajewski, 2015; Briner et al., 2016), using early pollen studies (Fredskild, 1973; Kelly and Funder, 1974; Fredskild, 1983). Southwest Greenland (Figure 1.3 – B) may have been subject to multiple climate trends or the immigration of *Alnus* could have modified these reconstructions (Gajewski, 2015).

In the Kangerlussuaq region (Figure 1.3 – B) palaeolimnological studies suggest reduced effective moisture during the early to middle Holocene (McGowan et al., 2003; Anderson and Leng, 2004; Aebly and Fritz, 2009; Anderson et al., 2012; Briner et al., 2016), although in-lake processes (e.g. ontogeny and conductivity) were responsible for more change than climate (Anderson et al., 2008; McGowan et al., 2008; Law et al., 2015). The ostracod species *Ilyocypris bradyi* has been used as a marker of the HTM (between 7.2 and 6.3 ka BP) with pronounced declines in the last 1,000 ka BP (Bennike et al., 2010). Neoglacial conditions were variable but cooler (D'Andrea et al., 2011) and regulated by the North Atlantic Oscillation (Olsen et al., 2012).

In Northwest Greenland (Figure 1.3 – B) pollen based temperature reconstructions placed peak summer warmth between 7.5 and 5.5 ka (Fredskild, 1985; Gajewski, 2015) and the extralimital thermophiles *Colymbetes dolabratus* (beetle) and *Gasterosteus aculeatus* (stickleback) which are no longer present were found in sediments from ~8.8 to 7.5 ka (Fredskild, 1985; Briner et al., 2016). Additionally, warmer climate during the early and middle Holocene was interpreted in sediments on an island in the North Water Polynya (Bennike et al., 2008) which had a maritime moderating effect (Figure 1.3 – B) and evidence of reduced algal abundance since in a lake ~4.5 ka on Kap Inglefield (Figure 1.3 – B) indicative of the Neoglacial (Blake et al., 1992; Briner et al., 2016).

1.6 Holocene deglaciation of Disko Island and the Disko Bugt region

Bennike and Björck (2002) combined all ice margin published radiocarbon dates from Greenland adjacent to the Greenland Ice Sheet (GIS) to provide minimum dates to constrain ice sheet recession over the Holocene (Figure 1.7). Dated shells from raised marine and littoral deposits, and the transition between glacial clays and organic matter in sediment cores have been used to track ice retreat. Disko Bugt was found to have had a later deglaciation than Umanak Fjord to the north and Scoresby Sund in east Greenland (Bennike and Björck, 2002). At present the Jakobshavn Isbræ (Ilulissat) provides the largest ice inlet into Disko Bugt, and is the largest ice outlet from the inland ice (Funder, 1989).

1.6.1 Holocene ice dynamics of Disko Island

On Disko Island the oldest ^{14}C date on geomorphological deposits is calibrated to 10.3 cal. ka BP, providing a minimum age for local deglaciation (Figure 1.7) (Bennike and Björck, 2002). The early Godhavn Stade featured the Greenland Ice Sheet (GIS) over the east and south of Disko Island with glaciation to the west and ice retreat is dated to reach the marine limit (due to isostatic uplift) by c. 9.25 – 9 ^{14}C yr BP (Ingólfsson et al., 1990). This was evidenced by a large asymmetrical moraine present in the Blæsedalen glacial valley, that was deposited by an ice tongue in Disko Bugt (Ingólfsson et al., 1990) (Figure 1.8). The later Disko Stade readvance during the Neoglacial is evidenced by truncated moraines stemming from glacial valleys, caused by changes in local climate providing increased precipitation, enabling expansion of the ice cap on Disko Island, but the maintenance of the GIS close to the mainland (Ingólfsson et al., 1990).

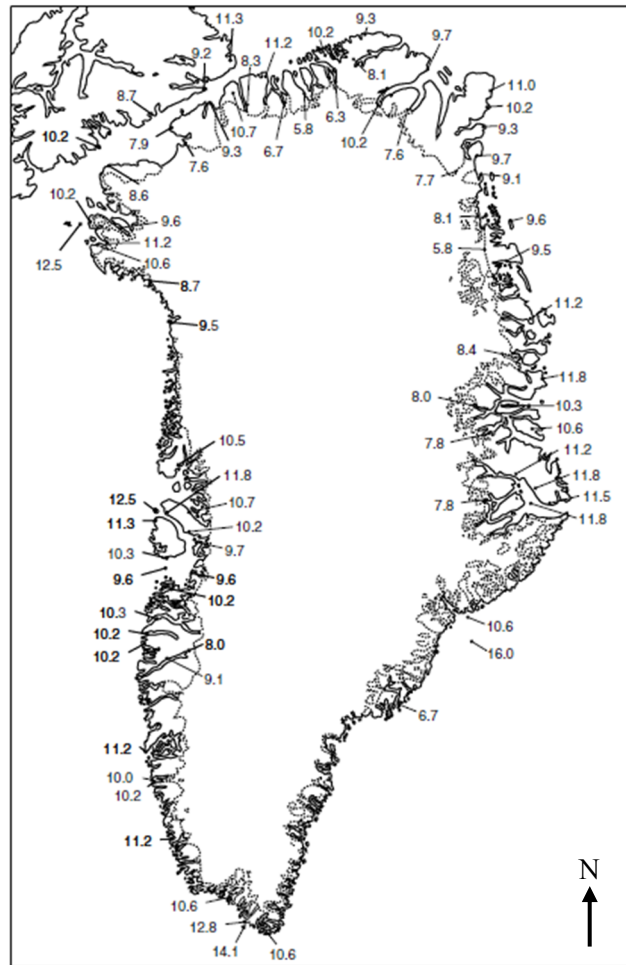


Figure 1.7: Deglaciation of Greenland from the last glacial maximum (LGM). The distribution of oldest radiocarbon dates from the ice-free parts of Greenland, the continental shelf and eastern Ellesmere Island. Dates in cal. kyr BP. Modified from Bennike and Björck (2002).

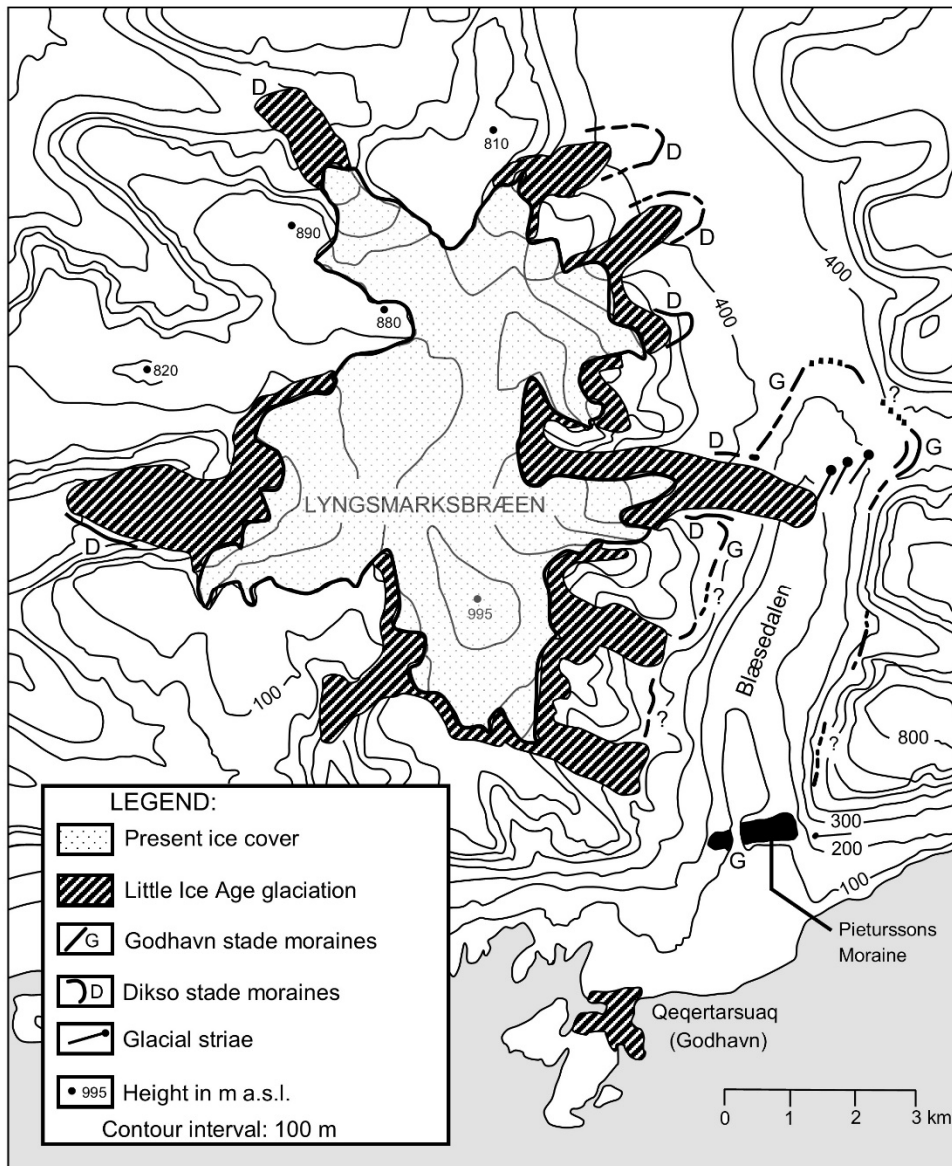
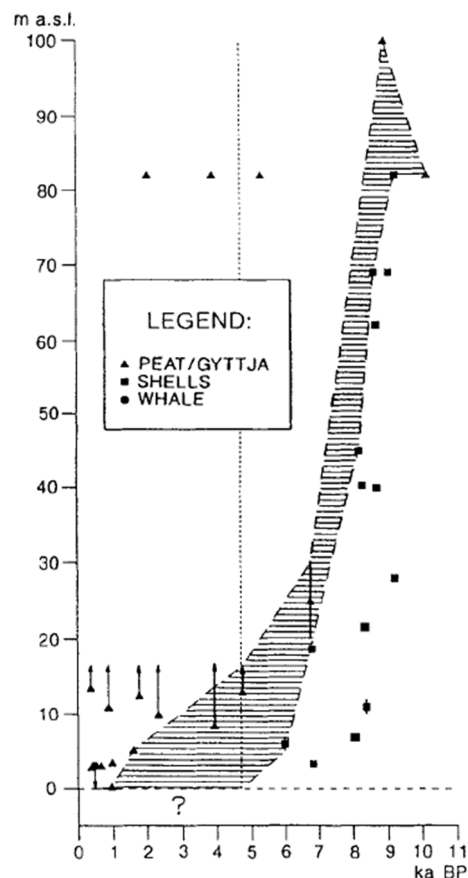


Figure 1.8: The extent of glacial advance and retreat in the study region of Disko Island. The Godhavn stade moraines indicate ice provision from a glacial tongue from the main GIS extending from Disko Bugt northwards up Blæsedalen. Redrawn from Ingólfsson et al. (1990).

1.6.2 Deglaciation of the Disko Bugt region

Later deglaciation of Disko Bugt than Scoresby Sund (Figure 1.6 – P) to the east and Uummannaq Fjord to the north suggests considerable ice flow may have persisted for longer in this bay than elsewhere in Greenland, with deglaciation only reaching the inner fjords of the Jakobshavn Isbrae (Figure 1.6 – ice sheet near A) by 10 ka BP (Roberts et al., 2015). At the start of the Holocene the GIS retreated rapidly with a higher marine limit around the Jakobshavn Isbræ near the centre of Disko Bugt (Long et al., 2006). A deglaciated Disko Bugt allowed warmer more saline flows to enter the bay and undercut cooler, less saline meltwater flows from the GIS (Lloyd et al., 2005). Deglaciation of Disko Bugt increased the orographic effect of Disko Island, acting as a pronounced barrier to airflow from the southwest, inducing air masses to diverge around the island (Humlum, 1985), bringing more maritime air masses and enhanced precipitation, potentially contributing to early Holocene glacier readvance (Ingólfsson et al., 1990). The maximum marine limit to assess the relative sea level of the landscape has been found to be ~60 m a.s.l. in the northwest of Disko to ~80-90 m a.s.l. in the southwest of Disko Island (Ingólfsson et al., 1990; Rasch and Nielsen, 1995) (Figure 1.9).

Figure 1.9: Age-altitude diagram showing ^{14}C (uncalibrated) dates from the south of Disko Island and Kitsissut. The shaded zone indicates the area in which the relative sea level curve should lie, with upward arrows denoting dated gyttja samples from lake sediments. From Rasch and Nielsen (1995).



1.7 Thesis outline

This chapter has reviewed the key literature on carbon cycling, limnological processes, the study area, Holocene environmental change and arctic landscape processes and set the projects aims and hypotheses. In subsequent chapters the principal methods utilised in the thesis are reviewed (chapter 2) and their use in the project described (chapter 3). A hydro-geomorphic catchment survey of the study areas is then completed together with an assessment of catchment land cover and a detailed geochemical assessment of catchment samples (chapter 4). Palaeolimnological investigations of the upland cirque lake (Disko 2 - chapter 5), Blæsedalen U-shaped valley lake (Disko 1 - chapter 5), and Ipraatsi feeder valley-bottom lake (Disko 4 - chapter 7) are then presented in elevation order, followed by a final synthesis (chapter 8).

Chapter 2: Literature review of key methods used in this thesis

This chapter provides a review of the principal methods used in the thesis including pigment analysis, lipid biomarkers, bulk carbon isotope ratios ($\delta^{13}\text{C}_{\text{TOC}}$), C/N ratios and the role of compound-specific $\delta^{13}\text{C}$ analysis. The aim of this chapter is to explain the background of these complementary palaeolimnological methods to aid interpretation of the thesis results.

2.1 Sedimentary pigment analysis

In this study, pigment analysis helps quantify the total and group-specific biological production of Arctic lakes, contributing to knowledge of catchment specific changes in autochthonous versus allochthonous production. Chlorophylls (Chls), carotenoids, their derivatives and associated photo-protective compounds are excellent sedimentary biomarkers of photosynthetic organisms both within the lake (e.g. algae, macrophytes, invertebrates and bacteria) and externally from the catchment (e.g. higher plants, inputs of degraded terrestrial material) (McGowan, 2013). Pigments are present in all photoautotrophic organisms and have good taxonomic specificity which can be effectively interpreted when biogeochemical and depositional processes are taken into account. Detailed studies of pigment taphonomy have determined that β -carotene, pheophytin *a* and chlorophyll *a* are good indicators of total algal abundance (although chlorophyll *a* is less stable), and can be found in all algal groups, higher plants and macrophytes (Leavitt, 1993; Cuddington and Leavitt, 1999). The chemical structure of chlorophyll *a* is shown in Figure 2.1.

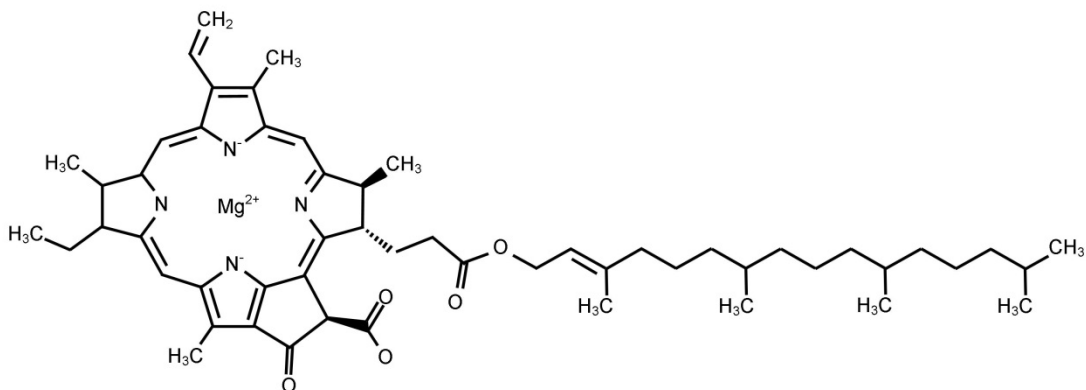


Figure 2.1: Chemical structure of chlorophyll *a* (indicator of total algal production).

Alloxanthin is a unique biomarker compound for cryptophytes, while okenone can help reconstruct changes in purple sulphur bacteria and, therefore, anoxia. Diatoxanthin, diadinoxanthin and fucoxanthin may all indicate diatoms, but can also indicate chrysophytes and other algal groups. Cyanobacteria can be indicated by canthaxanthin, echinenone, myxoxanthophyll, oscillaxanthin, scytonemin and zeaxanthin pigments. Degradation or derivative compounds may also be detected. Pheophytin *a* and *b* are derivatives of chlorophyll *a* and *b* respectively, with ratios of chlorophyll *a* / pheophorbide *a* often used to indicate degradation. Table 2.1 presents the affinity of selected pigments and their estimated stability based on Leavitt and Hodgson (2001), updated in McGowan (2013).

In some lakes it may also be possible to detect the pigment scytonemin which is produced in the extra cellular sheath of many cyanobacteria (Bianchi and Canuel, 2011) and acts as a photo protectant, from the potentially harmful effects of UV radiation (Leavitt et al., 1997; Leavitt et al., 2003). For example, in alpine lakes in British Columbia and Banff National Park, Canada Leavitt et al. (2003) found that algal abundance was lower after initial deglaciation due to high levels of UV damage in a low DOM environment (clear water). However, in other lakes the relationship may be more complex as the release of grazing pressure from invertebrates such as larval chironomids, may permit increases in algal abundance as the former may be more sensitive to UVB (Bothwell et al., 1994).

Table 2.1: The stability of pigments typically detected in the water column and sediments of lakes. The stability of pigments are presented from most stable (1) to least stable (4), with (-) indicating unknown stability. Stability determined by mass-balance studies and mesocosm experiments in Leavitt (1993).

Pigment	Affinity	Stability
Chl <i>a</i>	All photosynthetic algae, higher plants	3
Chl <i>b</i>	Green algae, euglenophytes, higher plants	2
Chl <i>c</i>	Dinoflagellates, diatoms, chrysophytes	4
Bchls <i>a</i> and <i>b</i>	Purple sulphur and nonsulphur bacteria	-
Bchls <i>c</i> , <i>d</i> , and <i>e</i>	Green sulfur bacteria	-
Pheophytin <i>a</i>	Chl <i>a</i> derivative	1
Pheophytin <i>b</i>	Chl <i>b</i> derivative	2
Pheophorbide <i>a</i>	Grazing, senescent diatoms	3
Pyro-pheo (pigments)	Derivatives of <i>a</i> and <i>b</i> phorbins	2
Steryl chlorin esters	Chlorophyll derivatives from grazing	-
β -Carotene	Most algae and plants	1
α -Carotene	Cryptophytes, prochlorophytes, rhodophytes	2
Alloxanthin	Cryptophytes	1
Fucoxanthin	Diatoms, prymnesiophytes, chrysophytes, raphidophytes, several dinoflagellates	2
Diadinoxanthin	Diatoms, dinoflagellates, prymnesiophytes, chrysophytes, raphidophytes, euglenophytes, cryptophytes	3
Diatoxanthin	Diatoms, dinoflagellates, chrysophytes	2
Peridinin	Dinoflagellates	4
Canthaxanthin	Colonial cyanobacteria, herbivore tissues	1
Echinenone	Colonial cyanobacteria	1
Myxoxanthophyll	Colonial cyanobacteria	2
Oscillaxanthin	Cyanobacteria (<i>Oscillatoriaceae</i>)	2
Scytonemin	Colonial cyanobacteria	-
Zeaxanthin	Cyanobacteria	1
Lutein	Green algae, euglenophytes, higher plants	1
Neoxanthin	Green algae, euglenophytes, higher plants	4
Violaxanthin	Green algae, euglenophytes, higher plants	4
Isorenieratene	Green sulfur bacteria	1
Okenone	Purple sulfur bacteria	1
Rhodopinal	Purple sulfur bacteria	-
Astaxanthin	Herbivore tissue, N-limited green algae	4

Stability estimates from Leavitt and Hodgson (2001), in McGowan (2013).

2.1.1 Pigment preservation and stability

Pigment preservation is dependent on the stability of the constituent molecule, its rate of production, sinking rate, the depth of algae in the water column and burial rate in sediments (Cuddington and Leavitt, 1999), such that typically 95% of pigments have degraded prior to sedimentation (Leavitt and Hodgson, 2001; McGowan, 2013). Pigment degradation increases with lake depth and O₂ penetration as chlorophyll and carotenoids are acutely sensitive to chemical oxidation, microbial decomposition and

the damaging effects of UVA and UVB photosynthetic radiation. The pathway to deposition can be direct algal senescence or involve grazing (e.g. by zooplankton) which can introduce a variety of transformational processes (e.g. production of steryl chlorin esters) combined with the faecal sinking rate which can be different from the direct algal sinking rate (Figure 2.2). Once pigments become buried in sediments they may undergo further rapid chemical and biological processes, particularly at the sediment-water surface interface. This is typically highlighted by exponential increases in easily degradable pigments (Table 2.1) at the top of sediment cores (McGowan, 2013). Over longer timescales, changes in pigment abundance are typically more stable and can remain intact for thousands of years, although over periods such as the Holocene (or longer) sediment infilling connected with ontogenetic processes (lake development) should be taken into account as water depth is a key control of initial pigment degradation (Cuddington and Leavitt, 1999). To check for the stability of pigment abundance, ratios of pheophytin *a* to Chl *a* have proved useful as a large variation may indicate poor reliability of the apparent reconstructed depositional environment.

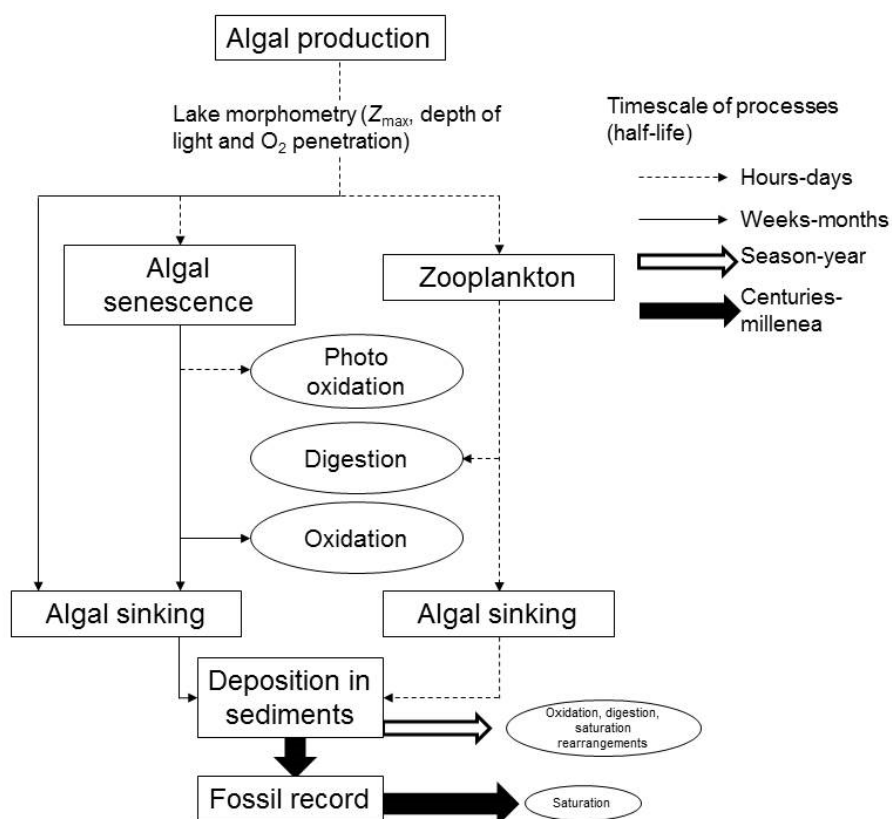


Figure 2.2: Pathways of pigment production, transformation and degradation in lakes redrawn from McGowan (2013), based on Leavitt (1993).

2.1.2 Application of pigment analysis in palaeolimnological investigations of carbon cycling

Numerous palaeolimnological studies have used chlorophyll and carotenoid pigments to elucidate our understanding of carbon cycling. For example, the acidification of lakes in the experimental lakes area, Ontario have demonstrated decreasing pH can cause reductions in DOC (decrease in water clarity), and reductions in fucoxanthin (indicative of dinoflagellates, diatoms and chrysophytes), but increasing pigments from green algae (chlorophyll *b*, pheophytin *b*, lutein-zeaxanthin), changing the ecological communities and signature of carbon buried in these sediments (Leavitt et al., 1999). Pigments provided evidence of land-use change and nutrient enrichment in Lake Windermere, England suggesting more autochthonous carbon burial, with marked increases in cyanobacteria closest to pollution point sources in the south basin (McGowan et al., 2012). A more autochthonous carbon signature in lake sediments has been demonstrated in a synthesis study of multiple lakes across the north temperate-subarctic, with increases in cyanobacterial pigments (myxoxanthophyll) linked primarily to N and P fertilisation (Taranu et al., 2015).

In glacier fed-lakes of the Rocky Mountains changes in algal pigments were found to correspond with the MCA and LIA, linked to N-enriched runoff and changes in glacier volume (Slemmons et al., 2015). This highlighted close coupling of pigment records to the catchment as nutrients stimulated some algal groups, affecting the origin of the carbon deposited in these upland lakes. In Arctic west Greenland pigment records over Holocene timescales also helped track source origin, showing changes between mixed and meromictic lake status linked to lake morphology and proportions of benthic to pelagic production (McGowan et al., 2008). Highlighting the role of changes in terrestrial vegetation on the source of organic carbon deposited in Arctic lakes, and resulting ecosystem cascade, the arrival of *Betula* (6500 yr BP) due to succession caused abrupt increases in green algae, higher plants, colonial cyanobacteria and all algae (Anderson et al., 2008).

In a lake on Baffin Island higher chlorophyll *a* concentrations corresponded with warmer periods including the HTM and 20th century warming, suggesting clear links between climate and biological production (increased autochthonous carbon) (Michelutti et al., 2005). In a further lake on Baffin Island (Qivitu Highlands), the main primary producer community shifted from one based on ‘green’ taxa in the HTM based on chlorophytes, higher plants and bryophytes, to a mid-late Holocene abundance of ‘brown’ taxa based on diatoms and chrysophytes as the primary

producers (Florian et al., 2015). These interpretations were based on sedimentary pigment biomarkers, highlighting the changing signature of organic carbon, linked to changes in Holocene vegetation and temperature.

In the northern Swedish subarctic, Holocene records of algal pigments in Lake Seukokjaure were tightly coupled with changes in tree-line influencing terrestrial vegetation, soil development and inputs of terrestrial carbon (e.g. DOM), regulating the light regime of the lake (Reuss et al., 2010b). Here, the algal communities were productive after deglaciation between ~9700 and 7800 cal.yr BP, but declined ~3200 cal. yr BP coincident with local retreat in the treeline and more destabilised soils (Reuss et al., 2010b). Changes in light and nutrient regimes from 1750 cal. yr BP to present caused a transition from diatom dominance to chlorophytes (increase in lutein-zeaxanthin), potentially caused by aquatic moss abundance. This highlights how pigments can track varying inputs, contributing to interpretations about the source and quality of carbon.

2.2 Lipid biomarkers

Lipids are a diverse range of compounds which have been widely used in palaeolimnological studies both to track the source of carbon and the transformation processes that occur prior to and during sedimentation. Detailed reviews of lipid biomarkers that have relevance to carbon cycling are provided by Meyers and Ishiwatari (1993), Matsuda and Koyama (1977), Cranwell et al. (1987), Volkman (1986), Meyers and Teranes (2001), Meyers (1997), Meyers (2003) and recently in Bianchi and Canuel (2011), Castañeda and Schouten (2011) and Ouyang et al. (2015). This sub-section provides a summary of the interpretive, transformative and analytical considerations for the key lipid biomarkers utilised in this study (*n*-alkanes, *n*-alkanols, *n*-acids and sterols) for reconstructing changes in carbon cycling.

In this study, lipids help characterise the quantity and quality of autochthonous versus allochthonous carbon buried in Arctic lakes. Since the structure of compounds synthesised by aquatic algae and bacteria are different to those sourced from terrestrial vascular plants, in some lake systems by combining multiple approaches it may be possible to interpret the relative contributions of organic matter from in-lake versus external catchment sources (Meyers and Teranes, 2001). Lipids are all substances that are insoluble in water but possible to extract with solvents (Bianchi and Canuel, 2011).

2.2.1 Review of biomarker compounds, lipid ratios and equations in lakes

Detail on the lipid *n*-alkane (hydrocarbon) compounds typically detected in sediments of lakes and catchment samples is provided in Table 2.2, fatty acids in Table 2.3 and *n*-alkanols/sterols in Table 2.4. The *n*-alkanes (alkanes have strong single bonds) are typically less susceptible to diagenesis than fatty acids and *n*-alkanols (due to the presence of oxygen).

Table 2.2: Lipid *n*-alkane (hydrocarbon) compounds typically detected in the sediments of lakes and catchment plant/soil samples. Presented together with the general interpretation of each proxy/source indicator and commonly used lipid ratios and equations. Full details of lipid ratios and equations are provided in Appendix A. Note – source attributions in this table are general, with specific Disko 2 catchment sample survey outcomes detailed in sections 4.7.2 and 4.8.4.

Compound	General interpretation
All <i>n</i>-alkanes	Typically less susceptible to diagenesis than fatty acids/alkanols to microbial degradation due to their single carbon-carbon bonds (Meyers and Teranes, 2001).
C ₁₇ <i>n</i> -alkane maxima	Algae and photosynthetic bacteria (Cranwell et al., 1987) (Appendix A – Figure A.1).
C ₂₇ , C ₂₉ or C ₃₁ maxima	Vascular plants on land or at edge of lake (Cranwell et al., 1987).
C ₂₁ , C ₂₃ or C ₂₅ maxima	Some submerged macrophytes (Ficken et al., 2000).
C ₃₁ maxima	Some grass inputs (Cranwell, 1973).
C ₂₇ and C ₂₉ maxima	Higher plant tree inputs (Cranwell, 1973).
Unresolved Complex Mixture (UCM)	Delivery of petroleum residues to sediments, where conventional GC separation is difficult (Meyers and Takeuchi, 1981; Bourbonniere and Meyers, 1996a).
Carbon Preference Index (CPI) and CPI 2 Index	To distinguish recent ‘fresh’ hydrocarbons (odd predominance) from older more petroleum-like compounds (Bray and Evans, 1961; Cooper and Bray, 1963; Marzi et al., 1993) (see Appendix A – Equation A1 & A2).
Average Chain Length (ACL)	Terrestrial plants may synthesise shorter chain plant waxes in cooler climates, but more long chain waxes in tropical environments (Poynter et al., 1989; Ouyang et al., 2015). May also indicate changes in temperature and humidity (Zhou et al., 2005) (see Appendix A – Equation A6).
Terrigenous to aquatic source contribution (TAR _{HC})	Higher values of long chain C ₂₇ , C ₂₉ and C ₃₁ compounds indicate terrestrial contributions (Bourbonniere and Meyers, 1996a), but may over-represent these contributions as long-chain compounds are less easily degraded (Meyers, 1997) (see Appendix A – Equation A.7).
Proxy for submerged and floating macrophytes (P_{aq})	Floating leaved and submerged macrophytes usually have maximum abundance in the mid-chain C ₂₃ and C ₂₅ <i>n</i> -alkanes (Ficken et al., 2000). P_{aq} has also been linked with changes in water level and effective precipitation (Ouyang et al., 2015) (see Appendix A – Equation A.9).
Proxy for waxy hydrocarbons (P_{WAX})	High P_{WAX} values indicate greater contributions from terrestrial plants or emergent macrophytes by comparing C ₂₇ , C ₂₉ & C ₃₁ <i>n</i> -alkanes with total hydrocarbons (Zheng et al., 2007; Ouyang et al., 2015) (see Appendix A – Equation A.10).

Table 2.3: Lipid *n*-fatty acid compounds typically detected in the sediments of lakes and catchment plant/soil samples. Presented together with the general interpretation of each proxy/source indicator and commonly used lipid ratios and equations. Full details of lipid ratios and equations are provided in Appendix A. Note – source attributions in this table are general, with specific Disko 2 catchment sample survey outcomes detailed in sections 4.7.2 and 4.8.4.

Compound	General interpretation
All <i>n</i>-fatty acids (Also referred to as carboxylic acids)	Typically more susceptible to diagenesis than <i>n</i> -alkanes due to weaker bonds (Meyers and Teranes, 2001).
C _{14:0} , C _{16:0} & C _{18:0} (short chain compounds)	Non-specific as present in all organisms, but are dominant components of algae (Meyers, 1997) (C ₁₆ <i>n</i> -fatty acid, Appendix A – Figure A.4).
C _{24:0} , C _{26:0} , C _{28:0} & C _{30:0} (longer chain compounds)	Longer-chain fatty acids are typically specific to higher vascular plants (Meyers, 1997).
Ratio of unsaturated to saturated <i>n</i> -fatty acid (e.g. C _{16:1} / C _{16:0} & C _{18:1} / C _{18:0})	Indicator of preservation as unsaturated compounds are more effectively degraded by microbes both during and after sedimentation (Cranwell, 1976). Could be temperature regulated, with microbial alteration of the unsaturated acid accelerated under warm conditions (Zhou et al., 2005).
C _{15:0} fatty acid	In some settings linked to a bacterial origin (Duan et al., 1997; Zheng et al., 2007).
Ratio between ‘normal’ and ‘anteiso’ (branched) C ₁₅ <i>n</i> -fatty acids.	May provide an indicator of microbial reworking and biomass (Robinson et al., 1987; Meyers, 2003).
Branched / cyclic <i>n</i> -fatty acids	Bacterial origins generally, but also identified in fungi, molluscs and phytoplankton (Perry et al., 1979).
Carbon Preference Index (CPI _H , CPI _L & CPI _T)	Adaptions of <i>n</i> -alkane CPI index for fatty-acid compounds (Matsuda and Koyama, 1977). Includes C ₁₂ -C ₁₈ for lower molecular weight compounds (CPI _L), ≥C ₂₀ for higher molecular weight compounds (CPI _H) and for the entire range of saturated fatty acids detected (CPI _T). CPI _L is high in most plants (12-100), but CPI _H is lower (0.9-8) as long-chain odd carbon acids are abundant in some land plants (Meyers and Ishiwatari, 1993). Can also be an indicator of bacterial processing as CPI values decrease with microbial activity (see Appendix A – Equation A.3, A.4 & A.5).
Terrigenous to aquatic fatty acid ratio (TAR _{FA})	Higher values of long chain C ₂₄ , C ₂₆ & C ₂₈ compounds indicate terrestrial contributions, although fatty acids are more susceptible to diagenesis compared with <i>n</i> -alkanes, particularly with the shorter chain compounds (Meyers, 1997) (see Appendix A – Equation A.8)..

Table 2.4: Lipid *n*-alkanol and some sterol compounds detected in the sediments of lakes and catchment plant/soil samples. Presented together with the general interpretation of each proxy/source indicator and commonly used lipid ratios and equations. Full details of lipid ratios and equations are provided in Appendix A. Note – source attributions in this table are general, with specific Disko 2 catchment sample survey outcomes detailed in sections 4.7.2 and 4.8.4.

Compound	General interpretation
All <i>n</i>-alkanols	Typically more susceptible to diagenesis than <i>n</i> -alkanes due to the presence of oxygen (Robinson et al., 1987).
C ₁₆ to C ₂₂ (short chain compounds)	Dominant in algae and bacteria (Meyers, 2003). Shorter chain compounds preferentially degrade compared with longer chain compounds (Robinson et al., 1987) (Appendix A – Figure A.2).
C ₂₂ to C ₃₀ (longer chain compounds)	Indicative of terrestrial plants (Meyers, 2003).
Phytol (3,7,11,15-tetramethyl-2-hexadecen-1-ol)	Derived from chlorophyll and is an indicator of photoautotrophy and so an indicator of all algae (Meyers, 2003) (Appendix A – Figure A3.).
Phytone / phytol ratio (6,10,14-trimethylpentadecan-2-one / 3,7,11,15-tetramethyl-2-hexadecen-1-ol)	Phytone is an early degradation product of phytol and so this ratio can help explore changes in lipid degradation and the presence of cyanobacterial and bacterial mats (Pearson et al., 2007).
All sterols	Sterols have a wide distribution, so assigning precise source origins can sometimes be difficult (Volkman, 1986). Sterols are tetracyclic alcohols that rigidify cell membranes with the presence or absence of double bonds at various positions on the carbon framework (Meyers and Ishiwatari, 1993).
Cholesterol / β -sitosterol ratio (cholest-5-en-3 β -ol / 24-ethylcholest-5-en-3 β -ol)	Cholesterol is primarily sourced from algae, but β -sitosterol is more dominant in emergent water plants and terrestrial vegetation (Nishimura and Koyama, 1977; Meyers, 1997).
Epicholestanol (5 α (H)-cholestan-3 α -ol)	Linked to anoxia in a sediment core in Lake Lemán, Switzerland (Mermoud et al., 1985).
Tetrahymanol (gammaceran-3 β -ol)	Associated with cyanobacterial mats (Pearson et al., 2007), including ciliates, protozoa, phototrophic and green/purple sulphur bacteria (Sinninghe Damsté et al., 1995).
Brassicasterol (24-methylcholesta-5,22-dien-3 β -ol)	Found in algal mats, diatoms and brassicas (Volkman et al., 1998; Pearson et al., 2007) (Appendix A – Figure A.5).

2.2.2 Selecting appropriate lipid biomarkers for the Disko 2 reconstruction

The review of biomarker lipid ratios and equations in lakes (Section 2.2.1, Tables 2.2, 2.3 & 2.4) was used, combined with the catchment survey (Section 4.7.2, 4.8.4 & Appendix B) to suggest nine key biomarkers suitable for plotting down-core in Disko 2 summary diagrams (Figure 5.16 and 5.20).

For *n*-alkanes the CPI 2 index was selected (Marzi et al., 1993) as it is a relatively robust indicator for distinguishing ‘fresh’ hydrocarbons which are more likely to be sourced from algae or young plant growth, compared with older more ‘petroleum-like’ soils or geological deposits (Table 2.2). The CPI 2 index, rather than the original CPI index was selected as this revision is more effective at distinguishing the slight variations in the chain length dominance of organic matter (Marzi et al., 1993). Also selected from the *n*-alkanes was the TAR_{HC} index to distinguish long chain terrestrial contributions from shorter chain aquatic impacts as this ratio combines a range of potential carbon chain lengths (Bourbonniere and Meyers, 1996a). TAR_{HC} was selected as it can track autochthonous from allochthonous inputs, enabling a comparison with C/N ratio. The *P*_{WAX} index (Zheng et al., 2007; Ouyang et al., 2015) has also been selected as this ratio compares long chain C₂₇, C₂₉ and C₃₁ compounds with total hydrocarbons, providing an indicator of broad terrestrial contributions. Although an even compound (odd compounds have greater abundance in *n*-alkanes), the C₂₆ to total *n*-alkanes ratio was selected, based not on the literature review (Table 2.2), but on the source study investigation as an excellent indicator of soils (Section 4.7.2 & 4.8.4).

Although less resistant to diagenesis than *n*-alkanes, fatty acid ratios were also selected as use of multiple compounds can strengthen interpretations. The CPI_T index (Matsuda and Koyama, 1977; Meyers, 1997) was selected as it can indicate how ‘fresh’ or ‘petroleum-like’ the fatty acids are as plants and algae tend to contain less degraded organic matter, and are subject to less microbial reworking than soils (Table 2.3). This index can also help distinguish between autochthonous and allochthonous sources of organic matter when compared with source inputs (Section 4.7.2 and 4.8.4). The ratio of the C₃₀ *n*-fatty acid to total fatty acids was also selected as longer chains are indicative of terrestrial plants (Table 2.3) and so should be a good indicator of fresh plants and soils (Section 4.7.2 & 4.8.4).

For *n*-alkanols, the ratio of C₁₆ to total *n*-alkanols was selected as short chain compounds are typically dominant in algae and bacteria (Meyers, 2003) (Table 2.4). A challenge with the interpretation of the shorter chain compounds is that they

preferentially degrade compared with longer chain compounds (Robinson et al., 1987) and so need to be considered with other proxies (e.g. pigments, C/N ratios and short-chain *n*-alkanes). For contrast, the ratio of longer chain C₂₄ *n*-alkanols to total *n*-alkanols was also selected as these compounds are typically indicative of higher plants (Meyers, 2003) (Table 2.4). Finally, the ratio of brassicasterol to total sterols was also selected as since this compound is often found in algal mats and diatoms (Volkman et al., 1998; Pearson et al., 2007) (Table 2.4), it is probably a good biomarker to compare with pigment indicators of total algal production (e.g. β -carotene, see Figure 5.20).

2.2.3 Palaeolimnological studies using lipid biomarkers for carbon cycling

Examples of palaeolimnological studies using lipid biomarkers relevant to carbon cycling include a study of Holocene vegetation in Lake Steisslingen, Germany where dominant tundra pioneer vegetation was indicated by the C₃₁, birch arrival by the C₂₇ and diverse deciduous forests to the C₂₉ *n*-alkane dominance (Schwark et al., 2002). As the catchment vegetation community changed, the *n*-alkane signature within lake sediments also changed, reflecting the origin of the carbon deposited. In sediments from lake El'gygytgyn in East Russia plant leaf wax *n*-alkanes, TAR/CPI ratios of *n*-alkanes and the compound dinosterol (indicator dinoflagellates) demonstrated higher tree cover and greater algal aquatic productivity (increased autochthonous production) during interglacial periods (D'Anjou et al., 2013).

In sediments of a lake in the Sierra Nevada, California there was a shift towards short chain length C₂₅ *n*-alkanes between ~3.1 and 2.9 ka BP as water levels increased, interpreted as causing an expansion in submerged aquatic plants and changing the source of the carbon deposited (Street et al., 2013). Glaciolacustrine clays in Lake Huron and Lake Ontario were found to have less land derived (long chain compounds) than recent deposits due to post-glacial forest expansion (Meyers et al., 1980; Silliman et al., 1996). This has relevance for understanding carbon cycling as it shows allochthonous inputs were lower in the early Holocene (more autochthonous) compared with more recent higher plant, forest derived deposits. In lake Lake Ontario changes in the *n*-alkanoic TAR ratio increased in coincident with deforestation (delivery of terrestrial material), while recent increases in the C₁₇ *n*-alkane were linked cultural eutrophication (from anthropogenic nutrient inputs) since the 1950s (Bourbonniere and Meyers, 1996b). This highlights how shorter chain *n*-alkanes are more indicative of carbon from in-lake autochthonous production (e.g. algae) whereas

longer chain compounds can be indicators of terrestrial (allochthonous) carbon delivery.

2.3 Organic carbon stable isotope ratios ($\delta^{13}\text{C}_{\text{TOC}}$) and C/N ratios

The $\delta^{13}\text{C}$ of total organic carbon (the ratio of ^{13}C to ^{12}C) in lake sediments is an indicator of the organic matter source, past lake productivity and the biosynthetic pathway of carbon both within lakes and externally. The use of $\delta^{13}\text{C}_{\text{TOC}}$ in sedimentary lacustrine sequences have been previously reviewed in Meyers (1994), Meyers (1997), Meyers and Lallier-Vergès (1999), Meyers and Teranes (2001), Meyers (2003), Leng and Marshall (2004), Leng et al. (2006) and more recently in Bianchi and Canuel (2011). In this study, $\delta^{13}\text{C}_{\text{TOC}}$ and C/N ratio helps elucidate how biological production and differences between catchments (presence of glaciers, permafrost and varying vegetation inputs) might influence the quality and quantity of autochthonous versus allochthonous carbon buried in Arctic lakes. This sub-section outlines the applicability of $\delta^{13}\text{C}_{\text{TOC}}$ for elucidating changes in carbon cycling in palaeolimnological studies.

Atmospheric CO_2 is composed of 99% the isotope carbon-12, but only ~1% of the isotope carbon-13. Since the uptake of ^{12}C requires less energy than ^{13}C in plants and algae the proportion of ^{13}C taken up is usually less than in the atmospheric ratio. However, significant differences in isotopic fractionation exist between photosynthetic pathways. The majority of plants and algae follow the C_3 Calvin pathway which uses the enzyme RuBP carboxylase to preferentially take up ^{12}C , approximately -20‰ lower than the $^{13}\text{C}/^{12}\text{C}$ of the inorganic (e.g. bicarbonate, HCO_3^-) or atmospheric (CO_2 source). (Meyers and Lallier-Vergès, 1999; Meyers and Teranes, 2001). Atmospheric CO_2 has a $\delta^{13}\text{C}$ of $\sim -7\text{‰}$, whereas HCO_3^- has a $\delta^{13}\text{C}$ of $\sim 0\text{‰}$, which means when algae fix HCO_3^- it may be reflected in a slightly higher $\delta^{13}\text{C}$ value (Bianchi and Canuel, 2011). However, in lakes where dissolved CO_2 ($\text{CO}_2(\text{aq})$) is in isotopic equilibrium with the atmosphere, and algae primarily use $\text{CO}_2(\text{aq})$, then $\delta^{13}\text{C}$ produced from C_3 algae or C_3 plants may be isotopically indistinguishable (Meyers and Lallier-Vergès, 1999; Meyers and Teranes, 2001). In contrast, terrestrial plants or aquatic macrophytes that utilise the C_4 Hatch-Slack pathway fractionate between -4 to -6‰ , compared with the CO_2 source (Meyers and Lallier-Vergès, 1999). This means that in environments where the proportion of C_4 plants have increased then $\delta^{13}\text{C}_{\text{TOC}}$ would be expected to become higher (Lamb et al., 2004). The precise $\delta^{13}\text{C}_{\text{TOC}}$ value sedimented

is therefore linked to the size of the terrestrial catchment (and land productivity) relative to the volume of the water body (and algal production) and the mixture of these inputs.

In large and deep lakes carbon isotopes have also been used in palaeolimnology to reconstruct algal palaeoproductivity (Schelske and Hodell, 1995; Brenner et al., 1999) and other in-lake organisms such as macrophytes (Aichner et al., 2010a). When $\delta^{13}\text{C}$ is primarily contributed by aquatic algae, values can become higher if $\text{CO}_{2(\text{aq})}$ is limited and if algae switch to primary usage of HCO_3^- which has a higher $\delta^{13}\text{C}$ value ($\sim 0\text{‰}$) than $\text{CO}_{2(\text{aq})}$. This is likely to occur during periods of high photosynthetic activity when CO_2 is limited, but algal production promoted, for example by nutrient input (Hollander and McKenzie, 1991; Bernasconi et al., 1997). However, complexity emerges, as over time related to catchment processes the $\delta^{13}\text{C}$ of DIC (including HCO_3^-) can vary and pH and temperature may influence uptake. For example, at higher water temperatures there is less $\text{CO}_{2(\text{aq})}$ in comparison with dissolved HCO_3^- as the solubility of CO_2 in H_2O at 0°C is 2.5 times higher than at 30°C (Nakai, 1972) (Table 2.5). With higher pH and more alkaline water there is more HCO_3^- available for carbon fixation, but calcium carbonate precipitate may cause pH to decline.

In recent sediments, decreases in the $\delta^{13}\text{C}_{\text{TOC}}$ value may be associated with the trend for increased atmospheric CO_2 known as the Seuss effect, coincident with industrialisation and the burning of fossil fuels to have lower $\delta^{13}\text{C}_{\text{TOC}}$ values (Keeling et al., 2013). Corrections have been made for the historic depletion of ^{13}C in atmospheric CO_2 at the global scale in some palaeolimnological studies to enable the contemporary interpretation of the lake specific interpretations of carbon cycling (Schelske and Hodell, 1995; Verburg, 2007). A summary of the potential controls on bulk $\delta^{13}\text{C}_{\text{TOC}}$ in lakes is provided in Table 2.5.

Table 2.5: Summary of the potential controls on bulk $\delta^{13}\text{C}_{\text{TOC}}$ in lakes collated by the author.

Control	Mechanism
Algal productivity/nutrient supply	CO_2 (aq) levels are insufficient to meet the requirements of photosynthesis so algae utilise HCO_3^- which has a higher $\delta^{13}\text{C}$ value (Hodell and Schelske, 1998).
C_3 versus C_4 photosynthesis	C_3 plants and C_4 algae are isotopically indistinguishable. But C_4 photosynthesis uses a different biosynthetic pathway resulting in higher $\delta^{13}\text{C}$ (Meyers and Teranes, 2001).
Stomatal diffusion and CO_2 absorption processes	The specific plant or algal diffusion processes may influence the process of CO_2 uptake due to chemical and physical properties of the organism (Diefendorf et al., 2010).
Concentration and isotopic composition of HCO_3^-	The isotopic composition and concentration of HCO_3^- dissolved in lake waters from the catchment can vary (Leng and Marshall, 2004).
Composition of algae in lake	Shifts in algal groups, communities or abundance may vary the ability for uptake of CO_2 (aq) or HCO_3^- (McGowan et al., 2012).
Wind mixing and in-lake water mixing regime	Wind mixing, water residence time and groundwater connectivity changes the concentration of CO_2 (aq) available to algae and aquatic plants (Gu et al., 2004).
Trophic interactions	With a change in food-web pathway, such as an additional consumer there can be an additional 1 to 2% enrichment (Parsons and Lee Chen, 1995).
Rising atmospheric CO_2 concentrations	The Suess effect is a recent phenomenon linked with industrialisation caused by the release of CO_2 which is depleted in ^{13}C . Corrections are reviewed in Verburg (2007).
Effect of temperature	With higher water temperature there is reduced CO_2 (aq) in comparison to dissolved HCO_3^- . The solubility of CO_2 in water at 0 °C is 2.5 times greater than at 30 °C (Nakai, 1972).
Effect of pH	Higher pH results in lower CO_2 availability compared with dissolved HCO_3^- (Håkansson, 1985).
Methanogenesis/respiration processes	When the water column is depleted in CO_2 (aq) anoxia can result in the bottom waters and sediments. Methanogenesis releases isotopically light CH_4 which forms CO_2 (aq) and can be utilised by algae or macrophytes (Brenner et al., 1999).
Terrestrial supply of organic carbon	Organic carbon can be supplied directly from the catchment, which may either be buried (as POC) or subsidise algal production directly or via the microbial loop (Pace et al., 2007).

2.3.1 Preservation and diagenesis of $\delta^{13}\text{C}_{\text{TOC}}$

Although diagenesis, remineralisation and biological degradation results in the majority of carbon in lakes ‘escaping’ sedimentation, the $\delta^{13}\text{C}$ values of organic matter are generally regarded as being resistant to change (Meyers, 1994). Bulk $\delta^{13}\text{C}_{\text{TOC}}$ values are weighted averages of multiple components, with each part potentially degrading at different rates. For example, in sediment traps positioned in Lake Michigan, organic algal compounds were found to degrade preferentially compared with the more recalcitrant components, such as long-chain *n*-alkanes (Meyers et al., 1984). However, diagenetic effects of $\delta^{13}\text{C}$ have been demonstrated in annually varved sediments with the majority of change (decrease with sedimentation) occurring within the first 5-10 years (Gälman et al., 2009).

Hodell and Schelske (1998) demonstrated that although diagenetic processes had an effect on organic carbon accumulation, it did not change $\delta^{13}\text{C}_{\text{TOC}}$ values in the zone of oxic pore waters. However, this is not always the case as it has been demonstrated that when methanogenesis is active in the upper sediments due to anoxia, this can release light CH_4 and isotopically heavy $\text{CO}_2(\text{aq})$, which is transferred to the upper water column and is fixed by algae (Gu and Schelske, 1996; Brenner et al., 1999). But oxidation of the lower $\delta^{13}\text{C}$ methane released from sediments can also lead to lower $\text{CO}_2(\text{aq})$ and lower $\delta^{13}\text{C}$ values of DIC, which can in turn be fixed by algae (Hollander and Smith, 2001; Vreca and Muri, 2006). This highlights that the role of methanogenesis can be complex and highly lake specific. The analysis of $\delta^{13}\text{C}$ on chironomid fossil head capsules has been demonstrated as a mechanism to help interpret past changes in methane flux at the sediment water interface in lakes (van Hardenbroek et al., 2010; van Hardenbroek et al., 2011).

The microbial loop (whereby bacteria metabolise carbon) and variations in the input of terrestrially derived organic carbon may provide an additional supplement of carbon to algae that are able to fix carbon by mixotrophic or heterotrophic processes (Jones, 2000; Burkholder et al., 2008; Reuss et al., 2010a). The $\delta^{13}\text{C}$ of source organic carbon (e.g. organic detritus, bacteria) is then subsequently incorporated into algae, influencing the isotopic composition of these organisms (Finlay, 2001). The interpretation of $\delta^{13}\text{C}_{\text{TOC}}$ is therefore a combined indicator of productivity, source input and diagenetic processes. A lake-specific interpretation is required, as the processes (see Table 2.5) taking place in each lake are uniquely coupled to ecology, geomorphology, climate and hydrology.

2.3.2 C/N ratios

The ratio of C/N in sediments is routinely used as an additional proxy to confirm the source of organic matter in carbon cycling investigations. Since the majority of $\delta^{13}\text{C}$ analyses are now conducted by an EA coupled to an IRMS, measurements of C/N ratios are combined (Meyers and Teranes, 2001). Low C/N ratios that are typically between 4 and 10 are indicative of algae as there is an absence of cellulose, but relatively high levels of protein (Meyers and Lallier-Vergès, 1999; Meyers, 2003). High C/N ratios that are usually greater than 20 indicate terrestrial inputs as vascular land plants contain greater amounts of cellulose, but proportionately less protein (Meyers and Lallier-Vergès, 1999; Meyers, 2003). This makes the C/N ratio an excellent confirmatory indicator of the algal or terrestrial source, especially when $\delta^{13}\text{C}$ values indicate C_3 plants or C_3 algae that may be hard to distinguish the primary source without combining with C/N ratios. C/N ratios are routinely plotted against $\delta^{13}\text{C}$ to effectively interpret source inputs and identify groupings amongst plants, algae and palaeolimnological samples (Figure 2.10).

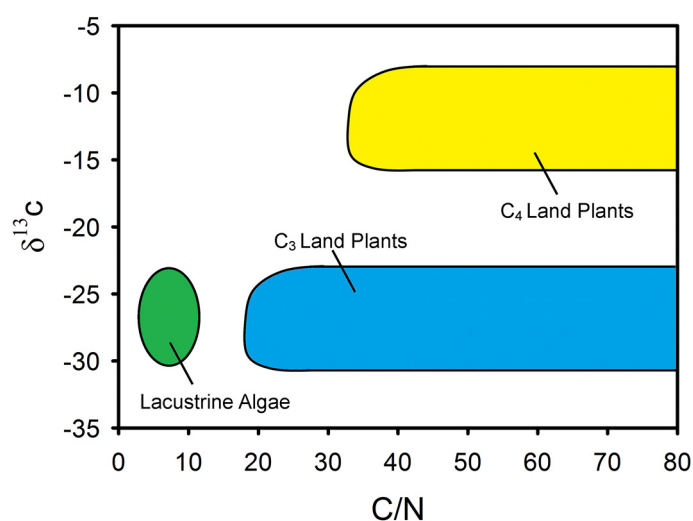


Figure 2.3: Plot of $\delta^{13}\text{C}$ against C/N values to highlight expected zones for organic matter sourced from lacustrine algae, C_3 land plants and C_4 land plants. Redrawn from Meyers and Lallier-Vergès (1999).

There are a number of diagenetic factors that need to be considered when interpreting C/N ratios. Early diagenesis may selectively degrade sugars and lipids causing C/N ratios of woody matter to be higher at depth (Meyers et al., 1995). Studies of varved sediments (27 years) in northern Swedish lakes have shown the N content of organic matter tends to preferentially degrade compared with the C content of recent sediments causing C/N ratios to increase with depth (Gälman et al., 2008). Algal C/N ratios may also increase during water column sinking and sedimentation, as proteins

high in nitrogen are more vulnerable to degradation (Meyers and Lallier-Vergès, 1999). However, the opposite can occur (C/N ratio decreasing with depth) in the sediments of oligotrophic lakes if anaerobic activity is promoted. In these conditions anaerobic activity can convert OM to the gases CO₂ and CH₄ which reduces the TOC concentration. In contrast, nitrogen in OM is converted to NH₄⁺ which is often locked in sediments as it is absorbed by clay minerals (Lallier-Vergès and Albéric, 1990; Meyers and Lallier-Vergès, 1999).

Similar changes resulting in declines in C/N ratios may occur in soils as microbial activity can release nitrogenous material and at the same time remineralise carbon (Sollins et al., 1984; Meyers and Lallier-Vergès, 1999). However, the effects of these diagenetic changes are usually relatively minor in contrast to the significant differences between C/N from aquatic algae and vascular land plants. Further, although sediment trap investigations have revealed large drops in the total amount of OM, the final sedimented C/N ratios tend to reflect inputs. However, during sinking there can be variations in C/N ratio, with often greater losses of algal matter, as algal matter is generally more fresh than terrestrial inputs which may have undergone diagenesis on land (Meyers and Eadie, 1993; Meyers and Lallier-Vergès, 1999).

Care needs to be taken when interpreting C/N ratios with very small C_{org} percentages (<0.3%). This is particularly important if measurements are made on organic carbon that has had carbonate carbon removed as inorganic nitrogen will remain (Meyers and Teranes, 2001). Usually, inorganic nitrogen comprises a very small percentage and so its effect is negligible. However, with such small organic concentrations this residual nitrogen could mean C/N ratios are unexpectedly low. Most lake sediments contain more than 1% TOC so values are usually reliable (Meyers and Teranes, 2001). It is important to follow a standardised methodology for the acidification and removal of inorganic carbon for all sediment and catchment samples as analytical precision depends not only on environmental variability, but also on acid pre-treatment and the composition of any residual inorganic carbon (Brodie et al., 2011). Although source input studies are recommended as there are some exceptions to the general trends. For example, some riparian and aquatic plants like *Carex* spp. may have high C/N ratios, and chlorophytes (e.g. *Botryococcus braunii*) may have very high C/N ratios similar to terrestrial matter (Lamb et al., 2004).

2.3.3 Example palaeolimnological studies using $\delta^{13}\text{C}$ and C/N to interpret carbon cycling

The majority of studies in palaeolimnology have used $\delta^{13}\text{C}_{\text{TOC}}$ and C/N ratios to reconstruct eutrophication related changes in productivity (Schelske and Hodell, 1995; Hodell and Schelske, 1998; Brenner et al., 1999) or changes in C_3 versus C_4 vegetation (Lamb et al., 2004). However, in Arctic environments eutrophication is unlikely in lakes above settlements (such as in all lakes in this study) and C_4 vegetation is not a major component of Arctic vegetation. In a west Greenland lake near Sisimiut $\delta^{13}\text{C}_{\text{TOC}}$ and C/N ratios were tightly coupled to glacial retreat and postglacial hydrological flushing between 11 and 8.5 ka BP, followed by more stable conditions and then further fluctuations in C/N ratio with the neoglacial and delivery of terrestrial organic matter from destabilised soils (Leng et al., 2012). At lakes in continental southwest Greenland near Kangerlussuaq $\delta^{13}\text{C}_{\text{TOC}}$ helped identify that the organic matter sedimented was predominantly autochthonous, with variability in C/N ratio linked to nitrogen deficiency in the lake (Olsen et al., 2013).

In subarctic Sweden, changes in $\delta^{13}\text{C}_{\text{TOC}}$ in lake records have been linked to treeline retreat around 3200 BP, with records becoming more variable due to lowered input of ^{13}C depleted DIC due to reduced soil respiration from the absence of trees (Reuss et al., 2010b). More recent shifts to lower, more algal C/N ratios since ~1750 probably reflects natural deforestation linked to declining temperatures (Reuss et al., 2010a). Changes in carbon and nutrient cycling can also result from disturbed permafrost, leading to increased nutrient inputs into lakes and lower more algal C/N ratios (Kokfelt et al., 2010), with in some systems high summer precipitation in permafrost covered landscapes leading to elevated DIC inwash and depletion (higher) $\delta^{13}\text{C}_{\text{TOC}}$ associated with mire export events (Kokfelt et al., 2009).

In the western Russian Arctic treeline retreat around 4000 ^{14}C yr BP led to increases in sedimentary $\delta^{13}\text{C}_{\text{TOC}}$ as atmospheric CO_2 became the dominant source of organic matter, with reduced decomposition rates and a switch to more algal (lower) C/N ratios (Wolfe et al., 1999). The closed and open basin connectivity of a lake in the Northwest Territories, Canada was the main control on sedimentary $\delta^{13}\text{C}$, linked to treeline advance. In this lake, during hydrological closure $\delta^{13}\text{C}$ became enriched due to declining $\text{CO}_{2(\text{aq})}$ and the need for algae to fix carbon using $\delta^{13}\text{C}_{\text{DIC}}$. Together, these studies highlight the role of the catchment in determining $\delta^{13}\text{C}_{\text{TOC}}$ and C/N ratios in Arctic lakes.

2.4 Compound specific carbon isotope analysis

Compound specific isotope analysis (CSIA) is increasingly being used in palaeolimnology as isotope values of specific molecules are likely to more accurately represent specific origins of organic matter compared with bulk values (see Tables 2.2, 2.3 & 2.4 for varying interpretations of lipid source specificity). CSIA is reviewed for palaeoenvironmental applications in Castañeda and Schouten (2011), Evershed et al. (2007), Leng and Henderson (2013) and briefly in Leng et al. (2006). The straight chain homologous series of hydrocarbon and hydrocarbon-like molecules of *n*-alkanes, *n*-alkanols and *n*-alkanoic acids can separate terrestrial epicuticular waxes (long chain) from algal lipids (short chain) to provide more source-specific $\delta^{13}\text{C}$ (Leng and Henderson, 2013).

2.4.1 Carbon isotopes on terrestrial leaf wax lipids

The largest number of palaeolimnological studies using CSIA $\delta^{13}\text{C}$ use long chain *n*-alkanes (C_{27} , C_{29} and C_{31}), *n*-alkanols (C_{24} , C_{26} and C_{28}) and *n*-acids (C_{26} , C_{28} and C_{30}) to reconstruct changes in C_3 to C_4 vegetation. This is possible because most plants use the C_3 pathway of CO_2 fixation (Hatch-Slack) and have $\delta^{13}\text{C}$ values around -35‰ , whereas other plants particularly grasses sometimes use the C_4 pathway of CO_2 fixation (Rubisco) and have $\delta^{13}\text{C}$ values of around -20‰ (Huang et al., 2000). Under current CO_2 concentrations, particularly in high aridity C_3 photosynthesis is disadvantaged and plants with C_4 pathways are more successful as they have a CO_2 concentrating mechanism and a higher water use efficiency, requiring less water consumption (Boom et al., 2002). Since plant leaf waxes are primarily of long chain lengths, the $\delta^{13}\text{C}$ values of these compounds more accurately represent terrestrial carbon cycling than bulk $\delta^{13}\text{C}$ (Rieley et al., 1991). For example, long chain leaf wax lipid $\delta^{13}\text{C}$ have helped interpret C_3 to C_4 vegetation change in Lake Wandakara, Uganda to human activity and climate change (Russell et al., 2009), in Lake Quexil, Guatemala linked to Mayan forest clearance (Huang et al., 2001) and in a lake near Mt Kilimanjaro to vegetation change linked to variations in precipitation (Sinninghe Damsté et al., 2011).

2.4.2 Carbon isotopes on short chain algal and mid chain macrophyte lipids

The $\delta^{13}\text{C}$ values of short chain algal lipids and mid-chain lipids from aquatic macrophytes are increasingly being used in palaeolimnological studies to understand the different parts of the carbon cycle within lake systems (Castañeda and Schouten, 2011; Leng and Henderson, 2013). Although the $\delta^{13}\text{C}$ values of bulk organic carbon have been widely attributed to aquatic productivity (higher $\delta^{13}\text{C}$ values) e.g. (Hollander and McKenzie, 1991; Brenner et al., 1999; Leng and Marshall, 2004), the $\delta^{13}\text{C}$ of TOC can also be influenced greatly by C_4 dominated terrestrial organic matter, limitation of dissolved CO_2 leading to algal utilisation of bicarbonate (HCO_3^-) and changes in pH (Meyers, 2003; Leng and Henderson, 2013). Additionally, breakdown of organic matter at the sediment surface interface can lead to lower $\delta^{13}\text{C}$ values of CO_2 , which can counteract the effect of increased productivity, and the presence of aquatic macrophytes may utilise both CO_2 from the atmosphere and from inorganic carbon in water (Leng and Henderson, 2013).

In contrast, compound-specific analyses of short chain (algal) and mid chain (macrophyte) *n*-alkanes, *n*-alkanols and *n*-acids are more source specific and so less likely to be influenced by these confounding factors. For example, Aichner et al. (2010b) used $\delta^{13}\text{C}$ values of C_{23} *n*-alkanes to help interpret changes in aquatic macrophytes, higher algal abundance and carbon limitation in Lake Koucha on the eastern Tibetan Plateau. Declines in the $\delta^{13}\text{C}$ values of C_{17} , C_{19} and C_{21} *n*-alkanes marked the Younger Dryas interval (~11.8 kyr BP) in Lake Malawi, East Africa linked to changes in wind induced upwelling providing ^{13}C -depleted CO_2 from decomposition in deeper waters (Castañeda et al., 2009). In Sky Pond, the Rocky Mountains recent changes in the $\delta^{13}\text{C}$ value of the C_{21} *n*-alkane was linked to enhanced in-lake or talus algal abundance due to nitrogen deposition since the 1950s (Enders et al., 2008).

2.5 Summary – methods literature review

This chapter has explored the literature to help select and interpret the most appropriate organic geochemical techniques for application in a palaeolimnological study, focused on reconstructing pigments (Section 2.1), lipid biomarkers (Section 2.2), organic $\delta^{13}\text{C}_{\text{TOC}}$ (Section 2.3), C/N ratio (Section 2.3) and compound-specific $\delta^{13}\text{C}$ (Section 2.4). A multi-proxy approach has been selected, as each set of proxies can contribute information that together offers the best potential to interpret carbon cycling on Disko.

The review suggests pigments are good indicators of photoautotrophy, particularly in algae but that these biomarkers may also be responsive to some plant and macrophyte inputs, enabling reconstructions of broad shifts in groups to be made. Some pigments are taxonomically specific including alloxanthin (cryptophytes), diatoxanthin (mostly diatoms) and canthaxanthin (cyanobacteria) (Section 2.1), however a limitation is that identification is not possible to species level compared with more direct palaeoecological proxies (e.g. macrophytes, diatoms and pollen). Although the stability of pigments is varied there are agreed approaches to assess the possibility of diagenesis in lakes (see Section 2.1.1), aiding interpretation. Pigments have been used successfully in previous northern latitude palaeolimnological investigations, including those focused on the source of organic carbon, changes from benthic to pelagic production, changes in primary production and the effects of nutrients and DOC from catchment change (see Section 2.1.2).

The review considered a wide range of potential biomarker compounds (Section 2.2.1), prior to selecting key compounds (Section 2.2.2) for use in Disko 2 summary diagrams (Figures 5.16 & 5.20). Compared with pigments, lipid biomarkers can provide clearer differentiation between autochthonous and allochthonous components of organic matter. However, lipid biomarkers are subject to varying degrees of diagenesis, with *n*-alkanes less susceptible than *n*-alkanols or *n*-fatty acids to these processes (Section 2.2.1). Among the *n*-alkanes three indexes were selected (Section 2.2.2) to distinguish autochthonous from allochthonous production, with a further ratio selected (C_{26} *n*-alkane) as it indicates soil inputs (and some vegetation contributions) in this system (see Sections 4.7.2 & 4.8.4). The ratios selected from the *n*-fatty acids and *n*-alkanols also had some differentiation in the source study investigations and brassicasterol was an excellent indicator of algae (see Sections 4.7.2 & 4.8.4). Lipids have been used successfully in previous studies to investigate relative autochthonous and allochthonous inputs, particularly in lakes with vegetated catchments (Section

2.2.3). As Disko is an environment with limited vegetation (Section 4.2 & 4.3) this adds an additional challenge to the proxy interpretations, but the catchment survey will help to mitigate this (see Sections 4.7.2 & 4.8.4).

The review also assessed the utility of $\delta^{13}\text{C}$ and C/N as proxies for reconstructing carbon cycling. Down-core $\delta^{13}\text{C}_{\text{TOC}}$ can either be indicative of productivity or the source of carbon, with multiple potential controls (Table 2.5) and varying susceptibility to diagenesis depending on the lake environment (Section 2.3.1). Although C/N ratio is generally a robust indicator of autochthonous versus allochthonous production, both C/N and $\delta^{13}\text{C}_{\text{TOC}}$ can be challenging to interpret in the uppermost sediments (Sections 2.3.1 & 2.3.2) making comparison with other proxies important. Both C/N and $\delta^{13}\text{C}_{\text{TOC}}$ have been widely used in Arctic lakes to indicate autochthonous versus allochthonous production, the impact of treeline on catchment soils and basin closed or open connectivity (Section 2.3.4). Compound-specific $\delta^{13}\text{C}$ enables interpretations to be tied to compounds, some of which can have specific origins, helping to provide more robust interpretations.

Chapter 3: Methods

This chapter outlines the principal methods used during the research presented in this thesis. Where slight variations in the methods are present, this is detailed in the relevant chapter.

3.1 Site selection

Lakes suitable for coring on Disko Island (Qeqertarsuaq) were selected from 1:100,000 scale maps and aerial imagery in consultation with Arktisk Station leader Dr Ole Stecher and Chief of Logistics Kjeld Mølgaard (see Figure 4.1 for detailed location map). Access to lake sites was provided by snowmobile with coring conducted through the ice in April 2013. Lake sites were selected to follow a broad landscape gradient from a high-elevation cirque lake with a small catchment (Disko 2) to two larger lakes at lower elevations (Disko 1 and 4). A range of lakes were sampled to address the landscape scale objectives of this study. All lakes were well above the local marine limit which ranges between 60 and 90 m.a.s.l on Disko Island (Ingólfsson *et al.*, 1990). In total, four lakes were cored (named Disko 1-4). For the purposes of this project sediments from three lakes (Disko 1, 2 & 4) have been investigated. Short cores were taken from lake Disko 3 but these cores are not used in this thesis.

3.2 Sediment coring

Sediment coring was conducted on Disko Island (Qeqertarsuaq), West Greenland between 17/04/13 and 21/04/13 (temperatures at Qeqertarsuaq (Godhavn) were -3 to -15 °C during this period), with cores taken from four sites (Disko 1-4). Replicate ‘chamber-type’ 10 cm diameter Russian corers (Anderson *et al.*, 2000; Glew *et al.*, 2001) were used to obtain overlapping sequences comprising ~ 1 m sections, to facilitate large sample sizes for subsequent analyses and avoid the freezing issues associated with Livingstone rod-driven piston techniques. Sediment coring was conducted from ice covered lakes in April 2013 at the deepest part of each lake, which was determined by the drilling of a series of ice holes with depths measured using an echo sounder to develop a basic basin bathymetry. Russian sediment cores were extruded onto boards covered with aluminium foil and wrapped in plastic film before being securely shipped to the University of Nottingham. To obtain an undisturbed

sediment-water interface HON-Kajak coring was conducted as close as possible to the entry point of the Russian drives (within ~3 m). HON-Kajak cores were extruded in the field into plastic sampling bags at 0.5 cm intervals. Water samples were taken through the ice at a depth of 1 m, kept refrigerated and filtered on the day of sampling at Arktisk Station with Whatman G/C filter papers (where necessary).

3.3 Sediment lithology, sectioning and LOI

At the University of Nottingham Russian sediment cores were photographed with a digital camera (Sony DSC-W300) and the top 1-2 mm of the surface was scraped off to account for potential disturbance to the core surface during extrusion and transport. Coloured fixing pins were placed at 5 to 10 cm intervals to account for potential shrinking of the core during sampling. Detailed core lithology descriptions were made with reference to clay banding, sediment type (e.g. gyttja, silt, sand-based) and visible particles, described using Munsell colour and textures, similar to descriptions used in Schnurrenberger et al. (2003). Sediments were transported from Disko Island by cargo ship to Denmark and then forwarded to the University of Nottingham where sediments were unpacked and stored refrigerated at 3-5 °C. On arrival cores were sub-sectioned for pigment, lipid and isotopic analyses at 1 cm intervals in batches. Percentage dry weight (DW) was estimated by drying sediment at 105 °C (Equation 3.1). Organic content was determined using weight-loss-on-ignition (LOI) at 550 °C (Equation 3.2) and for estimating carbonate (CaCO₃) content at 925 °C (Equation 3.3), in both Russian and HON-Kajak sediment cores using 1 to 2 cm³ volumes (Dean, 1974, Heiri *et al.*, 2001).

$$\% \text{ Dry weight (\% DW)} = 100 \cdot \frac{105 \text{ }^\circ\text{C dry sediment mass}}{\text{wet sediment mass}}$$

Equation 3.1: Calculation of sediment % dry weight (DW).

$$\% \text{ LOI (550 }^\circ\text{C)} = 100 \cdot \frac{105 \text{ }^\circ\text{C dry sediment mass} - 550 \text{ }^\circ\text{C sediment mass}}{105 \text{ }^\circ\text{C dry sediment mass}}$$

Equation 3.2: Calculation of %LOI 550 °C (OM).

$$\% \text{ CaCO}_3 = 1.36 \cdot \left(100 \cdot \frac{550^\circ\text{C sediment mass} - 950^\circ\text{C sediment mass}}{105^\circ\text{C dry sediment mass}} \right)$$

Equation 3.3: Calculation of carbonate content (CaCO_3).

3.4 Hydro-geomorphological survey and catchment sampling

The three study lakes (Disko 1, 2 & 4) were re-visited during the summer 2013 ice-free season to conduct a hydro-geomorphic survey of the catchment and collect samples from the field (02/08/13 to 07/08/13) to assess the composition of catchment inputs. Sketch maps of the lake catchments were drawn (Figures 4.2, 4.6 & 4.9) and plant, soil and water samples (Tables 4.3 to 4.7) were taken for subsequent analyses. C/N, $\delta^{13}\text{C}_{\text{TOC}}$ and lipid (*n*-alkane, *n*-fatty acid methyl esters (FAMES), *n*-alkanols and sterols) analyses were conducted on plant, soil and macrophyte samples. Pigment analyses were also conducted on algal filter paper samples from summer 2013 (Table 4.4), and compound-specific $\delta^{13}\text{C}$ FAMES analyses on selected catchment samples from Disko 2 (Table 4.9).

Water samples were taken as far as possible from the lake edge (~3-5 m) using a modified (rope-bottle) sample collector, filtered using Whatman G/C filter papers, refrigerated and taken back to the University of Nottingham for water chemistry analysis. Whatman G/C filter papers were wrapped in foil, sealed in polythene and stored at -20°C for pigment and chlorophyll analyses. Additional in situ measurements of temperature ($^\circ\text{C}$), dissolved oxygen (mg/L), conductivity ($\mu\text{S cm}^{-1}$) and pH were taken using a YSI multi-probe at the lakes edge (YSI measurements only in summer 2013) (Section 3.4).

At each lake catchment five 10x10 m plots (Disko 1) or three 10x10 m plots (Disko 2 and 4) were surveyed for vegetation at locations indicated in Figures 4.2, 4.6 & 4.9. Within each 10x10 m plot selected to represent vegetation differences in the catchment, five 1x1 m quadrats were placed randomly and broad percentage cover of plant functional types were estimated. Each quadrat was also photographed for subsequent reference (Section 4.1) and plant/soil samples were taken for the catchment $\delta^{13}\text{C}$, C/N and lipid analyses (Section 4.6). The catchment sampling strategy included the collection of multiple representative plant, soil, grass and bryophyte (lichen and mosses) from each plot. In the lab samples representing potential allochthonous inputs were subsequently analysed for C/N and $\delta^{13}\text{C}_{\text{TOC}}$ (Disko

1 N = 21, Disko 2 N = 30 & Disko 4 N = 12), with a smaller subset at Disko 2 analysed for lipid biomarkers (N = 11).

Where possible, plant species were identified following Rune (2011). The vegetation composition surveys of the lakes local catchments were presented as average percentages within the plots and quadrats and grouped into three groups of ‘total moss/lichen’, ‘total plants’ and ‘total bare ground’. Combining field notes, aerial imagery (LANDSAT & QuickBird through Google Earth) and mapping (Disko Island, Qeqertarsuaq 1:100,000 Hiking Map) the percentage cover of alpine vegetation, bare ground, snow cover and glaciers were estimated for the whole catchment by manually tracing the areas using the 2D area function in Google Earth Pro 7 (see Section 4.2).

Vegetation composition surveys include species identifications with varying confidence. Lichens were identified by lichenologist Dr Erika Hogan. Mosses are not identified but described based on colour (green moss, brown moss etc.) The aquatic moss *Calliergon giganteum* identification should be considered provisional. *Potamogeton* spp. was identified by Sarah Roberts. *Saxifraga* spp. and *Carex* spp. were identified by the author but are large groups with numerous species. The plants *Chamerion latifolium* and *Harrimanella hypnoides* were identified based on Rune (2011) and should be considered provisional.

3.5 Water chemistry analysis

The following analyses were provided by external laboratories:

DOC was measured using a Shimadzu TOC-VCSN analyser at Loughborough University, with DOC calculated as the sum of organically bound carbon present in water that originate from compounds which can pass through a 0.45 µm filter.

TN (total nitrogen) was additionally analysed for the summer 2013 samples at the Environment Agency, Nottingham using automated colorimetry.

The following analyses were conducted at the University of Nottingham, School of Geography:

TP (total phosphorus), SRP (soluble reactive phosphorus) and NH_4^+ (ammonium) were measured using the methods in Mackereth et al. (1978). Samples for TP (unfiltered water) were digested with sulphuric acid and potassium persulphate in a pressure cooker at ~1.5 psi, with colorimetric analysis (relative to blank at 885nm in a

spectrophotometer) to detect ortho-phosphate through the molybdate blue and ascorbic acid method. Samples for SRP (filtered water) were also analysed using the same spectrophotometric settings.

NH_4^+ (filtered water) was analysed by reacting with phenol, sodium nitroprusside and oxidizing solution (alkaline solution & sodium hypochlorite) and comparison against the reagent blank at 640nm using a spectrophotometer (Mackereth et al., 1978).

SiO_3 (silicate) was measured (on unfiltered water) by sodium molybdate yellow reaction and subsequent spectrophotometry at 365nm (compared with calibration standard) to detect total dissolved silicon, including colloidal silicon (Eaton *et al.*, 2005).

Cations (sodium, Na^+ , potassium, K^+ , magnesium, Mg^{2+} , calcium, Ca^{2+}) and anions (chloride, Cl^- , nitrate NO_3^- , sulphate, SO_4^{2-}) were determined using a Metrohm Basic 792 ion chromatography unit connected to a Metrosep C2-150 column (cations) and Metrosep A Supp 4-250 column (anions), with concentrations determined relative to standard calibration curves.

Total alkalinity (in mequiv L^{-1}) was measured using phenolphthalein and BDH universal indicators on unfiltered water (Golterman, 1978).

Chlorophyll *a* (chl *a*) was measured spectrophotometrically against an extraction solvent blank, after extracting Whatman G/C filters in acetone overnight (Jeffrey and Humphrey, 1975). The following equation was used to calculate chl *a* concentration (in $\mu\text{g L}^{-1}$) (Equation 3.4).

$$\text{Chl A } \mu\text{g L}^{-1} = (11.85(A_{665} - A_{750}) - 1.54(A_{645} - A_{750}) - 0.08(A_{630} - A_{750})) \bullet E/V$$

Where A = wavelength detected, E = the volume of the extraction solvent (ml) and V = the total volume of water filtered (L).

Equation 3.4: Calculation of chl *a* concentration in lake waters.

3.6 Pigment analysis

Chlorophylls, carotenoids and their derivatives were analysed at the University of Nottingham, School of Geography using an Agilent 1200 series HPLC equipped with a quaternary pump, autosampler, ODS Hypersill column (250x4.6mm; 5 μm particle size) and a photo-diode array detector (350-750nm), as described in Leavitt and

Hodgson (2001). For sediments, freeze-dried samples were weighed (0.2-1.0 g) and extracted overnight at $-20\text{ }^{\circ}\text{C}$ in 5 ml of extraction solvent containing (80% acetone; 15% methanol and 5% deionised H_2O). For water samples Whatman G/C filter papers were carefully cut to increase surface area and submerged in 5 ml of the same extraction solvent. After 12 hours, samples were filtered using a $0.22\text{ }\mu\text{m}$ Whatman G/C syringe filter and dried down under a gentle stream of N_2 . Samples were then dissolved into injection solution containing 70 % acetone, 20 % ion-pairing reagent and 5% methanol, with the volume selected per sample based on the visual colour intensity of the pigments. Samples were then injected using an auto sampler into the Agilent 1200 HPLC with runs lasting ~ 52 minutes across a solvent gradient based on a modified version of Chen et al. (2001). The HPLC solvent gradient programme used is described in Table 3.1.

Table 3.1: HPLC solvent programme for pigment analysis based on a modified version of Chen et al. (2001).

Time (mins)	% Solvent A	% Solvent B	% Solvent C	Flow ($\text{ml}/\text{min}^{-1}$)
0	100	0	0	1
4	0	100	0	1
38	0	25	75	1
39	0	25	75	1
43	100	0	0	1
52	100	0	0	1

Eluted pigments were passed through a photo-diode array detector which includes the detection of UV and visible wavelengths. All analyses were conducted in a darkened laboratory, to reduce light induced pigment degradation. Sedimentary pigments were calibrated using authentic standards (DHI Denmark) and were expressed in either n moles pigment g^{-1} organic sediment weight (where LOI at 550°C was conducted), n moles pigment g^{-1} dry weight (where dry weight was determined by drying overnight at $105\text{ }^{\circ}\text{C}$) or n moles pigment g^{-1} organic carbon (where organic carbon was analysed). Analytical procedure is summarised in Figure 3.1. Pigments from lake waters were expressed in n moles pigment per litre. Pigment identification was conducted using Agilent Chemstation (Version B, 3.01) and is based on commercial standards, absorbance spectra and retention time in comparison with reference materials (Jeffrey et al., 1997; Roy et al., 2011).

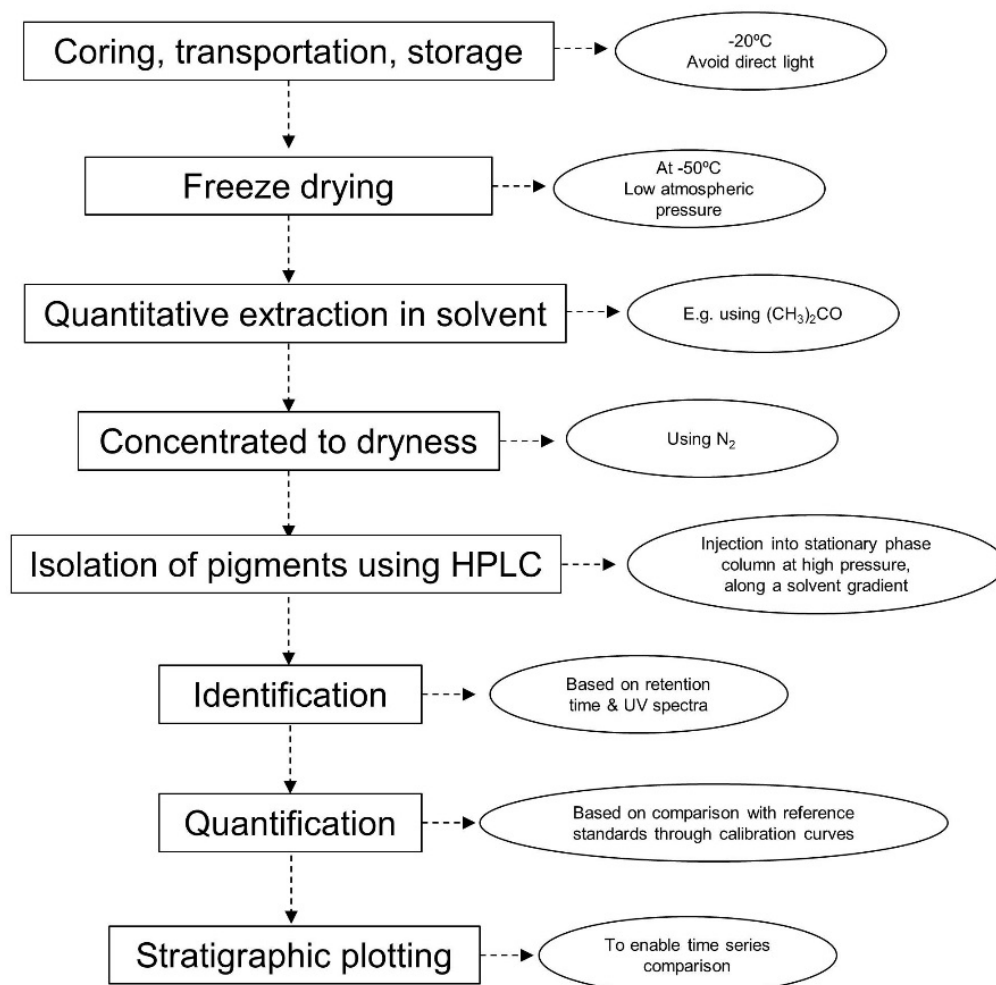


Figure 3.1: Flowchart of the analytical procedure for pigment analysis using HPLC.

3.7 Carbon isotope and elemental C/N analysis

Carbon isotope analysis ($\delta^{13}\text{C}_{\text{TOC}}$) to quantify the ratio of carbon-13 to carbon-12 was conducted at the NERC Isotope Geosciences laboratory (NIGL) on sedimentary and catchment samples (vegetation & soils) (Grants: IP-1393-1113 & IP-1516-1114) with wet chemistry pre-preparation conducted at the University of Nottingham. For sediments and soils, to remove potential carbonate samples were digested in excess HCl (hydrochloric acid) (5%) overnight and subsequently filtered three times using deionised H₂O onto Whatman filters. Drying was at 40 °C and all samples were homogenised with an agate pestle and mortar. To remove potential carbonate vegetation samples (plants and bryophytes) were placed in 5% HCl for 5 minutes, checked for a visible reaction and then washed in deionised H₂O three times and

ground to powder by freezer milling using liquid nitrogen. Sample powder was then placed into tin (Sn) capsules which were tightly packed to exclude air. TOC, TN (C/N ratios) and $\delta^{13}\text{C}_{\text{TOC}}$ analyses were performed online using a Costech ECS4010 elemental analyser (EA) coupled to a VG Triple Trap and a VG Optima dual-inlet mass spectrometer. Ratios of ^{13}C to ^{12}C ($\delta^{13}\text{C}$ values) were calibrated to the VPDB (Vienna Pee Dee Belemnite) scale using within-run laboratory standards which were subsequently calibrated against NBS-18, NBS-19 and NBS-22 international standards (Equation 3.5). Approximately 30 samples were completed per run, complete with 10 replicates of the internal NIGL standard BROCC 2 and 2 replicates of the external standard Soil B. Analytical precision was to within $\pm < 0.1\text{‰}$ (1 SD). Recent samples were not corrected for the Suess effect to avoid ambiguity in the interpretations.

$$\delta^{13}\text{C} = \frac{R(^{13}\text{C})_{\text{sample}}}{R(^{13}\text{C})_{\text{reference}}} - 1$$

where $R(^{13}\text{C})_{\text{sample}}$ is the $^{13}\text{C}/^{12}\text{C}$ ratio in a given sample, and $R(^{13}\text{C})_{\text{reference}}$ is the $^{13}\text{C}/^{12}\text{C}$ ratio in the standard reference material (VPDB standard) (Coplen, 2011).

Equation 3.5: Calculation of carbon isotope ratios.

3.8 Lipid biomarker analysis

Freeze dried sediment and catchment samples (~2g) from Disko 2 were crushed, homogenised and extracted in 15ml HPLC grade 3:1 dichloromethane (CH_2Cl_2) to methanol (CH_3OH) using a CEM MARS 5 microwave system in Teflon vessels. Prior to microwaving, internal standards (20-60 μl) 5 β -cholanic acid and C_{40} *n*-alkane were added to enable potential future calculation of concentration. Samples were heated over a temperature gradient to 70°C for 5 minutes, held at 70°C for further 5 minutes and then cooled for ~30 minutes. The total lipid extract (TLE) was centrifuged for 3 minutes at 3,500 RPM, followed by decanting of the supernatant into a round bottomed flask, which was subsequently concentrated using a Büchi rotary evaporator and dried down under a gentle stream of N_2 . The sample was then hydrolysed using 6% potassium hydroxide (KOH) in CH_3OH at 70°C for 1 hour and overnight at room temperature. The neutral compounds were extracted by repeatedly mixing with hexane ether (at least 3 times), centrifuging and concentrating the supernatant with a rotary evaporator, followed by dry down under N_2 . Excess salts were removed prior to

concentration with ultrapure CH_2Cl_2 extracted water to remove excess salts. To extract the acid fraction, CH_2Cl_2 extracted 1M hydrochloric acid (HCl) was added to the remaining sample until it reached pH 2, followed by the same hexane ether extraction procedure as applied to the neutral fraction. The neutral fraction was distilled with bis(trimethylsilyl)trifluoroacetamide (BSTFA) ~ 1 week prior to analysis to form trimethylsilyl esters. Esterification was performed on the acid fraction with 10% boron trifluoride in methanol ($\text{BF}_3/\text{CH}_3\text{OH}$) which was subsequently extracted as methyl esters by hexane. One sample blank was run in every batch of 12 samples to assess for within sample contamination. The lipid biomarker analytical procedure is shown in Figure 3.2.

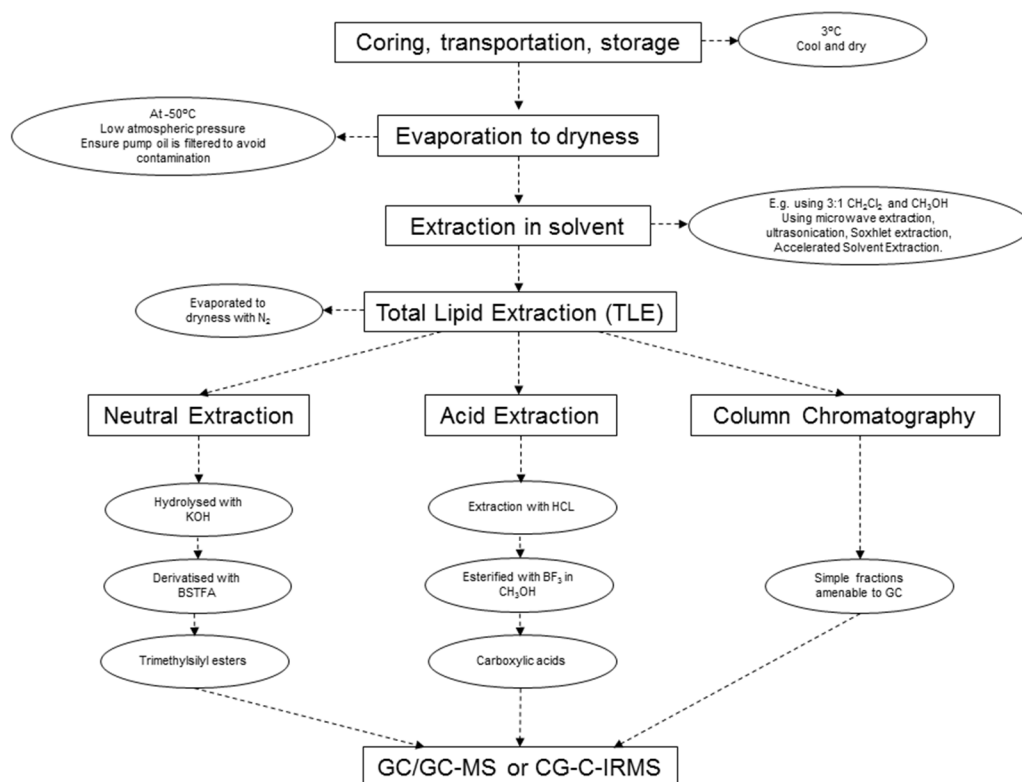


Figure 3.2: Flowchart of the analytical procedure for lipid analysis using GC/GC-MS or GC-C-IRMS.

Acid and neutral fractions were analysed on an Agilent 7890A GC coupled to a 5975C MS at the School of Civil Engineering and Geosciences and an Agilent 7890B GC coupled to a 5977A MS at the School of Geography, Politics and Sociology at Newcastle University due to machine availability. In both machines samples were injected in pulsed splitless mode at 280 °C in CH_2Cl_2 using a HP DB5-MS (30m x 0.25 mm i.d: 0.25 μm film thickness) column. Helium (He) was used as the carrier gas with the temperature program for the neutrals rising from 60 °C at 0 minutes, followed by 10 °C per minute to a 140°C hold for 1 minute followed by 4°C to 310 °C for 18.5

minutes (total run time 70 minutes). A faster ramp program was used for the acid fraction, rising from 60 °C for 1 minute, followed by a 20 °C rise per minute to a 160 °C hold for 1 minute and a 5 °C/minute rise for 15 minutes (total run time 52 minutes). Full scan mode was used (m/z 50-550) with a 1 s cycle time for MS data acquisition with compound identification based on a combination of mass spectra and peak retention time, in reference to published data and reference compounds. Since samples were run on a two machines, to ensure similar data trends selected samples were run on both machines (Figure 3.3).

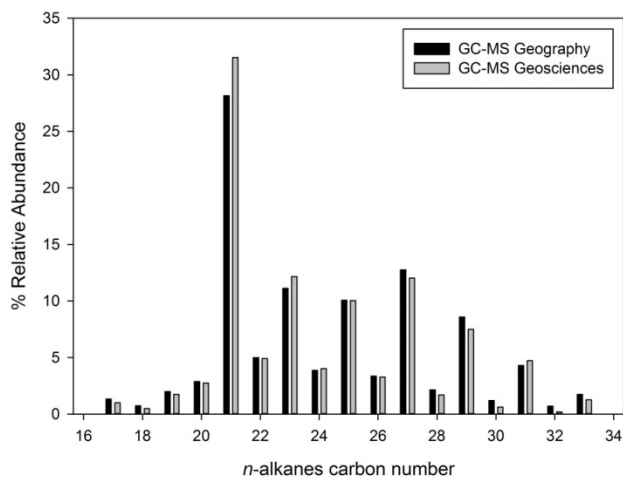


Figure 3.3: Comparisons of Newcastle University Geography and Geoscience GC-MS relative abundance results for *n*-alkanes, showing the similar distributions when using different machines.

Identification was completed in the GC-MS software Xcalibur™ (Thermo Finnigan, 2001 - version 1.3) in ‘Qual Browser’ mode. A combination of lipid concentrations and ratios were used for the comparison of sedimentary and catchment samples. Detected compounds included fatty acid methyl esters (FAMES) in the acid fraction. In the neutral fraction detected compounds included sterols, *n*-alkanes and *n*-alkanols. In this study selected lipid biomarker ratios and equations were presented.

3.9 Compound specific $\delta^{13}\text{C}$ analysis of FAMES

50% aliquots of the acid fraction of selected catchment and sedimentary FAME samples were taken to China University of Geoscience, Wuhan for the compound specific analysis of $\delta^{13}\text{C}$. 1 μl samples were spiked with squalene and injected (temperature 290 °C) in splitless mode to a Thermo Finnigan Trace GC coupled to a Thermo Finnigan Delta Plus XP isotope ratio mass spectrometer using a combustion interface (GC-C-IRMS). A HP DB-5MS column (30m x 0.35mm i.d: 0.25 μm film

thickness) was used to separate FAME compounds with He used as the carrier gas (1.4 mL min⁻¹). Oven temperature ranged from 50 °C (for one minute) increasing 10 °C per minute to 220 °C followed by a 20 minute hold and a final ramp to 310 °C at 10 °C per minute, followed by a final 20 minute hold. Samples were run in at least duplicate, with reproducibility achieved to at least ±0.5 ‰ (SD). An *n*-alkane standard was used as a within-run laboratory standard with known δ¹³C values (Chiron, Norway) and daily combined isotopic reference samples from C₁₂ to C₃₂ (Indiana University). Similar to bulk analyses ¹³C to ¹²C (δ¹³C values) were reported in the δ-notation (‰, per mil), relative to the VPDB standard reference gas. Recent samples were not corrected for the Suess effect to avoid ambiguity in the interpretations and for comparison to δ¹³C_{TOC}. Analytical precision was to within ±<0.5‰ (standard deviation).

3.10 Sedimentary dating techniques

3.10.1 Radiocarbon dating

In total 17 accelerator mass spectrometry (AMS) radiocarbon (¹⁴C) dates were obtained from the three lake sequences (Disko 1, 2 and 4). Three ¹⁴C dates were obtained for Disko 2 K1 (2 bulk sediment, 1 macrofossil) from Queens University, Belfast (QRA-¹⁴CHRONO Centre Radiocarbon Dating Award), 5 dates (all bulk sediment) were obtained for Disko 2 R1-1 from the NERC Radiocarbon Facility NRCF010001 (allocation number 1843.1014 to GEA Swann) analysed by AMS at SUERC in East Kilbride, with a further date (on bulk sediment) obtained from Beta Analytic (Miami, Florida). 8 samples were ¹⁴C dated from Disko 1 and 4 sequences (four each, 6 macrofossils and 2 bulk sediment) at the NERC Radiocarbon Facility (RCF) NRCF010001 (allocation number 1757.1013 to GEA Swann) which prepared the samples to graphite, but were subsequently dispatched to the Keck Carbon Cycle AMS Facility, University of California, Irvine for AMS measurement, courtesy of Dr X. Xu. All dates were fraction corrected for δ¹³C with measured values analysed using an IRMS for all the AMS dates from Beta Analytic and SUERC via the NERC RCF. For the dates analysed at the Keck Carbon Cycle AMS Facility and Queens University Belfast δ¹³C was modelled by comparison to the Craig (1957) ¹³C/¹²C value for PDB.

All dating samples were acid pretreated, although there were slight variations between laboratory procedures. At the NERC RCF samples were digested in 2M HCl at 80 °C for 4 hours to remove carbonates, followed by a rinse with deionised water, drying in

a vacuum oven at 40 °C and homogenisation. Carbon was recovered as CO₂ by heating with Copper(II) oxide (CuO) in a sealed quartz tube, which was subsequently concentrated to graphite by iron/zinc (Fe/Zn) reduction. Samples analysed at the Keck Carbon Cycle AMS Facility were corrected for modern carbon contamination based on data from process background and standard materials, and the effect of old carbon (for samples <100 µgC) based on a NIST Oxalic acid II standard. Calibration of 2-sigma radiocarbon ages before present (cal. yr BP) was performed in CALIB 7.0 (Stuiver et al., 2013), according to the latest IntCal 13 calibration database (Reimer et al., 2013) to derive 2-sigma age ranges. For Disko 2 S1 dates on bulk organic matter a reservoir correction of 834 years was applied based on the offset between macrofossil and bulk dates on core S2 R2-2. All dates were calibrated using IntCal 13 (Reimer et al., 2013) to derive 2-sigma age ranges, in Bacon v 2.2.

3.10.2 Recent dating (²¹⁰Pb, ¹³⁷Cs, ²⁴¹Am)

Recent dating techniques were applied to the most recent sediments from Disko 2 and 4. The Disko 2 HON-Kajak short core (Disko 2 K1) was analysed for lead-210 (²¹⁰Pb), radium-226 (²²⁶Ra), caesium-137 (¹³⁷Cs) and americium-241 (²⁴¹Am) by direct gamma assay using an ORTEC HPGe GWL Series well-type coaxial low background germanium detector at the UCL Environmental Radiometric Facility, by Dr H. Yang. Analysis was completed after three weeks storage in sealed containers to allow radioactive equilibration to occur. Total ²¹⁰Pb was measured by gamma emissions at 46.5keV, with ²²⁶Ra measured by the combined daughter isotope emissions of 295keV and 325keV to infer ‘supported’ ²¹⁰Pb. ¹³⁷Cs and ²⁴¹Am were measured by emissions at 662keV and 59.5keV (Appleby et al., 1986), with absolute efficiencies determined by comparison with known standards.

For the Disko 2 short core (K1) the constant rate of ²¹⁰Pb supply (CRS) model was used as the constant initial concentration (CIC) model was unsuitable due to slight departures from a monotonic declining trend in ²¹⁰Pb activity. A composite model was produced based on the 1963 peak in ¹³⁷Cs and ²⁴¹Am from radioactive fallout at 3.25 cm, as the ²¹⁰Pb placed this slightly earlier at 5 cm and so needed correcting (Appleby, 2001).

The Disko 4 HON-Kajak short core (Disko 4 K2) was analysed for lead-210 (²¹⁰Pb), caesium-137 (¹³⁷Cs) and americium-241 (²⁴¹Am) by direct gamma assay using a Canberra high purity germanium detector system (GL2015R) at the School of

Biosciences, University of Nottingham, under the direction of Prof G. Shaw and Mr I. Thawatchai. Total ^{210}Pb was measured by gamma emissions at 46.5keV. Calibration was performed using International Atomic Energy Agency certified reference material (IAEA-447). It was not possible to directly measure unsupported ^{210}Pb based on ^{226}Ra as this area of the spectra had not been calibrated. However, since background levels of total ^{210}Pb were extremely low it was possible to estimate this based on the minimum baseline value of supported ^{210}Pb to derive unsupported ^{210}Pb . ^{137}Cs and ^{241}Am were measured by emissions at 662keV and 59.5keV (Appleby et al., 1986).

For the Disko 4 short core the constant rate of ^{210}Pb supply (CRS) model was also used as the constant initial concentration (CIC) model was unsuitable due to departures from a monotonic declining trend in ^{210}Pb activity. Since the ^{210}Pb dating model gave a date consistent with the expected 1963 radioactive fallout peak interpreted from ^{137}Cs , a composite model was not required and the ^{210}Pb model was accepted.

3.10.3 Age-depth modelling

Age-depth models were produced using Bacon v 2.2 (Blaauw and Christen, 2013) using the R programming language (R Core Team, 2013). For Disko 1 the 2-sigma age (2σ) ranges of recent dates on terrestrial macrofossils were all within the last ~300 years, which limited the applicability of ^{14}C dating in this core and so further age-depth modelling could not be undertaken.

For the Disko 2 main sequence (cores Disko 2 K1 and Disko 2 R1-D1) an old carbon reservoir effect of 834 ^{14}C years was applied to bulk dates based on a paired macrofossil-bulk ^{14}C date in a neighbouring sequence from the same lake and radiometric dating provided a chronology for the upper sediments. Radiocarbon dates which were too old in comparison to recent dating or reflected instantaneous events were removed from the model. Three corrected bulk radiocarbon dates were retained in the model together with the uppermost and lowermost recent dates (Section 5.1.3).

The Disko 4 age-depth model used ^{14}C dates on terrestrial macrofossils together with the uppermost and lowermost recent dates (Section 7.1.4). The older paired bulk date was not used in the model which probably reflects input of old carbon from the catchment, compared with the younger terrestrial macrofossil which has known provenance.

3.11 Graphical and numerical

Stratigraphic plots were produced in SigmaPlot 12.5 (SYSTAT Software Inc.) and C2 (Juggins, 2003). Zones were determined for all cores using optimal partitioning in Zone version 1.2 (Juggins, 1991). The selected variables for zone calculations are provided in each figure caption. Principal components analysis (PCA) was conducted on $\log(x+1)$ transformed, standardised and centred pigment data in Canoco v4.51 as detrended correspondence analysis (DCA) produced short gradient lengths (ter Braak and Smilauer, 2002). Eigenvectors are provided in the figure captions and on the relevant diagrams. The ratio of pheophytin *a* to chlorophyll *a* was calculated to assess pigment degradation. Exploration of additional pigment ratios were also undertaken to identify differences in pigment response.

For Disko 2 sediment samples (selected for lipid analysis) a large number of lipid ratios and equations were considered (Appendix C) with only those most diagnostic of key changes used in down-core summary diagrams (Figure 5.16 & 5.20), with the rationale for selection based on the catchment sample survey (discussed in Section 4.7.2). For the *n*-alkanes selected ratios and equations included the Carbon Preference Index (CPI 2) (Marzi et al., 1993), the Terrigenous to Aquatic ratio (TAR_{HC}) (Bourbonniere and Meyers, 1996a) and the P_{WAX} index of waxy *n*-alkanes to total hydrocarbons (Zheng et al., 2007). Additionally, the C₂₆ *n*-alkane as a ratio of total *n*-alkanes was selected. For the *n*-fatty acids (FAMES) selected lipid indicators included the carbon preference index of total compounds (CPI_T) (Matsuda and Koyama, 1977), and the long chain C₃₀ *n*-fatty acid as a ratio of total fatty acids. For the *n*-alkanol compounds the C₁₆, and C₂₄ *n*-alkanols as a ratio of total *n*-alkanols were selected. For sterols the ratio of brassicasterol (24-methylcholesta-5,22-dien-3 β -ol) / total sterols were selected.

3.12 Additional analyses provided by UCL for core Disko 2 K1

3.12.1 Diatom analysis

Diatoms were prepared and counted by A.Young for core Disko 2 K1 under the supervision of Dr V.Jones (UCL) following standard methods (Battarbee et al., 2001). Briefly this comprised using 30% hydrogen peroxide (H₂O₂) to remove organic matter and 50% hydrochloric acid (HCl) to dissolve carbonates, prior to the addition of weak ammonia (NH₃) solution to prevent diatom clumping and keep clays in suspension.

Diatom samples were mounted on slides using Naphrax. Samples were counted to at least 300 diatom valves at 1000x magnification and presented as concentration with the aid of microspheres. Krammer and Lange-Bertalot (1986), were used for diatom identifications.

3.12.2 XRF analysis

A Spectro XLAB2000 X-ray fluorescence (XRF) spectrometer was used to detect geochemical elements and heavy metals (in % and $\mu\text{g/g}$) for core Disko 2 K1 by A.Young under the supervision of Dr V.Jones. Sediments were freeze-dried and homogenised and filled into nylon cups using 0.5 – 2.5 g of milled sediment with a 4 μm thick prolene foil base. Analytical reproducibility through use of reference standards was to within $\pm 5\%$ (Buffalo River Sediment, NIST-RM8704; Canadian Certified Reference Materials Project (CCRMP)-LKSD-2).

3.13 Overall methods summary

This chapter has provided an overview of the methods used in the hydrogeomorphic catchment survey (Chapter 4) and subsequent sediment core sequence chapters (Disko 2 – Chapter 5, Disko 1 – Chapter 6 & Disko 4 – Chapter 7). The chapter has provided detail on the methods used in the thesis including: site selection, sediment preparation, catchment hydro-geomorphic survey, catchment sampling, water chemistry analysis, proxy analysis, radiometric dating techniques and various numerical approaches used to explore these data. Methods used were primarily organic (pigments, lipids and organic carbon isotopes), although complementary approaches including the catchment source study, stratigraphic descriptions and XRF/diatoms (externally provided for the most recent sediments in Disko 2) are also used.

Chapter 4: Hydro-geomorphic vegetation catchment survey and site information

This chapter provides a detailed hydro-geomorphic and vegetation catchment survey of the three study lakes on Disko Island (Disko 1, 2 and 4). The methods used in this chapter have been described in Section 3.4 and help develop an understanding of the catchment and potential impacts for subsequent sediment sequence chapters (5, 6 &7). Lakes are presented in this chapter along a decreasing elevation gradient.

4.1 Location and local setting of the study lakes

Figure 4.1 presents the study lake locations on Disko Island in context of key catchment factors including glaciers, vegetation and topography. Disko 2 is situated within a glacial cirque basin to the east of the Kuussuaq valley (Section 4.1.1), Disko 1 to the east of the Lyngmarksbræen ice cap, within the Blæsedalen (Itinneq Kanglilleq) U-shaped valley (Section 4.1.2), and Disko 4 to the south of the Ipraatsi valley (Section 4.1.3). For detail on site selection, the hydromorphological survey and selection of catchment samples see Section 3.1 and 3.4.

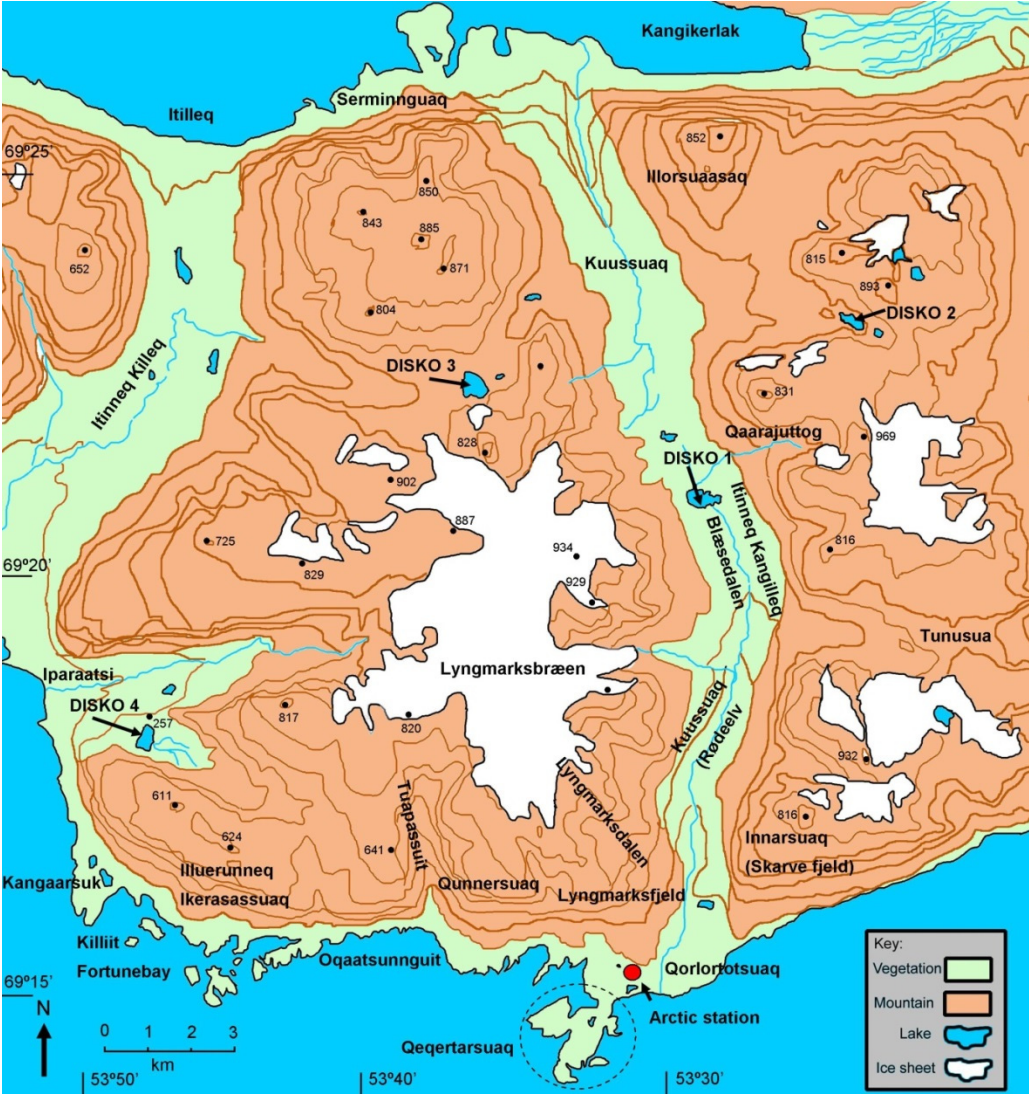


Figure 4.1: Location map of the area of Disko Island selected for this study. Lakes Disko 1-4 are indicated on the map, with lakes Disko 2, 1 & 4 part of this study.

4.1.1 Lake Disko 2

Lake Disko 2 (69° 23.342' N, 53° 24.085' W, Figures 4.2-4.4) is approximately 450 long and x 250 m wide and is located at an elevation of 575 m a.s.l. in a glacial cirque basin that runs west into the Kuussuaq incised valley, extending to the north of Blæsedalen (Figures 4.1 & 4.2). The characteristically glacially carved, over-deepened basin is dammed either by a moraine or rock lip and is fed from above by a smaller cirque lake (Figure 4.2). The catchment survey helped to identify a particularly active north facing scree slope, with scree extending into the Disko 2 lake. Rock falls during the summer fieldwork were noted. It is possible that this active freeze-thaw slope may have some similarities to rock glaciers previously noted in this region (Humlum, 1996, 1997, 2000). Although the presence of permanent ice is uncertain, some summer snow cover was visible (Figure 4.3). Wetland areas are indicated in Figure 4.2 containing algal benthic mats and *Potamogeton* aquatic macrophytes. Disko 2 is an open system, although the outflow is through an area of scree covered wetland (see white arrow, Figure 4.3).

The vegetation in the catchment of Disko 2 was extremely sparse, owing to the high altitude (575 m a.s.l.) and poorly developed soils. During April coring maximum lake depth was found to be 13.4 m by drilling through the ice, but proved too deep for coring which was completed at depths of between 10.3 and 10.6 m. A 35 cm HON-Kajak core was retrieved adjacent to the first Russian sequence (S1) of two drives (Figures 4.2 & 4.3). A second Russian sequence (S2) of two drives was taken from a similar depth, but closer to the scree slope (Figure 4.2 & 4.3). On the day of sampling (19/04/13) the ice thickness was 1 m and snow depth 8 cm.

Disko 2 has been selected for an extended study of lipid biomarker samples (Section 4.7) to help interpret sedimentary reconstructions (Chapter 5). This information is able to assist with understanding catchment specific signatures of algae and terrestrial inputs, which can vary between sites depending on the taxa present.

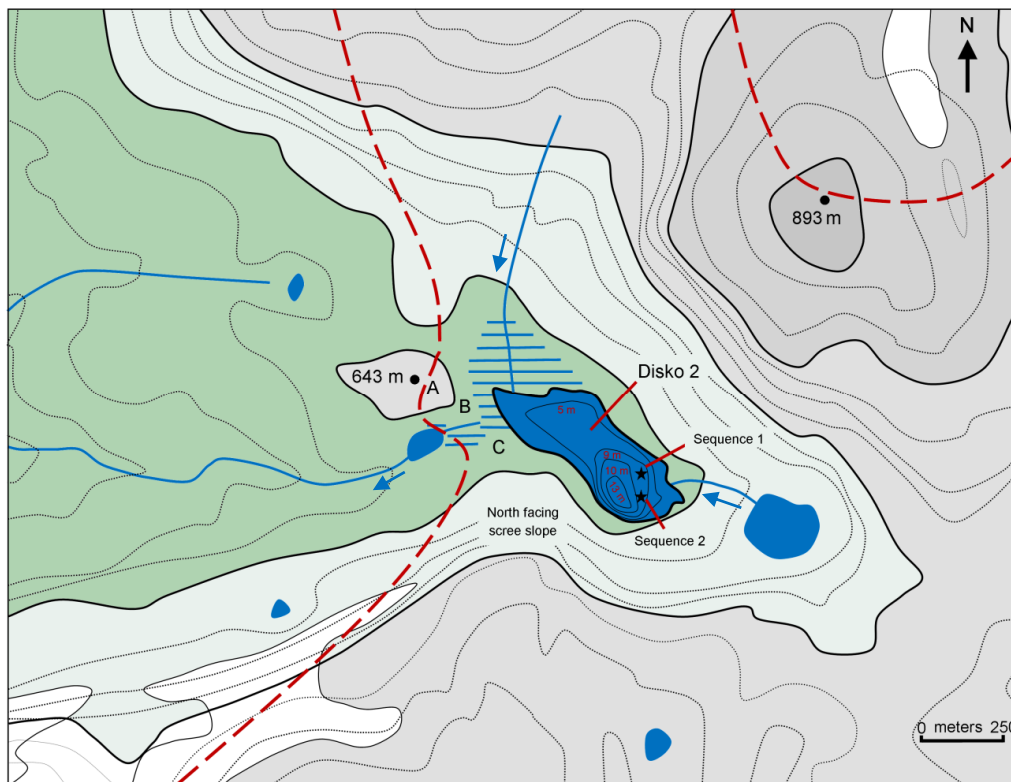


Figure 4.2: Map of Disko 2 cirque lake study area (~575 m a.s.l; 69°23.342'N, 53°24.085' W) set above the Blæsedalen (Itinneq Kanglilleq) and Kuussuaq valleys. A-C denote vegetation surveys. White fill denotes catchment glaciation, with green fill symbolising the upper limits of limited Arctic fell-field vegetation. Blue fill indicates lakes and rivers while the grey fill indicates areas of high elevation. Dashed blue fill indicates the lakes shallow margin. Red dashed line denotes the approximate catchment area boundary. Disko 2 is an open system, with outfall during summer sampling over an area of scree covered wetland. Blue arrows indicate flow direction.

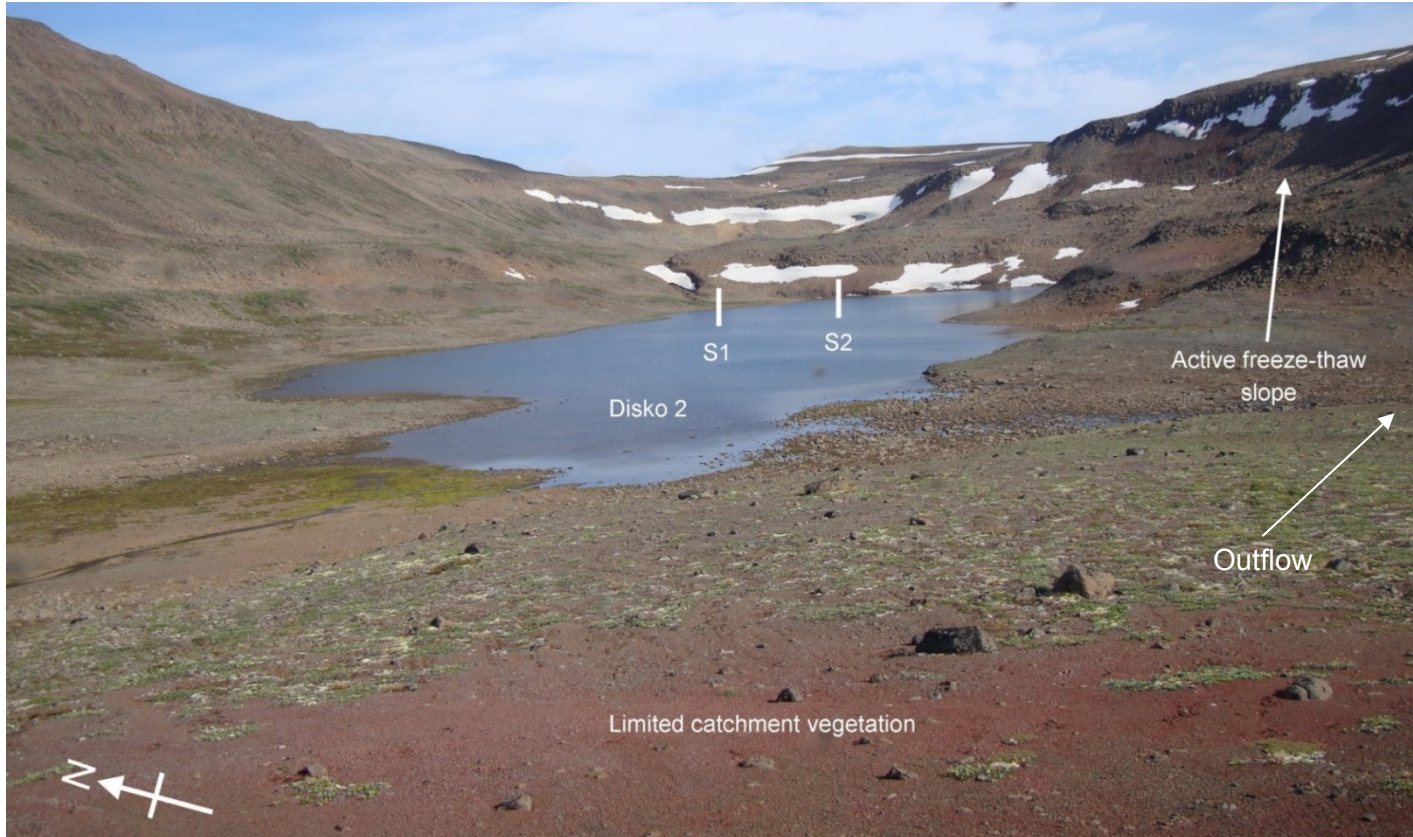


Figure 4.3: Image in an easterly direction of the Disko 2 cirque lake. Note the contrast between the southerly facing gentle slope on the left of the image, compared with northerly facing sharp, angular and debris-laden slope on the right of the image. Approximate location of core sequences (S1 & S2) indicated with ~50 m distance between drives. Freeze-thaw processes are clearly visible on the right hand side of the image, near the outflow (indicated). Photographer M.Stevenson. Date of photograph 03/08/2013.

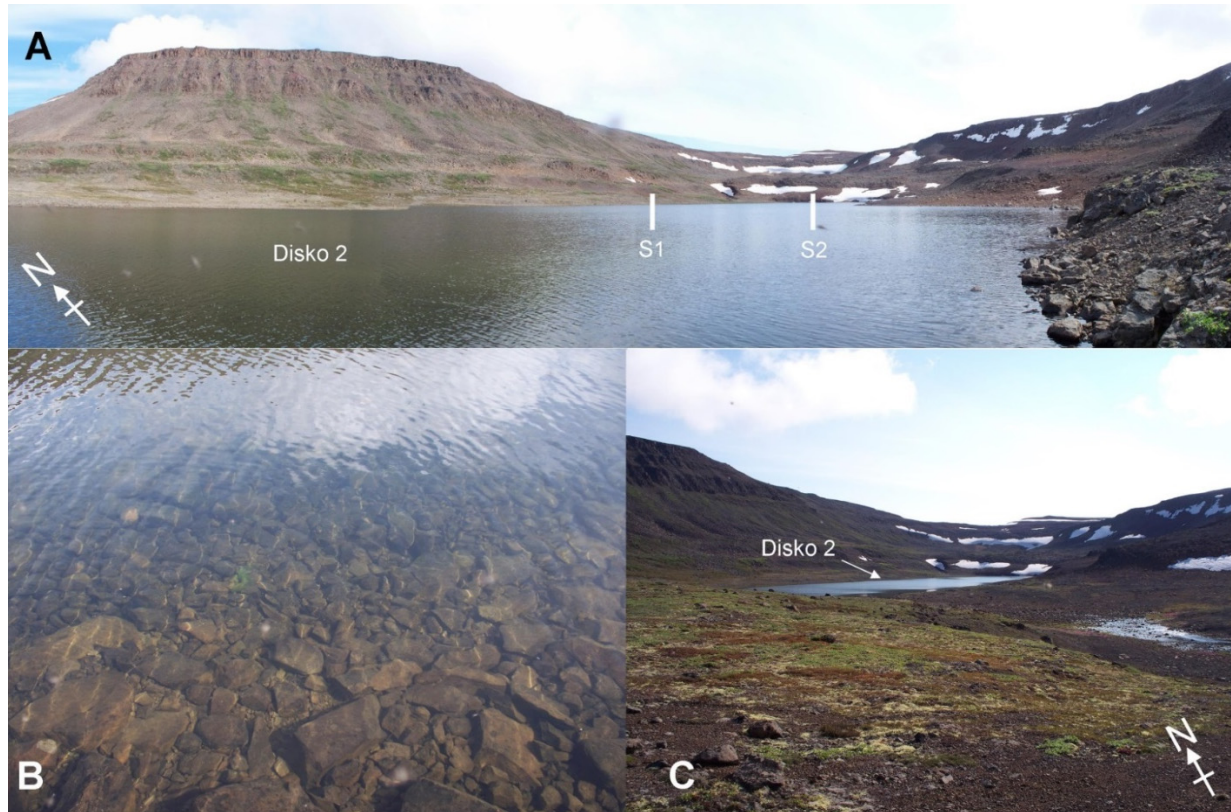


Figure 4.4: Multi-panel figure for the Disko 2 cirque lake. **A** – Panoramic image at the lake edge facing north-west complete with approximate locations of core sequences (S1& S2) approximately 50 m apart. Photographer J. Bailey. **B** – Image of high water clarity at the lake edge of Disko 2. Image taken from the south-east shoreline Photographer M.Stevenson. **C** – Image of lake Disko 2 in a north east direction. Note the limited catchment vegetation. Photographer J.Bailey. Date of photographs 03/08/2013.

4.1.2 Lake Disko 1

Disko 1 (69° 21.204' N, 53° 29.421' W, Figures 4.5-4.8) is approximately 900 m long by 200-300 m wide and located at an elevation of ~299 m a.s.l. in the Blæsedalen (Itinneq Kanglilleq) U-shaped valley, approximately 12 km north of the town of Qeqertarsuaq (Godhavn). The maximum lake depth found by drilling through the ice was 5.9 m, with a snow depth of 10 cm and an ice thickness of 110 cm. The geomorphic survey identified that Disko 1 lies at the centre of an area of arctic wetland, characterised both by peat deposits in depressions and glacial outwash in areas of rapid flow. A glacial outwash plain, complete with terminal and lateral moraines stems from a glacier that originates in the Lyngmarksbræen ice cap, which forms a moraine dammed lake and consecutively feeds into the Disko 1 valley lake (Figure 4.5). The Blæsedalen valley has a large presence of hummocky terrain and there is evidence of periglacial landforms including solifluction and freeze-thaw, especially on the steep basaltic valley sides (Figures 4.6, 4.7 & 4.8). A 25 cm HON-Kajak core was obtained from Disko 1 on 17/04/13 at the lakes maximum water depth of 5.9 m, followed by two overlapping replicate Russian core drives. The location of these drives (S1 and S2, Figure 4.6) was taken in adjacent positions also at the depth of 5.9 m. During the summer survey the water was visibly turbid, likely due to upstream inflows and the outflow was, relatively wide indicating increased flows during early spring melt.

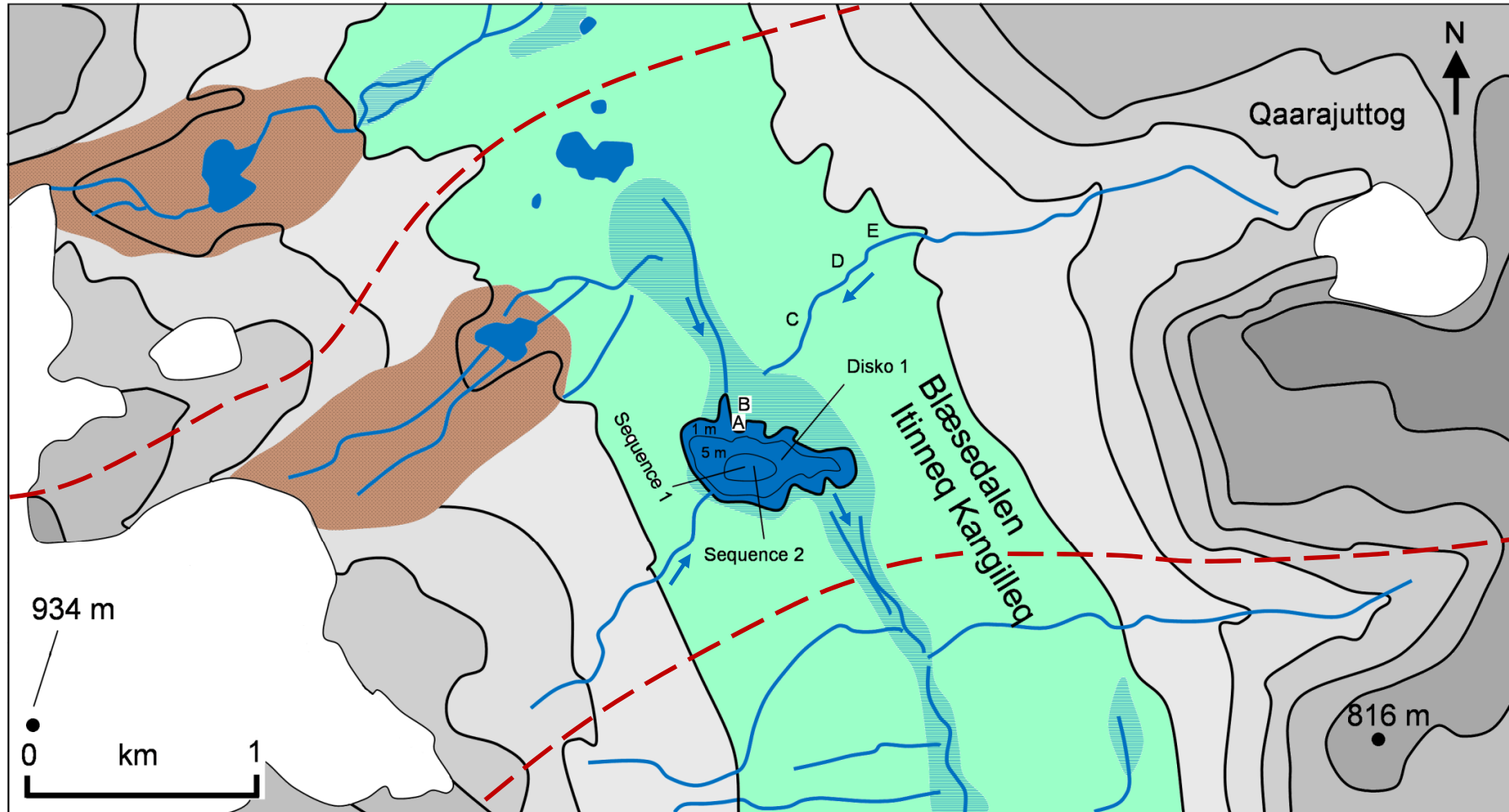


Figure 4.5: Map of Disko 1 lake (elevation ~299 m a.s.l.; 69°21.204'N, 53°29.421'W) study catchment in the Blæsedalen (Itinneq Kanglilleq) U-shaped valley. A-E denote catchment vegetation surveys. White fill denotes catchment glaciers, brown fill symbolises glacially scoured outwash plain and active moraines. Blue fill denotes lakes and rivers, with wetland areas in dark green. The valley base is shaded in green, with higher elevation basalt plateaus shaded in grey. Red dashed line denotes the approximate catchment area boundary. Disko 1 is an open system, with outfall during summer sampling over a wide outwash plain, which becomes more channelised ~50 m further south. Blue arrows indicate flow direction.

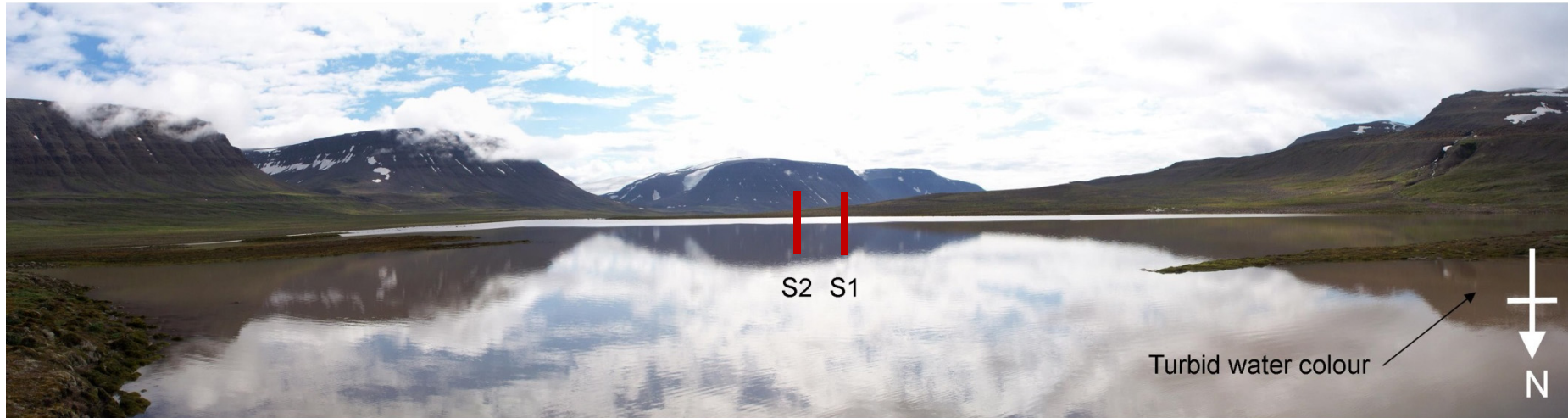


Figure 4.6: Panoramic image in a southerly direction of Lake Disko 1 in the Blæsedalen (Itinneq Kanglilleq) U-shaped valley. Approximate locations of sequence 1 (S1) and sequence 2 (S2) are indicated which were cored within 15 m. Note that in the areas without reflection, the water in this lake downstream of the valley glacier appears turbid. Photographer J.Bailey. Photograph taken 02/08/2013.



Figure 4.7: Panoramic image in a westerly direction of the Blæsedalen (Itinneq Kanglilleq) U-shaped valley from the hiking shelter (left foreground). To the left of the background is lake Disko 1 (indicated) and to the right a glacial outflow from the Lyngmarksbræen ice cap (indicated). Photographer J.Bailey. Date of photograph 02/08/2013.



Figure 4.8: Image in a south-westerly direction of lake Disko 1 in the Blæsedalen (Itinneq Kanglilleq) U-shaped valley. Note the contrast between the vegetated valley bottom and the steep basaltic valley sides. Photographer M.Stevenson. Date of photograph 02/08/2013.

4.1.3 Lake Disko 4

Disko 4 (69° 17.841'N, 53° 48.548'W, Figures 4.9-4.11) is approximately 400 m long by 900 m wide and is located at an elevation of ~214 m a.s.l. in a previously glaciated valley, although it was not possible to determine if the lake is moraine dammed or if it resides in a scoured and over-deepened basin with a rock lip. There are extensive wetlands present to the east of the lake that derive from plateau arctic moorlands, incised streams and a series of glaciers that connect to the Lyngmarksbræen ice sheet. Due to the complexity of the topography in this catchment, notably the presence of the Tuapassuit valley, it is uncertain if the glacier outwash that feeds into Disko 4 is directly connected, or independent of the Lyngmarksbræen ice sheet. Disko 4 has a steep north facing valley side with evidence of freeze-thaw and periglacial processes (Figure 4.9, 4.10 & 4.11.B). A direct outflow from the lake flows into the adjacent Ipraatsi valley and the Laksebugt bay. During summer 2013 fieldwork there was some evidence of remnant snow cover, particularly at higher elevations (Figure 4.10). Coring was conducted on 21/04/13 at an ice depth of 104 cm and a snow depth of 8 cm. The deepest part of the lake (6.8 m) was selected for sediment coring. Replicate HON-Kajak short cores were taken in addition to two replicate Russian sequences (each with two drives). The Disko 4 coring site is indicated in Figures 4.9-4.11. Both the primary and replicate cores were taken from within a ~10 m radius.

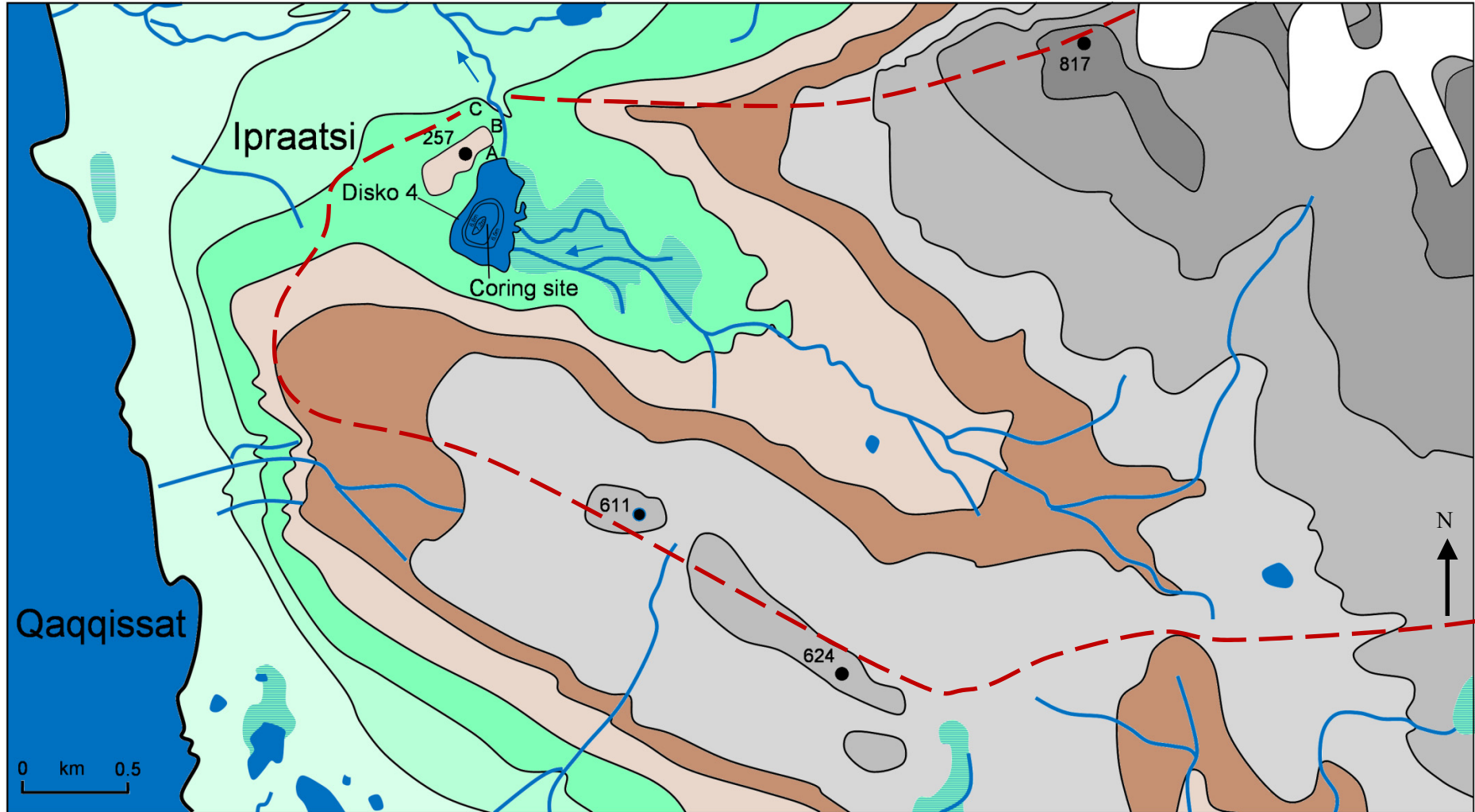


Figure 4.9: Map of Disko 4 study site adjacent to the Ipraatsi valley (214 m a.s.l.; 69°17.841'N, 53°48.548'W). A-C denote catchment vegetation surveys. White fill denotes catchment glaciation, blue fill denotes lakes and rivers, with wetland areas in dark green. The valley base is shaded in green, mid-elevation shaded in brown and higher elevation basalt plateaus shaded in grey. Red dashed line denotes the catchment area boundary and blue line indicates flow direction.



Figure 4.10: Panoramic image of the Disko 4 study lake facing south. Note the steep scoured valley sides now subject to freeze-thaw erosion, and to the left of the lake in the background the wetland source of the lake and in the foreground the lakes outflow. Photographer J.Bailey. Date of photograph 07/08/2013.

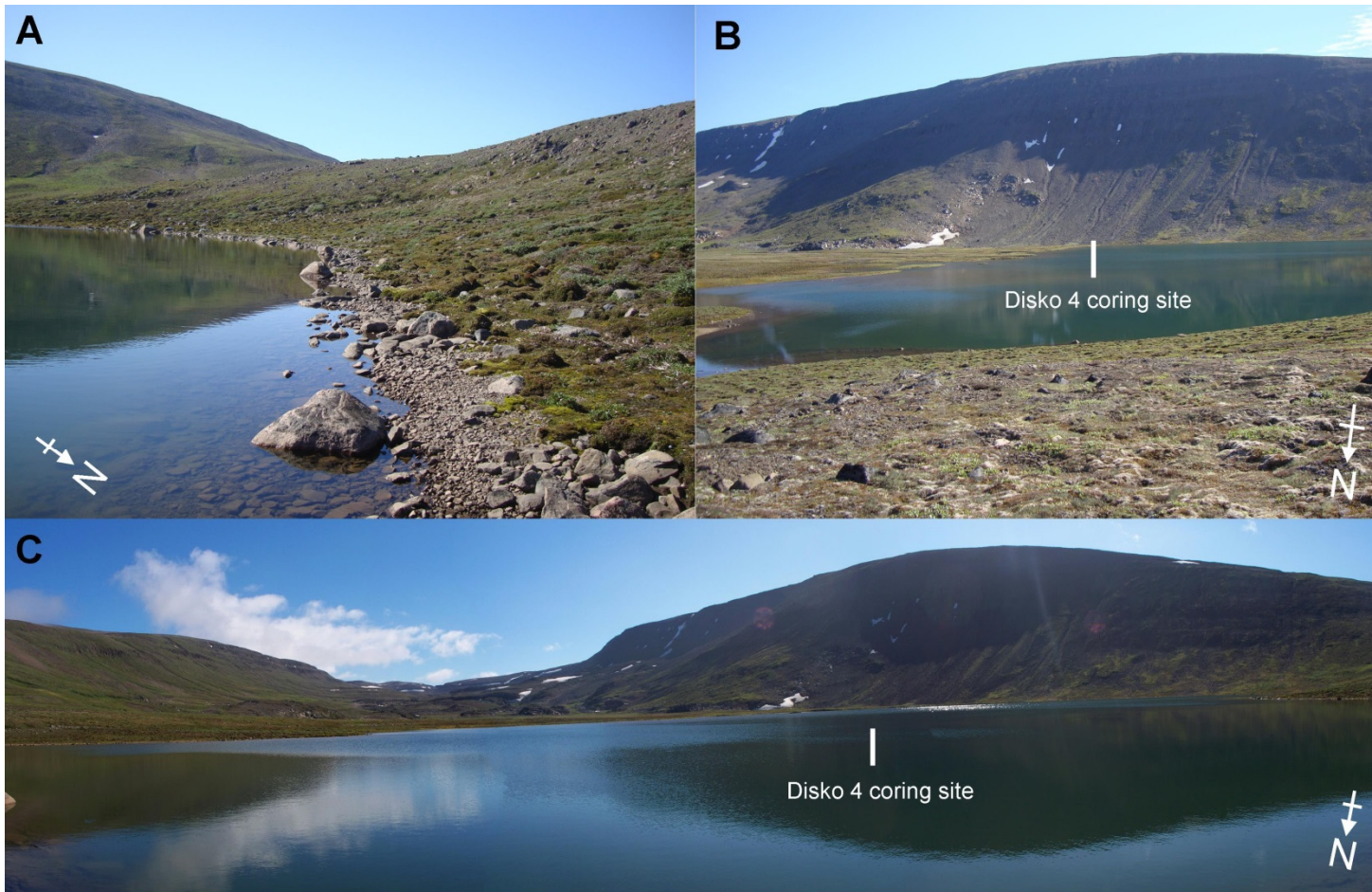


Figure 4.11: Multi-panel figure for the Disko 4 lake. A – Panoramic image at the lake edge facing south east. Note the clear water in this lake and the possible moraine with angular debris to the right. Photographer M.Stevenson. B – Lake Disko 4 facing south. Note the steep scoured valley north facing slope subject to freeze-thaw erosion. Photographer M. Stevenson. C – Panoramic image of lake Disko 4 showing the feeder valley/wetlands, and U-shaped valley sides highlighting the effect of glacial erosion in the formation of this landscape. Photographer J.Bailey. Date of photograph 07/08/2013.

4.2 Land cover characteristics

Key land cover characteristics for each lake catchment are shown in Table 4.1, compiled following methods outlined in Section 3.4. Disko 2, the cirque lake is at a higher elevation (575 m a.s.l) than Disko 1 (U-shaped valley lake) and Disko 4 (valley-end lake) of 299 and 214 m a.s.l respectively, with lake core sequences presented in subsequent catchments (Chapter 5-7) according to an elevation gradient. Disko 4 was found to have the largest catchment (1,829 ha), whereas Disko 2 the smallest catchment (358 ha). Although Disko 1 was expected to have the largest catchment due to its prominent U-shaped valley, this was not the case as is higher in the landscape gradient compared with Disko 4.

The land cover characteristics at the landscape scale were found to differ substantially between the three catchments (Table 4.1). For example, Disko 1 had the largest percentage of vegetation (39%), while Disko 2 had only 13% coverage. Bare earth was the most common land cover class of all the study catchments, with 79% and 68% present at Disko 2 and Disko 4 respectively. Characterisation of local scale vegetation plot composition at each site is described in Section 4.3 (Table 4.2). Permanent ice and glacier coverage was highest in the Disko 1 catchment (14%) due to the proximity to the Lyngmarksbræen ice cap (Figure 4.1, 4.2 & 4.4) but only 3.6% in the Disko 4 catchment. The largest lake was Disko 1 of 22 ha, while Disko 2 and Disko 4 were found to be 8 and 15 ha respectively.

To elucidate potential catchment input differences between the catchments it can be more appropriate to consider ratios of land cover classifications, to enable relative comparisons potential terrestrial inputs (Table 4.1). Disko 4 was found to have the largest catchment to lake area ratio of 122:1, whereas the ratio for Disko 2 was 45:1. The smallest vegetation to lake area ratio was at Disko 2 of 6:1, while the largest was found to be at Disko 4 with 33:1. Similarly, the smallest ice/glacier to lake area ratio was at Disko 2 (2:1), while the largest accounting for the presence of the Lyngmarksbræen ice cap was at Disko 1 (9:1). Bare earth to lake area ratio was highest in the Disko 4 catchment (83:1), while was less than half in the Disko 1 catchment (29:1).

Table 4.1: Study lake characteristics derived from in-field and imagery based land cover classification.

	Disko 2		Disko 1		Disko 4	
Lake coordinates	69°23.342'N, 53°24.085' W		69°21.204'N, 53°29.421'W		69°17.841'N, 53°48.548'W	
Elevation (m. s.a.l)	575		299		214	
Lake type	Cirque lake		U-shaped valley bottom lake		Valley-end lake	
Outflow type	Over scree covered shallow wetlands		Wide braided wetland outflow – <i>more marked channel ~50 m d/s</i>		Direct outflow	
Total catchment area (ha)	358		1,455		1,829	
Vegetation (ha)	46	13%	569	39%	497	27%
Bare earth/rock (ha)	284	79%	650	45%	1,250	68%
Permanent ice/glacier (ha)	17	5%	203	14%	67	3.6%
Study lake (ha)	8	2.2%	22	1.5%	15	0.8%
All lakes in area (ha)	11	3.1%	33	2.3%	15	0.8%
Catchment : lake area ratio	45:1		66:1		122:1	
Vegetation : lake area ratio	6:1		26:1		33:1	
Ice/glacier: lake area ratio	2:1		9:1		4:1	
Bare earth/ rock : lake area ratio	36:1		29:1		83:1	
Outflow type	Over scree covered shallow wetlands		Wide braided wetland outflow – <i>more marked channel ~50 m downstream</i>		Direct outflow	

4.3 Vegetation composition surveys of the study lakes local catchments

Although the proportions of total vegetation cover may differ between the catchments, it is also important to consider the vegetation composition within each study site as the local classification (plant, lichen and moss communities) between sites can be very different (Figure 4.12, Table 4.2). These sites are the same locations as the samples collected for C/N and $\delta^{13}\text{C}_{\text{TOC}}$ analysis (Section 4.6). The average percentage of quadrats covered by moss and lichen was similar at Disko 1 and Disko 4 (37.5% and 37% respectively), while it was lower at Disko 2 (27.3%) (Table 4.2). Within the Disko 1 moss/lichen class white and green moss were the most abundant (15.3% and 12.2% respectively), while within the Disko 2 moss/lichen class yellow moss (13.7%) and *Cetraria nivalis* lichen (6.8%) were the most abundant (Table 4.2). In the Disko 4 moss/lichen class white lichen (16.4%) and green moss (7.9%) were the most frequently present sub-groups (Table 4.2).

The percentage of total plants in the quadrat surveys differed between the three catchments (Table 4.2). Disko 2 had the lowest total plant cover (19.2%), while Disko 4 had the highest total plant cover (44.4%), Disko 1 had a moderate percentage plant cover of 32.7% (Table 4.2). Within the Disko 1 plant class *Salix arctica* seedlings were the most commonly present land cover (11%), followed by sedge species in the *Carex* genus (5.8%) (Table 4.2). *Salix arctica* plants (5.2%) and *Poaceae* grass (5.1%) were also present (Table 4.2). Similarly, in the Disko 2 plant class *Salix arctica* seedlings also had the highest percentage cover within the plant class (6%), closely followed by *Salix arctica* (5.3%) and *Saxifraga* sp. (4.8%) (Table 4.2). *Salix arctica* seedlings appeared to be newly germinated. Disko 4 was also predominantly covered by *Salix arctica* seedlings within the plant class (14%), followed by *Saxifraga* sp. (10.1%), *Salix arctica* (8.9%) and *Carex* spp. (4.7%) (Table 4.2). The presence of dead leaves and branches was much higher in Disko 1 and Disko 4 (2.4 and 2.2% respectively) compared with 0.7% in Disko 2 (Table 4.2). Plant roots were exposed in 0.6% of the Disko 2 catchment study plots (Table 4.2).

The percentage of total bare ground (including guano, bare organic soil and bare rock/gravel) differed between catchments in the quadrat survey. Disko 4 had the smallest percentage of total bare ground (18.6%) compared with 29.8% in Disko 1 and 53.5% in Disko 2 (Table 4.2). Compared with the overall land cover classifications from landscape imagery (see Section 4.2 & Table 4.1), the quadrats showed lower bare earth percentages, reflective of their position closer to the lake, in less exposed

locations. In the Disko 2 catchment all bare ground was described as bare rock and gravel, while in Disko 1 and Disko 4 substantial proportions were described as bare organic soil (16.1% and 5.2% respectively) (Table 4.2). Guano was present in 3% of the land cover in the Disko 1 catchment (Table 4.2).

Table 4.2: Vegetation composition surveys of the three study lakes local catchments.

	Disko 2 (%)	Disko 1 (%)	Disko 4 (%)
Total moss/lichen	27.3	37.5	37.0
White moss		15.3	
Grey moss		3.7	
Green moss	1.3	12.2	7.9
Dead/decaying moss	1.2	3.6	
Long green moss		2.1	
Yellow moss	13.7	0.6	2.3
<i>Cetraria nivalis</i> lichen	6.8		3.2
<i>Cladonia arbuscular</i> lichen			5.2
<i>Umbilicaria</i> -type lichen	3.5		2.0
White lichen	0.7		16.4
Total plants	19.2	32.7	44.4
<i>Salix arctica</i>	5.3	5.2	8.9
<i>Salix arctica</i> seedling	6.0	11.0	14.0
<i>Poaceae</i>	1.6	5.1	2.1
Dead leaves/branches	0.7	2.4	2.2
<i>Carex</i>		5.8	4.7
<i>Eriophorum spp.</i>		0.4	
<i>Saxifraga</i>	4.8	2.8	10.1
Plant roots	0.6		
<i>Chamerion latifolium</i>			2.4
Total bare ground	53.5	29.8	18.6
Guano		3.0	0.1
Bare organic soil		10.8	13.2
Bare rock/gravel	53.5	16.1	5.2
No. 10x10m plots	3	5	3
No. of 1x1m quadrats	15	25	15

All values are percentages derived as estimated mean values per study catchment from repeated randomised quadrat surveys of the lower catchments ($N=5$) within each 10 x 10 m study area ($N=3$ to 5). Locations of study plots are indicated in lake catchment maps A-E (Disko 1) and A-C (Disko 2 & 4).

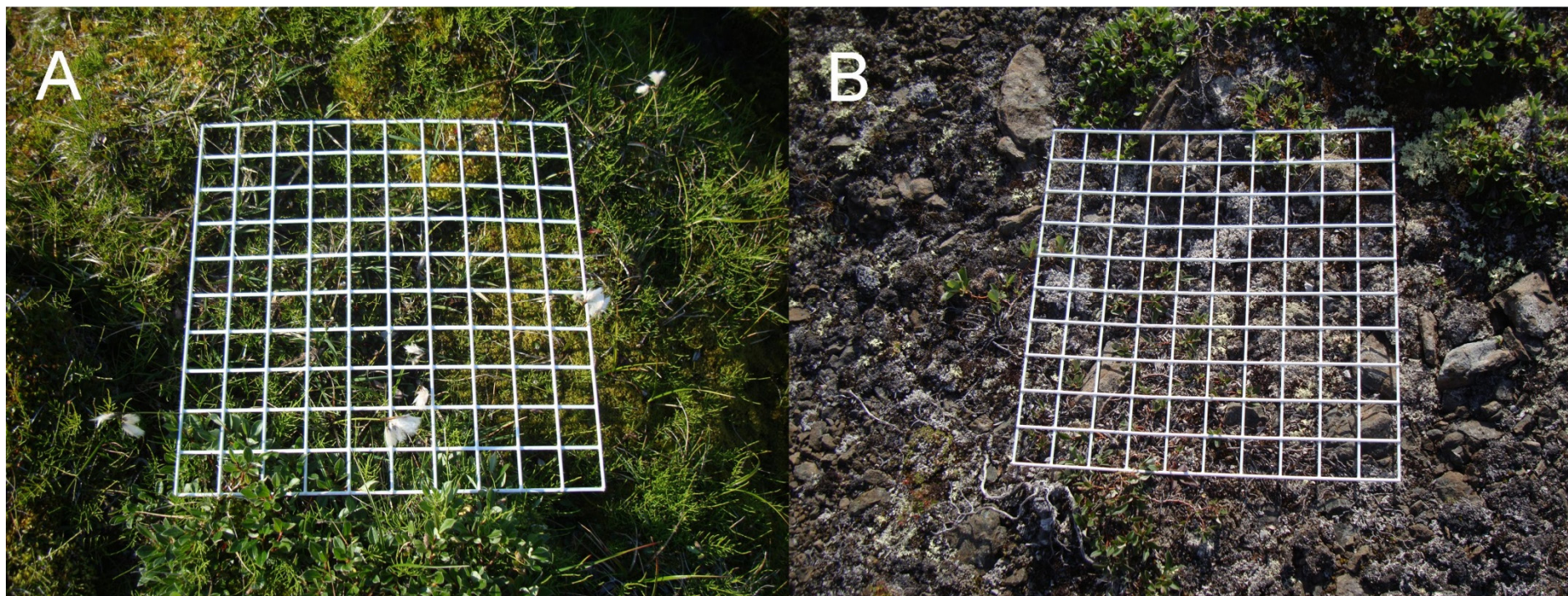


Figure 4.12: Example contrasting quadrats from the catchment of Disko 1 (A) and Disko 2 (B).

4.4 Water chemistry analyses

Water chemistry samples were taken for each study lake in both April and August 2013 (see Section 3.4). April measurements were taken from 1 m under the ice during coring (using a sample bottle attached to a 1 m pole), while August samples were taken at ~3 m from the shore using a rope and bottle sampler (Table 4.3). Cation and anion concentrations were generally low for all lakes during both sampling periods, although there were some variations. Cl^- was higher in all lakes in April compared with August. For example, Cl^- values were 4.0 mg L^{-1} in April in Disko 4, compared with 2.1 mg L^{-1} in August in Disko 4. SO_4^{2-} values were higher in April in Disko 1 (2.7 mg L^{-1}) but only 0.3 mg L^{-1} in August. In contrast, SO_4^{2-} values were higher in August in Disko 2 and Disko 4 (0.7 to 1.2 mg L^{-1} and 0.9 to 1.3 mg L^{-1} respectively). A high Na^+ value in April in Disko 1 (13.2 mg L^{-1}) contrasted with lower values in August in Disko 1 and the other sites at both sample periods. Values of K^+ and Mg^{2+} were low in both April and August samples and Ca^{2+} values did not vary substantially (all $\sim 5 \text{ mg L}^{-1}$).

Nutrients SRP (soluble reactive phosphorus) and TP (total phosphorus) however showed more variation (Table 4.3). In all lakes SRP was higher in April than in August. In Disko 1 SRP values were $59.8 \text{ } \mu\text{g L}^{-1}$ but just $13.8 \text{ } \mu\text{g L}^{-1}$ by August, while in Disko 2, SRP values declined from $10.5 \text{ } \mu\text{g L}^{-1}$ in April to just $0.7 \text{ } \mu\text{g/L}^{-1}$ in August, which was similar to the change in Disko 4 from $16.3 \text{ } \mu\text{g L}^{-1}$ to $1.9 \text{ } \mu\text{g L}^{-1}$ over the same time period. TP levels were similar in Disko 1 in April ($67.9 \text{ } \mu\text{g L}^{-1}$) and August ($67.8 \text{ } \mu\text{g L}^{-1}$). TP levels in Disko 2 declined from $37.5 \text{ } \mu\text{g L}^{-1}$ in April to $2.9 \text{ } \mu\text{g/L}^{-1}$ in August. TP values declined from an extremely high $164.8 \text{ } \mu\text{g L}^{-1}$ in Disko 4 in April to just $2.9 \text{ } \mu\text{g L}^{-1}$ in August. Alkalinity was relatively low, although reached 0.5 mequiv/L in Disko 1 in April. Chlorophyll *a* measurements were low, but higher in April than in August in Disko 1 and 2 ($1.0 \text{ } \mu\text{g L}^{-1}$ versus $0.4 \text{ } \mu\text{g L}^{-1}$ and $0.9 \text{ } \mu\text{g L}^{-1}$ versus $0.7 \text{ } \mu\text{g L}^{-1}$ respectively). In Disko 4 chlorophyll *a* was higher in August in Disko 4 ($1.0 \text{ } \mu\text{g L}^{-1}$) compared with April values ($0.1 \text{ } \mu\text{g L}^{-1}$). When analysed in August total N was low and BDL ($<0.1 \text{ mg/L}^{-1}$) in all lakes. Since NO_3^- values were extremely low in all samples dissolved inorganic nitrogen (DIN) was calculated ($\text{NH}_4^+ + \text{NO}_3^-$) with the highest value in Disko 1 in August (11.57 mg L^{-1}) and in Disko 2 also in August (3.19 mg/L^{-1}).

DOC was low in all lakes in both April and August sampling (Table 4.3). The highest value recorded was 1.5 mg L^{-1} in April in Disko 4, while the largest values were in April in Disko 1 (0.6 mg L^{-1}) and Disko 2 (0.6 mg L^{-1}). The temperature of Disko 1 in

August (9.9 °C) was slightly lower than Disko 2 and Disko5 4 (10.9 and 10.6 °C respectively). Dissolved oxygen (DO) was slightly higher in Disko 1 in August (11.9 ppm) compared with 9.6 ppm in Disko 2 and 9.7 ppm in Disko 4. Conductivity varied between the catchments but was low. It was highest in Disko 4 in August (33.7 $\mu\text{S cm}^{-1}$) and lowest in Disko 2 in August (23.5 $\mu\text{S cm}^{-1}$). The pH was measured in August and was indicative of neutral conditions in Disko 4 (pH 7.1) and alkaline conditions in Disko 1 (pH 7.7) and Disko 2 (pH 8.0).

Table 4.3: Water chemistry spot samples from Disko Island lakes in April and August 2013. Dashes denoting missing values, BDL = below detection limit.

Lake	Disko 2		Disko 1		Disko 4	
	April	August	April	August	April	August
2013 sampling						
Cl ⁻ (mg L ⁻¹)	2.0	1.7	2.9	1.2	4.0	2.1
NO ₃ ⁻ (µg ml ⁻¹)	10	40	50	30	20	40
SO ₄ ²⁻ (mg L ⁻¹)	0.7	1.2	2.7	0.3	0.9	1.3
Na ⁺ (mg L ⁻¹)	3.5	2.2	13.2	2.3	4.3	3.1
K ⁺ (mg L ⁻¹)	0.2	BDL	0.1	BDL	0.3	BDL
Mg ²⁺ (mg L ⁻¹)	1.0	0.8	1.1	0.8	1.6	1.2
Ca ²⁺ (mg L)	4.2	5.3	5.0	5.1	5.4	5.4
SRP (µg L ⁻¹)	10.5	0.7	59.8	13.8	16.3	1.9
TP (µg L ⁻¹)	37.5	2.9	67.9	67.8	164.8	2.9
NH ₄ ⁺ (µg L ⁻¹)	BDL	3.15	BDL	11.54	BDL	BDL
DIN (NH ₄ ⁺ + NO ₃ ⁻) (mg L ⁻¹)	0.01	3.19	0.05	11.57	0.02	0.04
Total alkalinity (mequiv L ⁻¹)	0.3	0.3	0.5	0.2	0.4	0.2
Chl <i>a</i> (µg L ⁻¹)	0.9	0.7	1.0	0.4	0.1	1.0
Total N (mg L ⁻¹)	–	<0.1	–	<0.1	–	<0.1
DOC (mg L ⁻¹)	1.0	0.6	0.6	0.9	1.5	0.8
Temperature (°C)	–	10.9	–	9.9	–	10.6
DO (ppm)	–	9.6	–	11.9	–	9.7
Specific conductivity (µS/cm)	–	23.5	–	28.5	–	33.7
pH	–	8.0	–	7.7	–	7.1
Date of collection	19/04	03/08	17/04	02/08	21/04	07/08

Note: appropriate units selected (e.g. mg L⁻¹/µg ml⁻¹) based on measurement magnitude.

4.5 Water chlorophyll and carotenoid pigment analysis

Concentrations of chlorophyll and carotenoid pigments from shoreline water samples (taken at ~3 m from the shore using a bottle and rope sampler), analysed by HPLC (see Section 3.4 & 3.6) were low in all three lakes in August 2013 (Table 4.4). This analysis was not conducted in the April 2013 field season. In Disko 1 pheophytin *b* had the highest concentration (0.95 nmol L⁻¹) relative abundance (22.2%), which is a chlorophyll *b* derivative and indicates chlorophytes, euglenophytes and higher plants. In Disko 2 and 4 chlorophyll *a* had the highest relative abundance (24.1% and 23.9% respectively), reflecting high August spectrophotometrically determined chlorophyll *a* in these lakes (Table 4.3). Pheophytin *b* was also abundant in Disko 2 and Disko 4 with 14.2% and 11.9% respectively, while chlorophyll *a* was 10.9% in Disko 1. Diatoxanthin concentrations were significantly higher in Disko 1 (0.63 nmol L⁻¹) compared with Disko 2 (0.05 nmol L⁻¹) and Disko 4 (0.08 nmol L⁻¹) and are indicative mainly of diatoms. However, fucoxanthin concentrations (also indicative mainly of diatoms) were highest in Disko 4 (0.34 nmol L⁻¹) compared with 0.17 and 0.11 nmol L⁻¹ in Disko 1 and 2. Alloxanthin concentrations indicative of cryptophytes were low in all lakes, but higher (2.4%) in Disko 2, compared with Disko 1 (0.7%) and Disko 4 (0.2%). Lutein concentrations were similar across all lakes (0.11 - 0.10 nmol L⁻¹) and are indicative of green algae, euglenophytes and higher plants.

Table 4.4: HPLC pigment analysis of filtered water samples from Disko Island study lakes in August 2013.

Sample	Disko 2		Disko 1		Disko 4	
	nmol pigment L ⁻¹	%RA*	nmol pigment L ⁻¹	%RA*	nmol pigment L ⁻¹	%RA*
Chlorophyll c ₂	0.03	1.3	0.03	0.6	0.04	1.5
Fucoxanthin	0.11	4.7	0.17	3.9	0.34	11.5
Neoxanthin	0.05	2.1	0.04	0.8	0.07	2.5
Diadinoxanthin	0.02	0.8	0.05	1.3	0.07	2.4
Alloxanthin	0.06	2.4	0.03	0.7	0.01	0.2
Diatoxanthin	0.05	2.3	0.63	14.7	0.08	2.8
Lutein	0.10	4.4	0.11	2.6	0.10	3.3
Chlorophyll <i>b</i>	0.08	3.7	0.03	0.7	0.05	1.9
Chlorophyll <i>a'</i>	0.30	13.0	0.26	6.2	0.33	11.5
Chlorophyll <i>a</i>	0.55	24.1	0.46	10.9	0.85	29.3
Chlorophyll <i>a''</i>	0.10	4.2	0.06	1.5	0.08	2.6
Pheophytin <i>b</i>	0.33	14.2	0.95	22.2	0.35	11.9
Pheophytin <i>b</i> ₂	0.26	11.5	0.63	14.9	0.17	6.0
Pheophytin <i>a</i>	0.09	3.8	0.32	7.4	0.16	5.3
β -carotene	0.01	0.6	0.03	0.7	0.05	1.6
Pyropheophytin <i>a</i>	0.16	7.0	0.46	10.8	0.17	5.7
Date of sampling	03/08/2013		02/08/2013		07/08/2013	

*%RA denotes % relative abundance.

Chlorophyll *a'* & chlorophyll *a''* denote chlorophyll *a*-like spectra (exact compound unknown, quantified with chlorophyll *a* standard).

Pheophytin *b*₂ denote pheophytin *b*-like spectra (exact compound unknown, quantified with chlorophyll *a* standard).

4.6 Catchment sample survey

Plant, bryophyte, soil and lake macrophyte/algae samples were taken from the catchment of each study lake on Disko Island and analysed for $\delta^{13}\text{C}_{\text{TOC}}$ and C/N ratios (methods in Section 3.4 & 3.7) to gain an improved understanding of potential catchment source inputs at each locality.

4.6.1 Disko 2

Disko 2 catchment end-member sample results are presented in Table 4.5 and C/N versus $\delta^{13}\text{C}_{\text{TOC}}$ plotted in Figure 4.13 (30 samples). At Disko 2 the $\delta^{13}\text{C}_{\text{TOC}}$ values were mostly within or near the C_3 plant range, although there is a notable exception. The aquatic macrophyte *Potamogeton* sp. had a $\delta^{13}\text{C}_{\text{TOC}}$ value of -6.4‰ , while the next lowest $\delta^{13}\text{C}_{\text{TOC}}$ values in the ‘black moss with white spots’ sample (-21.2‰) and the ‘algal benthic rock scrape’ (-22.6‰). Plants had fairly consistent $\delta^{13}\text{C}_{\text{TOC}}$ values ranging from -26.6‰ to -30.5‰ , but values in lichens and mosses were lower (-20.7‰ to -24.6‰). Soil generally had $\delta^{13}\text{C}_{\text{TOC}}$ values within the range of lichen and moss (-24.1‰ to -26.2‰). The grass sample (Poaceae) had a $\delta^{13}\text{C}_{\text{TOC}}$ value of -27.6‰ , within the range of other C_3 plant samples. There was low range in $\delta^{13}\text{C}_{\text{TOC}}$ values between the constituent parts (stem, bark, leaf) of *Salix arctica* (-27.3‰ to -29.6‰) and little variability between the two repeated samples of the plant *Harrimanella hypnoides* (-29.7‰ to -30.2‰).

Carbon content ranged between 31.8% in the Plant D root sample and 66.3% in the stem of *Salix arctica*. The lowest carbon content was in soils which ranged from 0.1% to 15.9% carbon. Lichen and moss carbon content ranged widely from 28.5% (*Cetraria nivalis* root) to 44.9% (*Cetraria nivalis* – bulk sample). Algal and aquatic macrophyte samples had lower carbon contents than lichen, moss and plants, with the ‘algal benthic rock scrape’ sample reporting a percentage carbon content of 24.5% and the aquatic macrophyte, *Potamogeton* a carbon content of 32.1%. Percent nitrogen content was variable, ranging from 0% in some samples to a maximum of 2.7% in the plant *Chamerion latifolium*. C/N ratios varied considerably, but were generally lower in algae, aquatic macrophytes and soils, compared with plants, lichen and moss. For example, the C/N ratio of *Potamogeton* sp. was 9.7 and for the ‘algal benthic rock scrape’ was 16.8. C/N ratios in soil samples ranged from 8.3 to 15.1, whereas C/N ratios ranged from 196 in the *Cetraria nivalis* lichen to 30 in the lichen *Stereocaulon alpinum*. There was significant within species variability in the lichen *Cetraria nivalis* ranging from a C/N ratio of 196 to just 33.3 in the root of the same species. Plants

ranged in C/N ratio widely from 12.2 in the *Chamerion latifolium* sample to 133.6 in the *Salix arctica* stem sample. There was also considerable within species variation in C/N ratio in *Salix arctica* with differences between stem samples (30.9 to 133.6), bark (96) and leaf samples (17.4). Similarly, there was within species variation in the plant *Harrimanella hypnoides* (122.8 – 32) and the stem in Plant D had a C/N ratio of 53.4, whereas the root had a C/N ratio of 23.4.

Table 4.5: End-member $\delta^{13}\text{C}_{\text{TOC}}$, TOC (%), N (%) and C/N results from the Disko 2 catchment.

Sample type	Description	$\delta^{13}\text{C}_{\text{TOC}}$	TOC (%)	N (%)	C/N
Algae	Algal benthic rock scrape*	-22.6	24.5	1.5	16.8
Aquatic macrophyte	<i>Potamogeton</i> sp.*	-6.4	32.1	3.3	9.7
Lichen	<i>Cetraria nivalis</i>	-23.6	44.9	0.2	196.0
	<i>Umbilicaria</i> -type lichen	-20.7	41.4	0.7	61.5
	<i>Cetraria nivalis</i>	-22.8	43.9	0.2	190.2
	<i>Cetraria nivalis</i> (root)	-25.5	28.5	0.9	33.3
	<i>Stereocaulon alpinum</i>	-22.2	43.8	1.5	30.0
Moss	Black moss with white spots*	-21.2	40.9	1.2	35.2
	Green moss*	-24.6	34.9	0.4	78.7
Plant	<i>Salix arctica</i> (leaf)*	-27.3	47.0	2.7	17.4
	<i>Salix arctica</i> (bark)	-29.4	49.3	0.5	96.0
	<i>Salix arctica</i> (stem)	-28.8	66.3	0.5	133.6
	<i>Salix arctica</i> (stem)	-28.0	50.5	1.6	30.9
	<i>Chamerion latifolium</i> (partly decomosed)*	-29.6	33.1	2.7	12.2
	<i>Harrimanella hypnoides?</i> (A)*	-30.2	43.0	0.4	115.5
	<i>Harrimanella hypnoides?</i> (B)	-29.7	47.2	0.4	122.8
	<i>Harrimanella hypnoides?</i> (C)*	-30.0	42.4	1.3	32.0
	Plant A (small leaf)	-29.0	49.2	0.8	59.2
	Plant A (stem)	-28.7	49.5	1.3	38.0
	Plant A (stem & leaf)*	-29.1	48.2	0.6	78.3
	Plant B	-26.6	43.1	1.1	38.8
	Plant C	-26.3	47.3	1.8	26.6
	Plant D (stem)	-30.5	52.8	1.0	53.4
	Plant D (root)	-25.7	31.8	1.4	23.4
	Plant E	-28.1	56.6	0.7	85.9
Grass	<i>Poaceae</i>	-27.6	46.7	0.7	66.2
Soil	PLOT A - Soil	-26.2	15.9	1.1	15.1
	PLOT B - Soil	-23.7	1.5	0.2	9.9
	PLOT C - Soil*	-26.1	0.1	BDL	8.3
	Catchment - Soil* [†]	-24.1	0.3	BDL	10.2

* Indicates sample selected for lipid biomarker and compound-specific isotopic studies.

[†] Catchment sample taken from near the highest point in Disko 2 catchment (893 m) (Figure 4.6).

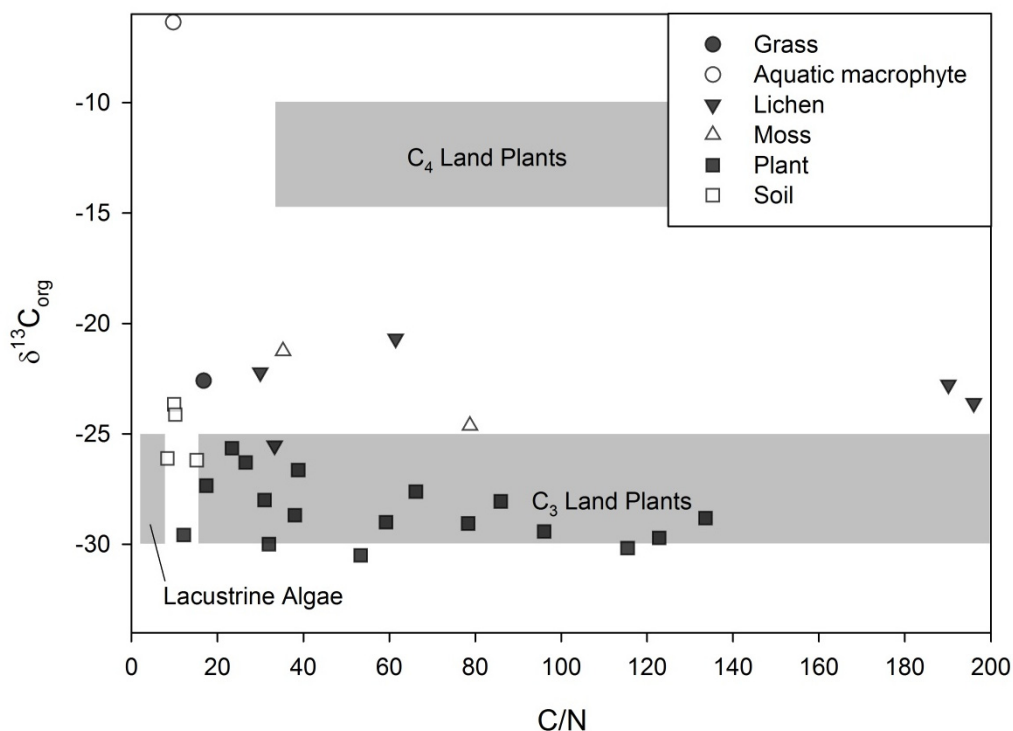


Figure 4.13: C/N vs $\delta^{13}\text{C}_{\text{TOC}}$ for catchment end-member samples from Disko 2. With expected zones for C_4 land plants, C_3 land plants and lacustrine algae from Meyers and Teranes (2001).

4.6.2 Disko 1

At Disko 1, a total of 21 samples (18 from catchment & 3 from the lake) were analysed and classified based on the contents of the single or mixed sample (Table 4.6, Figure 4.14). The $\delta^{13}\text{C}_{\text{TOC}}$ value of all samples from Disko 1 ranged between -24‰ and -31‰ which is near to, or within the range expected for C_3 land plants (as indicated in Figure 4.14). The lowest $\delta^{13}\text{C}_{\text{TOC}}$ value of -24‰ was present in the lichen *Cetraria nivalis*. The Plot D soil sample also had a similar $\delta^{13}\text{C}_{\text{TOC}}$ value of -24.8‰ , and the highest $\delta^{13}\text{C}_{\text{TOC}}$ values were in one of the *Chamerion latifolium* samples (-28‰) and both *Potamogeton* (-30.3‰) and algal mat samples A/B (-30.7‰).

Carbon content at Disko 1 was generally the highest in plant samples (for example, 50.8% in Plant A) but much lower in soil samples (between 0.3 and 20.1%), although the soil directly under moss and roots was much higher with $\sim 30.5\%$ carbon. Carbon content was also low in one of the *Potamogeton* and algal mat samples (C) at 18.5%. Nitrogen content was more variable than carbon content, and was lower in soil, moss

and lichen samples compared with plant samples. C/N ratios were also variable between sample classifications. 'Brown' and 'green moss' presented the highest C/N ratios (112.9 versus 127.9 respectively), while the lichen *Cetraria nivalis* also had a high C/N ratio of 120.5. The lowest C/N ratios were in catchment soil plots ranging from 8.9 to 16, although it was much higher in the soil directly under moss and roots (24.4). Plant C/N values ranged between 18.8 and 58.2, with within species differences present in *Chamerion latifolium* (18.8 – 33.4). Grass C/N ratios ranged from 11.8 to 58.1.

Table 4.6: End-member $\delta^{13}\text{C}_{\text{TOC}}$, %TOC, %N and C/N results from the Disko 1 catchment.

Class	Description	$\delta^{13}\text{C}_{\text{TOC}}$	%TOC	%N	C/N
Grass	Grass A	-27.3	38.9	3.3	11.8
	Grass B	-26.6	44.0	0.8	58.1
Lichen	<i>Cetraria nivalis</i>	-24.1	44.6	0.4	120.5
	Mix of <i>Cladonia arbuscula</i> & <i>Cladonia rangiferina</i>	-26.2	39.8	0.5	85.7
Macrophyte & algae	Potamogeton & algal mat A	-30.3	26.9	0.8	33.0
	Potamogeton & algal mat B	-28.5	36.4	1.0	35.9
	Potamogeton & algal mat C	-30.7	18.5	0.6	29.6
Moss	Brown moss	-27.8	44.5	0.4	112.9
	Green moss	-28.5	47.8	0.4	127.9
Moss/Lichen	Moss, with <i>cladonia</i> -like lichen fruiting body	-27.6	40.3	1.1	36.8
Plant	<i>Salix arctica</i> (stem)	-28.7	46.8	1.3	36.7
	<i>Eriophorum</i> spp.	-26.9	48.7	2.5	19.2
	<i>Chamerion latifolium?</i> (partly degraded)	-27.9	48.0	2.6	18.8
	<i>Chamerion latifolium?</i> (partly degraded)	-28.0	46.9	1.4	33.4
	Plant A	-30.8	50.8	0.9	58.2
	Plant B	-29.5	37.0	1.1	32.4
Soil	Soil under moss and roots	-26.4	30.5	1.2	24.4
	PLOT A - soil	-26.5	0.9	0.1	16.0
	PLOT B - soil	BDL	0.3	BDL	8.9
	PLOT C - soil	-26.2	20.1	1.3	15.6
	PLOT D - soil	-24.8	0.9	0.1	14.7

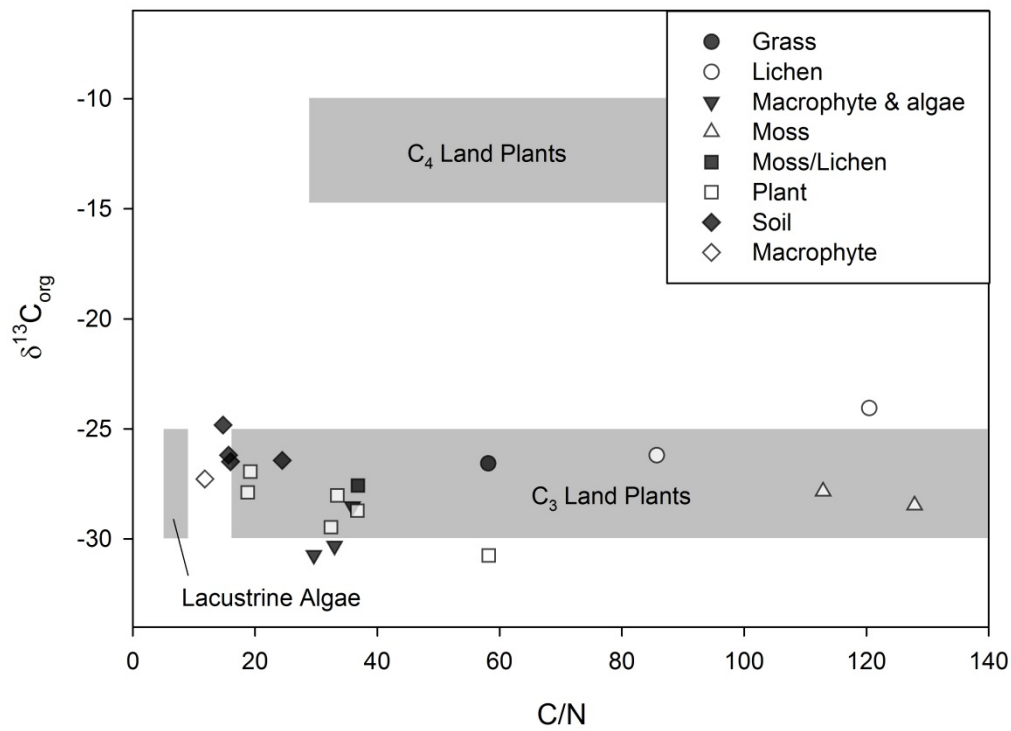


Figure 4.14: C/N vs $\delta^{13}C_{TOC}$ for catchment end-member samples from Disko 1. With expected zones for C₄ land plants, C₃ land plants and lacustrine algae from Meyers and Teranes (2001).

4.6.3 Disko 4

12 samples were analysed from the Disko 4 catchment, grouped into classifications (Table 4.7) and C/N values plotted against $\delta^{13}\text{C}_{\text{TOC}}$ (Figure 4.15). The $\delta^{13}\text{C}_{\text{TOC}}$ values of plant samples from the Disko 4 catchment ranged between -27.3‰ and -29.8‰ , with a slight difference between *Salix arctica* seedlings -29.0‰ and the *Salix arctica* stem (-27.4‰). The lowest $\delta^{13}\text{C}_{\text{TOC}}$ values in Disko 4 catchment samples were the ‘benthic algal rock scrape’ (-20.5‰) and the ‘black rock lichen’ attached to rocks in the catchment (-21.0‰). Both aquatic (*Calliergon giganteum*) and terrestrial ‘green moss’ samples had similar $\delta^{13}\text{C}_{\text{TOC}}$ values of -25.8‰ and -26.1‰ respectively. The guano sample $\delta^{13}\text{C}_{\text{TOC}}$ value was high in compared to the two other soil samples (-25.3‰ and -25.9‰)

Carbon content was lowest in the benthic algal rock scrape (1.5%) and the two conventional soil samples (0.4-1.3%), but higher in guano, plant, moss and lichen samples (35.4% - 54.1%). In the plant samples carbon content was the highest in the *Betula nana* leaf and stem sample (54.1%), the *Harrimanella hypnoides* sample (52.8%) and the *Salix arctica* samples (52.3% - 46.0%). The nitrogen content of samples from Disko 4 was variable, with the lowest nitrogen content found in the *Salix arctica* seedlings (3%). There was also considerable variation in the C/N ratios in the Disko 4 catchment samples. For example, the lowest values were in the ‘benthic algal rock scrape’ (9.2) and both the conventional soil samples (11.6 – 12.1), while the highest C/N ratio was in the ‘black rock lichen’ (102), but was also high in the *Harrimanella hypnoides* plant sample (70.6), the aquatic moss *Calliergon giganteum* (56), the guano sample (52.4) and the plant *Juniperus communis* (49).

Table 4.7: End-member $\delta^{13}\text{C}_{\text{TOC}}$, TOC (%), N (%) and C/N results from the Disko 4 catchment.

Class	Description	$\delta^{13}\text{C}_{\text{TOC}}$	TOC (%)	N (%)	C/N
Algae	Benthic algae rock scrape	-20.5	1.5	0.2	9.2
Aquatic moss	<i>Calliergon giganteum</i>	-25.8	35.4	0.6	56.0
Lichen	Black rock lichen	-21.0	42.8	0.4	102.0
Moss	Green moss	-26.1	45.5	1.0	45.1
Plant	<i>Juniperus communis</i>	-27.3	43.9	0.9	49.0
	<i>Betula nana</i> (leaf & stem)	-29.8	54.1	2.0	26.8
	<i>Harrimanella hypnoides?</i>	-27.7	52.8	0.7	70.6
	<i>Salix arctica</i> (seedlings)	-29.0	52.3	3.0	17.4
	<i>Salix arctica</i> (stem)	-27.4	46.0	1.9	24.3
Soil	Guano (likely from geese)	-33.6	41.5	0.8	52.4
	Soil	-25.3	1.3	0.1	11.6
	PLOT C - soil	-25.9	0.4	BDL	12.1

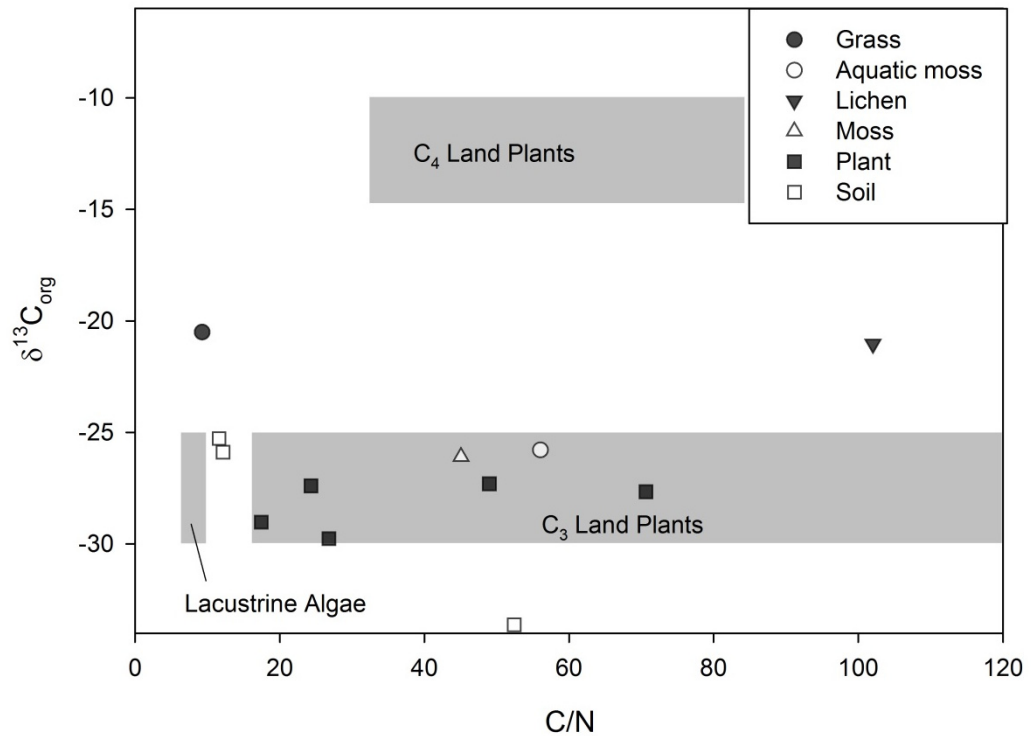


Figure 4.15: C/N vs $\delta^{13}C_{TOC}$ for catchment end-member samples from Disko 4. With expected zones for C₄ land plants, C₃ land plants and lacustrine algae from Meyers and Teranes (2001).

4.6.4 Comparative trends in catchment samples

Figure 4.16 combines the C/N and $\delta^{13}C_{TOC}$ catchment end-member samples from all three lake catchments. Most samples were in the range of C₃ land plants, or approach the range of lacustrine algae ($N=2$), with the exception of one aquatic macrophyte sample (Disko 2 *Potamogeton* sp. 6.4 ‰) and some lichen, moss and soil samples that have lower $\delta^{13}C_{TOC}$ values (~ 20 ‰) compared with C₃ plants. Lichen had the greatest range in C/N values ranging from ~ 25 to nearly 200 across all three catchments. Terrestrial plants had C/N ratios ranging from ~ 15 to ~ 130 , while soil samples were found to have lower C/N ratios, with the exception of those samples attached to lichen, moss or derived from guano. The algal samples did have low C/N ratios, but were not in the conventional lacustrine algal range (usually -25 to -30 ‰) as $\delta^{13}C_{TOC}$ values in these two samples were higher than -25 ‰. This suggests that cycling of $\delta^{13}C$ is more nuanced in this system due to the relatively low density vegetation (e.g. bryophytes) and the presence of in-lake carbon concentrating mechanisms (e.g. for some aquatic macrophytes).

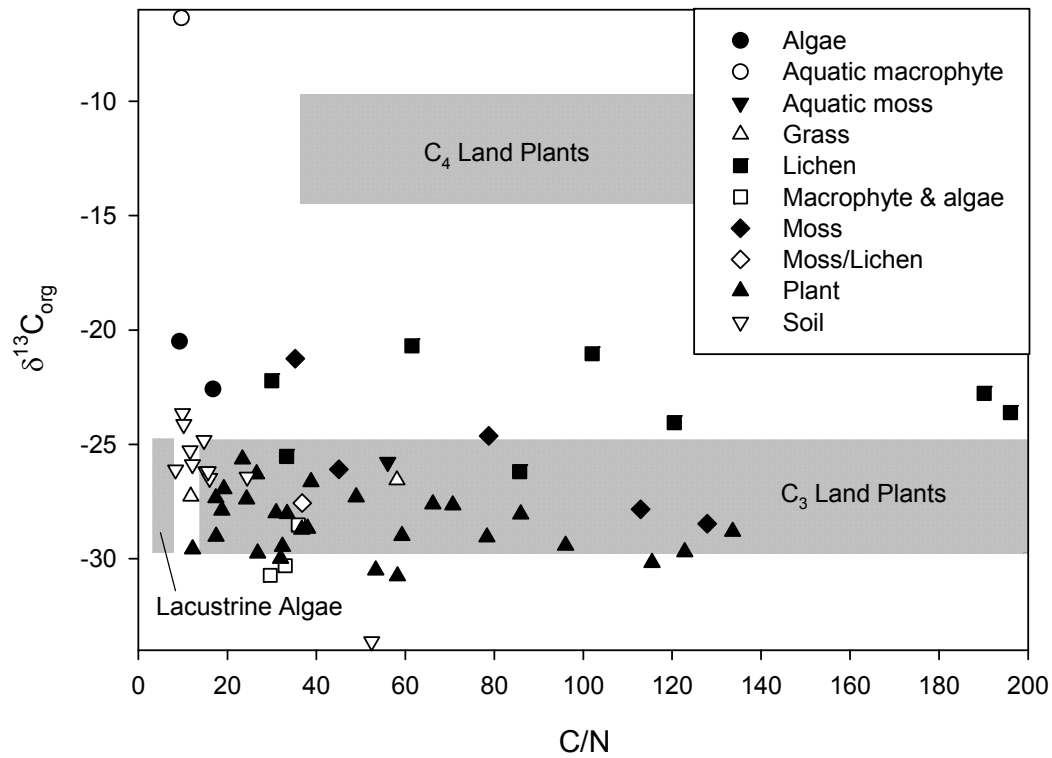


Figure 4.16: C/N vs $\delta^{13}C_{TOC}$ for catchment end-member samples from all three Disko catchment study areas. With expected zones for C₄ land plants, C₃ land plants and lacustrine algae from Meyers and Teranes (2001).

4.7 Lipid biomarker characterisation of selected samples from Disko 2

4.7.1 Carbon chain length distributions

n-alkanoic acids (FAMES, Fatty Acid Methyl Esters)

Figures 4.17, 4.18 and 4.19 present saturated *n*-alkanoic acids analysed by GC-MS for selected catchment samples from Disko 2. For the *n*-alkanoic acids the C₁₆ saturated carbon chain length was dominant in 9 of 11 samples from the catchment. All *n*-alkanoic acid samples were found to have an even dominance of carbon chain length. The *n*-acid distribution of *Harrimanella hypnoides* (C), a terrestrial plant was found to be dominant in the 16 carbon chain length (45% relative abundance (RA)), but there were also peaks at C₂₂ (8% RA) and C₂₈ (9% RA). Comparatively, Plant A was dominant at C₂₂ (30% RA) and had peaks additionally at C₂₀ (27% RA) and C₁₆ (17% RA). Since Plant A had a low relative abundance between the larger peaks for the C₁₈ compound (3%), it had a bimodal distribution (the two peaks were separated). The 'black moss with white spots' sample was strongly unimodal around the C₁₆ compound (85% RA), with the next highest peak at C₁₈ (<10% RA).

The *Harrimanella hypnoides* (A) terrestrial plant had a contrasting saturated *n*-acid chain length distribution to the *Harrimanella hypnoides* (C) previously described. *Harrimanella hypnoides* (A) was dominant in the C₁₈ homologue (45% RA) followed by the C₁₆ compound (35% RA) and has a bimodal distribution as there was found to be an arrangement of long-chain even compounds around C₂₆ (4% RA). The *Potamogeton* sample had a unimodal *n*-acid distribution around the C₁₆ even carbon number compound (76% RA), with a secondary peak at C₁₄ (18% RA). In contrast, the 'green moss' sample had a bimodal *n*-alkanoic acid distribution with peaks in the C₁₆ (38% RA) and C₂₄ (25% RA) compounds. The algal benthic rock scrape had a unimodal *n*-acid distribution which was strongly dominant in the C₁₆ (75% RA) compound, while the *Chamerion latifolium* plant had an extended bimodal distribution with *n*-acid peaks at C₁₆ (38% RA) and C₂₆ (11% RA).

The most common shrub in the Disko 2 catchment, *Salix arctica* had a bimodal distribution for the *n*-acid compounds, peaking at C₁₆ (64% RA) and C₂₄ (11% RA). This contrasted with the unimodal distribution of the 'catchment soil' sample which peaked at C₁₆ (35% RA). The *n*-acid Plot C soil sample had similar maxima at C₁₆ (35%

RA) and C₁₈ (28% RA) but was bimodal due to the arrangement of even compounds around the higher C₂₄ compound (6% RA).

n-alkanes

Saturated *n*-alkanes analysed by GC-MS are presented in Part B of Figures 4.17, 4.18 and 4.19 for selected catchment samples from Disko 2. Most *n*-alkane samples were found to have an odd over even preference of saturated carbon compounds (termed CPI, see Section 4.7.2). Where exceptions are present this is mentioned in the text. In contrast to the *n*-alkanoic acids (with dominance around the C₁₆ compound), for *n*-alkanes there was a unimodal distribution around the long-chain C₂₉ (52% RA) and C₃₁ (35% RA) compounds for *Harrimanella hypnoides* (C). Similarly, Plant A was dominant in the C₂₉ *n*-alkane (74% RA), with smaller peaks at C₂₇ (9% RA) and C₃₁ (8% RA). While the ‘black moss with white spots’ sample had a much less clearly visible dominant *n*-alkane signature, with compounds ~4% RA distributed across the entire range. However, the largest peaks were at C₂₂ (11.5% RA) and C₂₅ (11% RA). In contrast, *Harrimanella hypnoides* (A) sample had a clear unimodal *n*-alkane distribution with dominance in the C₂₉ (RA 35%) and C₃₁ (RA 41%) compounds. This was similar to *Harrimanella hypnoides* (C), although the C₃₁ compound had a higher % RA than the C₂₉ compound.

The *Potamogeton* sp. sample had the highest *n*-alkane relative abundance in the C₃₁ carbon number (17% RA), however the distribution extends across the entire range, with for example the lower chain C₂₁ and C₂₃ compounds found to have relative abundances of ~5%. Similarly, the ‘green moss’ sample had an *n*-alkane dominance in C₃₁ (~25% RA) and also had a distribution of mostly odd number predominance, extending across the entire range, with the exception of C₁₈ (8% RA). While the ‘algal benthic rock scrape’ sample was found to have highest peaks in the C₂₃ *n*-alkane (20% RA), and similarly had a wide distribution of odd chain length compounds. For example, there were peaks at C₂₁ (14% RA), C₂₅ (12% RA) and C₂₉ (8% RA). While the *Chamerion latifolium* sample had a bimodal distribution, with peaks at C₂₅ (26% RA) and in the even C₃₂ compound (18% RA).

In contrast, the *Salix arctica* leaf sample had a unimodal distribution with dominance in the neighbouring C₂₇ (29% RA) and C₂₉ (34% RA) carbon number chain lengths, although there was a small peak in the C₂₂ carbon chain length of <5% RA. The *n*-alkane distribution of the catchment soil sample had a unimodal distribution peaking at C₂₉ (29% RA) and C₃₁ (36% RA), although additionally was found to have a smaller peak in the C₂₇ compound (10% RA). This contrasts substantially with the *n*-alkane

distribution for the Plot C soil sample which appears to have no dominant pattern. Between C₂₁ and C₃₃ chain length compounds in the plot C soil sample all percent relative abundances were greater than 4%, except for C₃₂ (~3% RA). The highest chain length compounds for the Plot C soil sample were C₂₃, C₂₅, C₂₇ and C₂₉, all of which were found to have percent relative abundances > 10%.

n-alkanols

Saturated *n*-alkanols analysed by GC-MS are presented in Part C of Figures 4.17, 4.18 and 4.19 for selected catchment samples. Most *n*-alkanols were found to have an even dominance of carbon chain length, although there are some notable exceptions which are discussed below. The *Harrimanella hypnoides* sample (C) had a clear dominance of the C₂₂ *n*-alkanol compound (25% RA), with the second highest abundance in the C₂₄ homologue (14% RA). However, there was a second less dominant distribution around the C₁₇ *n*-alkanol compound (11.5% RA), and compounds with a percent relative abundance >5 were found to extend into the higher chain length C₂₆, C₂₈ and C₃₀ even compounds. Plant A was found to have a similar dominance of *n*-alkanols in the C₂₂ carbon number (50% RA), but is unimodal as the neighbouring peaks were sub-dominant (C₂₀, 18% RA). The ‘black moss with white spots’ sample had a very pronounced dominance of the C₁₈ *n*-alkanol compound (80% RA).

While all other compounds had percent relative abundances of < 5%, with the exception of the C₁₂ compound (~8% RA). The *Harrimanella hypnoides* (A) sample, contrasted in *n*-alkanol distribution compared with the *Harrimanella hypnoides* (C) sample. There was a peak in the C₂₆ (28% RA) and the C₂₈ (22% RA) even carbon numbers for the *n*-alkanols in the *Harrimanella hypnoides* (A) sample, however, the C₁₇ and C₁₉ compounds were dominant in the lower chain lengths, albeit at lower relative abundances (4% and 6% respectively). The *Potamogeton* sample had a strong dominance of the C₁₇ odd carbon number for the *n*-alkanols (52% RA), which was followed by the C₁₅ compound (11% RA). While in some higher *n*-alkanol chain lengths there was an even predominance (C₂₂, C₂₄, C₂₆, ~10% RA). The *n*-alkanol distribution for ‘green moss’ was primarily around the even C₂₆ carbon number (34% RA), including the C₂₂, C₂₄ and C₂₈ compounds. There was additionally single dominance of the lower chain length C₁₇ compound, which proportionately was less significant with a RA of <10%.

The ‘algal benthic rock scrape’ had a similar *n*-alkanol chain length distribution with a peak in the C₂₆ compound (40% RA) and high levels of the C₂₂ and C₂₄ compounds. There was also similarly the single dominance of the C₁₇ compound (17% RA). The

Chamerion latifolium sample had dominance in the C₂₄ *n*-alkanol compound (RA of 28%), followed by high levels of the even C₂₂ (25% RA) and C₂₆ (16% RA) compounds. There was additionally a small peak in the lower chain compounds of a dominant C₁₇ odd carbon chain length peak (~2.5% RA). Similarly, the *Salix arctica* (leaf) sample also had *n*-alkanol dominance in the C₂₄ compound (40% RA), with secondary peaks in the C₂₂ (30% RA), C₂₄ (21% RA) and C₂₆ (16% RA) compounds. However, the even chain length compounds were widely distributed, for example amongst the C₁₈ (7% RA) and C₃₀ (4% RA) compounds. In contrast, the soil sample from Plot C had a markedly different chain length distribution for the *n*-alkanols, dominated by a peak in the 18:0 compound (38% RA). Secondary peaks were fairly uniform with chain lengths of C₂₂, C₂₄, C₂₆ and C₂₈ (~5 – 1% RA).

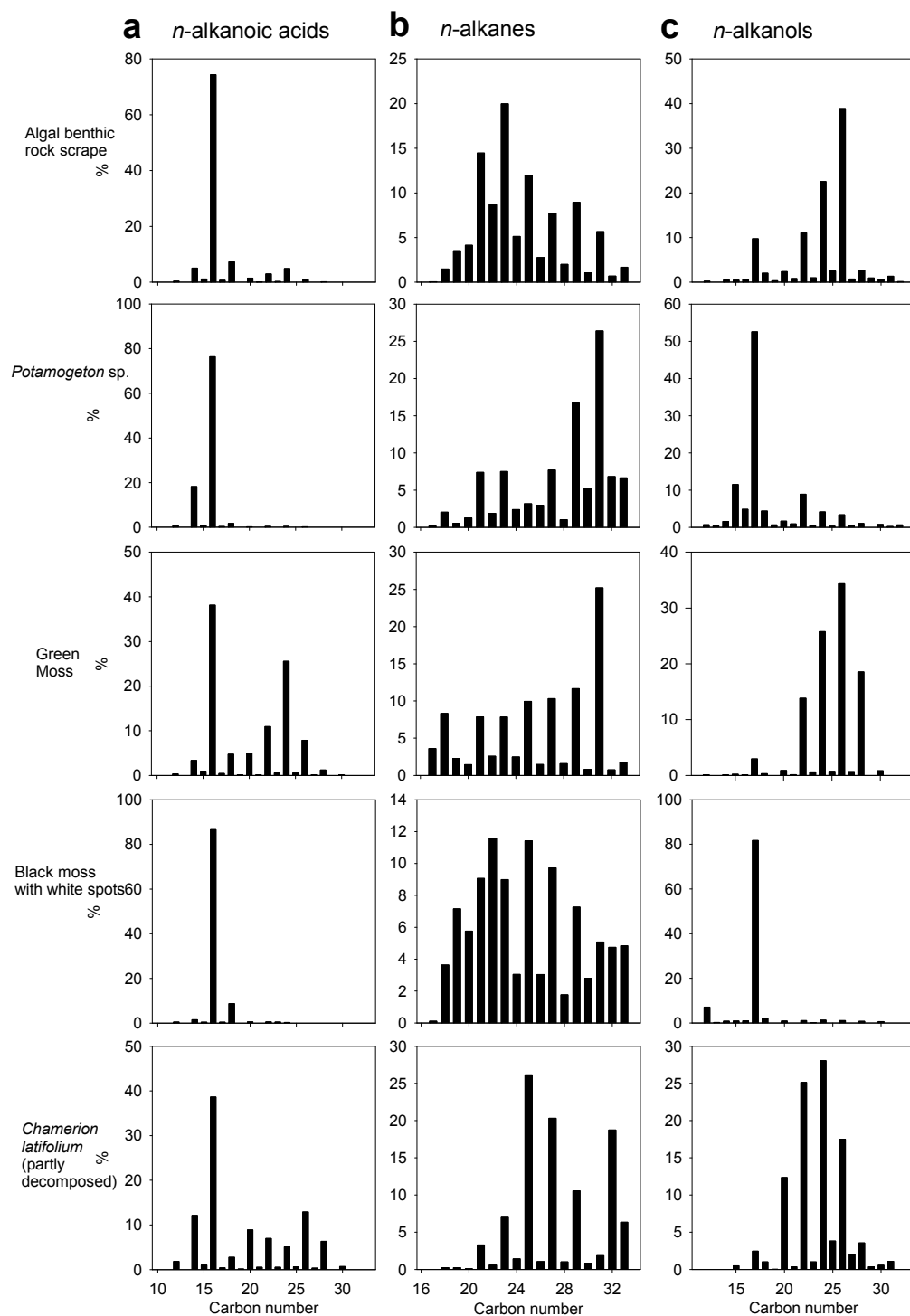


Figure 4.17: Part 1 of lipid distribution histograms for saturated (a) *n*-alkanoic acids, (b) *n*-alkanes and (c) *n*-alkanols for selected catchment plants analysed using GC-MS. Plotted as a percentage of total straight chain abundance.

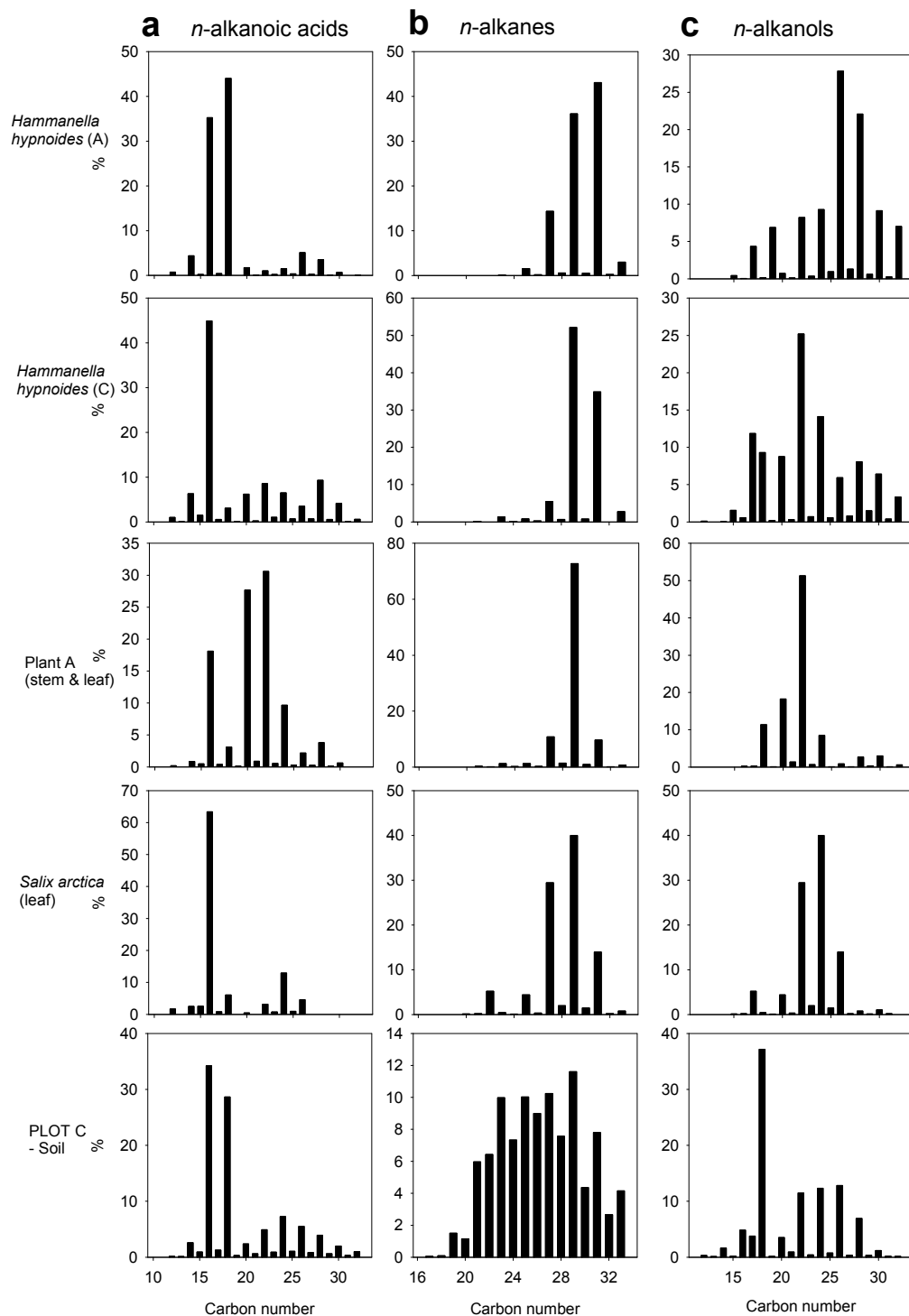


Figure 4.18: Part 2 of lipid distribution histograms for saturated (a) *n*-alkanoic acids, (b) *n*-alkanes and (c) *n*-alkanols for selected catchment plants and soils analysed using GC-MS. Plotted as a percentage of total straight chain abundance.

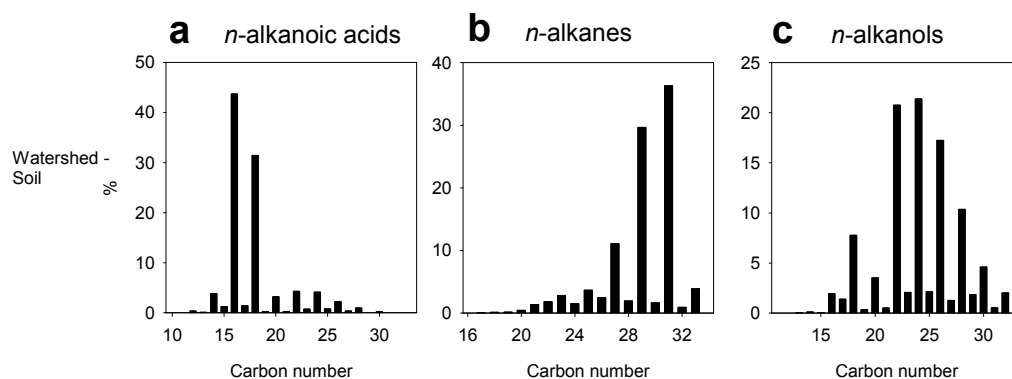


Figure 4.19: Part 3 of lipid distribution histograms for saturated (a) *n*-alkanoic acids, (b) *n*-alkanes and (c) *n*-alkanols for selected catchment soils analysed using GC-MS. Plotted as a percentage of total straight chain abundance.

4.7.2 Selected lipid ratios and equations for Disko 2 catchment samples

Table 4.8 presents selected key lipid ratios and equations for Disko 2 catchment samples for proxies that have been directly used in summary diagrams (Figure 5.16 and 5.20) and are referred to in the Disko 2 S1 combined sequence proxy interpretation (Section 5.3.3). Additional ratios for the same samples, not presented in proxy summary diagrams are in Appendix B. Diagnostic markers (Table 4.8) have been selected for comparison with other proxies (Figure 5.16 & 5.20) based on a detailed review of potential compounds (Section 2.2) and either because they are indicative of clear changes within proxies, or are amongst the clearest biomarkers for identifying source inputs, such as distinguishing autochthonous from allochthonous inputs.

n-alkanes

The CPI 2 index (Carbon Preference Index 2) (Marzi et al., 1993) for *n*-alkanes was a good indicator in the Disko 2 catchment of a broad range of terrestrial plants, including woody and herbaceous varieties (Table 4.8). CPI 2 had higher values among catchment plants than algae, moss and soil. For example, the catchment soil and Plot 3 soil samples had CPI values of just 0.3 and 0.1 respectively, while in plant samples like *Salix arctica* (18.5), Plant A (25.9) and *Harrimanella hypnoides* (39.6 – 27.6) CPI values were significantly higher. Moderate CPI values were obtained in algal, moss and macrophyte samples including 3.5 for the ‘algal benthic rock scrape’ sample and 5.4 for the ‘green moss’ sample.

The terrestrial and aquatic hydrocarbon ratio (TAR HC) (Bourbonniere and Meyers, 1996a) was an excellent indicator of herbaceous plants which formed part of the catchment soil sample (Table 4.8). TAR HC had extremely high values for leafy vascular plants including *Harrimanella hypnoides* (18,899.2 – 2,980.3) and Plant A (1,523.1). This contrasted with much smaller values for ‘black moss with white spots’ (3.0), ‘green moss’ (8.0) and the ‘algal benthic rock scrape’ (6.2). *Potamogeton* had a higher TAR HC ratio (68.5), while the *Salix arctica* sample had a lower value (19.6) than the other plants. The catchment soil sample had a much higher TAR_{HC} ratio (357.7) than the Plot C soil sample (18.9).

The P_{WAX} index (Zheng et al., 2007) was a good indicator of multiple terrestrial inputs, with slightly higher values in herbaceous plants (Table 4.8). *Harrimanella hypnoides* (1.2-1.0), Plant A (1.1) and the catchment soil sample all had P_{WAX} values greater than 1, while the lowest P_{WAX} value was in the ‘algal benthic rock scrape’ sample (<0.5). The $n-C_{26}$ to total saturated n -alkanes ratio was a good indicator of soils, algae and aquatic macrophytes, with the highest values in the Plot C soil sample (9.0) (Table 4.8). Herbaceous plant samples such as *Harrimanella hypnoides* displayed the lowest contributions (0.2), with moderate contributions from the *Salix arctica* (leaf) sample (1.1).

n-fatty acids

The CPI_T ratio (Carbon Preference Index for total n -fatty acids) (Matsuda and Koyama, 1977) was a good indicator of aquatic macrophyte and moss contributions (Table 4.8). CPI_T ratio was high in *Potamogeton* (74.3), and the ‘black moss with white spots’ samples (69.7), but relatively low in other samples including the catchment soil (15.1) and Plot C soil samples (11.7). The ratio of $n-C_{30}$ to total saturated n -fatty acids was a good indicator of some non-woody herbaceous terrestrial inputs and some soil samples. For example, *Harrimanella hypnoides* (C) had the highest ratio of $n-C_{30}$ to total saturated n -fatty acids (4.2), which was followed by the Plot C soil sample (2.0). In contrast the $n-C_{30}$ ratio of the catchment soil sample was much lower (0.2), highlighting localised variations in these patchy soils.

n-alkanols and sterols

The $n-C_{16}$ to total saturated n -alkanol ratio was a good indicator of aquatic macrophytes and catchment soils. *Potamogeton* and the Plot C soil samples had the highest n -alkanol $n-C_{16}$ ratios (both 4.9), with also some algal contributions relevant to this index (0.7). In contrast, the ratio of $n-C_{24}$ to total saturated n -alkanols was a good

indicator of more woody terrestrial plants such as *Salix arctica* and secondary contributions in green moss. *Salix arctica* had the highest values (40.0) followed by 'green moss' (25.8). The n -C₂₆ n -alkanol to total saturated n -alkanols ratio was a good indicator of 'green moss' (34.3) and the 'algal benthic rock scrape' (38.9), with some secondary contributions from herbaceous plants. The ratio of brassicasterol (24-methylcholesta-5,22-dien-3 β -ol) to total sterols was a clear indicator of algae and moss contributions, with high contributions in the 'algal benthic rock scrape' (57.8) and 'black moss with white spots' samples (56.6), but only minor contributions from the most woody terrestrial plants such as *Salix arctica* (0.4).

Table 4.8: Selected lipid ratios for catchment samples from Disko 2 analysed using GC-MS.

Sample	TOC %	<i>n</i> -alkane ratios			<i>n</i> -fatty acid (FAMES) ratios		<i>n</i> -alkanol ratios		Sterol (Brassicasterol /total sterols) *1000	
		CPI 2 ⁽¹⁾	TAR HC ⁽²⁾	<i>P</i> _{WAX} ⁽³⁾	<i>n</i> -C ₂₆ / total <i>n</i> -alkanes	CPI _T ⁽⁴⁾	<i>n</i> -C ₃₀ / total <i>n</i> -fatty acids	<i>n</i> -C ₁₆ / total <i>n</i> -alkanols		<i>n</i> -C ₂₄ / total <i>n</i> -alkanols
<i>Harrimanella hypnoides?</i> (A)	43.0	39.6	18899.2	1.2	0.2	43.2	0.7	0.1	9.3	6.4
<i>Harrimanella hypnoides?</i> (C)	42.4	27.6	2980.3	1.0	0.3	15.3	4.2	0.6	14.1	16.3
Plant A (stem & leaf)	49.2	25.9	1523.1	1.1	0.3	24.3	0.6	0.3	8.5	7.1
Black moss with white spots	40.9	3.7	3.0	0.7	3.0	69.7	0.0	0.9	1.3	56.6
Potamogeton	32.1	3.6	68.5	0.9	3.0	74.3	0.0	4.9	4.2	14.5
Green moss	34.9	5.4	8.0	0.9	1.5	32.4	0.1	0.1	25.8	44.2
Algal benthic rock scrape	24.5	3.5	6.2	0.5	2.8	40.6	0.0	0.7	22.6	57.8
<i>Chamerion latifolium</i> (partly decomposed)	33.1	15.7	119.8	0.7	1.1	27.5	0.7	0.0	28.1	3.5
<i>Salix arctica</i> (leaf)	47.0	18.5	19.6	0.9	1.1	17.3	0.0	0.2	40.0	0.4
Catchment - Soil	0.3	5.2	357.7	1.1	2.5	15.1	0.2	1.9	21.4	20.4
PLOT C - Soil	0.1	1.3	18.9	0.8	9.0	11.7	2.0	4.9	12.3	44.7

⁽¹⁾CPI 2 – Carbon Preference Index 2 (Marzi et al., 1993) = $((C_{23}+C_{25}+C_{27})+(C_{25}+C_{27}+C_{29}))/2*(C_{24}+C_{26}+C_{28})$

⁽²⁾TAR_{HC} – Terrigenous to Aquatic Ratio (Bourbonniere and Meyers, 1996a) = $(C_{27}+C_{29}+C_{31})/(C_{15}+C_{17}+C_{19})$

⁽³⁾*P*_{WAX} – Index of waxy *n*-alkanes to total hydrocarbons (Zheng et al., 2007) = $(C_{27}+C_{29}+C_{31})/(C_{23}+C_{25}+C_{29}+C_{31})$

⁽⁴⁾CPI_T – Carbon Preference Index (for the entire range) (Matsuda and Koyama, 1977) =

$0.5*((C_{12}+C_{14}+C_{16})+(C_{22}+C_{24}+C_{26}+C_{28}+C_{30}))+((C_{14}+C_{16}+C_{18})+(C_{24}+C_{26}+C_{28}+C_{30}+C_{32}))/((C_{13}+C_{15}+C_{17})+(C_{23}+C_{25}+C_{27}+C_{29}+C_{31}))$

Brassicasterol = 24-methylcholesta-5,22-dien-3β-ol

4.7.3 Compound specific $\delta^{13}\text{C}_{\text{FAMES}}$ on Disko 2 catchment samples

Compound-specific $\delta^{13}\text{C}_{\text{FAMES}}$ (fatty acid methyl esters) on catchment plant, soil and bryophyte samples (Table 4.9) were generally lower between C_{16} and C_{30} compared with their bulk value ($\delta^{13}\text{C}_{\text{TOC}}$). The lowest value was in the C_{30} compound for the *Harrimanella hypnoides* (C) sample ($\delta^{13}\text{C}_{30:0} = -39.1 \text{ ‰}$) and the highest was in the 16 monounsaturated *a* compound for the black moss with white spots sample ($\delta^{13}\text{C}_{16:1a} = -25.4 \text{ ‰}$). The $\delta^{13}\text{C}$ values on FAMES were reflective of relatively depleted C_3 land plants, except for the black moss with white spots sample which had slightly higher $\delta^{13}\text{C}_{\text{FAMES}}$ values (range -29.6 to -37.8 ‰). The $\delta^{13}\text{C}$ values on FAMES of the catchment soil sample were, where present, generally intermediate between that of terrestrial plants (e.g. *Salix arctica*) and the bryophyte samples (e.g. Black moss with white spots).

Table 4.9: Selected compound-specific catchment samples from Disko 2 analysed for $\delta^{13}\text{C}_{\text{FAMES}}$ compared with $\delta^{13}\text{C}_{\text{TOC}}$. All values in per mille (‰) relative to VPDB. FAMES were derived using BF_3 in methanol ($\delta^{13}\text{C} = -42.85$ ‰) with a mass balance correction applied from Boschker et al. (1999) following Rieley (1994). Compound-specific analyses analysed in duplicate. Only compound-specific data points with duplicates <0.5 SD are plotted, which accounts for the missing compounds.

Sample name	$\delta^{13}\text{C}_{\text{TOC}}$	16 mon <i>a</i>	16n	18 mon <i>a</i>	18 mon <i>b</i>	18n	20n	22n	24n	26n	28n	30n
<i>Harrimanella hypnoides?</i> (C)	-30.0		-33.2	-30.1			-33.3	-33.6	-36.8		-38.0	-39.1
Plant A (stem & leaf)	-29.1		-36.4	-31.1			-33.0	-32.4	-34.5		-37.3	
Black moss with white spots	-21.2	-25.4	-26.4	-25.4	-28.8	-25.6		-27.3				
<i>Chamerion latifolium</i>	-29.6	-29.6	-35.3				-37.9	-33.0	-38.4	-37.6	-37.8	
<i>Salix arctica</i>	-27.3		-36.1	-33.6		-35.2		-32.8	-38.0	-36.5	-34.4	-34.7
Catchment - Soil	-24.1		-28.9	-29.9		-29.9		-28.7		-35.8		

Abbreviations: ‘mon’ denotes ‘monounsaturated’, ‘n’ denotes saturated FAME (e.g. FAME_{16:0}).

4.8 Discussion

4.8.1 Hydro-geomorphic position of the study catchments

Based on the manual field map and imagery based land cover classification (Table 4.1) of each lake catchment, there were found to be differences between each site at the entire catchment scale. For example, the reduced vegetation coverage of Disko 2 (13%) compared with Disko 1 (39%) from the field map and imagery based survey could mean a reduced potential for vegetation leachate to be released from, or activated in permafrost, potentially reducing microbial phosphorus leaching during spring thaw (Buckeridge et al., 2015). Extensive wetlands observed at Disko 1 (Figure 4.3) and Disko 4 (Figures 4.10 & 4.11) are indicative of arctic environments where waterlogging might lead to methanogenic activity, terrestrial organic matter recycling and decomposition (Hobbie et al., 2000). This is in contrast to the Disko 2 catchment from the map and imagery based survey which is characterised by 79% bare earth, compared with Disko 1 (45%) and Disko 4 (68%).

Although Disko 2 has a smaller catchment to lake area ratio (45:1), compared with Disko 1 (66:1) and Disko 4 (122:1) identified from the map and imagery based survey, this does not appear to be the dominant control on catchment land cover. Instead, elevation (575 m a.s.l. at Disko 2, compared with 299 m a.s.l. at Disko 1 and 214 m a.s.l. at Disko 4) appears to be the dominant factor influencing catchment vegetation development, when combined with the lake's local geomorphological setting (cirque lake, compared with U-shaped valley bottom and valley end lake). This evidence of landscape heterogeneity between the study catchments is consistent with previous findings of significant diversity among high arctic wetlands (Woo and Young, 2006).

Another major difference between the study catchments, identified through the map and imagery based survey is the percentage of permanent ice and glaciation present in each catchment (Table 4.1). Disko 1 is directly fed by an outflow glacier from the Lyngmarksbræen ice cap which, combined with the permanent ice above the Qaarajuttog valley (Figure 4.2) constitutes 14% of the catchment, compared with just 5% at Disko 2 and 3.6% at Disko 4. The intensity of glacial meltwater activity present in each catchment may influence the water chemistry in each lake. For example, although all lakes were dilute ($<34 \mu\text{S cm}^{-1}$) and DOC concentrations were low ($<1.5 \text{ mg L}^{-1}$), there was evidence of high phosphorus concentrations in all lakes in one or both of April and August 2013 (Table 4.3). SRP concentrations were highest in April compared with August, which suggests nutrients are present under the ice but have

just not been used, probably due to low light levels. Any biological activity that is taking place under the ice in the winter (indicated by chlorophyll *a* – Table 4.4) is likely to be of a higher nutritional quality than during the summer (Hampton et al., 2015) due to the high SRP concentrations. However, TP concentrations remain high in both April ($59.8 \mu\text{g L}^{-1}$) and August ($67.8 \mu\text{g L}^{-1}$) and therefore the high summer values point to the high nutrient loads that can be released from glaciers during melt (Slemmons et al., 2013). Nitrate (NH_4^+) values were higher (but not unexpectedly high) in August in Disko 1 ($11.54 \mu\text{g L}^{-1}$), which is similar to observations in glacier fed lakes in the Rocky Mountains of North America (Slemmons and Saros, 2012). Low total N was below detection limits (BDL) in all lakes on Disko Island were similar to values obtained from coastal lakes near Sisimiut, South-West Greenland (Whiteford et al., 2016).

The low DOC values in all three lakes ($<1.5 \text{ mg L}^{-1}$) partly reflect the low level of soil maturity and development in these catchments and is consistent with values obtained from sites above the arctic treeline ($<2 \text{ mg L}^{-1}$) (Rautio, 2001; Rautio and Vincent, 2006). DOC values in continental west Greenland (near Kangerlussuaq) were higher ($>100 \text{ mg L}^{-1}$), but coastal values near Sisimiut were more similar to values on Disko ($1.5\text{-}3.6 \text{ mg L}^{-1}$) (Whiteford et al., 2016) due to the shorter retention time near the coast (more dilute). Conductivities on Disko probably driven by dissolved inorganic carbon (DIC) were slightly higher (23.5 to $33.7 \mu\text{S cm}^{-1}$) than Qivitu Highlands lake (13 to $14 \mu\text{S cm}^{-1}$) (Florian et al., 2015) and similar to values in Fogg Lake both on Baffin Island ($20.6 \mu\text{S cm}^{-1}$). A limitation of this suite of water chemistry observations is the absence of DIC measurements which could have been useful for reconstructing glacial inputs.

Water chemistry measurements presented in Table 4.3 are broadly comparable with those obtained by Christoffersen et al. (2004) from other lakes sampled on southern Disko Island which found TP concentrations ranged from 6 to $32 \mu\text{g L}^{-1}$ in all lakes except one ($201 \mu\text{g L}^{-1}$) in close proximity to the Qeqertarsuaq village. In the study by Christoffersen et al. (2004) lakes were at lower positions in the landscape and with less significant glacial inputs than Disko 1. Chlorophyll *a* concentrations (1.5 to $10.22 \mu\text{g L}^{-1}$) were slightly higher in the previous study compared with our observations (0.1 – $1.0 \mu\text{g L}^{-1}$), again likely due to the position of Disko 1, 2 and 4, higher in the landscape gradient. The slightly lower temperature of $9.9 \text{ }^\circ\text{C}$ in Disko 1, compared with 10.9 and $10.6 \text{ }^\circ\text{C}$ in Disko 2 and 4 respectively could be attributed to the proportionally greater meltwater inputs into Disko 1, and the lakes shorter expected residence time due to the large flows into the lake observed in August 2013. Similarly,

the higher dissolved oxygen (DO) (11.9 ppm) in Disko 1, compared with 9.6 ppm and 9.7 ppm in Disko 2 and 4 could be due to fluvial turbulence from hydrological glacial activity upstream in the Disko 1 catchment.

Pigment concentrations were dominated by chlorophyll *a* in Disko 2 (24.1 % RA) and Disko 4 (29.3 %RA), whereas pheophytin *b* (a chlorophyll *b* derivative) dominated pigment abundance in Disko 1 (22.2% RA) (Table 4.4). This indicates either there were significant differences between the algal communities, or speculatively that degradation caused by UVR damage (due to the low DOC concentrations) was greater in Disko 1. The Disko 1 lake downstream of significant glacial activity (14% of catchment, Table 4.6) was noticeably turbid (Figure 4.3), compared with Disko 2 (Figure 4.4 - B) and Disko 4 (Figure 4.11 - A), which could be responsible for altering the light regime of Disko 1 making it more suited to flagellates, or green algae which produced chlorophyll *b*, which degrades into pheophytin *b*. However, pheophytin *b* can also be supplied by catchment vegetation, which is higher in Disko 1 compared with Disko 2 (Table 4.2).

There was a much higher concentration of diatoxanthin (0.63 nmol L^{-1}) in Disko 1 compared with Disko 2 (0.05 nmol L^{-1}) and Disko 4 (0.08 nmol L^{-1}) (Table 4.4), which is a biomarker of diatoms, dinoflagellates and chrysophytes, highlighting the difference in algal composition or abundance between lakes. Diatoxanthin is also a degradation product of diadinoxanthin so its production could be regulated by degradation due to the low level of DOC and the fact Disko 1 is shallow (max depth = 5.9 m) with no depth refuge from harmful UVR radiation for organisms. The lack of UVR pigment in these lakes could be linked to the low nitrogen (N) levels as mycosporine-like amino acids (MAA) produced by organisms for photo-protection contain N.

Compared with average total phytoplankton pigment concentrations ($\sim 0.13 - 0.33 \text{ nmol L}^{-1}$) found in south-west Greenland across coastal, inland and ice sheet margin lakes near Kangerlussuaq, west Greenland (Whiteford et al., 2016), concentrations on Disko were higher. For example, individually the pigments pheophytin *b* in Disko 1 (0.95 nmol L^{-1}) and Disko 2 (0.55 nmol L^{-1}) and chlorophyll *a* at Disko 4 (0.85 nmol L^{-1}) were higher than the total averages for the values reported in Whiteford et al. (2016). The higher chlorophyll *a* concentration in Disko 4 (214 m a.s.l.), compared with Disko 2 (575 m a.s.l.) could be linked to the lakes lower position in the landscape gradient, with more nutrient inputs from multiple glacial and periglacial features,

combined with more complex catchment vegetation stimulating terrestrially controlled nutrient cycling.

Disko Island is a botanically diverse area of west Greenland with 213 species of higher plants reported in the area (Daugbjerg, 2003). The vegetation communities found in the catchments of Disko 1, 2 and 4 (Tables 4.2, 4.5, 4.6, 4.7) were broadly comparable with previous studies on Disko e.g. (Daugbjerg, 2003; Callaghan et al., 2011) and regionally (Fredskild, 2000), but were restricted due to the higher altitude of the catchments. Although the vegetation plots surrounding the three study lakes did not seek to identify rare species present, the plants with broad coverage identified included *Salix arctica*, *Carex* spp., *Eriophorum* spp, *Saxifraga* spp. and *Chamerion latifolium*, together with a wide variety of moss and lichen species (Table 4.2). The higher proportion of bare ground within the study plots at Disko 2 (53.5%) compared with Disko 1 (29.8%) and Disko 4 (18.6%) likely reflects the higher elevation of Disko 2 (575 m a.s.l.) compared with 299 – 214 m a.s.l. in the other catchments. Further, Disko 1 (10.8%) and Disko 4 (13.2%) have a proportion of organic soil exposed, while all bare ground in Disko 2 was bare rock and gravel (53.5%). Organic soils are indicative of faster recycling rates of organic matter and detritus compared with minerogenic soils.

Total organic carbon (TOC) in all soil samples analysed from the three catchments was variable. For example, at Disko 1 TOC varied from 0.3% in Plot B (a very minerogenic soil) to 30.5% in soil (more organic) found directly under moss and roots (Table 4.6), while TOC varied from 0.1% to 15.9% in Disko 2 (Table 4.5), highlighting the patchy nature of Arctic soil and wetlands at the local scale (Woo and Young, 2006). At the local scale decomposition can be key in regulating soil loss or retention in Arctic sites mediated by climate (temperature and moisture), but also litter quality and the soil food web (Wookey et al., 2009). *Betula nana* and *Juniperus communis* did not comprise a significant proportion of any study plot (Table 4.2), but were both present and sampled in other parts of the Disko 4 catchment (Table 4.7). An explanation might be the slightly weaker tolerance of *Betula nana* and *Juniperus communis* to the exposed and poorly drained soils of the higher elevation Disko 1 and Disko 2 sites, and the closer proximity to the coastline at Disko 4 which is known to have high plant diversity (Callaghan et al., 2011; Hollesen et al., 2015).

4.8.2 Catchment samples ($\delta^{13}\text{C}_{\text{TOC}}$, $\delta^{13}\text{C}_{\text{FAMES}}$ and C/N)

For higher plants $\delta^{13}\text{C}_{\text{TOC}}$ varied between -25.7‰ and -30.5‰ in Disko 2 (Table 4.5, Figure 4.13), -26‰ and -30‰ in Disko 1 (Table 4.6, Figure 4.14), and -27.3‰ and -29.8‰ in Disko 4 (Table 4.7, Figure 4.15), which is broadly comparable with the $\delta^{13}\text{C}$ values reported in previous studies (Meyers, 1990; Hammarlund et al., 1997; Meyers and Lallier-Vergès, 1999) and reflects photosynthesis which utilises atmospheric CO_2 . While on-land bryophytes (mosses & lichens) had $\delta^{13}\text{C}_{\text{TOC}}$ values that covered a slightly broader range from -20.7‰ to -24.6‰ on Disko 2 (Table 4.5, Figure 4.13), -24.1‰ to -27.8‰ for Disko 1 (Table 4.6, Figure 4.14) and -21.0‰ to -26.1‰ on Disko 4 (Table 4.7, Figure 4.15). This slightly larger range in $\delta^{13}\text{C}_{\text{TOC}}$ values reflects the more varied carbon fixation pathways in bryophytes which can have a CO_2 concentration mechanism (Glime, 2007; Hanson et al., 2014). The $\delta^{13}\text{C}_{\text{TOC}}$ values of soil reflected either a predominant bryophyte (moss/lichen) contribution (e.g. Disko Plot B -23.7‰), or a mixed contribution primarily from terrestrial plants ($\delta^{13}\text{C}_{\text{TOC}} > -25\text{‰}$).

The slightly lower (relatively depleted) $\delta^{13}\text{C}_{\text{FAMES}}$ values in higher plants (e.g. -39.1‰ in C_{30} FAMES sample) in Disko 2 samples (Table 4.9) is probably related primarily to the diffusional effects of plant physiology (Farquhar et al., 1989). Evaporative control of higher plants and the effect of humidity and precipitation (Diefendorf et al., 2010; Kohn, 2010) in the high arctic catchment may also play a role, although studies which suggest this were analysed $\delta^{13}\text{C}$ on *n*-alkanes, and the mechanism is currently debated. The higher (relatively enriched) value of the ‘black moss with white spots’ sample is indicative of different carbon-concentrating mechanisms in bryophytes as moss species lack a stomata and so the reduced ability to coordinate the water balance within plant cells can result in varying isotopic fractionation, typically closer to atmospheric CO_2 (e.g. -25.4‰ in C_{16} and C_{18} monounsaturated *a* FAMES).

There was wide variation in $\delta^{13}\text{C}_{\text{TOC}}$ amongst the aquatic samples. For example, although the mixed *Potamogeton* and algal matt samples in Disko 1 had $\delta^{13}\text{C}_{\text{TOC}}$ values of -28.5‰ to -30.7‰ , the Disko 2 ‘algal benthic rock scrape’ had a $\delta^{13}\text{C}_{\text{TOC}}$ value of -22.6‰ and the *Potamogeton* had a very high $\delta^{13}\text{C}_{\text{TOC}}$ value of -6.4‰ . Benthic algae is probably accessing ^{12}C released from breakdown of organic matter at the sediment surface, which might explain the high $\delta^{13}\text{C}_{\text{TOC}}$ value of -6.4‰ , close to atmospheric CO_2 . The varying $\delta^{13}\text{C}_{\text{TOC}}$ values for benthic algae (-20.5 to -22.6‰) between samples point to possible physicochemical variations between local in-lake habitat (James et al., 1999; Jones et al., 2000). The aquatic moss *Calliergon giganteum*

had a higher $\delta^{13}\text{C}_{\text{TOC}}$ value (-25.8‰) which was consistent with the $\delta^{13}\text{C}_{\text{TOC}}$ value of other aquatic mosses found in Zachenberg, East Greenland (~ -22.5 to -25‰) (Riis et al., 2016).

The majority of samples across all three catchments had C/N values between ~ 30 and 200 and so are indicative of higher plants or aquatic macrophytes (Tables 4.5-4.7) and show similar trends to those reported in Sisimiut, south-west Greenland (Leng et al., 2012). However, there were some exceptions amongst terrestrial plants for C/N ratio, with for example, Grass A (11.8) in Disko 1, *Eriphorium spp* (C/N 19.2) and *Chamerion latifolium* (18.8) in Disko 2, *Salix arctica* (leaf) (C/N 24.3) and *Salix arctica* (seedlings) in Disko 4 (17.4). The lower C/N ratios in these plant samples likely reflect new growth made possible during the short summer arctic growth season. The large within species variability in *Salix arctica*, *Chamerion latifolium*, *Harrimanella hypnoides* and Plant D may reflect the lignin proportions of plant matter at different growth stages. Variations could partly reflect the propensity of samples to respond to inorganic carbon removal during acidification (Brodie et al., 2011), although reaction time was controlled for all samples (Section 3.7).

The low C/N ratios of minerogenic soils (8.3-10.2) compared with more organic soils (11.6-24.2) reflect local proximity to vegetation patches and rapid hydrological flushing expected in the steep Disko 2 catchment (Table 4.5). The ‘algal benthic rock scrape’ in Disko 2 (16.8) and Disko 4 (9.2) together with the Disko 2 aquatic macrophyte (9.7) have lower C/N ratios (Table 4.5 & 4.7) consistent with values reported in aquatic algae in multiple studies (Meyers and Teranes, 2001). This confirms that benthic contributions of organic matter are likely to have low C/N ratios in these lakes. A limitation of this study is the absence of an end-member from the lake plankton contributions, however other studies have shown the typical values to be between -27 and -31‰ (Meyers and Teranes, 2001).

Summary

Taken together, $\delta^{13}\text{C}_{\text{TOC}}$ and C/N trends in catchment sampling in all catchments were relatively complex (Figure 4.16) due to the presence of limited catchment vegetation and substantial cover of bryophytes (Table 4.2) which have varying carbon concentrating mechanisms affecting $\delta^{13}\text{C}$ values. Despite this complexity, there are some trends that can be used to help interpret down-core changes. $\delta^{13}\text{C}_{\text{TOC}}$ in terrestrial plants overall ranged between -30.8‰ and -25.7‰ which is a reasonably narrow range to interpret source inputs. Algae $\delta^{13}\text{C}_{\text{TOC}}$ values were slightly higher (less negative) ranging from -22.6‰ to -20.5‰ and so higher values may indicate

increased algal contributions, although some caution needs to be acknowledged as this is based on two spot samples. One aquatic macrophyte in Disko 2 (*Potamogeton* sp.) had a very high (less negative) $\delta^{13}\text{C}_{\text{TOC}}$ value of -6.4‰ , close to atmospheric CO_2 and so increases in $\delta^{13}\text{C}_{\text{TOC}}$ in sediments could indicate macrophyte expansion, although caution should be made in this interpretation as it is based on one sample.

C/N ratio was a fairly good discriminator between algae and the more woody vascular plants (Figure 4.16), however due to the limited vegetation development across all sites, new growth had C/N ratios approaching the range of algae (some samples of herbaceous new growth ~ 12). Bryophyte C/N ratios ranged widely, depending on the growth strategies of each species. Some soils had C/N ratios close to aquatic algae (as they likely contain algae) which may complicate sedimentary interpretations, as these limited soils, unlike in more conventional systems may not have been formed predominantly by higher plants.

4.8.3 Lipid biomarker characterisation of Disko 2 catchment samples

There were diverse lipid distributions in the catchment samples which were not always consistent with the generalities reported in the literature, which makes applying a local context particularly important (Figures 4.17-4.19). This section addresses how representative the catchment samples are on Disko 2, compared with previous studies.

n-alkanoic acids

Among the *n*-alkanoic acids, the C_{16} saturated chain length compound was dominant in 9 of 11 compounds, which is consistent with our understanding that this is a ubiquitous non-source specific compound present in bacteria, algae, land plants and other microbes (Meyers, 1997). Longer chain length *n*-alkanoic acids are the major component of the waxy coatings on land plants, leaves and pollen (C_{24} , C_{26} & C_{28}) (Rieley et al., 1991), but in the Disko 2 catchment samples no plants have overall dominance in this part of the chromatogram (Figures 4.17-4.19). However, a number of plants did have secondary distributions around the higher compounds. For example, the C_{28} compound in *Harrimanella hypnoides* (C), the C_{26} and C_{28} compounds in *Harrimanella hypnoides* (A), the C_{26} compound in *Chamerion latifolium* and the C_{24} compound in *Salix arctica*, were all higher than the neighbouring peaks and sometimes reflect a bimodal distribution. Therefore, higher chain length *n*-alkanoic

acids in this system are more likely to be representative of terrestrial plants or moss ('green moss' = secondary dominance around C₂₄ compound).

In contrast, the aquatic *Potamogeton* spp. 'algal rock scrape' and 'black moss with white spots' samples did not have higher chain length peaks, but instead had arrangements tightly around C₁₆. The Plant A sample had its dominance around C₂₂ which complicates higher plant inputs. The catchment soil and Plot C *n*-alkanoic acid distributions suggested a mixed (although dominant C₁₆ and C₁₈) contribution with some minor peaks at C₂₂ and C₂₄, reflecting terrestrial plant/moss inputs. The higher chain length distribution (extending to C₃₂) in the Plot C soil sample potentially reflects its position close to vegetation inputs, compared with the more exposed position of the catchment sample.

n-alkanes

The majority of catchment samples had *n*-alkane dominances > 29 with the exception of the 'black moss with white spots' sample, the 'algal benthic rock scrape' and the *Chamerion latifolium* samples. Higher chain length (C₂₇, C₂₉ and C₃₁) *n*-alkanes are generally associated with vascular plants either at the lake edge or on land (Cranwell, 1984; Meyers, 2003), while mid-chain (C₂₁, C₂₃ and C₂₅) chain lengths have been associated with submerged and floating macrophytes (Cranwell, 1984; Ficken et al., 2000). In contrast, the source of the C₁₇ *n*-alkane has been linked to aquatic algae particularly phytoplankton. In the Disko 2 catchment samples we did not find any aquatic samples that maximised around the C₁₇ *n*-alkane, although this may be because no phytoplankton end-member was sampled.

Catchment plant distributions were generally consistent with dominance >C₂₇ (e.g. *Harrimanella hypnoides*, Plant A and *Salix arctica*), although the *Potamogeton* spp. sample (C_{MAX} 33) had an *n*-alkane dominance much higher than would be expected (usually C₂₁ – C₂₅ for floating macrophytes). Although high *n*-alkane maxima have been found in *Potamogeton natans* (C_{MAX} = 29) from the Sierra Nevada, California (Street et al., 2013), which is similar to the Disko 2 sample (peaks at C₂₉ and C₃₁ (dominant)) *P. natans* has floating leaves whereas the *Potamogeton* spp. sample on Disko 2 is a narrow submerged narrow leaved specimen. In contrast, in Tibetan lakes Aichner et al. (2010a) found *Potamogeton* spp. that maximised at C₂₃ and C₂₅ which is markedly different to the Disko 2 sample.

Both Zech et al. (2010) and Street et al. (2013) reported *n*-alkane *Salix* maxima at C₂₇, which is similar to the Disko 2 *Salix* maximum of C₂₉, with secondary dominance of

the C₂₇ compound. For *Salix* the slight difference between dominance of C₂₇ or C₂₉ may depend on the part of the plant sampled, or differences between arctic (e.g. *Salix arctica*) and temperate species. ‘Green moss’ from the Disko 2 catchment had *n*-alkane dominance in the C₃₁ compound, which contrasts significantly with *Sphagnum* mosses which have been reported to have a predominance of the C₂₃ and C₂₅ chain lengths (Bush and McInerney, 2013), although other moss species have reported higher C_{MAX} values such as in the C₃₃ *n*-alkane for the moss species *Hypnum revolutum* (Huang et al., 2010). The ‘black moss with white spots’ sample had C maxima at C₂₂ and C₂₅ for the *n*-alkanes which is consistent with previous reports of *Sphagnum* (Bush and McInerney, 2013), although it is within the range of aquatic and floating emergent macrophytes (C₂₁-C₂₅) (Ficken et al., 2000), which could complicate palaeolimnological interpretations.

The ‘algal benthic rock scrape’ has a distribution in the mid chain lengths, although unusually has dominance of the C₂₂ compound which could present as a useful biomarker for this input. Similarly, the *Chamerion latifolium* sample has a dominance in the mid chain lengths (C_{MAX} 25), although the presence of secondary dominance of the C₃₂ *n*-alkane (within the terrestrial range) suggests the partly decomposed nature of this sample could have caused the mid-chain distribution. The secondary maximum at the C₃₂ carbon chain length is unusual (even) dominance for an *n*-alkane and could also act as a diagnostic marker for this plant. The catchment soil sample was more strongly dominant in the higher chain length compounds in comparison to the Plot C soil sample. This suggests soil closer to the Disko 2 lake is likely to have more varied plant inputs than at higher more exposed positions in the catchment.

n-alkanols

The *n*-alkanol distributions were particularly diverse in the Disko 2 catchment samples. Waxes of land plants are expected to have an even dominance in the range of C₂₂ to C₃₀ (Eglinton and Hamilton, 1967; Rieley et al., 1991; Meyers, 2003), which differ from algae and bacteria which are conventionally highest in C₁₆ to C₂₂ compounds (Robinson et al., 1984; Volkman et al., 1999). Interestingly, the *Potamogeton* and ‘black moss with white spots’ samples both had a C_{MAX} in the odd C₁₇ compound which is unusual for an *n*-alkanol distribution. In sediments of Disko 2, the C₁₇ compound may act as a useful biomarker for moss and *Potamogeton* inputs, although the presence of the C₁₇ compound is also noted in many other samples which have maxima between C₂₂ and C₂₆.

Although other terrestrial plants including *Salix arctica* and *Chamerion latifolium* do have *n*-alkanol dominance >22 (indicative of higher plant inputs), the ‘algal benthic rock scrape’ had an almost identical distribution (dominating around the C₂₆ compound) which hinders the ability for the *n*-alkanols to clearly distinguish between terrestrial and aquatic inputs in this system. Algal mats also include bacteria and other microbes such as protozoans which could be utilising terrestrially derived material through heterotrophy or the microbial loop. The catchment soil *n*-alkanol distribution is diagnostic of the majority of catchment plant inputs (C₂₂-C₂₆ maximum), but the Plot C soil sample has an unusual maximum in the C₁₈ carbon number, which is not dominant in any catchment sample and might indicate the possible presence of fungi or bacteria in soils. The C₁₈ compound could be a by-product of degradation (*n*-alkanols are known to be less resistant to degradation than *n*-alkanes) or it is possible a key end-member has been missed in the catchment samples.

4.8.4 Key interpretations from selected Disko 2 biomarker catchment samples

This section interprets the lipid carbon chain length distributions from section 4.7.1 (Figures 4.17, 4.18 & 4.19) and lipid ratios from section 4.7.2 (Table 4.8), with focus on the specific key diagnostic markers that are directly used in Disko 2 summary diagrams (Figures 5.16 & 5.20) and are referred to in the Disko 2 S1 combined sequence proxy interpretation (Section 5.3.3).

n-alkanes

The CPI 2 index (used down-core in Figure 5.16) indicates how petrogenic (petrol-like, degraded) or ‘fresh’ the waxy *n*-alkane signature is (Marzi et al., 1993). The high values in leafy catchment plants (Table 4.8) makes CPI 2 a good indicator of non-woody vascular plants, for example *Harrimanella hypnoides* (27.6-39.6) and Plant A (25.9) in contrast to the lowest values in the ‘black moss with white spots’ sample (3.7) and ‘soil Plot C’ which are more petrogenic in signature. In moss, the petrogenic signature probably indicates the presence of dead or decaying biomass in the moss structure and the presence of ‘old’ carbon.

The TAR_{HC} ratio (used down-core in Figure 5.16) was developed to indicate higher ratios for terrestrial inputs and lower ratios for aquatic algae. In this system the TAR_{HC} ratio effectively provides high values for the plants *Harrimanella hypnoides*

(18,899.2-2,980.3) and Plant A (1,523.1), but is biased towards these non-woody inputs as *Salix arctica* provides a low ratio of 19.6 (Table 4.8). Effectively, the TAR_{HC} ratio provides a low ratio for the ‘algal benthic rick scrape’ (6.2), but the ‘black moss with white spots’ sample also has a low ratio (Table 4.8). Overall, the TAR_{HC} ratio is a good autochthonous versus allochthonous indicator but is biased towards non-woody plant inputs and moss inputs provide a similar signature to algae.

The P_{WAX} (used down-core in Figure 5.20) is the ratio of waxy *n*-alkanes to selected total *n*-alkanes (Zheng et al., 2007) and so higher values should indicate proportionately more terrestrial inputs. In Disko 2 the highest values were in fresh non-woody vascular plant material (*Harrimanella hypnoides* (1.2-1), Plant A (1.1)), the catchment soil sample (1.1), the aquatic macrophyte *Potamogeton* (0.9) and ‘green moss’ samples (Table 4.8). Although the P_{WAX} ratio in this system cannot distinguish the specific terrestrial input, the low contributions from the ‘algal benthic rock scrape’ sample (0.5), make the index a good indicator of general terrestrial inputs, combined with changes in aquatic macrophytes (Table 4.8).

The C₂₆ ratio to total saturated *n*-alkanes (used down-core in Figure 5.16) was a good indicator of soil samples as the highest contributions was in the Plot C (9.0) soil sample. This makes the *n*-alkane C₂₆ ratio a good indicator of allochthonous soil disturbance.

n-fatty acids

Although source attributions for *n*-fatty acids (FAMES) were comparatively less clear (Appendix B - Table B2) than *n*-alkanes (Appendix B – Table B1), the CPI index while not a good indicator for a specific sub-group is a good indicator of general increases in productivity (used down-core in Figure 5.20). For the CPI_T index of total fatty acids (T), even compounds are expressed against odd compounds as a way to determine the relative ‘fresh’ or petrogenic nature of the sample (Matsuda and Koyama, 1977). Highest contributions of CPI_T were in the aquatic macrophyte *Potamogeton* (74.3), black moss (69.7) and the ‘algal benthic rock scrape’ (40.3) (Table 4.8). Since fatty acids are more prone to diagenesis than *n*-alkanes, changes in CPI_T can probably be interpreted as a bulk change in productivity.

The long-chain C₃₀ fatty acid (FAMES) contributions (used down-core in Figure 5.16) were highest in in the *Harrimanella hypnoides* (C) (4.2) and the Plot C soil sample (2.0) (Table 4.8), making this ratio a good indicator of non-woody vascular plant and soil terrestrial inputs in Disko 2.

n-alkanols and sterols

The C₁₆ *n*-alkanol ratio (used down-core in Figure 5.20) is a good indicator of the aquatic macrophyte *Potamogeton* (4.9) and Plot C soil samples (4.9) (Table 4.8), but can also probably be interpreted as a bulk productivity indicator as short chain *n*-alkanols are also more susceptible to diagenesis than *n*-alkanes (Cranwell, 1981).

In contrast, the C₂₄ *n*-alkanol ratio (used down-core in Figure 5.16) is a good indicator of higher plants like *Salix arctica* (29.4) and *Chamerion latifolium* (25.1). This suggests the C₂₄ *n*-alkanol is an effective indicator of mixed and mid-chain inputs, primarily of allochthonous origin.

Brassicasterol (24-methylcholesta-5,22-dien-3 β -ol) is known to be high in samples containing cyanobacteria, algal mats, diatoms and brassicas (Pearson et al., 2007). In Disko 2 the ratio of brassicasterol to total sterols (used down-core in Figure 5.20) was highest in the ‘algal benthic rock scrape’ sample (58.7), with similar high contributions in the ‘black moss with white spots’ sample (56.6). However, in Disko 2 the darker moss, classified as dead/decaying had only minimal coverage (1.2%) of the quadrat surveys (see Table 4.2) and so the ratio of brassicasterol to total sterols is probably an indicator of algae in this system. This interpretation is corroborated by minor contributions from woody terrestrial plants such as *Salix arctica* (0.4).

Summary – Disko 2 catchment sample interpretations

Nine key lipid ratios and equations which were most diagnostic among the catchment source study assessment (see Appendix B) have been interpreted and are subsequently used down-core in Disko 2 summary diagrams (Figures 5.16 & 5.20). For *n*-alkanes both the CPI₂ index and TAR_{HC} ratio were good indicators of general higher plant inputs, with the *P*_{WAX} ratio also probably indicative of changes in aquatic macrophytes. The C₂₆ *n*-alkane ratio was a good indicator of allochthonous soil disturbance. For the *n*-fatty acids (FAMES) the CPI_T index provided a general indicator of productivity (probably associated with algae and aquatic macrophytes) and the C₃₀ fatty acid a good indicator of non-woody vascular plants and soil inputs. For the *n*-alkanols, the C₁₆ ratio was a good indicator of aquatic macrophyte, soil inputs and bulk productivity, while the C₂₄ *n*-alkanol ratio was an effective indicator of mixed woody and non-woody plant inputs. Both fatty acids and *n*-alkanols are more susceptible than *n*-alkanes to diagenesis. In this system the ratio of brassicasterol to total sterols is primarily an indicator of aquatic algae.

4.9 Summary – hydro-geomorphic catchment survey

The detailed hydro-geomorphic survey of the three study catchments, including combined land cover and quadrat surveys found that the highest elevation Disko 2 lake with the smallest catchment was substantially less vegetated than Disko 1 and 4, which have extensive wetlands and ice cover in their catchments. Differences between the land cover of each catchment suggests that despite close proximity between lakes there is considerable landscape heterogeneity due to variations in elevation, geomorphology, ice cover, soil development and wetlands (Section 4.8.1).

Interpretation of water chemistry spot samples suggest that the algal community dominated by the degradation product pheophytin *b* in Disko 1 might be related to glacier inputs as this lake was visibly turbid at the time of sampling (14% of Disko 2 covered by permanent ice and glaciers). All lakes had low DOC which is consistent with poorly developed soils and restricted vegetation development further north than Arctic tree-line. Permafrost and glacier melt cycles are probably key regulators of in-lake water quality, with evidence of a wide outlet at Disko 1 indicative of increased spring meltwater flows.

Nutrient concentrations (TP) were highest in Disko 1 which is probably linked to the cover of permanent ice and glaciers in the catchment, but may also be indicative of increased nutrient cycling from the extensive wetlands in the low gradient U-shaped Blæsedalen valley adjacent to the lake. April sampled under ice nutrients were also high, probably reflecting the low light levels available for production under the ice, although moderate chlorophyll *a* values (Table 4.3) did indicate under-ice algal communities were present.

Carbon isotope ($\delta^{13}\text{C}_{\text{TOC}}$) and C/N distributions were consistent with C_3 land plants in plant samples, while bryophytes had more wide-ranging values reflective of varying carbon concentrating mechanisms present in species of this group (Section 4.6.4, 4.8.2 & Figure 4.16). Despite the complexity, some generalisations can be applied to help interpret down-core changes. Across all sites, terrestrial plants had $\delta^{13}\text{C}_{\text{TOC}}$ values ranging from -30.8‰ to -25.7‰ , whereas algae had slightly higher (less negative) values ranging from -22.6‰ to -20.5‰ . One aquatic macrophyte had a $\delta^{13}\text{C}_{\text{TOC}}$ value close to atmospheric CO_2 , suggesting higher (less negative) $\delta^{13}\text{C}_{\text{TOC}}$ may cautiously indicate macrophyte expansion. C/N ratio was found to be a good discriminator between algae and the more woody vascular plants, but bryophyte ratios ranged widely and some soils had ratios similar to aquatic algae.

A thorough survey of multiple lipid ratios and equations for Disko 2 (Appendix B) was followed by the selection (Section 4.7.2 & Table 4.8) and interpretation (Section 4.8.4) of nine key indexes, subsequently applied in down-core summary diagrams (Figures 5.16 & 5.20). Lipid end-member distributions were diverse and *n*-alkanes are more source specific than *n*-fatty acids or *n*-alkanols as they are less susceptible to diagenesis. Allochthonous soil disturbance is indicated by the C₂₆ *n*-alkane ratio, whereas the CPI 2 index and TAR_{HC} index are all indicators of general plant inputs, with the *P*_{WAX} ratio also suggestive of aquatic macrophytes. The *n*-fatty acid CPI_T index is probably a general indicator of productivity due to its contributions from both algae and aquatic macrophytes, with the long-chain C₃₀ fatty acid indicative of non-woody vascular plants and soils. Due partly to diagenesis, the *n*-alkanol C₁₆ ratio is probably indicative of bulk productivity (including aquatic macrophytes and soils), with the longer chain C₂₄ *n*-alkanol ratio an indicator of both woody and non-woody plant inputs, whereas brassicasterol is primarily an indicator of algae. The catchment survey has helped understand the most appropriate indexes to apply down-core and assist with interpretations.

Chapter 5: Disko 2 – Results and discussion

This section presents (Section 5.1 & 5.2) and discusses (Section 5.3) the results from the analysis of sediment cores from lake Disko 2. At Disko 2 sediments from two overlapping sequences (S1 and S2) from different positions in the basin were analysed and were each found to have individualistic profiles. Sequence 1 cores have been correlated based on a thorough assessment of all overlapping proxies, helping to derive a dated master sequence. Sequence 2 cores were taken from a part of the basin, which appears to be disturbed to a greater extent and so are presented individually as these core drives did not present a convincing overlap. Lake Disko 2 is within a higher elevation (575 m.a.s.l) glacial cirque basin which runs west into the Kuussuaq incised valley, extending to the north of Blæsedalen (Figure 4.6). The lake receives intermittent discharge from a small upstream lake and some small areas of ice cover within the catchment. Within the hydrogeomorphic and lake-landscape framework of this thesis, Disko 2 is presented as the first lake due to its comparative high-elevation and small catchment (Table 4.1).

In the catchment sample survey (see Section 4.8.2 for full interpretation) $\delta^{13}\text{C}_{\text{TOC}}$ ranged between -25.7‰ and -30.5‰ for higher plants in Disko 2 (Table 4.6, Figure 4.14), was -22.6‰ for the ‘algal benthic rock scrape’ sample but much higher (less negative) -6.4‰ in the aquatic macrophyte *Potamogeton* sp. sample. Bryophytes had a broad range from -20.7‰ to -24.6‰ , with soils ranging from -23.7‰ to -26.2‰ . C/N values ranged between ~ 30 and ~ 135 for most catchment plant samples, except those reflective of new growth (e.g. *Salix arctica* leaf fragment or the plant *Chamerion latifolium*). The aquatic macrophyte *Potamogeton* sp. had the lowest C/N ratio (9.7), with similar low values in soil samples (8.3 to 15.1) and a moderate value in the ‘algal benthic rock scrape sample’ (16.8) (Table 4.6 & Figure 4.14). The summer 2013 water pigment spot sample was dominated by chlorophyll *a* and the degradation product pheophytin *b* (Table 4.4).

Key lipid ratios and equations for Disko 2 have been selected (Section 4.7.2 & Table 4.8), interpreted (Section 4.8.4) and are applied in down-core summary diagrams in this chapter (Figures 5.16 & 5.20). To summarise, the C_{26} *n*-alkane ratio is a good indicator of allochthonous soil disturbance, CPI 2 index and TAR_{HC} index can help reconstruct changes in different plant contributions, with the P_{WAX} index additionally able to indicate aquatic macrophyte inputs. For *n*-fatty acids which compared with *n*-alkanes are more susceptible to diagenesis, the CPI_{T} index is probably a general

indicator of bulk productivity together with aquatic macrophytes and soils, whereas the longer chain C₂₄ *n*-alkanol probably indicates both woody and non-woody plant inputs. Brassicasterol in the Disko 2 lake is primarily an indicator of algae.

5.1 Results – Disko 2 Sequence 1

5.1.1 Core correlations

Sequence 1 (S1) (location – Figure 4.6, 4.7 & 4.8A) comprised two overlapping Russian drives (R1-1 and R1-2) and a HON-Kajak (K1) core to recover the upper sediments (Figure 5.1). The S1 sequence was taken from a depth of ~10.6 m as close to the deepest part of the basin (~13.4 m) as coring equipment would allow. The combined sequence was ~178 cm, with further coring prevented by a consolidated stone layer (Figure 5.1). The distance between the two Russian core drives was ~2.5 m.

The sequence comprised primarily homogeneous olive-brown gyttja and brown silt interspersed with rock and grit layers throughout, and in R1-2 thin strands of aquatic macrofossils and rootlets (Figure 5.1). The overlapping of K1 with R1-1 was based on a thorough assessment of all overlapping proxies together with stratigraphy. Overlapping of OM, DW (Appendix C, Figure C1), C/N and $\delta^{13}\text{C}_{\text{TOC}}$ (Appendix C, Figure C2) was regarded as more appropriate than pigments (Appendix C, Figure C3, 4 & 5) which have some differential susceptibility to preservation. In particular, C/N and $\delta^{13}\text{C}_{\text{TOC}}$ showed excellent overlap between R1-1 and K1 (Appendix C, Figure C2).

As less proxy data was available, the overlapping of R1-1 with R1-2 was made on the basis of the transition from brown gyttja to olive-brown gyttja at ~94 cm in the combined sequence (Figure 5.1). A wide range of geochemical proxies were analysed for K1 and R1-1, however only bulk measures were analysed in core R1-2 (OM, DW & CaCO₃) which are presented in Appendix C (Figure C1).

5.1.2 Stratigraphic descriptions

Brown gyttja (Figure 5.1) was present from the bottom of R1-2 (~178 cm) to ~134 cm where thin strands of aquatic macrofossils were present during a distorted change to dark brown silt (between ~125 and ~123 cm). Stone layers were present at ~174 cm and between ~153 and ~149 cm (Figure 5.1 – Image F). The brown silt was also interspersed by grit and gravel layers at ~166 cm, ~163 cm and between ~140 and

~148 cm. There was a small marled change to olive-brown gyttja at ~116 cm after a layer of dense aquatic macrofossil rootlets and orange oxidation-like particles (Figure 6.1 - Image D). Olive-brown gyttja continued until ~106 cm where it changed to brown silt to the top of the core at ~83 cm, with an intermediate fine clay layer at ~97 cm. Core R1-1 comprised olive-brown gyttja with red gravel from the bottom of the core (~116 cm) to ~106 cm where there was a change to brown silt. The brown silt was interspersed by coarse gravel at ~107 cm, ~92 cm, ~80 cm, between ~62 and 70 cm and between ~53 and ~57 cm. A large (~2 cm) red cobble (mudstone) was present at ~67 cm (Figure 5.1 – Image B) and a series of olive-brown marls within brown silt were present between ~61 and ~57 cm depth (Figure 5.1 – Image A). At ~42 cm there was a marled change to olive brown gyttja to the top of the core which was distorted and stretched. The overlapping K1 short core comprised homogenous olive brown gyttja from its base at ~31 cm with visible aquatic plant macrofossils at the sediment-water interface.

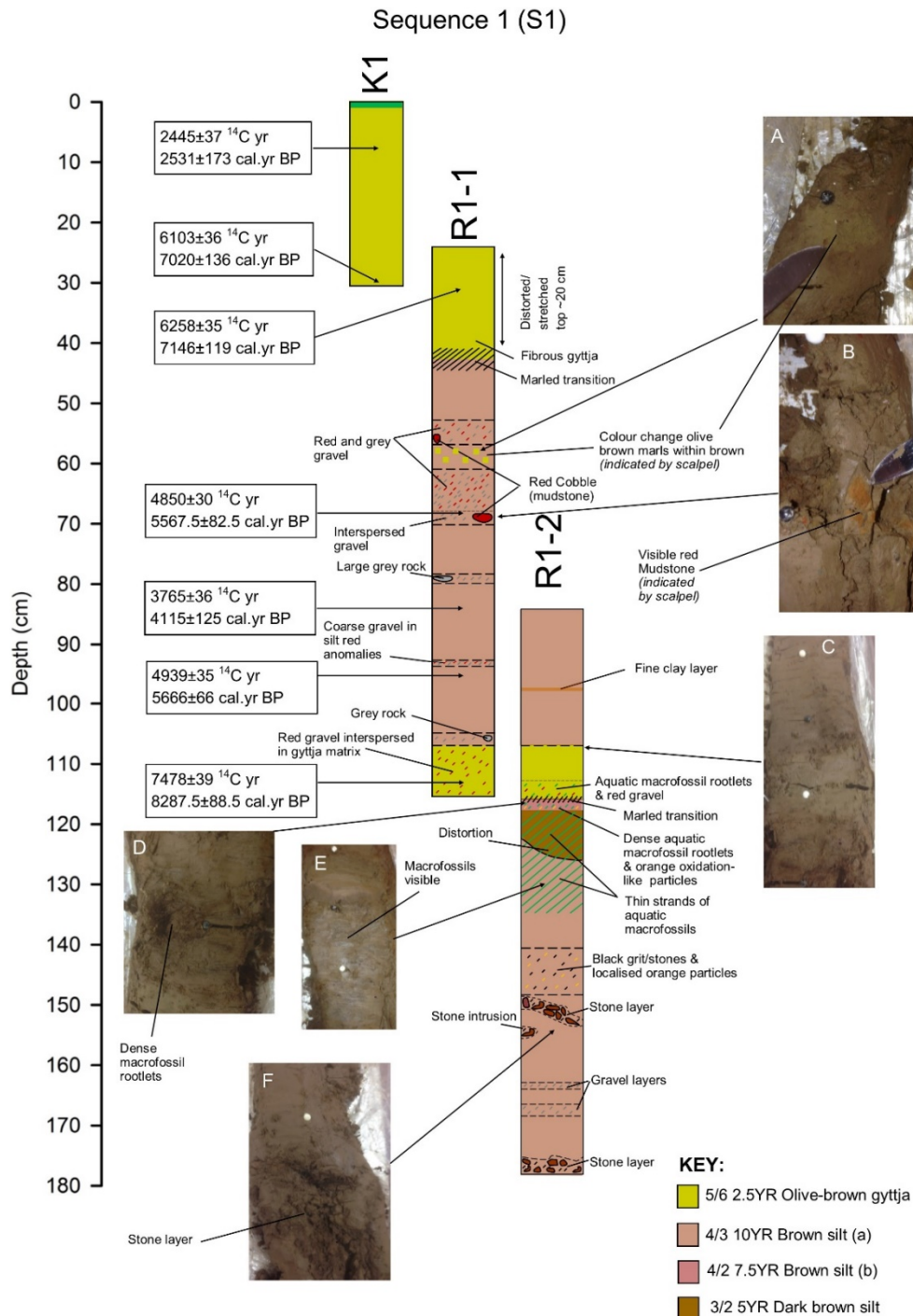


Figure 5.1: Stratigraphy for sequence 1 (S1) comprising lake Disko 2 R1-1 & R1-2 overlapping Russian and K1 HON-Kajak core drives with proposed depth matching sequence. Sediment is described based on identified descriptions provided in the Munsell colour system. Overlapping is based primarily on the geochemistry for K1 with R1-1 until ~31 cm and olive brown gyttja at ~96 – 103 cm for R1-1 with R1-2 (not confirmed with geochemistry). Photographs (A-F) display key macrofossil, clay and grit/stone layers at relevant parts of the sequence. White and black pins reflect 5 and 10 cm depths in core to aid description. Colours and textures used in the diagram are exaggerated to aid interpretation. Radiocarbon dating results are indicated in square boxes with arrows to indicate the source of the sample, with middle calibrated age given (2 σ) together with error range. All dates for S1 were on bulk organic matter.

5.1.3 Radiometric dating and removal of instantaneous events

An age-depth model was developed using a combination of ^{210}Pb , ^{137}Cs and ^{241}Am for the most recent sediments and ^{14}C for deeper sections of the sequence. As sequence 1 (combined K1 and R1-1) was found to have a number of catchment related instantaneous events (Figure 5.1) an adjusted master sequence was devised to remove samples from the stratigraphy associated with these events and derive a more appropriate chronology, taking into account all available evidence. Radiocarbon dates are listed in Table 5.1 and appended to the stratigraphic diagram (Figure 5.1). Corrected radiocarbon dates, together with identification of the master sequence based on an adjusted age-depth model is presented in Table 5.2, with reference to removal of instantaneous events in Figure 5.2. ^{210}Pb activity is plotted against depth (Figure 5.3), compared with ^{137}Cs and ^{241}Am measurements (Figure 5.4) and plotted with sedimentation rate (Figure 5.5). The final age-depth model using both recent and radiocarbon dating is plotted in Figure 5.6 against adjusted depth, following removal of instantaneous events.

Radiocarbon dating (^{14}C)

Radiocarbon dating measurements (n=7) were all made on bulk sediment for Disko 2, sequence 1 as macrofossils in these cores were only aquatic and so would not have yielded enough carbon for reliable dates to be made at high resolution (Table 5.1). To identify if radiocarbon dates were adjacent to instantaneous events, or too old based on recent dating, corrected and calibrated dates were plotted against master sequence depth (Figure 5.2), with dates suitable for inclusion in the model (n=3) listed in Table 5.2. A reservoir offset of 834 years was applied to all bulk dates in Table 5.2 which is based on the terrestrial macrofossil to bulk offset in core D2 R2-2 at 84-85 cm from the same lake (Table 5.3; Section 5.3.2) and is consistent with dating offsets in lakes in the wider area (~850 years in Disko 1). Three radiocarbon dates used in the model were at 77.5-78.5 cm, 88.5-89.5 cm and 104.5-105.5 cm in the adjusted master sequence and are listed in Table 5.2.

Table 5.1: Radiocarbon dating results from Disko 2 (S1) sediment sequences (K1 & R1-1). Analyses prepared at the NERC Radiocarbon laboratory (East Kilbride) and analysed at the SUERC AMS Laboratory under the supervision of Dr L.M. Cisneros-Dozal (sample code SUERC), at the BETA Analytic Laboratory (Miami) under the supervision of Darden Hood (sample code Beta) and at the ¹⁴CHRONO Centre, Queens University Belfast under the supervision of Prof. Paula Reimer (sample code UBA). Calibrations performed in Calib 7.04 using IntCal 13 (Reimer et al., 2013). Carbon isotope values $\delta^{13}\text{C}_{\text{VPDB}}$ analysed using IRMS indicated by *, all other values derived by AMS.

Publication code	Sample identifier	Master sequence depth	Sample type	¹⁴ C Enrichment (% Modern $\pm 1\sigma$)	AMS Radiocarbon Age (years BP $\pm 1\sigma$)	Carbon content (% by wt.)	$\delta^{13}\text{C}_{\text{VPDB}}$ ‰	Max cal age BP (2 σ)	Min cal age BP (2 σ)	Mid cal age BP (2 σ)	Cal age error \pm
SUERC-59781	D2 K1 7-7.5 cm	S1 7-7.5 cm	Bulk sediment	73.76 \pm 0.34	2445 \pm 37	2.1	-26.2	2704	2358	2531	173
SUERC-59784	D2 K1 30-30.5 cm	S1 30-30.5 cm	Bulk sediment	46.78 \pm 0.21	6103 \pm 36	2.3	-22.9*	7156	6884	7020	136
SUERC-59782	D2 R1-1 6-7 cm	S1 30.5-31.5 cm	Bulk sediment	45.88 \pm 0.20	6258 \pm 35	4.3	-25.2*	7265	7027	7146	119
Beta-420931	D2 R1-1 43-44 cm	S1 67.5-68 cm	Bulk sediment	n/a	4850 \pm 30	n/a	-24.4	5650	5485	5568	83
UBA-25170	D2 R1-1 60-61 cm	S1 84.5-85.5 cm	Bulk sediment	62.58 \pm 0.28	3765 \pm 36	n/a	-23.3	4240	3990	4115	125
SUERC-59785	D2 R1-1 71-72 cm	S1 95.5-96.5 cm	Bulk sediment	54.08 \pm 0.24	4939 \pm 35	1.91	-24.9*	5732	5600	5666	66
SUERC-59786	D2 R1-1 89-90 cm	S1 113.5-114.5 cm	Bulk sediment	39.42 \pm 0.19	7478 \pm 39	5.2	-21.8*	8376	8199	8288	89

Table 5.2: Corrected radiocarbon dating results from Disko 2 sediment sequences and selection decision for retention or exclusion from age-depth model. Corrections applied based on the 834 ¹⁴C yr offset between paired macrofossil and bulk date from Disko 2 core R2-2 (sequence 2, Section 5.3.2). Calibrations performed on corrected ¹⁴C yr dates in Calib 7.04 using IntCal 13 (Reimer et al., 2013). The adjusted master sequence depth is provided for dates retained in the model after removal of instantaneous events.

Publication code	Sample identifier	Master sequence depth	AMS Radiocarbon Age (years BP ± 1σ)	AMS Corrected Radiocarbon Age - less 834 ¹⁴ C yr (years BP ± 1σ)	Max cal age BP (2σ) - Corrected	Min cal age BP (2σ) - Corrected	Mid cal age BP (2σ) - Corrected	Cal age error ± - Corrected	Included in the model?	Adjusted Master sequence depth
SUERC-59781	D2 K1 7-7.5 cm	S1 7-7.5 cm	2445±37	1611±37	1594	1406	1500	94	No – too old based on recent dating (²¹⁰ Pb & ¹³⁷ Cs) at 9.75 cm depth.	N/A
SUERC-59784	D2 K1 30-30.5 cm	S1 30-30.5 cm	6103±36	5269±36	6180	5936	6058	122	No – too old & corroborated by date SUERC-59782. (30-31.5 cm removed as age-indicated instantaneous event)	N/A
SUERC-59782	D2 R1-1 6-7 cm	S1 30.5-31.5 cm	6258±35	5424±35	6296	6133	6215	82	No – too old & corroborated by date SUERC-59784. (30-31.5 cm removed as age-indicated instantaneous event)	N/A
Beta-420931	D2 R1-1 43-44 cm	S1 67.5-68 cm	4850±30	4016±30	4567	4419	4493	74	No – too old & within instantaneous event removed from stratigraphy.	N/A
UBA-25170	D2 R1-1 60-61 cm	S1 84.5-85.5 cm	3765±36	2931±36	3179	2692	2936	244	Yes – in stratigraphic order.	77.5-78.5
SUERC-59785	D2 R1-1 71-72 cm	S1 95.5-96.5 cm	4939±35	4105±35	4815	4452	4634	182	Yes – in stratigraphic order.	88.5-89.5
SUERC-59786	D2 R1-1 89-90 cm	S1 113.5-114.5 cm	7478±39	6644±39	7583	7444	7514	70	Yes – in stratigraphic order.	104.5-105.5

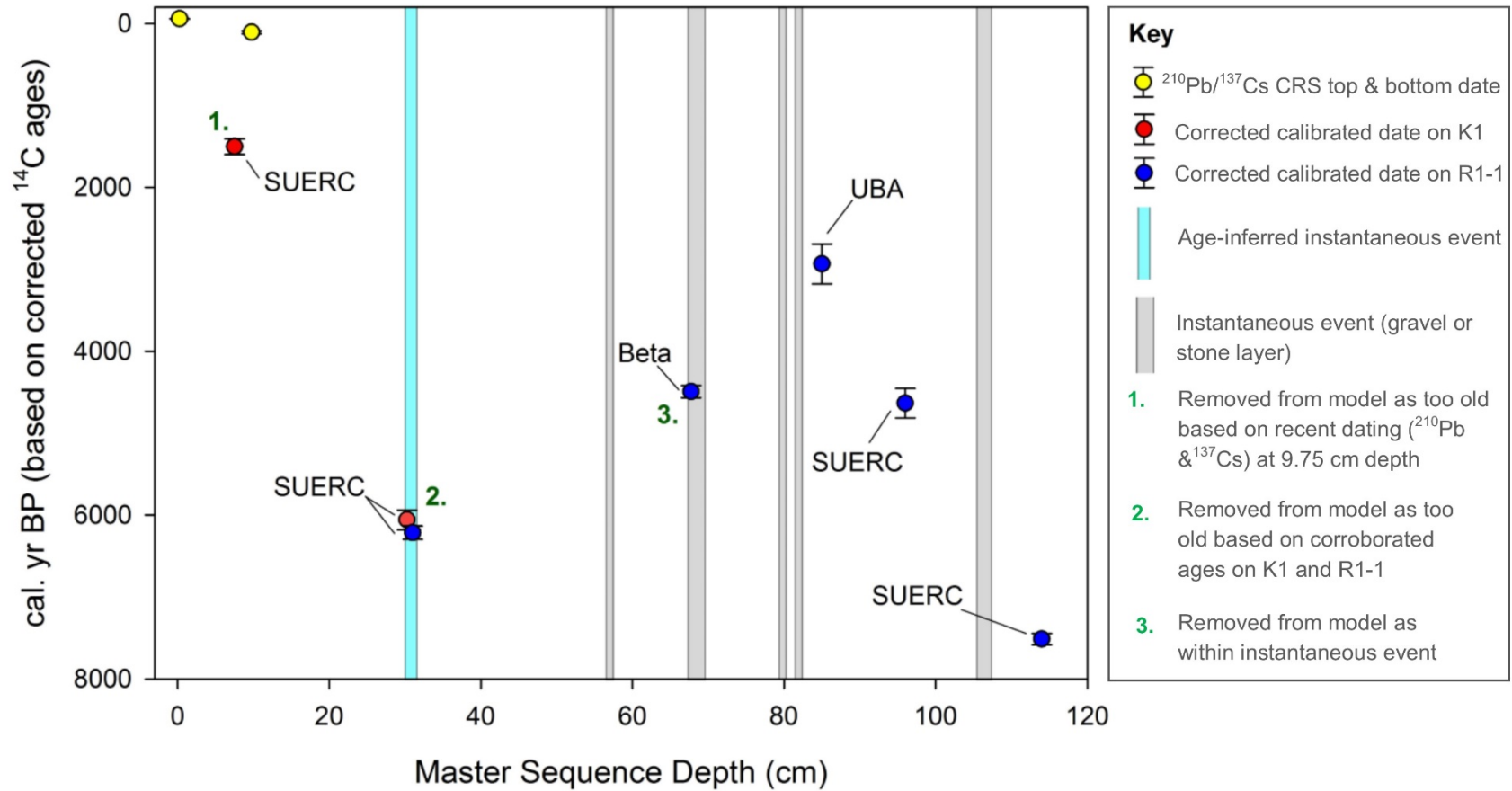


Figure 5.2: Corrected and calibrated ^{14}C dates (cal. yr BP) with top and bottom date from $^{210}\text{Pb}/^{137}\text{Cs}$ CRS recent model plotted against master sequence depth (K1 & R1-1). Corrections applied based on the 834 ^{14}C yr offset between paired macrofossil and bulk date from Disko 2 core R2-2 (sequence 2). Figure provides rationale for removal of dates which are too old or coincident with instantaneous events (coarse particle indicated or corroborated old age-indicated). For calibrated ^{14}C dates (cal. yr BP) laboratory code is appended to the diagram.

Recent dating (^{210}Pb , ^{137}Cs , ^{241}Am)

Supported ^{210}Pb activity generally declined from the top of the Disko 2 short core (K1) throughout the profile, with a slight departure from a monotonic trend at ~ 3.25 cm depth. ^{210}Pb activity declined from ~ 840 Bq/kg $^{-1}$ at ~ 0.25 cm to ~ 160 Bq/kg $^{-1}$ by ~ 3.25 cm, prior to a slight increase to ~ 200 Bq/kg $^{-1}$ by 3.75 cm, followed by a gradual decline to background levels by 9.75 cm. The CRS model was used to develop the age model, due to the slight departure from a monotonic trend (Appleby, 2001), with supported ^{210}Pb measurements modeled from ^{226}Ra . Measurements of ^{137}Cs peaked between ~ 2.75 cm and ~ 3.25 cm at ~ 145 Bq/kg $^{-1}$ acting as a marker for the AD 1963 bomb peak. ^{241}Am measurements also peaked around ~ 1.25 cm and between 2.75 and 4.25 cm, corroborating the ^{137}Cs zone of activity. Since the 1963 bomb peak (^{137}Cs) was slightly offset from the expected modelled ^{210}Pb , a corrected CRS date was adjusted to take into account the age of 1963 at ~ 3.75 cm (Figure 5.5). The sedimentation rate peaked slightly at 55 yr before coring (2013) from 0.01 g cm $^{-2}$ yr $^{-1}$ to 0.03 g cm $^{-2}$ yr $^{-1}$, before plateauing around ~ 0.02 g cm $^{-2}$ yr $^{-1}$. Only top (0.25 cm) and bottom (9.75 cm) dates were included from the corrected CRS model (Figure 5.5) in the final age-depth model (Figure 5.6).

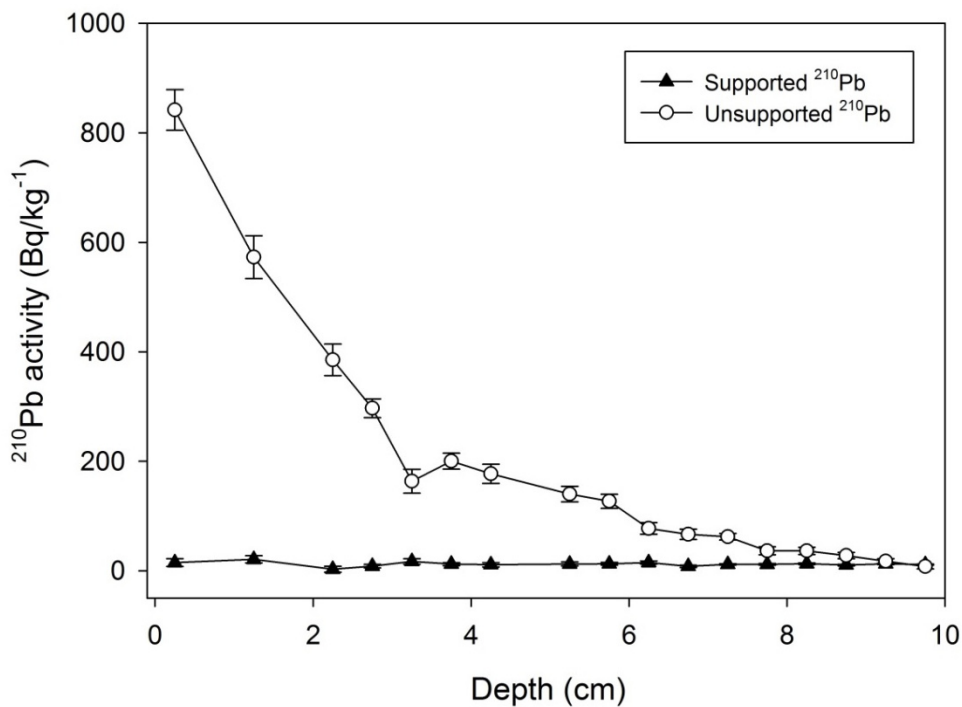


Figure 5.3: ^{210}Pb supported and unsupported activity plotted against depth for the Disko 2 K1 short core. Standard errors (1σ) were calculated from the counting statistics. Samples analysed by Dr Handong Yang, Environmental Change Research Centre, UCL, London.

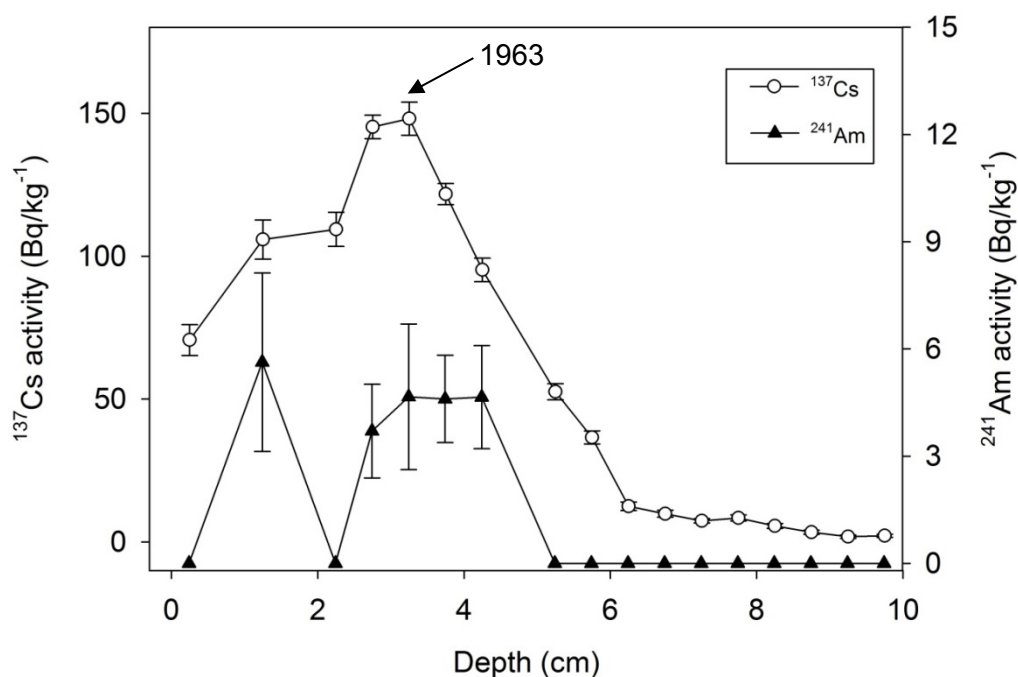


Figure 5.4: ^{137}Cs and ^{241}Am activity plotted against depth for the Disko 2 K1 short core. Standard errors (1σ) were calculated from the counting statistics. Samples analysed by Dr Handong Yang, Environmental Change Research Centre, UCL, London.

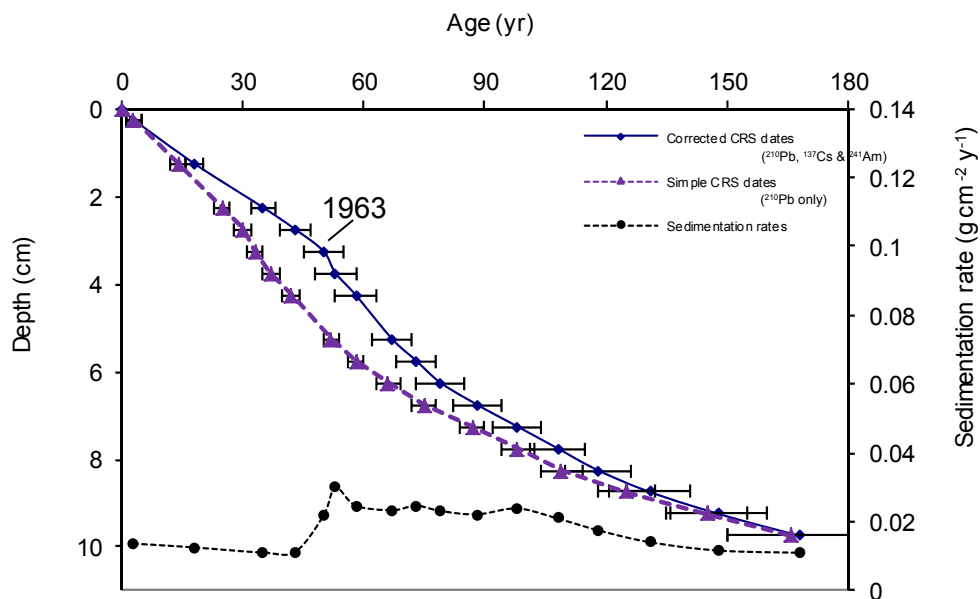


Figure 5.5: Age depth models and sedimentation rates for the Disko 2 K1 short core. The simple CRS (constant rate of supply) model derived from ^{210}Pb dating only is indicated by pink triangles. The corrected CRS (constant rate of supply) model is derived from a ^{210}Pb base, with manual splice corrections based on the ^{137}Cs 1963 peak indicated by purple circles. The general period of increased activity in ^{241}Am is between 2.75 and 4.25 cm (Figure 5.4). Samples analysed and composite plot produced by Dr Handong Yang, Environmental Change Research Centre, UCL, London.

Age-depth model

The final age-depth model (Figure 5.6) was produced using Bayesian statistics in Bacon v 2.2 (Blaauw and Christen, 2011, 2013) in the R programming language. The model is a composite of the corrected CRS dates from the K1 short core (top and bottom dates only) from Figure 5.5 and the three corrected bulk ^{14}C dates (calibrated to cal. yr BP) once dates coincident with instantaneous events had been removed (Table 5.2 and Figure 5.2). The widest 95% confidence interval was present between the final corrected ^{210}Pb date and the first corrected ^{14}C date at ~78 cm in the adjusted master sequence, however, below this the 95% confidence interval was narrower, accounting for the more closely spaced ^{14}C dates. From the final date (104.5-105.5 cm) to the bottom of the adjusted master sequence (107 cm) the model was extrapolated. Model fitting included the use of 22 sections within the calculation.

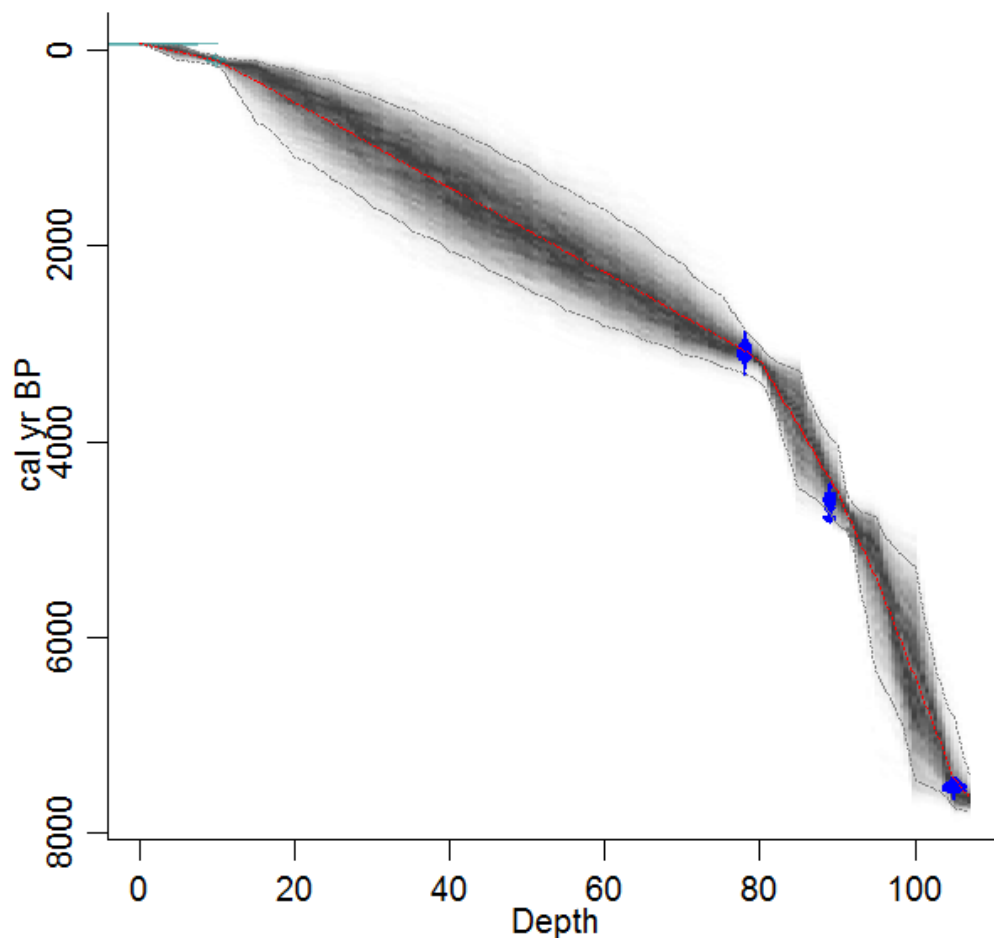


Figure 5.6: Age-depth model for Disko 2 S1 combined HON-Kajak (K1) and Russian (R1-1) adjusted master sequence. Produced using Bayesian statistics in Bacon v2.2 (Blaauw and Christen, 2011, 2013). Dates in green at shallow depths are from recent ^{210}Pb , ^{137}Cs and ^{241}Am radiometric dating (top and bottom dates only) on the K1 short core. All ^{14}C dates (blue) were calibrated using IntCal 13 (Reimer et al., 2013), with the shape of the date reflecting the proportional likelihood of an age falling within the relevant part of the calibration curve. All dates are on bulk sediment due to the generally low carbon content of the core sequence and absence of terrestrial macrofossils, corrected by using an age of 834 years based on the offset between macrofossil and bulk dates on sequence 2 (D2 R2-2) presented in section 5.2.3. The red line indicates the mean age-depth model selected, with the grey fill indicating the 95% confidence interval age-range. For model fitting 22 sections were included in the calculation.

5.1.4 Disko 2 Sequence 1– pigment results

The final combined stratigraphic pigment diagrams for Disko 2 S1 include K1 samples from 0 to 28.25 cm and R1-1 samples from 29 to 107 cm in the adjusted master depth (Figure 5.7). The plot was split into 5 zones using optimal partitioning in Zone 1.2 (Juggins, 1991) from 107-98.5 cm (E), 98.5-39.5 cm (D), 39.5-24.5 cm (C), 24.5-8.5 cm (B) & 8.5-0 cm (A). All pigments are expressed against TOC.

Zone E

Although variable, pigment concentrations in zone E were relatively high for diatoxanthin, alloxanthin, diadinoxanthin, lutein-zeaxanthin, canthaxanthin and pheophorbide *a*. There was a generally decreasing trend from 107 cm to 98.5 cm, which was particularly pronounced in pheophorbide *a*. Concentrations were relatively low in fucoxanthin, okenone and chlorophyll *a*.

Zone D

A clear group of pigments including alloxanthin, diadinoxanthin, lutein-zeaxanthin, canthaxanthin and pheophorbide *a* displayed a marked decrease in concentration into zone D. For example, alloxanthin (cryptophytes) decreased from >50 nmol pig g⁻¹ TOC in zone E to <25 nmol pig g⁻¹ TOC between 90 and 80 cm depth. In contrast, pheophytin *a* displayed a marked increase from ~1,250 nmol pig g⁻¹ TOC in zone E to a peak of >1,600 nmol pig g⁻¹ TOC in zone D at ~85 cm depth. β -carotene had a intermittent variable trend and was variable to ~50 cm in zone D.

Zone C

There was a slight increase in zone C in alloxanthin, diadinoxanthin, lutein-zeaxanthin and canthaxanthin in line with changes in TOC. Fucoxanthin, okenone, chlorophyll *a* and β -carotene were all low and stable in zone C. There was a marked decrease in pheophytin *a* from ~1000 nmol pig g⁻¹ TOC in zone D to fluctuations around ~750 nmol pig g⁻¹ TOC in zone C. Pheophorbide *a* was higher in zone C (~750 nmol pig g⁻¹ TOC) compared with the previous zone, where this pigment was intermittent.

Zone B

Concentrations of fucoxanthin, diatoxanthin, okenone, chlorophyll *a*, β -carotene and pheophorbide *a* were all very low throughout zone B. There was a pronounced peak in alloxanthin, diadinoxanthin, lutein-zeaxanthin and canthaxanthin around ~18 cm depth. Pheophytin *b*, pheophytin *a* and pyropheophytin *a* were all lower in concentration than

the previous zone. Pyropheophytin *a* declined to its lowest concentration (~ 250 nmol pig g⁻¹ TOC) in zone B.

Zone A

There were clear increases in pigment concentration in fucoxanthin, diadinoxanthin, pheophytin *b*, chlorophyll *a*, and pheophytin *a* in zone A, peaking in the uppermost samples. The increase in fucoxanthin was pronounced increasing from a minimum of <50 nmol pig g⁻¹ TOC to $>1,900$ nmol pig g⁻¹ TOC at the top of the core. Pigments diatoxanthin, alloxanthin, lutein-zeaxanthin, canthaxanthin, β -carotene, pyropheophytin *a* and pheophorbide *a* did not show consistent increases. A pulse was present in okenone at ~ 1.75 cm to >250 nmol pig g⁻¹ TOC.

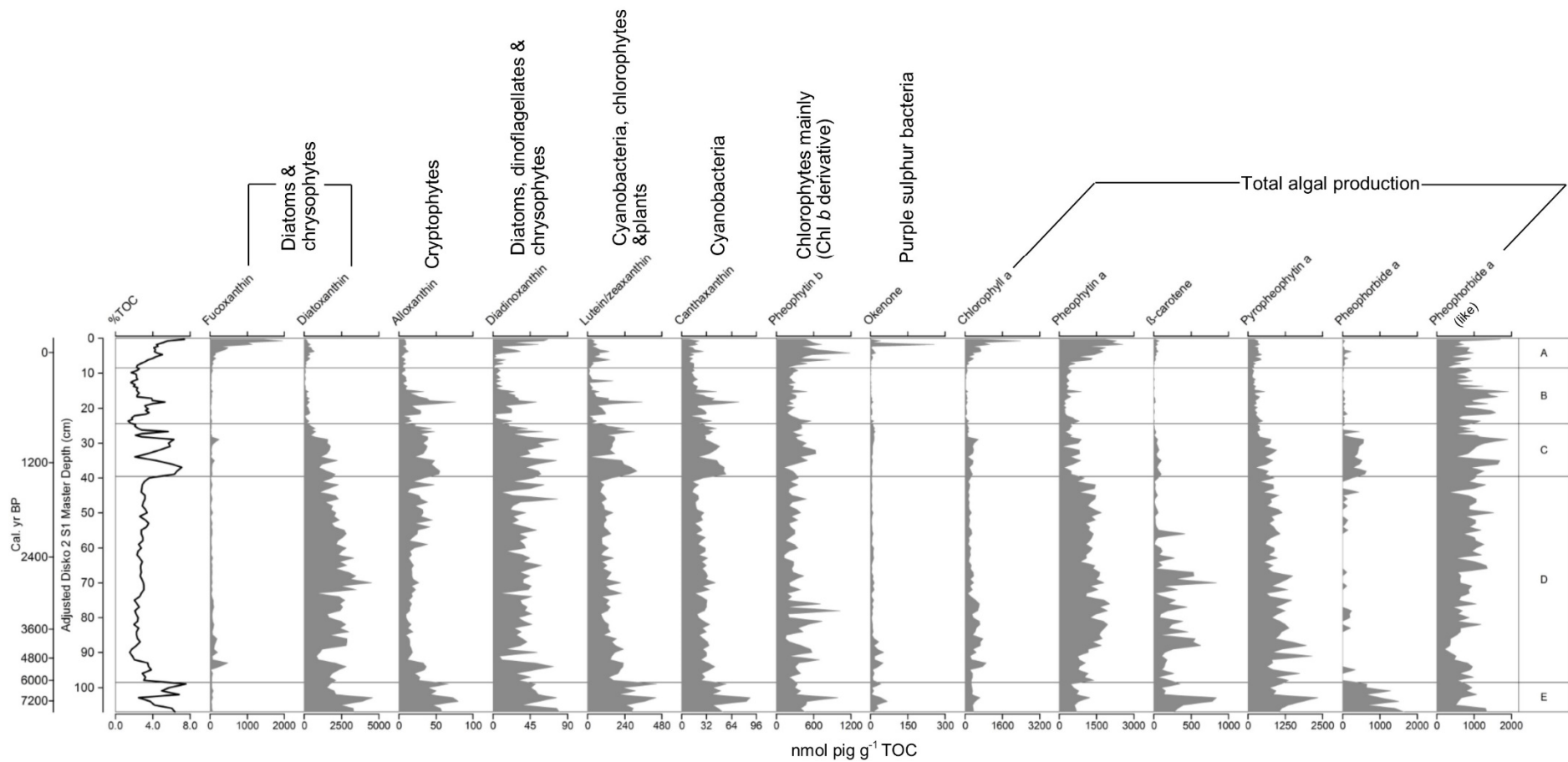


Figure 5.7: Stratigraphic plot for Disko 2 S1 pigment concentrations expressed against TOC. Plotted against (S1) master depth and age (cal. yr BP). Zones (A, B, C, D & E) were based on optimal partitioning resulting in 5 zones. Zone calculations included all variables in the figure above in addition to those sampled at full resolution CaCO_3 , OM, $\delta^{13}\text{C}_{\text{TOC}}$, TOC, N & C/N.

5.1.5 Exploratory statistics – Disko 2 Sequence 1

The Disko 2 S1 PCA ordination biplot with pigments (as species) plotted against samples (both log transformed, centred and standardised) had eigenvectors of 0.46 for PCA axis 1 and 0.20 for PCA axis 2 (Figure 5.8). Pigments were widely distributed, particularly in the two left hand quadrants. Pyropheophytin *a*, okenone and diatoxanthin were the three pigments most closely correlated with PCA axis 1, associated with change in zones D and E. Pheophorbide *a* and the pheophorbide *a*-like compound (pheophorbide *a*2) were the two pigments correlated with PCA axis 2, associated with change in zone C. Pigments mid-way between axes in the lower left quadrant included diadinoxanthin, lutein-zeaxanthin, canthaxanthin and alloxanthin associated with change in zones C and E. Pigments mid-way between axes in the upper left quadrant included β -carotene, chlorophyll *a*, pheophytin *a* and fucoxanthin associated with change in zone D. Both axes orientated away from samples in zone A and B.

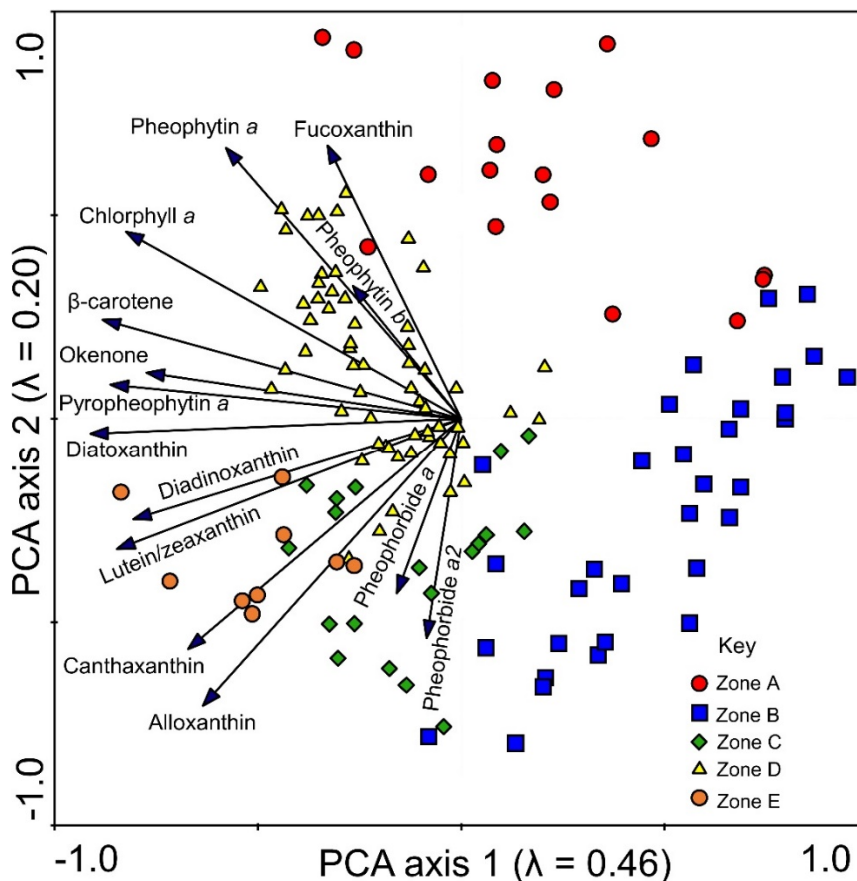


Figure 5.8: PCA ordination biplot for Disko 2 S1. Complete with pigments (as species) plotted against samples. Sample zone origins are listed in the figure key. Eigenvectors are 0.46 for PCA 1 and 0.20 for PCA axis 2. PCA was selected as DCA had low gradient lengths < 2.5 (DCA gradient length 1 = 0.57, DCA gradient length 2 = 0.54).

5.1.6 Disko 2 Sequence 1 – geochemical data, pigment ratios and PCA scores

Pigment trends were summarised using principal components analysis (PCA) on $\log(x+1)$ transformed data, standardised and centred and standardised, (Figure 5.9) as detrended correspondence analysis (DCA) produced gradient lengths <2.5 . Geochemical data (TOC, N, C/N and $\delta^{13}\text{C}_{\text{TOC}}$) were presented against pigment ratios to explore groups with the clearest response.

Zone E

TOC was relatively high reaching $\sim 7.5\%$ at ~ 99 cm depth following a drop to $<3\%$ at ~ 103 cm depth, with N following a similar trend to TOC. CMAR (carbon mass accumulation rate) decreased from ~ 6 to $2 \text{ g C m}^{-2} \text{ yr}^{-1}$. C/N ratio was relatively low, rising from ~ 8 at the base of the core to ~ 9 by 99 cm depth. $\delta^{13}\text{C}_{\text{TOC}}$ was relatively high ($\sim -20\text{‰}$) and both pigment PCA axis 1 and 2 were negative (<0). The chlorophyll *a*: pheophytin *a* ratio was stable (~ 0.5), with similar low values in all other ratios.

Zone D

There was a marked decline in TOC to 3% at the start of the zone (99 cm) reducing to $\sim 1.5\%$ by 90 cm, followed by a gradual increase to $\sim 3.5\%$ by 40 cm depth. N followed a trend similar to TOC, from 0.2% at 90 cm to 0.4% by 40 cm depth. CMAR increased from $\sim 2 \text{ g C m}^{-2} \text{ yr}^{-1}$. C/N ratio varied between 8 and 10.5 with the highest values reached at ~ 65 cm depth. $\delta^{13}\text{C}_{\text{TOC}}$ displayed a marked decrease from the previous zone maximum of -21‰ to $\sim -27\text{‰}$ by ~ 81 cm, followed by a stepped increase to $\sim -22\text{‰}$ by the top of the zone (~ 39.5 cm). Although variable, PCA axis 1 increased slightly from a maximum of -1.2 at 94 cm depth to a maximum of ~ 0.5 by 41 cm depth. PCA axis 2 increased more markedly from -1.3 at the top of the previous zone to a maximum of 1.5 by ~ 89 cm, followed by a gradual decline to ~ 0 by the top of the zone. Ratios chlorophyll *a*: pheophytin *a*, fucoxanthin: diatoxanthin and alloxanthin: diatoxanthin were comparatively low throughout this zone. There were some increases in the ratio of alloxanthin: chlorophyll *a* above ~ 74 cm depth.

Zone C

There were three pulses in TOC and N in zone C around 37 cm, 29 cm and 27 cm depth. TOC ranged from 2-7% and N ranged from 0.2 to 0.8 %. C/N ratio ranged between 8 and 10 throughout the zone and $\delta^{13}\text{C}_{\text{TOC}}$ was higher than the previous zone

reaching -20% at 38 cm and 27 cm, in a similar pattern to TOC. There was a peak in CMAR to $\sim 14 \text{ g C m}^{-2} \text{ yr}^{-1}$ at ~ 29 cm depth, followed by a return to previous levels ($\sim 6 \text{ g C m}^{-2} \text{ yr}^{-1}$). Both PCA axis 1 and 2 were variable, with a notable decrease in PCA 2 to -1.5 at ~ 37 cm depth coincident with increases in TOC. A pulse in chlorophyll *a*: pheophytin *a* ratio at ~ 31 cm depth was clearly marked together with a slight general increase in the ratio throughout the zone. Both fucoxanthin: chlorophyll *a* and fucoxanthin: diatoxanthin ratios were low. The alloxanthin: diatoxanthin ratio was slightly higher above 27.5 cm, with similar trends in the ratio of alloxanthin: chlorophyll *a*.

Zone B

TOC increased from $<1.4\%$ at the start of the zone (24 cm) to a pulse of $\sim 5\%$ at 18.25 cm, followed by a decline to $\sim 2\%$ by the top of the zone (8.5 cm). N followed a similar trend, ranging from a minimum of 0.16% to a maximum of 0.5% . CMAR increased slightly to $\sim 11 \text{ g C m}^{-2} \text{ yr}^{-1}$ by the top of the zone (8.5 cm). C/N ratio was high at the start of the zone (~ 24 cm) reaching >12 with values ranging between 9 and 11 above 21 cm. Similar to TOC, $\delta^{13}\text{C}_{\text{TOC}}$ peaked around 18 cm to -20% , from a minimum of -24% at ~ 24 cm and a further minimum of -24% at the top of the zone (8.75 cm). Both PCA 1 and 2 were variable, but featured declines around ~ 18 cm prior to increases by the top of the zone (8.75 cm). The ratio of chlorophyll *a*: pheophytin *a* was low and stable throughout the zone, with only minor increases in fucoxanthin, but there was a marked increase in the ratios of fucoxanthin: chlorophyll *a*, alloxanthin: diatoxanthin and alloxanthin: chlorophyll *a*.

Zone A

Clear increases in TOC were present increasing from $\sim 2\%$ at 8.5 cm to $\sim 8\%$ by the top of the core. N followed a similar trend increasing from 0.2 to $\sim 1\%$ by 0 cm. CMAR reached its highest levels in zone A, fluctuating between ~ 7 and $18 \text{ g C m}^{-2} \text{ yr}^{-1}$. There was a clear decline in C/N ratio from a pulse of ~ 12 at 7 cm depth to ~ 7.5 above 2.5 cm. $\delta^{13}\text{C}_{\text{TOC}}$ featured a clear decline from -24% at ~ 9 cm to -28% from ~ 6 cm to the top of the core. PCA 1 displayed a clear decline (to ~ 0), with a clear increase present in PCA 2 to the top of the core (to ~ 2.5). Chlorophyll *a*: pheophytin *a* was relatively stable, although there were clear and pronounced peaks in the ratio of fucoxanthin: chlorophyll *a* and fucoxanthin: diatoxanthin at the top of zone A. Both the ratios of alloxanthin: diatoxanthin and alloxanthin: chlorophyll *a* were lower than the previous zone.

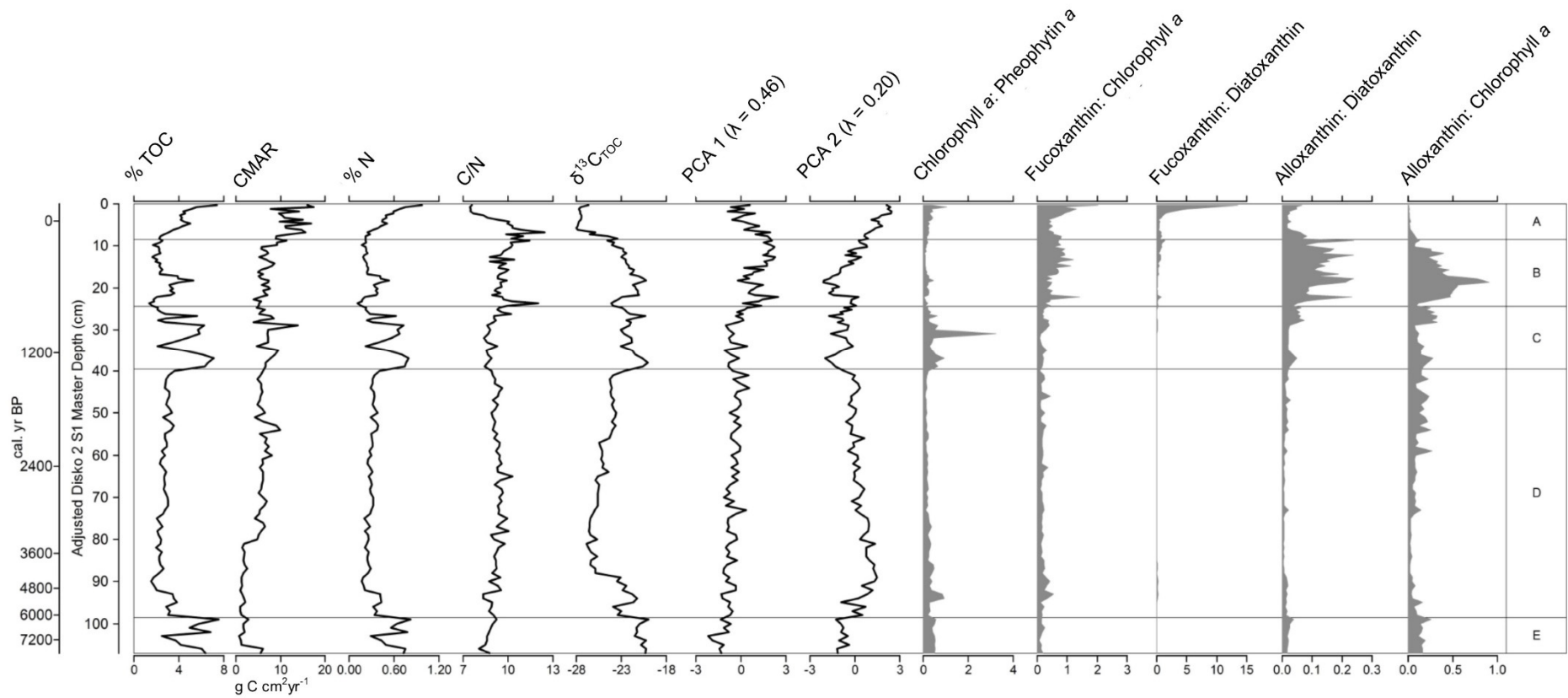


Figure 5.9: Stratigraphic sequence 1 (S1) geochemical data (TOC, N, C/N, $\delta^{13}\text{C}_{\text{TOC}}$), carbon mass accumulation rate (CMAR) pigment PCA 1 ($\lambda = 0.46$) and PCA 2 ($\lambda = 0.20$) scores and key pigment ratios. Both the sequence 1 (S1) adjusted master depth and age model (cal. yr BP) are provided.

5.1.7 Disko 2 S1 compound-specific fatty acid (FAMES) $\delta^{13}\text{C}$ results

Figure 5.10 presents the compound specific fatty acid (FAMES) analysis plotted against high resolution $\delta^{13}\text{C}_{\text{TOC}}$ for Disko 2 S1. The dominant compound in all samples was the C_{16} fatty acid. For bulk $\delta^{13}\text{C}_{\text{TOC}}$ the analytical precision was to within 0.1 ‰, whereas the analytical precision for $\delta^{13}\text{C}_{\text{FAMES}}$ was to within 0.5 ‰ (SD) based on duplicate analyses. Only compound-specific data points with duplicates <0.5 SD are plotted, which accounts for variations in sample resolution in the plot. The specific $\delta^{13}\text{C}$ values between $\delta^{13}\text{C}_{\text{TOC}}$ and $\delta^{13}\text{C}_{\text{FAMES}}$ differed. For example, $\delta^{13}\text{C}_{\text{TOC}}$ ranged from a max of -20 ‰ to a minimum of -26.9 ‰ (a difference of 6.9 ‰). However, the largest difference was in the $\delta^{13}\text{C}_{21:0}$ fatty acid which ranged from a maximum of -30.1 ‰ to a minimum of -45.6 ‰ (a difference of 15.6 ‰). In contrast, the $\delta^{13}\text{C}$ value of the $\text{C}_{17:0}$ fatty acid ranged from a maximum of -28.1 ‰ to a minimum of -34.2 ‰ (a difference of 6.1 ‰).

The trends in $\delta^{13}\text{C}_{\text{FAMES}}$ in many compounds mirrored $\delta^{13}\text{C}_{\text{TOC}}$, with higher values in zones B, C and E, compared with zones A and D. A similar trend to $\delta^{13}\text{C}_{\text{TOC}}$ was found to be present in $\delta^{13}\text{C}_{14:0}$, $\delta^{13}\text{C}_{15:0}$, $\delta^{13}\text{C}_{16:0}$, $\delta^{13}\text{C}_{17:0}$, $\delta^{13}\text{C}_{20:0}$, $\delta^{13}\text{C}_{21:0}$, $\delta^{13}\text{C}_{24:0}$, $\delta^{13}\text{C}_{26:0}$, and $\delta^{13}\text{C}_{28:0}$. The remaining $\delta^{13}\text{C}$ values of $n\text{-C}_{16:1a}$ monounsaturated a, $n\text{-C}_{18:1a}$ monounsaturated a and $n\text{-C}_{18:0}$ all featured variable profiles.

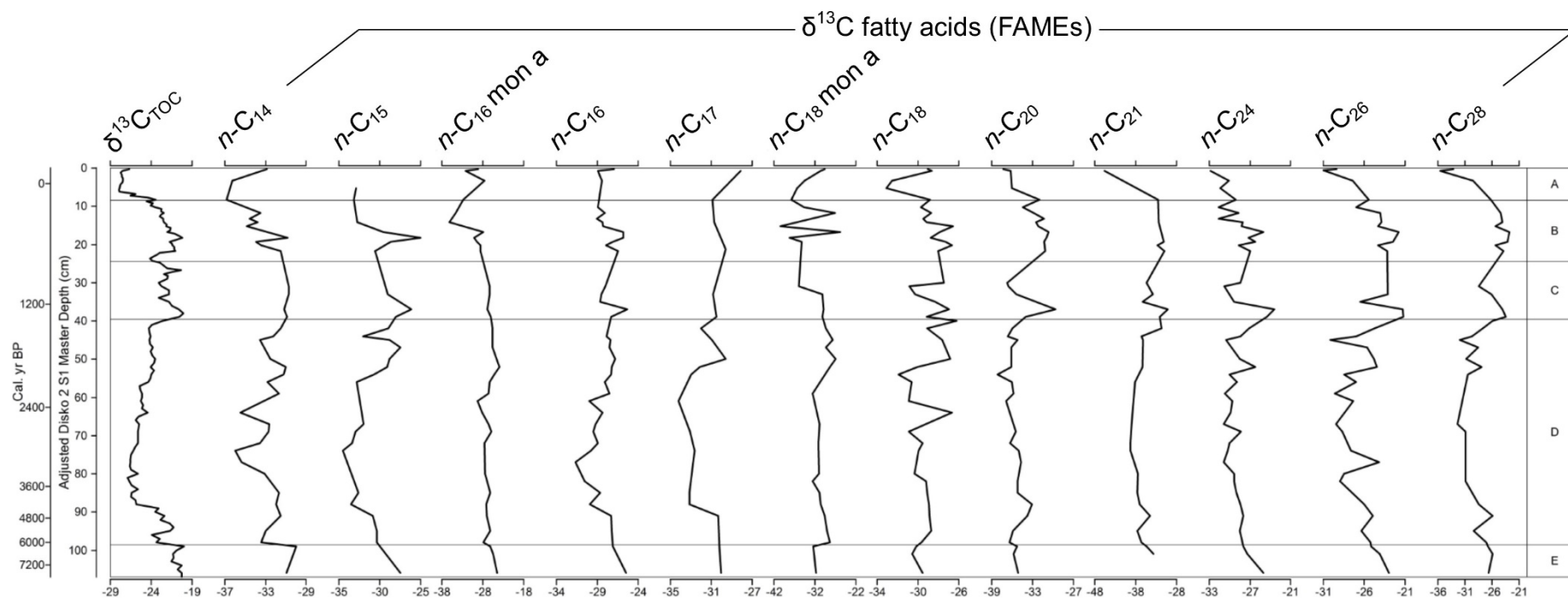


Figure 5.10: Stratigraphic sequence 1 (S1) Disko 2 compound specific fatty acid (FAMES) $\delta^{13}\text{C}$ data plotted against $\delta^{13}\text{C}_{\text{TOC}}$. FAMES derived using BF_3 in methanol ($\delta^{13}\text{C} = -42.85 \text{ ‰}$) with a mass balance correction applied from Boschker et al. (1999) following Rieley (1994). Both the sequence 1 (S1) adjusted master depth and age model (cal. yr BP) are plotted. Compound-specific analyses analysed in duplicate. Only compound-specific data points with duplicates <0.5 SD are plotted, which accounts for the varying sample resolution between compounds. Compounds with insufficient $\delta^{13}\text{C}$ data points to derive clear trends are not presented. Ratios presented in Section 2.2.5.

5.1.8 Disko 2 S1 lipid biomarker ratios – *n*-alkanes

The *n*-alkane equations are presented in Figure 5.11 together with ratios of selected *n*-alkanes versus total saturated *n*-alkanes that displayed key changes. The Carbon Preference Index 2 (CPI 2) of Marzi et al. (1993) displayed a pronounced decrease in zone E (from ~6 to ~3) followed by relatively stable values (~3) in zone D and further peaks at ~40 cm and ~18 cm depth. Higher CPI 2 values generally indicate fresher, less petrogenic inputs. In contrast, the Terrigenous to Aquatic Ratio (TAR_{HC}) of Bourbonniere and Meyers (1996a) was low in zone E (~6), but increased in zone D. Higher TAR_{HC} values generally indicate increased land plant contributions. There were fluctuations in TAR_{HC} around ~33 cm and a pulse to ~30 at 13 cm depth, prior to a decrease to the top of the core. The aquatic macrophyte ratio (P_{aq}) of Ficken et al. (2000) was generally very low (<1), although was slightly higher at two pulses around 40 cm and 18 cm depth. Higher P_{aq} values have in some studies been found to indicate increased submerged and floating macrophytes. The index of waxy *n*-alkanes to total hydrocarbons (P_{WAX}) was slightly lower at the base of zone E (~0.6), compared with the peak of 0.8 at ~75 cm in zone D. There were sharp declines in the P_{WAX} index to ~0.4 at 39 cm and 18.25 cm depth, prior to ~0.8 by the top of the core in zone A. Higher values generally indicate greater contributions from terrestrial plants and emergent macrophytes.

The ratio of the *n*-C₁₇ *n*-alkane to total saturated *n*-alkanes was characterised by a pulse to ~2.5 in zone E and a further pulse to ~3.6 in zone A with more stable values in other zones ranging between 0.1 and 1.5. In contrast, the C₁₉ *n*-alkane ratio declined from zone E to D until ~55 cm where it increased to a peak of ~3.5 in zone C at ~35 cm depth. There was a decline in *n*-C₁₉ values by ~13 cm (to ~0.9) prior to a pulse in zone A at ~3 cm depth (to ~3.5). The *n*-alkane *n*-C₂₄, *n*-C₂₆, *n*-C₂₉ and *n*-C₃₁ compounds all featured similar trends with slightly lower values in zone E to zone D and a series of pulses at 33 cm, 20 cm and 13 cm depths.

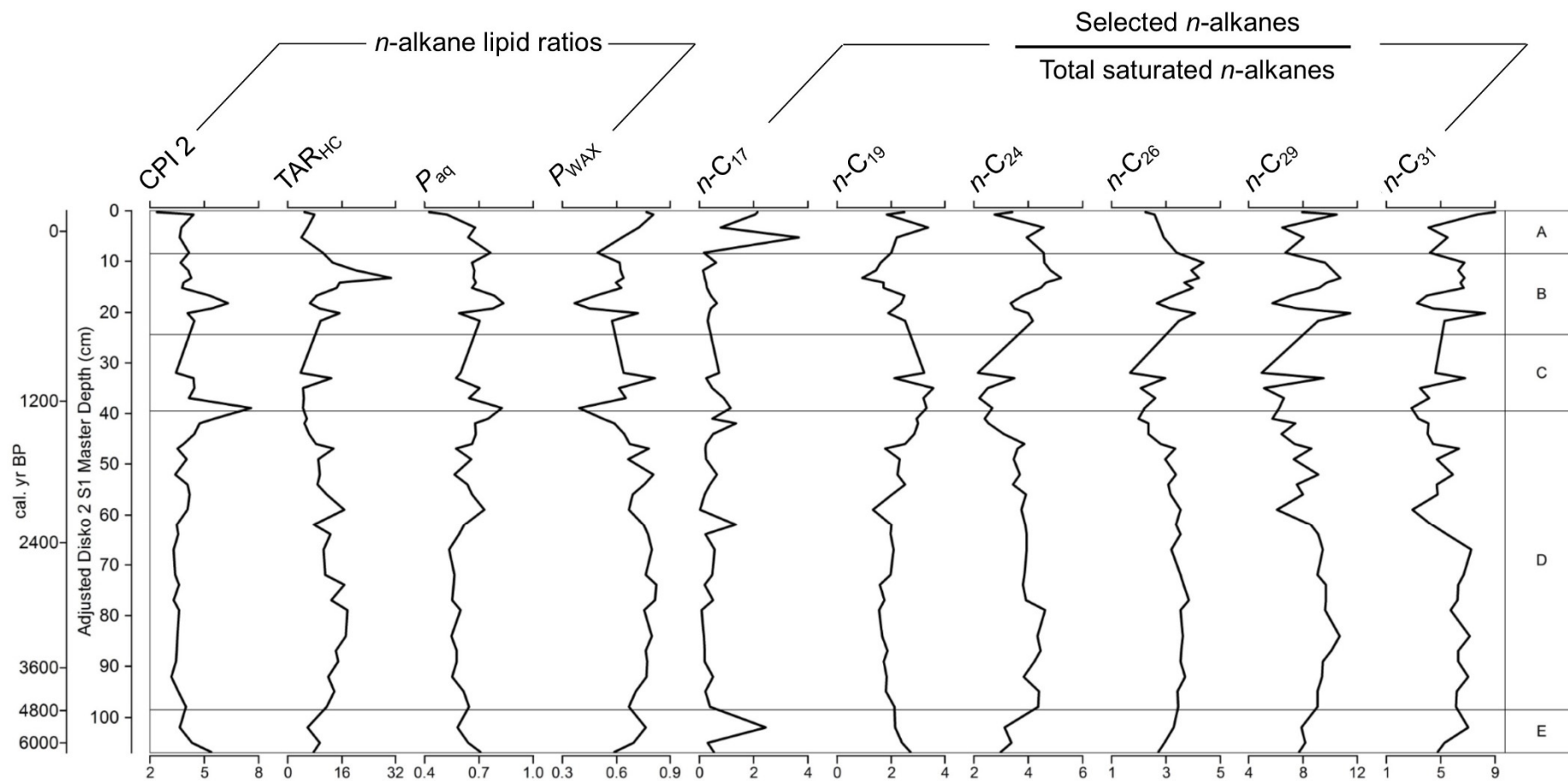


Figure 5.11: Stratigraphic Disko 2 sequence 1 (S1) *n*-alkane lipid biomarker data. Variables include key lipid ratios and ratios of selected *n*-alkanes to total saturated *n*-alkanes. Both the sequence 1 (S1) adjusted master depth and age model (cal. yr BP) are plotted. Only ratios with visible trends (changes) are presented. Ratios presented in Section 2.2.5.

5.1.9 Disko 2 S1 lipid biomarker ratios – *n*-fatty acids (FAMES)

The *n*-fatty acids equations are presented in Figure 5.12 together with selected *n*-fatty acids (FAMES) versus total saturated *n*-fatty acids that displayed key changes. Higher fatty acid CPI indexes generally indicate fresher, less petrogenic inputs although the diagenetic susceptibility of fatty acids can make this index challenging to interpret. The carbon preference index (CPI_L) of lower molecular weight compounds (Matsuda and Koyama, 1977) primarily fluctuated around ~15, with the exception of an intermittent variable increase to ~35 at ~35 cm. The CPI_H index of higher molecular weight compounds displayed a clear decrease in zone E from ~10.5 at 106 cm to ~7 by zone D, followed by fluctuations between ~5 and 9 in zones C and B, increasing to ~12 by the top of zone A. The CPI_T index of the entire range of *n*-fatty acid saturated hydrocarbons was highly variable, with a slight increasing trend from zone E to D. Zone A featured a clear increase in CPI_T to ~25 by the top of the core. In contrast, the terrigenous to aquatic fatty acid ratio (TAR_{FA}) featured a slight decline from a peak of (~ 0.7) in Zone E to fluctuations around ~0.4 throughout zone B. In zone B there were clear pulses in TAR_{FA} at ~12 cm and ~19 cm depth (to ~1.4). Higher values of the TAR_{FA} index generally suggest increased terrestrial contributions, although fatty acids can be susceptible to diagenesis.

The ratio of the C_{18:1a} monounsaturated (a) compound to the C_{18:0} saturated compound (C_{18:1a}/C_{18:0}) was dominated by a clear increase to ~12.5 in zone A (~ 5 cm) compared with < 0.2 in all other zones. The C_{16:1a} monounsaturated a ratio was also characterised by a peak in zone A, reaching ~112 by ~5 cm and ~280 by the top of the core. The C_{16:1d} monounsaturated d ratio reached relatively high ratios in zone B at ~20 cm, ~15 cm and ~8 cm compared with low detection in the previous zones.

The ratio of *n*-C₁₄ fatty acid to total saturated *n*-fatty acids was characterised by a peak in zone D between ~80 and ~55 cm and a further peak in zone A to ~24 at ~3 cm depth. The *n*-C₁₆ fatty acid was characterised by fluctuations between ~20 and ~50 and a clear increase in zone A to ~65 by the top of the core. The fatty acid *n*-C₂₄, *n*-C₂₆, *n*-C₂₈ and *n*-C₃₀ compounds all featured similar trends, changing from higher values in zone E to lower values in zone D, prior to intermittent variable increases in zone C and B, prior to a decline in zone A to the top of the core.

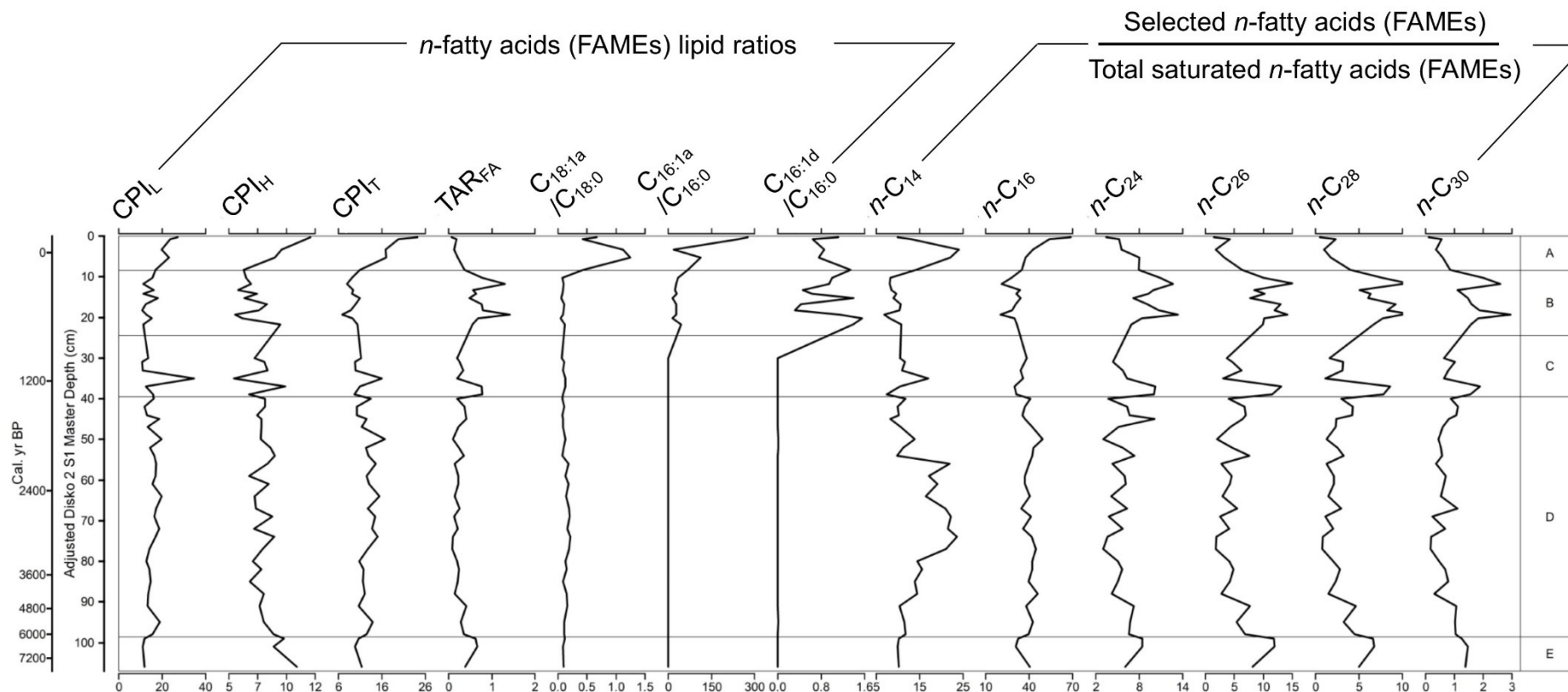


Figure 5.12: Stratigraphic Disko 2 sequence 1 (S1) *n*-fatty acid (FAMES) lipid biomarker data. Variables include key lipid ratios and ratios of selected *n*-fatty acids (FAMES) to total saturated *n*-fatty acids (FAMES). Both the sequence 1 (S1) adjusted master depth and age model (cal. yr BP) are plotted. Only ratios with visible trends (changes) are presented. Ratios presented in Section 2.2.5.

5.1.10 Disko 2 S1 lipid biomarker ratios – *n*-alkanols, sterols and ketones

Selected *n*-alkanol, sterol and ketone ratios that displayed key changes are presented in Figure 5.13. The terrigenous to aquatic *n*-alkanol ratio (TAR *n*-alkanol) displayed a slight increase from zone E to D to fluctuations around ~20, prior to a decline to ~2 at ~56 cm depth. Although the TAR *n*-alkanol ratio was highly variable there was a clear peak in zone B at ~12 cm, followed by a decline to ~3 by the top of the core. The C₁₆ *n*-alkanol to total saturated *n*-alkanol ratio featured peaks at ~37 cm and ~20 cm depth, followed by a marked increase to the top of the core (~13). The *n*-C₂₂ ratio featured a slight decline from zone E to D where it fluctuated around ~24, prior to a pulse to ~35 at ~30 cm depth and a further pulse to ~45 at 3 cm depth. Although the *n*-C₂₄ ratio was highly varied, there was a clear increase from zone E to D, followed by a general but fluctuating decline to the top of the core. An opposite trend was present in the C₂₆ *n*-alkanol ratio with a slight decline in zone D and in zone B, prior to a decline in zone A to the top of the core.

Three key sterol ratios of cholest-5-en-3 β -ol (cholesterol) / 24-ethylcholest-5-en-3 β -ol (β -sitosterol), cholesta-5,22E-dien-3 β -ol / total sterols and cholest-5-en-3 β -ol (cholesterol) / total sterols all displayed declines from a peak in zone E to fairly stable lower levels in zone D, followed by increases in zone C and declines in zones B and A. In contrast, the 24-methylcholesta-5,22-dien-3 β -ol (brassicasterol) / total sterols ratio was dominated by a clear peak in the uppermost ~5 cm of zone A. These key sterol ratios are potentially good indicators of cyanobacteria and other algal inputs. The 6,10,14-trimethylpentadecan-2-one (phytone) / 3,7,11,15-tetramethyl-2-hexadecen-1-ol (phytol) ratio was very low, with the exception of a key pulse at ~56 cm depth and further smaller pulses in zones D, C and B. The compound phytone is an early oxidation product of phytol so is a good index for exploring degradation processes, cyanobacteria and purple sulphur bacteria (Pearson et al., 2007).

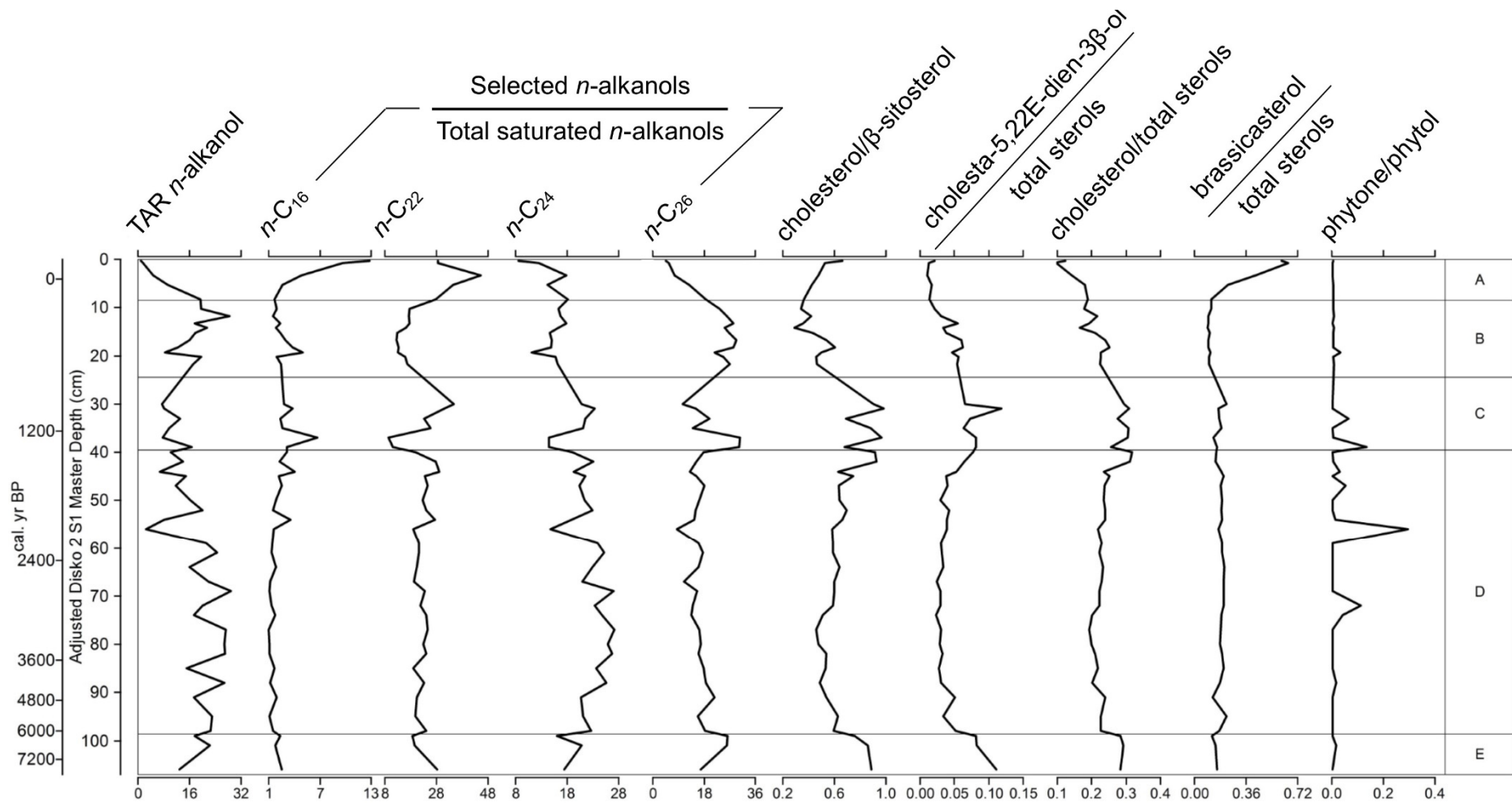


Figure 5.13: Sequence 1 (S1) Disko 2 R1-1 *n*-alkanol, sterol, ketone and phytol lipid biomarker data. Variables include key lipid ratios and ratios of selected *n*-alkanols to total saturated *n*-alkanols. Only ratios with visible trends (changes) are presented. Ratios presented in Section 2.2.5.

5.1.11 Disko 2 S1 diatom results

Diatom results provided by A. Young and V. Jones (UCL) are presented in Figure 5.14.

Zone B (AD 1253 (shown from 1700)-1867)

There were high concentrations of *Fragilaria* around AD ~1760 (including *F. brevistriata*, *F. capucina*, *F. constricta*, *F. construens*, *F. elliptica* and *F. pinnata*) along with *Synedra rumpens* and *Pinnularia biceps*, which all decreased in concentration by ~1828 AD. For example, *F. brevistriata* decreased from a maximum of $\sim 42 \cdot 10^6$ valves/g dry wt. in AD 1763 to a minimum of $\sim 9.8 \cdot 10^6$ valves/g dry wt in AD 1828. In contrast, there was almost a complete absence of *Aulacoseria subarctica* (not present), *Eunotia rhomboidea* (not present) and *Nitzschia microcephala* ($< 2 \cdot 10^6$ valves/g dry wt). There were comparatively low concentrations of *Achnantes helvetica* ($< 10 \cdot 10^6$ valves/g dry wt) and *Aulacoseria distans* ($< 8 \cdot 10^6$ valves/g dry wt), and a slight decreasing trend in *Pinnularia balfouriana*. *Meridion circulare* was present, decreasing in concentration to the top of the zone (from ~ 16 to $< 5 \cdot 10^6$ valves/g dry wt).

Zone A (AD 1867-2011)

There was a large increase in the concentration of multiple diatom species. *A. distans*, *F. brevistriata*, *F. construens* and *F. pinnata*, *S. rumpens* (agg.) and *P. biceps* all increased consistently. For example, *F. brevistriata* increased from $\sim 30 \cdot 10^6$ valves/g dry wt in AD 1931 to $\sim 130 \cdot 10^6$ valves/g dry wt by AD 1986. The diatoms *A. helvetica*, *A. subarctica*, *F. elliptica* and *N. microcephala* all increased slightly later after AD ~1960 to ~1982.

A. helvetica, *F. capucina* and *P. biceps* all increased further above AD ~1960 to the top of the core. For example, *A. helvetica* reached $\sim 43 \cdot 10^6$ valves/g dry wt in AD 2002. *E. rhomboidea* was present for the first time above AD ~1986, increasing to the top of the core (between ~ 9 and $\sim 15 \cdot 10^6$ valves/g dry wt). There were slight declines in *F. brevistriata*, *F. constricta*, *F. construens*, *F. elliptica*, *F. pinnata*, *S. rumpens* (agg.) and *N. microcephala*. *M. circulare*, *A. distans* and *P. balfouriana* were not present above ~1980. *A. subarctica* was present until AD ~1994 but absent in the uppermost sample.

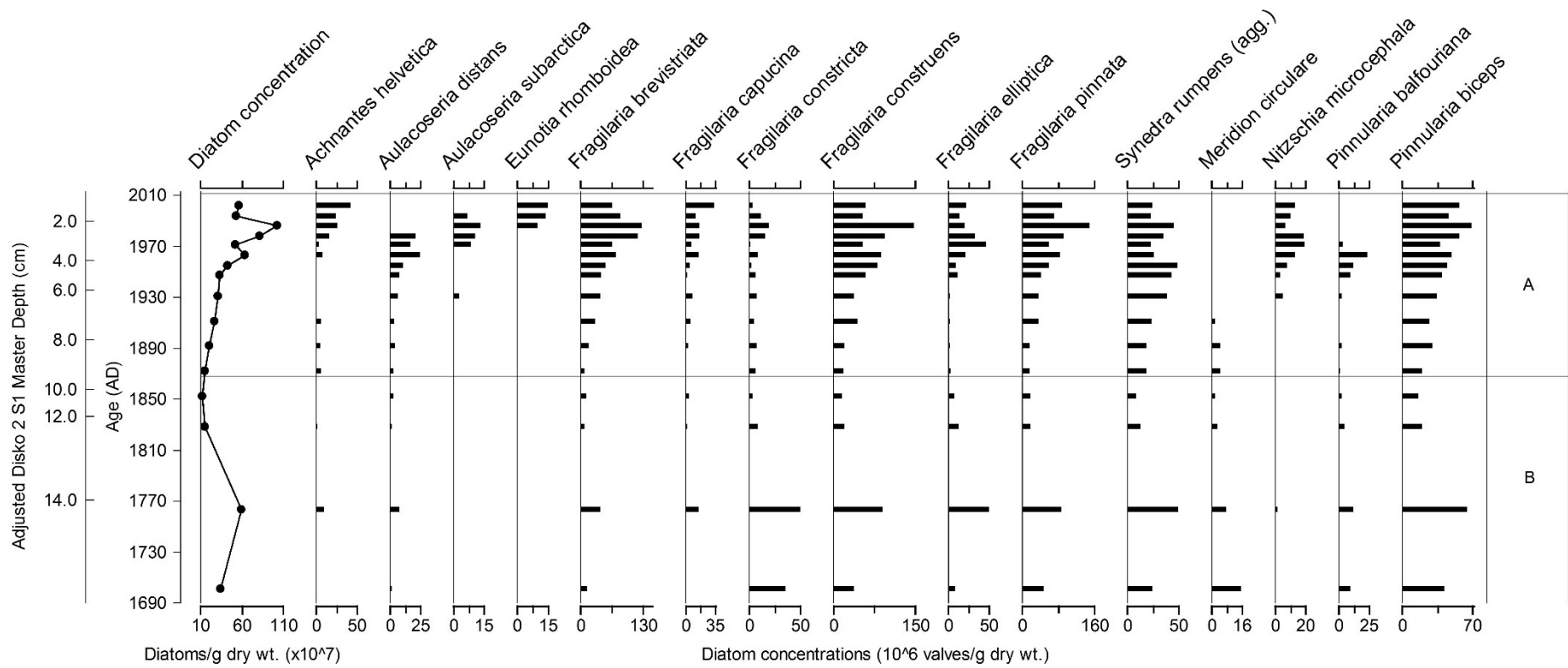


Figure 5.14: Disko 2 S1 key diatom concentration data supplied by A.Young and V.Jones, plotted against both date and depth from zone A and the upper parts of zone B. Presented taxa include the most abundant and ecologically informative species. Diatoms were identified at 0.5 cm intervals to 4 cm, 1 cm intervals to 10 cm and 2 cm intervals to 14 cm depth. Zones (A&B) presented remain the same as in previous diagrams, calculated based on pigment and selected geochemical data (CaCO_3 , OM, $\delta^{13}\text{C}_{\text{TOC}}$, TOC, N & C/N).

5.1.12 Disko 2 S1 XRF data

The XRF data for Disko 2 K1 provided by A.Young and V.Jones (UCL) is presented in Figure 5.15 plotted against percentage (%) or concentration ($\mu\text{g/g}$) where indicated. There were limited directional trends in all elements in zones C & B, although strontium (Sr) had a clearly visible decrease (from ~ 240 to ~ 180 $\mu\text{g/g}$) around AD ~ 1500 . A clear group of elements including titanium (Ti), iron (Fe), calcium (Ca), aluminium (Al) and strontium (Sr) were all found to decline in zone A from around ~ 1850 onwards, accelerating to the top of the core.

In contrast, the opposite trend was present in a number of other elements. Silicon (Si) increased from ~ 26 % in AD 1900 to a peak of ~ 32 % by AD 1994, prior to a decline to the top of the core. Similarly, lead (Pb) concentrations also increased, starting from ~ 3.6 $\mu\text{g/g}$ in ~ 1810 (zone B), rising gradually to ~ 1900 , followed by an accelerated increase to ~ 9.9 by AD 1920 and a decline to the top of the core from AD ~ 1987 . Bromine (Br) increased from a minimum of ~ 9.5 $\mu\text{g/g}$ in AD ~ 1843 to an initial peak of ~ 29 $\mu\text{g/g}$ by ~ 1931 , prior to a slight decline to ~ 21 $\mu\text{g/g}$ by AD ~ 1978 , followed by a sharp increase to ~ 44 $\mu\text{g/g}$ by the top of the core. Phosphorus (P) increased from ~ 0.14 % in AD ~ 1940 to ~ 0.38 % at the top of the core. Cadmium (Cd) values fluctuated variably between ~ 0.8 $\mu\text{g/g}$ and ~ 3.5 $\mu\text{g/g}$ until ~ 1980 , increasing consistently in from ~ 1 $\mu\text{g/g}$ to ~ 9 $\mu\text{g/g}$ by the top of the core. The Pb/Ti ratio displayed a similar trend to the Pb concentration graph, increasing from a minimum in AD ~ 1850 to a maximum of 14 by AD 1920, prior to a slight fluctuating decline in the upper sediments.

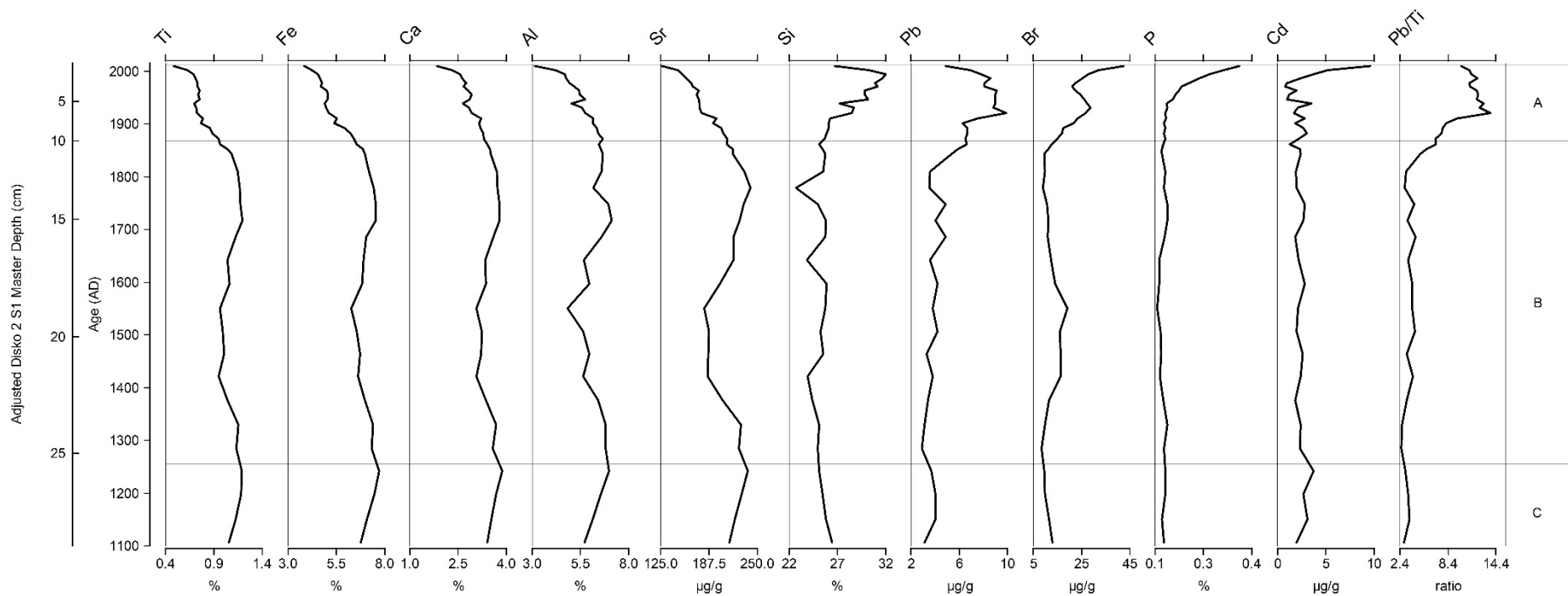


Figure 5.15: Disko 2 S1 XRF data supplied by A.Young and V.Jones (UCL) presented as percentage (%) (Ti, Fe, Ca, Al, Si, P) and in $\mu\text{g/g}$ (Sr, Pb, Br, Cd). XRF analysis was conducted at 0.5 cm intervals until 10 cm depth, followed by 1 cm depth until the bottom of the core (~31 cm). Zones (A – C) presented remain the same as in previous diagrams, calculated based on pigment and selected geochemical data (CaCO_3 , OM, $\delta^{13}\text{C}_{\text{TOC}}$, TOC, N & C/N). Plotted against both date and depth from zones A, B and the upper parts of zone C.

5.1.13 Disko 2 S1 Synthesis

Key proxies to summarise change in Disko 2 S1 were selected to facilitate cross comparison and are presented in Figure 5.16.

Zone E (7643 to 6113 cal. yr BP)

TOC, canthaxanthin (cyanobacteria), alloxanthin (cryptophytes) and diatoxanthin (mostly diatoms) were all higher in zone E compared with D. Less negative (higher) $\delta^{13}\text{C}$ values on bulk organics, short ($\delta^{13}\text{C}_{16:0}$) and long ($\delta^{13}\text{C}_{24:0}$) chain fatty acids were also present in zone E compared with D and a similar trend was present in the *n*-alkane CPI 2 index of odd or even chain dominance. There was also a slight decline in *n*-fatty acid C_{30} ratio. In contrast, chlorophyll *a* concentrations, the ratio of brassicasterol to total sterols, *n*-alkanol C_{24} ratio, *n*-alkane C_{26} ratio, C/N ratio and *n*-alkane TAR_{HC} equation were all low in zone E.

Zone D (6113 to 1382 cal. yr BP)

TOC, canthaxanthin (cyanobacteria) and alloxanthin (cryptophytes) all declined in zone D. Changes in alloxanthin were in line with TOC, increasing slightly above ~ 2500 cal. yr BP. Diatoxanthin concentrations were initially lower in zone D (minimum of ~ 100 nmol pig g^{-1} TOC at ~ 2700 cal. yr BP), followed by a peak to ~ 4600 nmol pig g^{-1} TOC at ~ 2700 cal. yr BP and a decline to the top of the zone. Chlorophyll *a* was also slightly higher in zone D. There was a decline in bulk, short-chain and long-chain fatty acid $\delta^{13}\text{C}$ in zone D, together with slight decreases in *n*-alkane CPI 2 and *n*-fatty acid C_{30} ratio. The ratio of brassicasterol to total sterols increased slightly in zone D, together with more marked increases in *n*-alkanol C_{24} ratio, *n*-alkane C_{26} ratio, C/N ratio and the *n*-alkane TAR_{HC} index.

Zone C (1382 to 676 cal. yr BP)

There were increases in TOC (to $\sim 7\%$) at ~ 1300 and ~ 900 cal. yr BP with more modest increases in canthaxanthin (cyanobacteria) and alloxanthin (cryptophytes) at the same age, with a slight peak in chlorophyll *a* in zone C. In contrast, there was an increase in bulk $\delta^{13}\text{C}_{\text{TOC}}$, reaching -20% by ~ 1300 cal. yr BP and slight increases in fatty acid $\delta^{13}\text{C}_{16:0}$ and $\delta^{13}\text{C}_{24:0}$. Both the *n*-alkane CPI 2 and *n*-fatty acid C_{30} ratio peaked around ~ 1300 cal. yr BP, although the ratio of brassicasterol: total sterols was fairly stable. The *n*-alkanol C_{24} ratio and *n*-alkane TAR_{HC} ratio both featured declines in zone C.

Zone B (676 to 83 cal. yr BP)

TOC, canthaxanthin (cyanobacteria) and alloxanthin (cryptophytes) all peaked around ~420 cal. yr BP prior to a slight decline. In contrast, diatoxanthin concentrations were markedly lower, with similar decreases in chlorophyll *a* and the ratio of brassicasterol: total sterols. Peaks were present around ~420 cal. yr BP in $\delta^{13}\text{C}_{\text{TOC}}$, *n*-alkane CPI 2 index and *n*-fatty acid C₃₀ ratio. The *n*-alkanol C₂₄ ratio was slightly lower in zone B, in contrast to the *n*-alkane C₂₆ ratio which was higher. C/N ratio was characterised by peaks at the top and bottom of the zone, with the *n*-alkane TAR_{HC} ratio reaching a peak at ~200 cal. yr BP.

Zone A (83 to -60 cal. yr BP; AD 1867 to 2010)

TOC concentrations increased markedly in zone A reaching ~8%, in contrast with relatively low levels of canthaxanthin (cyanobacteria) and alloxanthin (cryptophytes). There was a minor pulse in diatoxanthin around ~ AD 1950, but concentrations remained comparatively low to the high levels in zone D. Both chlorophyll *a* and the ratio of brassicasterol: total sterols showed a marked increase in zone A, in contrast to a marked decrease in $\delta^{13}\text{C}_{\text{TOC}}$, *n*-fatty acid C₃₀ ratio, *n*-alkane C₂₆ ratio, C/N ratio and the TAR_{HC} equation.

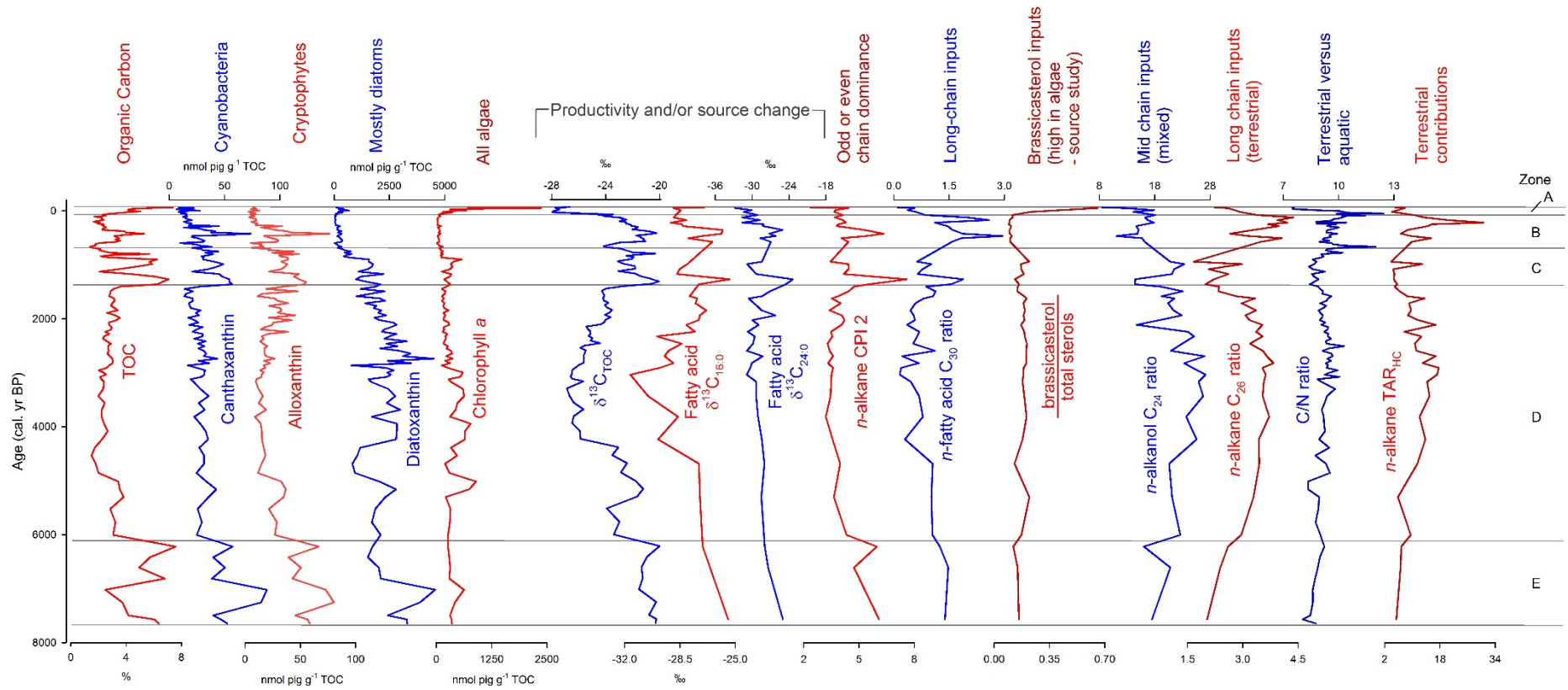


Figure 5.16: Summary diagram for multi-proxy study of Disko 2 Sequence 1 presented against age (cal. yr BP). Proxies include TOC, canthaxanthin (cyanobacteria), pheophorbide *a* (degradation product of all algae - may indicate grazing and senescent diatoms), diatoxanthin (mostly diatoms), chlorophyll *a* (all algae), $\delta^{13}\text{C}_{\text{TOC}}$, compound specific fatty acid $\delta^{13}\text{C}_{16:0}$, compound specific fatty acid $\delta^{13}\text{C}_{24:0}$, *n*-alkane CPI 2 index (Marzi et al., 1993), *n*-alkane C₃₀ ratio, ratio of brassicasterol/total sterols (brassicasterol = 24-methylcholesta-5,22-dien-3 β -ol), *n*-alkanol C₂₄ ratio, *n*-alkane C₂₆ ratio, C/N ratio and *n*-alkane TAR_{HC} ratio (Bourbonniere and Meyers, 1996a).

5.2 Results – Disko 2 – Sequence 2

5.2.1 Core correlations – Disko 2

Sequence S2 (Location – Figure 4.6, 4.7 & 4.8A) comprised two Russian cores (R2-1 & R2-2) presented in Figure 5.17. The S2 Sequence was taken from a depth of ~10.1 m as close to the deepest part of the basin (~13.4 m) as available coring rods would permit. Overlapping of R2-1 with R2-2 was not possible as both cores had unique stratigraphies (Figure 5.17). Although occasional clay-like orange intrusions and small fragments of gravel within the primarily olive-brown gyttja and brown silt matrix were explored as potential overlap markers, these did not provide a convincing overlap when combined with bulk measures (OM, DW, CaCO₃) and so each drive has been presented separately.

Similar to cores from S1 (R1-2) the R2-2 core reached consolidated material at its base, influenced by gravel deposits (Figure 5.17). Multiple core correlations were considered, but no overlap satisfied all robust measures (stratigraphy, OM, DW, CaCO₃). A summary of key changes in OM and selected pigments for R2-1 is presented in Figure 5.18 and for R2-2 is presented in Figure 5.19. The R2-2 core has proved particularly useful due to the paired terrestrial macrofossil-bulk date (Table 5.3) that helped derive an offset for the S1 master stratigraphy (Section 5.1.3).

5.2.2 Stratigraphic descriptions

The R2-2 core consisted of reddish brown gyttja from the base at ~90 cm to a band of reddish black clay/gyttja at ~85 cm depth with a small gravel layer (Figure 5.17 – Image F). This was followed by a change to brown clay/silt at ~85 cm and reddish brown gyttja until a fluctuating change around ~54 cm to olive-brown gyttja. There was a smeared change at ~27 cm to brown clay/silt to the top of the core (Figure 5.17 – Image B). In addition, there was a dark reddish-grey layer at ~42 cm (Figure 5.17 – Image C), orange clay oxidation marls around ~33 cm, organic fibrous rootlets at ~28 cm and small fragments of grey/red gravel at ~61 cm.

The R2-1 core extended from ~88 cm and comprised homogenous olive-brown gyttja throughout. There was a discontinuous dark reddish-grey organic layer at ~82 cm depth (Figure 5.17 – Image D) and a slanted orange clay intrusion at ~60 cm. There was also an orange clay-like intrusion at ~40 cm across half of the core (Figure 5.17 – Image A), an orange gravel layer at ~40 cm and two further orange clay intrusions at ~12 cm (halfway across the core) and at ~6 cm depth.

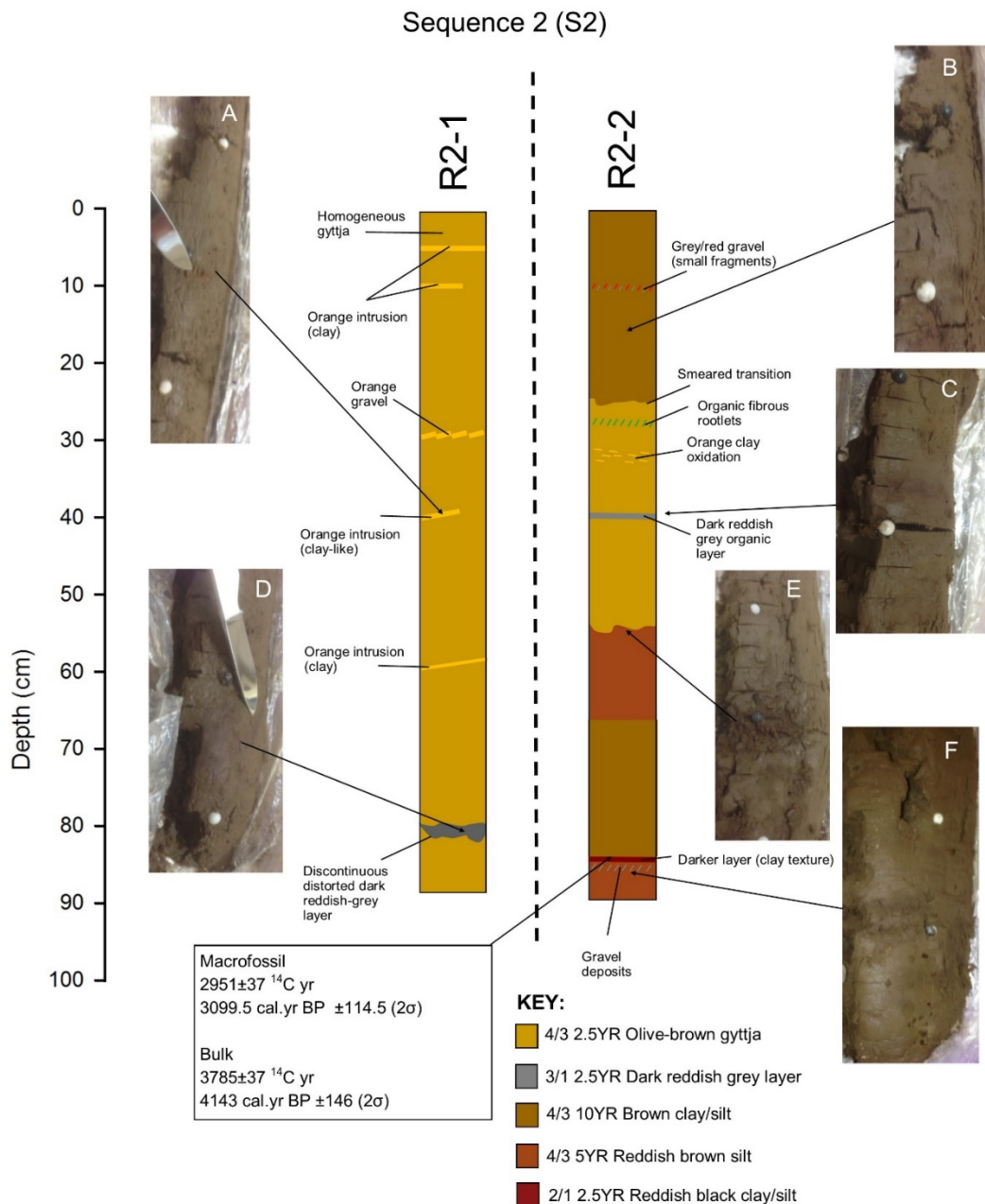


Figure 5.17: Stratigraphy for sequence 2 (S2) comprising lake Disko 2 R2-1 and R2-2 Russian core drives presented separately. Sediment is described based on identified descriptions provided in the Munsell colour system. Overlapping was not possible as each stratigraphy was unique, probably related to localised differences in sedimentation linked to debris input from steep cirque headwall. Photographs (A-F) display key macrofossil, clay and grit/stone layers at relevant parts of the sequence. White and black pins reflect 5 and 10 cm depths in the core to aid description. Colours and textures used in the diagram are exaggerated to aid interpretation. Radiocarbon dating results are indicated in square boxes with arrows to indicate the source of the sample, with middle calibrated age given (2σ) together with error range. Paired dates for S2 were on a terrestrial macrofossil (woody fragment) and bulk organic matter and were used in the S1 (Section 5.1.3) calibrated age-depth model to correct ^{14}C dates.

5.2.3 Radiocarbon dating – Sequence 2

Two dates were obtained from near the base of the Disko 2 R2-2 core (depth 84-85 cm) on both bulk organic matter and an unidentified macrofossil (twig/woody fragments, most likely *Salix* spp.) (Table 5.3). Both dates were analysed at Queens University Belfast (sample code UBA) with the methods detailed in Section 3.10. The youngest date was on the terrestrial macrofossil which yielded a ^{14}C AMS radiocarbon age of 2951 ± 37 years BP. When calibrated the 2σ central estimate was 3100 cal. yr BP with an expected error of ± 11.5 cal. yr BP. The oldest date was on bulk sediment which yielded a ^{14}C AMS radiocarbon age of 3785 ± 37 years BP. When calibrated the 2σ central estimate was 4143 cal. yr BP with an expected age range of ± 146 cal. yr BP.

Since the overlap of R2-1 with R2-2 was problematic and there was no dating of the top of R2-2, an age-depth model was not produced for this sequence. The calibrated central estimate of the macrofossil date on R2-2 at 84-85 cm (3100 cal. yr BP, Table 5.3) was found to be similar to the calibrated date once corrected at 84.5-85.5 cm in the S1 adjusted master sequence (2935.5 cal. yr BP). This suggests that although not fully modelled, both S1 and S2 cores probably have similar sedimentation rates and that R2-2 is unlikely to have extended much deeper than R2-1. The shallow positioning of R2-2 is confirmed by field measurements which show that the base of R2-2 reached ~ 130 cm below the sediment-water interface.

Table 5.3: Radiocarbon dating results from Disko 2 S2 sediment sequence. Analyses prepared at the ^{14}C CHRONO Centre, Queens University Belfast under the supervision of Prof. Paula Reimer (sample code UBA). Calibrations performed in Calib 7.04 using IntCal 13 (Reimer et al., 2013). Carbon isotope values ($\delta^{13}\text{C}_{\text{VPDB}}$) derived by calculations from AMS. The ^{14}C offset between bulk and macrofossil dates of 834 years was used in the S1 (Section 5.1.3) calibrated age-depth model to correct ^{14}C dates.

Publication code	Sample identifier	Sample type	^{14}C Enrichment (% Modern $\pm 1\sigma$)	Conventional Radiocarbon Age (years BP $\pm 1\sigma$)	Carbon content (% by wt.)	$\delta^{13}\text{C}_{\text{VPDB}}$ ‰	Max cal age BP (2σ)	Min cal age BP (2σ)	Mid cal age BP (2σ)	Cal age error \pm
UBA-25168	D2 R2-2 84-85 cm	Macrofossil (unidentified twig)	69.26 \pm 0.32	2951 \pm 37	n/a	-29.4	3214	2985	3100	115
UBA-25169	D2 R2-2 84-85 cm	Bulk sediment	62.42 \pm 0.28	3785 \pm 37	n/a	-21.1	4289	3997	4143	146

5.2.4 Disko 2 R2-1 Russian core – bulk organics & pigment concentrations

Figure 5.18 displays a summary of key proxies from the Disko 2 R2-1 Russian core including stratigraphy, OM and six pigments plotted against core depth. OM ranged between ~6 and ~23% with slightly lower values in zone D compared with C. The dark reddish-grey stratigraphy at ~81 cm depth was coincident with a slight decline in OM and a peak in fucoxanthin. Diatoxanthin and β -carotene concentrations were slightly higher in zone D, compared with C, but there were no clear trends in alloxanthin, lutein-zeaxanthin and canthaxanthin. Fucoxanthin, diatoxanthin and β -carotene concentrations were slightly lower in zones C and B. The orange clay-like intrusion (see Figure 5.17) at ~41 cm depth was coincident with a decrease in organic matter and simultaneous increase in all pigments, at the boundary between zones B and A. OM increased consistently in zone A, reflected by similar increases in lutein-zeaxanthin and canthaxanthin.

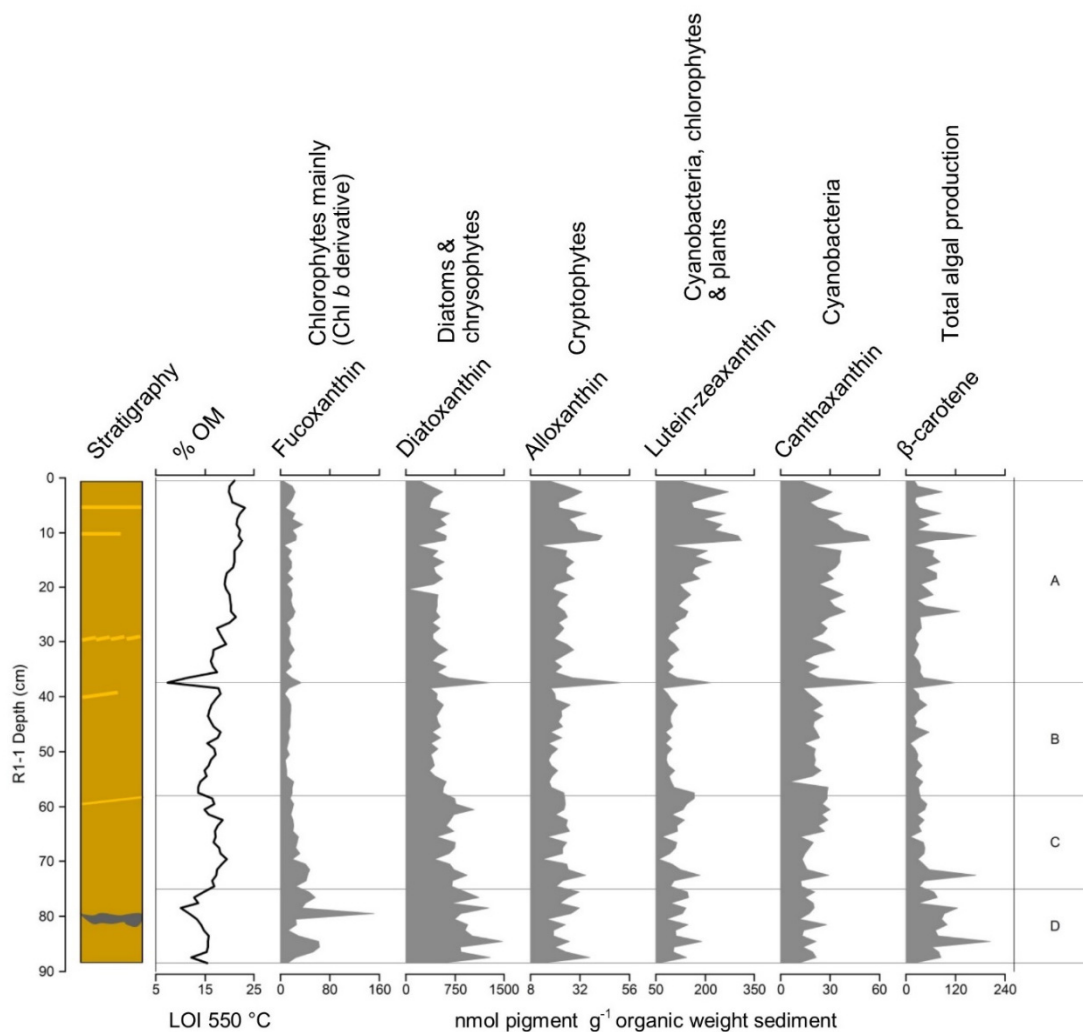


Figure 5.18: Stratigraphic plot for Disko 2 R2-1 Russian core of selected pigment concentrations expressed against OM (LOI 550 °C). Zones (A, B, C & D) were based on optimal partitioning resulting in 4 zones. Zone calculations included a full suite of 13 pigments analysed in addition to CaCO₃, OM & DW. Age depth model was not calculated due to the difficulty in overlapping cores for this sequence (see Figure 5.17 & Section 5.2.1). Key for stratigraphy fill in Figure 5.17.

5.2.5 Disko 2 R2-2 Russian core – bulk organics & pigment concentrations

Figure 5.19 displays a summary of key proxies from the Disko 2 R2-2 Russian core including stratigraphy, OM and six pigments presented against depth. OM was comparatively low (5-10%) in zone D, until an increase in zones C and B (to ~17%), coincident with the transition to more organic orange-brown gyttja and a decline to the top of the core with the return to brown clay/silt (~7%). Fucoxanthin and diatoxanthin concentrations were higher in zone D, with a further peak in diatoxanthin in zone B (reaching ~1,100 nmol pig g⁻¹ org sed. weight). Alloxanthin, lutein-zeaxanthin and canthaxanthin were all markedly higher in zone A. For example canthaxanthin concentrations increased from <10 pig g⁻¹ org sed. weight to >50 pig g⁻¹ org sed. weight by ~18 cm depth. β -carotene concentrations fluctuated throughout, although there was a slight decline in concentration to <30 nmol pig g⁻¹ org sed. weight at ~50 cm depth.

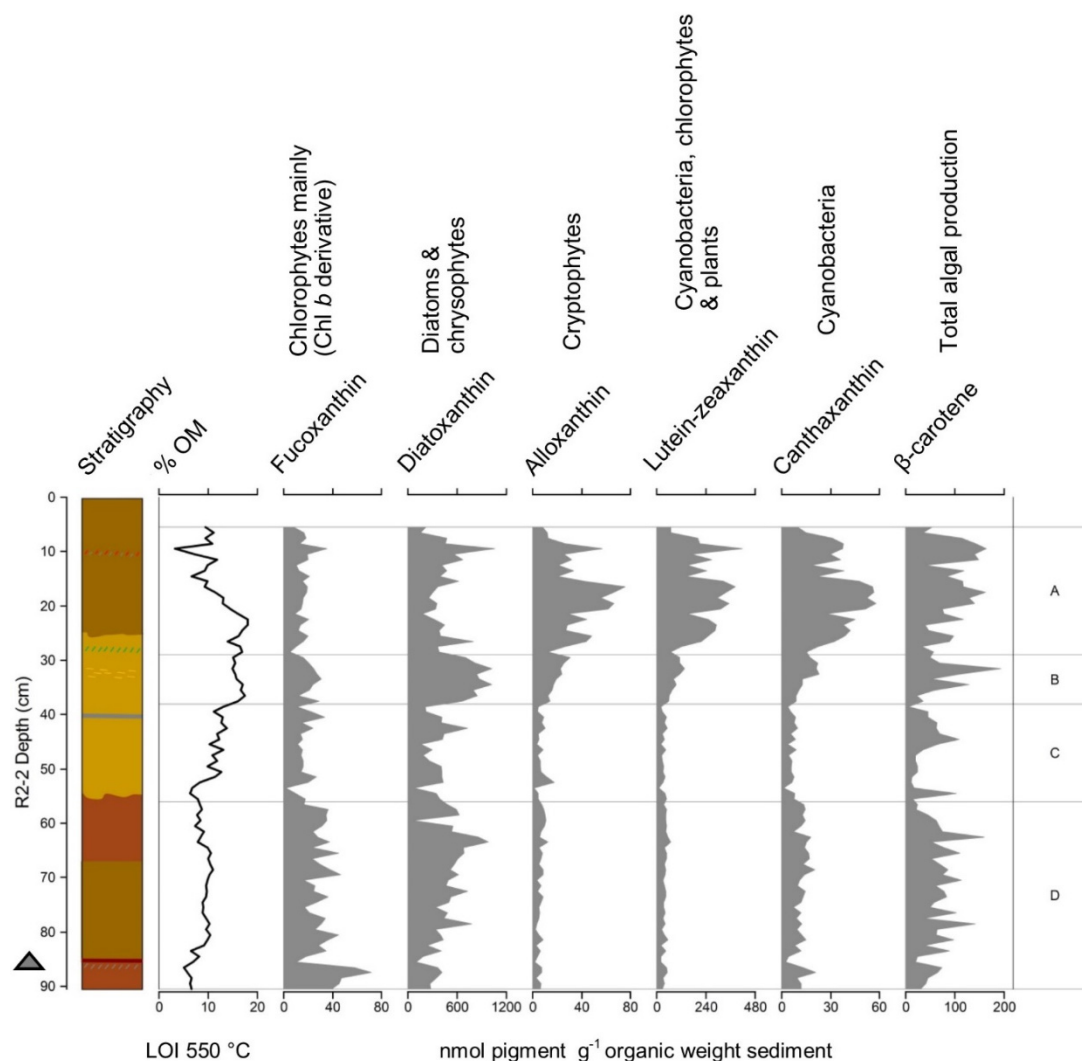


Figure 5.19: Stratigraphic plot for Disko 2 R2-2 Russian core of selected pigment concentrations expressed against OM (LOI 550 °C). Zones (A, B, C & D) were based on optimal partitioning resulting in 4 zones. Zone calculations included all variables in the figure above in addition to CaCO₃, OM & DW. Zone calculations included a full suite of 13 pigments analysed in addition to CaCO₃, OM & DW. Filled triangle indicates position of paired terrestrial macrofossil & bulk date. Macrofossil = 2951±37 ¹⁴C yr, 3100 cal.yr BP ±115 (2σ). Bulk = 3785±37 ¹⁴C yr, 4143 cal.yr BP ±146 (2σ). The ¹⁴C offset between bulk and macrofossil dates of 834 years was used in the S1 (Section 5.1.3) calibrated age-depth model to correct ¹⁴C dates. Table 5.3 provides additional radiocarbon dating information. Key for stratigraphy fill in Figure 5.17.

5.3 Disko 2 Discussion

5.3.1 Stratigraphy, core correlations and bulk measures

Both sequence 1 (S1) and sequence 2 (S2) from lake Disko 2 (Figures 5.1 & 5.17) were individual profiles at different core sites within the basin (Figure 4.6, 4.7 & 4.8) and did not share similar trends. This suggests that in Disko 2 sediment focusing across the basin is highly heterogeneous. The presence of a north facing steep slope (to the south of Disko 2) was identified during the summer 2013 field survey to be a key source of angular freeze-thaw broken rocks (Figure 4.7). Although most of Disko is present on granite and basalt geology, the rock slope to the south of Disko 2 was observed to be a mudstone intrusion, potentially accounting for the brittle nature of the instantaneous events sampled in the sediment cores.

Sequence 1 (S1) had multiple bands of rock and gravel deposits at periodic intervals throughout (Figure 5.1) which were likely sourced from the observed slope, prior to deposition. The distortions found in core R1-2 and angular stone layers suggest that deposits may have formed inconsistently on the lake floor, due to the supply of debris from the south facing slope. In contrast, S2 did not have as many gravel and stone layers, but had clay-like intrusions at multiple depths (Figure 5.17). This suggests the position of S1 received gravel and rock deposits to a greater extent than S2. The clay intrusions could be sourced from ice activity as 5% of the catchment currently has permanent ice cover (Table 4.4, Figure 4.6). Variable sediment focusing in glacier-fed lakes have been demonstrated in Bow Lake, Alberta Canada through multiple core studies (Smith, 1981). Although Disko 2 is not presently a glacier fed lake, there is permanent ice cover present in the catchment and the north facing scree slope may have a rock glacier-like characteristic which could be responsible for the supply of finer particles. Rock glaciers are common on Disko Island and can take the form of a lobe or tongue shaped feature (Humlum, 1996). The Disko 2 slope of angular freeze-thaw debris is not a full rock glacier, but may have similar properties, potentially with a permanent ice centre facilitating mass wasting and rock flow into the lake. Delivery of clays can also be associated with solifluction lobes which were observed in the catchment and is a process of gradual mass wasting associated with freeze thaw activity in periglacial environments.

Sequence 1 (S1) correlations were good when based on lithostratigraphic and geochemical variables and so a combined sequence was derived (Figure 5.1, Appendix C – Figure C1 & C2). The low OM (generally 4-16%, with the exception of a rise to

~24% at the top of the core, Figure 5.7 & 5.8) is indicative of a relatively low productivity system, typical in Arctic upland catchments with the majority of sediment supplied from minerogenic sources. Low CaCO₃ (0-8% in R1-1 and R1-2) is consistent with the local non-carbonate geology which would be unlikely to precipitate calcium carbonate and may not actually reflect any carbonate due to as this technique is known to be influenced by water from clays (Heiri et al., 2001).

Correlating S2 was more challenging due likely to localised sediment focusing (between ~3 m position of drives) which can disrupt sedimentation in small basins (Lehman, 1975), but has provided invaluable information associated with the geomorphology of the lake. For this reason, cores from S2 (R2-1 and R2-2) are discussed separately. Although an overlap was considered based on the dark reddish grey organic layer at ~80 cm, as the brown clay/silt layers in R2-2 were not present in R2-1 (Figure 5.17) it was not possible to derive a combined S2 sequence with high confidence. It is possible that the brown clay/gyttja layer was caused by sediment slumping associated with disturbance in the lake from rock-fall. Sediment focusing studies in Mirror Lake, New Hampshire (Davis and Ford, 1982), demonstrated silts and sands were deposited over 85% of the basin. But this phenomenon leaves a significant proportion of the lake bed with reduced sedimentation which could account for the differences between R2-1 and R2-2. Organic-rich sediments (which tend to preserve higher pigment concentrations) have been found to be focused into the deepest part of the basin in some studies (Davis and Ford, 1982).

In Disko 2 coring could not be conducted in the deepest part of the lake (13.4 m) due to limitations in the length of coring equipment available and so all sequences are likely to be from zones of partial sediment deposition (10 m), rather than solely deposition at the deepest part of the basin. The presence of weak orange clay intrusions at multiple levels in R2-1, compared with just once in R2-2 (Figure 5.17), suggest R2-1 may have been more susceptible to localised clay plumes brought in during inwash events from periglacial or snowpack/small permanent ice activity in the catchment. Basin shape can also affect sedimentation patterns. The bathymetry was relatively low resolution (Figure 4.6) and so may not have picked up micro-topographical features, particularly associated with the freeze-shattered north-facing slope, as this could cause complex irregularities resulting in uneven sedimentation (Lehman, 1975). The basin is characteristic of an over-deepened cirque lake (Figure 4.7) due to its position at ~575 m a.s.l, above the Blæsedalen (Itinneq Kanglilleq) and Kuussuaq valleys. It is possible that the deeper middle part of the basin could be less disrupted than the areas sampled (S1 & S2).

5.3.2 Radiometric dating

The majority of radiocarbon dates ($n = 7$) were concentrated on sequence 1 (Figure 5.1 and Table 5.1 & 5.2) as this core was selected as the main high-resolution multi-proxy sequence to make regional carbon cycling interpretations. Although some dates did not present in stratigraphic order it was possible to remove dates associated with instantaneous events and where recent dating suggested a younger model (Table 5.2, Figure 5.2). Possible explanations for the dating challenges include a variable hard-water reservoir effect, slumping/resuspension of sediments within the lake and the supply of old organic carbon from the catchment. Evidence for an offset between bulk dates and terrestrial macrofossils of 834 years was found in the R2-2 core (Table 5.3 and Figure 5.19) which was applied to all dates in the final age-depth model (Figure 5.6). The effect of old bicarbonate in the lake water (Shotton, 1972) is a less likely scenario as carbonate (CaCO_3) was relatively low (~0.1-8% in S1) and samples were acidified prior to ^{14}C analysis. However, evidence for disturbance was present throughout S1 with the presence of gravel, rock and stone layers throughout, suggesting the reworking of carbon in the catchment (Figure 5.1). Catchment samples confirmed the presence of organic carbon within catchment soils ranging from 15.9 to 0.3% (Table 4.6 & Figure 4.14) and so delivery of old organic carbon in the catchment may have contributed to making radiocarbon dates older than expected. Disturbance from the north facing scree slope direct to the lake was observed during the summer 2013 field season so this may also have contributed to sediment resuspension, leading to the movement of old profundal sediments to deeper parts of the lake.

A complementary explanation could be that algae from preserved ice in the catchment or within deeply frozen permafrost may be released hydrologically at a significant delay since carbon fixation. There was probably a small glacier on the north facing slope that has subsequently retreated, changing the sources to the sediment considerably. Snow cover was observed during summer 2013 so some permanent ice does remain within the small catchment (~5%, Table 4.1, Figure 4.6), which likely continues to be a source of entrained algae or ancient labile DOC (Lawson et al., 2014b; Hood et al., 2015) to the lake. The $\delta^{13}\text{C}$ values on radiocarbon dating samples (range -21.8 ‰ to -26.5 ‰) were within the range of C_3 land plants, algae and bryophytes identified during catchment end-member investigations of the lake (Table 4.6, Figure 4.14). The highest value of -21.8 ‰ may reflect a contribution from the exceptionally high (less negative) $\delta^{13}\text{C}$ value of a *Potamogeton* sample (-6.4 ‰) identified in the catchment as bulk dates integrate carbon from multiple sources. It is

possible that the oldest dates in the S1 master sequence reflect periods of enhanced catchment activity or erosion (see Figure 5.2).

Wide diurnal temperature fluctuations in the ice-free season would likely provide the most active freeze-thaw activity (Coutard and Francou, 1989), facilitating delivery of material into the lake. Based on the adjusted S1 master age depth model (Figure 5.6), based on the oldest corrected date of 6644 ± 39 ^{14}C years (calibrated to 7514 ± 70 cal. yr BP) at 104.5-105.5 cm this could place the lowermost samples (see Figure 5.16) towards the end of the spatially variable and heterogeneous Holocene Thermal Maximum (HTM). Aquatic macrofossil rootlets in R1-2 between ~113 cm and ~134 cm could have been deposited during the HTM in a more favourable lake environment, with the base of R1-2 potentially restricted from early Holocene glacial deposits (see stone layer at ~177 cm, Figure 6.5).

Sedimentation rates which were highest in the uppermost samples of S1 were relatively low (Figure 5.5; between ~0.02 and $0.01 \text{ g cm}^{-2}\text{yr}^{-1}$) and were consistent with the geomorphology as a small upland lake (catchment area = 358 ha) of high elevation (~575 m. a.s.l) with limited sparse catchment vegetation (Figure 4.7). This sedimentation rate is lower than two previously dated sedimentary sequences on Disko Island (Qivittut and Fortune Bay lakes) which were cored at lower elevations and had larger catchments (Bennike, 1995). Although it was not possible to derive an age-depth model for S2 as core R2-1 did not overlap appropriately with R2-2, sedimentation rates are likely to be similar with S1 as explained in Section 5.2.3.

5.3.3 Disko 2 S1 Combined Sequence – Proxy interpretation

The Disko 2 S1 multi-proxy geochemical data is summarised in Figure 5.16 and shows evidence of changes in all proxies in lake Disko 2 since ~7650 cal. yr BP. This section of the discussion initially uses key geochemical indicators to gain insight into the lake ecosystem and understand how this might have changed over time. Proxies are then interpreted to understand the role of organic carbon for tracking algal production in the system, including the delivery of this externally to the lake and processing within the lake. As multiple proxies have been used from a variety of sources comment is then made on transformations and diagenesis to assess the relative value of proxies, with reference to catchment sampling. The role of external catchment drivers in mediating these trends is then highlighted, together with comment on the wider palaeoclimate periods known from this region.

Disko 2 lake ecosystem

Proportionally diatoxanthin was the pigment with the highest concentration (Figure 5.7 & 5.16), suggesting diatoms constitute a major proportion of the algae sedimented in Disko 2, despite being only a small part of the planktonic modern sample (Table 4.4). XRF indicated silica (Si) was also found to be relatively high (23-31%), which is a major element required for development of silica frustules in diatoms (Figure 5.15). Chlorophyll *a* and DOC concentrations were found to be low (Table 4.3), suggesting high water clarity and so a significant proportion of the diatom contributions are likely to be sourced from benthic surfaces including sediments, macrophytes, filamentous microbial communities and detritus. Diatom communities found in the uppermost samples were consistent with an oligotrophic environment, with the majority of these diatoms from a benthic source, particularly attached sediment-dwelling species. An example is *Meridion circulare* which is known to be common on stream epilithic substrates, which then becomes deposited into lakes (Antoniades and Douglas, 2002).

A clear group of pigments including canthaxanthin (cyanobacteria) and alloxanthin (cryptophytes) followed a similar trend to TOC (Figure 5.7, 5.8 & 5.16) suggesting that in this lake system the availability of carbon could have some effect on stimulating algae and the presence of a tightly coupled microbial loop. The input of enhanced DOC to the lake may have facilitated the growth of heterotrophic algae (e.g. cryptophytes indicated by alloxanthin) resulting in a preference for communities with mixotrophic abilities (Jones, 2000). In contrast, pigments such as fucoxanthin (diatoms and chrysophytes) and pheophytin *a* (total algal production, indicator of degradation) followed different trends, unrelated to TOC and reflect changes in wider

lake ecology. This is likely dominated by contributions from benthic macrophytes, which may have changed more gradually over time as the lakes littoral zone became gradually expanded with lake infilling from the erosion of cirque headwall.

Other algal groups appear to be associated with more abrupt changes in community dynamics. Clear shifts in pigments between zones (Figures 5.7 & 5.16) suggest re-organisation of algal communities, with for example, diatoxanthin concentrations displaying trends independent of TOC. Evidence that all pigments fluctuated between adjacent samples (Figure 5.7 & 5.16) is consistent with an Arctic landscape environment where material is delivered intermittently, in line with melt phases, influencing community structure. For example, there were pulses of pheophytin *b* (chlorophytes mainly) and chlorophyll *a* (all algae) below ~70 cm depth (~2800 cal. yr BP), which could indicate a re-organisation of algal communities and changes in in-lake ecology (Figure 5.7, Zone D). The relatively abrupt changes between zones in pigments (Figure 5.7 & 5.16), indicates distinct changes in algal community, which is probably indicative of a simple trophic structure in this high elevation relatively low productivity upland lake (Figure 4.6, Table 4.1) with a low DOC status (Table 4.3).

Role of organic carbon for algal production – within lake processing and terrestrial inputs

The percentage of TOC and some pigments (including canthaxanthin and alloxanthin) showed similar trends, however comparisons with other pigments show that the cycling of carbon in this system is more nuanced. As TOC and N are higher in zones E, C & B (Figure 5.9 & 5.16) the $\delta^{13}\text{C}_{\text{TOC}}$ value increase could be due to algal productivity increases, with insufficient ^{12}C available, requiring the fixation of ^{13}C (Hodell and Schelske, 1998). Alternatively, the differences may reflect a change in the source of the sediment. Compound-specific $\delta^{13}\text{C}_{\text{FAMES}}$ analysis showed similar trends to $\delta^{13}\text{C}_{\text{TOC}}$ in both short chain (predominantly algae, $\delta^{13}\text{C}_{16:0}$) and long chain fatty acids (terrestrial contributions $\delta^{13}\text{C}_{24:0}$) suggesting that in this system, source inputs external to the lake are the main driver of changes in $\delta^{13}\text{C}_{\text{TOC}}$. This implies that at least some of the change in $\delta^{13}\text{C}_{\text{TOC}}$ can be attributed to carbon supplied external to the lake, weakening the likelihood that all the trends in $\delta^{13}\text{C}_{\text{TOC}}$ might be linked to the insufficient supply of ^{12}C . This also helps support similar trends in cryptophytes (indicated by alloxanthin) which may be responding in part to inputs of DOC from the catchment. The absence of these trends in the $\delta^{13}\text{C}$ values of the $\text{C}_{16:1a}$ and $\text{C}_{18:1a}$ monounsaturated compounds (Figure 5.12) is understandable as these compounds are more unstable compared with saturated *n*-fatty acids (Table 2.3).

Differences in the specific $\delta^{13}\text{C}$ values of individual fatty acids is likely explained by biological ^{13}C discrimination in the original allochthonous and autochthonous sources to the sediments (Figure 5.12). For C_3 plants (no C_4 plants identified in the Disko 2 catchment) the CO_2 utilised for carbon fixation is directly proportional to atmospheric CO_2 and the ability for this to diffuse through the plant stomata which is linked to temperature, plant phylogeny, growth and leaf traits (Diefendorf et al., 2010). Additionally, precipitation is closely coupled to the ability for stomata to uptake CO_2 affecting the $\delta^{13}\text{C}$ of the organism (Kohn, 2010). The $\delta^{13}\text{C}$ values of individual lipid biomarkers in sediments are productivity weighted (Diefendorf et al., 2010), meaning that even compound-specific $\delta^{13}\text{C}$ values have multiple non-specific sources, particularly in catchments (such as Disko 2) dominated by C_3 plants with similar $\delta^{13}\text{C}$ values. The end-member survey identified an exceptionally high $\delta^{13}\text{C}$ value of -6.4‰ in the *Potamogeton spp.* sample in Disko 2 (Table 4.6), suggesting that changes in aquatic macrophyte abundance may also have the potential to change $\delta^{13}\text{C}_{\text{TOC}}$, which could be linked to lake level change.

Overall, C/N ratio was relatively low throughout the sequence (~ 7.5 to ~ 13.5) suggesting that the main contributor of organic matter is algae and aquatic macrophytes (Figure 5.9 & 5.16) (Meyers and Teranes, 2001). In this system algae (16.8) and aquatic macrophytes (9.7) had low ratios, whereas ratios were much higher in most plants (up to 133.6 in *Salix arctica* stem samples) (Table 4.6 & 4.14). Slightly higher values in zone D and at ~ 665 cal. yr BP and ~ 48 cal. yr BP may reflect pulses of terrestrial material brought into the catchment associated with catchment dieback (Leng et al., 2012) or could reflect proportional decreases in algal production. Due to the limited catchment vegetation and poorly developed soils in the Disko 2 catchment (see Figure 4.7, 4.8 & 4.6) both processes are likely occurring together. For example, there is a large increase in chlorophyll *a* and the ratio of brassicasterol to total sterols (indicator of algae & moss mainly in this system, Table 4.8) in zone A, which is coincident with a more algal signature in C/N ratio (~ 7.5). The simultaneous decline in $\delta^{13}\text{C}_{\text{TOC}}$ to values more in line with terrestrial plants as observed in the end-member investigations (see Table 4.6) helps confirm the tight coupling between terrestrial inputs and within lake processing in this system.

Lipid indexes and ratios also helped support the closer coupling of terrestrial inputs with in-lake algal production. For *n*-alkanes the CPI 2 index (Table 2.2) presented opposite trends to the TAR_{HC} index (Figure 5.11 & 5.16) suggesting a more nuanced response to terrestrial inputs. In line with TOC, canthaxanthin (cyanobacteria) and alloxanthin (cryptophytes) the CPI 2 index was higher in zones E compared with D

and there were pulses in the ratio around ~1270 and 423 cal. yr BP. Higher CPI 2 index values indicate fresher material with stronger odd over even predominance (Marzi et al., 1993). This means that with higher values less diagenesis has taken place as lower values (~1) are characteristic of crude oil. In this system the source study demonstrated that higher CPI 2 ratios were associated with higher plants including *Salix arctica* (Table 4.8), providing further evidence that terrestrial material may be higher in the same periods as increased algal production (Figure 5.16).

However, the TAR_{HC} index (Table 2.2) which is often used to track allochthonous versus autochthonous contributions showed the opposite trend (as vascular plants are dominated by C₂₇, C₂₉ and C₃₁ *n*-alkanes and algae by C₁₇ *n*-alkanes), supporting changes in C/N ratio. The TAR_{HC} index in the source study investigation indicated increased higher plants, but specifically more leafy plants and soils, rather than woody plants like *Salix arctica* (Table 4.8), as herbaceous plants would probably be more susceptible to catchment dieback during harsh conditions. Similar trends were present in the *n*-alkane C₂₆ ratio (Figure 5.11 & 5.16) which was most closely associated with catchment soils in the source study investigation (Table 4.8), suggesting catchment dieback may also have been linked to soil instability despite the lower TOC in zone D. The lack of a pigment response in zone D suggests the quality of carbon may have been more bioavailable in zones E and parts of C, promoting within lake algal production in some groups (cyanobacteria and cryptophytes).

Biomarker transformations and diagenesis

Prior to the interpretation of external drivers of change in this system it is important to acknowledge the varying susceptibility to diagenesis and preservation in some biomarker proxies. The *n*-fatty acid (FAMES) lipid ratios (Figure 5.12 & 5.16) are complex and often challenging to interpret (Table 2.3). Fatty acids are more susceptible to diagenesis than *n*-alkanes with maximum proportions centring around the C₁₆ *n*-fatty acid which are present in all organisms but dominant in algae (Meyers, 1997). Although the *n*-C₁₆ compound fluctuates throughout the core, the *n*-C₁₄ compound peaks in zone D & A could reflect increased diagenesis of longer chain compounds reducing in chain length or inputs of diatoms/other algae (Figure 5.12). *Potamogeton* spp. was found to be the greatest contributor proportionately of the C₁₄ *n*-fatty acid in the source study investigation (Table 4.8), however fatty acids are more susceptible to diagenesis which may have partly contributed to the rise. The longer-chain C₂₄, C₂₆, C₂₈ and C₃₀ *n*-fatty acids all featured opposite trends to the long chain *n*-alkane compounds. This would in isolation suggest terrestrial contributions are

higher, but is contrary to the C/N ratio evidence and *n*-alkane results which are more robust and less susceptible to diagenesis. It is likely that the deposits that constitute most of zone D have undergone more diagenesis (brown gyttja, Figure 5.1), compared with the olive-brown gyttja elsewhere in the core.

Monounsaturated compounds in some sedimentary systems can be used to interpret microbial activity (Table 2.3). Although previous studies have linked lower C_{18:1}/C_{18:0} ratios to warmer temperatures and more microbial activity (Zhou et al., 2005), it appears in Disko 2 all monounsaturated compounds reduce to background levels by ~30 cm depth (Figure 5.12). This is informative as it shows some long-term diagenesis has occurred in these cores and that trends in monounsaturated compounds are unlikely to be a good palaeoenvironmental indicator in this system.

Pigments also have varying levels of stability (Table 2.1) which needs to be considered in interpretations (Leavitt and Hodgson, 2001; McGowan, 2013). Although canthaxanthin (cyanobacteria) and alloxanthin (cryptophytes) are fairly stable, chlorophyll *a* is less stable (summary diagram, Figure 5.16). The clear peak in chlorophyll *a* at the top of zone A could be linked to increased algal production (summer 2013 filter spot sample was dominated by chlorophyll *a*, Table 4.4), but it could also be indicative of degradation. The relatively low concentrations of okenone, increasing only in the upper sediments at ~1.75 cm is unlikely to be indicative of lake bottom water anoxia (Hodgson et al., 1998), but instead probably indicates post-depositional within-sediment degradational processes, leading to some anoxia within the sediment-water matrix but not necessarily within the water column (Figure 5.7). The chlorophyll *a*: pheophytin *a* ratio increased to a pulse of ~1 in 2003 AD approximately 10 years prior to coring. This ratio assesses the diagenetic susceptibility of chlorophyll *a* and therefore suggests that caution should be taken when interpreting pigments with poor stability (Leavitt and Hodgson, 2001; Leavitt et al., 2003). Peaks in 2003 are also present in fucoxanthin, diadinoxanthin and β-carotene. However, these pigment trends are generally variable and fluctuating, consistent with natural variability and are not consistent with a continuous declining trend which might weaken interpretations.

External catchment drivers and paleoclimate

Change ~7640 to 6113 cal. yr BP (Zone E)

Together all available sedimentary, geomorphic and geochemical proxy data from S1 point to a close coupling of the catchment with in-lake biogeochemistry since ~7640

cal. yr BP. Despite the latest global proxy synthesis providing evidence for an overarching early Holocene warming (10,000 to 5,000 cal. yr BP) (Marcott et al., 2013) which may act as an overarching driver, Holocene climate is understood to be heterogeneous, regionally complex and tightly linked to the responsiveness of specific proxy records (Briner et al., 2016). The more algal signature of organic matter (TOC) and higher concentrations of algae which are likely to have responded to terrestrial inputs (e.g. cyanobacteria and cryptophytes) in zone E (7640 – 6113 cal. yr BP) (Figure 5.16) probably reflect increased catchment nutrient cycling associated with permafrost melt and glacier activity, rather than lengthening of the ice free season. Although the S1 dating model has some limitations (due to removal of dates linked with instantaneous events, see Table 5.2), if broadly correct this would place Disko 2 peak catchment-responsive algal production (canthaxanthin and alloxanthin) slightly earlier than reconstructions at North Lake near Ilulissat which suggest warmest summers between ~6 and 4 ka (Axford et al., 2013; Briner et al., 2016).

Change ~6113 to 1381 cal. yr BP (zone D)

Proxies in the S1 reconstruction provide evidence of changes in catchment carbon cycling, linked to terrestrial inputs and resulting changes in lake biology. By considering the impact of climate on catchment processes (reduced nutrient cycling) it is possible to link minimum TOC concentration (1.3%) dated to ~4200 - 4800 cal. yr BP, broadly with the “4.2 ka event” (Figure 5.17). This is concordant with findings at a similar latitude in the nearby Ilulissat North Lake (Axford et al., 2013) and may reflect connectivity between West Greenland’s climate with this more widely documented event (Booth et al., 2005). In zone D the generally lower TOC and less algal (higher) C/N ratios indicates reduced overall algal production (Figure 5.10) with pulses of longer chain *n*-alkanols and *n*-alkanes suggesting catchment dieback (Table 4.8 and 4.10) during harsher conditions. This period in the reconstruction (~6100 to 1380 cal. yr BP) could reflect some elements of the late Holocene Neoglaciation (Kelly, 1980), where some catchments remained covered by permanent ice for longer periods in the year, restricting the release of DOC and nutrients. However, it is also now acknowledged that the Neoglacial cooling trend is not a single event, but rather a spatially heterogeneous process with very different trends in for example, eastern Beringia (NW America) (Kaufman et al., 2016), compared with west Greenland (Briner et al., 2016).

Change ~1382 to 83 cal. yr BP (zones C & B)

Change in sedimentary proxies in zones C and B (~1382 to 83 cal. yr BP, Figure 5.16) reflect a period of greater variability in lake Disko 2 proxies, which includes change during many spatially heterogeneous climatic phases such as the Medieval Climate Anomaly (MCA) and Little Ice Age (LIA). Increases in TOC and multiple pigments in zone C (including canthaxanthin and alloxanthin, Figure 5.16) may correspond with increased catchment activity supplying DOC and nutrients during periods with greater climate variability or longer length of the ice-free season. In zone B a similar increase in these proxies centred around ~423 cal. yr BP could mark the spatially variable MCA, which is known to be complex (Mann et al., 2009) and probably increased catchment nutrient cycling resulting in corresponding increases in algal production (Figure 5.16). The reduced algal production and TOC between ~330 and ~68 cal. yr BP (~AD 1620-1882) probably reflects the regional Greenland LIA, which is generally accepted as extending from AD 1150-1920 (Humlum, 1999; Yde and Knudsen, 2007). Fluctuations were also present in $\delta^{13}\text{C}_{\text{TOC}}$ and multiple lipid indicators (Figure 5.16), indicating changes in carbon source origin (see Section 4.8.2). On balance, considering the geomorphic position of lake Disko 2 (Figure 4.7), combined with changes in these proxies, although shorter length of the ice-free season is a potential control restricting algal growing time, a more likely explanation is reduced inputs of DOC and nutrients from longer frozen permafrost and reduced disturbance from periglacial activity (e.g. solifluction) and movement of ice within the catchment.

Recent change since AD ~1867 (Zone A)

Zone A reflects the most recent changes in key proxies since ~1867 (Figure 5.16), with change summarised since ~AD 1880 in Figure 5.20. The boundary between zone B and A (~1867) corresponds closely to the end of the Greenland LIA (Humlum, 1999) and is marked by a major re-organisation of algal communities and change in inorganic proxies (Figure 5.7, 5.15, 5.16 & 5.20). XRF evidence supports a general reduction in the supply of catchment derived elements since AD ~1860 (Ti, Fe, Ca, Al and Sr), roughly coincident with the later part of the LIA (Figure 5.15), but increased P likely sourced from glacial or permafrost melt (Slemmons and Saros, 2012; Slemmons et al., 2013). This probably indicates reduced erosion from less ice in the Disko 2 catchment, but export of P stored within ice, stimulating algal production as indicated by β -carotene (all algae) and pigment PCA 2 scores (Figure 5.20). Increases in multiple pigments were found in the most recent sediments on Baffin Island

(Michelutti et al., 2005; Florian et al., 2015) to the west of Disko. Similar trends correlating with climate have been observed in *Betula nana* tree ring reconstructions on Disko (Holleisen et al., 2015), although an indirect link is the most likely scenario, with algae responding to increased nutrient and/or DOC supply following ice retreat and intensification of periglacial activity during warming.

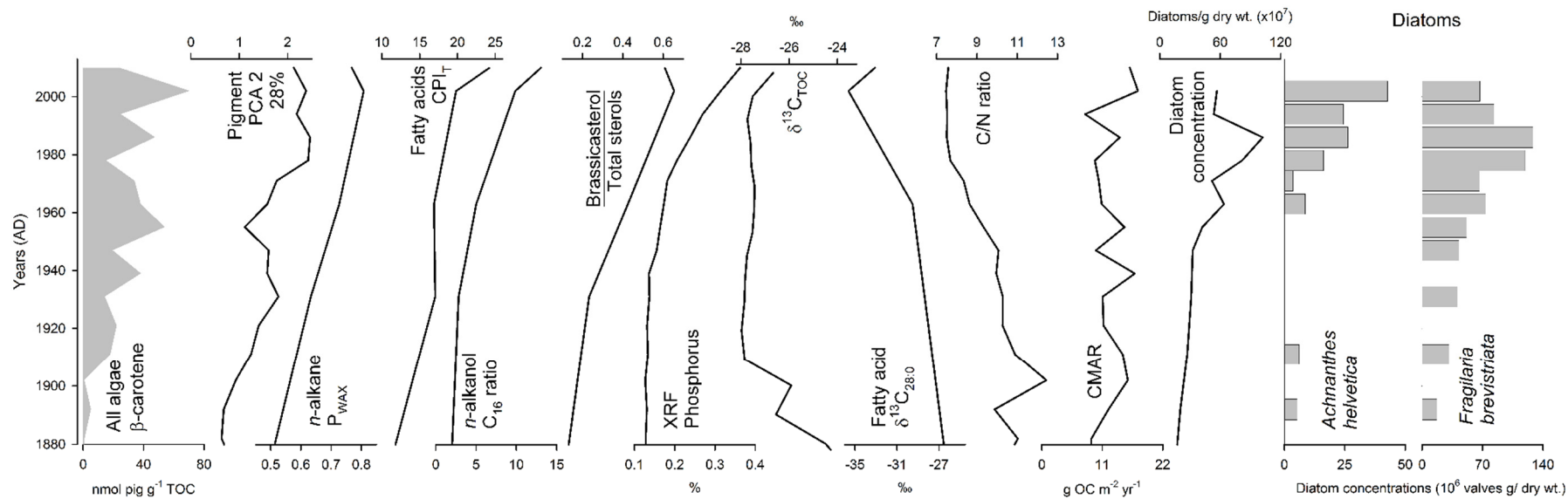


Figure 5.20: Disko 2 S1 sequence key proxies plotted against year (AD). Proxies include β -carotene (all algae), pigment PCA 2 scores (28%), n -alkane P_{WAX} index (Zheng et al., 2007), fatty acid CPIT index (Matsuda and Koyama, 1977), n -alkanol C_{16} ratio, ratio of brassicasterol/total sterols (brassicasterol = 24-methylcholesta-5,22-dien-3 β -ol), XRF derived % Phosphorus, $\delta^{13}C_{TOC}$, compound specific fatty acid $\delta^{13}C_{28:0}$, C/N ratio, carbon mass accumulation rate (CMAR), diatom concentration and the diatoms *Achnanthes helvetica* and *Fragilaria brevistriata*.

The decrease in C/N ratio to ~ 7.5 in the uppermost sediments is low and probably primarily algal in origin (Meyers and Teranes, 2001) together possibly with increases in aquatic macrophytes (Table 4.6), supporting pigment evidence (Figure 5.20). The slight increase in C/N ratio to ~ 13 around AD 1920 may reflect in-wash of plant material (Leng et al., 2012) as catchments thawed following the LIA (plant material up to ~ 135 in Disko 2 catchment, Table 4.6). Declines in $\delta^{13}\text{C}_{\text{TOC}}$ to ~ -27 ‰ are coincident with the end of the LIA and reflect a period of stability at high resolution (sampled at 0.5 cm intervals) which is probably explained by a change in the source of the organic matter. In Disko 2 terrestrial plants were found to have $\delta^{13}\text{C}_{\text{TOC}}$ values of around ~ -27 ‰ (Table 4.6). Although part of the decline in $\delta^{13}\text{C}_{\text{TOC}}$ (up to ~ 1.5 ‰) can be explained by the Suess effect (Tans et al., 1979; Verburg, 2007) a decline in up to ~ 7 ‰ could not have caused this. This supports the scenario of algal response (as C/N ratio was low) to changes in the catchment following the LIA. Long chain fatty acid compounds *n*-C₂₀, *n*-C₂₁, *n*-C₂₆ & *n*-C₂₈ also displayed decreases in $\delta^{13}\text{C}_{\text{TOC}}$ to the top of the core (Figure 5.10, *n*-C₂₈ also in Figure 5.20). This probably indicates that some of the carbon utilised for the decline in $\delta^{13}\text{C}_{\text{TOC}}$ was originally terrestrial in source.

Supporting recent increases in algal production the brassicasterol (24-methylcholesta-5,22-dien-3 β -ol)/total sterols ratio increased unambiguously since \sim AD 1880 (Figure 5.20). In the source study investigation (Table 4.8) this ratio was linked to soil, algae and moss contributions, potentially corroborating the change in algal community at the top of the core. The more pronounced response of brassicasterol could be due to the high diatom concentrations in Disko 2 which is known to contain this compound, although contributions could also derive from microalgae and algal mats (Volkman et al., 1998; Pearson et al., 2007). Diatom concentrations peaked in \sim AD 1986 (Figure 5.7 & 5.20) suggesting a general increase in siliceous algal production. Diatoms present were consistent with an oligotrophic environment, with the majority of diatoms from a benthic source, particularly attached to sediment-dwelling species. The absence of the diatom *Meridion circulare* above \sim AD 1910 suggests reduced ice or glacier activity in the catchment, as this diatom has been found attached as mucilaginous colonies to benthic debris often in flowing water (Krejci and Lowe, 1987; Antoniadis and Douglas, 2002). Increased lake level associated with observed debris near the outflow may also have contributed to this change (Figure 4.7). Changes above \sim AD 1975 include disappearance of *Aulacoseria distans* and *Pinnularia balfouriana* (Figure 5.14), corroborating the changes in algal community to the top of the core indicated by fucoxanthin, diadinoxanthin and chlorophyll *a* (Figure

5.7). The timing of these changes are consistent with diatom transitions across the northern hemisphere linked to recent warming and length of the ice free season (Smol et al., 2005; Smol and Douglas, 2007), however at Disko 2 an indirect climate mechanism through nutrients and DOC from the retreat of ice in the catchment, and changes in lake level are a more likely explanation.

Other biomarker proxies indicated both increased terrestrial and increased aquatic carbon in the most recent sediments. The increasing *n*-alkane P_{WAX} index (Figure 5.11 & 5.20) provides evidence of recent increased contributions of waxy *n*-alkanes from terrestrial sources (Zheng et al., 2007), which is supported in the end-member samples by high contributions in soils, plants for this index (Table 4.8). Vegetation in the catchment is limited (Figure 4.9 & Table 4.2) with *n*-alkanes probably sourced from both catchment increases in terrestrial vegetation and increased dust deposition (Schefuß et al., 2003). Increases in fatty acid carbon preference indexes (CPI_L , CPI_H & CPI_T) suggested the uppermost sediments were fresher (Figure 5.12 & 5.20) as these samples had clearer dominance of even chain lengths (Matsuda and Koyama, 1977). This could be due to the increased algal abundance in the uppermost sediments (Figure 5.20) or could be an indicator of diagenesis (decomposition/oxidation of OM), as compared with *n*-alkanes, fatty acids are more susceptible (Canuel and Martens, 1996). The *n*-alkanol C_{16} ratio increase in the uppermost samples supports recent changes in algal abundance (a general indicator of productivity, Table 4.8), but also could be influenced partly by diagenesis to the longer chain compounds (Figure 5.13 & 5.20).

There is also evidence of long range atmospheric deposition of contaminants in the most recent sediments of Disko 2. The increase in Pb since ~AD 1900 is likely the result of long-range atmospheric deposition of anthropogenic contaminants associated with leaded petroleum. Similar increases have been observed in lake sediment across the northern hemisphere in the UK (Yang and Rose, 2005), Sweden (Renberg et al., 2002), north-eastern United States (Graney et al., 1995) and the Kangerlussuaq and Sisimiut areas of western Greenland (Bindler et al., 2001). In Disko 2 the concentrating effect of recent permanent ice loss in the catchment probably influenced these increases in contaminants. The slight decline in Pb deposition to the top of the core is likely explained by the recent transition to unleaded fuels and is confirmed by the Pb/Ti ratio which corrects change to Ti which is catchment derived. The recent increases in Cd could also be associated with the hemispheric-scale burning of fossil fuels (Johansson et al., 2001), with increases in Br probably linked in this system to increased OM (Ziegler et al., 2008), rather than burning of fossil fuels. P also

increases from ~AD 1950 but is unlikely to reflect long range phosphorus deposition (Camarero and Catalan, 2012) to the lake, due to its position far from major sources of agriculture, with release from ice and permafrost melt a more likely explanation.

S1 Combined Sequence – Summary

Pigment and diatom evidence from S1 suggest that the Disko 2 lake ecosystem is relatively unproductive, primarily benthic and probably has a simple trophic structure. As pigments from cyanobacteria and cryptophytes all follow trends similar to TOC this has been interpreted as evidence of a tightly coupled microbial loop, where autochthonous algae responds to the delivery of allochthonous material external to the lake. Algal changes provide evidence of clear shifts in community dynamics, probably in line with catchment inputs rather than length of the ice-free season, bringing variable amounts of bioavailable carbon into the lake. Changes in both bulk and long-chain $\delta^{13}\text{C}$, confirmed with catchment calibrations suggest that allochthonous inputs are important in driving algal change in this system. Biomarker compounds are all variably susceptible to diagenesis, although in this system algal pigments are fairly robust (confirmed by ratios), with interpretation of trends strengthened by the use of multiple proxies (e.g. C/N, *n*-alkanes, *n*-alkanols & *n*-fatty acids).

Indirect catchment mediated drivers include changes in permafrost carbon and nutrient cycling, variations in catchment permanent ice cover and lake level change associated with deposition of eroded rock near the lakes outfall. The more algal signature of organic matter in S1 between ~7640 and 6113 cal. yr BP was found to be broadly in line with the later part of the spatially heterogeneous HTM, but slightly earlier than lakes near Ilulissat (Axford et al., 2013). Minimum TOC concentrations were found to be present around the '4.2 ka event' suggesting some connectivity regionally with this more widely documented event. Pulses in C/N indicating catchment dieback during the harsher Neoglacial was supported by long chain *n*-alkane and *n*-alkanol lipids. The reduced algal production and TOC between ~330 and ~68 cal. yr BP (~AD 1620-1882) probably reflects the Greenland LIA of maximum catchment ice extent and minimum permafrost melt, resulting in less in-lake algal production. Recent change is marked by a major re-organisation of algal communities, more algal OM and increases in algal indicating lipids (e.g. short chain C_{16} alkanols and ratio of brassicasterol to total sterols). At the same time, some proxies such as *n*-alkanes (P_{WAX} index) and $\delta^{13}\text{C}$ (bulk and compound specific long chain fatty acids) suggest recent increases in terrestrial material, which may be partly responsible for stimulating algae. Recent increases in algal production are probably driven by a

combination of increased lake level due to rock fall near the lakes outfall (explaining recent trend to slightly more planktonic diatoms), and greater permafrost nutrient cycling/catchment ice melt associated with warming.

5.3.4 Disko 2 – Sequence 2 – Proxy Interpretation

Both Disko 2 R2-1 (Figure 5.18) and R2-2 (Figure 5.19) cores from Sequence 2 are discussed individually as the overlap between these cores was not satisfactory. This suggests that catchment processes are important in lake Disko 2 as despite their close proximity (taken within ~2 m), both cores had unique stratigraphies (Figure 5.17, 5.18 & 5.19). The R2-2 core was particularly valuable for deriving the sequence 1 age-depth model (Figure 5.19) as it contained a paired terrestrial macrofossil and bulk date, which enabled the correction of bulk dates (Figure 5.6, Table 5.2).

In R2-1 pigment records were found to fluctuate rapidly, linked to variations in OM, probably associated with delivery of DOC and nutrients from the catchment from permafrost thaw and changes in ice melt (Figure 5.18). Bands of clay in the stratigraphy, including at the boundary between zones B and A (~37.5 cm) are marked by a pulse in algal production across multiple pigments, providing evidence for catchment solifluction and delivery of labile carbon. Pigments which suggest an algal community dominated by diatoms (fucoxanthin and diatoxanthin) are highest in the two lowest zones (C & D), whereas pigments which suggest an algal community dominated by cyanobacteria (canthaxanthin and lutein/zeaxanthin) are highest in zone A. This reflects a major change in algal community structure and is probably related to catchment processes and lake benthic ecology. Since Disko 2 is known to receive inputs of freeze-thaw debris from the observed scree slope (Figure 4.7 & 4.8), the changes in algal production (Figure 5.18) could be related to variations in the source of aquatic macrophytes on the lakebed and over time with lake infilling (Hannon and Gaillard, 1997; Rasmussen and Anderson, 2005). More recent increases in algal production and the trend towards cyanobacteria could be associated with lake level increase, from infilling at the outflow which appears to have been partly filled by scree (Figure 4.7).

In R2-2 the core is dominated by a pronounced increase in pigments from cryptophytes (alloxanthin) and cyanobacteria (lutein-zeaxanthin and canthaxanthin) in zone A (Figure 5.19). This marks a major shift in community structure towards more open water taxa, despite only modest increases in pigments for all algae (e.g. β -carotene). Although there is a single date at 84-85 cm in the core (Table 5.3, Figure 5.19) and age-depth model has not been derived as the position of the sediment-water interface is unclear, and so it is not possible to relate these changes to known climate periods (e.g. MCA or RW). The change in algal community structure in zone A is coincident with a shift to brown clay/silt in the stratigraphy. A potential mechanism

could be the increased supply of nutrients and DOC from the catchment, linked to temperature and precipitation, made possible by enhanced terrestrial soil microbial activity (Hobbie, 1996) or release from glaciers (Slemmons et al., 2013), potentially increasing mixotrophic algae such as cryptophytes (alloxanthin) and cyanobacteria (canthaxanthin) (Jones, 2000; Burkholder et al., 2008). An alternative or complementary explanation for the shift in algal community structure could be the presence of deposits originating from a different part of the lake (from erosion or disturbance), variations in pigment preservation or changes in lake level. Coincident with the transition from zone A to B in the pigment profile is the transition from brown clay/silt to olive brown gyttja (Figure 5.17 & 5.19), which may each have different pigment preservation factors (Leavitt, 1993). Both alloxanthin and canthaxanthin are among the most stable pigments (Leavitt and Hodgson, 2001) and so this is probably not the main explanation for the increase. More likely, the brown clay/silt layer might include macrophyte focusing from the littoral areas which may have varied over time with lake infilling (Rasmussen and Anderson, 2005), together with lake level change linked to deposition of scree near the outfall (Figure 4.7).

5.4 Disko 2 summary

Two locations (S1 and S2) were cored in lake Disko 2, each displaying individualistic responses in all proxies, providing evidence of catchment disturbance derived from its geomorphological position within a cirque basin. Overall, work on Disko 2 has highlighted the presence of basin heterogeneity in this disturbed upland Arctic lake, together with the importance of benthic processes and possible lake-level change in this relatively unproductive environment. Despite the challenges preventing the development of an age-depth model for S2, it was possible to use a paired terrestrial macrofossil-bulk date from S2 to calibrate bulk dates on S1. This, combined with removal of dates coincident with instantaneous events and dates which were too old compared with recent dating (^{210}Pb and ^{137}Cs) helped derive an appropriate age-depth model for S1 to ~7640 cal. yr BP.

The Disko 2 lake ecosystem was found to be relatively unproductive, primarily benthic with a simple trophic structure, reflected in the high diatom abundance (diatoxanthin) and relatively abrupt changes in algal community. Similar trends in both pigments from algae and cryptophytes with TOC suggest a tightly coupled microbial loop where autochthonous algae responds to allochthonous inputs. $\delta^{13}\text{C}$ values in both bulk TOC and compound specific long-chain fatty acids follow similar trends, suggesting potential terrestrial stimulation of algae. Despite varying susceptibility to diagenesis, pigment records in this system are interpreted as robust, particularly when combined with multiple proxies. Although changes in the length of the ice free season may play a role in regulating the length of the algal growing season, the observed physical disturbances to the lake, combined with periodic delivery of allochthonous carbon probably outweighs this effect.

In S1 the more algal signature of OM between ~7640 and 6113 cal. yr BP was found to be broadly in line with the later part of the spatially heterogeneous HTM. A likely explanation is that during warmer periods there was greater catchment nutrient and DOC cycling, leading to more stimulation in in-lake algae. Minimum TOC levels are broadly in line with the 4.2 ka event suggesting some potential connectivity with the North Atlantic, although it is acknowledged that this event is spatially complex. Fluctuating increases in C/N ratio together with some long chain lipids (e.g. *n*-alkane C_{26} ratio) provide evidence of catchment dieback during harsher conditions, probably during the complex and spatially variable neoglaciation. A further minimum in production (~AD 1620 – 1882), particularly in cyanobacteria and cryptophytes probably reflects the Greenland LIA. The mechanism for reduced algal production is

likely that with maximum ice extent and minimum summer permafrost melt, organic release from the catchment was reduced (nutrients and DOC) resulting in less in-lake algal production. Most recently, coincident with regional warming there has been clear increases in algal production reflected in both pigment and lipid indicators (e.g. short chain alkanols and ratio of brassicasterol to total sterols). This is probably driven both by more permafrost nutrient cycling and catchment ice melt (increased P release observed) together with possible increases in lake level due to deposition of scree near the outfall.

Chapter 6: Disko 1 Results and Discussion

This chapter presents (Section 6.1), and discusses (Section 6.2) the sediment core results from lake Disko 1. Lake Disko 1 is situated within the U-shaped Blæsedalen valley at an elevation of 299 m. a.s.l, receiving predominant discharge stemming from the ice cap and is adjacent to mossy wetlands. Within the hydrogeomorphic and lake-landscape framework of this thesis, Disko 1 is present as the second lake due to its comparative mid-elevation and moderate sized catchment (Table 4.1).

Although C/N ratio and $\delta^{13}\text{C}_{\text{TOC}}$ was not analysed down-core in Disko 1 it is useful to summarise these findings to reflect the diverse autochthonous and allochthonous signatures at this site (see Section 4.8.4). In the catchment sample survey $\delta^{13}\text{C}_{\text{TOC}}$ ranged between -26‰ and -30‰ for higher plants in Disko 1 and mixed *Potamogeton* sp. and algal mat samples between -28.5‰ and -30.7‰ (Table 4.5, Figure 4.13). Bryophytes had a slightly broader range from -24.1‰ to -27.8‰ , with soils ranging from -24.8‰ to -26.5‰ . C/N values ranged between ~ 30 and 130 for the majority of catchment plant samples, except for some which were degraded or had new growth (Table 4.5, Figure 4.13). Soils had the lowest C/N ratios probably indicative of soil algal communities, with moderate C/N ratios in *Potamogeton* and algal mat samples (29.6 to -35.9‰). The degradation product pheophytin *a* and diatoxanthin (indicator of diatoms) were the most abundant pigments in summer 2013 filtered water samples (Table 4.4).

6.1 Results – Disko 1

6.1.1 Core correlations – master stratigraphy

The Disko 1 combined sequence comprised the K1 HON-Kajak core from S1 location together with two overlapping Russian drives (R2-1 and R2-2) from S2 location (Figures 4.2 & 4.3). The Russian sequences were selected from S2 location as compared with S1 it had fewer distortions and had clearer visual overlap. All cores were obtained from a water depth of 5.9 m, with a total combined sequence length of 163 cm (Figure 6.1). The sequence was predominantly dark reddish-brown silty clay, with fine, often well preserved laminations or varves present in some sections of the sequence.

The overlap of R2-1 with R2-2 was made on the basis of a combination of stratigraphic (Figure 6.1) and bulk geochemical measures through % organic matter at 550 °C (OM), % dry weight at 105 °C (DW) and % carbonate at 925 °C (CaCO₃) (Figure 6.3). Narrow macrofossil rich layers at ~66 cm helped tie R2-1 to R2-2, which was corroborated by a yellowish-brown clay intrusion at ~78 cm depth (Image B - Figure 6.1). The five final OM samples on R2-1 (blue) also overlapped clearly with the second peak in OM ~81 cm, (Figure 6.3).

Although the OM, DW and CaCO₃ measurements were offset between the HON-Kajak and the Russian cores (Figure 6.1), pigment trends when overlapped showed similar trends (Appendix D, Figure D1, D2 & D3). The final combined sequence used samples from the K1 HON-Kajak core (where available) until ~22 cm due to the higher (0.5 cm) sample resolution of the core and inclusion of samples to the sediment-water interface.

6.1.2 Stratigraphic descriptions

The base of the R2-2 sequence (~163 cm) comprised dark reddish brown silty clay with fine (<0.5 cm) fluctuations of highly distorted light brown silty clay laminations (Figure 6.1 – Image D). These laminations became clearer (Figure 6.1 – Image C) at ~123 cm until ~93 cm with more pronounced light brown silty clay bands. There was a macrofossil rich layer at ~163 cm and yellowish-brown clay layers at ~154 cm, ~143 cm and ~123-125 cm. Further yellowish brown clay bands were present at ~111 cm depth and between ~103 and ~101 cm. Above ~93 cm the dark reddish-brown silty clay was not clearly banded. A wider yellowish-brown clay layer was present at ~76 and 79 cm depth although it did not permeate the full width of the core and was slanted (Figure 6.1 – Image B) and a macrofossil rich layer was present at ~66 cm depth.

The R2-1 sequence was ~83 cm in length and comprised dark reddish brown silty clay. There were yellowish-brown clay layers present between ~76 and ~79 cm, at ~73 cm and also at ~63 cm depth. A macrofossil rich layer was present at ~66 cm depth. The dark reddish-brown silty clay continued until a yellowish-brown clay layer (~50 cm) and a gradual change to dark greyish-brown silt that was lighter by ~36 cm. Laminations were present (each <0.5 cm) from ~36 cm to ~21 cm of dark reddish-brown and light brown silty clay (Figure 6.1 – Image A). From ~21 cm to ~17 cm there was a light brown silty clay layer, a yellowish-brown clay layer (~17 cm) and from ~17 cm to 11 cm, dark reddish brown and light brown silty clay bands, changing

to dark reddish brown silty clay with minor fluctuating bands of light brown above ~11 cm to the top of the core.

The K1 sequence was ~22 cm in length and comprised primarily dark reddish brown silty clay with minor fluctuating bands of light brown silty clay. Macrofossils were present at the sediment-water interface.

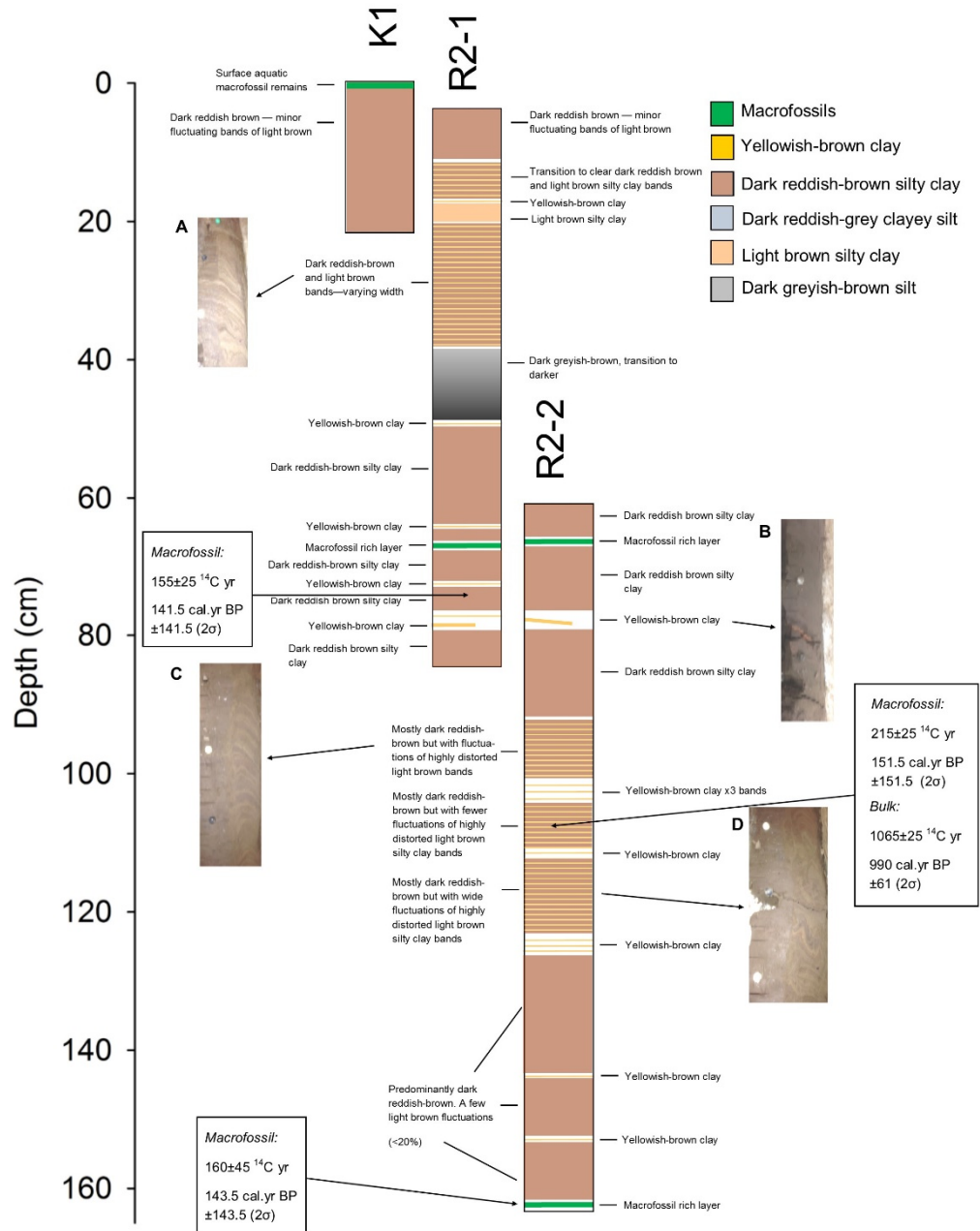


Figure 6.1: Stratigraphy for Disko 1 R2-1 and R2-2 overlapping Russian and K1 HON-Kajak core drives and proposed depth matching sequence. Sediment is described based on identified descriptions provided in the Munsell colour system. Overlapping is based primarily on the feint macrofossil rich layers ~65 cm and the yellowish-brown clay intrusions ~75 cm, confirmed by comparison with measured depth and geochemical analyses (%LOI 550 °C). Photographs display laminations (often distorted and fluctuating) at relevant parts of the sequence. Colours and textures used in the diagram are exaggerated to aid interpretation. Radiocarbon dating results (calibrated with IntCal 13 (Reimer et al., 2013) & uncalibrated) are indicated in square boxes with arrows to indicate the origin of the sample.

6.1.3 Radiometric dating

Radiocarbon dating results are appended to the stratigraphic diagram (Figure 6.1), listed in table format according to publication code (Table 6.1) and plotted with uncertainty bars (2σ calibrated error; 1σ uncalibrated ^{14}C error) against depth (Figure 6.2). Calibrations were made using IntCal 13 (Reimer et al., 2013). Radiocarbon dating results on terrestrial macrofossils yielded relatively recent ages, and did not order chronologically with depth. The single bulk date was older than the paired macrofossil, likely due to old organic carbon deposited from the catchment (see Section 6.2.3). ^{210}Pb or ^{137}Cs for recent radiometric dating was not analysed on Disko 1 sediments.

The lowermost depth that was dated was near the bottom of the sequence, on a terrestrial *Salix* macrofossil at a master sequence depth of 161.25-162.25 cm. This date yielded an uncalibrated ^{14}C age of 160 years BP ± 45 . When calibrated, (2σ) this age yielded a maximum age of 288 cal. yr BP, a minimum age of 1 cal. yr BP and a middle age of 143.5 cal. yr BP, with an error of ± 143.5 cal. yr BP. The $\delta^{13}\text{C}$ value modelled by AMS for this macrofossil was -18.6‰ . At 108.25-109.25 cm depth in the master sequence both a *Salix* macrophyte leaf fragment and a bulk sediment sample were analysed for radiocarbon. The plant macrofossil yielded a younger age of 215 ± 25 ^{14}C years BP, compared with the bulk sediment which yielded an age of 1065 ± 25 years BP. When calibrated, the age range (2σ) of the *Salix* macrofossil extended from a minimum of 1 cal. years BP to a maximum of 304 cal. yr BP, and a middle age of 151.5 cal. yr. BP, with an error also of ± 151.5 cal. yr. BP.

This contrasted with the calibrated age range of the bulk sediment from a maximum of 1051 cal. yr BP to a minimum of 929 cal. yr BP, and a middle age of 990 cal. yr BP, with a calibrated error range of ± 61 cal. yr BP. The $\delta^{13}\text{C}$ value measured by AMS for the plant macrofossil was -25.1‰ , whereas this was lower for the bulk sample (-21.2‰) from the same depth. The first date was on a *Salix* leaf fragment plant macrofossil at a depth of 73.5-74.25 cm which yielded a ^{14}C uncalibrated radiocarbon age of $155 \text{ BP} \pm 25$ years. The calibrated 2σ age range for this sample ranged from a maximum of 284 cal. yr BP, to a minimum of 1 cal. yr BP, with a middle expected age of 141.5 cal. yr BP and an error of ± 141.5 cal. yr BP. The $\delta^{13}\text{C}$ value for this sample was -23.7‰ . All samples for dating were taken from the undisturbed centre of the core. A reservoir effect was not applied to the dating results.

Figure 6.2 (A) shows the uncalibrated ^{14}C age ranges plotted against depth. The age of the bulk sediment was much older, compared with the plant macrofossil at 108.25-

109.25 cm depth in the master sequence. Figure 6.2 (B) displays the calibrated middle dates and 2σ age ranges. The three terrestrial macrofossils all had calibrated ages that extended to 0 cal. yr. BP, resulting in errors in the modelling software (Calib 7.04). Dating more recently than 0 cal yr BP (~1950 AD) is beyond the applicability of the IntCal 13 calibration method. Similar to the uncalibrated ^{14}C age, the calibrated age was also older in the bulk sample compared with the plant macrofossil at 108.25-109.25 cm depth. An assessment of the reliability of this dating is provided in Section 6.2.3.

Table 6.1: Radiocarbon dating results from Disko 1 Russian sediment sequences R2-2 and R2-1. Analyses prepared at the NERC Radiocarbon laboratory (East Kilbride) under the supervision of Dr L.M. Cisneros-Dozal with samples measured by AMS at the Keck Carbon Cycle AMS Facility, University of California, Irvine under the supervision of Dr X. Xu. Calibrations performed in Calib 7.04 using IntCal 13 (Reimer et al., 2013).

Publication code	Sample identifier	Master sequence depth	Sample type	^{14}C Enrichment (% Modern $\pm 1\sigma$)	Uncalibrated Radiocarbon Age (years BP $\pm 1\sigma$)	Carbon content (% by wt.)	$\delta^{13}\text{C}_{\text{VPDB}}$ ‰ AMS online	Max cal age BP (2σ)	Min cal age BP (2σ)	Mid cal age BP (2σ)	Cal age error \pm
UCIAMS-154516	D1 R2-1 70-71 cm	73.25- 74.25 cm	<i>Salix</i> spp. Macrofossil	98.09 \pm 0.27	155 \pm 25	52.6	-23.7	284	1	141.5	141.5
UCIAMS-154520	D1 R2-2 50-51 cm	108.25- 109.25 cm	<i>Salix</i> spp. Macrofossil	97.36 \pm 0.26	215 \pm 25	51.5	-25.1	304	1	151.5	151.5
UCIAMS-154521	D1 R2-2 50-51 cm	108.25- 109.25 cm	Bulk sediment	87.60 \pm 0.24	1065 \pm 25	0.21	-21.2	1051	929	990	61
UCIAMS-154512	D1 R2-2 103-104 cm	161.25- 162.25 cm	<i>Salix</i> spp. Macrofossil	98.05 \pm 0.50	160 \pm 45	53.2	-18.6	288	1	143.5	143.5

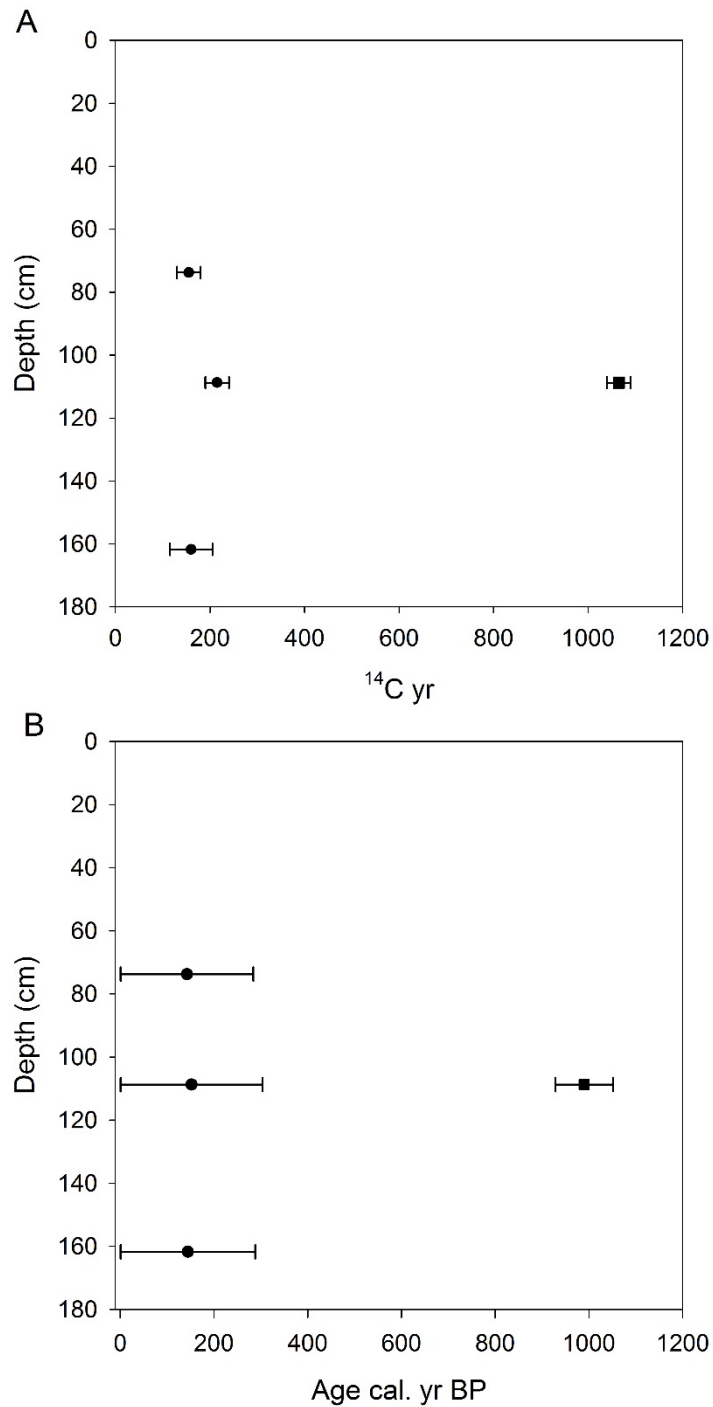


Figure 6.2: Radiocarbon dating results plotted against depth. A - presents uncalibrated radiocarbon ^{14}C years BP $\pm 1\sigma$ error. B - presents calibrated radiocarbon years BP $\pm 2\sigma$ error age-ranges. Circular symbols denote date on terrestrial macrofossils, square symbols denote date on bulk sediment. Errors presented in B that reach 0 cal. yr BP are uncertain beyond this point, due to limitations in the calibration method.

6.1.4 Bulk measures

The bulk OM measured using LOI 550 °C for the overlapping Disko 1 Russian sequences (R2-1 and R2-2) ranged between ~3% and ~8% (Figure 6.3). At the start of the sequence the OM fluctuated around ~4% (~163 cm), before an abrupt decline at 143 cm to ~2.5% until between ~139 cm to 133 cm where it peaked, reaching ~5%. The OM then remained fairly stable around ~3.5%, until ~100 cm where it increased gradually until ~83 cm (~4.5%). Following this, there was a peak in OM reaching ~8% at ~81 cm depth, before a decline to ~4% around ~75 cm. The R2-1 core then reached a maximum peak of ~8 cm, compared with just 5.5% in R2-2 at around ~70 cm. OM then declined to ~4% by 60 cm depth and fluctuated until ~35 cm, before rising to ~4.5% between 23 cm and the top of the core. The HON-Kajak (K1) bulk OM ranged between ~2% at 24 cm depth to ~3% by 9 cm, declining to ~2% by 4.5 cm. This was followed by a peak at ~4 cm to ~3.5%, declining to ~2% by the top of the core.

Bulk DW for the overlapping Disko 1 Russian sequences R2-1 and R2-2 ranged between ~68% and ~77% between 163 cm and ~130 cm, followed by successive step increases to ~75% (by 128 cm), and 79% (by 138 cm). This was followed by a gradual but variable increase to ~80 % DW by ~82 cm, followed by an abrupt decline to ~69% by ~81 cm. At ~70 cm the R2-1 and R2-2 cores DW values were found to overlap. Although the raw values in both cores ranged between ~70 and ~81% during the overlap (~81 – 61 cm), the patterns were found to be broadly similar (Figure 6.3). Above ~61 cm DW increased to ~84% by 56 cm, followed by a decline to ~76% by ~46 cm. Above 40 cm DW remained stable around ~77% to ~28 cm, where it declined gradually until around ~71% at ~13 cm depth, followed by a slight increase to a peak of ~74% at ~7 cm depth. K1 bulk DW ranged from ~75% at ~21 cm depth, variably to ~62% by ~8 cm. This was followed by a peak to ~68% by 5% and a variable decline to ~55% by the top of the core.

Throughout the combined R2-1 and R2-2 sequence the amount of carbonate (CaCO₃) was fairly low ranging from a minimum of <1% to a maximum of 2.5%, remaining relatively stable within this narrow range. Between ~163 and ~108 cm the CaCO₃ fluctuated between ~1 and ~2%, with an increase abruptly after ~108 cm to fluctuations between ~1.5% and ~2.5% until ~50 cm. The overlaps between R2-1 and R2-2 between ~81 cm and ~61 cm were generally consistent. CaCO₃ levels continued to fluctuate between ~1 and ~2% to the top of the core. K1 bulk CaCO₃ was slightly higher, ranging between ~3 and 4%, with a peak to ~4.7% at ~18 cm depth.

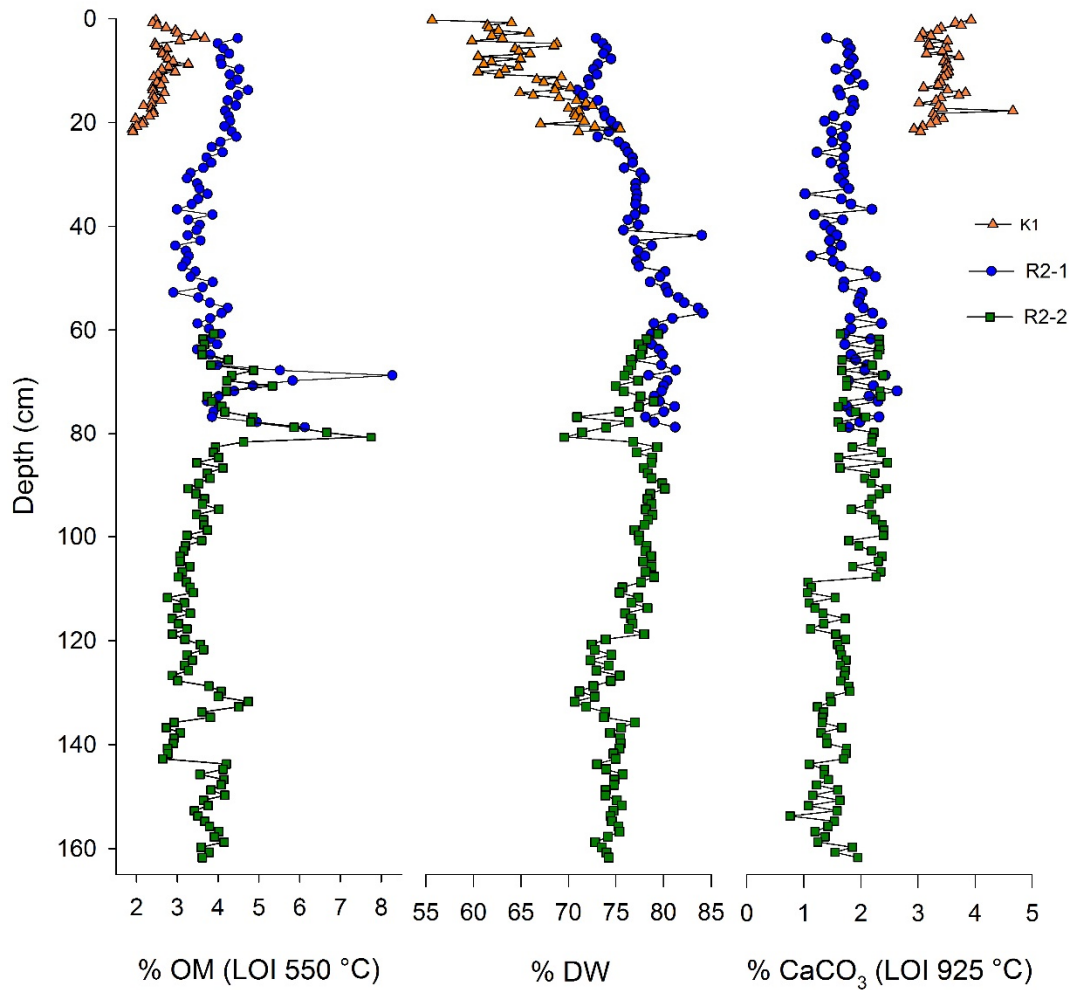


Figure 6.3: Stratigraphic diagram for Russian (R2-1 & R2-2) and HON-Kajak (R1-1) overlapping sequences from lake Disko 1. Presented measures include: organic matter content ((OM) loss-on-ignition at 550 °C for 5 hours (LOI 550°C)), percentage dry-weight after drying at 105 °C overnight (DW) and loss-on-ignition at 925 °C for 2 hours with carbonate correction (CaCO₃ (LOI 925 °C)).

6.1.5 Disko 1 sequence – Pigment results

The final combined stratigraphic pigment diagram including the two overlapping Russian drives and HON-Kajak short core was formed from R2-1 until 75 cm, R2-2 until 21.75 cm, followed by a switch to K1 to the end of the sequence (Figure 6.4). Optimal partitioning using Zone v 2.1 (Juggins, 1991) was used to split the sequence into three zones, using all variables in Figure 6.4 in addition to DW and CaCO₃. Three zones from 0-21.5 cm (R2-A), 21.5-92.25 cm (R2-B) and 92.25-163 cm (R2-C) were used to describe changes in pigment concentration expressed relative to organic matter.

Zone C

Pigment concentrations were generally low and slightly less variable in zone C compared with the other two zones. Concentrations of fucoxanthin, diatoxanthin, alloxanthin and pyropheophytin *a* were all low between ~0 and ~2 nmol pig g⁻¹ org w. sed. Diatoxanthin had three minor peaks at ~134 cm and ~120 cm and ~108 cm to ~2 nmol pig g⁻¹ org w. sed. and was also generally low. The minor peak at ~134 cm and a more pronounced peak at ~108 cm was also visible in lutein-zeaxanthin, chlorophyll *a* and β-carotene, but generally concentrations in these sequences were relatively low. Canthaxanthin and pheophytin *b* (to a greater extent) had a more fluctuating profile during zone R2-C, with the highest concentration in canthaxanthin at ~158 cm and in pheophytin *b* at ~163 cm.

Zone B

Fucoxanthin and diatoxanthin were also found to have low concentrations in zone B throughout the sequence with only minor fluctuations present. Although proportionately smaller peaks were found at the same depth for diatoxanthin and alloxanthin, two clear peaks between ~67 cm to ~72 cm, and ~78 to ~85 cm were found in lutein-zeaxanthin and chlorophyll *a*, which was mirrored by the two peaks in OM. Similar but less pronounced peaks were present at the same depths in diatoxanthin and β-carotene, and at ~75 cm to 82 cm in alloxanthin. Minor fluctuations between ~40 cm and 44 cm were present in diatoxanthin, alloxanthin, lutein-zeaxanthin, canthaxanthin, pheophytin *b* and β-carotene.

Zone A

Most pigments (except lutein-zeaxanthin, diatoxanthin and β-carotene which remained low) displayed a pronounced increase in Zone A compared with the previous two

zones. For example, diadinoxanthin increased from ~0-1 to ~15 nmol pig g⁻¹ org w. sed. at its peak at ~5 cm depth. Alloxanthin, canthaxanthin, pheophytin *b*, pheophytin *a* and pyropheophytin *a* all peaked in concentration at ~4-6 cm depth. Pheophytin *a* had the highest concentration in Zone R2-A (reaching >90 nmol pig g⁻¹ org w. sed.), followed by pyropheophytin *a* (reaching >25 nmol pig g⁻¹ org w. sed.) and chlorophyll *a* (reaching >20 nmol pig g⁻¹ org w. sed.). Chlorophyll *a* had peaks at ~1 cm and ~3 cm depth. Canthaxanthin reached its peak of ~1.3 nmol pig g⁻¹ org w. sed. at ~7 cm depth, followed by a slight decline to <0.8 nmol pig g⁻¹ org w. sed. to the top of the core.

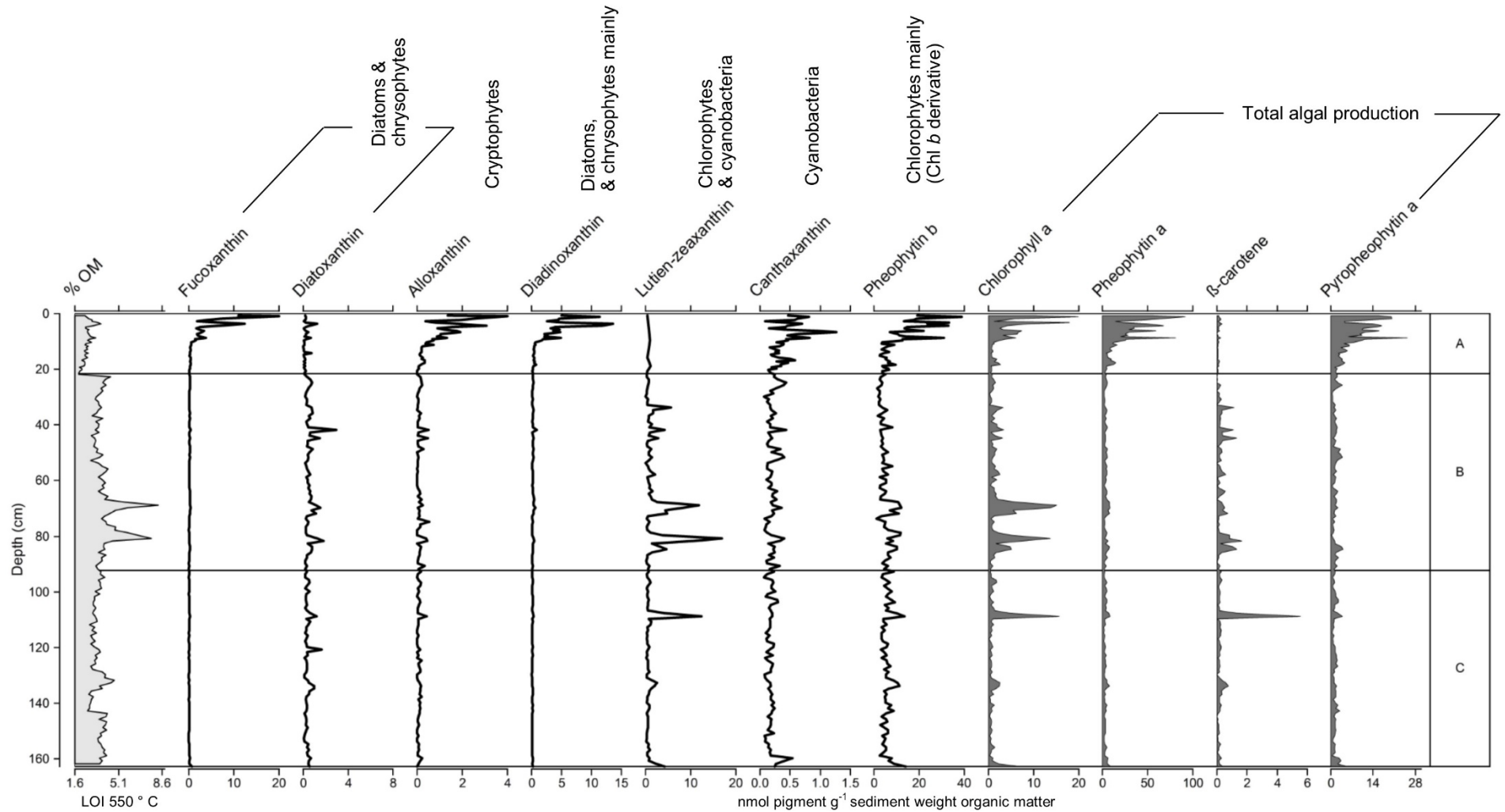


Figure 6.4: Stratigraphic pigment diagram for final combined core sequence from lake Disko 1. Split into three Zones (A, B & C) using optimal partitioning. Zone calculations included all variables in the figure above in addition to DW and CaCO₃.

6.1.6 Exploratory statistics – Disko 1 sequence

The PCA ordination biplot for the Disko 1 combined stratigraphy with pigments (as species) plotted against samples had eigenvectors of 0.58 for PCA axis 1 and 0.25 for PCA axis 2 (Figure 6.5). Among pigments three clear groups were present. The pigments pheophytin *b*, canthaxanthin, pheophytin *a*, alloxanthin, diadinoxanthin, fucoxanthin and pyropheophytin *a* were most closely associated with PCA axis 1 (0.58), whereas lutein-zeaxanthin, β -carotene and diatoxanthin were most closely associated with PCA axis 2 (0.25). In contrast, chlorophyll *a* was located mid-way between the two axes. Samples from zone A were co-located predominantly within the space occupied by the pigments associated with PCA axis 1, whereas samples from zone B and C were located in a trajectory adjacent to PCA axis 2. Lutein-zeaxanthin, β -carotene and diatoxanthin (PCA 2) reflect long-term change throughout the core, whereas pheophytin *b*, canthaxanthin, pheophytin *a*, alloxanthin, diadinoxanthin, fucoxanthin and pyropheophytin *a* (PCA 1) reflect the most strongly responsive pigments to recent change.

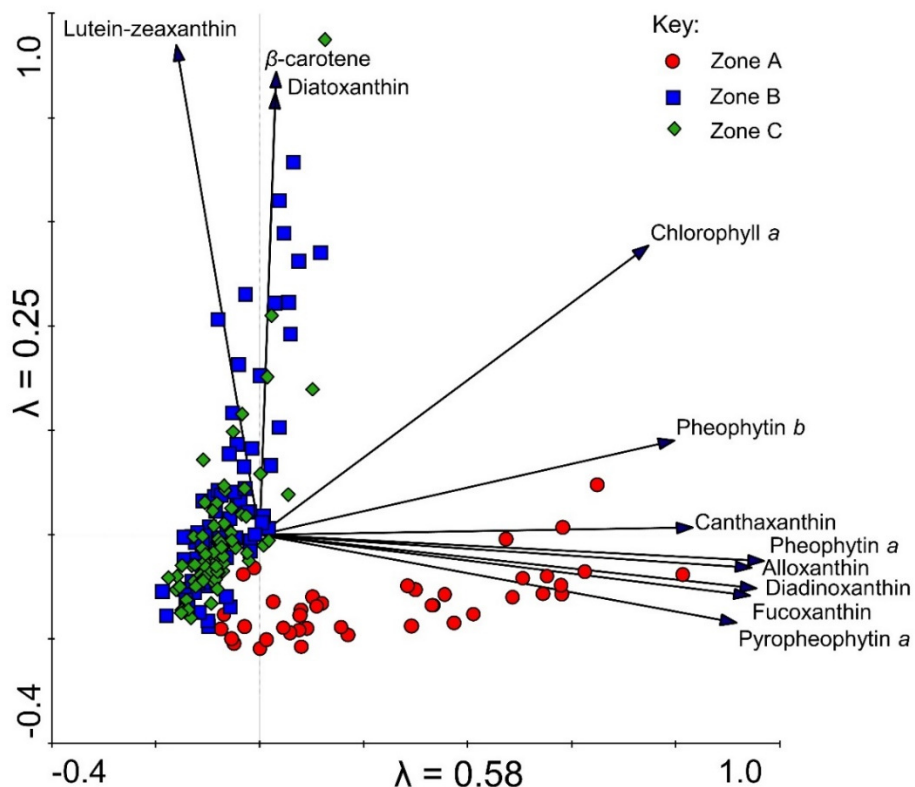


Figure 6.5: PCA ordination biplot for Disko 1 combined stratigraphy. Complete with pigments (as species) plotted against samples. Red circles denote samples from zone A, blue squares samples from zone B and green diamond zone C. Eigenvectors are 0.58 for PCA 1 and 0.25 for PCA 2. Data were log transformed, centred and standardised prior to analysis. PCA was selected as DCA had low gradient lengths < 2.5 (DCA gradient length 1 = 1.26, DCA gradient length 2 = 0.92).

6.1.7 Pigment ratios and PCA scores – Disko 1 sequence

To elucidate the key changes in pigment data principal components analysis (PCA) (Figure 6.6) was performed because detrended correspondence analysis (DCA) produced gradient lengths < 2.5 S.D. Key pigment ratios were also explored to assess variation both between algal groups (e.g. alloxanthin: diatoxanthin, for cryptophytes: diatoms) and within algal groups (e.g. fucoxanthin: diatoxanthin, for two potential comparative indicators of diatoms and chrysophytes).

Zone C

PCA axis 1 and 2 scores were generally low, fluctuating around ~ 0 from ~ -1 to ~ 1 (likely due to scaling). There were also minor peaks at the bottom of the core (~ 163 cm) and at ~ 133 cm, both to ~ 2 cm in PCA 2. The ratio of lutein-zeaxanthin to diatoxanthin similarly had peaks at the bottom of the core (~ 163 cm) of ~ 7 and at ~ 133 cm of ~ 5 . The ratios of chlorophyll *a*: pheophytin *a*, fucoxanthin: diatoxanthin, alloxanthin: diatoxanthin and fucoxanthin: chlorophyll *a* fluctuated around comparatively low values. In contrast, the ratio alloxanthin: chlorophyll *a* fluctuated widely throughout the zone with sharp peaks every ~ 2 cm, reaching > 0.60 . A clear peak at ~ 108 cm depth was present in PCA 2, the ratio of lutein-zeaxanthin: diatoxanthin and chlorophyll *a*: pheophytin *a*.

Zone B

PCA axis 1 scores remained low in zone B, fluctuating around ~ 0 (from -1 to 1). Peaks > 2 were present in PCA 2 at ~ 81 cm, ~ 69 cm and ~ 34 cm. Both the ratio of lutein-zeaxanthin: diatoxanthin and chlorophyll *a*: pheophytin *a* had peaks at similar depths to PCA axis 2, with the largest peaks at ~ 81 cm (lutein-zeaxanthin: diatoxanthin = > 14 ; chlorophyll *a*: pheophytin *a* = > 4). There were no major peaks in the ratio of fucoxanthin: chlorophyll *a* (all fluctuating $\sim 0.3-0.5$) although there was a slight noticeable increasing trend from the minimum at ~ 71 cm (~ 0) to the end of the zone at ~ 21 cm (~ 0.5). Similar to the previous zone, both fucoxanthin: diatoxanthin and alloxanthin: diatoxanthin ratios had very low values, with only very few minor fluctuations around ~ 74 cm. In contrast, the ratio of alloxanthin: chlorophyll *a* was much more varied and fluctuating, with two peaks > 0.40 at ~ 91 cm and ~ 74 cm. Above ~ 73 cm the ratio of alloxanthin: chlorophyll *a* continued to fluctuate, but the variability was slightly less pronounced.

Zone A

PCA axis 1 was characterised by a pronounced increase from ~1 at the start of the zone, peaking at ~8 cm with a value of ~4, followed by an intermittent variable increase to ~4.5 by ~1.5 cm depth. PCA axis 2 was slightly lower than the previous zone and fluctuated between -1 to ~0. The ratio lutein-zeaxanthin: diatoxanthin had intermittent variable peaks to ~7 (at ~19 cm) and ~15 (at ~19 cm) depth. Chlorophyll *a*: pheophytin *a* was low throughout the zone (~0 to 3). The ratios fucoxanthin: chlorophyll *a*, fucoxanthin: diatoxanthin and alloxanthin: diatoxanthin all featured similar, but fluctuating increasing ratios, with the highest values in the top ~5 cm. There were peaks in the ratio alloxanthin: chlorophyll *a* at ~11 cm and ~4 cm.

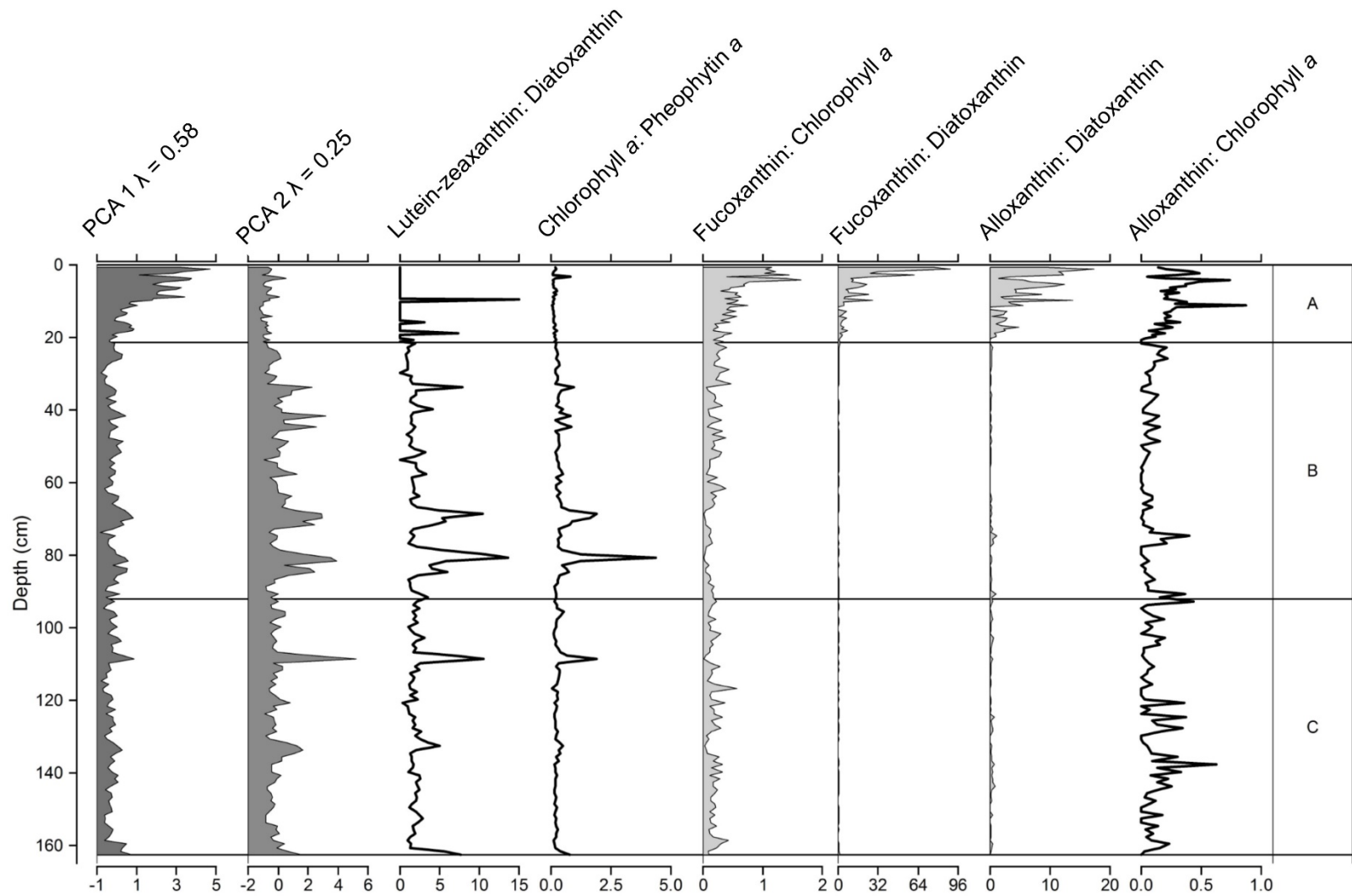


Figure 6.6: Disko 1 final combined core sequence pigment PCA 1 & 2 scores on \log^{10} transformed data (centred and standardised) and key pigment ratios. Eigenvectors are 0.58 (PCA 1), and 0.25 (PCA 2).

6.2 Discussion of sedimentary sequence from Disko 1

6.2.1 Stratigraphy

The stratigraphy based on overlapping bulk measures for the Russian drives (R2-1 and R2-2, Figure 6.3) and pigment trends for the Kajak overlap (Figures D1-3) fluctuates between fine laminations and deposits of more homogeneous silty clays, suggesting sediments derive from a mixed minerogenic glacial and arctic wetlands source (Figure 6.1). Both freshwater and marine sediments particularly those downstream of glacial and periglacial landforms are often laminated in this region (Anderson et al., 1999; Long et al., 2011). Laminations form when there are distinct inputs within each year such as peaks in algal production or variations in meltwater inputs. However, it is uncertain if the fine laminations in the Disko 1 sequence are varve couplets with finer particles settled during winter ice cover, or are tied to specific non-seasonal catchment events as these bands are intermittent (Figure 6.1).

The middle part of the Qivittut Lake record on Disko Island (Bennike, 1995) consists of laminated silt and some layers in the sequence from a lake on Qeqertarsuaq Island to the south of Disko were found to be laminated in places (Fredskild, 2000). Similarly, further south at Sisimiut (Leng et al., 2012) and Kangerlussuaq (McGowan et al., 2003; Anderson and Leng, 2004) sediments have been found to also be composed of finely laminated sediments, although these cores were more highly organic.

For laminations to be preserved optimal conditions are required including low benthic invertebrate populations, deep water and sometimes an anoxic hypolimnion (Anderson et al., 1999). However, many of the laminations in the Disko 1 sequence are variably distorted (e.g. Image D – Figure 6.1) which could be due to the Russian coring method used leading to potential coring artefacts or possible slumping of the cores during transportation. However, some fluctuations are extremely contorted and more likely to be a result of variable sediment focusing within the basin (Lehman, 1975). Disko 1 is a highly non-uniform basin (Figure 4.2), with multiple inflows from known glaciers in the catchment. As entrained material enters the lake from different inflows, combined with seasonal variations in hydrology this would lead to riverine-like proglacial bed-forms (Church and Gilbert, 1975). During summer 2013 the surface currents in Disko 1 were noticeably originating from the northern inflow, potentially influencing sedimentation in a radial manner (Figure 4.2 – flow origin indicated). Further, complex basin shapes are more likely to affect sediment focusing and deposition (e.g.

frustum or hyperboloid-like) than simpler basin shapes (e.g ellipsoid or sinusoid-like) (Lehman, 1975). Since Disko 1 is located <1 km from upstream glaciers, on both a yearly and seasonal basis, particularly during spring melt there would be wide hydrological variations. This would likely alter the connectivity of the basin to its 'mossy' adjacent wetlands (Hooke, 2003), varying the entrainment of organic matter which can become re-deposited in lake sediments. Evidence of water tolerant species across much of the Disko 1 basin and significant waterlogging suggests that during flood pulse events (Junk et al., 1989), the Disko 1 lake will become part of a braided glacial 'riverscape' (Malard et al., 2006), with much higher landscape connectivity. Clay bands present at varying intervals in the stratigraphy (Figure 6.1) are likely due to fluvial erosion following glacial retreat.

6.2.2 Bulk measures

The low OM (~2-8 %) is consistent with a relatively unproductive system, with a predominance of minerogenic inputs (Figure 6.3). The pulses in OM at ~78 and 70 cm are associated with macrofossil layers noted in the stratigraphy (Figure 6.3) and are likely the result of localised catchment disturbance from erosive glacial or periglacial processes, disturbing and entraining plant material. The high DW values (~57-84 %) confirm the dominance of minerogenic material, but there was poor overlap of absolute values, between ~73 and 83 cm (Figure 6.3). However, the patterns at the same depth between R2-1 and R2-2 were similar. This is because the DW value is reliant on the moisture content of the sediment during sampling, which due to transportation was ~4 months after coring. The low CaCO₃ (~1-4 %) composition of the sediments is consistent with the granite and basaltic geology, which will not have promoted significant calcium carbonate precipitate and reflects values probably below the detection limit (BDL) of the method. The low CaCO₃ which is unlikely to be a detrital source, could reflect the loss of water from clays, as loss-on-ignition at 925°C is a method for estimating CaCO₃ composition, rather than directly measuring it (Heiri et al., 2001).

6.2.3 Radiocarbon dating

There were no ²¹⁰Pb or ¹³⁷Cs measurements available for sediments from Disko 1 and so interpretations are reliant on radiocarbon dating. Dates did not show evidence of

^{14}C enrichment so there was no clear post-bomb effect and so reflect dates prior to AD 1950. However, all radiocarbon dates yielded relatively recent dates which suggests a fairly high sedimentation rate at Disko 1 (Table 6.1, Figure 6.2). The relatively high sedimentation rate for an Arctic lake is likely due to local catchment factors such as the presence of a high percentage of the catchment (~14%) covered with glaciers or permanent snow cover. The younger ages on plant *Salix* macrofossils (155 ± 25 ^{14}C yr to 215 ± 25 ^{14}C yr), compared with a much older date on bulk sediment (1065 ± 25 ^{14}C yr) could be due to the hard water effect which causes ages to be too old if the source (e.g. algae/aquatic plant) utilises old bicarbonate in the lake water (Shotton, 1972). However, the low sedimentary CaCO_3 in this system (Figure 6.3), possibly below detection limits (BDL) of the method, supported by low in-lake Ca^{2+} (Table 4.3) makes this explanation unlikely.

A more likely scenario is that old organic carbon, released from periodic permafrost or glacier melt in the catchment is influencing the bulk ^{14}C ages (Singer et al., 2012). At the depth of 108.25-109.25 cm a paired macrofossil was analysed together with bulk sediment, yielding an uncalibrated ^{14}C age offset of 850 years (based on the middle ^{14}C ages of both samples). An alternative explanation that the denser terrestrial macrofossils might have sunk through the sediment matrix is unlikely, both due to the likely high sedimentation rate in this sequence and the presence of finely laminated sediments above sampled macrofossils.

The mixed order (with increasing depth) of the ^{14}C dates on the *Salix* plant macrofossils may partly be due to the fact that slow growing woody *Salix* macrofossils are relatively long-lived (Oswald et al., 2005) and may be sequentially re-buried from other parts of the catchment, prior to final deposition together with the overlapping age ranges which is expected with dates from a narrow time range. Further, the $\delta^{13}\text{C}_{\text{AMS}}$ value of the plant macrofossil at 161.25 – 162.25 cm in the master sequence was only -18.6‰ , which is less negative than expected for C_3 terrestrial plants (expected -23 to -30‰ , (Meyers and Teranes, 2001)). The less negative $\delta^{13}\text{C}$ value suggests the macrofossil may potentially be contaminated partly with C_3 algae and that the acid pre-treatment was insufficient, as *Salix* macrofossils in the source study investigations had more negative $\delta^{13}\text{C}$ values (Table 4.5, 4.6 & 4.7).

Despite the challenges with interpreting the dates on terrestrial macrofossils, the bulk date has been discounted from this model as the older date is likely more erroneous due to the influence of old organic carbon from the catchment. For the dates from Disko 1 deriving an age-depth model was problematic as calibrated age ranges for the

more source specific terrestrial macrophytes overlap significantly (Figure 5.3 – B), and so for this sequence pigment results were plotted against depth.

6.2.4 Disko 1 geochemical interpretation

Since the radiocarbon dating results were relatively young, the combined sequence will be discussed in terms of recent change on Disko Island. A summary diagram combining selected geochemical measurements from Disko 1 to assist comparison is presented in Figure 6.7. The marked increase in algal production in zone A (Figure 6.4, 6.6 & 6.7) in the majority of pigments suggests a major reorganisation of algal communities in the top ~21.5 cm of the core. Despite high pheophytin *a* in water samples (Table 4.4, see Section 4.8.1), pigment degradation within the sediment matrix is unlikely to be the main driver of these increases as the ratio of chlorophyll *a*: pheophytin *a* (Figure 6.6) remains stable throughout the top 21.5 cm (an indicator of degradation). Increases in other pigments tend to fluctuate, rather than systematically increase only in the uppermost samples (which may indicate preferential degradation). Further, the changes in stratigraphy at the top of the core are only minor and are unlikely to reflect a major change in sediment type which might affect preservation.

Increases in algal production in the most recent sediments of temperate lakes are primarily associated with catchment modifications and nutrient concentrations (McGowan et al., 2012; Taranu et al., 2015). However, in Arctic environments such as on Disko Island there is limited recent direct human modification of the relatively undisturbed catchments, with the only catchment activities of low density summer hiking and winter hunting unlikely to have affected algal production to this extent. Although speculative, Arctic ‘greening’ is one possible explanation whereby warming temperatures or changes in seasonality have led to expansion of shrubs across the Arctic (Sturm et al., 2001; Tape et al., 2006). Such growth of vegetation can over-time improve soils, increasing recycling rates and methanogenic activity, increasing the release of DOC (potential source for heterotrophy) and nutrients into aquatic systems. Increased temperature can deepen the seasonal permafrost active layer and activate microbial activity (Hobbie et al., 2002).

An alternative explanation could be that recent climate warming has led to an expansion of the ice-free season, providing greater potential for algal production, or shifts in species composition (e.g. Smol et al., 2005). Both of these scenarios could be responsible for increases in algal production, but it is uncertain if they could promote the large increases found in key pigments such as alloxanthin, diatoxanthin and pheophytin *a* (Figure 6.4 & 6.7). For example, alloxanthin increases four-fold from <1 to ~4 nmol pig g⁻¹ org w. sed, diatoxanthin 7 fold from <2 to ~15 nmol pig g⁻¹ org w. sed and pheophytin *a* 7 fold from <10 to >70 nmol pig g⁻¹ org w sed. There is some

evidence that temperature, specifically winter warming on Disko Island may directly lead to increased *Betula nana* growth. Dendroclimatological records from *Betula nana* on Disko Island less than 10 km from Disko 1 suggest the importance of winter warming between AD 1910 –1930, and again between AD 1990 and 2011, where thawing occurred earlier and where there were higher numbers of growing degree-days (Hollesen et al., 2015). These dendroclimatological records also show a pronounced change in the last 20 years with increases in *Betula nana* linked to warmer winter and spring air temperatures.

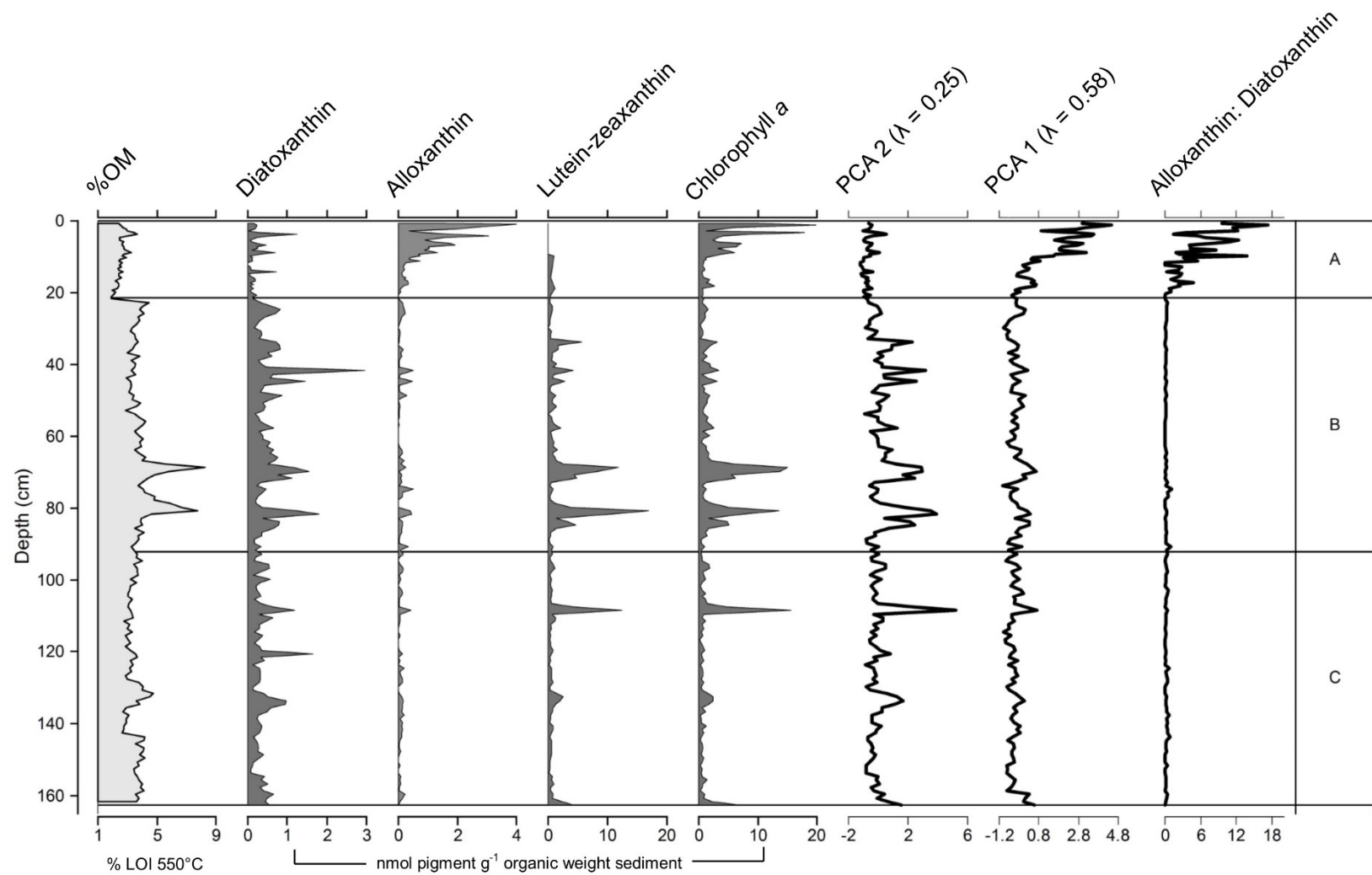


Figure 6.7: Disko 1 summary diagram combining OM, selected pigments (diatoxanthin, alloxanthin, lutein-zeaxanthin & chlorophyll *a*), pigment PCA axes (1 & 2) and the ratio of alloxanthin: diatoxanthin for clear comparison.

However, changes in temperature may also indirectly lead to catchment changes such as the retreat of glaciers. Disko Island has geomorphological evidence of retreat in the majority of glaciers since the end of the Little Ice Age (LIA) (AD ~1880). The positions of glaciers, particularly those extending from the Lyngmarksbræen ice cap have been regularly surveyed, for example by Steenstrup (1901) who compared the photographs of glacier position between AD 1880 and AD 1898, and Jost (1940) who compared his observations from an AD 1913 survey of the central valley glaciers to a survey in AD 1931-33. More recently, Weidick (1968) and Humlum (1987) have used aerial photography, to track glacier retreat on Disko with satellite imagery used to update these records (Yde and Knudsen, 2007). The current understanding is that recession rates were highest during the first half of the century (AD 1920-1940), followed by a stationary phase (AD 1953-1964) and an active phase of recession (1964-1985), although more recently most have remained stationary (AD 1985-2005), but with some continuing to recede (Yde and Knudsen, 2007). Each glacier responds independently to changes in climate, snowfall and wind-direction.

It is likely the glacier that primarily feeds the Disko 1 lake retreated as there is a clearly visible moraine and extensive non-vegetated eroded material in a scoured path, suggesting recent retreat (Figure 4.4). This extent of retreat since the LIA, for the primary glacier that feeds Disko 4 is estimated in Ingólfsson et al. (1990) to be up to 1 km according to an outline map in the study, highlighting evidence of recent changes in the catchment. Although there were some changes in the Disko 1 stratigraphy to more extensive dark reddish brown silty clay, with minor fluctuations of light brown silty clay at the top of the sequence (Figure 6.1), the analysis of particle size may helped to confirm the possible glacial origin of these sediments.

A possible explanation for the significant increases in algal production in the majority of pigments from Disko 1 (Figure 6.4), also suggested by PCA axis 1 scores (Figure 6.6 & 6.7) is the role of glacial retreat. The retreat of glaciers can modify the hydrological regime of downstream lakes, particularly during spring melt and if continuous during the ice-free season can increase the water depth, facilitating enhanced planktonic production. Disko 1 is a relatively shallow lake (April 2013 maximum depth 5.9 m) and so it is possible increased melt may have changed the average ice-free season water depth. An alternative mechanism could be that increased glacial melt has brought in enhanced nutrient concentrations, stimulating algal production. This scenario is consistent with the relatively high phosphorus concentrations (Table 4.4) recorded in Disko 1 both directly under the ice and during the summer melt-free season. Both diatom assemblages and pigment abundance have

been influenced by nitrogen (N) enrichment in glacier-fed lakes of the US Rocky Mountains (Slemmons et al., 2015) and nitrate concentrations have been found to be higher in glacier fed lakes than snow-pack fed lakes in the same region (Slemmons and Saros, 2012).

Glaciers can be productive environments with sediments and algae able to build up in cryoconite holes on the surface, in moulins, or in the gaps between basal ice and rock (Paterson, 1994; Bagshaw et al., 2013). This biologically active material, often rich in low molecular weight (LMW) DOC can become stored in glacial ice during periods of stability or advance (e.g. during the LIA) and then released during melting (e.g. during retreat since the LIA). Much of this DOM which is released can be ancient and highly bio-available for downstream organisms (Lawson et al., 2014b). Measurements from the Greenland ice-sheet have demonstrated highly labile organic sources from glaciers can enter Arctic aquatic environments (Hood et al., 2015). DOM released from the Greenland Leverett glacier, West Greenland has been demonstrated to be N-rich, suggesting a microbial provenance of highly bioavailable DOM (Lawson et al., 2014a), that can be interpreted as a potential source of nutrition for downstream algal production.

The lack of a pigment response in the top 21.5 cm (zone A) (Figures 6.4, 6.6 & 6.7) of lutein-zeaxanthin and β -carotene (which is proportionally more common in cyanobacteria) suggest not all algae respond to the recent changes in the same way. Although β -carotene is diagnostic of total algal production, in this system it may be an indicator of a more specific group. The profile of β -carotene fluctuates to higher levels in zones C & B at similar levels to lutein-zeaxanthin (indicator of chlorophytes and cyanobacteria). Although chlorophyll *a* and pheophytin *a* do respond to increases in recent algal concentration (A), they also have similar fluctuations to β -carotene and lutein-zeaxanthin in zones C & B. The fluctuations in zones C & B likely reflect the temporary delivery of organic material, DOC and nutrient inputs, related to specific localised catchment events that are hydrologically mediated.

The two pulses in pigment concentration that were coincident with slight increases in OM (~70 cm and 78 cm depth) could reflect pigments from preserved aquatic or terrestrial macrophytes which were sampled in the catchment survey (Table 4.5). This would explain why the pulses are reflected in chlorophyll *a* and lutein-zeaxanthin, but not in for example, fucoxanthin or alloxanthin (Figure 6.6). The clear separation in the PCA ordination (Figure 6.7) between the groups reflects the distinct groups of pigments that respond to recent change. The variability in the ratio of alloxanthin:

chlorophyll *a* likely reflects the intermittent variable nature of complex processes in the catchment linked to glacial and periglacial hydrology. Whereas the fucoxanthin: diatoxanthin and alloxanthin: diatoxanthin ratios both exemplify the distinct re-organisation of algal community, likely related to a major change in the catchment due sustained glacial nutrient and labile DOM release from increases in recent discharges in glacial meltwater.

Without recent dating markers (e.g. ^{210}Pb or ^{137}Cs) it is not possible to confirm if the increase in algal production at the top of zone A (above ~10 cm depth, Figure 6.4, 6.6 & 6.7) is coincident with post-LIA glacial retreat or the more recent winter warming noted on Disko from dendroclimatological proxies (Hollesen et al., 2015). Similar recent increases in chlorophyll *a* pigment concentrations and also the ratio of lutein: diatoxanthin have been found in recent lake sediments on Eastern Baffin Island, ~300 km across Baffin Bay to the west of Disko (Florian et al., 2015). These changes were linked to Anthropocene warming supporting enhanced levels of ‘green’ algae, linked to wider pan-Arctic climate (Smol et al., 2005) or potential nitrogen deposition mediated forcings (Holtgrieve et al., 2011). Chlorophyll *a* concentrations reconstructed by reflectance spectrophotometry have also been found to increase in the most recent sediments in lakes near the Clyde River hamlet on east-central Baffin Island slightly further north (Michelutti et al., 2005). Increases in lake primary production in this study on Baffin Island were fairly coherent and monotonic, and so were linked directly to recent climate warming (Overpeck et al., 1997), driven by the length of the growing season, increased algal habitat availability and nutrients from the catchment (Douglas and Smol, 1999). Although the pigment trends at the top of the sequence do increase significantly in Zone A above 10 cm, the fluctuating nature of the response emphasises the role of the catchment (e.g. glacial activity) in mediating these trends.

6.3 Summary – Disko 1

The Disko 1 sequence was composed of a mixture of silty clay homogenous and laminated sediments which suggest a mixed glacial and Arctic wetland source, probably linked to catchment-mediated fluvial glacial meltwater cycles and seasonal limnology. Increases in multiple pigments in zone A (Figure 6.4, 6.6 & 6.7) in the uppermost sediments were pronounced and have been speculatively linked to catchment-mediated glacial retreat, which has been widely documented on Disko (e.g. Ingólfsson et al. 1990) and the probable release of labile DOC and nutrients (e.g. N & P), stimulating algae. Fluctuations in the pigment response, particularly towards the top of the sequence emphasise the role of the catchment as the dominant control on these algal communities, although the direct effect of warming on the length of the ice free season, or the indirect enhancement of catchment soil and permafrost nutrient cycling may also play a secondary role in the increase in algal production in the most recent sediments.

Dating these sediments was challenging as although radiocarbon dates did not present a clear post-bomb effect, and so reflect dates prior to AD 1950, all terrestrial macrofossil dates were found to overlap helping to suggest that the sediments are relatively recent. A radiocarbon date on bulk OM was offset compared with a terrestrial macrofossil by ~1850 ^{14}C years, highlighting the contribution of old carbon in these glacially influenced systems, and so was excluded from the development of an age-depth model. The peak in algal production at the top of the sequence could be coincident with the end of the LIA and glacial retreat, or more recent warming documented on Disko (e.g. (Hollesen et al., 2015). Future ^{210}Pb or ^{137}Cs dating could help identify the timing of the increase in algal production in the uppermost sediments from Disko 1 more robustly.

Chapter 7: Disko 4 – Results and discussion

This chapter presents (Section 7.1) and discusses (Section 7.2) the results of the analysis of sediment cores from lake Disko 4. Lake Disko 4 is a valley end lake situated in a basin prior to outflow into the Ipraatsi valley, fed by discharge through mossy wetlands from multiple areas of ice within the catchment. As lake Disko 4 is located at an elevation of 214 m. a.s.l. (lowest elevation) and has the largest catchment (1.829 ha) (Table 4.1) it is presented as the third lake in the hydrogeomorphic landscape framework of this thesis and is substantially less vegetated than Disko 2 (Table 4.1). For lake Disko 4 radiometric dating proved effective and it was possible to include all three terrestrial macrofossil dates, removing only a paired bulk date from the model.

In the catchment sample survey $\delta^{13}\text{C}_{\text{TOC}}$ ranged between -27.3‰ and -29.8‰ in Disko 4 (Table 4.7 & Figure 4.15), with higher values in the ‘benthic algal rock scrape’ sample (-20.5‰) and the aquatic moss (-25.8‰). Bryophytes had a broad range from -21.0‰ to -26.1‰ , with soils ranging from -25.3‰ to -25.9‰ . C/N ratios ranged between 24.3 and 70.6 for catchment plant samples, but with low C/N for the benthic algal rock scrape (9.2) and high C/N for the aquatic moss (56.0). Soils had low C/N ratios (11.6 to 12.1) close to aquatic algae (Table 4.7, Figure 4.15). Similar to lake Disko 2, Disko 4 also had a summer 2013 water pigment spot sample dominated by chlorophyll *a* and the degradation product pheophytin *b* (Table 4.4).

7.1 Results – Disko 4

7.1.1 Core correlations – master stratigraphy

The Disko 4 combined sequence comprised the K2 HON-Kajak core together with two overlapping Russian drives (R2-1 and R2-2) from the single Disko 4 coring location (Figure 4.9, 4.10 % 4.11 B-C). The R2 sequence was selected for further analysis from lake Disko 4 as the overlap was clearer and recovery was slightly deeper compared with R1. The R2 sequence was obtained from the deepest part of Disko 4 from a water depth of ~ 6.8 m and comprised two overlapping Russian drives (R2-1 and R2-2), with an overlapping HON-Kajak short core (Figure 7.1). The combined sequence was ~ 130 cm, with further coring prevented by consolidated material, although it is uncertain if this was bedrock. The sequence comprised predominantly homogenous very dark greyish-brown silt, interspersed with macrofossil and

yellowish-brown clay layers. The overlapping of K2 and R2-1 was made primarily on the basis of OM, DW and CaCO₃ measures (Figure 7.2), while the overlapping of R2-1 with R2-2 was based primarily on stratigraphic macrofossil and clay layers (Figure 7.1). The macrofossil layers at ~35 cm in R2-1 (Image C) and ~36 cm in R2-2 (Image B) of the master sequence were corroborated by clay bands at ~65 cm in R2-1 (Image E) and R2-2 (Image D). The top ~15 cm of the K2 core followed similar trends to the top of R2-1 for OM, DW and CaCO₃ variables (Figure 7.2). The final combined sequence used R2-2 from 130-66 cm, R2-1 from 65-15.5 cm and K2 from 15.25-0.25 cm. Although not used as the basis of the core overlaps (due to the potential for selective degradation), pigment overlaps showed similar general trends (Appendix E, Figures E1, E2 & E3).

A noticeable offset in the absolute values of OM was present from ~54 cm onwards in R2-2 (green), so key samples were repeated (red) resulting in lower values, implying slight LOI offsets which can occur with this bulk estimation technique (Figure 7.2). A corrected OM profile was created from ~54 cm onwards for R2-2 (Figure 7.3), based on the mean differences of repeated samples at ~68 cm, ~88 cm, ~103 cm, ~111 cm and ~127 cm depth. There was excellent agreement between OM in R1-1 and adjusted OM for R2-2 over the overlap from ~25 cm to ~80 cm (Figure 7.3). Additionally, there was excellent agreement for DW for the same overlap (Figure 7.2). However, there was a minor offset in CaCO₃ between ~30 cm to ~50 cm of ~0.5%. Excellent overlap in TOC and N was present between ~55 cm and ~78 cm and similar, although more fluctuating overlaps were present in $\delta^{13}\text{C}_{\text{TOC}}$ and C/N.

7.1.2 Stratigraphic descriptions

Core R2-2 (Figure 7.1) comprised predominantly very dark greyish-brown silt from the base (~130 cm) to the top of the core (~29 cm). Within this there was an indistinct clay layer at ~118 cm and two further clay layers at ~105 cm and ~91 cm (Figure 7.1 – Image F). There was a variable patterned clay band (~3 cm thick) at ~65 cm (Figure 7.1 – Image D) which helped tie R2-2 to R2-1. Macrofossil layers were present at ~62 cm, ~38 cm (Figure 7.1 – Image B) and ~35 cm (fine layer). Two fine sandy layers were present at ~56 and ~45 cm depths.

Core R2-1 also comprised predominantly very dark greyish-brown silt from the base (~79 cm) to the top of the core. Yellowish-brown clay layers were present at ~65 cm (Figure 7.1 – Image E), 62 cm and 46 cm. Bands at ~62 cm and ~46 cm were immediately preceded by fine sandy layers. There was a macrofossil layer at ~35 cm (Figure 7.1 – Image C) and two further yellowish-brown clay layers at ~32 and ~25

cm (Figure 7.1 – Image A). A further macrofossil layer (~ 9 cm thick) was present at ~20 cm prior to poor recovery to the top of the core. The K2 core also comprised homogenous very-dark greyish brown silt, with a visible macrofossil layer at the sediment-water interface.

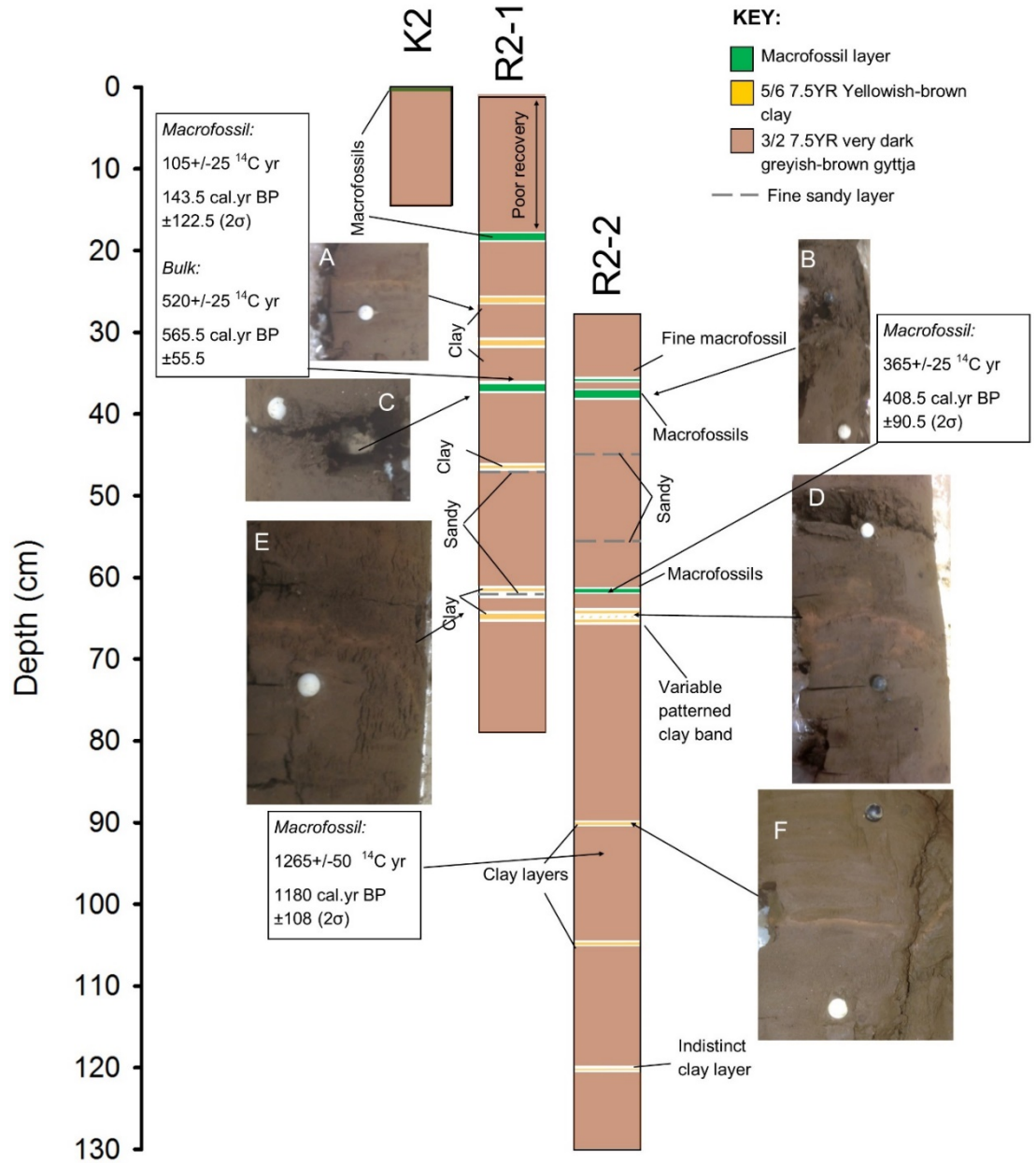


Figure 7.1: Stratigraphy for Disko 4 R2-1 and R2-2 overlapping Russian and K2 HON-Kajak core drives and proposed depth matching sequence. Sediment is described based on identified descriptions provided in the Munsell colour system. Overlapping is based primarily on the macrofossil rich layer ~36 cm and the yellowish-brown clay intrusions ~65 cm, confirmed by comparison with corrected measured depth and geochemical analyses (e.g. LOI 550 °C). Photographs display key macrofossil and clay layers at relevant parts of the sequence. Colours and textures used in the diagram are exaggerated to aid interpretation. Radiocarbon dating results are indicated in square boxes with arrows to indicate the source of the sample. White and black pins on core photographs indicate 5 and 10 cm depth intervals.

7.1.3 Bulk measures

OM is presented in Figure 7.2 and Figure 7.3, although the adjusted values in Figure 7.3 are described here. The bulk OM for the overlapping Disko 4 Russian (R2-1 and R2-2) and HON-Kajak (K2) sequences ranged mainly between ~4 and ~8%. Trends in OM generally changed in direction approximately every 5-10 cm, for example reaching a minimum of ~4% at ~120 cm, ~100 cm, ~92 cm, ~65 cm and ~45 cm, with maximum values of ~7-8 % OM found to be present at ~125 cm, ~95 cm, ~80 cm, ~55 cm and ~35 cm. Higher OM values were present in the Kajak core around ~14 cm (reaching ~8%), ~2 cm (reaching ~8%) and at the top of the core (>13%).

Bulk DW for the master sequence from Disko 4 is presented in Figure 7.2 with potential outliers removed in DW at ~124 cm, ~95 cm and ~22 cm and presented in Figure 7.3. DW ranged narrowly between ~60% and ~70% from the base (~130 cm) to ~15 cm in the sequence. Following a similar pattern to OM, trends in DW generally changed in direction approximately every 5-10 cm. For example, minimum DW (~60%) was present at ~115 cm, ~95 cm, ~85 cm, ~75 cm, ~60 cm and ~40 cm. Maximum values of ~70% DW were present at ~125 cm, ~110 cm, ~105 cm, ~90 cm, ~65 cm and ~35 cm. Above ~15 cm DW values declined to a minimum at ~10 cm (~40%), followed by fluctuations between 10 cm and 5 cm, (~50% – ~70%), and a final pronounced drop to <15% at the top of the core.

Bulk carbonate (CaCO_3) from the Disko 4 master sequence is presented in Figure 7.2 and was found to be very low throughout the sequence ranging between ~1.5% and 3%. Within the narrow range there was generally little variation, although minimum values (~1.5%) were present at ~130 cm, ~90 cm and between approximately 50 cm and 30 cm in the R2-2 core which was offset by ~0.5% in this part of the sequence. The maximum value of 3% CaCO_3 at ~124 cm depth was deemed to be an outlier due to its departure from the general trend. Slight peaks in CaCO_3 above this of ~2.5% were present at ~38 cm, ~22 cm ~15 cm and ~2 cm.

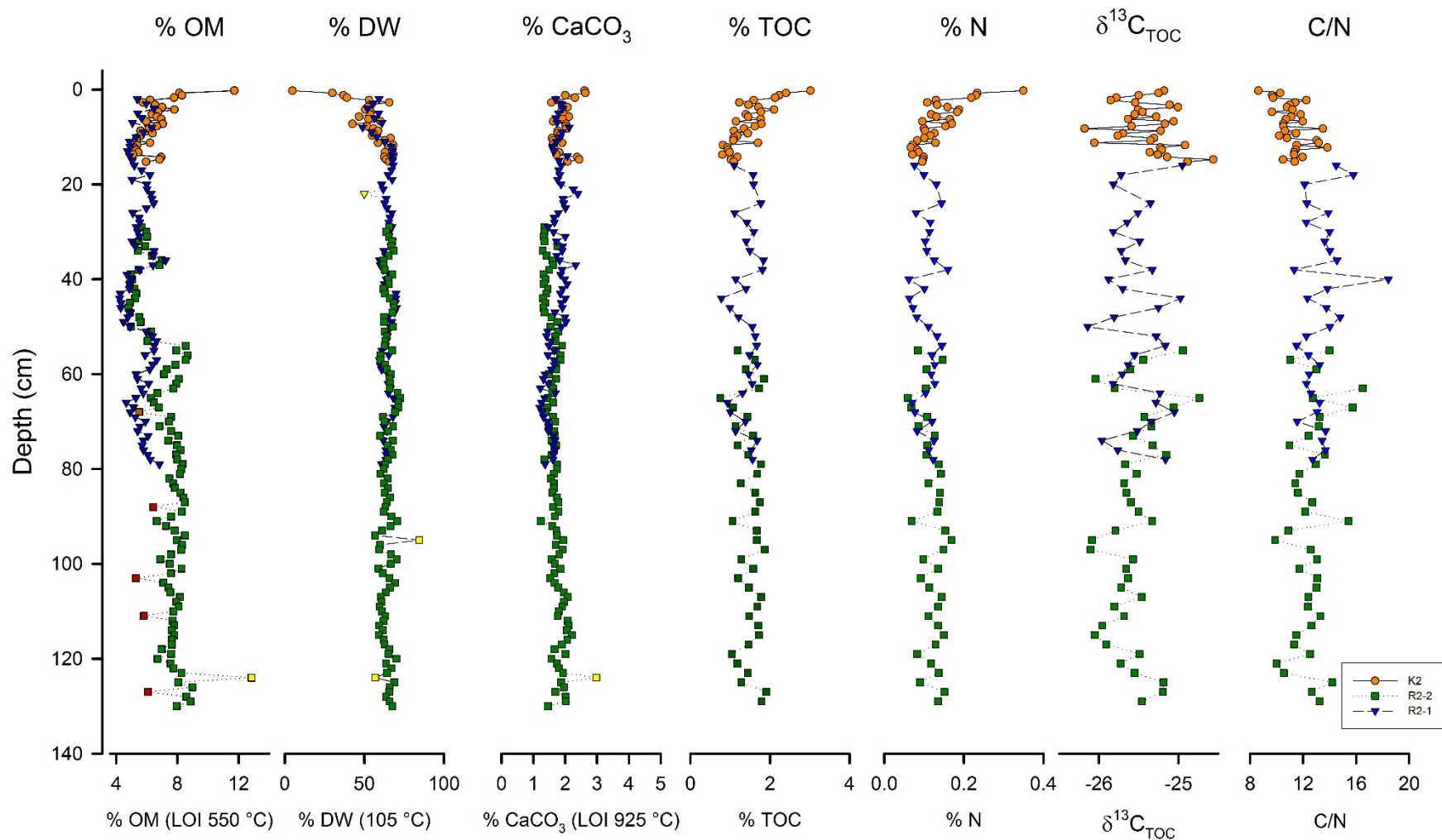


Figure 7.2: Stratigraphic diagram for Russian (R2-1 and R2-2) overlapping sequences and HON-Kajak (K2) core appended above. Variables include % OM (LOI 550 °C), % DW (105 °C), % carbonate ((% CO₃) LOI 925 °C), % TOC, % N, δ¹³C_{TOC} & C/N. Red samples denote repeated samples for % OM. Yellow samples indicate possible outliers removed (by taking the mean of adjacent samples) in subsequent graphs. Offset in OM from ~54 cm onwards in R2-2 most likely due to differences between the efficiencies of furnaces. Subsequent diagrams (Figure 7.3 onwards) resolve this offset.

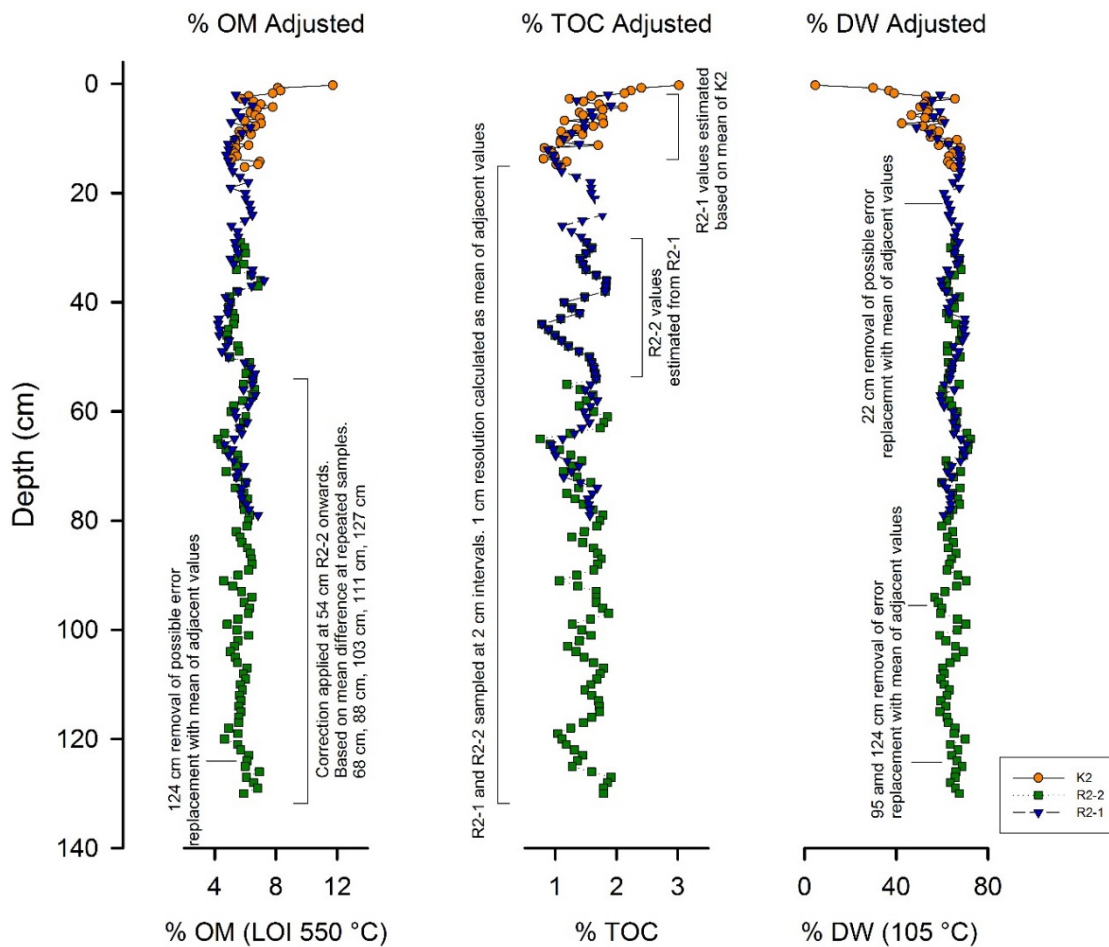


Figure 7.3: Stratigraphic diagram for adjusted values from Disko 4 for OM, TOC and DW which is used in subsequent graphs and expressed relative to pigment concentration. Due to the offset visible in Figure 7.2 for OM in R2-2 from 54 cm onwards a correction was applied based on the mean difference of repeated samples at 68 cm, 88 cm, 103 cm, 111 cm and 127 cm depth. Adjustments to TOC included increasing resolution from 2 cm to 1 cm intervals by calculating the missing values as the mean of adjacent values, estimating R2-2 values from the R2-1 overlap between 54 and 29 cm and estimating missing values between 2-15 cm based on the mean of adjacent TOC values from K2. DW adjustments included removal of outliers at 22 cm, 95 cm and 124 cm.

7.1.4 Radiometric dating

An age-depth model was developed for the Disko 4 combined sequence on the basis of ^{210}Pb , ^{137}Cs , and ^{241}Am measurements for the most recent sediments and AMS ^{14}C for the deeper sections of the core. Radiocarbon dates are appended to the stratigraphic diagram (Figure 7.1), listed in table format according to publication code (Table 7.1) and plotted as part of the age-depth model against depth (Figure 7.7). ^{210}Pb activity for the Disko 4 K2 short core is plotted against depth (Figure 7.4) and modelled as an age depth curve against ^{137}Cs (Figure 7.5) and ^{241}Am activity (Figure 7.6). The sedimentation rate for the Disko 4 K2 short core against depth is also presented (Figure 7.7).

Radiocarbon dating

At 34.5-35.5 cm in the master sequence both a *Salix* plant macrofossil sample and a paired bulk date were analysed to assess the local ^{14}C radiocarbon offset (Table 7.1). The *Salix* leaf fragment yielded a ^{14}C uncalibrated AMS radiocarbon age of 105 BP ± 25 years. The central estimate calibrated expected age was 143.5 cal. yr BP (based on maximum and minimum values) with an error of ± 122.5 cal. yr BP. In contrast, the bulk sample yielded a much older AMS radiocarbon age of 520 ^{14}C years BP ± 25 years. For this sample the calibrated central estimate age was 408.5 cal. yr BP (based on maximum and minimum values) with an error of ± 55.5 cal. yr BP. Further dating on *Salix* plant macrofossils were also made at 62.5-63.5 cm (365 ^{14}C years BP ± 25) and 117.5 – 118.5 cm (1265 ^{14}C years BP ± 50). All macrofossil samples were taken from samples within the core, avoiding the outer edge of the sediment. Full detail on calibrations, maximum/minimum age ranges and $\delta^{13}\text{C}$ values is provided in Table 7.1.

Table 7.1: Radiocarbon dating results from Disko 4 Russian sediment sequences R2-2 and R2-1. Analyses prepared at the NERC Radiocarbon laboratory (East Kilbride) under the supervision of Dr L.M. Cisneros-Dozal with samples measured by AMS at the Keck Carbon Cycle AMS Facility, University of California, Irvine under the supervision of Dr X. Xu. Calibrations performed in Calib 7.04 using IntCal 13 (Reimer et al., 2013).

Publication code	Sample identifier	Master sequence depth	Sample type	^{14}C Enrichment (% Modern $\pm 1\sigma$)	Uncalibrated Radiocarbon Age (years BP $\pm 1\sigma$)	Carbon content (% by wt.)	$\delta^{13}\text{C}_{\text{VPDB}}$ ‰ AMS online	Max cal age BP (2σ)	Min cal age BP (2σ)	Mid cal age BP (2σ)	Cal age error \pm
UCIAMS-154514	D4 R2- D2 89-90 cm	117.5- 118.5	Plant macrofossil (<i>Salix</i> spp.)	85.46 \pm 0.51	1265 \pm 50	56.7	-14.3	1288	1072	1180	108
UCIAMS-154517	D4 R2- D1 34-35 cm	34.5-35.5	Plant macrofossil (<i>Salix</i> spp.)	98.73 \pm 0.27	105 \pm 25	52.3	-23.6	266	21	143.5	122.5
UCIAMS-154519	D4 R2- D2 34-35 cm	62.5-63.5	Plant macrofossil (<i>Salix</i> spp.)	95.53 \pm 0.26	365 \pm 25	58	-22.8	499	318	408.5	90.5
UCIAMS-154524	D4 R2- D1 34-35 cm	34.5-35.5	Bulk	93.74 \pm 0.25	520 \pm 25	3.54	-23.3	621	510	565.5	55.5

Recent dating (^{210}Pb , ^{137}Cs and ^{241}Am)

^{210}Pb activity was higher towards the top of the Disko 4 short core compared with the measurements towards the bottom of the core (Figure 7.4), although the trend was not monotonic. Initially ^{210}Pb activity increased from ~290 Bq/kg at 0.75 cm depth to ~350 Bq/kg at 1.25 cm, prior to a sharp decline to ~45 Bq/kg at 2.75 cm depth. ^{210}Pb activity then increased until 3.75 cm depth (~160 Bq/kg), before declining to 5.25 cm depth (~61 Bq/kg). Measurements then plateaued between ~72 and ~67 Bq/kg until 7.25 cm depth before declining in a linear manner until 11.25 cm, with an activity of <0.5 Bq/kg. To develop the ^{210}Pb age-depth model the CRS model (Appleby, 2001) was used (Figure 7.5). Since the system was unable to detect ^{226}Ra , supported ^{210}Pb was estimated as being a small contribution (0.0004 Bq/g), slightly less than the minimum total ^{210}Pb activity. The depth of zero represented an age of 2013 AD based on coring, which was modelled to decline gradually to ~1993 AD by 3.25 cm.

The age declined at a slightly quicker rate to 1951 AD by 7.25 cm, followed by an increased decline to 1902 AD by 9.25 cm. ^{137}Cs activity to measure radioactive bomb fallout increased from <2 Bq/kg at 9.25 cm to ~80 Bq/kg at 6.25 cm, prior to declining to a minimum of ~7 Bq/kg by 2.25 cm depth (Figure 7.5). The maximum ^{137}Cs activity was coincident with the expected 1963 AD bomb peak and so the ^{210}Pb age was accepted. For ^{241}Am activity (Figure 7.6) most samples were below detection limits except for 6.75 cm and 6.25 cm which had ~17 and ~22 Bq/kg detected respectively and was present between ^{210}Pb modelled ages from 1956 AD to 1963 AD. The sedimentation rate was calculated from the ^{210}Pb age (Figure 7.7) and initially gradually increased from a minimum of ~0.007 g cm⁻²yr⁻¹ to ~0.05 g cm⁻²yr⁻¹ by 1951. It then fluctuated with peaks at ~1963 (~0.15 g cm⁻²yr⁻¹), ~1977 (~0.25 g cm⁻²yr⁻¹) and a major peak in ~1997 (~0.70 g cm⁻²yr⁻¹), prior to a decline to >0.08 g cm⁻²yr⁻¹ by 2012.

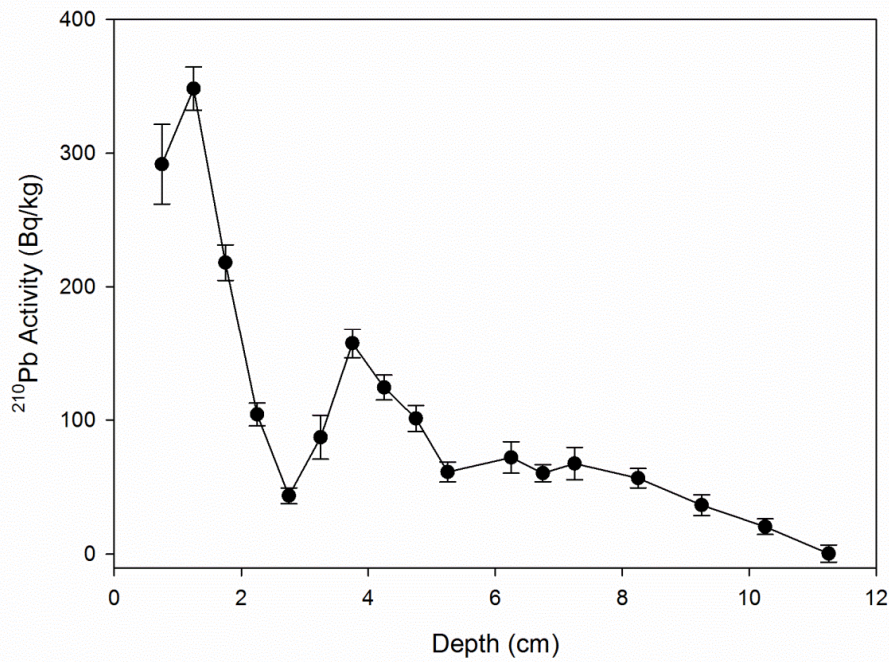


Figure 7.4: ²¹⁰Pb activity plotted against depth for the Disko 4 K2 short core.

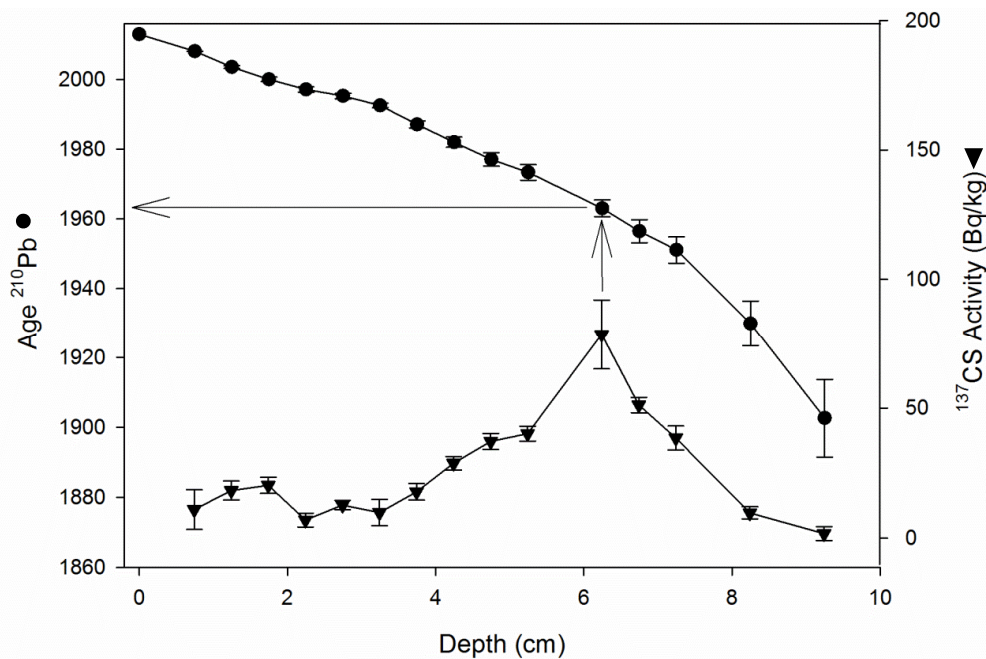


Figure 7.5: ²¹⁰Pb age and ¹³⁷Cs activity plotted against depth for the Disko 4 K2 short core. Model calculated using CRS model (Appleby, 2001). Supported ²¹⁰Pb was estimated as being a small contribution (0.0004 Bq/g), slightly less than the minimum total ²¹⁰Pb, activity as this system could not make ²²⁶Ra measurements. The peak in ¹³⁷Cs is coincident with the ~1963 bomb peak, corroborating the ²¹⁰Pb model.

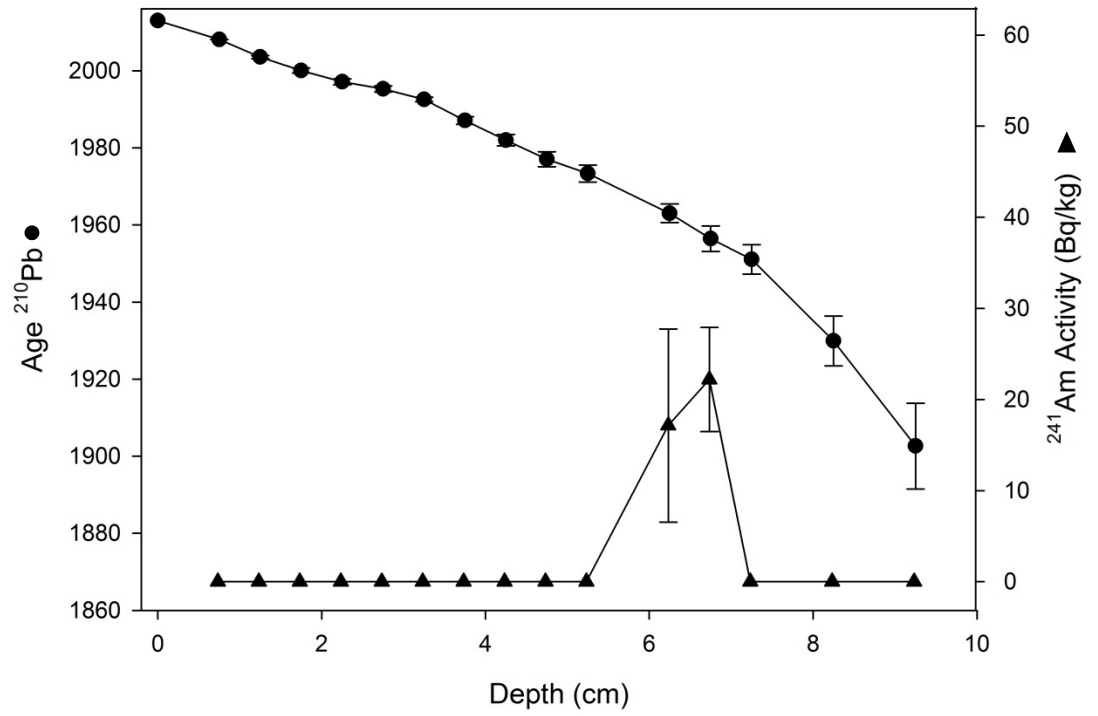


Figure 7.6: ^{210}Pb age and ^{241}Am activity plotted against depth (cm) for the Disko 4 K2 short core.

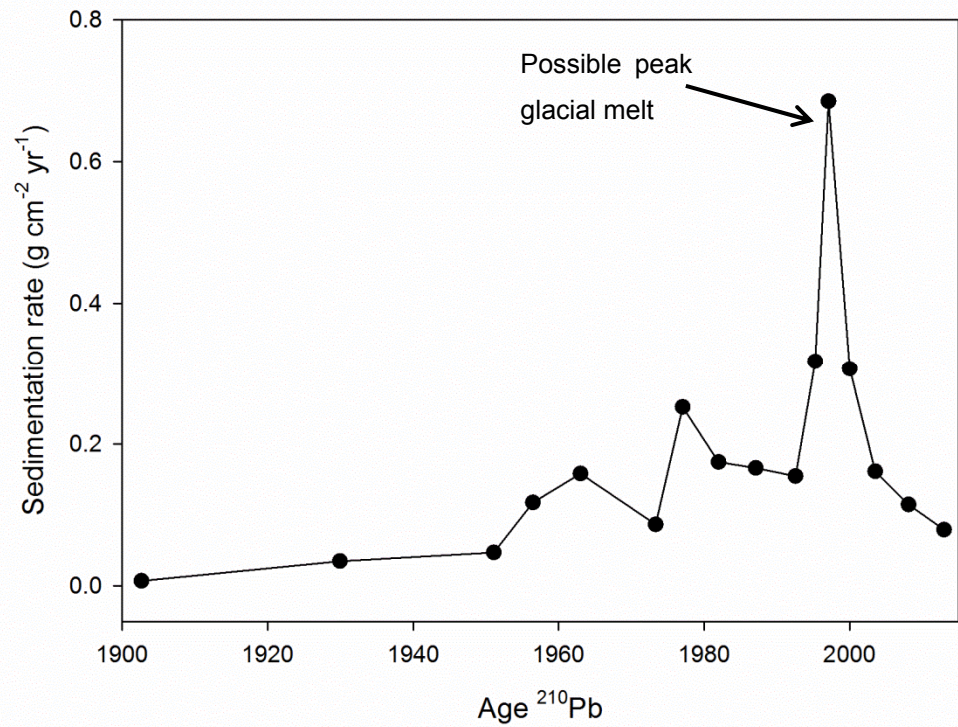


Figure 7.7: Sedimentation rate plotted against ^{210}Pb age for the Disko 4 K2 short core.

Age-depth model

The final age-depth model (Figure 7.8) was produced using Bayesian statistics in Bacon v 2.2 (Blaauw and Christen, 2011, 2013) in the R programming language. The model is a composite of the accepted ^{210}Pb model (top and bottom dates only) from the K2 short core and the ^{14}C dates on terrestrial macrofossils. The bulk date which was much older than the terrestrial macrofossil at 34.5-35.5 cm depth was removed from the model under the principal that younger dates reflect clear sources and avoid reservoir effects, especially when sourced from known terrestrial inputs (e.g. *Salix* spp.). The Bayesian model effectively smoothed the change in rate between the oldest ^{210}Pb dates and the youngest radiocarbon date age range at 34.5- 35.5 cm. Here the older extent of the 2σ age range was selected by the model to have a higher likelihood (red mean age on blue calibrated date). Similarly the mean age (red line) was found to pass through the older part of the 2σ age-range at 62.5 - 63.5 cm, whereas for the date at 117.5 - 118.5 cm the modelled mean age passed through the centre of the expected age range. The 95% confidence interval was narrower over the first 500 cal. yr BP, gradually widening from 500 cal. yr BP to the end of the model. From the final date onwards the mean modelled age was extrapolated to the base of the master sequence (~130 cm).

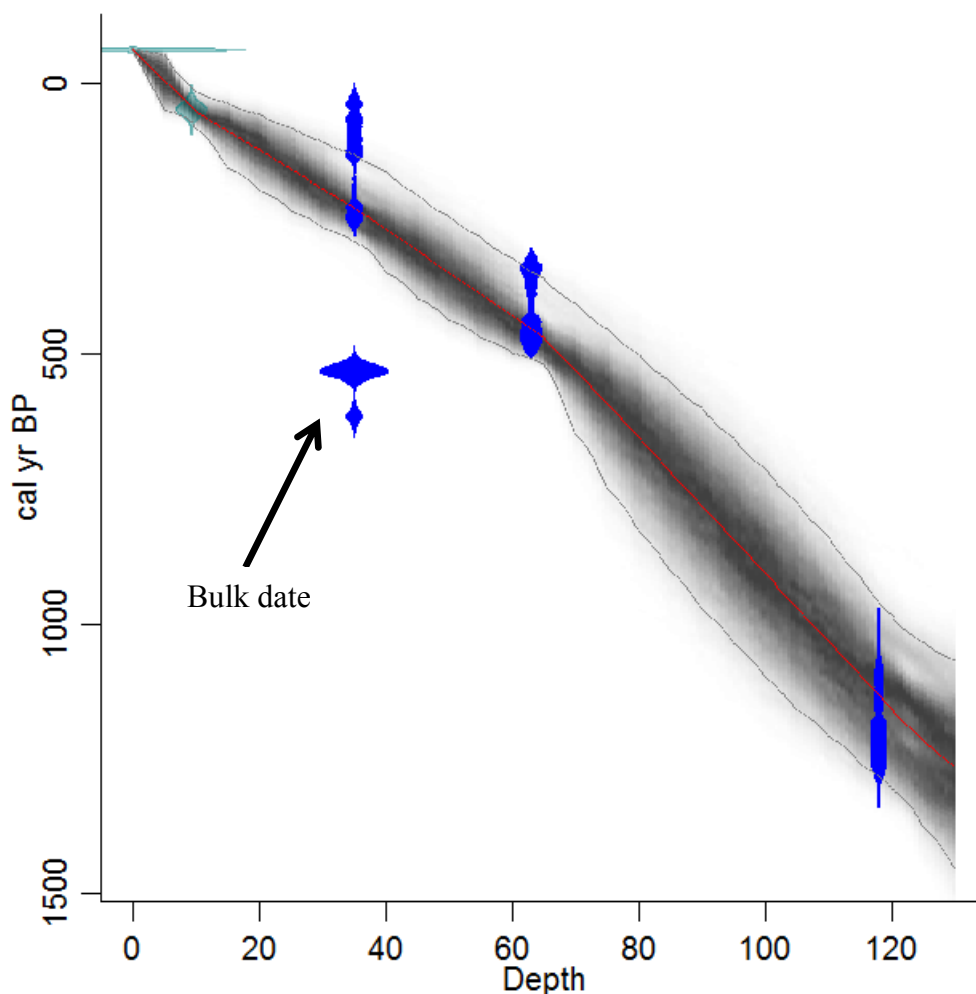


Figure 7.8: Age-depth model for Disko 4 combined HON-Kajak (K2) and Russian (R2-1 & R2-2) master sequence. Produced using Bayesian statistics in Bacon v2.2 (Blaauw and Christen, 2011, 2013). Dates in green at shallow depths are from recent ^{210}Pb radiometric dating on the K2 short core. Dates in blue reflect calibrated ^{14}C dates BP calibrated using IntCal 13 (Reimer et al., 2013), with the shape of the date reflecting the proportional likelihood of an age falling within the relevant part of the calibration curve. Calibrated ^{14}C dates are on *Salix* spp. terrestrial macrophytes, except for the bulk age which is older than the macrophyte at 34.5-35.5 cm in the master sequence (indicated). The red line indicates the mean age-depth model selected, with the grey fill indicating the 95% confidence interval age-range. For model fitting 27 sections were included in the calculation.

7.1.5 Disko 4 combined master sequence – pigment results

The final combined stratigraphic pigment diagrams for Disko 4 were formed from K2 from 0-15.25 cm, R2-1 from 16 cm to 65 cm and R2-2 from 65 cm to 130 cm (Figure 7.12). The plot was split into 5 zones using optimal partitioning from 0-2 cm (A), 2-68.5 cm (B), 68.5-92.5 cm (C), 92.5-114.5 cm (D) and 114.5-130 cm (E). All pigments were expressed against adjusted TOC (see Figure 7.3).

Zone E

Pigment concentrations were generally low at the base of the core (~130 cm), increasing to ~114.5 cm in a fluctuating pattern. For example, fucoxanthin increased from < 1 nmol pigment g⁻¹ TOC (nmol pig g⁻¹ TOC) at ~130 cm to ~70 nmol pig g⁻¹ TOC at the top of the zone. Similar large fluctuating increases were present in canthaxanthin which increased from ~2 nmol pig g⁻¹ at the bottom of the zone to ~20 nmol pig g⁻¹ at the top. In contrast, pigment concentrations remained relatively low and lutein-zeaxanthin did not substantially increase (fluctuating between ~0 and ~5 nmol pig g⁻¹ TOC) and the increase in okenone was only present above ~118 cm (increase from ~2 to ~14 nmol pig g⁻¹ TOC). All pigments were highly varied, but there were sharp peaks in β-carotene at ~120 cm, ~117 cm and ~115 cm. The pigments with the highest concentrations were pheophytin *a* (reaching ~120 nmol pig g⁻¹ TOC), the pheophytin *b*-like compound (reaching ~450 nmol pig g⁻¹ TOC) and pyropheophytin *a* (reaching ~640 nmol pig g⁻¹ TOC).

Zone D

Pigment concentrations were noticeably higher than the previous zone, although variable. Two pronounced declines in pigment concentration were present at ~104 cm and ~99 cm depth and there were shared peaks in pigment concentration at ~105 cm, ~102 cm, ~97 cm and ~94 cm depth. For example, in diadinoxanthin the maximum pigment concentration of ~500 nmol pig g⁻¹ was present at ~101 cm. The pigment profiles of lutein-zeaxanthin and okenone were slightly less varied compared with the other pigments which fluctuated more widely. Again pheophytin *a*, the pheophytin *b*-like compound and pyropheophytin *a* had the highest concentrations (all maximum concentrations > 600 nmol pig g⁻¹ TOC).

Zone C

Pigment concentrations were generally lower although continued to fluctuate widely. Peaks in pigment concentration were generally present at ~86 cm, ~81 cm and ~72 cm.

For example, in pheophytin *b* the maximum pigment concentration was at ~82 cm depth (~430 nmol pig g⁻¹ TOC), followed by a minimum pigment concentration at ~77 cm depth (~50 nmol pig g⁻¹ TOC). Fluctuations were less variable in lutein-zeaxanthin (~2-8 nmol pig g⁻¹ TOC). However, fluctuations were particularly variable in the pigments with the highest concentration including pheophytin *b* (concentration range ~430 to ~50 nmol pig g⁻¹ TOC), pheophytin *a* (concentration range ~1650 to ~80 nmol pig g⁻¹ TOC) and pyropheophytin *a* (concentration range ~1,000 to ~80 nmol pig g⁻¹ TOC).

Zone B

Pigments diatoxanthin, canthaxanthin, pheophytin *a*, β-carotene, and pyropheophytin *a* were markedly lower in concentration compared with the previous zone. The reduction in pigment concentration was pronounced between ~68 cm and ~72 cm where most pigments were comparatively low. This was then followed by a period of fluctuating but increased pigment concentrations from ~60 cm to ~20 cm in fucoxanthin, diatoxanthin, diadinoxanthin, the pheophytin *b*-like compound, chlorophyll *a*, pheophytin *a* and pyropheophytin *a*. Above 20 cm these pigments reduced in concentration, prior to a final increase from ~10 cm to the top of the core. In contrast, lutein-zeaxanthin had low concentrations at the start of the zone until a pulse at ~50 cm (reaching ~35 nmol pig g⁻¹ TOC), prior to a series of smaller pulses (approx. 5 cm intervals) until ~13.25 cm depth. Concentrations in canthaxanthin in were substantially lower, except above ~10 cm. In pheophytin *b* concentrations continued to fluctuate in a similar manner to the previous zone (between ~100 and ~300 nmol pig g⁻¹ TOC) until a minimum of ~50 nmol pig g⁻¹ TOC at ~15 cm depth. Okenone was characterised by a distinct large pulse of ~70 nmol pig g⁻¹ TOC at ~27 cm, with all previous fluctuations in this zone ranging between 0 and ~18 nmol pig g⁻¹ TOC. β-carotene had a pulse in concentration of ~50 nmol pig g⁻¹ TOC at ~31 cm depth.

Zone A

There were marked increases in the pigments fucoxanthin (to ~100 nmol pig g⁻¹ TOC), pheophytin *b* (to ~620 nmol pig g⁻¹ TOC), the pheophytin *b*-like compound (to ~1,300 nmol pig g⁻¹ TOC) and pheophytin *a* (to ~2,000 nmol pig g⁻¹ TOC). There were also more modest increases in canthaxanthin and chlorophyll *a*. Since lutein-zeaxanthin and okenone were not present in K2 these pigments did not extend to the top of the core. No major trends were present in diatoxanthin, diadinoxanthin, β-carotene or pyropheophytin *a*, although there was an increase in alloxanthin at ~0.25 cm.

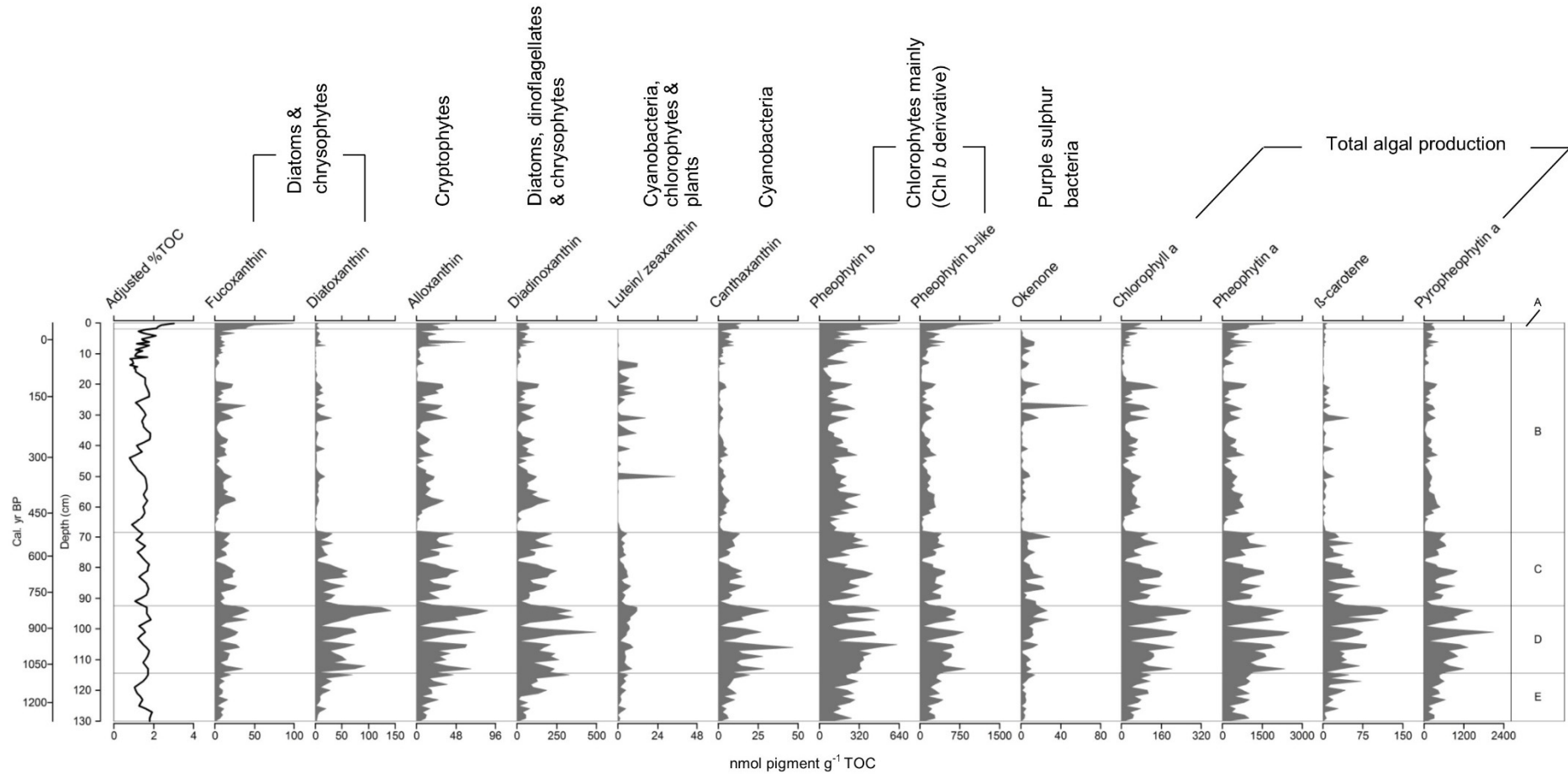


Figure 7.9: Stratigraphic plot for final combined HON-Kajak and Russian sequence (K2, R2-1 & R2-2) from Disko 4 of pigment concentrations expressed against TOC. Zones (A, B, C, D & E) were based on optimal partitioning resulting in 5 zones. Zone calculations included all variables in the figure above in addition to CaCO₃, OM, δ¹³C_{TOC}, TOC, N, C/N. Age depth model used from Figure 7.8.

7.1.6 Exploratory statistics – Disko 4 combined sequence

The PCA ordination biplot for the Disko 4 combined sequence with pigments (as species) plotted against samples had eigenvectors of 0.76 for PCA axis 1 and 0.12 for PCA axis 2 (Figure 7.10). Pigments were distributed fairly evenly in the two left hand quadrants. The pigments pheophytin *b*, pheophytin *b*2 (pheophytin *b*-like), pheophytin *a*, fucoxanthin, pyropheophytin *a*, diadinoxanthin, alloxanthin and canthaxanthin were all closely associated and present in the upper left quadrant. Chlorophyll *a* was the most strongly associated pigment with PCA axis 1. In contrast, the pigments diatoxanthin, β -carotene, okenone, and lutein-zeaxanthin were loosely grouped in the lower left quadrant and reflected more intermittent pulses in zone B. Lutein-zeaxanthin was the most closely associated pigment to PCA axis 2 (present at $\sim 45^\circ$ angle to axis 2). Samples from zone B (blue squares) were primarily located in the two right hand quadrants away from the main pigment gradients. Samples from zone C (green rotated squares), zone D (yellow triangles) and zone E (orange circles) were generally orientated in the space occupied by the lower left orientated pigments. In contrast, samples from zone A (red circle) were located in a cluster to the outer top of the ordination.

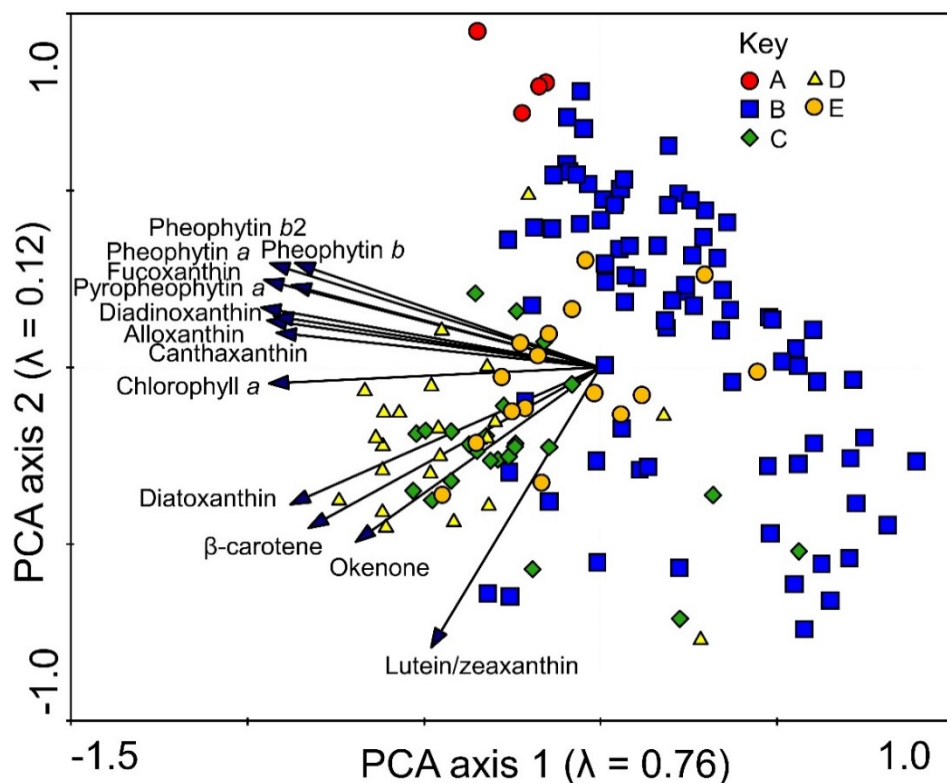


Figure 7.10: PCA ordination biplot for Disko 4 combined stratigraphy (R2-1, R2-2, K2). Complete with pigments (as species) plotted against samples. Sample zone origins are listed in the Figure key. Eigenvectors are 0.76 for PCA 1 and 0.12 for PCA axis 2.

7.1.7 Disko 4 combined master sequence – geochemical data, pigment ratios and PCA scores

To elucidate changes in pigment data principal components analysis (PCA) (Figure 7.10) was plotted by depth (Figure 7.11) because detrended correspondence analysis (DCA) produced gradient lengths < 2.5 SD. Geochemical data (TOC, N, C/N and $\delta^{13}\text{C}_{\text{TOC}}$) were also explored together with selected pigment ratios (Figure 7.13).

Zone E

There was little overall directional trends in geochemical data, pigment PCA 1 and 2 scores and key pigment ratios, except for the C/N ratio which fluctuated from ~ 14.2 at ~ 125 cm to ~ 10 at ~ 121 cm. TOC was low (range $\sim 1\%$ to $\sim 2\%$) and %N was also very low ($< 0.2\%$). The $\delta^{13}\text{C}_{\text{TOC}}$ varied between ~ -25 ‰ and ~ -26 ‰. CMAR (carbon mass accumulation rate) decreased from ~ 25 to $15 \text{ g C m}^{-2}\text{yr}^{-1}$. PCA 1 and 2 fluctuated around 0, but there was a slight decline towards the top of the zone in PCA 1 (114.5 cm). Pigment ratios were stable, with low ratios of lutein-zeaxanthin: diatoxanthin and fucoxanthin: diatoxanthin.

Zone D

There were only slight changes in geochemical, pigment PCA scores and pigment ratios. TOC continued fluctuating between $\sim 1\%$ and $\sim 2\%$ and N remained very low ($< 0.2\%$). C/N ratio fluctuated around ~ 13 , decreasing to < 10 at ~ 95 cm. $\delta^{13}\text{C}_{\text{TOC}}$ continued fluctuating between -26 ‰ and -25 ‰. CMAR fluctuated between ~ 5 and $16 \text{ g C m}^{-2}\text{yr}^{-1}$. PCA 1 scores were slightly lower and fluctuated around ~ -1 with the exception of peaks at ~ 99 and ~ 104 cm depth (0.5 and 0.75 respectively). PCA 2 mainly fluctuated around ~ 0 and then declined at ~ 99 cm (~ -2). Most pigment ratios were very similar to the previous zone with the exception of slight peaks at ~ 99 cm depth in both the chlorophyll *a*: pheophytin *a* and fucoxanthin: chlorophyll *a* ratios.

Zone C

Again only minor changes were present in geochemical, pigment PCA scores and pigment ratios in zone D4-C. TOC, N, C/N and $\delta^{13}\text{C}_{\text{TOC}}$ generally fluctuated around the ranges previously described, although there was a peak in C/N at ~ 91 cm (~ 15) and a slight decline at ~ 75 cm (~ 11). CMAR followed a generally stable pattern ranging between 7 and $17 \text{ g C m}^{-2}\text{yr}^{-1}$. PCA 1 scores were slightly higher than the end of the previous zone and fluctuated mainly around 0 with a peak at ~ 91 cm (to ~ 0.6) and ~ 78 cm (to ~ 1.5). PCA 2 scores also fluctuated variably around 0 with peaks at

~84 cm (~0.2), ~73 cm (~0.4) and 71 cm (~0.2). The only slight noticeable change in pigment ratios was in the ratio of alloxanthin: diatoxanthin which was slightly higher than the previous zone above ~77 cm. There was a slight peak in the ratio of chlorophyll *a* to pheophytin *a* at ~78 cm (~0.30 compared with ~0.15).

Zone B

TOC varied between ~0.8% and 1.8%, with minor fluctuations in this zone and a slight increasing trend above ~13 cm. N followed a similar trend to TOC but with fluctuations ranging between ~0.06% and ~0.16 % from ~69 cm prior to increasing fluctuations from ~13 cm to the top of the zone. CMAR increased from ~8.5 g C m⁻² yr⁻¹ at 68 cm depth to ~24 g C m⁻² yr⁻¹ by 16 cm depth, followed by an increase to <45 g C m⁻² yr⁻¹ between ~15 and 10 cm. C/N ratios fluctuated more widely compared to the previous zone, with a clear peak at ~40 cm depth (~18.5) and a minimum at ~38 cm depth (~11.3 %). Generally, $\delta^{13}\text{C}_{\text{TOC}}$ continued to fluctuate between -26 ‰ and -25 ‰, although there was a slight peak to -24.5 ‰ at ~14.75 cm depth. The PCA 1 profile fluctuated widely but reached a minimum at ~60 cm, ~50 cm, ~27 cm and ~20 cm and peaks at ~45 cm, ~35 cm and 14.75 cm, followed by a decline by ~3 cm depth. The PCA 2 profile was highly varied but increased from ~0 at the start of the zone to ~1.8 by ~59 cm. Wide fluctuations were then present until a final minimum of ~ -1.5 at 18 cm, followed by a gradual but fluctuating rise until the end of the zone.

The ratio of lutein-zeaxanthin: diatoxanthin was characterised by pulses at ~35 cm (to ~6.5), ~26 cm (to ~6.7), ~18 cm (to ~12) and ~13 cm (to ~18). Similarly, the ratio of chlorophyll *a* to pheophytin *a* had pronounced fluctuations at ~35 cm (to ~0.5) and ~18 cm (to ~0.6), followed by a steep decline to ~9 cm (<0.1). In the ratio of fucoxanthin: chlorophyll *a* there were fluctuations between ~0.1 and ~0.4 until ~16 cm, followed by a pronounced increase to ~1.3 by 13.75 cm. After this pulse the ratio reduced to ~0.5 by ~12 cm and increased to ~1.5% by ~9.5 cm, followed by a decline to ~0.3 by ~4-5 cm. There were more fluctuations in the ratio of fucoxanthin: diatoxanthin compared with the previous zone. The largest pulse was at ~8.75 cm depth (ratio of ~60) which was followed by a decline to ~2. The ratio of alloxanthin: diatoxanthin was more variable and higher compared with the previous zone, with a key pulse present at ~24 cm (ratio of ~36) compared with general fluctuations of <10. The alloxanthin: chlorophyll *a* ratio fluctuated around 0.5, with a minimum at ~18 cm and a maximum at ~6.25 cm (of ~1.7), prior to a gradual decline to the top of the zone.

Zone A

The upper zone of 2 cm was characterised by a pronounced increase in TOC (to ~3 %), N (to ~0.35%), PCA 2 (to ~3), fucoxanthin: chlorophyll *a* ratio (to ~1.5) and fucoxanthin: diatoxanthin ratio (to ~30). CMAR decreased to ~4 g C m⁻² yr⁻¹ by the top of the core. C/N ratios declined slightly (to ~8), but there was no clear directional change in $\delta^{13}\text{C}_{\text{TOC}}$.

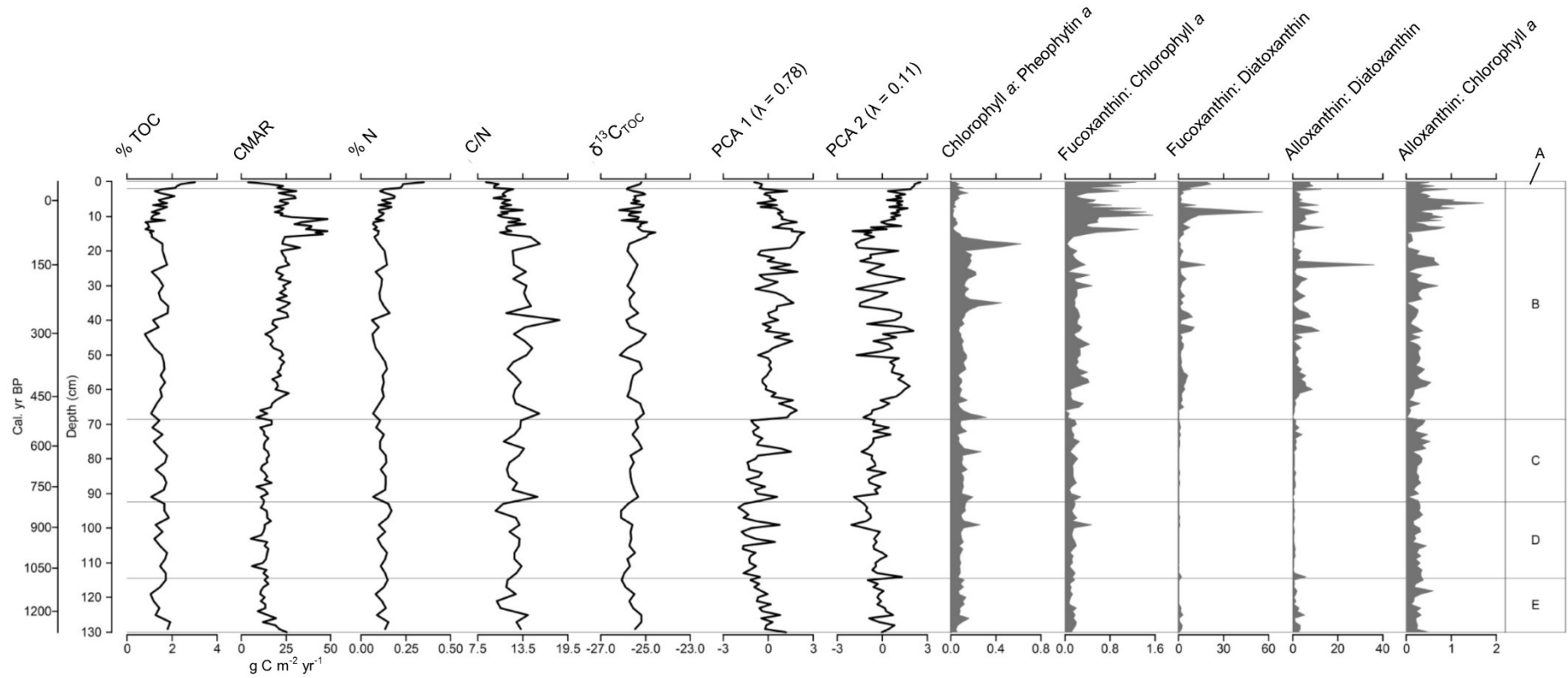


Figure 7.11: Stratigraphic Disko 4 geochemical data (% TOC, % N, C/N, $\delta^{13}\text{C}_{\text{TOC}}$), carbon accumulation rate (CMAR), pigment PCA 1 ($\lambda = 0.76$) and PCA 2 ($\lambda = 0.12$) scores and key pigment ratios. Plotted against both Cal. yr BP (adjusted axis) and depth (fixed scale axis). Age depth model used is presented in Figure 7.8.

7.2 Discussion Disko 4

7.2.1 Stratigraphy, core correlations and bulk measures

The combined master stratigraphy (K2, R2-1 and R2-2) which was found to be predominantly homogeneous silt with occasional macrofossil and clay layers is consistent with a mixed Arctic wetland source, without a single dominant source of material which might have led to laminations (Figure 7.1). Homogenous freshwater deposits, classified as silt or gyttja are often present in west Greenland lakes, including in isolation basins (Long et al., 2011) and was present in many layers of the sequence taken on the island of Qeqertarsuatsiaq directly to the south across Disko Bay (Fredskild, 2000) (Figure 1.6). The clay layers are likely of glacial erosive origin, developed under the ice present in the catchment (Figure 4.9, Table 4.1, 3.6% permanent ice/glacier), and then released to the catchment in pluses during local glacier meltwater cycles or retreat, or from periglacial processes including nivation hollows and solifluction. The individualistic nature of these clay layers point to the maritime climate of Disko and is similar to the catchment erosion processes experienced by lakes in the maritime influenced Sisimiut, further south along the south-west Greenland coast (Anderson et al., 2012; Law et al., 2015).

The macrofossil layers (up to ~1.5 cm thick) may be terrestrial in origin as these contained *Salix* spp. macrofossils (used for ¹⁴C dating) and were likely brought into the lake during a meltwater flood-pulse, probably growing bank-side in the braided riverscape (Malard et al., 2006) that feeds Disko 4 (Figure 4.9). The macrofossil layers could also partly be aquatic in origin and linked to local plant development on the lakebed, which can also affect sedimentation (Madsen et al., 2001). The fine sandy layers which sometimes precede clay layers (e.g. at ~63 cm and ~47 cm depth) likely reflect the fluvial entrainment of differing particle sizes from the catchment (Hjulstrøm, 1939) and the delivery of sorted particles to the lake based on event-linked seasonal variations in hydrology.

Good core overlapping was possible in Disko 4 sediments once minor variations were accounted for. There was a small offset in OM between R2-1 and R2-2 values from ~54 cm onwards (Figure 7.2), despite good agreement between lithostratigraphic measures (Figure 7.1). Repeated OM (LOI 550 °C values (red) were slightly lower (Figure 7.2) and so a corrected OM adjusted profile was devised, based on TOC measured using an elemental analyser which is more robust, compared with LOI. The offset in LOI was linked to slight differences in the efficiency of furnaces, which can

be problematic when OM is low (~4 – 8%). All LOI 550 °C batches were heated for exactly 5 h, but continuing this overnight could have helped correct for between-furnace differences in efficiency. Adjusted OM was fairly low (~4 – 8%) (Figure 7.3) suggesting a relatively unproductive system, with values similar to those in Disko 1 (Figure 6.3). Excellent agreement in TOC measurements between the overlaps of R2-1 and R2-2 helped confirm this part of the sequence. Slight differences in CaCO₃ between ~25 cm and ~45 cm likely could be artefacts of measuring such low percentages of CaCO₃ as LOI 925 °C is not accurate at this level (~1-2%), which is close to the error range of this technique (Heiri et al., 2001). Trends in OM and CaCO₃ in Disko 4, were more similar to Disko 1 (Section 6.1.4) compared with Disko 2 (Section 5.1.6), reflecting the substantially smaller catchment and higher elevation of Disko 2.

The HON-Kajak (K2) core had excellent agreement with OM, DW and CaCO₃ with the top of R2-2 and so the overlap was based on these measures (Figure 7.2). Minor offsets in pigment concentration between the two cores (Appendix E, Figure E1, E2 & E3) are likely related to the more flocculent nature of the upper ~15 to ~20 cm of the R2-1 Russian core, whereas the HON-Kajak coring system was able to take an undisturbed record of the water-sediment surface interface. The specifics of the HON-Kajak coring technique is outlined in Renberg (1991), with the overlapping of adjacent drives in Glew et al. (2001). Pigments are variably susceptible to diagenesis (Leavitt and Hodgson, 2001) and so are unsuitable to be the primary core correlation tool, although measures were taken to ensure both the HON-Kajak and Russian sequences were transported under similar conditions.

The potential for sediment focusing (Lehman, 1975) at Disko 4 was acknowledged as the main water inlets are concentrated on the south-eastern bank (Figure 4.9) due to the basin extending up a previously glacially scoured U-shaped valley. Sedimentation is likely to originate from these inputs in a radial manner which may be responsible partly for slight fluctuations in relatively closely adjacent (~ <10 m cores). Previous studies using biological proxies (diatoms) in multi-core comparison studies have found deposition variability throughout simple basins, closely linked to susceptibility to resuspension (Anderson, 1990) and the complicating influence of periphyton (Anderson, 1989). Benthic algal production is known to be a particularly large contributor to biomass in Arctic lakes (Vadeboncoeur et al., 2003), with may partly help to explain why there can be minor localised variations in pigment concentrations at different positions in the lake (Appendix E - Figure E1, E2 & E3).

7.2.2 Radiometric dating

The age-depth model (based on three accepted ^{14}C dates and ^{210}Pb recent dating of the uppermost sediments) when extrapolated to the base suggests that the entire sequence covers the last ~1260 cal. yr BP (Table 7.1, Figures 7.7 – 7.11). Consolidated material was reached at the base of R2-2, likely due to the limitations of the Russian coring system without applying force to reach deeper compacted sediments. Based on a calibrated central estimate age of 1180 cal. yr BP at ~118 cm this suggests an average (mean) sedimentation rate of ~0.1 cm² yr⁻¹ cm, which is relatively high for an Arctic lake at ~69° latitude. For example, at a similar depth of ~120 cm in lake Braya Sø the record extended to at least ~7,100 cal. yr BP and at lake SS6 at least ~5,500 cal. yr BP in Kangerlussuaq, West Greenland (McGowan et al., 2003). Directly to the north of Disko on Nussuaq a depth of 112-116 cm returned a central estimate date of ~2900 cal. yr BP (Bennike, 2000), with the depth of 126-130 cm reporting a date of ~5610 cal. yr BC (~7,560 BP) in the lake on Qeqertarsuaq (Fredskild, 2000).

Similar sedimentation rates to the one derived from Disko 4 were found in Qivittut and Fortune Bay lakes on Disko Island. For example, at 150 – 165 cm at Qivittut lake the central estimate age was 2190 cal. yr BP, while in Fortune Bay lake at 190-195 cm the central estimate age was ~2,350 BP (Bennike, 1995). This suggests the relatively high sedimentation rate in Disko 4 is not unusual for Disko Island and could be due to the substantial erosive capacity of the active Lyngmarksbræen ice cap and the prominent freeze-thaw weathered outcrops and periglacial activity present in the catchment (Figure 4.10 & 4.11 B & C). If coring was restricted at the base of R2-2 (~130 cm) by consolidated material then this could be explained by neoglacial deposits. Work is currently ongoing in a neighbouring valley to ascertain the extent of local fluctuations in glacial activity over the Holocene based on rock exposure dating (T. Lane and K. Adamson, personal communication), which could help understand local readvance.

Overall, the lake Disko 4 sequence was the best dated among all lakes in this study (Disko 2, Chapter 5 & Disko 1, Chapter 6), made possible by the use of three identified *Salix* macrofossils of terrestrial origin combined with robust ^{210}Pb dating of the uppermost sediments. The age-depth model rejected the older paired bulk date at 34.5-35.5 cm (510 – 621 cal. yr BP 2 σ range), instead using the younger macrofossil date as the key marker (21 – 266 cal. yr BP 2 σ range) (Table 7.1 and Figure 7.8). The rejection of the older date was made within Bacon v2.2 (Blaauw and Christen, 2011, 2013) on the basis that the youngest date on a terrestrial macrofossil is most likely to

represent the true age. The older date is unlikely to be due to the reservoir effect which causes ages to be erroneously old if the aquatic source utilises old bicarbonate in the lake water (Shotton, 1972), as water in this lake was relatively dilute (Table 4.3). Sedimentary carbonate (CaCO_3) was found to be extremely low in this system, so a more likely possibility is that entrained algae from soils or glaciers with an old signature is being buried directly in the lake sediments, or ancient labile DOC released from glacial melt water (Lawson et al., 2014b; Hood et al., 2015) is the source of $\text{CO}_{2(\text{aq})}$ through bacterial or light mediated decomposition. This could be the basis of a heterotrophic microbial web which provides nutrition to algae and in-lake macrophytes.

The $\delta^{13}\text{C}_{\text{AMS}}$ of the radiocarbon dates at 34.5 – 35.5 cm to 62.5 – 63.5 cm ranged between -22.8‰ and -23.6‰ and are within the range expected for either C_3 vascular plants or algae (Meyers and Teranes, 2001) (also see Table 4.7). However, the -14.3‰ value from the *Salix* spp. plant macrofossil at 117.5-118.5 cm (Table 7.1) was much lower than expected and within the range normally expected for C_4 plants. C_4 plants were not present in the catchment and so it is possible that the acid pre-treatment was insufficient, or that as the sample was a small leaf, different biological fractionation might have occurred. In the source study investigation, across all sites the highest (least negative) $\delta^{13}\text{C}$ value for *Salix* sp. was -27.3‰ (Disko 2, Table 4.6), suggesting the -14.3‰ value in this sample might be accessing CO_2 more directly from the atmosphere and there could have been some algae remaining in the sample, which was challenging to clean due to its small size. Despite the precise source origin of the final sample, overall the age model remains excellent.

7.2.3 Disko 4 geochemical interpretation

A multi-panel figure of proxies summarising key changes is presented in Figure 7.12. All pigment profiles (Figure 7.9 & 7.12) were highly variable throughout the sequence, although the majority of pigments reached higher maximum concentrations in Zones E, D and C (~1260 – 500 cal. yr BP) compared with zone B (~500 cal. yr BP – AD ~ 1995). The fluctuating manner of the entire sequence is likely due to tight coupling of the catchment to lake nutrient, DOC and hydrological regimes mediating algal communities. Disko 4 has a complex periglacial catchment with meltwater originating from the Lyngmarksbræen ice cap and other smaller glaciers on the headwall of the north-eastern part of the catchment (Figure 4.9, Table 4.1). Glacier mass balance is known to be closely coupled to climate on Disko, although the precise advance or retreat of individual glaciers can be highly dependent on local factors such as the supply of snowfall, aspect and glacier type (e.g. surging, rock, valley-type, individual or ice sheet connected) (Yde and Knudsen, 2007). Both rock type (Humlum, 1996) and surge-type (Yde and Knudsen, 2005; Yde et al., 2005) glaciers have been documented on Disko and are likely to provide contrasting sediment yields. In particular, surging glaciers may remain dormant during periods in their life-cycle, broken by periods of intensive activity and fluvial sedimentation. Previous monitoring of a surge-type glacier in Kuannersuit Kuussuat, Disko Island revealed a significant basaltic weathering regime with an absence of carbonate minerals (Yde et al., 2005), which is consistent with measurements in Disko 4 of negligible CaCO_3 .

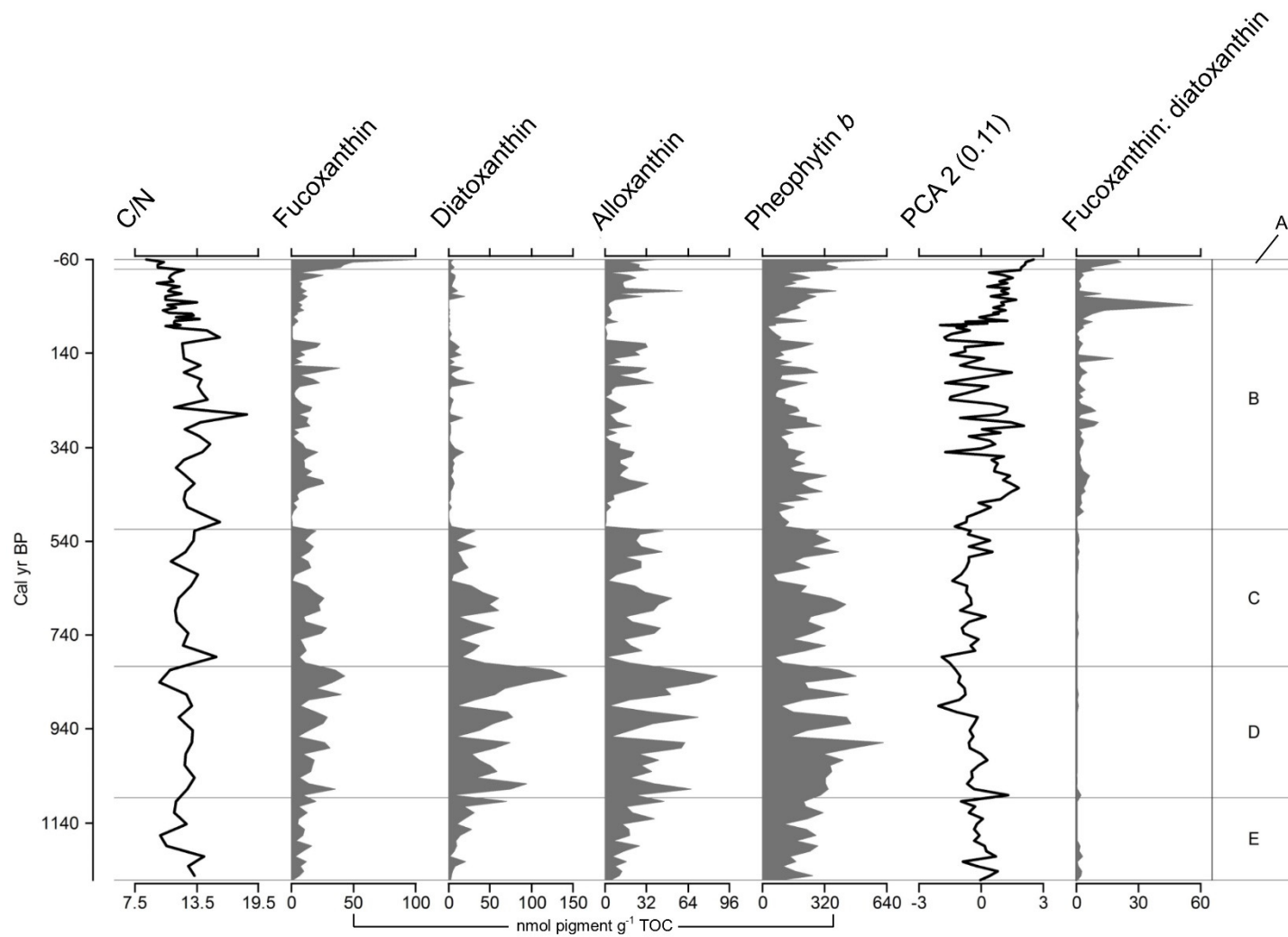


Figure 7.12: Disko 4 summary diagram of key changes combining C/N ratio, selected pigments (fucoxanthin, diatoxanthin, alloxanthin, pheophytin *b*), pigment PCA axis 1 and the ratio of fucoxanthin: diatoxanthin for clear comparison.

The pulses of pigment noted throughout the Disko 4 sequence (Figure 7.9 & 7.12) could either be linked to the delivery of algae or changes in in-lake conditions. Trends remained broadly similar when corrected for TOC, OM & DW (Appendix E – E1, E2 & E3) confirming algal change beyond variations in stratigraphy and delivery of inorganic and minerogenic material (suggested by percentage dry weight). During melt glaciers can store water in subglacial cavities, small ice dammed lakes and in cryoconite holes which can be biologically productive environments (Telling et al., 2012; Bagshaw et al., 2013). These fluvial deposits when released from the glacier likely sediment in downstream lakes such as Disko 4. Alternatively, glaciers during melt and periods of recession are known to release locally significant nutrient concentrations (Slemmons and Saros, 2012; Slemmons et al., 2013), which can stimulate downstream algal communities. Additionally, ancient and labile DOC (Lawson et al., 2014b; Hood et al., 2015) has the potential to support microbial activity and promote mixotrophy (Roberts et al., 2000; Laybourn-Parry and Marshall, 2003).

The presence of highly varied pigment profiles could also indicate wide variations in catchment permafrost melt which has been linked to the release of stored carbon (Schuur et al., 2009) and the stimulation of microbial decomposition (Jansson and Tas, 2014). The Disko 4 topography is rugged and complex with the presence of Arctic wetlands between braided channels and in extensive margins extending around the lake, particularly to the south-east up the valley (Figure 4.9). The vegetation survey noted a large moss and lichen component in the catchment (Table 4.2, 37%) which is often a key indicator of waterlogged conditions. Arctic soils and vegetation at a landscape scale are known to be highly complex and patchy (Hobbie et al., 2000) and so disturbance at the local level by permafrost melt or hydrological disturbance during flood flow is likely to have partly influenced the delivery of DOM to Disko 4.

Edaphic processes are likely to explain the variable nature of the general pigment profile, but there is probably an overall climate control on the higher maximum pigment concentrations reached in zones E, D and C, compared with B (Figure 7.9 & 7.12). The difference is present in all pigments but is particularly pronounced in diatoxanthin (diatoms), canthaxanthin (cyanobacteria) and β -carotene (total algae). This difference could reflect the transition between the Medieval Climate Anomaly (MCA) and the Little Ice Age (LIA) climate periods. Although both events are known to be spatially variable across the paleoclimate archive (Matthews and Briffa, 2005), the general period of the MCA from AD 950-1250 (~1000 – 750 BP) and the LIA from AD 1400-1700 (550-250 BP) (Mann et al., 2009) are broadly coincident with the

differences in maximum pigment concentration (Figure 7.9 & 7.12). The period marked as the MCA (~1000-750 BP) is directly coincident with the zone with the highest pigment concentrations (Zone D) and the start of the LIA (~550 BP (Mann et al., 2009)), is coincident with the boundary between zone C and B. The long-term cooling trend is linked to a gradual reduction in orbitally driven summer insolation, leading to the pan-arctic cooling trends of the LIA (Kaufman et al., 2009).

In the Disko 4 record the wide fluctuations are unlikely to have been driven solely by changes in the length of the ice-free period as this would not have resulted in such a wide variation in pigment concentration (Figure 7.9 & 7.12). It is more likely that the complex interplay of catchment glacier advance and retreat linked to precipitation, air currents (for snow deposition) and climate is regulating these changes. The period of increased maximum pigment concentration (zone D) is also coincident with warming interpreted from a sedimentary alkenone index derived from two lakes in Kangerlussuaq, south-west Greenland (D'Andrea et al., 2011). This warming from ca. 1,100 to 850 y BP was linked to climate amelioration and the Norse migration to Greenland and is followed in Kangerlussuaq by an abrupt temperature decline from ~850 y BP. This is broadly in line with the large drop in diatoxanthin and alloxanthin that marks the transition between zone D and C (~800 cal. yr BP) (Figure 7.9 & 7.12). A slightly later deterioration of temperature in Kangerlussuaq, compared with glacier-mediated pigment decline on Disko Island could be explained by its maritime proximity. However, since the comparison of independently dated age-depth models can propagate error, dating offsets are an alternative explanation.

The low TOC and N values (Figure 7.11 & 7.12) can be explained by the erosive nature of the Disko 4 catchment, the presence of glacier activity and evidence of freeze-thaw on exposed slopes (Figure 4.10, 4.11 B & C), providing large amounts of minerogenic material relative to organic matter and responsible for the relatively high sedimentation rates. The fluctuating C/N ratio (ranging between ~7.5 and ~19) likely reflects during peaks, macrofossil remains (e.g. *Salix* leaves) brought into the lake (*Salix* sp. ranged 17.4 to 133.6 depending on plant part across all sites, Table 4.5, 4.6 & 4.7), with the peaks at ~41 and ~18 cm, potentially associated with catchment dieback linked to harsh conditions (Leng et al., 2012). Slight declines in C/N above ~15 cm could reflect increasing algal contributions (as reflected in the source study (C/N 9.2), Table 4.7 & Figure 4.15) since the end of the LIA. The relatively narrow range in $\delta^{13}\text{C}_{\text{TOC}}$ (-26.5 ‰ to -24.5 ‰) reflect the C_3 contribution of organic matter from algal and terrestrial sources (Meyers and Teranes, 2001), although in this system could also reflect bryophyte inputs (ranged -21.0 ‰ to -26.1 ‰ in the source study,

Table 4.7 & Figure 4.15). Slight variations in $\delta^{13}\text{C}_{\text{TOC}}$ could either reflect fluctuations in algal productivity associated with the supply of nutrients and DOC at intermittent periods, linked to glacial outwash or may simply reflect slight differences in the $\delta^{13}\text{C}_{\text{TOC}}$ values of allochthonous inputs supplied to the lake (Table 4.7 & Figure 4.15). Both PCA axis 1 and 2 scores are highly varied (Figure 7.11 & 7.12) although the change between zone C & B could be explained by the broad shift in pigment maximum between these two zones as all gradients orientate against zone B (Figure 7.10) which has the least variability in raw pigment concentration.

The pulses in lutein-zeaxanthin (Figure 7.9 & 7.12) could reflect the presence of benthic algae and macrophytes (including aquatic bryophytes) that typically form in patches on the lake bed, made possible by the lakes relatively moderate (~6.8 m) depth. This may also explain the successively increasing pulses (~50 – 18 cm) in the ratio of lutein-zeaxanthin to diatoxanthin (Figure 7.9 & 7.12). The ratio of chlorophyll *a*: pheophytin *a* (an indicator of preservation) is high until ~15 cm where a decline occurs. As this decline is coincident with the switch to the HON-Kajak core it is likely an artefact of slightly different relative sediment focusing between the two cores, rather than a decline in preservation. The proportionally lower ratios of fucoxanthin: diatoxanthin and alloxanthin: diatoxanthin in zones E, F and C, compared with zone B indicate fucoxanthin and alloxanthin are relatively more abundant over the MCA compared with the LIA than for diatoxanthin. A possible explanation is that the algal group that indicates alloxanthin (cryptophytes) is able to function more effectively than diatoms during the less favourable conditions of the LIA (zone B). Cryptophytes can have the possibility to adopt mixotrophic strategies when $\text{CO}_{2(\text{aq})}$ is limited (Roberts and Laybourn-Parry, 1999), but labile DOC present, or the ability for these taxa to migrate through the water column using their flagella (Ojala et al., 1996). A similar explanation might apply in this system for fucoxanthin which can be an indicator of chrysophytes which can adopt similar strategies (Holen and Boraas, 1995).

The most recent sediments in the sequence, summarised in Figure 7.13 mark the end of the LIA and the spatially variable pan-arctic hemispheric warming trend that has been noted as reversing the long term cooling trajectory exerted by declining insolation (Kaufman et al., 2009), which is known to be both regionally and temporally heterogeneous (Briner et al., 2016; Kaufman et al., 2016). Although there is a pronounced increase in algal concentration around AD 1940, the profile overall is highly variable with multiple fluctuations (Figure 7.15). This is in contrast to diatom records across the circumpolar arctic (Smol et al., 2005), spectrally reconstructed chlorophyll *a* records (Michelutti et al., 2005) and individual pigment records from

Baffin Island across Baffin Bay, which show unambiguous directional increases or floristic change (Florian et al., 2015). The variability is likely explained by the complex interplay between catchment glacial advance and retreat and the release of nutrients and labile DOC from melting ice (Slemmons and Saros, 2012; Lawson et al., 2014a; Lawson et al., 2014b). The abrupt increase in diatoxanthin from AD ~1940 could be related to an increase in riverine diatoms (associated with meltwater flow) or diatoms from biological production on glaciers, which were stored overtime and then released along with bioavailable C, N and P during meltwater cycles (Bagshaw et al., 2013).

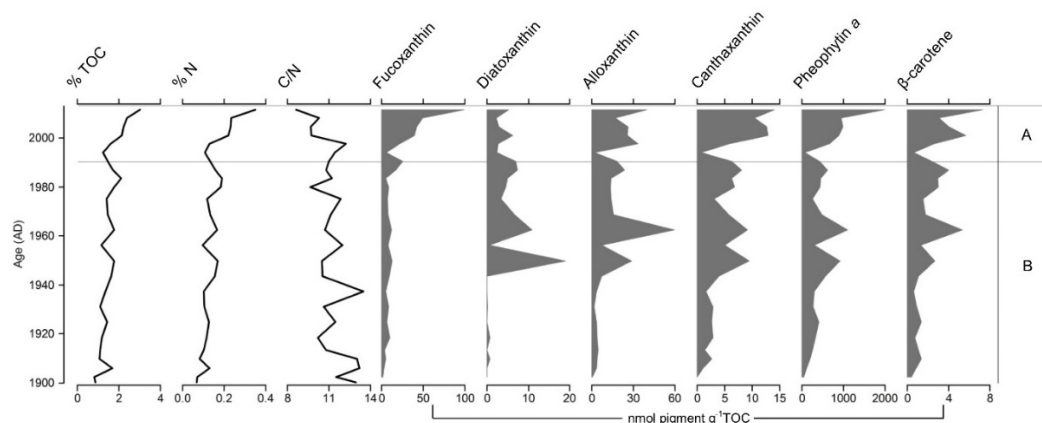


Figure 7.13: Disko 4 recent summary diagram of key changes combining TOC, N, C/N ratio and selected pigments (fucoxanthin, diatoxanthin, alloxanthin, canthaxanthin, pheophytin *a* & β -carotene) for clear comparison.

The gradual but fluctuating increase in TOC (Figure 7.13) could reflect enhanced carbon sequestration as a result of the increases in pigment concentration in the most recent sediments, be an artefact of diagenesis of TOC in the upper ~8 cm or may indicate benthic macrophyte rootlets which were visible in these sediments. Fucoxanthin increases gradually until the most recent ~20 years (~4 cm), where there is a more pronounced increase. It is possible that chrysophytes (which can contribute to fucoxanthin) are responding to the most recent change in the catchment, although diagenesis below this is possible. However, diagenesis does not appear to be a major problem in this system as there is not a trend of undifferentiated pigment concentration increase in the top deposits and the $\delta^{13}\text{C}_{\text{TOC}}$ value remains stable (Figure 7.11), fluctuating narrowly between ~ -26 ‰ and ~ -24.5 ‰, with no evidence of selective degradation (Meyers, 1994). The recent pigment changes from Disko 4 although highly varied are similar to the *Betula* tree-ring reconstructions present locally ($\sim < 8$ km) (Hollesen et al., 2015) and could be associated indirectly with recent warming trends noted at Ilulissat and Qeqertarsuaq, which have increased in rate since the 1990s (Box, 2002; Hansen et al., 2006).

7.2.4 Summary – Disko 4

The sequence from Disko 4 was well dated through the combination of terrestrial macrofossil samples from undisturbed parts of the core and ^{210}Pb dating, covering the past ~1260 cal. yr BP. This presents a moderately fast sedimentation rate of ~0.1 cm² yr⁻¹ for an Arctic lake, but is within the range of other lower elevation lakes in the region. The moderately fast sedimentation rate is likely due to extensive erosion present in the catchment (glaciers and periglacial processes including solifluction and freeze-thaw) which is probably associated with the high sedimentary DW, but low OM and TOC values. Deposits of homogenous silt with clay layers, rather than more organic deposits is consistent with the active glacial and periglacial processes in this catchment. Macrofossil layers in the sediments are likely linked to both the erosion of patchy terrestrial vegetation during meltwater flood pulses and the localised patchy nature of benthic macrophytes typical in Arctic lakes.

The fluctuating nature of the Disko 4 pigment record may be linked to the complex interplay between spatially varied advance and retreat of local catchment glaciers, permafrost and thin Arctic soils releasing old DOC and nutrients during melt, stimulating algal production. Although there is no independent proxy to confirm the variable delivery of old DOC and nutrients, a trend driven purely by small changes in the length of ice duration is unlikely to drive such large (up to 10 fold) increases in algae, given the importance of ecological nutrient stoichiometry. Therefore, the higher maximum pigment concentration reached during the MCA, compared with the LIA is likely explained primarily by an indirect climate forcing on glacial advance/retreat and the general insolation driven cooling trend noted in proxies across the Arctic (e.g. Kaufman 2009), while acknowledging heterogeneity (Briner et al., 2016; Kaufman et al., 2016). This means that increases in maximum pigment concentrations in the MCA and more recently since the end of the LIA, increasing in rate from ~AD 1940 is most likely explained by warming associated with enhanced glacial melt and the release of nutrients and labile DOC in meltwater. Changes in the length of the ice-free season may also play small a role during warming, but these changes are unlikely to be sufficient to explain such large fluctuations in pigment concentration present in Disko 4.

Chapter 8: Synthesis and discussion – Carbon cycling in Arctic lakes on Disko Island

This chapter provides a landscape-scale synthesis of the sediment core and hydro-geomorphic catchment survey elements of the thesis (chapters 4-7). The initial survey aims are revisited and the discussion provides a critical review on work completed to this point, together with selection of appropriate proxies for synthesis. The ecological trends across lakes on Disko are then considered, highlighting the importance of geomorphology and landscape position. This is followed by a synthesis of hemispheric, Arctic and regional scale proxies at multiple timescales. Reflections on the importance of these outcomes to carbon burial across the Arctic are then made, prior to an assessment of the projects limitations and scope for future improvements.

8.1 Project aims revisited

8.1.1 Primary aim

- Investigate the effect of catchment position on carbon cycling in lakes at different positions along a hydro-geomorphic landscape gradient on Disko Island, west Greenland.

8.1.2 Focused aims

- Understand how lake geomorphology, position and ecology regulate and mediate palaeolimnological trends in carbon cycling.
- Elucidate how differences between catchments (presence of glaciers, permafrost and varying vegetation inputs) might influence the quality and quantity of autochthonous versus allochthonous carbon buried in Arctic lakes.
- Use a detailed hydrogeomorphic survey to provide catchment information and calibration samples to help interpret down-core reconstructions.
- Link changes in catchment coupled carbon cycling in palaeolimnological sequences to known environmental change for:
 - Recent change – lakes Disko 2, 1 & 4
 - Change since ~1260 cal. yr BP – lake Disko 4
 - Change since ~7640 cal. yr BP – Lake Disko 2
- Compare the most effective proxies of carbon cycling in lakes on Disko Island with known local, regional and pan-Arctic reconstructions and syntheses.

- Use palaeolimnological records to interpret lakes metabolic status as a source or sink of carbon, linked to key periods of environmental change including recent warming.

8.2 Critical review and proxy synthesis selection

This section provides a critical appraisal of thesis data and outcomes to this point, based on the analyses presented and discussed in chapters 4 to 7. Taking account of the limitations of the proxies used, the proxies most suited for synthesis and comparison with regional, Arctic and hemispheric scale reconstructions are highlighted.

8.1.1 Catchment study

The catchment study (Chapter 4) was critical for developing a thesis framework as stemming from these data, a hydro-geomorphic elevation gradient was used to place sediment core chapters in decreasing elevation order (Disko 2, 1 & 4). The direct effects of elevation (e.g. climate) are probably minimal between the closely located lakes (Figure 4.1) (<20 km max), but lake position in the landscape helps explain catchment size, vegetation inputs, glacier coverage and the heterogeneity of Arctic land cover (see Sections 4.2 & 4.3).

Across all sites the relatively dilute water chemistry indicated all lakes are hydrologically connected systems and the low DOC levels are consistent with poorly developed soils and restricted soils north of Arctic treeline (Table 4.2). Some lakes had high under-ice April nutrient concentrations, modest chlorophyll *a* and there were higher relative abundances of degradation products (pheophytin *a*) in Disko 1 which had the greatest glacier inputs (Table 4.3), potentially linked to on-ice pigment degradation or the effects of glacial flour on in-lake algal production, through light limitation. However, these measurements were spot samples and do not take into account of changes in water chemistry values that might take place over time. Samples taken upstream and downstream of each lake and directly adjacent to each glacier input would be required to confirm these potential sources.

Catchment calibration samples of plant and soil samples included many bryophytes and mosses which form a large proportion of land cover across all sites (Table 4.2). Across all sites, C/N and $\delta^{13}\text{C}_{\text{TOC}}$ on catchment samples (Figure 4.16) was relatively

mixed as bryophytes have different carbon concentrating mechanisms compared with plants, and Arctic soils are rich in algal communities. Despite this, some discrimination between algae (higher, less negative) and terrestrial plants (lower, more negative) for $\delta^{13}\text{C}_{\text{TOC}}$ was possible (Section 4.8.2).

Lipid ratios were analysed for Disko 2 (Section 4.8.3 & 4.8.4), with the most diagnostic selected for comparison against other proxies (Figure 5.16 & 5.20). The focus on ratios was primarily on use of equations which enable interpretations to be based on multiple compounds (e.g. *n*-alkane CPI 2 index & TAR_{HC} ratio). Where individual compounds were presented relative to the sum of the entire homologous series (e.g. *n*-alkane C₂₆) these were presented only when linked closely to the source study investigation (Section 4.8.4). Future work could attempt to quantify these compounds to enable wider comparisons. The increased susceptibility to diagenesis for *n*-alkanols and *n*-fatty acids, compared with *n*-alkanes is a limitation of these proxies, but can help provide information about the lability of organic matter.

8.1.2 Lake Disko 2

Disko 2 (Chapter 5) is the first lake in the hydrogeomorphic elevation gradient (elevation 575 m.a.s.l), has the smallest catchment, but has the longest dated sequence of all lakes in the study (S1 dated to ~7650 cal. yr BP, section 5.1.3). A replicate sequence (S2) proximal to an active freeze-thaw slope (Figure 4.7) displayed individualistic proxy records which could not be overlapped (Section 5.2), but highlighted the role of catchment processes in this upland lake (Section 5.3.4). Although some dating uncertainty was present in the S1 record due to the presence of reversed dates on bulk organic matter, identification and removal of dates coincident with instantaneous events (Figure 5.2) helped derive a more robust chronology when combined with recent ¹³⁷Cs and ²¹⁰Pb dating (Figure 5.6). Overall, Disko 2 was interpreted as having a low production, slow sedimentation and simple ecological structure, compared with lakes at lower positions in the hydrogeomorphic elevation gradient (Section 5.3.3).

For synthesis of the full record since ~7650 cal. yr BP the pigments canthaxanthin (cyanobacteria), alloxanthin (cryptophytes), diatoxanthin (mostly diatoms) C/N ratio and $\delta^{13}\text{C}_{\text{TOC}}$ have been selected. As canthaxanthin and alloxanthin have similar trends to TOC (Figure 5.6), these pigments may be responding to delivery of organic matter which is then made available through the microbial loop, whereas diatoxanthin is

produced by both benthic and pelagic diatoms. Changes in $\delta^{13}\text{C}_{\text{TOC}}$ in Disko 2 probably reflect source origin (rather than productivity), but interpretation in a system such as Disko 2 with wide ranging sources, including bryophytes is challenging (Figure 4.16). The *n*-alkane CPI 2 ratio has also been selected as it helps confirm fresher, less degraded inputs. The *n*-alkanol and *n*-fatty acid compounds are not taken for further synthesis as compared with *n*-alkanes, these compounds are more susceptible to diagenesis. C/N ratio is also used in the synthesis as it can help indicate the delivery of catchment plant matter, also helping tailor interpretation of $\delta^{13}\text{C}$. For the synthesis of recent change β -carotene has been selected as compared with other indicators of total algal production (e.g. chlorophyll *a*) it is less susceptible to degradation (Table 2.1).

8.1.3 Lake Disko 1

Disko 1 (Chapter 6) is the second lake in the hydrogeomorphic elevation gradient (elevation 299 m.a.s.l.), with clear glacier inputs from the ice cap (Figure 4.2) resulting in turbid water delivery and is situated within a U-shaped valley, providing more developed waterlogged permafrost compared with Disko 2. Dating Disko 1 was the most problematic of the sequences, probably because the use of ^{14}C dating in isolation was less appropriate than recent dating techniques (e.g. $\text{Cs}^{137}/\text{Pb}^{210}$). Disko 1 probably has a faster sedimentation rate as the date of three terrestrial macrofossils (*Salix* spp) taken from within the cores (undisturbed by Russian coring) overlapped (Figure 6.2). The clear increase in algal production in the uppermost sediments probably links to the retreat of glaciers since the end of the LIA, which has been widely documented on Disko (Ingólfsson et al., 1990).

Based on the dating uncertainties, Disko 1 reconstructions are not plotted against proxies at regional or pan-hemispheric scales. However, Disko 1 sediments are probably relatively recent based on the more reliable dates on terrestrial macrofossils, compared with bulk dating which is more likely to be affected by delivery of old carbon from the catchment (Figure 6.2), and has a similar reservoir offset to Disko 2 of ~850 years.

8.1.4 Lake Disko 4

Disko 4 (Chapter 7) is the third and lowest elevation lake (214 m.a.s.l) in the hydro-geomorphic landscape gradient and is the best dated sequence of all records (to ~1260 cal. yr BP). The age-depth model combined $^{210}\text{Pb}/^{137}\text{Cs}$ for recent records with three dates on terrestrial macrofossils, rather than a bulk date which was older and is probably influenced by old carbon from the catchment (Figure 7.8). Compared with Disko 2, this lake was found to have a moderately high sedimentation rate, reflecting the larger catchment and more extensive vegetation cover in the land cover (Table 4.1) and quadrat surveys (Table 4.2).

For the synthesis of the full record since ~1260 cal. yr BP the pigments canthaxanthin (cyanobacteria), diatoxanthin (diatoms), alloxanthin (cryptophytes), the ratio of alloxanthin to diatoxanthin and C/N ratio have been selected. These pigments were selected as they are all relatively stable (Table 2.1) and reflect broad and varied algal groups, with the ratio of alloxanthin: diatoxanthin a possible indicator of increased diatom abundance (linked to pelagic production or benthic habitat) or the utilisation of carbon assisted by the microbial web (e.g. cryptophytes). For the entire sequence synthesis C/N ratio was selected as it can indicate source inputs and delivery of material from the catchment, but $\delta^{13}\text{C}_{\text{TOC}}$ was not selected as its range was too narrow to show clear trends (-24.6‰ to -26.2‰) (Figure 7.11). PCA 1 and 2 were also not selected for comparison with the full record as these summary indicators were highly variable (Figure 7.11), probably responding to delivery of material or the patchy growth of benthic macrophytes, rather than long-term trends. For the synthesis of recent change, β -carotene has also been selected as an indicator of total algal production that is relatively stable (Table 2.1).

8.3 Thesis synthesis

Together, palaeolimnological records of carbon cycling across all three lakes and lake catchments, highlight the importance of the catchment in regulating and mediating all trends. Each record (Disko 2 - Chapter 5, Disko 1 – Chapter 6 & Disko 4 – Chapter 7) presented individualistic records, highlighting the importance of the specific landscape position in regulating the delivery, production and burial of organic carbon in Arctic lakes on Disko. The gradient of elevation used as the framework for this thesis (Section 4.2, Table 4.1) is appropriate as it is closely linked to the catchment to lake area ratio which is smaller at higher elevations. This means lakes at higher positions in the catchment have less developed soils, smaller areas of ice meltwater input and simpler ecosystems. In contrast, more riverine lakes such as Disko 1 receive flows directly (Section 4.1.1, Figure 4.2), leading to faster deposition, such as during glacier melt phases. On Disko, climate exerts as a secondary, indirect overarching mediating factor, rather than a direct control.

8.3.1 Ecology

External to the lake there is a clear vegetation and soil development gradient, which controls the inputs of terrestrial allochthonous material to each lake. Lake Disko 2 at higher elevation was found to have very limited vegetation and thin soils, compared with Disko 4 (lowest elevation), which had more developed soils, thicker permafrost and greater plant cover (Section 4.2, Table 4.1 & 4.2). Lake Disko 1 (mid elevation) had similar vegetation cover to Disko 4, but its catchment inputs were found to be dominated by glacier outwash. The catchment survey elements of this thesis highlight the high levels of landscape heterogeneity on Disko associated with catchment to lake area ratio and elevation. This demonstrates in lakes, relationships that are already known in Arctic river ecosystems, including the diversity and structure of plant richness along the river corridor (Gould and Walker, 1997, 1999) and the differences in ecology between glacier and Arctic tundra streams (Huryn et al., 2005). In many parts of the Arctic ‘greening’ of shrub expansion, linked to recent climate change is known to be occurring (Tape et al., 2006), although pre-existing soil conditions predispose parts of the landscape to support increased shrub abundance (Tape et al., 2012), such as lower down the landscape gradient where soils are more developed. On Disko there is localised evidence of winter warming as a co-driver of *Betula nana* growth <15 km from the lake study sites, in response to recent climate change (Hollesen et al., 2015).

Within each lake there were differences in ecosystem closely coupled to position in the landscape. Lake Disko 2 with its smaller catchment had a relatively simple algal community structure with multiple pigments including canthaxanthin (cyanobacteria) and alloxanthin (cryptophytes) found to change coincident with TOC and $\delta^{13}\text{C}_{\text{TOC}}$, suggesting these pigments are closely coupled to delivery of organic matter (Section 5.1.13, Figure 5.16). This provides evidence for the microbial loop whereby allochthonous dissolved or particulate organic matter can provide an energy source for pelagic bacteria (Tranvik, 1992), which in turn can be utilised by cryptophytes and cyanobacteria as these taxa may adopt mixotrophic strategies (Jones, 2000; Burkholder et al., 2008). Changes in other pigments probably reflected transitions in algal community structure (Figure 5.7), linked to lake development and in-lake biotic interrelationships, with only a minor mediating role for climate (Anderson et al., 2008). Benthic communities were a large contributor to total algal production, with diatom communities in Disko 2 primarily benthic (Figure 5.14), typical of Arctic lakes (Vadeboncoeur et al., 2002; Vadeboncoeur et al., 2003). Differences between replicate cores such as in Disko 2 probably reflect in part, the role of benthic macrophytes which may form a patchy mosaic on the lake bed.

At lakes lower down the hydrogeomorphic elevation gradient the lake ecosystem was found to be closely tied to more developed catchment soils, greater vegetation development and probably faster nutrient cycling. In Disko 4 most pigments fluctuated together (Figure 7.9 & 7.12), highlighting the importance of nutrients as a limiting factor for algal production, probably coupled to permafrost cycling, periglacial processes and glacier mass balance. More developed catchment soils are likely to be highly susceptible to localised leaching (Hobbie et al., 2002) and solifluction (Draebing and Eichel, 2017), resulting in increased DOC, N and P release stimulating all algal groups. This helps explain the intermittent fluctuating algal community response in Disko 4 (Figure 7.9 & 7.12), which is in marked contrast to more varied changes in Disko 2 (Figures 5.7 & 5.16).

There was also evidence of possible mixotrophic activity in lakes at lower positions in the landscape, with alloxanthin (cryptophytes) and fucoxanthin (multiple indicators, including chrysophytes) found to have proportionately higher production than diatoxanthin (mostly diatoms) during periods of low production. Facultatively mixotrophic cryptophytes may respond through heterotrophy to DOM and particulate matter (Jones, 2000; Burkholder et al., 2008; Stevenson et al., 2016), stimulating primary production indirectly through ingestion of bacterioplankton (Tranvik, 1990)

or be linked to consumption of phagotrophic heterotrophs through release of dissolved nutrients by herbivores (Sanders et al., 1990).

The length of the ice-free season may play a role in mediating the time available for biological production, altering the species composition of some algae (Smol et al., 2005). However, on Disko the catchment is likely the main control on algal production, through the mechanism of nutrient limitation and availability of DOC. This is key as the large (up to >10 fold) fluctuations in diatoxanthin pigments in Disko 4 (Figure 7.12), highlight the role of nutrients and/or DOC as limiting factors, rather than the more subtle effect of length of the ice-free season, which would be unlikely to result in diatom fluctuations of this magnitude.

8.3.2 Geomorphology

Geomorphology exerted a clear controlling influence on all lake ecosystems samples, although the nature and intensity of this varied with lake position. Figures 8.1, 8.2 and 8.3 provide schematic diagrams for Disko 2, 1 and 4 respectively, highlighting the individuality of each lake catchment. Sedimentation rate was found to be closely associated with catchment to lake area ratio and the presence of erosive glaciers (ice cover) in the catchment (Section 4.2, Table 4.1). Sedimentation rate was the slowest in Disko 2 at the highest position in the landscape, with a simple catchment, but considerably faster in Disko 4 at the lowest position in the landscape and a more complex catchment. In Disko 1 sedimentation was the fastest, probably linked to delivery of material from a glacier stemming from the Lyngmarksbræen ice cap which is known to be in retreat since its maximum extent during the LIA (Ingólfsson et al., 1990). Although dating of this sequence was uncertain (Section 6.1.3 & 6.2.3), and the precise sedimentation rate is unknown, all reasonable age-depth scenarios would indicate fast sedimentation compared with lakes Disko 2 and 4. Disko 1 sediments featured a marked increase in algal production across multiple pigments in the uppermost sediments, probably in response to glacier retreat (and release of nutrients N & P) highlighting close coupling of geomorphology with in-lake algal production.

Geomorphology also determines the availability of habitat for vegetation communities, which is greater in the more sheltered and waterlogged U-shaped valleys in the catchments of Disko 1 and 4, compared with Disko 2 (Section 4.1 and Figure 4.1). In Disko 4 C/N ratio reached higher maximum values, compared with Disko 2, highlighting the more developed vegetation which would be delivered during periodic

meltwater events. Geomorphology also controls the extent and diversity of periglacial and glacial features present in each catchment. Lake Disko 2 sits in an over-deepened cirque basin with clear delivery of material from a frost shattered headwall, which probably supported a single glacier (possibly rock-type) in the LIA. (Figure 8.1). In contrast, lake Disko 4 at its lower position in the landscape (Figure 8.3) receives material derived from multiple glaciers, which may all advance and retreat independently, linked to localised accumulation on the varied and rugged topography (Yde and Knudsen, 2007). The larger Disko 4 catchment with some areas of thicker soil development also explains how multiple periglacial processes and features (e.g. solifluction and freeze-thaw weathering) result in a diverse mixture of material delivered to the lake, often entraining patchy vegetation with these flows. Together, these glacier, periglacial, soil and vegetation factors help explain why the Disko 4 response across all proxies fluctuated to a greater extent than Disko 2.

Lake Disko 2 - cirque lake

Elevation 575 m.a.s.l

Catchment area 358 ha

Catchment: lake area ratio 45:1

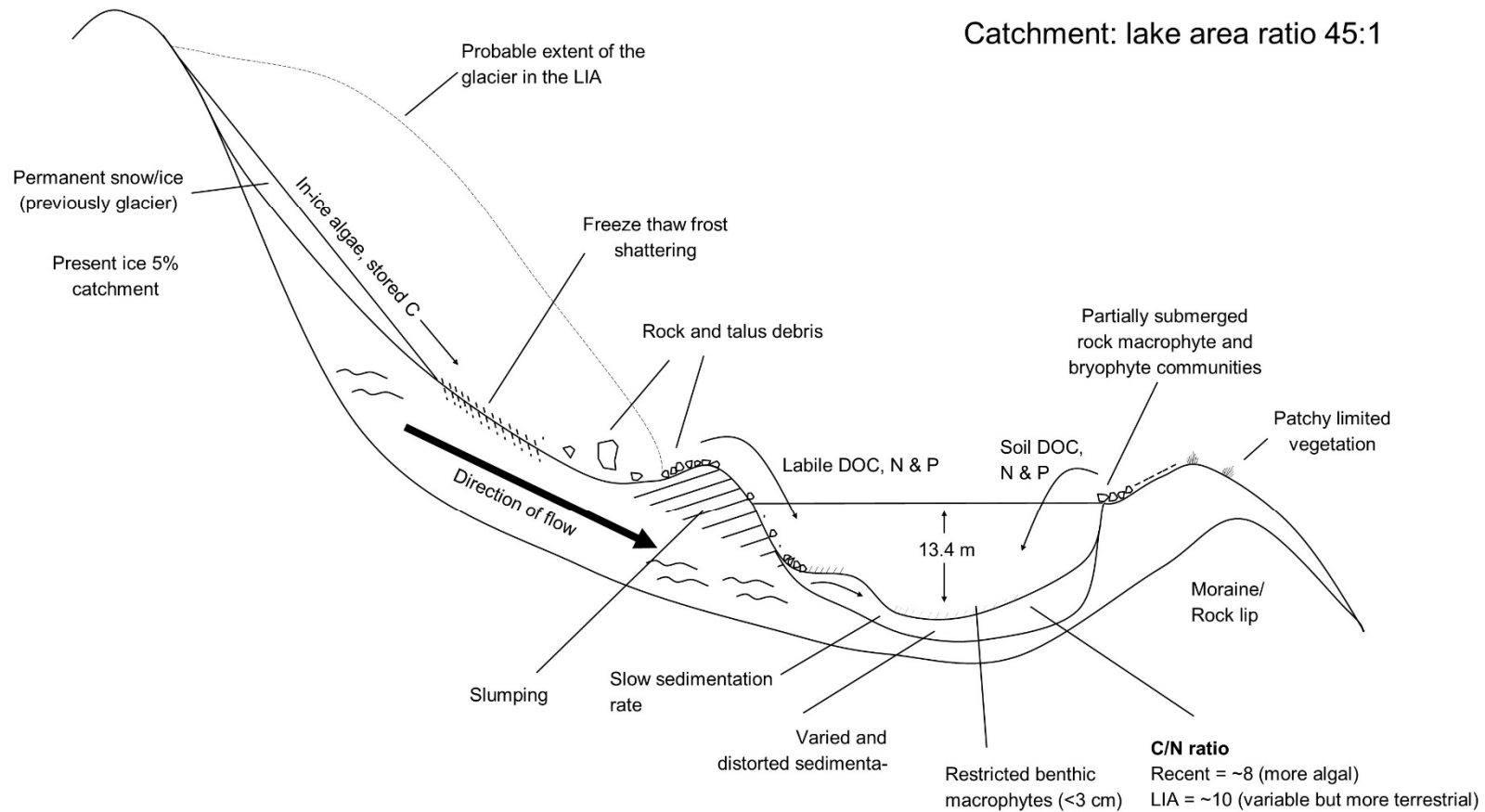


Figure 8.1: Schematic diagram of lake Disko 2 (cirque lake) positioned above Kaussuaq incised valley, extending to the north of the Blæsedalen (Itinneq Kanglilleq) valley. Sedimentation has been slow (Chapter 6) and the small catchment of patchy limited vegetation supplies limited amounts of nutrients (N & P) and DOC supplemented by bryophytes and microbial soil leaching. Additional concentrations of labile DOC, N & P are likely supplied from the permanent ice in the catchment (previously cirque glacier in colder periods). Recent increases in algal production are likely related to more active movement (and release of labile DOC, N & P) from the freeze thaw scree slope/debris flow. Past extent of the glacier in the LIA is not to scale.

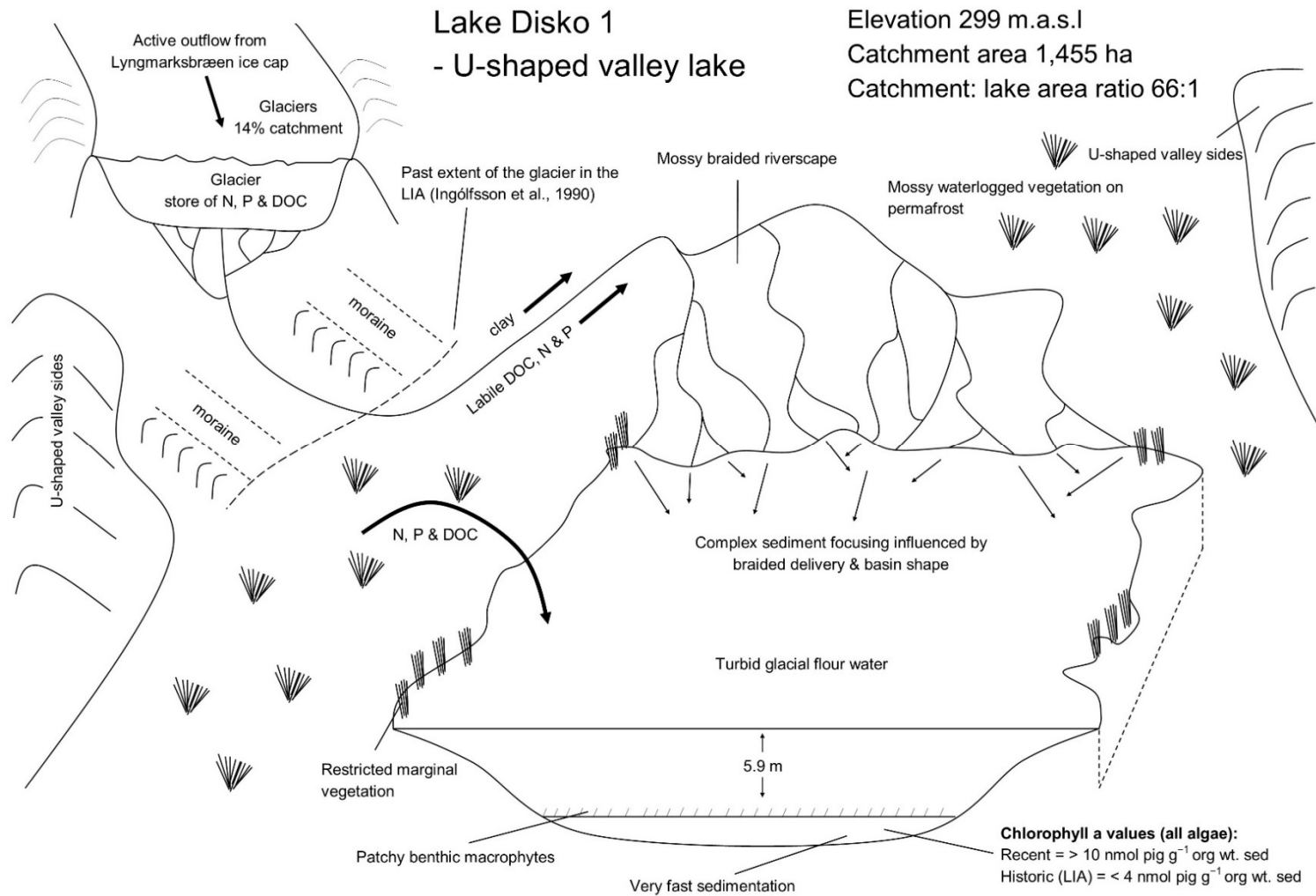


Figure 8.2: Schematic diagram of lake Disko 1 and its position in the Blæsedalen (Itinneq Kanglilleq) U-shaped valley. Sedimentation has been fast and dominated by the input from a large outflow glacial tongue from the Lyngmarksbræen ice cap. The sedimentary record encompassing only recently dated deposits (Chapter 5) is marked by recent increases in algal production linked primarily to release of labile DOC, and nutrients N & P from the glacier. Additional contributions of DOC, N & P are likely supplied from the waterlogged permafrost catchment. Past extent of the glacier in the LIA is not to scale.

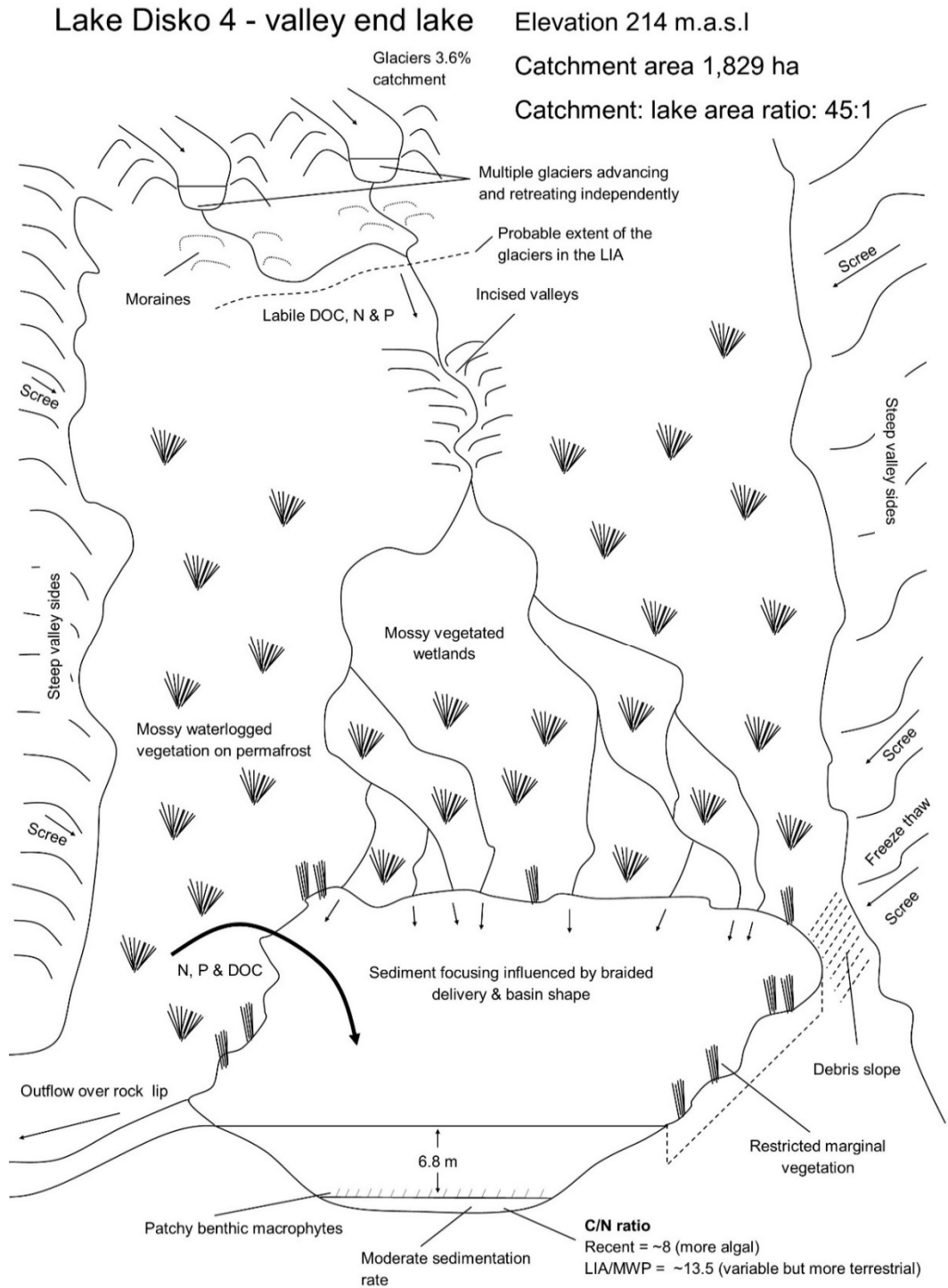


Figure 8.3: Schematic diagram of lake Disko 4 (valley end lake) positioned above the Ipraatsi valley and feeding into Laksebugt bay. Sedimentation has been moderate (Chapter 7) with the large catchment interpreted as supplying complex and variable pulses of DOC and nutrients (N & P) to stimulate an intermittent variable record of algal production since the MCA. Biological activity in the mossy vegetated wetlands on permafrost, carbon supplied from active freeze thaw weathering on steep valley sides and outflows from multiple localised glaciers (some potentially connected indirectly to the Lyngmarksbræen ice cap) are all interpreted as contributing DOC, N and P to the lake stimulating algae in an intermittent variable manner. Past extent of the glacier in the LIA is not to scale.

8.3.3 Pan-Arctic synthesis

The Disko 2 reconstruction (Chapter 5) provides changes in key lipid, pigment and $\delta^{13}\text{C}_{\text{TOC}}$ ratios since ~ 7640 cal. yr BP and so is suitable for comparison with pan-Arctic and hemispheric scale reconstructions (Figure 8.4). Across much of the northern hemisphere ($90\text{--}30^\circ$ N) temperature is known to have decreased since the end of the HTM to the end of the LIA, followed by recent warming (Figure 8.4 – A) (Marcott et al., 2013), with the trend to the end of the LIA broadly following changes in insolation (Figure 8.4 – C). However, pan-Arctic changes in temperature are now known to be regionally and spatially heterogeneous due to the complex locally specific responses to insolation, changes in the extent of the Laurentide and Greenland ice sheets, variations in oceanographic currents and the role of the catchment on proxy response (Briner et al., 2016; Kaufman et al., 2016; Sejrup et al., 2016). Despite the identification of heterogeneity across the pan-Arctic, each region has a set of composite records, presenting key trends including the Canadian Arctic Islands, Greenland and mainland Canada north of 66° N (Briner et al., 2016), an Eastern Beringia synthesis (Kaufman et al., 2016) and a North Atlantic Fennoscandian synthesis (Sejrup et al., 2016), all with considerable within-composite heterogeneity (Figure 8.4).

There was a similar decline in diatoxanthin in Disko 2 (indicator of diatoms) from ~ 2700 cal. yr BP onwards (Figure 8.4 – E) to the Canadian, Greenland Canada composite (Figure 8.4 – C) (Briner et al., 2016) and Qivitu Highlands Lake $\delta^{13}\text{C}$ record on Baffin Island (Figure 8.4 – D), however prior to this point the fluctuations in diatoxanthin are not consistent with these proxies. There could be a climate control on diatoms from ~ 2700 cal. yr BP onwards, but in-lake processes and catchment are probably the main drivers prior to this. The $\delta^{13}\text{C}_{\text{TOC}}$ record on Disko 2 (Figure 8.4 – H) did not follow a similar trend to diatoxanthin or composite reconstructions which is understandable as $\delta^{13}\text{C}_{\text{TOC}}$ in this system has been interpreted as an indicator of organic matter source, rather than climate directly (Section 5.3.3). Despite this, there is a decline in $\delta^{13}\text{C}_{\text{TOC}}$ from the start of the record to ~ 4500 cal. yr BP, which is similar to declines in the Eastern Beringia synthesis (Figure 8.4 – F) and PC1 of the North Atlantic Fennoscandian synthesis (Figure 8.4 – G). These declines could indicate an early HTM and links to the West Greenland Current, or may be a factor in sampling resolution of $\delta^{13}\text{C}_{\text{TOC}}$.

Later pulses in $\delta^{13}\text{C}_{\text{TOC}}$ from ~ 1300 cal. yr BP onwards probably reflect the spatially varied MCA (Mann et al., 2009), with the decline since ~ 100 cal. yr BP probably

reflecting in-lake changes to the LIA and trend to recent warming, also seen in the northern hemisphere (90-30° N) reconstruction (Figure 8.4 – A) (Marcott et al., 2013). The lipid *n*-alkane CPI 2 indicator of ‘fresher’ less degraded inputs (Figure 8.4 – I) had a similar trend to $\delta^{13}\text{C}_{\text{TOC}}$, but with more abrupt pulses from ~1300 cal. yr BP, highlighting the proxy-specific nature of each response. Overall, at the pan-Arctic scale since ~7640 cal. yr BP there is no evidence of a direct climate driver on proxy trends for the entire record. Some similarities between Disko 2 proxies and composite records at specific times could be lined to climate mechanisms, but their intermittent expression confirms the importance of the catchment.

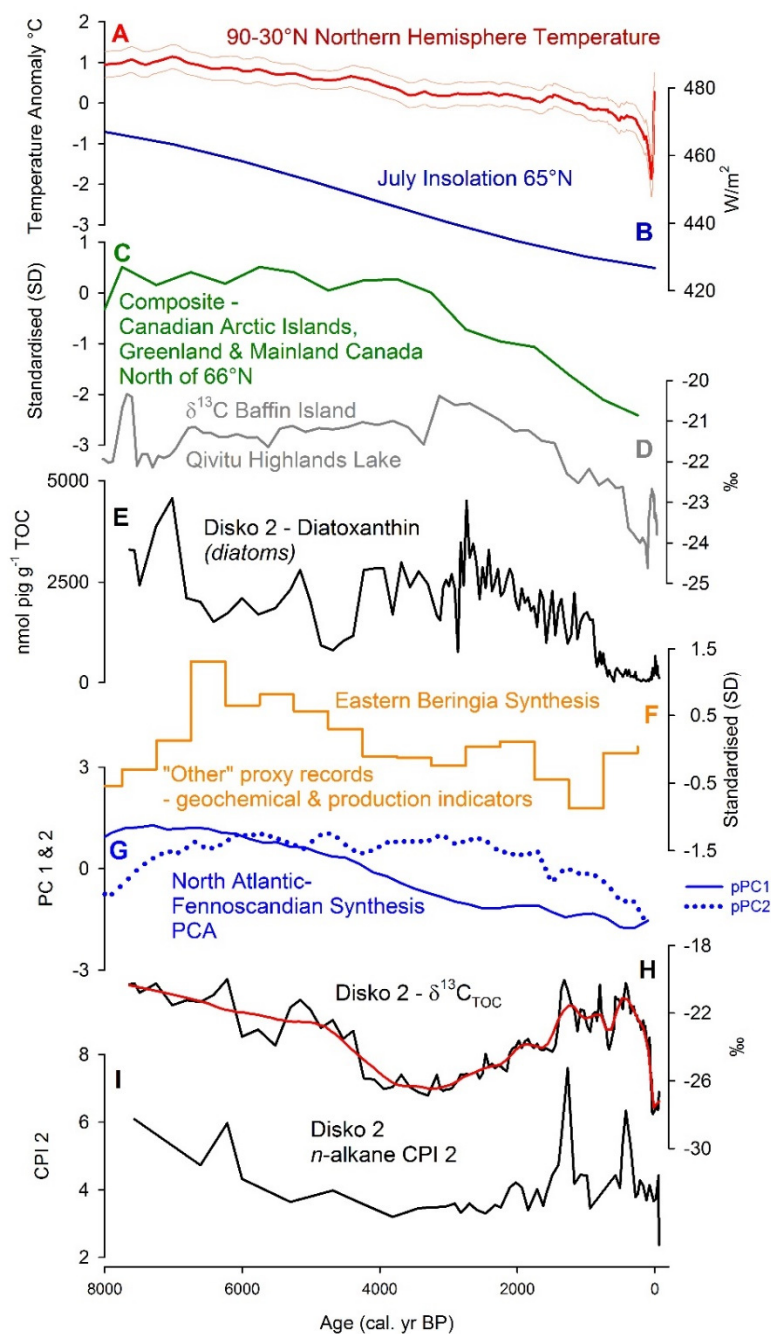


Figure 8.4: Pan-Arctic and hemispheric scale synthesis – comparing selected lake Disko 2 reconstructions with existing pan-Arctic and northern hemisphere proxies. **A.** Northern hemisphere (90-30° N) temperature synthesis calculated with 5x5 grid with 1 σ uncertainty (Marcott et al., 2013); **B.** July insolation at 65° N (Berger and Loutre, 1991); **C.** Composite of temperature sensitive records north of 66° N from the Canadian Arctic Islands, Greenland & Mainland Canada (Briner et al., 2016); **D.** $\delta^{13}\text{C}$ record from Qivitu Highlands Lake, Baffin Island (Florian et al., 2015); **E.** Disko 2 diatinoxanthin (diatoms); **F.** Eastern Beringia synthesis of ‘other’ proxy records including geochemical and production indicators (Kaufman et al., 2016); **G.** North Atlantic- Fennoscandian synthesis PCA components 1 and 2, highlighting inter-regional heterogeneity (Sejrup et al., 2016); **H.** Disko 2 $\delta^{13}\text{C}_{\text{TOC}}$ with smoothed polynomial trend line (loess, sampling proportion = 0.1, polynomial degree = 1) and **I.** Disko 2 *n*-alkane CPI 2 index.

8.3.4 Greenland scale synthesis

Comparing Disko 2 reconstructions since ~7640 cal. yr BP with existing pan-Greenland reconstructions (Figure 8.5) highlights some secondary links to regional forcings, but underlines the dominant effect of the catchment. The trend in the Greenland Ice Sheet surface area reconstruction (Figure 8.5 – A) (Lecavalier et al., 2014; Larsen et al., 2015), broadly follows trends in smoothed alloxanthin (indicator of cryptophytes) (Figure 8.5 – B) until ~1300 cal. yr BP and $\delta^{13}\text{C}_{\text{TOC}}$ until ~400 cal. yr BP (Figure 8.5 – D). Glacier mass balance in the Disko 2 catchment may be broadly in line with changes in the Greenland Ice Sheet at longer timescales, becoming decoupled during the spatially and temporally complex MCA and LIA (Mann et al., 2009). A potential mechanism is that with increased permanent ice in the catchment there could be greater biological production on glaciers (Anesio et al., 2009; Telling et al., 2012), which could increase nutrient cycling in the catchment, stimulating algae (Slemmons et al., 2013; Slemmons et al., 2015). But the Greenland Ice Sheet reconstruction is relatively low resolution and does not include the shorter cycle fluctuations that would be expected in smaller glaciers as found on Disko. C/N ratio (Figure 8.5 – C) has a slight inverse relationship with alloxanthin, indicating catchment dieback (disturbance of terrestrial plants during cool periods) but has no similarity to any regional Greenland proxy.

GRIP (Greenland Ice Core Project) borehole temperature (Dahl-Jensen et al., 1998) from the Greenland interior (Figure 8.5 – E, location Figure 1.6) was offset from trends in Disko 2 $\delta^{13}\text{C}_{\text{TOC}}$ (Figure 8.5 – D), although some patterns were similar. The minimum temperature at GRIP was later (~2000 cal. yr BP) than the changing organic matter source indicated by $\delta^{13}\text{C}_{\text{TOC}}$ (~3500 cal. yr BP). Again, this supports the role of the catchment in individually integrating complex processes. The peak in GRIP borehole temperature at ~1300 to 1000 cal. yr BP (Figure 8.5 – E), generally linked to the MCA is reflected in part by changes in $\delta^{13}\text{C}_{\text{TOC}}$ source composition (more algal), although again the trend is nuanced and temporally offset (Figure 8.5 – D). Although variable, there was some similarity between declines in diatoxanthin (diatoms) from ~2700 cal. yr BP onwards (Figure 8.5 – F) and GISP 2 (Greenland Ice Sheet Project) temperature (Figure 8.5 – G). Cooler temperatures may have limited permafrost nutrient cycling, leading to in-lake species interactions, making autotrophic taxa like diatoms less competitive. Length of the ice free season may also contribute in part (Smol et al., 2005), although such large >10 fold reductions in diatom production (Figure 8.5 – F) could not be explained by temperature alone. The different trends reconstructed in the lake Braya Sø Uk'37 index (Figure 8.5 – H) (D'Andrea et al.,

2011), highlight the spatial heterogeneity of climate on Greenland and the more continental position of Kangerlussuaq, compared with Disko.

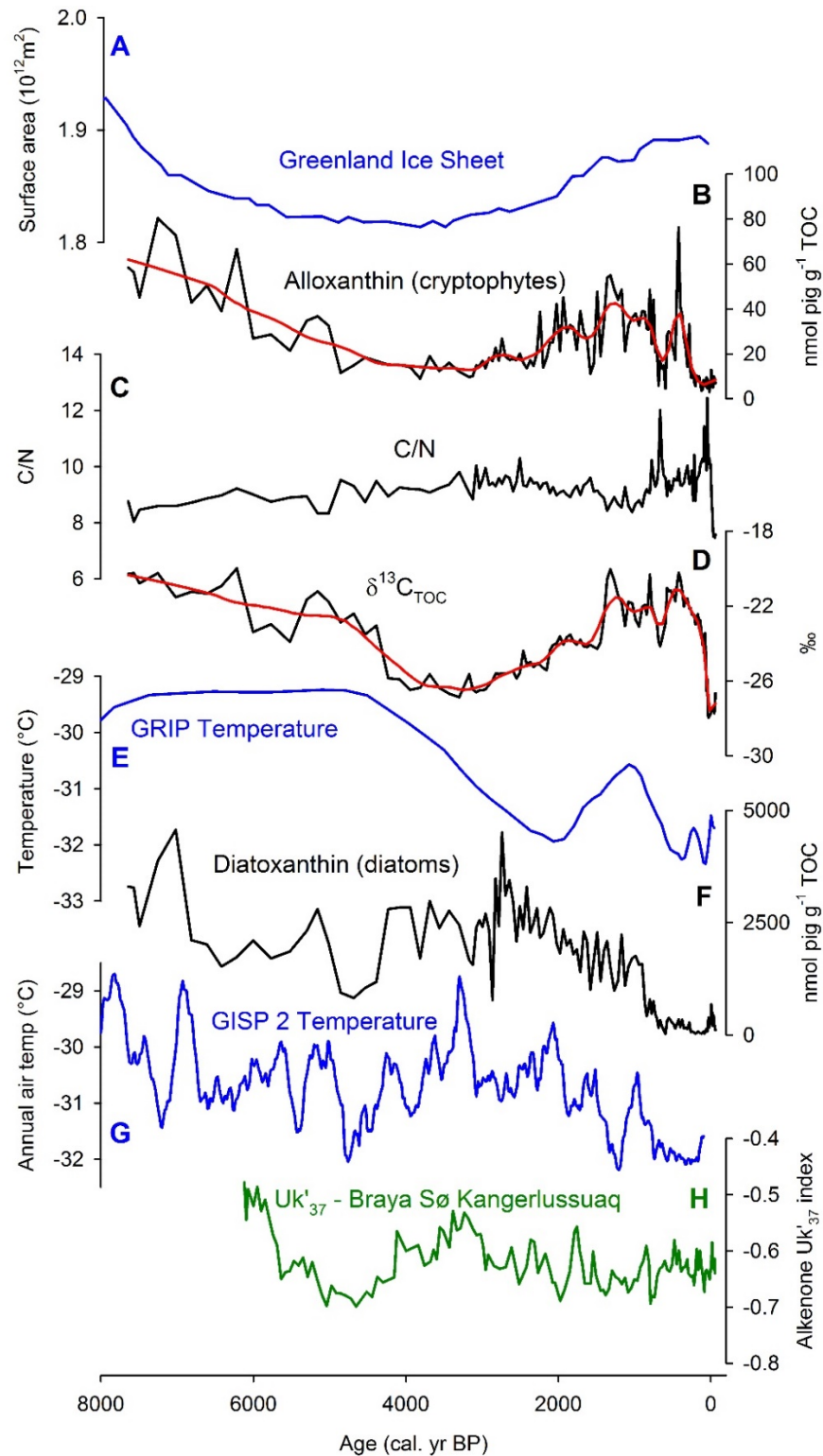


Figure 8.5: Greenland synthesis – comparing selected lake Disko 2 reconstructions with existing pan-Greenland proxies. **A.** Greenland Ice Sheet modelled area (Lecavalier et al., 2014; Larsen et al., 2015); **B.** Disko 2 alloxanthin (cryptophytes); **C.** Disko 2 C/N ratio; **D.** Disko 2 $\delta^{13}\text{C}_{\text{TOC}}$; **E.** GRIP temperature reconstruction (Dahl-Jensen et al., 1998); **F.** Disko 2 diatoxanthin (diatoms) and **G.** Uk^{37} alkenone reconstruction from lake Braya Sø, Kangerlussuaq (D'Andrea et al., 2011). Disko 2 alloxanthin and $\delta^{13}\text{C}_{\text{TOC}}$ smoothed with polynomial trend line (loess, sampling proportion = 0.1, polynomial degree = 1).

8.3.5 Regional scale synthesis

At the regional scale for Disko 2 since ~7640 cal. yr BP there was also evidence for considerable heterogeneity in proxy response to climate (Figure 8.6). Regionally there were some similarities between cryptophyte (alloxanthin, Figure 8.6 – A), cyanobacteria (canthaxanthin, Figure 8.6 – B) and Disko Bugt (Bay) reconstructions, with warmer water indicating benthic foraminifera (*I.norcrossi*) (Figure 8.6 – C) prior to 6000 cal. yr BP and after ~2700 cal. yr BP, similar to increased alloxanthin and $\delta^{13}\text{C}_{\text{TOC}}$. However, the sustained increase in warm water benthic foraminifera between ~5600 and ~3300 cal. yr BP (Figure 8.6 – C) was not resolved in pigments alloxanthin and diatoxanthin, highlighting oceanographic forcings may be out of phase. The alkenone $\text{C}_{37:4}$ indicator of meltwater production (Figure 8.6 – D) (Moros et al., 2016) had a similar trend to canthaxanthin and $\delta^{13}\text{C}_{\text{TOC}}$ from ~2600 cal. yr BP onwards, supporting the notion that meltwater production may be stimulating both oceanographic algae and production in lakes at high positions in the landscape at similar times. However, caution should be applied when using the alkenone $\text{C}_{37:4}$ index as it can be influenced by multiple factors and trends were dissimilar to alloxanthin and diatoxanthin prior to ~6000 cal. yr BP (Figure 8.6 – A, D & E).

At Ilulissat (location – Figure 1.3), the North Lake chironomid temperature reconstruction (Figure 8.6 – F) (Axford et al., 2013) did not resolve the complexity present from ~2800 cal. yr BP onwards in other proxies, but did show convincing evidence for minimum temperatures in the LIA. Evidence for minimum temperatures in the LIA is present in other proxies of production and source, including alloxanthin (Figure 8.6 – A), canthaxanthin (Figure 8.6 – B) and $\delta^{13}\text{C}_{\text{TOC}}$ (Figure 8.6 – E). Both LOI and $\delta^{13}\text{C}_{\text{TOC}}$ reached minimum levels at ~4200 cal. yr BP, although overall trends were dissimilar. The declining diatoxanthin trend from ~2700 cal. yr BP onwards (Figure 8.6 – G), except for minimum values during the LIA, was not resolved clearly in any regional proxy. Overall, Disko 2 appears to be integrating multiple regional and pan-Arctic trends, modified through the catchment. Disko 2 is probably more influenced by oceanographic changes in Disko Bugt than Ilulissat (Axford et al., 2013) which is closer to the ice sheet margin, although the response is highly proxy specific.

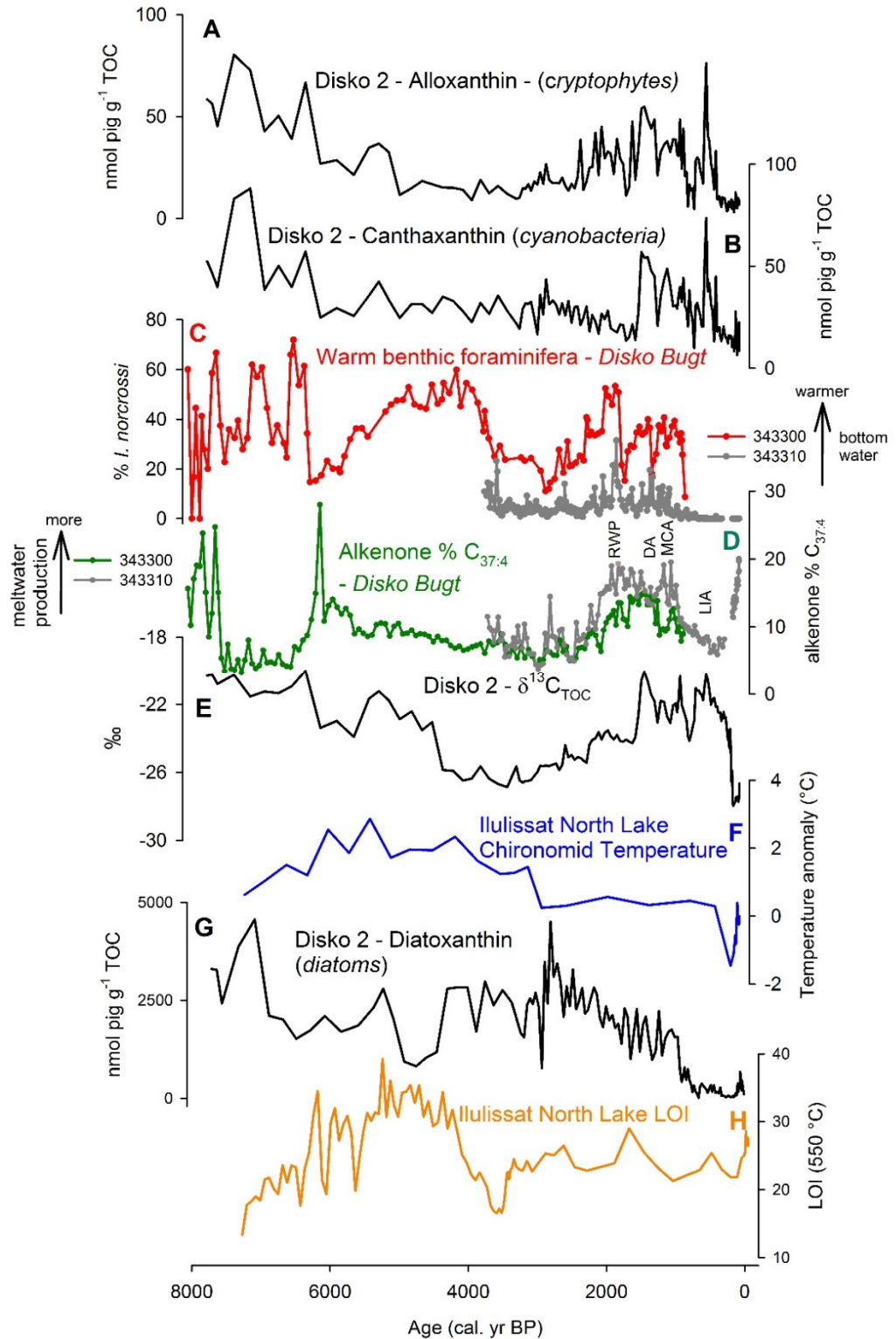


Figure 8.6: Regional synthesis - comparing selected lake Disko 2 reconstructions with existing regional proxies. **A.** Disko 2 alloxanthin (cryptophytes); **B.** Disko 2 canthaxanthin (cyanobacteria); **C.** Disko Bugt warm benthic foraminifera (*I. norcrossi*) from cores 343300 and 343310 (Moros et al., 2016); **D.** Disko Bugt alkenone % $C_{37:4}$ index of meltwater production from cores 343300 and 343310 (Moros et al., 2016); **E.** Disko 2 $\delta^{13}C_{TOC}$; **F.** Ilulissat North Lake chironomid temperature anomaly (Axford et al., 2013); **G.** Disko 2 diatoxanthin (diatoms) & **H.** Ilulissat North Lake loss on ignition (LOI) reconstruction (Axford et al., 2013).

8.3.6 Lower elevation lake synthesis

There was evidence of sensitivity to regional and pan-Arctic trends in a lake at a lower position in the landscape (Disko 4, Chapter 7), since ~1260 cal. yr BP (Figure 8.7). In lake Disko 4 there was convincing evidence for expression of the spatially and temporally heterogeneous LIA and MCA as demonstrated in regions across the Arctic (Briner et al., 2016; Kaufman et al., 2016; Sejrup et al., 2016). Specifically on Disko these trends appear to be consistent with the northern hemispheric dynamic range for the MCA as reported in Mann et al. (2009) as between ~ AD 950 and ~1250 (or 1000 to 700 cal. yr BP), which corresponds to maximum concentrations of most pigments in Disko 4, while noting spatial and temporal heterogeneity (Figure 8.7). The coldest temperatures of the LIA at the northern hemispheric scale are between ~ AD 1400 and 1700 (550 to 250 cal.yr BP) (Mann et al., 2009), although the wider period of the LIA based on glacial geomorphological evidence on Greenland spans the period ~AD 1150-1920 (800-30 cal.yr BP) (Humlum, 1999), with direct evidence on Disko corroborating this (Yde and Knudsen, 2007).

Throughout the LIA there was a major decrease in most algal pigments in Disko 4 (Figure 8.7, Zone B) coincident with the decline in summer insolation (Berger and Loutre, 1991) and fluctuations in the Dye 3 bore hole temperature reconstruction (Dahl-Jensen et al., 1998). The reduction in pigment concentration is more in phase with changes in Disko Bugt oceanographic proxies (alkenone % $C_{37:4}$ meltwater production and U_{37}^k index relative sea surface temperature) than the North Lake chironomid mean temperature reconstruction from near Ilulissat (Axford et al., 2013). This could be due to chironomids being highly sensitive to water temperatures which rebound in the Dye 3 temperature record, combined with the relatively low resolution North Lake record which may not have sampled the reduction in temperature around 550 cal.yr BP (Figure 8.2). The large >2 fold fluctuating decreases in algal production between the MCA and LIA evidenced by multiple pigments point to reductions in the delivery of nutrients and organic carbon from the catchment, as the direct effect of temperature would cause more subtle changes in whole algal community structure (Fritz and Anderson, 2013). A likely mechanism is reduced nutrient cycling following reduced permafrost melt (Hobbie et al., 2002) and less active glacier melt cycles which can be closely coupled to algal production (Slemmons et al., 2013; Slemmons et al., 2015).

Diatoxanthin (mainly diatoms) and canthaxanthin (cyanobacteria) show two of the largest decreases in pigment abundance during the LIA (Figure 8.7). Although still

decreasing substantially, proportionally the decrease for alloxanthin between the MCA (zones E - C) is not as large into the LIA (zone B). This is exemplified by the variable increase in the ratio of alloxanthin: diatoxanthin in the LIA (zone B), which suggests when nutrients are limited cryptophytes are proportionally (compared with diatoms) able to take advantage of improved conditions, perhaps by migrating through the water column to benthic microbial mats or by using mixotrophy as a way to utilise organic carbon and take advantage of the microbial loop (Roberts and Laybourn-Parry, 1999; Laybourn-Parry, 2002). Slight intermittent variable increases in C/N ratio in zone B probably from catchment dieback of vegetation during cold periods (Leng et al., 2012) could indicate supply of carbon from the catchment for in-lake microbial processing and heterotrophy. The lack of coherence with the Braya Sø Alkenone reconstruction (Figure 8.2) from Kangerlussuaq is likely due to Disko Island's more northerly position and maritime sensitivity to regional forcings, compared with the continentality of the inland position of Søndre Strømfjord and is consistent with the regional heterogeneity expected (Briner et al., 2016).

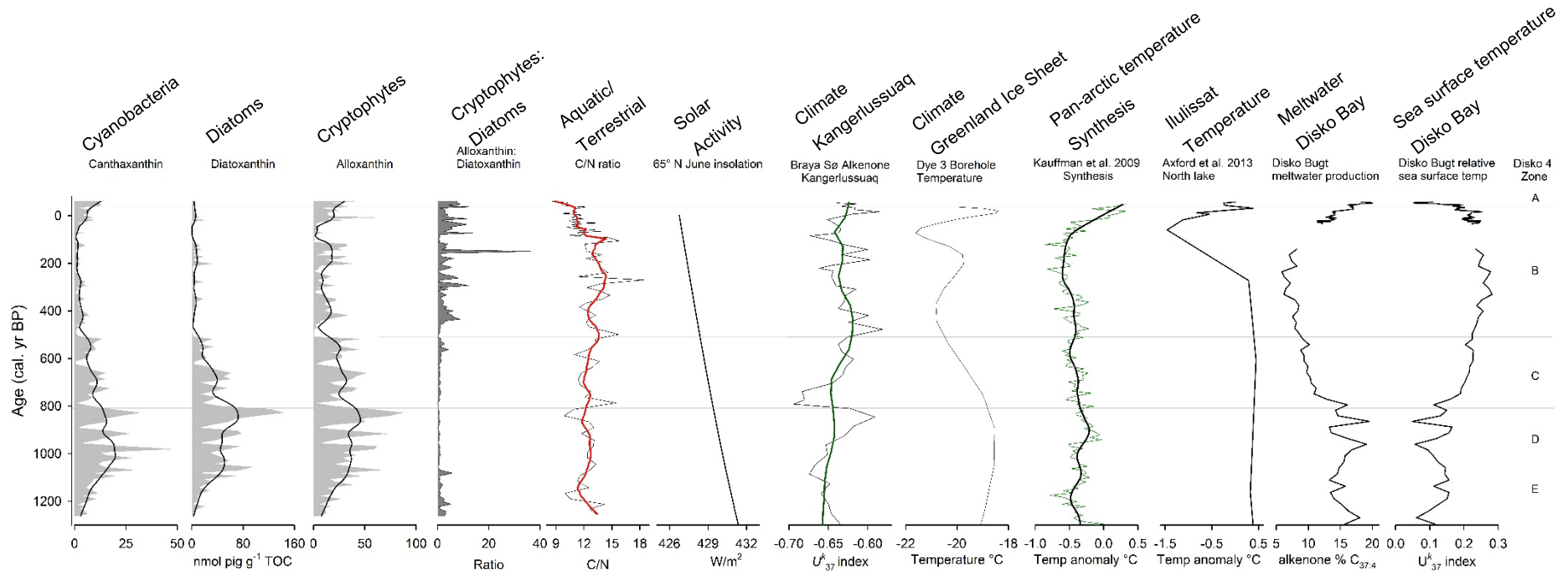


Figure 8.7: Disko 4 combined sequence summary diagram of pigments canthaxanthin, diatoxanthin, alloxanthin, ratio of alloxanthin: diatoxanthin and C/N ratio. Presented against 60°N June insolation (Berger and Loutre, 1991), Braya Sø U_{37}^k alkenone based reconstruction, Kangerlussuaq West Greenland (D'Andrea et al., 2011), temperature anomaly pan-arctic synthesis (Kaufman et al., 2009), chironomid based temperature reconstruction from North lake, near Ilulissat, west Greenland (Axford et al., 2013), Disko Bugt alkenone %C_{37:4} meltwater production reconstruction from site 343310 (Moros et al., 2016) and Disko Bugt U_{37}^k relative sea surface temperature reconstruction also from site 343310 (Moros et al., 2016). Where present, smoothed trend lines were calculated using a polynomial loess function in Sigmaplot v.12.5 (sampling proportion = 0.1; polynomial degree = 1).

8.3.7 Recent change synthesis

The end of the LIA locally on Disko Island marked a pronounced recession of most glaciers since the beginning of the 20th century (Yde and Knudsen, 2007). Recent warming has been observed in multiple proxies across the Arctic, reversing the long term cooling trend of the LIA (Kaufman et al., 2009). Although some Arctic studies have linked changes in algal communities to direct forcing driven by the increased length of the ice free season with warming (Michelutti et al., 2005; Smol et al., 2005), all three lakes on Disko Island provided evidence of a catchment mediated mechanism of recent change, despite contrasting catchments.

Algal production increased in the uppermost sediments in Disko 1, becoming more autochthonous (Figure 6.4 & 6.7). Although the precise dating of this sequence was problematic, sedimentation was clearly faster than in other lakes (see Chapter 6). The increased algal production is probably the result of nutrient release from an adjacent upstream glacier which has retreated since the LIA (Yde and Knudsen, 2007), together with increased nutrient cycling from permafrost melt associated with warming (Schuur et al., 2008). A catchment mechanism is proposed as the large response in some pigments such as alloxanthin (indicator of cryptophytes) and all algae was >4 fold which would not be ecologically possible from just lengthening of the ice-free season or temperature without the lifting of nutrient limitation.

Figure 8.8 presents a recently dated synthesis of Disko 2 and 4 sequences since ~1870 AD presented against NAO index, Disko mean temperature and algal reconstructions in a lake on Baffin Island (Florian et al., 2015). Both Disko 2 and 4 showed trends of increased algal production in all algae (β -carotene) and diatoms (diatoxanthin) around ~AD 1925 coincident with an increase in mean temperature by ~1.5 °C, compared with the period AD 1870 to 1925 (Hansen et al., 2006; Hollesen et al., 2015), probably indicating a switch to a more autochthonous system. Similar fluctuating increases to the Disko 1 response (clear increases in most pigments) suggest a catchment driver, although in these catchments lower sedimentation rates, and smaller percentages of permanent ice/glaciers suggest that terrestrial soils and permafrost may also release nutrients and DOC into the lakes, to a greater extent proportionally than Disko 1.

The lack of a response around AD 1925 AD in cryptophytes (alloxanthin) and cyanobacteria (canthaxanthin) in Disko 2 in response to warming (Figure 8.8) but a clear response in Disko 4, point to the different algal groups being stimulated. In Disko 4 the response to cryptophytes (alloxanthin) and cyanobacteria (canthaxanthin) could indicate comparatively greater inputs of labile organic carbon, compared with

Disko 2. The C/N ratio decline in Disko 2, confirms a more algal response in the most recent sediments but there was no clear change in Disko 4. Possible explanations for lake Disko 2 responding slightly differently to Disko 4 include the larger catchment of Disko 2 (catchment to lake area ratio 122:1), with more diverse catchment inputs at a lower position in the landscape (575 m.a.s.l) and a shallower lake depth (6.8 m) enabling greater benthic algal biological activity (Vadeboncoeur et al., 2003). In contrast, Disko 2 is a cirque lake at a high position in the landscape (214 m.a.s.l), with a smaller catchment to lake area ratio (66:1), limited terrestrial vegetation and a much deeper maximum lake depth (13.4 m). Phosphorus also increased in the most recent sediments in Disko 2 (Section 5.3.3, Figure 5.20) which suggests nutrient limitation may have been relaxed, leading to increased production as a result of increased leaching from permafrost and ice melt. At Disko 2 catchment erosion near the lakes outfall may also have increased lake level, contributing to a more planktonic diatom signature (Section 5.3.3, Figures 5.20 & 5.14). There was no convincing relationship between NAO index and pigment concentration, highlighting that underlying climate factors at sub-decadal levels are insignificant compared with the more dominant catchment processes of glacier and permafrost nutrient and DOC release.

Comparison of Disko 2 and 4 recent change records with increased algal production documented on Baffin Island (Florian et al., 2015), show that despite the robust dating of these records, recent increases in algal production, although present are not temporally synchronous across the Arctic. Recent change leads to highly individualised responses as algal communities reorganise to changes in nutrient input, DOC and light regime associated with catchment processes and changes in the length of the ice free season. On Disko catchment processes clearly dominate due to the >4 fold increases across multiple algal groups and in multiple lakes, which suggests limiting factors such as nutrients or DOC are controlling these changes.

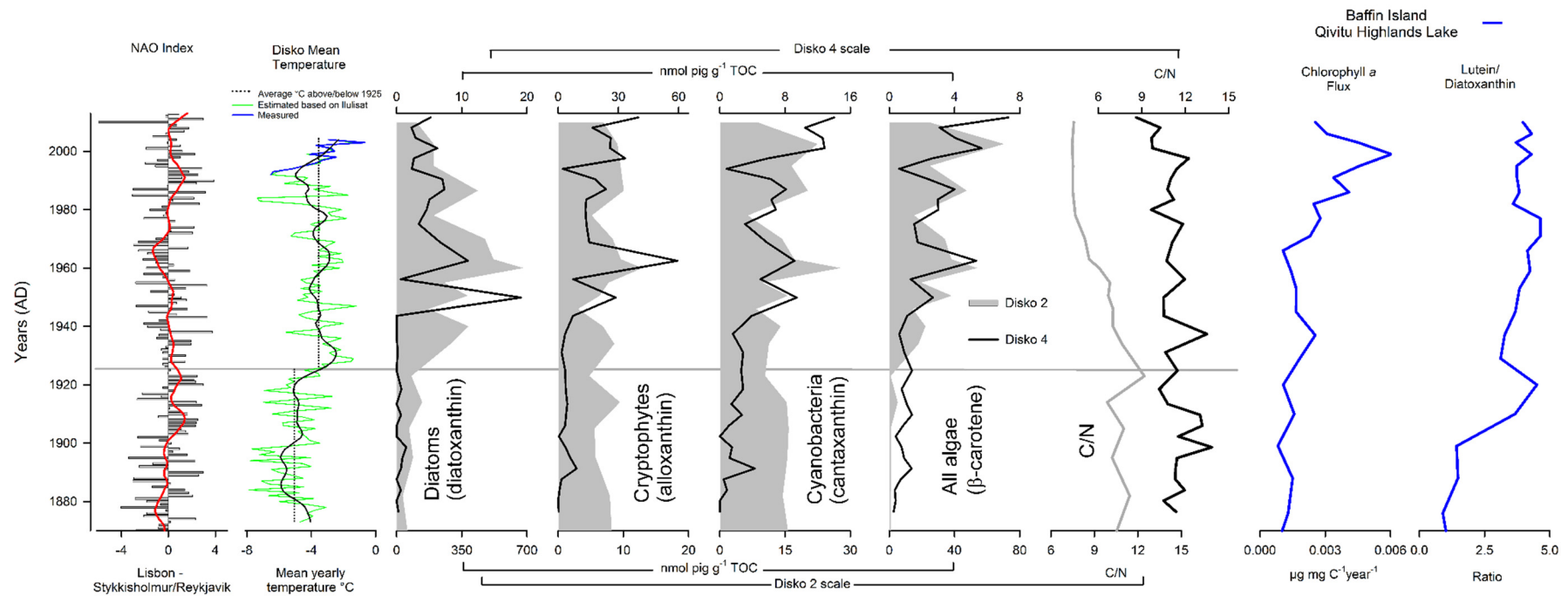


Figure 8.8: Recent change summary diagram for Disko 2 and 4 short cores. The mean annual North Atlantic Oscillation (NAO) index based on the difference of normalized sea level pressure between Lisbon, Portugal and Stykkisholmur/Reykjavik, Iceland (Hurrell and Deser, 2009) and Disko mean yearly temperature, based on local measurements (1992-2004) and estimated based on Ilulissat temperatures since 1873, following Hansen et al. (2006) and Hollesen et al. (2015). The smoothed trend lines (NAO index and mean temperature) were calculated using a polynomial loess function in Sigmaplot v.12.5 (sampling proportion = 0.1; polynomial degree = 1). Horizontal line represents mean temperature above and below 1925. Presented against dated (^{210}Pb , ^{137}Cs and ^{241}Am) reconstructions for lakes Disko 2 (grey) and Disko 4 (black) for diatoms (diatoxanthin), cryptophytes (alloxanthin), cyanobacteria (canthaxanthin), all algae (β -carotene) and C/N ratio. Also shown for regional comparison are recent chlorophyll *a* and lutein/diatoxanthin reconstructions from Qivitu Highlands Lake, Baffin Island (Florian et al., 2015).

8.3.8 Implications for carbon cycling

This study has demonstrated that all lakes on Disko Island investigated have recent increases in algal production, although these changes are highly lake specific and individual to each catchment. Most lakes are net-heterotrophic, processing the carbon delivered from allochthonous sources through physical, chemical and biological processes (e.g. respiration, heterotrophy) and then releasing this through aerobic (CO_2) or anaerobic (CH_4) conditions (Cole et al., 2007; Prairie, 2008; McGowan et al., 2016). Qualitatively, the increased production identified in all three lakes is unlikely to have caused a transition to overall net-autotrophic status, because the lakes all appear to be responding to increased catchment derived nutrients and DOC rather than temperature. However, the recent sediments in these lakes can be considered as an increased carbon sink as the switch to increased algal production is accompanied by increased carbon mass accumulation rate (CMAR) in Disko 2 and 4 (Figure 8.9). Although there was evidence for increased cyanobacteria and cryptophyte production in the most recent sediments of Disko 4 (Figure 8.8) which can be mixotrophic (Jones, 2000; Burkholder et al., 2008), in these low DOC systems this is probably contributing to nutrient and labile carbon bioavailability supporting further autotrophic production, rather than making the lake metabolic balance ‘more’ heterotrophic.

Catchment position was closely linked with the amount of carbon burial and also the individual response (and timing) of each lake to external drivers. Lake Disko 2 at a higher position in the hydrogeomorphic elevation gradient (575 m a.s.l.) had an average CMAR approximately half ($\sim 8.2 \text{ g OC cm}^{-2}\text{yr}^{-1}$) that of Disko 4 ($\sim 19.6 \text{ g OC cm}^{-2}\text{yr}^{-1}$) at a lower position (214 m a.s.l.) in the landscape since $\sim 1265 \text{ cal. yr BP}$ (Figure 8.9). The greater catchment to lake area of Disko 4 (Section 4.2, Table 4.1), together with its more developed vegetation and multiple glacier inputs helps explain this lake’s increased carbon burial compared with Disko 4. Maximum carbon burial rate in Disko 2 is coincident with recent warming, but is slightly earlier in Disko 4 ($\sim \text{AD } 1880\text{-}1900$) around the end of the LIA (Figure 8.9). This highlights the role of the catchment in filtering allochthonous inputs and highlights the pronounced effect of the LIA on Disko Island glacier mass balance (Yde and Knudsen, 2007) and permafrost nutrient and DOC release across the Arctic (Schuur et al., 2008). Disko 4 average CMAR is at least twice the rate compared with lakes further south near continental Kangerlussuaq (Figure 1.3), highlighting the more active glacial geomorphology on the more maritime influenced Disko and its faster permafrost nutrient cycling linked to greater hydrological flushing.

Algal production increases in recent sediments, or changes in community structure have now been detected in multiple studies across the Arctic including on Baffin Island (Michelutti et al., 2005; Florian et al., 2015) and potentially across the Canadian Arctic (Smol et al., 2005). This suggests more widely that recent warming, modified through the catchment to varying extents (depending on location) may be leading to increased carbon storage if consistent with increases in carbon burial as on Disko Island (Figure 8.9). These lakes probably act as a small sink of some of the carbon released from destabilised catchments as a result of permafrost degradation (Schuur et al., 2008) and glacier retreat (Yde and Knudsen, 2007), after processing by in-lake algae.

Across the Arctic, large quantities of organic carbon in permafrost are currently at risk from release (as CO₂ and CH₄) due to climate warming either directly (Schuur et al., 2008) or through downstream waterbodies (Tranvik et al., 2009), potentially acting as a global climate warming feedback (Walter et al., 2006; Koven et al., 2011; Schuur et al., 2015). However, although greater algal production is probably leading to increased carbon burial in lakes on Disko, Arctic lakes generally have low organic carbon burial efficiency relative to organic carbon deposition (Sobek et al., 2014). This is understandable as much of the organic carbon released from glaciers and ice is not sedimented at inland waters, but is delivered to the oceans (Hood et al., 2009; Hood et al., 2015), although carbon sequestered in lakes on Disko, may if upscaled across the Arctic represent a substantial sink, which should be integrated in future climate models. However, this trend to increased pelagic algal production will result in wider reductions in benthic diversity, through cascading effects on in-lake processes, reducing biodiversity in these sensitive Arctic lakes.

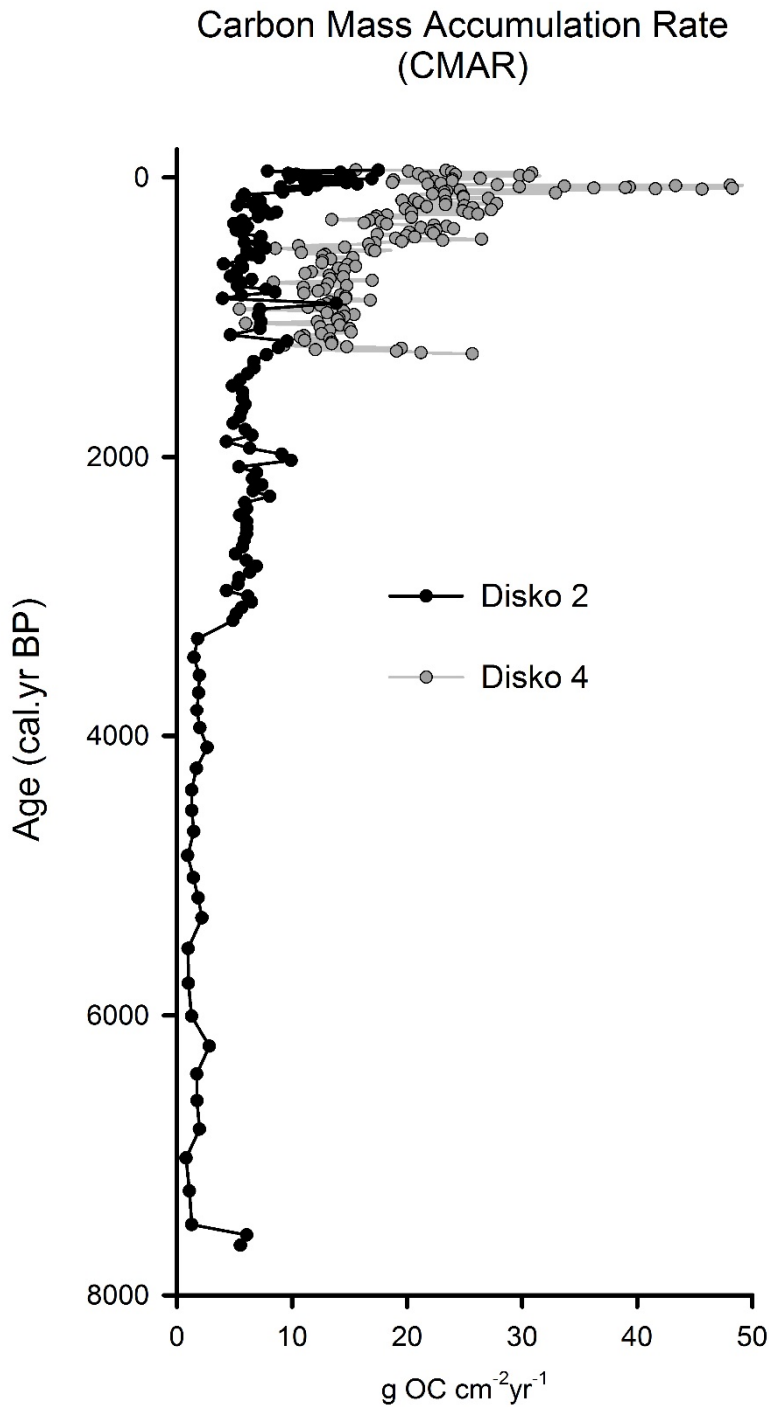


Figure 8.9: Comparing organic carbon mass accumulation rate (CMAR) for dated lake Disko 2 and 4 records. The mean accumulation rate from ~1265 cal.yr BP to the top of the sequence is ~8.2 g OC cm⁻²yr⁻¹ for Disko 2 (elevation 575 m a.s.l) and ~19.6 g OC cm⁻²yr⁻¹ for Disko 4 (214 m a.s.l).

8.4 Project challenges and future directions

Overlapping of cores was focused on bulk measures and stratigraphy which helped develop robust sequences, but where this was not possible in Disko 2 (S2) this was linked to catchment processes and the presence of a slope providing scree (Section 5.3.1). Radiocarbon dating was very effective at producing a robust chronology for Disko 4 due to the presence of identifiable terrestrial macrofossils (Section 7.1.4). Challenges were encountered in the radiocarbon dating of Disko 2 (S1), although it was possible to produce a revised chronology through the removal of instantaneous events and the correction of bulk dates using a paired macrofossil-bulk date offset on an adjacent sequence. Developing a chronology for Disko 1 was more problematic as although relatively recent ^{14}C dates were derived from terrestrial macrofossils taken within the core, without recent ^{210}Pb or ^{137}Cs dating it is not possible to confirm the high sedimentation rate interpreted from this core.

The combination of methods used in this thesis have helped address the initial aims (Section 1.3). The calculation of land cover data and vegetation quadrat surveys (Chapter 4) helped set the hydrogeomorphic elevation gradient which has been the key framework for this thesis, helping address the primary aim to consider the effect of catchment position on lake carbon cycling. Carbon cycling has been reconstructed through the calculation of carbon burial rates and by interpreting the source inputs, and variations in algal production that will have led to changes in $\delta^{13}\text{C}_{\text{TOC}}$ and C/N ratios. Changes in lake ecology and algal production have been interpreted through the taxonomic specificity of some pigments such as alloxanthin (indicator of cryptophytes), canthaxanthin (indicator of cyanobacteria) and diatoxanthin (indicator of diatoms). Interpretations of the quantity and quality of carbon deposited in lake sediments has been interpreted through the comparison of $\delta^{13}\text{C}_{\text{TOC}}$, C/N and lipid ratios (where present).

A limitation in the lipid biomarker reconstructions is that these techniques were only applied to one core and so between-lake comparison was not possible. Additionally, quantification prior to calculation of ratios would have been more robust, accounting for potential variations over time in the running of the GC-MS. However, samples were randomised prior to injection into the GC-MS and replicability between the two machines used was high (Section 3.8, Figure 3.3). Selected lipid biomarker compounds in Disko 2 have been interpreted together with changes in C/N ratio, helping to make use of these valuable data (Section 5.1.13 & 5.3.3, Figure 5.16). The analysis of catchment samples was useful for down-core reconstructions, however

bryophytes which make up a large proportion of vegetation cover on Disko had mixed $\delta^{13}\text{C}_{\text{TOC}}$, C/N and lipid ratios which means source attributions are not as definitive as in environments with greater higher plant contributions (Chapter 4). Despite these challenges it was possible to select a number of lipid biomarker compounds with good source attributions (Section 4.8.4) and apply these to Disko 2 down-core summary reconstructions (Figure 5.16 & 5.20).

To compare reconstructions on Disko with previous regional and pan-Arctic syntheses $\delta^{13}\text{C}_{\text{TOC}}$, C/N ratio and key pigment indicators were most useful, as together these techniques were able to track algal community change and variations in the source origin of carbon, at high resolution across multiple lakes. The final aim to identify changes in the lakes metabolic status (source or sink) of carbon has been addressed by combining changes in recent algal production with carbon burial rate calculations (Section 8.3.8). This has helped contribute to a wider discussion of potential implications across the Arctic.

Other techniques might also help address the projects primary aim, to investigate the effect of catchment position on carbon cycling in Arctic lakes on Disko (Section 1.3.1). Vegetation expansion and changes could be interpreted regionally using pollen analysis or directly in the catchment using macrofossil reconstructions. The advantage of these techniques compared with lipid analysis is that they are taxonomically specific and are not reliant on challenging catchment calibration studies. However, they are susceptible to preservation (macrophytes) or paint a regional rather than catchment specific signal of change due to dispersal (pollen). Extended use of diatom analysis (currently presented only for Disko 2 recent sediments, Figure 5.14 and 5.20) might have provided additional insight into lake development over time and the balance between planktonic and benthic diversity over periods of past heterogeneous environmental change (e.g. LIA & MCA). To complement pigment reconstructions which can be susceptible to degradation (Table 2.1) the pigment diatoxanthin (indicator of diatoms) could be compared with biogenic silica.

To enable a more direct reconstruction of past DOC change (UVR pigments were not detected in this core) future studies on Disko could subject pore waters to bioavailability experiments (Lawson et al., 2014b). Spectrophotometric and spectrofluorescence methods may also help elucidate overall changes in the bioavailability of DOC (Lepane et al., 2004; Leeben et al., 2008), whereas in this study the biomarker approach has considered changes in very specific compounds, which reflect only part of the carbon cycled in Arctic lakes.

Temperature reconstructions would also be useful, especially for plotting against the longer-term syntheses since ~7640 cal. yr BP (Figure 8.4, 8.5 & 8.6). Temperature reconstructions can be derived from for example, pollen (Seppä and Birks, 2001), chironomids (Axford et al., 2013), GDGTs (glycerol dialkyl glycerol tetraethers) (Pearson et al., 2011) and lipid alkenones (D'Andrea et al., 2011). Future extensions of the project could include the identification of alkenones from existing chromatograms (confirmed to be present in the Disko 2 cores) to develop a temperature reconstruction (U_{37}^k) that could be compared with the oceanographic reconstructions in Disko Bugt (Moros et al., 2016) and the Braya Sø reconstruction to the south at Kangerlussuaq (D'Andrea et al., 2011).

Use of inorganic methods may also have complemented the study, in particular by more effectively considering glacier inputs. XRF (X-ray fluorescence) was used to provide an elemental reconstruction of the most recent sediments on Disko 2 (Figure 5.15), but could be expanded throughout the sequence to consider the effects of catchment derived elements (e.g. Ti) over the full record. As glaciers produce distinctive outputs, particle size analysis could help identify if glacier inputs or permafrost leaching of nutrients are more closely related to recent increases in algal production (Figure 8.8). Finally, XRF analysis could be used to identify more closely layers of gravel (delivered the from the Disko 2 catchment scree slope), helping reconstruct past periods of erosion in the catchment and the delivery of this material to the lake.

8.5 Final conclusions

At the landscape scale this thesis presents palaeolimnological sequences, across a hydrogeomorphic landscape and elevation gradient from three lakes on Disko Island, West Greenland, each with unique catchments and contrasting reconstructions of carbon cycling. It underscores the importance of local factors including basin shape, sediment focusing and inputs of allochthonous versus autochthonous carbon in regulating lake biogeochemistry and the resulting signature of organic matter deposited in lakes. Although, Holocene climate variability is a key regulator of overarching trends in carbon cycling, in these lakes catchment factors including glacier activity, position in the landscape and the development of terrestrial vegetation modified the response, resulting in individualistic records.

Lakes at high positions with poorly developed soils and lower glacier coverage such as Disko 2 had simple algal communities that responded to changes the catchment, but the response since ~7640 cal. yr BP was heterogeneous compared with global northern hemispheric climate (Figure 8.5), consistent with current knowledge of Arctic environmental change (Briner et al., 2016; Kaufman et al., 2016; Sejrup et al., 2016). Upland geomorphic processes influence Arctic lakes, with proximity to rock and talus debris flow found to result in disturbed records proximal to these inputs. Spatially and temporally heterogeneous climate processes led to small changes in catchment vegetation, permafrost melt, glacier response and microbial activity, influencing nutrient/DOC regimes, impacting algal abundance in this lake. Some similarities between Greenland ice sheet surface area and pigment biomarkers of cryptophytes (alloxanthin), suggest ice variation on Disko in phase with Greenland may regulate nutrient and DOC release from catchments, stimulating algae (Figure 8.5).

Lake Disko 1 at a mid-elevation position in the catchment receives meltwater to a large retreating glacier. The recent increases in algal production in the sediments of Disko 1 is probably related to the retreat of this glacier since the end on the LIA and the increase in nutrients (N & P) and labile DOC, although permafrost and soil development in the U-shaped valley of this lake is thicker compared with Disko 2. Improved dating (using $^{210}\text{Pb}/^{137}\text{Cs}$) and an inorganic proxy of glacier inwash (e.g. particle size) would be required to identify if the recent increase in algal production is more closely related with glacier retreat or permafrost melt.

In Disko 4 at the lowest position in the landscape gradient the complex, varied pigment response is tightly coupled to local catchment factors with multiple glacier

sources in the catchment and a large wetland area, both supplying nutrients and DOC to the lake, regulated by extent of permafrost melt and local, varied hydrological regimes. In this lake higher maximum pigment concentrations were coincident with the broad extent of the spatially and temporally heterogeneous expression of the MCA and recent warming, with lower pigment concentrations coherent with the LIA.

Together, these records highlight the active geomorphological processes on Disko Island (glaciers, permafrost, periglacial processes & wetlands) that drive local carbon cycling and the delivery of allochthonous material to support algal production in lakes. Climate variability is important primarily in driving these catchment factors which regulate the release and delivery (cycling) of nutrients and DOC to support aquatic production. However, the precise integrator of external forcings in these lakes on Disko Island is the catchment, with position in the landscape, proximity to glaciers, basin shape, vegetation development and the relative allochthonous to autochthonous supply of organic matter all key regulators of local in-lake carbon cycling in these lakes.

Recent increases in algal production in all three lakes, although individual to each catchment, when combined with recent increases in carbon burial (Figure 8.9) suggests that these lakes are becoming increased carbon sinks. Although the majority of carbon released from glaciers and permafrost cycling into inland waters is released to the oceans, the increases in carbon burial in lakes associated with recent warming could be significant if upscaled across the Arctic and should be considered in future models. With future climate warming, recent changes in algal community structure and function in lakes across the Arctic could intensify. Evidence from Disko suggests the catchment will play a pronounced role in mediating future change in Arctic lakes.

References

- Aebly, F.A., Fritz, S.C., 2009. Palaeohydrology of Kangerlussuaq (Søndre Strømfjord), west Greenland during the last~ 8000 years. *The Holocene* 19, 91-104.
- Aichner, B., Herzsuh, U., Wilkes, H., 2010a. Influence of aquatic macrophytes on the stable carbon isotopic signatures of sedimentary organic matter in lakes on the Tibetan Plateau. *Organic Geochemistry* 41, 706-718.
- Aichner, B., Wilkes, H., Herzsuh, U., *et al.*, 2010b. Biomarker and compound-specific $\delta^{13}\text{C}$ evidence for changing environmental conditions and carbon limitation at Lake Koucha, eastern Tibetan Plateau. *Journal of Paleolimnology* 43, 873-899.
- Aislabie, J.M., Chhour, K.L., Saul, D.J., *et al.*, 2006. Dominant bacteria in soils of Marble Point and Wright Valley, Victoria Land, Antarctica. *Soil Biology and Biochemistry* 38, 3041-3056.
- Algesten, G., Sobek, S., Bergström, A.K., *et al.*, 2004. Role of lakes for organic carbon cycling in the boreal zone. *Global Change Biology* 10, 141-147.
- Alley, R.B., Meese, D., Shuman, C., *et al.*, 1993. Abrupt increase in Greenland snow accumulation at the end of the Younger Dryas event. *Nature* 362, 527-527.
- Andersen, C., Koc, N., Jennings, A., *et al.*, 2004. Nonuniform response of the major surface currents in the Nordic Seas to insolation forcing: implications for the Holocene climate variability. *Paleoceanography* 19.
- Anderson, N., 1990. Variability of diatom concentrations and accumulation rates in sediments of a small lake basin. *Limnology and Oceanography* 35, 497-508.
- Anderson, N.J., 1989. A Whole-Basin Diatom Accumulation Rate for a Small Eutrophic Lake in Northern Ireland and its Palaeoecological Implications. *Journal of Ecology* 77, 926-946.
- Anderson, N.J., Bennike, O., Christoffersen, K., *et al.*, 1999. Limnological and palaeolimnological studies of lakes in south-western Greenland. *Geology of Greenland Survey Bulletin* 183, 68-74.
- Anderson, N.J., Brodersen, K., Ryves, D., *et al.*, 2008. Climate Versus In-Lake Processes as Controls on the Development of Community Structure in a Low-Arctic Lake (South-West Greenland). *Ecosystems* 11, 307-324.
- Anderson, N.J., Clarke, A., Juhler, R.K., *et al.*, 2000. Coring of laminated lake sediments for pigment and mineral magnetic analyses, Søndre Strømfjord, southern West Greenland. *Geology of Greenland Survey Bulletin* 186, 83-87.
- Anderson, N.J., D'Andrea, W., Fritz, S.C., 2009. Holocene carbon burial by lakes in SW Greenland. *Global Change Biology* 15, 2590-2598.
- Anderson, N.J., Leng, M.J., 2004. Increased aridity during the early Holocene in West Greenland inferred from stable isotopes in laminated-lake sediments. *Quaternary Science Reviews* 23, 841-849.

- Anderson, N.J., Liversidge, A.C., McGowan, S., *et al.*, 2012. Lake and catchment response to Holocene environmental change: spatial variability along a climate gradient in southwest Greenland. *Journal of Paleolimnology* 48, 209-222.
- Anderson, N.J., Saros, J.E., Bullard, J.E., *et al.*, 2017. The Arctic in the Twenty-First Century: Changing Biogeochemical Linkages across a Paraglacial Landscape of Greenland. *BioScience* 67, 118-133.
- Andresen, C.S., Björck, S., Bennike, O., *et al.*, 2004. Holocene climate changes in southern Greenland: evidence from lake sediments. *Journal of Quaternary Science* 19, 783-795.
- Andresen, C.S., McCarthy, D.J., Dylmer, C.V., *et al.*, 2010. Interaction between subsurface ocean waters and calving of the Jakobshavn Isbræ during the late Holocene. *The Holocene* 21, 211-224.
- Anesio, A.M., Hodson, A.J., Fritz, A., *et al.*, 2009. High microbial activity on glaciers: importance to the global carbon cycle. *Global Change Biology* 15, 955-960.
- Anesio, A.M., Laybourn-Parry, J., 2012. Glaciers and ice sheets as a biome. *Trends in Ecology & Evolution* 27, 219-225.
- Antoniades, D., Douglas, M.S., 2002. Characterization of high arctic stream diatom assemblages from Cornwallis Island, Nunavut, Canada. *Canadian Journal of Botany* 80, 50-58.
- Appleby, P.G., 2001. Chronostratigraphic Techniques in Recent Sediments, In: Last, W.M., Smol, J.P. (Eds.), *Tracking Environmental Change Using Lake Sediments*. Springer Netherlands, pp. 171-203.
- Appleby, P.G., Nolan, P.J., Gifford, D.W., *et al.*, 1986. ²¹⁰Pb dating by low background gamma counting. *Hydrobiologia* 143, 21-27.
- Ask, J., Karlsson, J., Persson, L., *et al.*, 2009. Whole - lake estimates of carbon flux through algae and bacteria in benthic and pelagic habitats of clear - water lakes. *Ecology* 90, 1923-1932.
- Axford, Y., Losee, S., Briner, J.P., *et al.*, 2013. Holocene temperature history at the western Greenland Ice Sheet margin reconstructed from lake sediments. *Quaternary Science Reviews* 59, 87-100.
- Bagshaw, E.A., Tranter, M., Fountain, A.G., *et al.*, 2013. Do Cryoconite Holes have the Potential to be Significant Sources of C, N, and P to Downstream Depauperate Ecosystems of Taylor Valley, Antarctica? *Arctic, Antarctic, and Alpine Research* 45, 440-454.
- Bardgett, R.D., Freeman, C., Ostle, N.J., 2008. Microbial contributions to climate change through carbon cycle feedbacks. *ISME J* 2, 805-814.
- Battarbee, R., Jones, V., Flower, R., *et al.*, 2001. Diatoms, In: Smol, J., Birks, H.J., Last, W., Bradley, R., Alverson, K. (Eds.), *Tracking Environmental Change Using Lake Sediments*. Springer Netherlands, pp. 155-202.
- Bennike, O., 1995. Palaeoecology of two lake basins from Disko, West Greenland. *Journal of Quaternary Science* 10, 149-155.

- Bennike, O., 2000. Palaeoecological studies of Holocene lake sediments from west Greenland. *Palaeogeography, Palaeoclimatology, Palaeoecology* 155, 285-304.
- Bennike, O., Anderson, N.J., McGowan, S., 2010. Holocene palaeoecology of southwest Greenland inferred from macrofossils in sediments of an oligosaline lake. *Journal of Paleolimnology* 43, 787-798.
- Bennike, O., Björck, S., 2002. Chronology of the last recession of the Greenland Ice Sheet. *Journal of Quaternary Science* 17, 211-219.
- Bennike, O., Goodsite, M., Heinemeier, J., 2008. Palaeoecology of Holocene peat deposits from Nordvestø, north-west Greenland. *Journal of Paleolimnology* 40, 557-565.
- Berger, A., Loutre, M.-F., 1991. Insolation values for the climate of the last 10 million years. *Quaternary Science Reviews* 10, 297-317.
- Bernasconi, S.M., Barbieri, A., Simona, M., 1997. Carbon and nitrogen isotope variations in sedimenting organic matter in Lake Lugano. *Limnology and Oceanography* 42, 1755-1765.
- Bertilsson, S., Tranvik, L.J., 2000. Photochemical transformation of dissolved organic matter in lakes. *Limnology and Oceanography* 45, 753-762.
- Bianchi, T.S., Canuel, E.A., 2011. *Chemical Biomarkers in Aquatic Ecosystems*. Princeton University Press, Princeton.
- Bindler, R., Renberg, I., Anderson, N.J., *et al.*, 2001. Pb isotope ratios of lake sediments in West Greenland: inferences on pollution sources. *Atmospheric Environment* 35, 4675-4685.
- Blaauw, M., Christen, J.A., 2011. Flexible paleoclimate age-depth models using an autoregressive gamma process. *Bayesian Analysis* 6, 457-474.
- Blaauw, M., Christen, J.A., 2013. Bacon Manual v2. 2.
- Blake, W.J., Boucherle, M., Fredskild, B., *et al.*, 1992. The geomorphological setting, glacial history and Holocene development of 'Kap Inglefield Sø', Inglefield Land, North-West Greenland. *Meddelelser om Grønland Geoscience* 27, 1-42.
- Bond, G., Kromer, B., Beer, J., *et al.*, 2001. Persistent Solar Influence on North Atlantic Climate During the Holocene. *Science* 294, 2130-2136.
- Bond, G., Showers, W., Cheseby, M., *et al.*, 1997. A Pervasive Millennial-Scale Cycle in North Atlantic Holocene and Glacial Climates. *Science* 278, 1257-1266.
- Boom, A., Marchant, R., Hooghiemstra, H., *et al.*, 2002. CO₂- and temperature-controlled altitudinal shifts of C4- and C3-dominated grasslands allow reconstruction of palaeoatmospheric pCO₂. *Palaeogeography, Palaeoclimatology, Palaeoecology* 177, 151-168.
- Booth, R.K., Jackson, S.T., Forman, S.L., *et al.*, 2005. A severe centennial-scale drought in midcontinental North America 4200 years ago and apparent global linkages. *The Holocene* 15, 321-328.

- Boschker, H., De Brouwer, J., Cappenberg, T., 1999. The contribution of macrophyte - derived organic matter to microbial biomass in salt - marsh sediments: Stable carbon isotope analysis of microbial biomarkers. *Limnology and Oceanography* 44, 309-319.
- Bothwell, M.L., Sherbot, D.M.J., Pollock, C.M., 1994. Ecosystem Response to Solar Ultraviolet-B Radiation: Influence of Trophic-Level Interactions. *Science* 265, 97-100.
- Bourbonniere, R.A., Meyers, P.A., 1996a. Anthropogenic influences on hydrocarbon contents of sediments deposited in eastern Lake Ontario since 1800. *Environmental Geology* 28, 22-28.
- Bourbonniere, R.A., Meyers, P.A., 1996b. Sedimentary geolipid records of historical changes in the watersheds and productivities of Lakes Ontario and Erie. *Limnology and Oceanography* 41, 352-359.
- Box, J.E., 2002. Survey of Greenland instrumental temperature records: 1873–2001. *International Journal of Climatology* 22, 1829-1847.
- Bradley, R.S., Hughes, M.K., Diaz, H.F., 2003. Climate in Medieval Time. *Science* 302, 404-405.
- Bray, E.E., Evans, E.D., 1961. Distribution of *n*-paraffins as a clue to recognition of source beds. *Geochimica et Cosmochimica Acta* 22, 2-15.
- Brenner, M., Whitmore, T., Curtis, J., *et al.*, 1999. Stable isotope ($\delta^{13}\text{C}$ and $\delta^{15}\text{N}$) signatures of sedimented organic matter as indicators of historic lake trophic state. *Journal of Paleolimnology* 22, 205-221.
- Briner, J.P., McKay, N.P., Axford, Y., *et al.*, 2016. Holocene climate change in Arctic Canada and Greenland. *Quaternary Science Reviews* 147, 340-364.
- Brodie, C.R., Casford, J.S., Lloyd, J.M., *et al.*, 2011. Evidence for bias in C/N, $\delta^{13}\text{C}$ and $\delta^{15}\text{N}$ values of bulk organic matter, and on environmental interpretation, from acid treatment methods. *Quaternary Science Reviews* 30, 3076–3087.
- Brutemark, A., Rengefors, K., Anderson, N.J., 2006. An experimental investigation of phytoplankton nutrient limitation in two contrasting low arctic lakes. *Polar Biology* 29, 487-494.
- Buckeridge, K.M., Schaeffer, S.M., Schimel, J.P., 2015. Vegetation Leachate During Arctic Thaw Enhances Soil Microbial Phosphorus. *Ecosystems* 19, 477-489.
- Burkholder, J.M., Glibert, P.M., Skelton, H.M., 2008. Mixotrophy, a major mode of nutrition for harmful algal species in eutrophic waters. *Harmful Algae* 8, 77-93.
- Bush, R.T., McInerney, F.A., 2013. Leaf wax *n*-alkane distributions in and across modern plants: implications for paleoecology and chemotaxonomy. *Geochimica et Cosmochimica Acta* 117, 161-179.
- Callaghan, T., Christensen, T., Jantze, E., 2011. Plant and Vegetation Dynamics on Disko Island, West Greenland: Snapshots Separated by Over 40 Years. *AMBIO* 40, 624-637.

- Camarero, L., Catalan, J., 2012. Atmospheric phosphorus deposition may cause lakes to revert from phosphorus limitation back to nitrogen limitation. *Nature Communications* 3, 1118.
- Canuel, E.A., Martens, C.S., 1996. Reactivity of recently deposited organic matter: Degradation of lipid compounds near the sediment-water interface. *Geochimica et Cosmochimica Acta* 60, 1793-1806.
- Carey, S.K., 2003. Dissolved organic carbon fluxes in a discontinuous permafrost subarctic alpine catchment. *Permafrost and Periglacial Processes* 14, 161-171.
- Carr, J.R., Stokes, C., Vieli, A., 2014. Recent retreat of major outlet glaciers on Novaya Zemlya, Russian Arctic, influenced by fjord geometry and sea-ice conditions. *Journal of Glaciology* 60, 155-170.
- Castañeda, I.S., Schouten, S., 2011. A review of molecular organic proxies for examining modern and ancient lacustrine environments. *Quaternary Science Reviews* 30, 2851-2891.
- Castaneda, I.S., Werne, J.P., Johnsona, T.C., 2009. Influence of climate change on algal community structure and primary productivity of Lake Malawi (East Africa) from the Last Glacial Maximum to present. *Limnology and Oceanography* 54, 2431-2447.
- Catalan, J., 1989. The winter cover of a high-mountain Mediterranean lake (Estany Redó, Pyrenees). *Water Resources Research* 25, 519-527.
- Chalmers, J.A., Pulvertaft, T.C.R., Marcussen, C., *et al.*, 1999. New insight into the structure of the Nuussuaq Basin, central West Greenland. *Marine and Petroleum Geology* 16, 197-224.
- Chapin, F.S., Walker, L.R., Fastie, C.L., *et al.*, 1994. Mechanisms of primary succession following deglaciation at Glacier Bay, Alaska. *Ecological Monographs* 64, 149-175.
- Chen, N., Bianchi, T.S., McKee, B.A., *et al.*, 2001. Historical trends of hypoxia on the Louisiana shelf: application of pigments as biomarkers. *Organic Geochemistry* 32, 543-561.
- Christoffersen, K.S., Hansen, R.B., Thomar, J., 2004. Plankton investigations in lakes at southern Disko, In: Anderson, A.M.H., Jørgensen, T.R., Rahe, K. (Eds.), Arctic Biology Field Course Qeqertarsuaq 2004. Faculty of Science, University of Copenhagen, pp. 124-129.
- Church, M., Gilbert, R., 1975. Proglacial fluvial and lacustrine environments, In: Jopling, A.V., McDonald, B.C. (Eds.), Glaciofluvial and glaciolacustrine sedimentation. Society of economic paleontologists and mineralogists. Special Publication, pp. 40-100.
- Clow, D.W., Stackpoole, S.M., Verdin, K.L., *et al.*, 2015. Organic carbon burial in lakes and reservoirs of the conterminous United States. *Environmental Science & Technology* 49, 7614-7622.
- Cole, J.J., Pace, M.L., Carpenter, S.R., *et al.*, 2000. Persistence of net heterotrophy in lakes during nutrient addition and food web manipulations. *Limnology and Oceanography* 45, 1718-1730.

- Cole, J.J., Prairie, Y.T., Caraco, N.F., *et al.*, 2007. Plumbing the Global Carbon Cycle: Integrating Inland Waters into the Terrestrial Carbon Budget. *Ecosystems* 10, 172-185.
- Coleman, K.A., Palmer, M.J., Korosi, J.B., *et al.*, 2015. Tracking the impacts of recent warming and thaw of permafrost peatlands on aquatic ecosystems: a multi-proxy approach using remote sensing and lake sediments. *Boreal environment research* 20.
- Cooper, J.E., Bray, E.E., 1963. A postulated role of fatty acids in petroleum formation. *Geochimica et Cosmochimica Acta* 27, 1113-1127.
- Coplen, T.B., 2011. Guidelines and recommended terms for expression of stable-isotope-ratio and gas-ratio measurement results. *Rapid communications in mass spectrometry* 25, 2538-2560.
- Coutard, J.P., Francou, B., 1989. Rock temperature measurements in two alpine environments: implications for frost shattering. *Arctic and Alpine Research*, 399-416.
- Cox, P.M., Betts, R.A., Jones, C.D., *et al.*, 2000. Acceleration of global warming due to carbon-cycle feedbacks in a coupled climate model. *Nature* 408, 184-187.
- Craig, H., 1957. Isotopic standards for carbon and oxygen and correction factors for mass-spectrometric analysis of carbon dioxide. *Geochimica et Cosmochimica Acta* 12, 133-149.
- Cranwell, P., 1981. Diagenesis of free and bound lipids in terrestrial detritus deposited in a lacustrine sediment. *Organic Geochemistry* 3, 79-89.
- Cranwell, P., 1984. Lipid geochemistry of sediments from Upton Broad, a small productive lake. *Organic Geochemistry* 7, 25-37.
- Cranwell, P.A., 1973. Chain-length distribution of *n*-alkanes from lake sediments in relation to post-glacial environmental change. *Freshwater Biology* 3, 259-265.
- Cranwell, P.A., 1976. Decomposition of aquatic biota and sediment formation: lipid components of two blue-green algal species and of detritus resulting from microbial attack. *Freshwater Biology* 6, 481-488.
- Cranwell, P.A., Eglinton, G., Robinson, N., 1987. Lipids of aquatic organisms as potential contributors to lacustrine sediments—II. *Organic Geochemistry* 11, 513-527.
- Crowther, T.W., Todd-Brown, K.E.O., Rowe, C.W., *et al.*, 2016. Quantifying global soil carbon losses in response to warming. *Nature* 540, 104-108.
- Cuddington, K., Leavitt, P.R., 1999. An individual-based model of pigment flux in lakes: implications for organic biogeochemistry and paleoecology. *Canadian Journal of Fisheries and Aquatic Sciences* 56, 1964-1977.
- D'Anjou, R.M., Wei, J.H., Castañeda, I.S., *et al.*, 2013. High-latitude environmental change during MIS 9 and 11: biogeochemical evidence from Lake El'gygytyn, Far East Russia. *Climate of the Past* 9, 567-581.
- D'Andrea, W.J., Huang, Y., Fritz, S.C., *et al.*, 2011. Abrupt Holocene climate change as an important factor for human migration in West Greenland. *Proceedings of the National Academy of Sciences* 108, 9765-9769.

- Dahl-Jensen, D., Mosegaard, K., Gundestrup, N., *et al.*, 1998. Past temperatures directly from the Greenland ice sheet. *Science* 282, 268-271.
- Dansgaard, W., Clausen, H., Gundestrup, N., *et al.*, 1982. A new Greenland deep ice core. *Science* 218, 1273-1277.
- Dansgaard, W., Johnsen, S., Clausen, H., *et al.*, 1993. Evidence for general instability of past climate from a 250-kyr ice-core record. *Nature* 364, 218-220.
- Daugbjerg, N., 2003. Some Vascular Plants in the Vicinity of Godhavn, Disko Island - July 2002. University of Copenhagen, pp. 93-101.
- Davis, M.B., Ford, M.S.J., 1982. Sediment focusing in mirror lake, New Hampshire. *Limnology and Oceanography* 27, 137-150.
- Denton, G.H., Broecker, W.S., 2008. Wobbly ocean conveyor circulation during the Holocene? *Quaternary Science Reviews* 27, 1939-1950.
- Desloges, J.R., Gilbert, R., Nielsen, N., *et al.*, 2002. Holocene glacial marine sedimentary environments in fiords of Disko Bugt, West Greenland. *Quaternary Science Reviews* 21, 947-963.
- Diefendorf, A.F., Mueller, K.E., Wing, S.L., *et al.*, 2010. Global patterns in leaf $\delta^{13}C$ discrimination and implications for studies of past and future climate. *Proceedings of the National Academy of Sciences* 107, 5738-5743.
- Douglas, M.S., Smol, J.P., 1999. Freshwater diatoms as indicators of environmental change in the High Arctic, In: Stoermer, E.F., Smol, J.P. (Eds.), *The diatoms: applications for the environmental and earth sciences*. Cambridge University Press, New York, pp. 227-244.
- Draebing, D., Eichel, J., 2017. Spatial Controls of Turf-Banked Solifluction Lobes and Their Role for Paraglacial Adjustment in Glacier Forelands. *Permafrost and Periglacial Processes* 28, 446-459.
- Duan, Y., Wen, Q., Zheng, G., *et al.*, 1997. Isotopic composition and probable origin of individual fatty acids in modern sediments from Ruergai Marsh and Nansha Sea, China. *Organic Geochemistry* 27, 583-589.
- Edmundson, J., Kyle, G., Carlson, S., *et al.*, 1997. Trophic-level responses to nutrient treatment of meromictic and glacially influenced Coghill Lake. *Alaska Fishery Research Bulletin* 4, 136-153.
- Edmundson, J.A., Mazumder, A., 2002. Regional and hierarchical perspectives of thermal regimes in subarctic, Alaskan lakes. *Freshwater Biology* 47, 1-17.
- Eglinton, G., Hamilton, R.J., 1967. Leaf Epicuticular Waxes. *Science* 156, 1322-1335.
- Elberling, B., 2007. Annual soil CO₂ effluxes in the High Arctic: The role of snow thickness and vegetation type. *Soil Biology and Biochemistry* 39, 646-654.
- Enders, S.K., Pagani, M., Pantoja, S., *et al.*, 2008. Compound-specific stable isotopes of organic compounds from lake sediments track recent environmental changes in an alpine ecosystem, Rocky Mountain National Park, Colorado. *Limnology and Oceanography* 53, 1468-1478.

- Engstrom, D.R., Fritz, S.C., Almendinger, J.E., *et al.*, 2000. Chemical and biological trends during lake evolution in recently deglaciated terrain. *Nature* 408, 161-166.
- Evershed, R.P., Bull, I.D., Corr, L.T., *et al.*, 2007. Compound-specific stable isotope analysis in ecology and paleoecology, In: Michener, R., Lajtha, K. (Eds.), *Stable isotopes in ecology and environmental science*, 2 ed. Blackwell, Malden, USA, p. 480.
- Farquhar, G.D., Ehleringer, J.R., Hubick, K.T., 1989. Carbon isotope discrimination and photosynthesis. *Annual review of plant biology* 40, 503-537.
- Felip, M., Sattler, B., Psenner, R., *et al.*, 1995. Highly active microbial communities in the ice and snow cover of high mountain lakes. *Applied and Environmental Microbiology* 61, 2394-2401.
- Ficken, K.J., Li, B., Swain, D.L., *et al.*, 2000. An *n*-alkane proxy for the sedimentary input of submerged/floating freshwater aquatic macrophytes. *Organic Geochemistry* 31, 745-749.
- Findlay, D.L., Kasian, S.E.M., Stainton, M.P., *et al.*, 2001. Climatic influences on algal populations of boreal forest lakes in the Experimental Lakes Area. *Limnology and Oceanography* 46, 1784-1793.
- Finlay, J.C., 2001. Stable-carbon-isotope ratios of river biota: implications for energy flow in lotic food webs. *Ecology* 82, 1052-1064.
- Fleitmann, D., Mudelsee, M., Burns, S.J., *et al.*, 2008. Evidence for a widespread climatic anomaly at around 9.2 ka before present. *Paleoceanography* 23, n/a-n/a.
- Florian, C.R., Miller, G.H., Fogel, M.L., *et al.*, 2015. Algal pigments in Arctic lake sediments record biogeochemical changes due to Holocene climate variability and anthropogenic global change. *Journal of Paleolimnology* 54, 53-69.
- Fréchette, B., de Vernal, A., 2009. Relationship between Holocene climate variations over southern Greenland and eastern Baffin Island and synoptic circulation pattern. *Climate of the Past* 5, 347-359.
- Fredskild, B., 1973. Studies in the vegetational history of Greenland. *Meddelelser om Grønland* 198, 1-245.
- Fredskild, B., 1983. The Holocene vegetational development of the Godthåbsfjord area, West Greenland. *Meddelelser om Grønland Geoscience* 10, 1-28.
- Fredskild, B., 1985. Holocene pollen records from West Greenland. *Quaternary environments: Eastern Canadian Arctic, Baffin Bay and Western Greenland*, edited by: Andrews, J.T., Allen and Unwin, Boston, 643-681.
- Fredskild, B., 2000. The Holocene vegetational changes on Qeqertarsuatsiaq, a West Greenland island. *Geografisk Tidsskrift-Danish Journal of Geography* 100, 7-14.
- Frey, K.E., McClelland, J.W., 2009. Impacts of permafrost degradation on arctic river biogeochemistry. *Hydrological Processes* 23, 169-182.
- Frey, K.E., Smith, L.C., 2005. Amplified carbon release from vast West Siberian peatlands by 2100. *Geophysical Research Letters* 32.

- Fritz, S.C., Anderson, N., 2013. The relative influences of climate and catchment processes on Holocene lake development in glaciated regions. *Journal of Paleolimnology* 49, 349-362.
- Fritz, S.C., Engstrom, D.R., Juggins, S., 2004. Patterns of early lake evolution in boreal landscapes: a comparison of stratigraphic inferences with a modern chronosequence in Glacier Bay, Alaska. *The Holocene* 14, 828-840.
- Funder, S., 1989. Quaternary geology of West Greenland, In: Fulton, R.J. (Ed.), Quaternary Geology of Canada and Greenland. Geological Survey of Canada.
- Funder, S., Weidick, A., 1991. Holocene boreal molluscs in Greenland - palaeoceanographic implications. *Palaeogeography, Palaeoclimatology, Palaeoecology* 85, 123-135.
- Gagosian, R.B., Peltzer, E.T., 1986. The importance of atmospheric input of terrestrial organic material to deep sea sediments. *Organic Geochemistry* 10, 661-669.
- Gajewski, K., 2015. Quantitative reconstruction of Holocene temperatures across the Canadian Arctic and Greenland. *Global and Planetary Change* 128, 14-23.
- Gälman, V., Rydberg, J., Bigler, C., 2009. Decadal diagenetic effects on $\delta^{13}\text{C}$ and $\delta^{15}\text{N}$ studied in varved lake sediment. *Limnol. Oceanogr* 54, 917-924.
- Gälman, V., Rydberg, J., de-Luna, S.S., *et al.*, 2008. Carbon and nitrogen loss rates during aging of lake sediment: Changes over 27 years studied in varved lake sediment. *Limnology and Oceanography* 53, 1076-1082.
- Glew, J.R., Smol, J.P., Last, W.M., 2001. Sediment Core Collection and Extrusion, In: Last, W.M., Smol, J.P. (Eds.), Tracking Environmental Change Using Lake Sediments. Springer Netherlands, pp. 73-105.
- Glime, J.M., 2007. Bryophyte Ecology. Volume 1. Physiological Ecology. Michigan Technological University and the International Association of Bryologists.
- Gould, W.A., Walker, M.D., 1997. Landscape-scale patterns in plant species richness along an arctic river. *Canadian Journal of Botany* 75, 1748-1765.
- Gould, W.A., Walker, M.D., 1999. Plant communities and landscape diversity along a Canadian Arctic river. *Journal of Vegetation Science* 10, 537-548.
- Graney, J., Halliday, A., Keeler, G., *et al.*, 1995. Isotopic record of lead pollution in lake sediments from the northeastern United States. *Geochimica et Cosmochimica Acta* 59, 1715-1728.
- Grogan, P., Chapin, F., 1999. Arctic soil respiration: effects of climate and vegetation depend on season. *Ecosystems* 2, 451-459.
- Grootes, P.M., Stuiver, M., White, J.W.C., *et al.*, 1993. Comparison of oxygen isotope records from the GISP2 and GRIP Greenland ice cores. *Nature* 366, 552-554.
- Gu, B., Schelske, C.L., Hodell, D.A., 2004. Extreme $\delta^{13}\text{C}$ enrichments in a shallow hypereutrophic lake: Implications for carbon cycling. *Limnology and Oceanography* 49, 1152-1159.

- Gu, B., Schelske, L., 1996. Temporal and spatial variations in phytoplankton carbon isotopes in a polymictic subtropical lake. *Journal of Plankton Research* 18, 2081-2092.
- Håkansson, S., 1985. A review of various factors influencing the stable carbon isotope ratio of organic lake sediments by the change from glacial to post-glacial environmental conditions. *Quaternary Science Reviews* 4, 135-146.
- Hammarlund, D., Aravena, R., Barnekow, L., *et al.*, 1997. Multi-component carbon isotope evidence of early Holocene environmental change and carbon-flow pathways from a hard-water lake in northern Sweden. *Journal of Paleolimnology* 18, 219-233.
- Hampton, S.E., Moore, M.V., Ozersky, T., *et al.*, 2015. Heating up a cold subject: prospects for under-ice plankton research in lakes. *Journal of Plankton Research* 37, 277-284.
- Hannon, G.E., Gaillard, M.-J., 1997. The plant-macrofossil record of past lake-level changes. *Journal of Paleolimnology* 18, 15-28.
- Hansen, B.U., Elberling, B., Humlum, O., *et al.*, 2006. Meteorological trends (1991–2004) at Arctic Station, Central West Greenland (69°15'N) in a 130 years perspective. *Geografisk Tidsskrift-Danish Journal of Geography* 106, 45-55.
- Hanson, D.T., Renzaglia, K., Villarreal, J.C., 2014. Diffusion Limitation and CO₂ Concentrating Mechanisms in Bryophytes, In: Hanson, T.D., Rice, K.S. (Eds.), *Photosynthesis in Bryophytes and Early Land Plants*. Springer Netherlands, Dordrecht, pp. 95-111.
- Heiri, O., Lotter, A., Lemcke, G., 2001. Loss on ignition as a method for estimating organic and carbonate content in sediments: reproducibility and comparability of results. *Journal of Paleolimnology* 25, 101-110.
- Hinkel, K., Nelson, F., 2003. Spatial and temporal patterns of active layer thickness at Circumpolar Active Layer Monitoring (CALM) sites in northern Alaska, 1995–2000. *Journal of Geophysical Research: Atmospheres* 108.
- Hinzman, L.D., Bettez, N.D., Bolton, W.R., *et al.*, 2005. Evidence and Implications of Recent Climate Change in Northern Alaska and Other Arctic Regions. *Climatic Change* 72, 251-298.
- Hinzman, L.D., Deal, C.J., McGuire, A.D., *et al.*, 2013. Trajectory of the Arctic as an integrated system. *Ecological Applications* 23, 1837-1868.
- Hjulstrøm, F., 1939. Transportation of debris by moving water, In: PD, T. (Ed.), *Recent marine sediments; a symposium: Tulsa, Oklahoma*. American Association of Petroleum Geologists, pp. 5-31.
- Hobbie, S.E., 1996. Temperature and Plant Species Control Over Litter Decomposition in Alaskan Tundra. *Ecological Monographs* 66, 503-522.
- Hobbie, S.E., Nadelhoffer, K.J., Högberg, P., 2002. A synthesis: The role of nutrients as constraints on carbon balances in boreal and arctic regions. *Plant and Soil* 242, 163-170.
- Hobbie, S.E., Schimel, J.P., Trumbore, S.E., *et al.*, 2000. Controls over carbon storage and turnover in high-latitude soils. *Global Change Biology* 6, 196-210.

- Hodell, D.A., Schelske, C.L., 1998. Production, sedimentation, and isotopic composition of organic matter in Lake Ontario. *Limnology and Oceanography* 43, 200-214.
- Hodgson, D., Wright, S., Tyler, P., *et al.*, 1998. Analysis of fossil pigments from algae and bacteria in meromictic Lake Fidler, Tasmania, and its application to lake management. *Journal of Paleolimnology* 19, 1-22.
- Hoegh-Guldberg, O., Mumby, P.J., Hooten, A.J., *et al.*, 2007. Coral Reefs Under Rapid Climate Change and Ocean Acidification. *Science* 318, 1737-1742.
- Hogan, E.J., McGowan, S., Anderson, N.J., 2014. Nutrient limitation of periphyton growth in arctic lakes in south-west Greenland. *Polar Biology* 37, 1331-1342.
- Holen, D.A., Boraas, M.E., 1995. Mixotrophy in chrysophytes, In: Sandgren, C.D., Smol, J.P., Kristiansen, J. (Eds.), *Chrysophyte algae: ecology, phylogeny and development*. Cambridge University Press, pp. 119-140.
- Hollander, D.J., McKenzie, J.A., 1991. CO₂ control on carbon-isotope fractionation during aqueous photosynthesis: A paleo-*p*CO₂ barometer. *Geology* 19, 929-932.
- Hollander, D.J., Smith, M.A., 2001. Microbially mediated carbon cycling as a control on the $\delta^{13}\text{C}$ of sedimentary carbon in eutrophic Lake Mendota (USA): new models for interpreting isotopic excursions in the sedimentary record. *Geochimica et Cosmochimica Acta* 65, 4321-4337.
- Hollesen, J., Buchwal, A., Rachlewicz, G., *et al.*, 2015. Winter warming as an important co-driver for *Betula nana* growth in western Greenland during the past century. *Global Change Biology* 21, 2410-2423.
- Holtgrieve, G.W., Schindler, D.E., Hobbs, W.O., *et al.*, 2011. A coherent signature of anthropogenic nitrogen deposition to remote watersheds of the northern hemisphere. *Science* 334, 1545-1548.
- Hood, E., Battin, T.J., Fellman, J., *et al.*, 2015. Storage and release of organic carbon from glaciers and ice sheets. *Nature Geoscience* 8, 91-96.
- Hood, E., Fellman, J., Spencer, R.G., *et al.*, 2009. Glaciers as a source of ancient and labile organic matter to the marine environment. *Nature* 462, 1044-1047.
- Hooke, J., 2003. Coarse sediment connectivity in river channel systems: a conceptual framework and methodology. *Geomorphology* 56, 79-94.
- Huang, X., Wang, C., Xue, J., *et al.*, 2010. Occurrence of diploptene in moss species from the Dajiuhe Peatland in southern China. *Organic Geochemistry* 41, 321-324.
- Huang, Y., Dupont, L., Sarnthein, M., *et al.*, 2000. Mapping of C₄ plant input from North West Africa into North East Atlantic sediments. *Geochimica et Cosmochimica Acta* 64, 3505-3513.
- Huang, Y., Street-Perrott, F.A., Metcalfe, S.E., *et al.*, 2001. Climate Change as the Dominant Control on Glacial-Interglacial Variations in C₃ and C₄ Plant Abundance. *Science* 293, 1647-1651.
- Humlum, O., 1985. The glaciation level in West Greenland. *Arctic and Alpine Research*, 311-319.

- Humlum, O., 1987. Glacier behaviour and the influence of upper-air conditions during the Little Ice Age in Disko, central West Greenland. *Geografisk Tidsskrift-Danish Journal of Geography* 87, 1-12.
- Humlum, O., 1996. Origin of rock glaciers: Observations from Mellemfjord, Disko Island, Central West Greenland. *Permafrost and Periglacial Processes* 7, 361-380.
- Humlum, O., 1997. Active layer thermal regime at three rock glaciers in Greenland. *Permafrost and Periglacial Processes* 8, 383-408.
- Humlum, O., 1998. Active Layer Thermal Regime 1991-1996 at Qeqertarsuaq, Disko Island, Central West Greenland. *Arctic and Alpine Research* 30, 295-305.
- Humlum, O., 1999. Late-Holocene climate in central West Greenland: meteorological data and rock-glacier isotope evidence. *The Holocene* 9, 581-594.
- Humlum, O., 2000. The geomorphic significance of rock glaciers: estimates of rock glacier debris volumes and headwall recession rates in West Greenland. *Geomorphology* 35, 41-67.
- Hurrell, J.W., Deser, C., 2009. North Atlantic climate variability: The role of the North Atlantic Oscillation. *Journal of Marine Systems* 78, 28-41.
- Huryn, A.D., Slavik, K.A., Lowe, R.L., *et al.*, 2005. Landscape heterogeneity and the biodiversity of Arctic stream communities: a habitat template analysis. *Canadian Journal of Fisheries and Aquatic Sciences* 62, 1905-1919.
- Ingólfsson, Ó., Frich, P., Funder, S., *et al.*, 1990. Paleoclimatic implications of an early Holocene glacier advance on Disko Island, West Greenland. *Boreas* 19, 297-311.
- James, C.S., Eaton, J.W., Hardwick, K., 1999. Competition between three submerged macrophytes, *Elodea canadensis* Michx, *Elodea nuttallii* (Planch.) St John and *Lagarosiphon major* (Ridl.) Moss, In: Caffrey, J., Barrett, P.R.F., Ferreira, M.T., Moreira, I.S., Murphy, K.J., Wade, P.M. (Eds.), *Biology, Ecology and Management of Aquatic Plants: Proceedings of the 10th International Symposium on Aquatic Weeds*, European Weed Research Society. Springer Netherlands, Dordrecht, pp. 35-40.
- Jansson, J.K., Tas, N., 2014. The microbial ecology of permafrost. *Nature Reviews Microbiology* 12, 414-425.
- Jansson, M., Bergström, A.K., Blomqvist, P., *et al.*, 2000. Allochthonous organic carbon and phytoplankton/bacterioplankton production relationships in lakes. *Ecology* 81, 3250-3255.
- Jansson, M., Karlsson, J., Jonsson, A., 2012. Carbon dioxide supersaturation promotes primary production in lakes. *Ecology Letters* 15, 527-532.
- Jeffrey, S.W., Humphrey, G.F., 1975. New spectrophotometric equations for determining chlorophylls *a*, *b*, *c*₁, *c*₂ in higher plants, algae, and natural phytoplankton. *Biochimie und Physiologie der Pflanzen* 167, 191-194.
- Jeffrey, S.W., Mantoura, R.F.C., Wright, S.W., 1997. *Phytoplankton Pigments in Oceanography: Guidelines to Modern Methods*. UNESCO Publishing.

- Jensen, L., Schmidt, L., Hollesen, J., *et al.*, 2006. Accumulation of Soil Organic Carbon Linked to Holocene Sea Level Changes in West Greenland. *Arctic, Antarctic, and Alpine Research* 38, 378-383.
- Jeppesen, E., Jensen, J.P., Jensen, C., *et al.*, 2003. The impact of nutrient state and lake depth on top-down control in the pelagic zone of lakes: a study of 466 lakes from the temperate zone to the arctic. *Ecosystems* 6, 313-325.
- Johansson, K., Bergbäck, B., Tyler, G., 2001. Impact of Atmospheric Long Range Transport of Lead, Mercury and Cadmium on the Swedish Forest Environment. *Water, Air and Soil Pollution: Focus* 1, 279-297.
- Johnsen, S., Dansgaard, W., Clausen, H., *et al.*, 1972. Oxygen isotope profiles through the Antarctic and Greenland ice sheets. *Nature* 235, 429-434.
- Johnsen, S.J., Dahl-Jensen, D., Gundestrup, N., *et al.*, 2001. Oxygen isotope and palaeotemperature records from six Greenland ice-core stations: Camp Century, Dye-3, GRIP, GISP2, Renland and NorthGRIP. *Journal of Quaternary Science* 16, 299-307.
- Jones, J.I., Eaton, J.W., Hardwick, K., 2000. The influence of periphyton on boundary layer conditions: a pH microelectrode investigation. *Aquatic Botany* 67, 191-206.
- Jones, R.I., 2000. Mixotrophy in planktonic protists: an overview. *Freshwater Biology* 45, 219-226.
- Jonsson, A., Karlsson, J., Jansson, M., 2003. Sources of Carbon Dioxide Supersaturation in Clearwater and Humic Lakes in Northern Sweden. *Ecosystems* 6, 224-235.
- Jørgensen, J.J., Johansen, K.M.L., Westergaard-Nielsen, A., *et al.*, 2015. Net regional methane sink in High Arctic soils of northeast Greenland. *Nature Geoscience* 8, 20-23.
- Jost, W., 1940. Gletscherschwankungen auf der Insel Disco in Westgrönland. *Z. Gletscherkd* 27, 20-28.
- Juggins, S., 1991. ZONE v.1.2. – Unpublished Computer Program, Department of Geography, University of Newcastle.
- Juggins, S., 2003. C2 user guide. *Software for ecological and palaeoecological data analysis and visualisation*. University of Newcastle, Newcastle upon Tyne, UK 69.
- Junk, W.J., Bayley, P.B., Sparks, R.E., 1989. The flood pulse concept in river-floodplain systems. *Canadian special publication of fisheries and aquatic sciences* 106, 110-127.
- Kaplan, M.R., Wolfe, A.P., 2006. Spatial and temporal variability of Holocene temperature in the North Atlantic region. *Quaternary Research* 65, 223-231.
- Kaplan, M.R., Wolfe, A.P., Miller, G.H., 2002. Holocene Environmental Variability in Southern Greenland Inferred from Lake Sediments. *Quaternary Research* 58, 149-159.
- Kaštovská, K., Elster, J., Stibal, M., *et al.*, 2005. Microbial assemblages in soil microbial succession after glacial retreat in Svalbard (High Arctic). *Microbial Ecology* 50, 396-407.

- Kastowski, M., Hinderer, M., Vecsei, A., 2011. Long - term carbon burial in European lakes: Analysis and estimate. *Global Biogeochemical Cycles* 25.
- Kaufman, D.S., Ager, T.A., Anderson, N.J., *et al.*, 2004. Holocene thermal maximum in the western Arctic (0–180°W). *Quaternary Science Reviews* 23, 529-560.
- Kaufman, D.S., Axford, Y.L., Henderson, A.C., *et al.*, 2016. Holocene climate changes in eastern Beringia (NW North America)—A systematic review of multi-proxy evidence. *Quaternary Science Reviews* 147, 312-339.
- Kaufman, D.S., Schneider, D.P., McKay, N.P., *et al.*, 2009. Recent Warming Reverses Long-Term Arctic Cooling. *Science* 325, 1236-1239.
- Kawamura, K., Ishiwatari, R., Yamazaki, M., 1980. Identification of polyunsaturated fatty acids in surface lacustrine sediments. *Chemical Geology* 28, 31-39.
- Keeling, C., Whorf, T., 2005. Atmospheric carbon dioxide record from Mauna Loa. *Trends: A Compendium of Data on Global Change. Carbon Dioxide Information Analysis Center, Oak Ridge National Laboratory, Oak Ridge, TN.*
- Keeling, C.D., Bacastow, R.B., Carter, A.F., *et al.*, 2013. A three-dimensional model of atmospheric CO₂ transport based on observed winds: 1. Analysis of observational data, Aspects of Climate Variability in the Pacific and the Western Americas. American Geophysical Union, pp. 165-236.
- Kelly, M., 1980. The status of the Neoglacial in western Greenland. 64.
- Kelly, M., Funder, S.V., 1974. The pollen stratigraphy of late Quaternary lake sediments of South-West Greenland. *Rapp. Grøn. Geol. Unders.*, 1-26.
- Klug, J.L., 2002. Positive and negative effects of allochthonous dissolved organic matter and inorganic nutrients on phytoplankton growth. *Canadian Journal of Fisheries and Aquatic Sciences* 59, 85-95.
- Kohn, M.J., 2010. Carbon isotope compositions of terrestrial C₃ plants as indicators of (paleo) ecology and (paleo) climate. *Proceedings of the National Academy of Sciences* 107, 19691-19695.
- Kokfelt, U., Reuss, N., Struyf, E., *et al.*, 2010. Wetland development, permafrost history and nutrient cycling inferred from late Holocene peat and lake sediment records in subarctic Sweden. *Journal of Paleolimnology* 44, 327-342.
- Kokfelt, U., RosÉN, P., Schoning, K., *et al.*, 2009. Ecosystem responses to increased precipitation and permafrost decay in subarctic Sweden inferred from peat and lake sediments. *Global Change Biology* 15, 1652-1663.
- Kortelainen, P., Pajunen, H., Rantakari, M., *et al.*, 2004. A large carbon pool and small sink in boreal Holocene lake sediments. *Global Change Biology* 10, 1648-1653.
- Koven, C.D., Ringeval, B., Friedlingstein, P., *et al.*, 2011. Permafrost carbon-climate feedbacks accelerate global warming. *Proceedings of the National Academy of Sciences* 108, 14769-14774.
- Krammer, K., Lange-Bertalot, H., 1986. Bacillariophyceae, Vol 1–4. Gustav Fischer Verlag, Stuttgart.

- Krawczyk, D.W., Witkowski, A., Lloyd, J., *et al.*, 2013. Late-Holocene diatom derived seasonal variability in hydrological conditions off Disko Bay, West Greenland. *Quaternary Science Reviews* 67, 93-104.
- Krejci, M.E., Lowe, R.L., 1987. The seasonal occurrence of macroscopic colonies of *Meridion circulare* (Bacillariophyceae) in a spring-fed brook. *Transactions of the American Microscopical Society*, 173-178.
- Kwok, R., Rothrock, D.A., 2009. Decline in Arctic sea ice thickness from submarine and ICESat records: 1958–2008. *Geophysical Research Letters* 36, n/a-n/a.
- Lallier-Vergès, E., Albéric, P., 1990. Optical and geochemical study of organic matter in present oxic sediments (equatorial North Pacific Ocean NIXO area). *Oceanologica Acta, Special issue* 10, 281-291.
- Lamb, A.L., Leng, M.J., Umer Mohammed, M., *et al.*, 2004. Holocene climate and vegetation change in the Main Ethiopian Rift Valley, inferred from the composition (C/N and $\delta^{13}\text{C}$) of lacustrine organic matter. *Quaternary Science Reviews* 23, 881-891.
- Lamb, H.H., 1965. The early medieval warm epoch and its sequel. *Palaeogeography, Palaeoclimatology, Palaeoecology* 1, 13-37.
- Lane, C.S., Brauer, A., Blockley, S.P.E., *et al.*, 2013. Volcanic ash reveals time-transgressive abrupt climate change during the Younger Dryas. *Geology*.
- Larsen, L.M., Pedersen, A.K., Pedersen, G.K., *et al.*, 1992. Timing and duration of Early Tertiary volcanism in the North Atlantic: new evidence from West Greenland. *Geological Society, London, Special Publications* 68, 321-333.
- Larsen, N.K., Kjær, K.H., Lecavalier, B., *et al.*, 2015. The response of the southern Greenland ice sheet to the Holocene thermal maximum. *Geology*.
- Law, A., Anderson, N., McGowan, S., 2015. Spatial and temporal variability of lake ontogeny in south-western Greenland. *Quaternary Science Reviews* 126, 1-16.
- Lawson, E.C., Bhatia, M.P., Wadham, J.L., *et al.*, 2014a. Continuous summer export of nitrogen-rich organic matter from the Greenland Ice Sheet inferred by ultrahigh resolution mass spectrometry. *Environmental Science & Technology* 48, 14248-14257.
- Lawson, E.C., Wadham, J.L., Tranter, M., *et al.*, 2014b. Greenland Ice Sheet exports labile organic carbon to the Arctic oceans. *Biogeosciences* 11, 4015-4028.
- Laybourn-Parry, J., 2002. Survival mechanisms in Antarctic lakes. *Philosophical Transactions of the Royal Society of London. Series B: Biological Sciences* 357, 863-869.
- Laybourn-Parry, J., Marshall, W.A., 2003. Photosynthesis, mixotrophy and microbial plankton dynamics in two high Arctic lakes during summer. *Polar Biology* 26, 517-524.
- Leavitt, P.R., 1993. A review of factors that regulate carotenoid and chlorophyll deposition and fossil pigment abundance. *Journal of Paleolimnology* 9, 109-127.
- Leavitt, P.R., Cumming, B.F., Smol, J.P., *et al.*, 2003. Climatic control of ultraviolet radiation effects on lakes. *Limnology and Oceanography* 48, 2062-2069.

- Leavitt, P.R., Findlay, D.L., Hall, R.I., *et al.*, 1999. Algal responses to dissolved organic carbon loss and pH decline during whole-lake acidification: Evidence from paleolimnology. *Limnology and Oceanography* 44, 757-773.
- Leavitt, P.R., Hodgson, D.A., 2001. Sedimentary pigments, In: Birks, H.J.B., Last, W.M. (Eds.), *Tracking Environmental Change using Lake Sediments. Terrestrial, Algal and Siliceous Indicators Volume 3*. Kluwer, Dordrecht, pp. 295-325.
- Leavitt, P.R., Vinebrooke, R.D., Donald, D.B., *et al.*, 1997. Past ultraviolet radiation environments in lakes derived from fossil pigments. *Nature* 388, 457-459.
- Lecavalier, B.S., Milne, G.A., Simpson, M.J.R., *et al.*, 2014. A model of Greenland ice sheet deglaciation constrained by observations of relative sea level and ice extent. *Quaternary Science Reviews* 102, 54-84.
- Lee, H., Schuur, E.A.G., Vogel, J.G., *et al.*, 2011. A spatially explicit analysis to extrapolate carbon fluxes in upland tundra where permafrost is thawing. *Global Change Biology* 17, 1379-1393.
- Leeben, A., Alliksaar, T., Heinsalu, A., *et al.*, 2008. Tracking changes in the organic matter in a lake palaeoecosystem: A spectrophotometric approach. *Organic Geochemistry* 39, 915-918.
- Lehman, J.T., 1975. Reconstructing the rate of accumulation of lake sediment: the effect of sediment focusing. *Quaternary Research* 5, 541-550.
- Leng, M.J., Henderson, A.C.G., 2013. Recent advances in isotopes as palaeolimnological proxies. *Journal of Paleolimnology* 49, 481-496.
- Leng, M.J., Lamb, A.L., Heaton, T.H., *et al.*, 2006. *Isotopes in lake sediments*. Springer.
- Leng, M.J., Marshall, J.D., 2004. Palaeoclimate interpretation of stable isotope data from lake sediment archives. *Quaternary Science Reviews* 23, 811-831.
- Leng, M.J., Wagner, B., Anderson, N.J., *et al.*, 2012. Deglaciation and catchment ontogeny in coastal south-west Greenland: implications for terrestrial and aquatic carbon cycling. *Journal of Quaternary Science* 27, 575-584.
- Lepane, V., Leeben, A., Malashenko, O., 2004. Characterization of sediment pore-water dissolved organic matter of lakes by high-performance size exclusion chromatography. *Aquatic Sciences* 66, 185-194.
- Lloyd, J., Moros, M., Perner, K., *et al.*, 2011. A 100 yr record of ocean temperature control on the stability of Jakobshavn Isbrae, West Greenland. *Geology* 39, 867-870.
- Lloyd, J.M., Kuijpers, A., Long, A., *et al.*, 2007. Foraminiferal reconstruction of mid-to late-Holocene ocean circulation and climate variability in Disko Bugt, West Greenland. *The Holocene* 17, 1079-1091.
- Lloyd, J.M., Park, L.A., Kuijpers, A., *et al.*, 2005. Early Holocene palaeoceanography and deglacial chronology of Disko Bugt, West Greenland. *Quaternary Science Reviews* 24, 1741-1755.
- Long, A.J., Roberts, D.H., Dawson, S., 2006. Early Holocene history of the west Greenland Ice Sheet and the GH-8.2 event. *Quaternary Science Reviews* 25, 904-922.

- Long, A.J., Woodroffe, S.A., Roberts, D.H., *et al.*, 2011. Isolation basins, sea-level changes and the Holocene history of the Greenland Ice Sheet. *Quaternary Science Reviews* 30, 3748-3768.
- Lupascu, M., Welker, J.M., Seibt, U., *et al.*, 2014. High Arctic wetting reduces permafrost carbon feedbacks to climate warming. *Nature Climate Change* 4, 51-55.
- Mackereth, F.J.H., Heron, J., Talling, J.F., 1978. Water analysis: some revised methods for limnologists. Freshwater Biological Association.
- Madsen, J.D., Chambers, P.A., James, W.F., *et al.*, 2001. The interaction between water movement, sediment dynamics and submersed macrophytes. *Hydrobiologia* 444, 71-84.
- Malard, F., Uehlinger, U., Zah, R., *et al.*, 2006. Flood-pulse and riverscape dynamics in a braided glacial river. *Ecology* 87, 704-716.
- Mann, M.E., Zhang, Z., Rutherford, S., *et al.*, 2009. Global Signatures and Dynamical Origins of the Little Ice Age and Medieval Climate Anomaly. *Science* 326, 1256-1260.
- Marcott, S.A., Shakun, J.D., Clark, P.U., *et al.*, 2013. A reconstruction of regional and global temperature for the past 11,300 years. *Science* 339, 1198-1201.
- Marshall, J.D., Lang, B., Crowley, S.F., *et al.*, 2007. Terrestrial impact of abrupt changes in the North Atlantic thermohaline circulation: Early Holocene, UK. *Geology* 35, 639-642.
- Marzi, R., Torkelson, B.E., Olson, R.K., 1993. A revised carbon preference index. *Organic Geochemistry* 20, 1303-1306.
- Mathewes, R.W., 1993. Evidence for Younger Dryas-age cooling on the North Pacific coast of America. *Quaternary Science Reviews* 12, 321-331.
- Matsuda, H., Koyama, T., 1977. Early diagenesis of fatty acids in lacustrine sediments - II. A statistical approach to changes in fatty acid composition from recent sediments and some source materials. *Geochimica et Cosmochimica Acta* 41, 1825-1834.
- Mathews, J.A., Briffa, K.R., 2005. The 'Little Ice Age': Re-evaluation of an evolving concept. *Geografiska Annaler: Series A, Physical Geography* 87, 17-36.
- Mayewski, P.A., Rohling, E.E., Curt Stager, J., *et al.*, 2004. Holocene climate variability. *Quaternary Research* 62, 243-255.
- McGowan, S., 2013. Pigment Studies. Elsevier, Amsterdam.
- McGowan, S., Anderson, N.J., Edwards, M.E., *et al.*, 2016. Long-term perspectives on terrestrial and aquatic carbon cycling from palaeolimnology. *Wiley Interdisciplinary Reviews: Water* 3, 211-234.
- McGowan, S., Barker, P., Haworth, E.Y., *et al.*, 2012. Humans and climate as drivers of algal community change in Windermere since 1850. *Freshwater Biology* 57, 260-277.
- McGowan, S., Juhler, R., Anderson, N.J., 2008. Autotrophic response to lake age, conductivity and temperature in two West Greenland lakes. *Journal of Paleolimnology* 39, 301-317.

- McGowan, S., Leavitt, P.R., Hall, R.I., *et al.*, 2005. Controls of algal abundance and community composition during ecosystem state change. *Ecology* 86, 2200-2211.
- McGowan, S., Ryves, D.B., Anderson, N.J., 2003. Holocene records of effective precipitation in West Greenland. *The Holocene* 13, 239-249.
- McGuire, A.D., Anderson, L.G., Christensen, T.R., *et al.*, 2009. Sensitivity of the carbon cycle in the Arctic to climate change. *Ecological Monographs* 79, 523-555.
- Mermoud, F., Gülaçar, F.O., Buchs, A., 1985. 5 α (H)-cholestan-3 α -ol in sediments: Characterization and geochemical significance. *Geochimica et Cosmochimica Acta* 49, 459-462.
- Meyers, P.A., 1990. Impacts of late Quaternary fluctuations in water level on the accumulation of sedimentary organic matter in Walker Lake, Nevada. *Palaeogeography, Palaeoclimatology, Palaeoecology* 78, 229-240.
- Meyers, P.A., 1994. Preservation of elemental and isotopic source identification of sedimentary organic matter. *Chemical Geology* 114, 289-302.
- Meyers, P.A., 1997. Organic geochemical proxies of paleoceanographic, paleolimnologic, and paleoclimatic processes. *Organic Geochemistry* 27, 213-250.
- Meyers, P.A., 2003. Applications of organic geochemistry to paleolimnological reconstructions: a summary of examples from the Laurentian Great Lakes. *Organic Geochemistry* 34, 261-289.
- Meyers, P.A., Bourbonniere, R.A., Takeuchi, N., 1980. Hydrocarbons and fatty acids in two cores of Lake Huron sediments. *Geochimica et Cosmochimica Acta* 44, 1215-1221.
- Meyers, P.A., Eadie, B.J., 1993. Sources, degradation and recycling of organic matter associated with sinking particles in Lake Michigan. *Organic Geochemistry* 20, 47-56.
- Meyers, P.A., Ishiwatari, R., 1993. Lacustrine organic geochemistry - an overview of indicators of organic matter sources and diagenesis in lake sediments. *Organic Geochemistry* 20, 867-900.
- Meyers, P.A., Lallier-Vergès, E., 1999. Lacustrine sedimentary organic matter records of Late Quaternary paleoclimates. *Journal of Paleolimnology* 21, 345-372.
- Meyers, P.A., Leenheer, M.J., Bourbonniere, R.A., 1995. Diagenesis of vascular plant organic matter components during burial in lake sediments. *Aquatic Geochemistry* 1, 35-52.
- Meyers, P.A., Leenheer, M.J., Eadie, B.J., *et al.*, 1984. Organic geochemistry of suspended and settling particulate matter in Lake Michigan. *Geochimica et Cosmochimica Acta* 48, 443-452.
- Meyers, P.A., Takeuchi, N., 1981. Environmental changes in Saginaw Bay, Lake Huron recorded by geolipid contents of sediments deposited since 1800. *Environmental Geology* 3, 257-266.
- Meyers, P.A., Teranes, J.L., 2001. Sediment Organic Matter, In: Last, W.M., Smol, J.P. (Eds.), *Tracking Environmental Change Using Lake Sediments. Volume 2: Physical and Geochemical Methods*. Springer Netherlands, pp. 239-269.

- Michelutti, N., Wolfe, A.P., Vinebrooke, R.D., *et al.*, 2005. Recent primary production increases in arctic lakes. *Geophysical Research Letters* 32.
- Moros, M., Jensen, K.G., Kuijpers, A., 2006. Mid-to late-Holocene hydrological and climatic variability in Disko Bugt, central West Greenland. *The Holocene* 16, 357-367.
- Moros, M., Lloyd, J.M., Perner, K., *et al.*, 2016. Surface and sub-surface multi-proxy reconstruction of middle to late Holocene palaeoceanographic changes in Disko Bugt, West Greenland. *Quaternary Science Reviews* 132, 146-160.
- Motyka, R.J., Truffer, M., Fahnestock, M., *et al.*, 2011. Submarine melting of the 1985 Jakobshavn Isbræ floating tongue and the triggering of the current retreat. *Journal of Geophysical Research: Earth Surface* 116.
- Muschitiello, F., Wohlfarth, B., 2015. Time-transgressive environmental shifts across Northern Europe at the onset of the Younger Dryas. *Quaternary Science Reviews* 109, 49-56.
- Nakai, N., 1972. Carbon Isotopic Variation and the Paleoclimate of Sediments from Lake Biwa. *Proceedings of the Japan Academy* 48, 516-521.
- Nishimura, M., Koyama, T., 1977. The occurrence of stanols in various living organisms and the behavior of sterols in contemporary sediments. *Geochimica et Cosmochimica Acta* 41, 379-385.
- O'Brien, S.R., Mayewski, P.A., Meeker, L.D., *et al.*, 1995. Complexity of Holocene Climate as Reconstructed from a Greenland Ice Core. *Science* 270, 1962-1964.
- Ojala, A., Heaney, S.I., Arvola, L., *et al.*, 1996. Growth of migrating and non-migrating cryptophytes in thermally and chemically stratified experimental columns. *Freshwater Biology* 35, 599-608.
- Olsen, J., Anderson, N.J., Knudsen, M.F., 2012. Variability of the North Atlantic Oscillation over the past 5,200 years. *Nature Geoscience* 5, 808-812.
- Olsen, J., Anderson, N.J., Leng, M.J., 2013. Limnological controls on stable isotope records of late-Holocene palaeoenvironment change in SW Greenland: a paired lake study. *Quaternary Science Reviews* 66, 85-95.
- Oswald, W.W., Anderson, P.M., Brown, T.A., *et al.*, 2005. Effects of sample mass and macrofossil type on radiocarbon dating of arctic and boreal lake sediments. *The Holocene* 15, 758-767.
- Ouellet-Bernier, M.-M., de Vernal, A., Hillaire-Marcel, C., *et al.*, 2014. Paleooceanographic changes in the Disko Bugt area, West Greenland, during the Holocene. *The Holocene* 24, 1573-1583.
- Ouyang, X., Guo, F., Bu, H., 2015. Lipid biomarkers and pertinent indices from aquatic environment record paleoclimate and paleoenvironment changes. *Quaternary Science Reviews* 123, 180-192.
- Overland, J.E., Wang, M., 2010. Large-scale atmospheric circulation changes are associated with the recent loss of Arctic sea ice. *Tellus A* 62, 1-9.
- Overpeck, J., Hughen, K., Hardy, D., *et al.*, 1997. Arctic environmental change of the last four centuries. *Science* 278, 1251-1256.

- Pace, M.L., Carpenter, S.R., Cole, J.J., *et al.*, 2007. Does terrestrial organic carbon subsidize the planktonic food web in a clear-water lake? *Limnology and Oceanography* 52, 2177-2189.
- Pages 2K Consortium, 2013. Continental-scale temperature variability during the past two millennia. *Nature Geoscience* 6, 339-346.
- Pålsson, C., Kritzberg, E.S., Christoffersen, K., *et al.*, 2005. Net heterotrophy in Faroe Islands clear-water lakes: causes and consequences for bacterioplankton and phytoplankton. *Freshwater Biology* 50, 2011-2020.
- Parsons, T.R., Lee Chen, Y.L., 1995. The Comparative Ecology of a Subarctic and Tropical Estuarine Ecosystem as Measured with Carbon and Nitrogen Isotopes. *Estuarine, Coastal and Shelf Science* 41, 215-224.
- Paterson, W.S.B., 1994. The physics of glaciers. Butterworth-Heinemann.
- Pearson, E.J., Farrimond, P., Juggins, S., 2007. Lipid geochemistry of lake sediments from semi-arid Spain: Relationships with source inputs and environmental factors. *Organic Geochemistry* 38, 1169-1195.
- Pearson, E.J., Juggins, S., Talbot, H.M., *et al.*, 2011. A lacustrine GDGT-temperature calibration from the Scandinavian Arctic to Antarctic: Renewed potential for the application of GDGT-paleothermometry in lakes. *Geochimica et Cosmochimica Acta* 75, 6225-6238.
- Perner, K., Moros, M., Jennings, A., *et al.*, 2013a. Holocene palaeoceanographic evolution off West Greenland. *The Holocene* 23, 374-387.
- Perner, K., Moros, M., Lloyd, J.M., *et al.*, 2011. Centennial scale benthic foraminiferal record of late Holocene oceanographic variability in Disko Bugt, West Greenland. *Quaternary Science Reviews* 30, 2815-2826.
- Perner, K., Moros, M., Snowball, I.A.N., *et al.*, 2013b. Establishment of modern circulation pattern at c. 6000 cal a BP in Disko Bugt, central West Greenland: opening of the Vaigat Strait. *Journal of Quaternary Science* 28, 480-489.
- Perry, G.J., Volkman, J.K., Johns, R.B., *et al.*, 1979. Fatty acids of bacterial origin in contemporary marine sediments. *Geochimica et Cosmochimica Acta* 43, 1715-1725.
- Post, E., Bhatt, U.S., Bitz, C.M., *et al.*, 2013. Ecological Consequences of Sea-Ice Decline. *Science* 341, 519-524.
- Poynter, J.G., Farrimond, P., Robinson, N., *et al.*, 1989. Aeolian-Derived Higher Plant Lipids in the Marine Sedimentary Record: Links with Palaeoclimate, In: Leinen, M., Sarnthein, M. (Eds.), *Paleoclimatology and Paleometeorology: Modern and Past Patterns of Global Atmospheric Transport*. Springer Netherlands, pp. 435-462.
- Prairie, Y.T., 2008. Carbocentric limnology: looking back, looking forward. *Canadian Journal of Fisheries and Aquatic Sciences* 65, 543-548.
- Prokushkin, A., Gleixner, G., McDowell, W., *et al.*, 2007. Source - and substrate - specific export of dissolved organic matter from permafrost - dominated forested watershed in central Siberia. *Global Biogeochemical Cycles* 21.

- Przytulska, A., Comte, J., Crevecoeur, S., *et al.*, 2016. Phototrophic pigment diversity and picophytoplankton in permafrost thaw lakes. *Biogeosciences* 13, 13-26.
- R Core Team, 2013. R: A language and environment for statistical computing. R Foundation for Statistical Computing, Vienna, Austria.
- Rasch, M., Nielsen, N., 1995. Coastal morpho-stratigraphy and Holocene relative sea level changes at Tuapaat, southeastern Disko Island, central West Greenland. *Polar Research* 14, 277-290.
- Rasch, M., Nielsen, N., Christiansen, C., *et al.*, 2003. Role of landscape parameters in riverine run-off, and sediment and organic matter yield on Disko Island, West Greenland. *Geografisk Tidsskrift Danish Journal of Geography* 103, 1-11.
- Rasmussen, P., Anderson, N.J., 2005. Natural and anthropogenic forcing of aquatic macrophyte development in a shallow Danish lake during the last 7000 years. *Journal of Biogeography* 32, 1993-2005.
- Rautio, M., 2001. Zooplankton Assemblages Related to Environmental Characteristics in Treeline Ponds in Finnish Lapland. *Arctic, Antarctic, and Alpine Research* 33, 289-298.
- Rautio, M., Vincent, W.F., 2006. Benthic and pelagic food resources for zooplankton in shallow high-latitude lakes and ponds. *Freshwater Biology* 51, 1038-1052.
- Reichstein, M., Bahn, M., Ciais, P., *et al.*, 2013. Climate extremes and the carbon cycle. *Nature* 500, 287-295.
- Reimer, P.J., Bard, E., Bayliss, A., *et al.*, 2013. IntCal13 and Marine13 radiocarbon age calibration curves 0-50,000 years cal BP. *Radiocarbon* 55.
- Renberg, I., 1991. The HON-Kajak sediment corer. *Journal of Paleolimnology* 6, 167-170.
- Renberg, I., Brännvall, M.-L., Bindler, R., *et al.*, 2002. Stable lead isotopes and lake sediments - a useful combination for the study of atmospheric lead pollution history. *Science of The Total Environment* 292, 45-54.
- Reuss, N., Leavitt, P.R., Hall, R.I., *et al.*, 2010a. Development and application of sedimentary pigments for assessing effects of climatic and environmental changes on subarctic lakes in northern Sweden. *Journal of Paleolimnology* 43, 149-169.
- Reuss, N.S., Hammarlund, D., Rundgren, M., *et al.*, 2010b. Lake ecosystem responses to Holocene climate change at the subarctic tree-line in northern Sweden. *Ecosystems* 13, 393-409.
- Ribeiro, S., Moros, M., Ellegaard, M., *et al.*, 2012. Climate variability in West Greenland during the past 1500 years: evidence from a high-resolution marine palynological record from Disko Bay. *Boreas* 41, 68-83.
- Rieley, G., 1994. Derivatization of organic compounds prior to gas chromatographic-combustion-isotope ratio mass spectrometric analysis: identification of isotope fractionation processes. *Analyst* 119, 915-919.

- Rieley, G., Collier, R.J., Jones, D.M., *et al.*, 1991. The biogeochemistry of Ellesmere Lake, U.K. - I: source correlation of leaf wax inputs to the sedimentary lipid record. *Organic Geochemistry* 17, 901-912.
- Riis, T., Christoffersen, K.S., Baattrup-Pedersen, A., 2016. Mosses in High-Arctic lakes: in situ measurements of annual primary production and decomposition. *Polar Biology* 39, 543-552.
- Roberts, D., Lane, T., Rea, B., *et al.*, 2015. New insights into West Greenland ice sheet/stream dynamics during the last glacial cycle, EGU General Assembly Conference Abstracts, p. 3528.
- Roberts, E.C., Laybourn-Parry, J., 1999. Mixotrophic cryptophytes and their predators in the Dry Valley lakes of Antarctica. *Freshwater Biology* 41, 737-746.
- Roberts, E.C., Laybourn-Parry, J., McKnight, D.M., *et al.*, 2000. Stratification and dynamics of microbial loop communities in Lake Fryxell, Antarctica. *Freshwater Biology* 44, 649-661.
- Robinson, N., Cranwell, P., Finlay, B., *et al.*, 1984. Lipids of aquatic organisms as potential contributors to lacustrine sediments. *Organic Geochemistry* 6, 143-152.
- Robinson, N., Cranwell, P.A., Eglinton, G., 1987. Sources of the lipids in the bottom sediments of an English oligo-mesotrophic lake. *Freshwater Biology* 17, 15-33.
- Rohling, E.J., Pälike, H., 2005. Centennial-scale climate cooling with a sudden cold event around 8,200 years ago. *Nature* 434, 975-979.
- Rosén, P., Hammarlund, D., 2007. Effects of climate, fire and vegetation development on Holocene changes in total organic carbon concentration in three boreal forest lakes in northern Sweden. *Biogeosciences* 4, 975-984.
- Roulet, N., Moore, T.R., 2006. Environmental chemistry - Browning the waters. *Nature* 444, 283-284.
- Roy, S., Llewellyn, C.A., Egeland, E.S., *et al.*, 2011. *Phytoplankton Pigments: Characterization, Chemotaxonomy and Applications in Oceanography*. Cambridge University Press.
- Rune, F., 2011. *Wild flowers of Greenland*. Gyldenlund, Denmark.
- Russell, J.M., McCoy, S.J., Verschuren, D., *et al.*, 2009. Human impacts, climate change, and aquatic ecosystem response during the past 2000 yr at Lake Wandakara, Uganda. *Quaternary Research* 72, 315-324.
- Sabine, C.L., Feely, R.A., Gruber, N., *et al.*, 2004. The Oceanic Sink for Anthropogenic CO₂. *Science* 305, 367-371.
- Sabine, C.L., Heimann, M., Artaxo, P., Bakker, D.C.E., Chen, C.T.A., Field, C.B., Gruber, N., Le Quéré, C., Prinn, R.G., Richey, J.E., Lankao, P.R., Sathaye, J.A., Valentini, R., 2004. Current Status and Past Trends of the Global Carbon Cycle, In: Field, C.B., Raupach, Michael R. (Ed.), *The Global Carbon Cycle: Intergrating Humans, Climate, and the Natural World*. Island Press, Washington.

- Sand-Jensen, K., Staehr, P.A., 2009. Net heterotrophy in small Danish lakes: a widespread feature over gradients in trophic status and land cover. *Ecosystems* 12, 336-348.
- Sanders, R.W., Porter, K.G., Bennett, S.J., 1990. Heterotrophic, autotrophic, and mixotrophic nanoflagellates: seasonal abundances and bacterivory in a eutrophic lake. *Limnology and Oceanography* 35, 1821-1832.
- Schefuß, E., Ratmeyer, V., Stuut, J.-B.W., *et al.*, 2003. Carbon isotope analyses of n-alkanes in dust from the lower atmosphere over the central eastern Atlantic. *Geochimica et Cosmochimica Acta* 67, 1757-1767.
- Schelske, C.L., Hodell, D.A., 1995. Using carbon isotopes of bulk sedimentary organic matter to reconstruct the history of nutrient loading and eutrophication in Lake Erie. *Limnology and Oceanography* 40, 918-929.
- Schimmel, D., Stephens, B.B., Fisher, J.B., 2015. Effect of increasing CO₂ on the terrestrial carbon cycle. *Proceedings of the National Academy of Sciences* 112, 436-441.
- Schmidt, S., Reed, S.C., Nemergut, D.R., *et al.*, 2008. The earliest stages of ecosystem succession in high-elevation (5000 metres above sea level), recently deglaciated soils. *Proceedings of the Royal Society of London B: Biological Sciences* 275, 2793-2802.
- Schmidt, S.K., Nemergut, D.R., Miller, A.E., *et al.*, 2009. Microbial activity and diversity during extreme freeze-thaw cycles in periglacial soils, 5400 m elevation, Cordillera Vilcanota, Perú. *Extremophiles* 13, 807-816.
- Schnurrenberger, D., Russell, J., Kelts, K., 2003. Classification of lacustrine sediments based on sedimentary components. *Journal of Paleolimnology* 29, 141-154.
- Schuur, E., McGuire, A., Schädel, C., *et al.*, 2015. Climate change and the permafrost carbon feedback. *Nature* 520, 171-179.
- Schuur, E.A.G., Bockheim, J., Canadell, J.G., *et al.*, 2008. Vulnerability of Permafrost Carbon to Climate Change: Implications for the Global Carbon Cycle. *BioScience* 58, 701-714.
- Schuur, E.A.G., Vogel, J.G., Crummer, K.G., *et al.*, 2009. The effect of permafrost thaw on old carbon release and net carbon exchange from tundra. *Nature* 459, 556-559.
- Schwark, L., Zink, K., Lechterbeck, J., 2002. Reconstruction of postglacial to early Holocene vegetation history in terrestrial Central Europe via cuticular lipid biomarkers and pollen records from lake sediments. *Geology* 30, 463-466.
- Sejrup, H.P., Seppä, H., McKay, N.P., *et al.*, 2016. North Atlantic-Fennoscandian Holocene climate trends and mechanisms. *Quaternary Science Reviews* 147, 365-378.
- Seppä, H., Birks, H.J.B., 2001. July mean temperature and annual precipitation trends during the Holocene in the Fennoscandian tree-line area: pollen-based climate reconstructions. *The Holocene* 11, 527-539.
- Sharp, M., Burgess, D.O., Cawkwell, F., *et al.*, 2014. Remote sensing of recent glacier changes in the Canadian Arctic, Global Land Ice Measurements from Space. Springer Berlin Heidelberg, pp. 205-228.

- Shotton, F.W., 1972. An Example of Hard-Water Error in Radiocarbon Dating of Vegetable Matter. *Nature* 240, 460-461.
- Sierszen, M.E., McDonald, M.E., Jensen, D.A., 2003. Benthos as the basis for arctic lake food webs. *Aquatic Ecology* 37, 437-445.
- Silliman, J.E., Meyers, P.A., Bourbonniere, R.A., 1996. Record of postglacial organic matter delivery and burial in sediments of Lake Ontario. *Organic Geochemistry* 24, 463-472.
- Singer, G.A., Fasching, C., Wilhelm, L., *et al.*, 2012. Biogeochemically diverse organic matter in Alpine glaciers and its downstream fate. *Nature Geoscience* 5, 710-714.
- Sinninghe Damsté, J.S., Kenig, F., Koopmans, M.P., *et al.*, 1995. Evidence for gammacerane as an indicator of water column stratification. *Geochimica et Cosmochimica Acta* 59, 1895-1900.
- Sinninghe Damsté, J.S., Verschuren, D., Ossebaar, J., *et al.*, 2011. A 25,000-year record of climate-induced changes in lowland vegetation of eastern equatorial Africa revealed by the stable carbon-isotopic composition of fossil plant leaf waxes. *Earth and Planetary Science Letters* 302, 236-246.
- Slemmons, K.E.H., Saros, J., Stone, J., *et al.*, 2015. Effects of glacier meltwater on the algal sedimentary record of an alpine lake in the central US Rocky Mountains throughout the late Holocene. *Journal of Paleolimnology* 53, 385-399.
- Slemmons, K.E.H., Saros, J.E., 2012. Implications of nitrogen-rich glacial meltwater for phytoplankton diversity and productivity in alpine lakes. *Limnology and Oceanography* 57, 1651-1663.
- Slemmons, K.E.H., Saros, J.E., Simon, K., 2013. The influence of glacial meltwater on alpine aquatic ecosystems: a review. *Environmental Science: Processes & Impacts* 15, 1794-1806.
- Smith, N.D., 1981. The Effect of Changing Sediment Supply on Sedimentation in a Glacier-Fed Lake. *Arctic and Alpine Research* 13, 75-82.
- Smol, J.P., Douglas, M.S.V., 2007. Crossing the final ecological threshold in high Arctic ponds. *Proceedings of the National Academy of Sciences* 104, 12395-12397.
- Smol, J.P., Wolfe, A.P., Birks, H.J.B., *et al.*, 2005. Climate-driven regime shifts in the biological communities of arctic lakes. *Proceedings of the National Academy of Sciences of the United States of America* 102, 4397-4402.
- Sobek, S., Anderson, N., Bernasconi, S., *et al.*, 2014. Low organic carbon burial efficiency in arctic lake sediments. *Journal of Geophysical Research: Biogeosciences* 119, 1231-1243.
- Sobek, S., Durisch-Kaiser, E., Zurbrügg, R., *et al.*, 2009. Organic carbon burial efficiency in lake sediments controlled by oxygen exposure time and sediment source. *Limnology and Oceanography* 54, 2243.
- Sollins, P., Spycher, G., Glassman, C., 1984. Net nitrogen mineralization from light- and heavy-fraction forest soil organic matter. *Soil Biology and Biochemistry* 16, 31-37.

- Solomina, O.N., Bradley, R.S., Jomelli, V., *et al.*, 2016. Glacier fluctuations during the past 2000 years. *Quaternary Science Reviews* 149, 61-90.
- Sommaruga, R., 2001. The role of solar UV radiation in the ecology of alpine lakes. *Journal of Photochemistry and Photobiology B: Biology* 62, 35-42.
- Staeher, P.A., Sand-Jensen, K., Raun, A.L., *et al.*, 2010. Drivers of metabolism and net heterotrophy in contrasting lakes. *Limnology and Oceanography* 55, 817-830.
- Steenstrup, K.J.V., 1901. Beretning om en undersøgelsesrejse til øen Disko i sommeren 1898. *Meddelelser om Grønland* 24, 249-306.
- Stevenson, M.A., McGowan, S., Anderson, N.J., *et al.*, 2016. Impacts of forestry planting on primary production in upland lakes from north - west Ireland. *Global Change Biology* 22, 1490-1504.
- Stewart, A.J., Wetzel, R.G., 1986. Cryptophytes and Other Microflagellates as Couplers in Planktonic Community Dynamics. *Archiv Fur Hydrobiologie* 106, 1-19.
- Street, J.H., Anderson, R.S., Rosenbauer, R.J., *et al.*, 2013. *n*-Alkane evidence for the onset of wetter conditions in the Sierra Nevada, California (USA) at the mid-late Holocene transition, ~ 3.0 ka. *Quaternary Research* 79, 14-23.
- Striegl, R.G., Dornblaser, M.M., Aiken, G.R., *et al.*, 2007. Carbon export and cycling by the Yukon, Tanana, and Porcupine rivers, Alaska, 2001–2005. *Water Resources Research* 43.
- Stroeve, J., Holland, M.M., Meier, W., *et al.*, 2007. Arctic sea ice decline: Faster than forecast. *Geophysical Research Letters* 34, 9.
- Stuiver, M., Reimer, P., Reimer, R., 2013. CALIB 7.0 manual [WWW document]. URL: <http://calib.qub.ac.uk/calib>.
- Sturm, M., Racine, C., Tape, K., 2001. Climate change: Increasing shrub abundance in the Arctic. *Nature* 411, 546-547.
- Tans, P.P., De Jong, A.F.M., Mook, W.G., 1979. Natural atmospheric ¹⁴C variation and the Suess effect. *Nature* 280, 826-828.
- Tape, K., Sturm, M., Racine, C., 2006. The evidence for shrub expansion in northern Alaska and the Pan-Arctic. *Global Change Biology* 12, 686-702.
- Tape, K.D., Hallinger, M., Welker, J.M., *et al.*, 2012. Landscape Heterogeneity of Shrub Expansion in Arctic Alaska. *Ecosystems* 15, 711-724.
- Taranu, Z.E., Gregory-Eaves, I., Leavitt, P.R., *et al.*, 2015. Acceleration of cyanobacterial dominance in north temperate-subarctic lakes during the Anthropocene. *Ecology Letters* 18, 375-384.
- Taylor, K.C., Mayewski, P.A., Alley, R.B., *et al.*, 1997. The Holocene-Younger Dryas Transition Recorded at Summit, Greenland. *Science* 278, 825-827.
- Telling, J., Anesio, A.M., Tranter, M., *et al.*, 2012. Controls on the autochthonous production and respiration of organic matter in cryoconite holes on high Arctic glaciers. *Journal of Geophysical Research: Biogeosciences* 117.

- ter Braak, C.J.F., Smilauer, P., 2002. CANOCO reference manual and CanoDraw for Windows user's guide : software for canonical community ordination (version 4.5). Biometris, Wageningen.
- Thies, H., Nickus, U., Mair, V., *et al.*, 2007. Unexpected Response of High Alpine Lake Waters to Climate Warming. *Environmental Science & Technology* 41, 7424-7429.
- Tranvik, L.J., 1990. Bacterioplankton Growth on Fractions of Dissolved Organic Carbon of Different Molecular Weights from Humic and Clear Waters. *Applied and Environmental Microbiology* 56, 1672-1677.
- Tranvik, L.J., 1992. Allochthonous dissolved organic matter as an energy source for pelagic bacteria and the concept of the microbial loop, Dissolved organic matter in lacustrine ecosystems. Springer, pp. 107-114.
- Tranvik, L.J., Downing, J.A., Cotner, J.B., *et al.*, 2009. Lakes and reservoirs as regulators of carbon cycling and climate. *Limnology and Oceanography* 54, 2298-2314.
- Tranvik, L.J., Sieburth, J.M., 1989. Effects of Flocculated Humic Matter on Free and Attached Pelagic Microorganisms. *Limnology and Oceanography* 34, 688-699.
- Vadeboncoeur, Y., Jeppesen, E., Zanden, M., *et al.*, 2003. From Greenland to green lakes: cultural eutrophication and the loss of benthic pathways in lakes. *Limnology and Oceanography* 48, 1408-1418.
- Vadeboncoeur, Y., Vander Zanden, M.J., Lodge, D.M., 2002. Putting the Lake Back Together: Reintegrating Benthic Pathways into Lake Food Web Models: Lake ecologists tend to focus their research on pelagic energy pathways, but, from algae to fish, benthic organisms form an integral part of lake food webs. *BioScience* 52, 44-54.
- van Hardenbroek, M., Heiri, O., Grey, J., *et al.*, 2010. Fossil chironomid $\delta^{13}\text{C}$ as a proxy for past methanogenic contribution to benthic food webs in lakes? *Journal of Paleolimnology* 43, 235-245.
- van Hardenbroek, M., Lotter, A., Bastviken, D., *et al.*, 2011. Relationship between $\delta^{13}\text{C}$ of chironomid remains and methane flux in Swedish lakes. *Freshwater Biology* 57, 166-177.
- Verburg, P., 2007. The need to correct for the Suess effect in the application of $\delta^{13}\text{C}$ in sediment of autotrophic Lake Tanganyika, as a productivity proxy in the Anthropocene. *Journal of Paleolimnology* 37, 591-602.
- Vincent, W.F., Hobbie, J.E., 2000. Ecology of Arctic lakes and rivers, In: Nuttall, M., T, C. (Eds.), *The Arctic: Environment, People, Policy*. Harwood Academic Publishers, Amsterdam, pp. 197-231.
- Vinther, B.M., Buchardt, S.L., Clausen, H.B., *et al.*, 2009. Holocene thinning of the Greenland ice sheet. *Nature* 461, 385-388.
- Volkman, J.K., 1986. A review of sterol markers for marine and terrigenous organic matter. *Organic Geochemistry* 9, 83-99.

- Volkman, J.K., Barrett, S.M., Blackburn, S.I., 1999. Eustigmatophyte microalgae are potential sources of C₂₉ sterols, C₂₂–C₂₈ *n*-alcohols and C₂₈–C₃₂ *n*-alkyl diols in freshwater environments. *Organic Geochemistry* 30, 307-318.
- Volkman, J.K., Barrett, S.M., Blackburn, S.I., *et al.*, 1998. Microalgal biomarkers: A review of recent research developments. *Organic Geochemistry* 29, 1163-1179.
- Vreca, P., Muri, G., 2006. Changes in accumulation of organic matter and stable carbon and nitrogen isotopes in sediments of two Slovenian mountain lakes (Lake Ledvica and Lake Planina), induced by eutrophication changes. *Limnology and Oceanography* 51, 781-790.
- Waddington, J., Roulet, N., 1996. Atmosphere - wetland carbon exchanges: Scale dependency of CO₂ and CH₄ exchange on the developmental topography of a peatland. *Global Biogeochemical Cycles* 10, 233-245.
- Walker, M., Johnsen, S., Rasmussen, S.O., *et al.*, 2009. Formal definition and dating of the GSSP (Global Stratotype Section and Point) for the base of the Holocene using the Greenland NGRIP ice core, and selected auxiliary records. *Journal of Quaternary Science* 24, 3-17.
- Walter, K.M., Edwards, M.E., Grosse, G., *et al.*, 2007. Thermokarst Lakes as a Source of Atmospheric CH₄ During the Last Deglaciation. *Science* 318, 633-636.
- Walter, K.M., Zimov, S., Chanton, J.P., *et al.*, 2006. Methane bubbling from Siberian thaw lakes as a positive feedback to climate warming. *Nature* 443, 71-75.
- Walvoord, M.A., Striegl, R.G., 2007. Increased groundwater to stream discharge from permafrost thawing in the Yukon River basin: Potential impacts on lateral export of carbon and nitrogen. *Geophysical Research Letters* 34.
- Wanner, H., Beer, J., Bütikofer, J., *et al.*, 2008. Mid- to Late Holocene climate change: an overview. *Quaternary Science Reviews* 27, 1791-1828.
- Wanner, H., Bütikofer, J., 2008. Holocene Bond Cycles: real or imaginary. *Geografie* 4, 338-349.
- Weidick, A., 1968. Observations on some Holocene Glacial Fluctuations in West Greenland. *Meddelelser om Grønland* 165, 133.
- Welker, J.M., Fahnestock, J.T., Jones, M.H., 2000. Annual CO₂ Flux in Dry and Moist Arctic Tundra: Field Responses to Increases in Summer Temperatures and Winter Snow Depth. *Climatic Change* 44, 139-150.
- Whiteford, E.J., McGowan, S., Barry, C.D., *et al.*, 2016. Seasonal and Regional Controls of Phytoplankton Production along a Climate Gradient in South-West Greenland During Ice-Cover and Ice-Free Conditions. *Arctic, Antarctic, and Alpine Research* 48, 139-159.
- Williams, M.W., Davinroy, T., Brooks, P.D., 1997. Organic and inorganic nitrogen pools in talus fields and subtalus water, Green Lakes Valley, Colorado Front Range. *Hydrological Processes* 11, 1747-1760.

- Williamson, C.E., Morris, D.P., Pace, M.L., *et al.*, 1999. Dissolved organic carbon and nutrients as regulators of lake ecosystems: resurrection of a more integrated paradigm. *Limnology and Oceanography* 44.
- Williamson, C.E., Saros, J.E., Schindler, D.W., 2009. Sentinels of Change. *Science* 323, 887-888.
- Wolfe, B.B., Edwards, T.W., Aravena, R., 1999. Changes in carbon and nitrogen cycling during tree-line retreat recorded in the isotopic content of lacustrine organic matter, western Taimyr Peninsula, Russia. *The Holocene* 9, 215-222.
- Woo, M.-k., Young, K.L., 2006. High Arctic wetlands: Their occurrence, hydrological characteristics and sustainability. *Journal of Hydrology* 320, 432-450.
- Wookey, P.A., Aerts, R., Bardgett, R.D., *et al.*, 2009. Ecosystem feedbacks and cascade processes: understanding their role in the responses of Arctic and alpine ecosystems to environmental change. *Global Change Biology* 15, 1153-1172.
- Yang, H., Rose, N., 2005. Trace element pollution records in some UK lake sediments, their history, influence factors and regional differences. *Environment International* 31, 63-75.
- Yde, J.C., Knudsen, N.T., 2005. Observations of debris - rich nales associated with a major glacier surge event, Disko Island, West Greenland. *Permafrost and Periglacial Processes* 16, 319-325.
- Yde, J.C., Knudsen, N.T., 2007. 20th-century glacier fluctuations on Disko Island (Qeqertarsuaq), Greenland. *Annals of Glaciology* 46, 209-214.
- Yde, J.C., Knudsen, N.T., Nielsen, O.B., 2005. Glacier hydrochemistry, solute provenance, and chemical denudation at a surge-type glacier in Kuannersuit Kuussuat, Disko Island, West Greenland. *Journal of Hydrology* 300, 172-187.
- Yu, S.-Y., Colman, S.M., Lowell, T.V., *et al.*, 2010. Freshwater Outburst from Lake Superior as a Trigger for the Cold Event 9300 Years Ago. *Science* 328, 1262-1266.
- Zech, M., Andreev, A., Zech, R., *et al.*, 2010. Quaternary vegetation changes derived from a loess - like permafrost palaeosol sequence in northeast Siberia using alkane biomarker and pollen analyses. *Boreas* 39, 540-550.
- Zhang, T., Barry, R.G., Knowles, K., *et al.*, 1999. Statistics and characteristics of permafrost and ground - ice distribution in the Northern Hemisphere 1. *Polar Geography* 23, 132-154.
- Zheng, Y., Zhou, W., Meyers, P.A., *et al.*, 2007. Lipid biomarkers in the Zoigê-Hongyuan peat deposit: Indicators of Holocene climate changes in West China. *Organic Geochemistry* 38, 1927-1940.
- Zhou, W., Xie, S., Meyers, P.A., *et al.*, 2005. Reconstruction of late glacial and Holocene climate evolution in southern China from geolipids and pollen in the Dingnan peat sequence. *Organic Geochemistry* 36, 1272-1284.
- Ziegler, M., Jilbert, T., de Lange, G.J., *et al.*, 2008. Bromine counts from XRF scanning as an estimate of the marine organic carbon content of sediment cores. *Geochemistry, Geophysics, Geosystems* 9, 1-6.

References

Zona, D., Gioli, B., Commane, R., *et al.*, 2016. Cold season emissions dominate the Arctic tundra methane budget. *Proceedings of the National Academy of Sciences* 113, 40-45.

Appendix A – Detailed review of lipid biomarker ratios and equations suitable for palaeolimnological studies

A1. Ratios and equations

There are a wide range of ratios that have been used in palaeolimnological investigations using lipid biomarkers, both for source apportionment and to assess diagenesis. This appendix supports the lipid biomarker summary tables in chapter 2 (Table 2.1, 2.2 & 2.3).

To identify if the dominant odd or even compounds are clearly higher in abundance the Carbon Preference Index (CPI) was developed (Equation A.1) (Bray and Evans, 1961; Cooper and Bray, 1963). In fresh hydrocarbons odd-numbered chains predominate, whereas for fatty acids and alcohols even numbered chains dominate chromatograms (Meyers and Ishiwatari, 1993). For example, *n*-alkane CPI values for ancient sediments should be lower than for recent sediments as 1.0 is characteristic of crude oil. Slight variations in this ratio can be helpful to assess the source and diagenesis within lake sediments.

$$\text{CPI} = \frac{1}{2} \left(\frac{\text{C}_{25} + \text{C}_{27} + \text{C}_{29} + \text{C}_{31} + \text{C}_{33}}{\text{C}_{24} + \text{C}_{26} + \text{C}_{28} + \text{C}_{30} + \text{C}_{32}} + \frac{\text{C}_{25} + \text{C}_{27} + \text{C}_{29} + \text{C}_{31} + \text{C}_{33}}{\text{C}_{26} + \text{C}_{28} + \text{C}_{30} + \text{C}_{32} + \text{C}_{34}} \right)$$

Equation A.1: The Carbon Preference Index (CPI) (Bray and Evans, 1961; Cooper and Bray, 1963).

The index has been adapted to improve effectiveness at distinguishing slight variations in the chain length dominance of organic matter by Marzi et al. (1993) (Equation A.2).

$$\text{CPI2} = \frac{(\text{C}_{23} + \text{C}_{25} + \text{C}_{27}) + (\text{C}_{25} + \text{C}_{27} + \text{C}_{29})}{2 \times (\text{C}_{24} + \text{C}_{26} + \text{C}_{28})}$$

Equation A.2: The modified Carbon Preference Index 2 (Marzi et al., 1993).

The CPI index has been adapted to suit fatty acids and to include source apportionment by Matsuda and Koyama (1977), who split the index into CPI_L (Equation A.3) for the lower molecular weight compounds (C₁₂-C₁₈), CPI_H (Equation 2.4) for higher molecular weight fatty acids (≥C₂₀) and CPI_T (Equation A.5) for the entire range of saturated fatty acids detected. Here, even carbon numbers are divided by odd carbon numbers.

$$\text{CPI}_L = \frac{1 \sum C_{12} - C_{16} + \sum C_{14} - C_{18}}{2 \sum C_{13} - C_{17}}$$

Equation A.3: Carbon Preference Index for low molecular weight compounds (CPI_L) (Matsuda and Koyama, 1977). $\text{CPI}_H = \frac{1 \sum C_{22} - C_{30} + C_{24} - C_{32}}{2 \sum C_{23} - C_{31}}$

Equation A.4: Carbon Preference Index for high molecular weight compounds (CPI_H) (Matsuda and Koyama, 1977). $\text{CPI}_T = \frac{1 (\sum C_{12} - C_{16} + \sum C_{22} - C_{30}) + (\sum C_{14} - C_{18} + \sum C_{24} - C_{32})}{2 \sum C_{13} - C_{17} + \sum C_{23} - C_{31}}$

Equation A.5: Carbon Preference Index for the entire range of saturated fatty acids detected (CPI_T) (Matsuda and Koyama, 1977). For *n*-alkanoic acids CPI_L values are high in most plants (12-100), but CPI_H values are lower (0.9-8) as there are typically some long chain odd-carbon acids in some land plants (Meyers and Ishiwatari, 1993). With bacterial processing CPI values decrease as microbial activity resynthesizes the original compositions.

The ratio of unsaturated to saturated fatty acids (e.g. C_{18:1}/C_{18:0}) can be a good indicator of microbial activity as unsaturated *n*-C₁₆ and *n*-C₁₈ acids when sourced from algae are rapidly degraded (Cranwell, 1976). This is due to the carbon-carbon double bonds that are less resistant and have been demonstrated both in Lake Haruna, Japan (Kawamura et al., 1980) and Lake Huron (Meyers et al., 1980). Ouyang et al. (2015) report this process might be temperature regulated, with microbial alteration of the unsaturated acid accelerated under warm conditions (Zhou et al., 2005). In some sedimentary settings the *n*-C_{15:0} fatty acid has been linked to a bacterial origin based on the light compound-specific carbon isotope composition in specific settings, relative to *n*-C_{16:0} to *n*-C_{28:0} acids (−37.2‰ vs −33.7‰) (Duan et al., 1997; Zheng et al., 2007).

The Average Chain Length (ACL) measure (Equation 2.6) takes the concentration weighted average chain length of the C₂₇ to C₃₃ *n*-alkanes (Poynter et al., 1989) to relate environmental conditions to the chain length distributions of plant waxes with higher chain lengths (Ouyang et al., 2015). Terrestrial plants may synthesise shorter chain compounds in cooler climates, but more long chain compounds in tropical environments due to waxy coatings (Gagosian and Peltzer, 1986) or be related to precipitation and humidity (Zhou et al., 2005).

$$ACL = \frac{\sum((C_i^*[C_i]))}{\sum[C_i]}$$

Equation A.6: The Average Chain Length (ACL) index of Poynter et al. (1989). Where $\sum[C_i]$ is the concentration of the *n*-alkanes with carbon number C_i , over C_{27} - C_{33} .

A robust indicator of the terrestrial to aquatic source contribution in lake sediments is the terrigenous to aquatic ratio TAR_{HC} (Equation A.7), which was first employed by Bourbonniere and Meyers (1996a).

$$TAR_{HC} = \frac{C_{27} + C_{29} + C_{31}}{C_{15} + C_{17} + C_{19}}$$

Equation A.7: Terrigenous to aquatic hydrocarbon ratio (TAR_{HC}) of Bourbonniere and Meyers (1996).

With higher values, terrestrial contributions are interpreted, however they may over represent terrestrial inputs as long chain compounds are less easily degraded (Meyers, 1997). The ratio has also been adapted to identify source contributions of fatty acids (TAR_{FA}) (Equation A.8).

$$TAR_{FA} = \frac{C_{24} + C_{26} + C_{28}}{C_{12} + C_{14} + C_{16}}$$

Equation A.8: Terrigenous to aquatic fatty acid ratio (TAR_{FA}) of (Meyers, 1997).

Again, higher values indicate increased terrestrial contributions, although it is emphasised that fatty acids are more susceptible to diagenesis, particularly with the short chain compounds (Meyers, 1997). The index can similarly be used for *n*-alkanol compounds as *n*-alkanols also usually have maximum abundance in the even numbered saturated compounds.

Since aquatic macrophytes (submerged and floating leaved) usually have maximum abundance in the mid chain length *n*- C_{23} , and *n*- C_{25} *n*-alkanes, a proxy (P_{aq}) has been developed (Equation A.9) which records these inputs, in comparison to terrestrial vegetation ($>C_{29}$) (Ficken et al., 2000).

$$P_{aq} = \frac{(C_{23} + C_{25})}{(C_{23} + C_{25} + C_{29} + C_{31})}$$

Equation A.9: Aquatic macrophyte ratio (P_{aq}) of Ficken et al. (2000). The P_{aq} proxy can reflect changes in the source contributions of submerged and floating macrophytes over time, but has also been linked with changes in water level and effective

precipitation (Ouyang et al., 2015). Higher values equal greater proportions of macrophytes. This ratio has been adapted to produce the P_{WAX} index (Equation A.10) which indicates the relative proportion of waxy n -alkane hydrocarbons from emergent macrophytes and terrestrial plants to total hydrocarbons (Zheng et al., 2007).

$$P_{WAX} = \frac{(C_{27} + C_{29} + C_{31})}{(C_{23} + C_{25} + C_{27} + C_{29} + C_{31})}$$

Equation A.10: The P_{WAX} index of waxy n -alkanes to total hydrocarbons.

High P_{WAX} values indicate greater contributions from terrestrial plants or emergent macrophytes (Zheng et al., 2007; Ouyang et al., 2015).

The ratio of the sterols cholesterol to 24-ethylcholest-5-en-3 β -ol (β -sitosterol) has also been used as a terrestrial to aquatic marker as cholesterol is primarily sourced from algae, whereas β -sitosterol is present in a greater abundance in emergent plants and catchment vegetation (Nishimura and Koyama, 1977; Meyers, 1997).

Pearson et al. (2007) modified the autochthonous to allochthonous ratios (Equation A.11) based on a thorough review of source inputs amongst a wide range of Spanish lakes. For acid compounds, the algal specific n -C₁₆ and n -C₁₈ compounds were expressed against a wider range of terrestrial compounds compared with the TAR_{FA} ratio.

$$\text{Aut/All ratio acid} = \frac{C_{16} + C_{18}}{C_{20} + C_{22} + C_{24} + C_{26} + C_{28} + C_{30}}$$

Equation A.11: The autochthonous to allochthonous ratio for acid compounds (Aut/All ratio acid) as presented by Pearson et al. (2007).

Here, higher values indicate increased autochthonous compounds. A similar approach was applied to the n -alkanols to consider a wider range of compounds (Equation A.12).

$$\text{Aut/All ratio alkanol} = \frac{C_{14} + C_{16} + C_{18} + C_{20}}{C_{22} + C_{24} + C_{26} + C_{28}}$$

Equation A.12: The autochthonous to allochthonous ratio for alkanol compounds (Aut/All ratio alkanol) as presented by Pearson et al. (2007).

Similarly, higher values indicate increased algal contributions. In contrast, based on the unambiguous source apportionment of the C₁₇ n -alkane (aquatic) to C₂₇ n -alkane (terrestrial), the ratio of C₁₇ to C₂₇ n -alkane was used (Pearson et al., 2007).

A2. Chemical structure of example lipid biomarkers

This appendix supports the lipid biomarker summary tables in chapter 2 (Table 2.1, 2.2 & 2.3) by providing the chemical structure of example compounds.

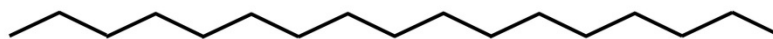


Figure A.1: Chemical hydrocarbon structure of C_{17} *n*-alkane ($C_{17}H_{36}$, heptadecane).



Figure A.2: Chemical structure of C_{16} *n*-alcohol ($C_{16}H_{34}O$, hexadecan-1-ol).

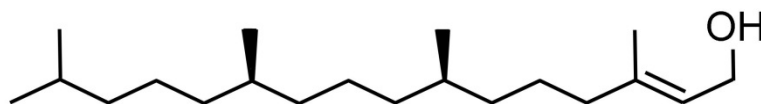


Figure A.3: Chemical structure of phytol ($C_{20}H_{40}O$, 3,7,11,15-tetramethyl-2-hexadecen-1-ol).

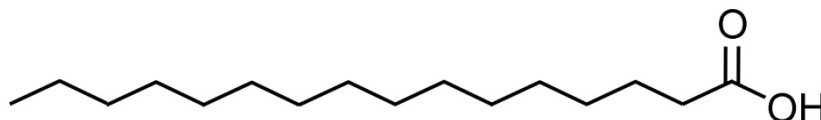


Figure A.4: Chemical structure of C_{16} *n*-fatty acid ($C_{16}H_{32}O_2$, hexadecanoic acid).

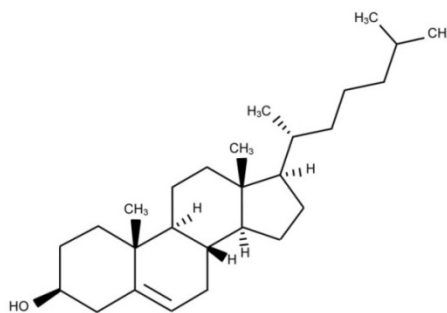


Figure A.5: Chemical structure of cholesterol ($C_{27}H_{46}O$, cholest-5-en-3 β -ol).

Appendix B – Supplementary tables from hydro-geomorphic vegetation catchment survey and site information

This appendix contains the full suite of biomarker ratios and equations for catchment samples from Disko 2. Selected *n*-alkane lipid ratios are presented in Table B1, with key *n*-fatty acid (FAMES) in Table B2 and *n*-alkanol, sterol, ketone and phytol ratios in Table B3. These ratios and equations are provided as a resource for future studies.

Table B.1: Selected *n*-alkane lipid ratios for catchment samples from Disko 2 catchment analysed using GC-MS.

Sample	TOC %	Key <i>n</i> -alkane lipid ratios				Selected <i>n</i> -alkane / total saturated <i>n</i> -alkanes					
		CPI 2 ⁽¹⁾	TAR HC ⁽²⁾	<i>P</i> _{aq} ⁽³⁾	<i>P</i> _{WAX} ⁽⁴⁾	<i>n</i> -C ₁₇	<i>n</i> -C ₁₉	<i>n</i> -C ₂₄	<i>n</i> -C ₂₆	<i>n</i> -C ₂₉	<i>n</i> -C ₃₁
<i>Harrimanella hypnoides?</i> (A)	43.0	39.6	18899.2	0.0	1.2	0.0	0.0	0.1	0.2	36.2	43.1
<i>Harrimanella hypnoides?</i> (C)	42.4	27.6	2980.3	0.0	1.0	0.0	0.0	0.2	0.3	52.2	34.9
Plant A (stem & leaf)	49.2	25.9	1523.1	0.0	1.1	0.0	0.1	0.2	0.3	72.7	9.7
Black moss with white spots	40.9	3.7	3.0	0.6	0.7	0.1	7.2	3.0	3.0	7.3	5.1
Potamogeton	32.1	3.6	68.5	0.2	0.9	0.2	0.5	2.4	3.0	16.7	26.4
Green moss	34.9	5.4	8.0	0.3	0.9	3.6	2.3	2.5	1.5	11.7	25.2
Algal benthic rock scrape	24.5	3.5	6.2	0.7	0.5	0.1	3.5	5.1	2.8	9.0	5.7
<i>Chamerion latifolium</i> (partly decomposed)	33.1	15.7	119.8	0.7	0.7	0.0	0.3	1.4	1.1	10.6	1.9
<i>Salix arctica</i> (leaf)	47.0	18.5	19.6	0.7	0.9	0.1	2.2	2.4	1.1	7.1	6.1
Catchment - Soil	0.3	5.2	357.7	0.1	1.1	0.1	0.2	1.5	2.5	29.6	36.3
PLOT C - Soil	0.1	1.3	18.9	0.5	0.8	0.1	1.5	7.3	9.0	11.6	7.8

⁽¹⁾CPI 2 – Carbon Preference Index 2 (Marzi et al., 1993) = $((C_{23}+C_{25}+C_{27})+(C_{25}+C_{27}+C_{29}))/2*(C_{24}+C_{26}+C_{28})$

⁽²⁾TAR_{HC} – Terrigenous to Aquatic Ratio (Bourbonniere and Meyers, 1996a) = $(C_{27}+C_{29}+C_{31})/(C_{15}+C_{17}+C_{19})$

⁽³⁾*P*_{aq} – Aquatic macrophyte ratio (Ficken et al., 2000) = $(C_{23}+C_{25})/(C_{23}+C_{25}+C_{29}+C_{31})$

⁽⁴⁾*P*_{WAX} – Index of waxy *n*-alkanes to total hydrocarbons (Zheng et al., 2007) = $(C_{27}+C_{29}+C_{31})/(C_{23}+C_{25}+C_{29}+C_{31})$

Table B.2: Selected *n*-fatty acid (FAMES) lipid ratios for catchment plant samples from Disko 2 catchment analysed using GC-MS.

Sample	Key <i>n</i> -fatty acid (FAMES) ratios						Selected <i>n</i> -fatty acids / total saturated <i>n</i> -fatty acids							
	TOC %	CPI _L ⁽¹⁾	CPI _H ⁽²⁾	CPI _T ⁽³⁾	TAR FA ⁽⁴⁾	C _{18:1a} / C _{18:0}	C _{16:1a} / C _{16:0} *1000	C _{16:1d} / C _{16:0} *1000	<i>n</i> -C ₁₄	<i>n</i> -C ₁₆	<i>n</i> -C ₂₄	<i>n</i> -C ₂₆	<i>n</i> -C ₂₈	<i>n</i> -C ₃₀
<i>Harrimanella hypnoides?</i> (A)	43.0	88.0	11.4	43.2	0.3	0.1	5.6	0.0	4.4	35.3	1.5	5.1	3.5	0.7
<i>Harrimanella hypnoides?</i> (C)	42.4	24.5	8.9	15.3	0.4	5.0	18.6	0.1	6.3	44.9	6.5	3.5	9.3	4.2
Plant A (stem & leaf)	49.2	22.8	25.3	24.3	0.8	0.8	9.2	0.7	0.8	18.1	9.7	2.2	3.8	0.6
Black moss with white spots	40.9	114.4	1.1	69.7	0.0	4.5	14.5	0.1	1.5	86.6	0.3	0.0	0.0	0.0
<i>Potamogeton</i>	32.1	79.0	11.5	74.3	0.0	9.6	52.6	0.9	18.2	76.4	0.4	0.2	0.1	0.0
Green moss	34.9	31.4	33.6	32.4	0.8	3.4	13.8	0.0	3.4	38.2	25.6	7.9	1.2	0.1
Algal benthic rock scrape	24.5	45.0	19.4	40.6	0.1	3.4	38.9	0.1	5.1	74.4	4.9	0.9	0.2	0.0
<i>Chamerion latifolium</i> (partly decomposed)	33.1	37.2	18.5	27.5	0.5	1.2	57.0	6.6	12.1	38.7	5.1	12.9	6.3	0.7
<i>Salix arctica</i> (leaf)	47.0	20.5	11.0	17.3	0.3	2.4	0.6	0.0	2.5	63.4	12.9	4.6	0.0	0.0
Catchment - Soil	0.3	22.4	4.9	15.1	0.2	0.1	110.0	0.5	3.8	43.7	4.2	2.3	1.0	0.2
PLOT C - Soil	0.1	21.4	5.6	11.7	0.5	0.2	9.3	0.0	2.6	34.2	7.3	5.5	3.9	2.0

⁽¹⁾CPI_L – Carbon Preference Index (lower molecular weight compounds) (Matsuda and Koyama, 1977) = $0.5 * ((C_{12} + C_{14} + C_{16}) + (C_{14} + C_{16} + C_{18})) / (C_{13} + C_{15} + C_{17})$

⁽²⁾CPI_H – Carbon Preference Index (higher molecular weight compounds) (Matsuda and Koyama, 1977) =

$$0.5 * ((C_{22} + C_{24} + C_{26} + C_{28} + C_{30}) + (C_{24} + C_{26} + C_{28} + C_{30} + C_{32})) / (C_{23} + C_{25} + C_{27} + C_{29} + C_{31})$$

⁽³⁾CPI_T – Carbon Preference Index (for the entire range) (Matsuda and Koyama, 1977) =

$$0.5 * ((C_{12} + C_{14} + C_{16}) + (C_{22} + C_{24} + C_{26} + C_{28} + C_{30})) / ((C_{14} + C_{16} + C_{18}) + (C_{24} + C_{26} + C_{28} + C_{30} + C_{32})) / ((C_{13} + C_{15} + C_{17}) + (C_{23} + C_{25} + C_{27} + C_{29} + C_{31}))$$

⁽⁴⁾ Terrigenous to aquatic fatty acid ratio (Bourbonniere and Meyers, 1996a) = $(C_{24} + C_{26} + C_{28}) / (C_{12} + C_{14} + C_{16})$

Table B.3: Selected *n*-alkanol, sterol and ketone versus phytol lipid ratios for catchment samples from Disko 2 catchment analysed using GC-MS.

Depth	TOC %	<i>n</i> -alkanols					Sterols				Ketone versus phytol ratio
		<i>n</i> -alkanol ratio	Selected saturated <i>n</i> -alkanols	<i>n</i> -alkanols/total			Sterol ratio	(Key sterol/total sterol)*1000			
		TAR ⁽¹⁾	<i>n</i> -C ₁₆	<i>n</i> -C ₂₂	<i>n</i> -C ₂₄	<i>n</i> -C ₂₆	Cholesterol / β -sitosterol	Stdehyd	Cholesterol	Brassicasterol	Phytone/phytol
Harrimanella hypnoides? (A)	43.0	556.8	0.1	8.2	9.3	27.8	3.1	0.0	3.0	6.4	21.3
Harrimanella hypnoides? (C)	42.4	37.2	0.6	25.2	14.1	5.9	14.7	0.9	13.7	16.3	21.6
Plant A (stem & leaf)	49.2	43.2	0.3	51.3	8.5	0.9	1.3	0.0	1.3	7.1	19.7
Black moss with white spots	40.9	0.3	0.9	1.1	1.3	1.1	522.6	6.2	217.7	56.6	5.5
Potamogeton	32.1	1.2	4.9	8.9	4.2	3.4	40.5	1.9	37.8	14.5	1.2
Green moss	34.9	316.7	0.1	13.8	25.8	34.3	109.2	0.2	41.7	44.2	6.0
Algal benthic rock scrape	24.5	44.3	0.7	11.1	22.6	38.9	185.8	7.2	111.8	57.8	2.3
Chamerion latifolium (partly decomposed)	33.1	930.0	0.0	25.1	28.1	17.5	0.1	0.0	0.1	3.5	1.1
Salix arctica (leaf)	47.0	234.1	0.2	29.4	40.0	13.9	0.0	0.0	0.0	0.4	6.4
Catchment - Soil	0.3	23.5	1.9	20.8	21.4	17.2	121.9	0.0	102.1	20.4	12.5
PLOT C - Soil	0.1	4.7	4.9	11.5	12.3	12.8	117.0	0.0	85.3	44.7	4.4

⁽¹⁾TAR - Terrigenous to aquatic *n*-alkanol ratio (Bourbonniere and Meyers, 1996a) = $(C_{24}+C_{26}+C_{28})/(C_{12}+C_{14}+C_{16})$

Abbreviations:

Cholesterol = cholest-5-en-3 β -ol

β -sitosterol = 24-ethylcholest-5-en-3 β -ol

Stdehyd (non-standard name) = cholesta-5,22E-dien-3 β -ol

Phytol = 3,7,11,15-tetramethyl-2-hexadecen-1-ol

Brassicasterol = 24-methylcholesta-5,22-dien-3 β -ol

Phytone = 6,10,14-trimethylpentadecan-2-one

Appendix C – Supplementary figures from lake Disko 2

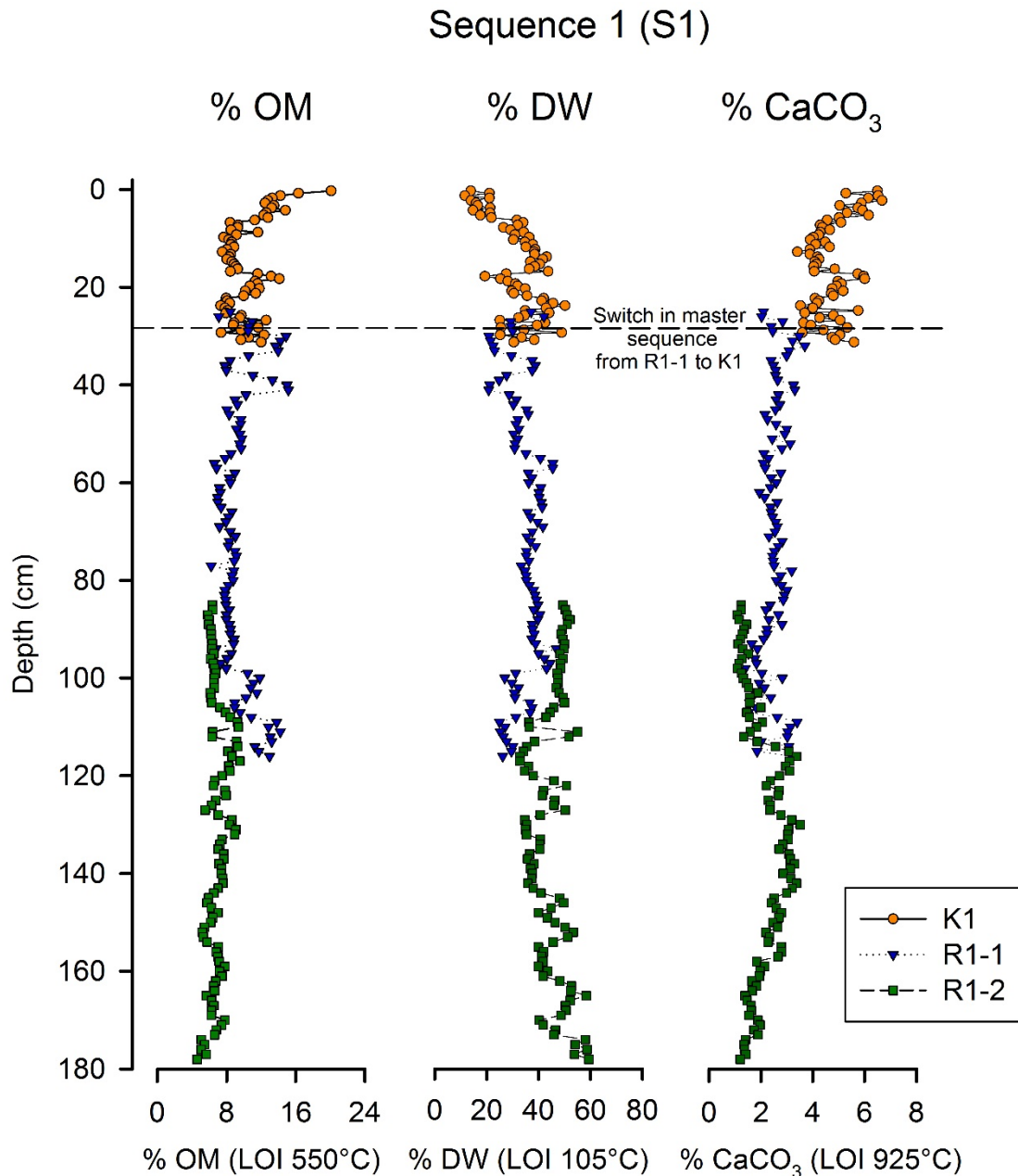


Figure C.1: Stratigraphic diagram of bulk measures for sequence 1 (S1) from lake Disko 2 including K1 (orange circles), R1-1 (blue triangles) and R1-2 (green squares). Presented measures include: organic matter content ((OM) loss-on-ignition at 550 °C for 5 hours (LOI 550°C)), percentage dry-weight after drying at 105 °C overnight (DW) and loss-on-ignition at 925 °C for 2 hours with carbonate correction (CaCO₃ (LOI 925 °C)). Dashed line indicates depth of 28.5 cm used to switch samples from core R1-1 to K1.

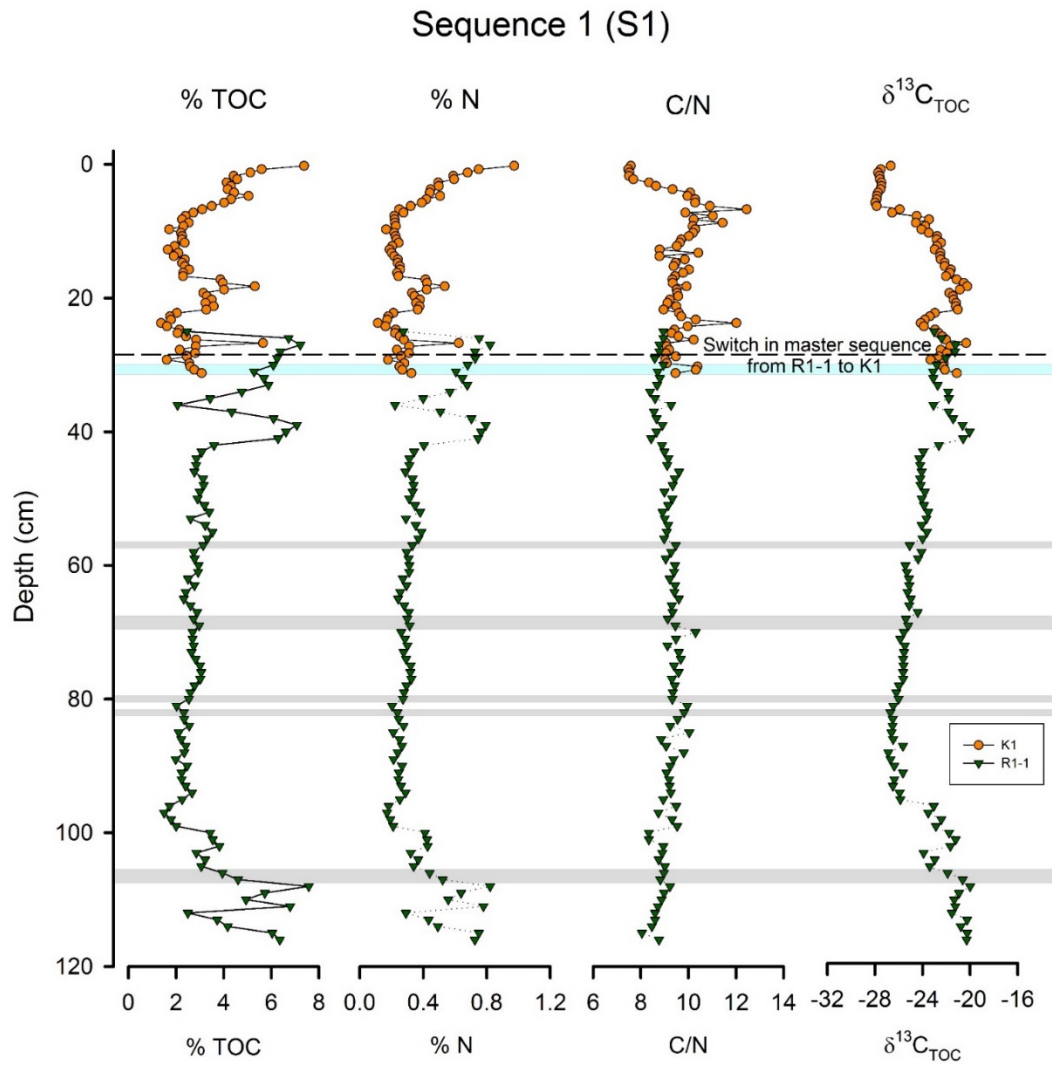


Figure C.2: Stratigraphic diagram of geochemical variables for overlapping sequence 1 (S1) from lake Disko 2 including K1 (orange circles) and R1-1 (green triangles). Presented variables include: TOC, N, C/N and $\delta^{13}\text{C}_{\text{TOC}}$. Dashed line indicates depth of 28.5 cm used to switch samples from core R1-1 to K1.

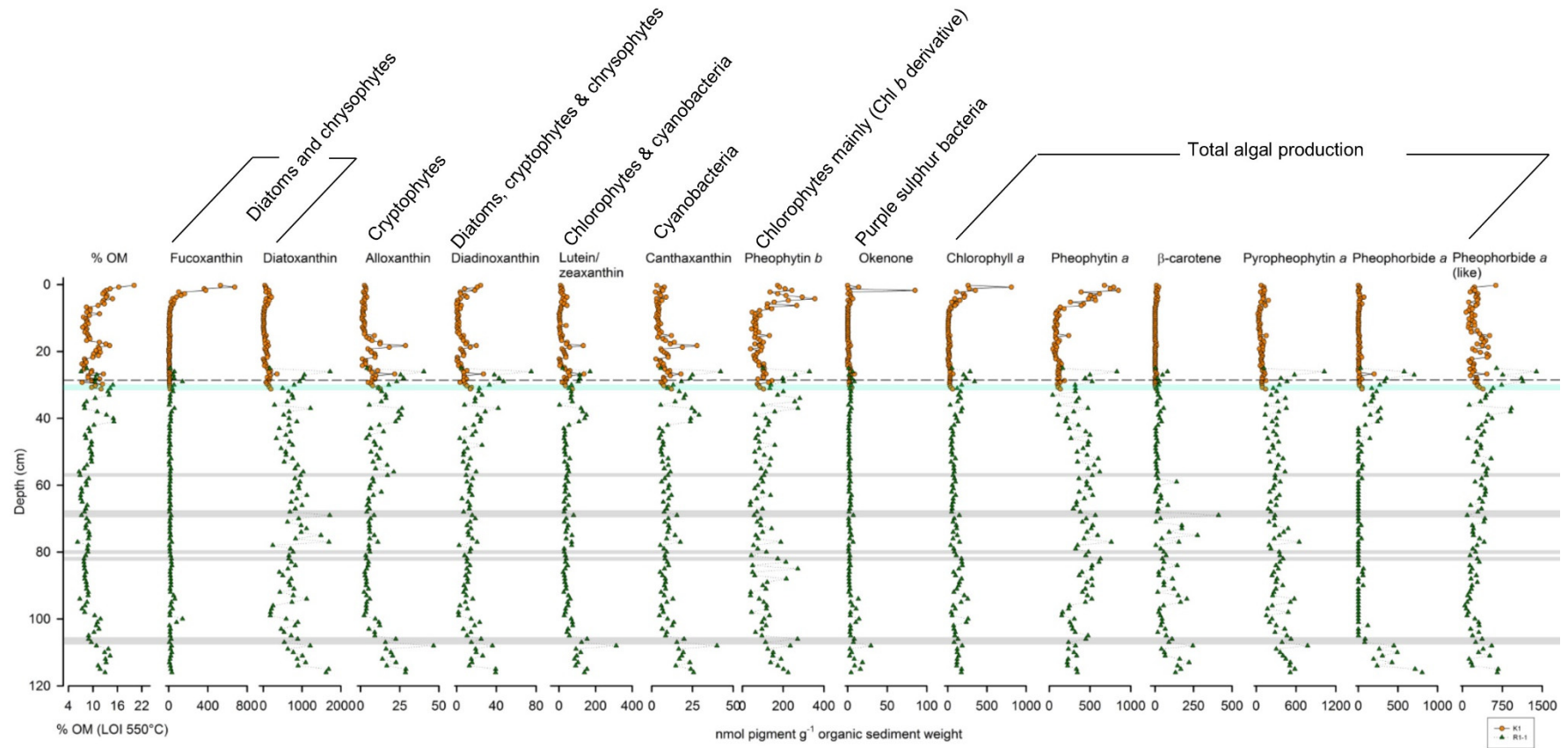


Figure C.3: Stratigraphic pigment diagram for HON-Kajak K1 (orange circles) and Russian R1-1 (green triangles) overlapping S1 sequence from lake Disko 2. Pigments fucoxanthin, diatoxanthin, alloxanthin, diadinoxanthin, lutein-zeaxanthin, canthaxanthin, pheophytin *b*, okenone, chlorophyll *a*, pheophytin *a*, β -carotene, pyropheophytin *a*, pheophorbide *a* and pheophorbide *a* (like) are presented with concentrations expressed relative to the organic matrix (% OM, LOI 550 °C). Instantaneous events indicated by green (age-suggested) and grey (stone/gravel layer) horizontal lines. Dashed line indicates depth of 28.5 cm used to switch samples from core R1-1 to K1.

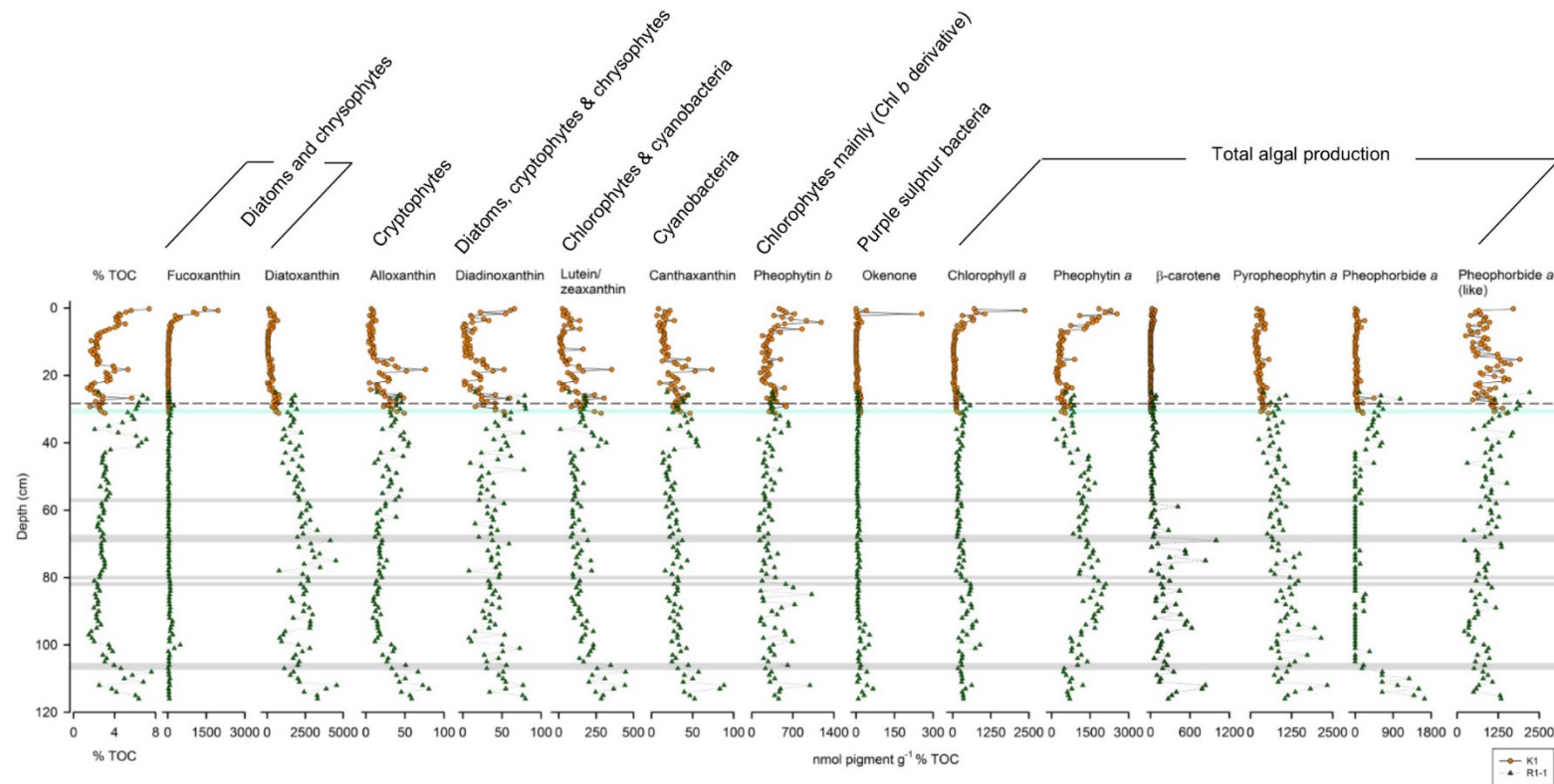


Figure C.4: Stratigraphic pigment diagram for HON-Kajak K1 (orange circles) and Russian R1-1 (green triangles) overlapping S1 sequence from lake Disko 2. Pigments fucoxanthin, diatoxanthin, alloxanthin, diadinoxanthin, lutein-zeaxanthin, canthaxanthin, pheophytin *b*, okenone, chlorophyll *a*, pheophytin *a*, β -carotene, pyropheophytin *a*, pheophorbide *a* and pheophorbide *a* (like) are presented with concentrations expressed relative to total organic carbon (% TOC). Instantaneous events indicated by green (age-suggested) and grey (stone/gravel layer) horizontal lines. Dashed line indicates depth of 28.5 cm used to switch samples from core R1-1 to K1.

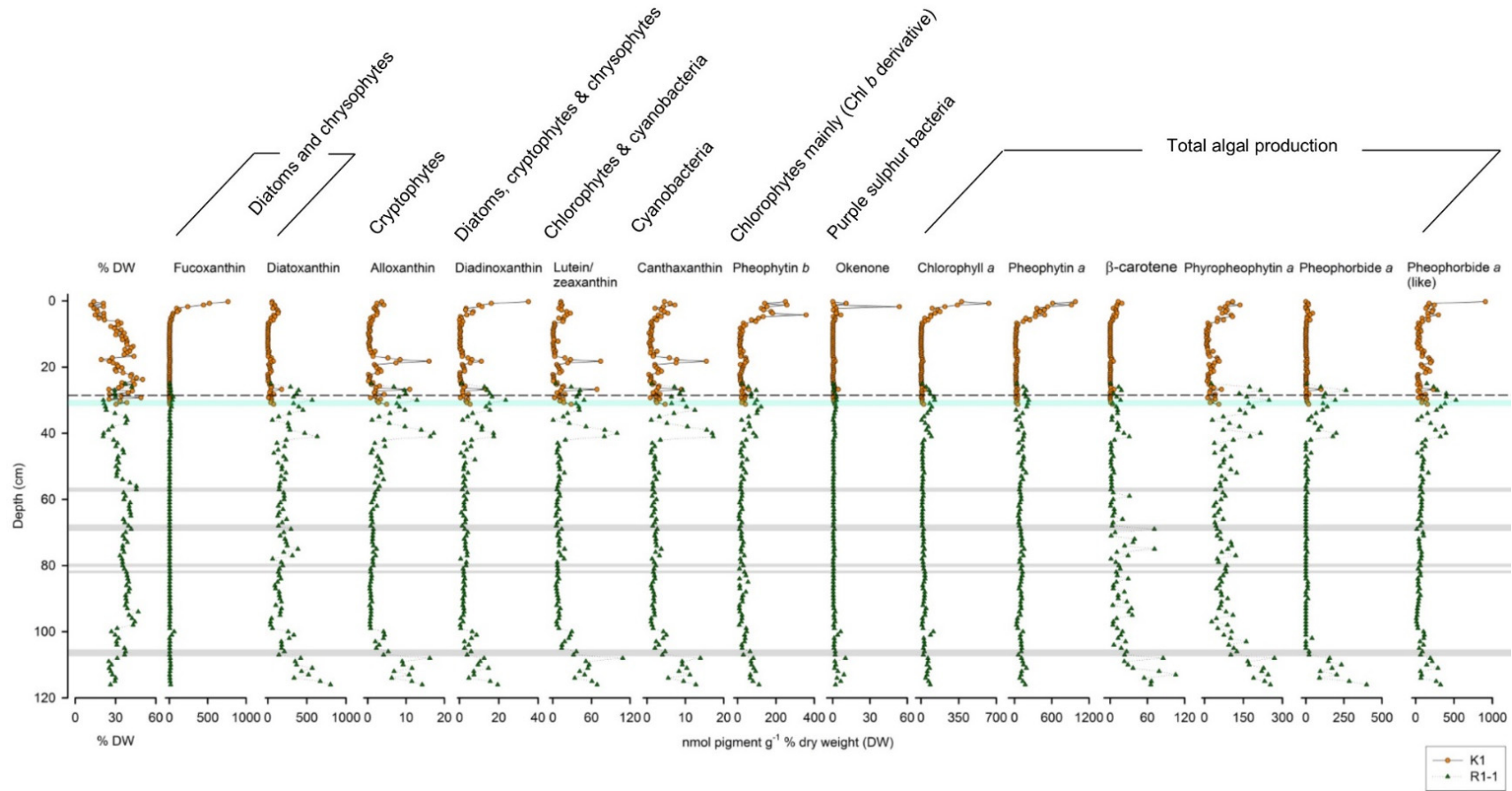


Figure C.5: Stratigraphic pigment diagram for HON-Kajak K1 (orange circles) and Russian R1-1 (green triangles) overlapping S1 sequence from lake Disko 2. Pigments fucoxanthin, diatoxanthin, alloxanthin, diadinoxanthin, lutein-zeaxanthin, canthaxanthin, pheophytin *b*, okenone, chlorophyll *a*, pheophytin *a*, β-carotene, pyropheophytin *a*, pheophorbide *a* and pheophorbide *a* (like) are presented with concentrations expressed relative to percentage dry weight (% DW). Instantaneous events indicated by green (age-suggested) and grey (stone/gravel layer) horizontal lines. Dashed line indicates depth of 28.5 cm used to switch samples from core R1-1 to K1.

Appendix D – Supplementary figures from lake Disko 1

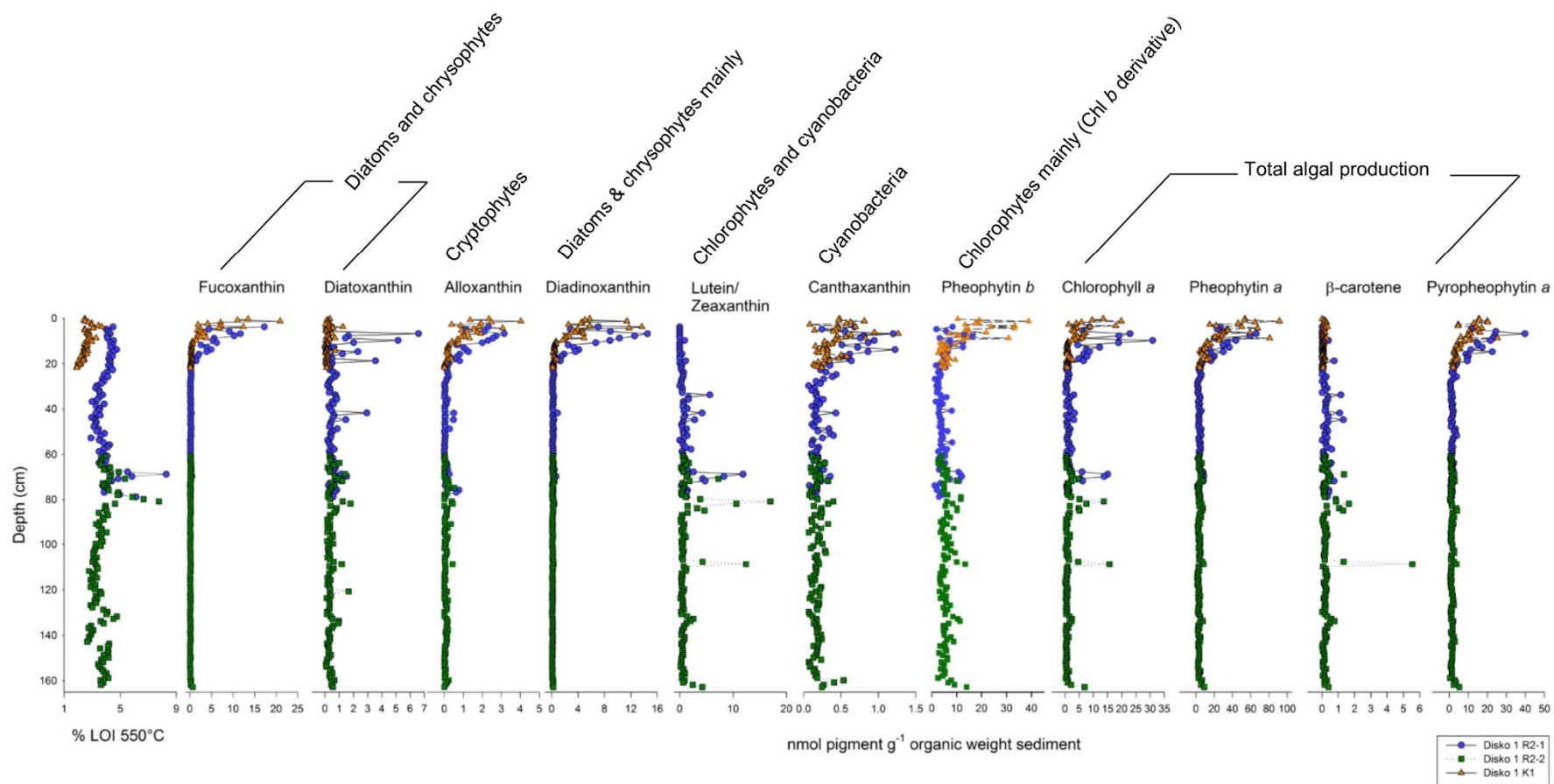


Figure D.1: Stratigraphic pigment diagram corrected by OM for overlapping K1 (orange triangles), R2-1 (blue circles) and R2-2 (green squares) sequences from lake Disko 1. Pigments fucoxanthin, diatoxanthin, alloxanthin, diadinoxanthin, lutein-zeaxanthin, canthaxanthin, pheophytin *b*, chlorophyll *a*, pheophytin *a*, β -carotene and pyropheophytin *a* are presented with concentrations expressed relative to the organic matrix (LOI 550 °C).

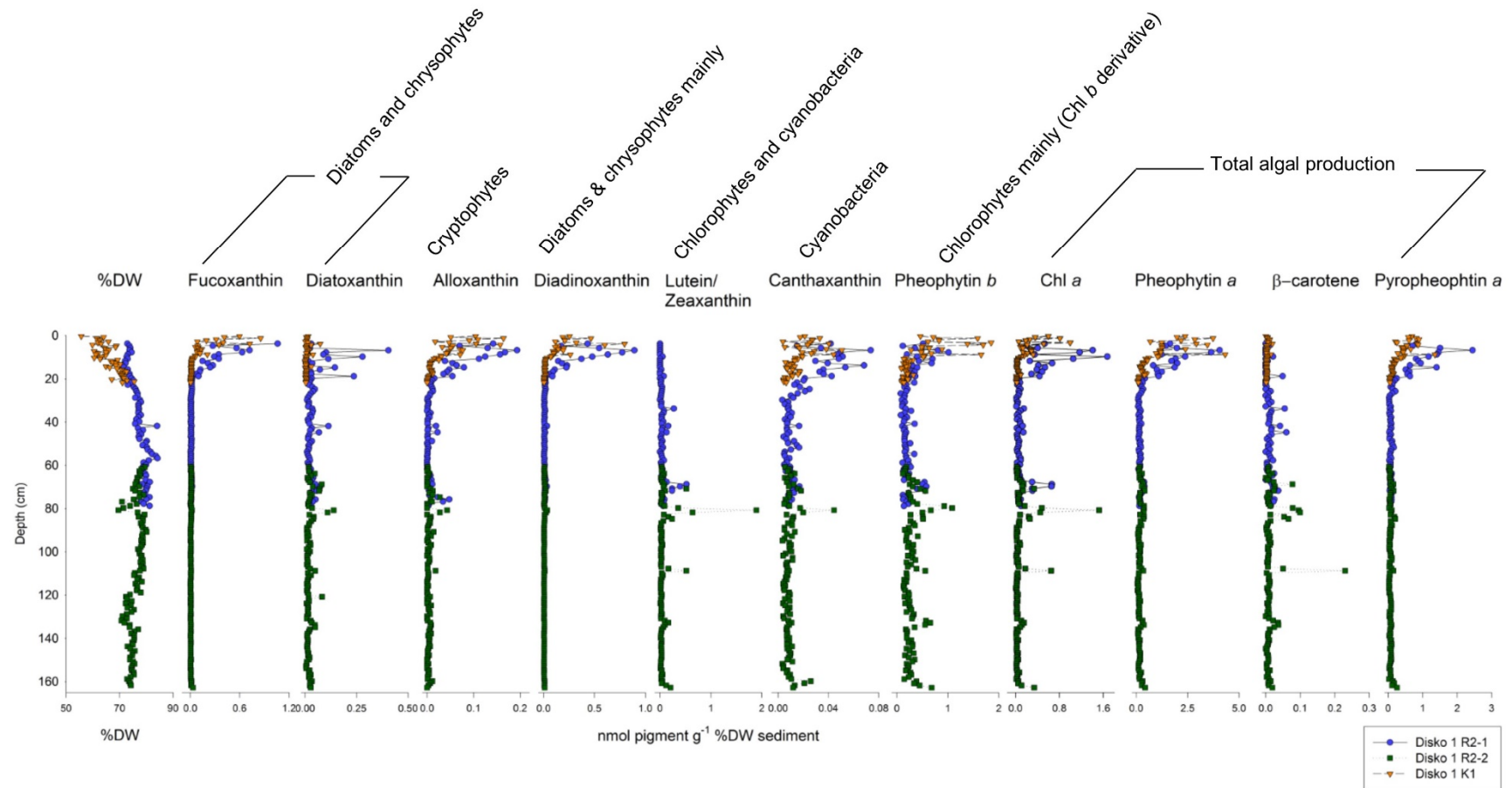


Figure D.2: Stratigraphic pigment diagram corrected by DW for overlapping K1 (orange triangles), R2-1 (blue circles) and R2-2 (green squares) sequences from lake Disko 1. Pigments fucoxanthin, diatoxanthin, alloxanthin, diadinoxanthin, lutein-zeaxanthin, canthaxanthin, pheophytin *b*, chlorophyll *a*, pheophytin *a*, β -carotene and pyropheophytin *a* are presented with concentrations expressed relative to percentage dry weight (% DW).

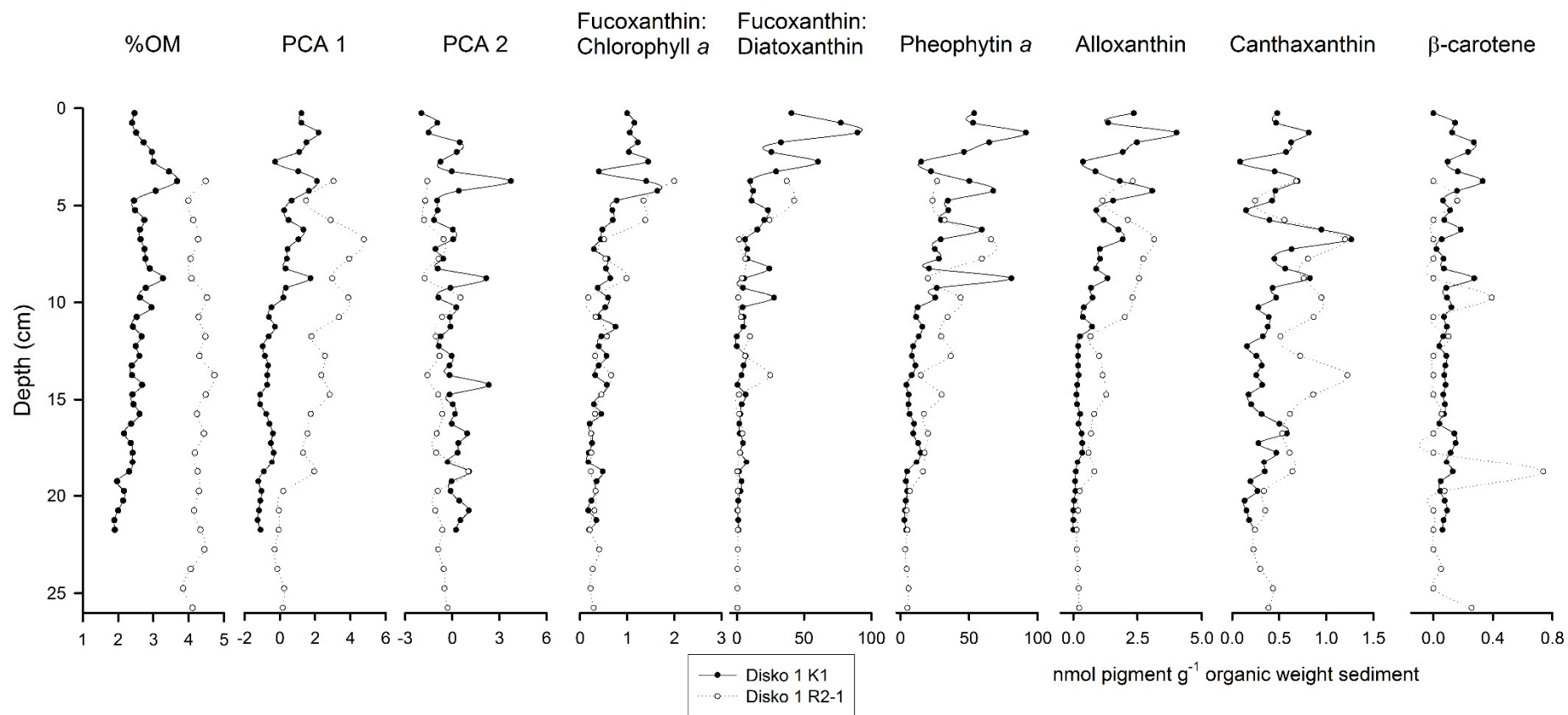


Figure D.3: Stratigraphic diagram to compare the HON-Kajak short core (K1) with the top of the upper Russian core (R2-1) for Disko. A suggested overlap is presented, although there was considerable distortion of the top of R2-1 and the OM values are ~2% lower in core K1.

Appendix E – Supplementary figures from lake Disko 4

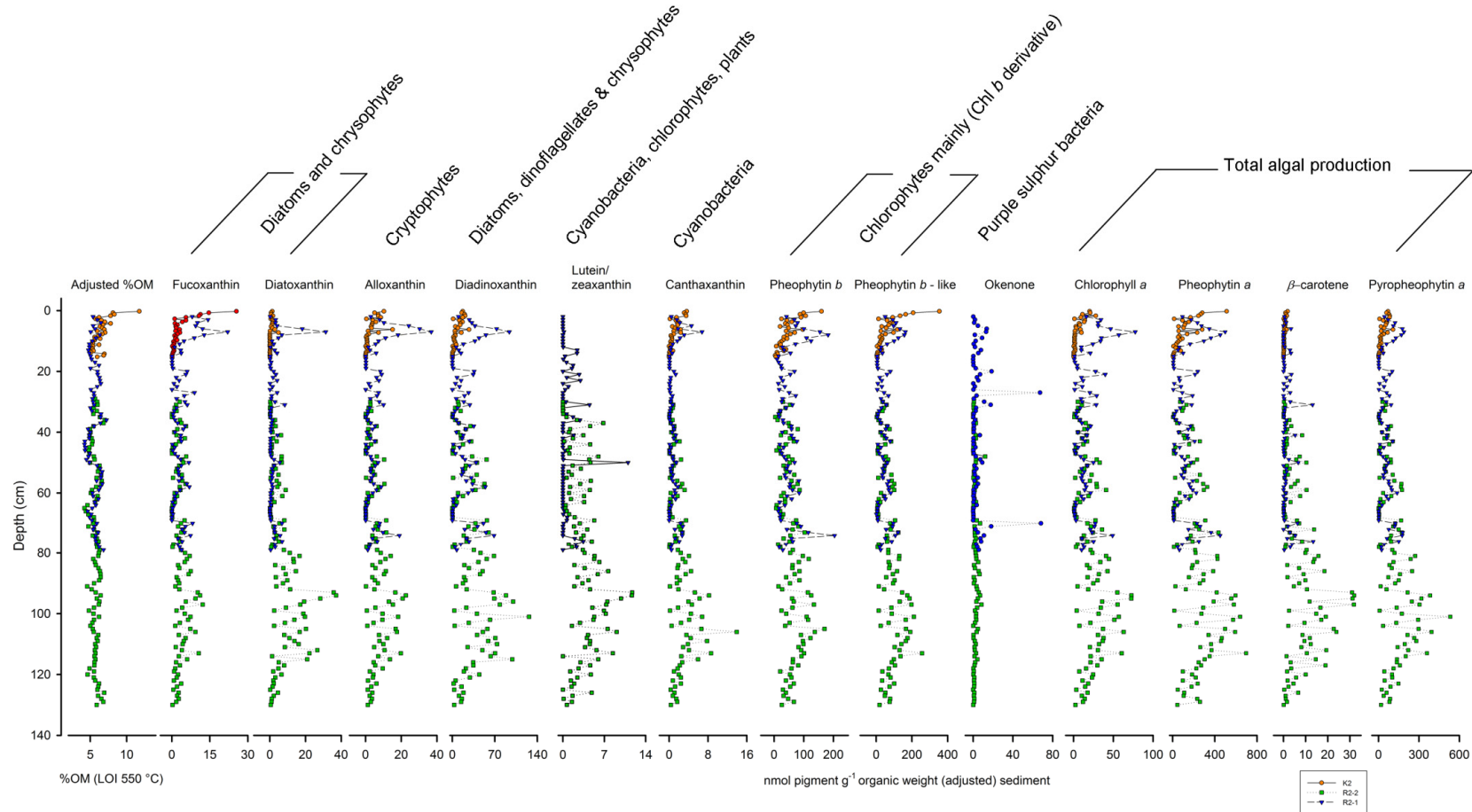


Figure E.1: Stratigraphic pigment diagram corrected by OM for HON-Kajak K2 (orange circles), Russian overlapping sequences R2-1 (blue triangles) and R2-2 (green squares) cores from lake Disko 4. Pigments fucoxanthin, diatoxanthin, alloxanthin, diadinoxanthin, canthaxanthin, pheophytin b, pheophytin b – like, okenone, chlorophyll a, pheophytin a, β-carotene and pyropheophytin a are presented with concentrations expressed relative to the adjusted organic matrix (OM, LOI 550 °C).

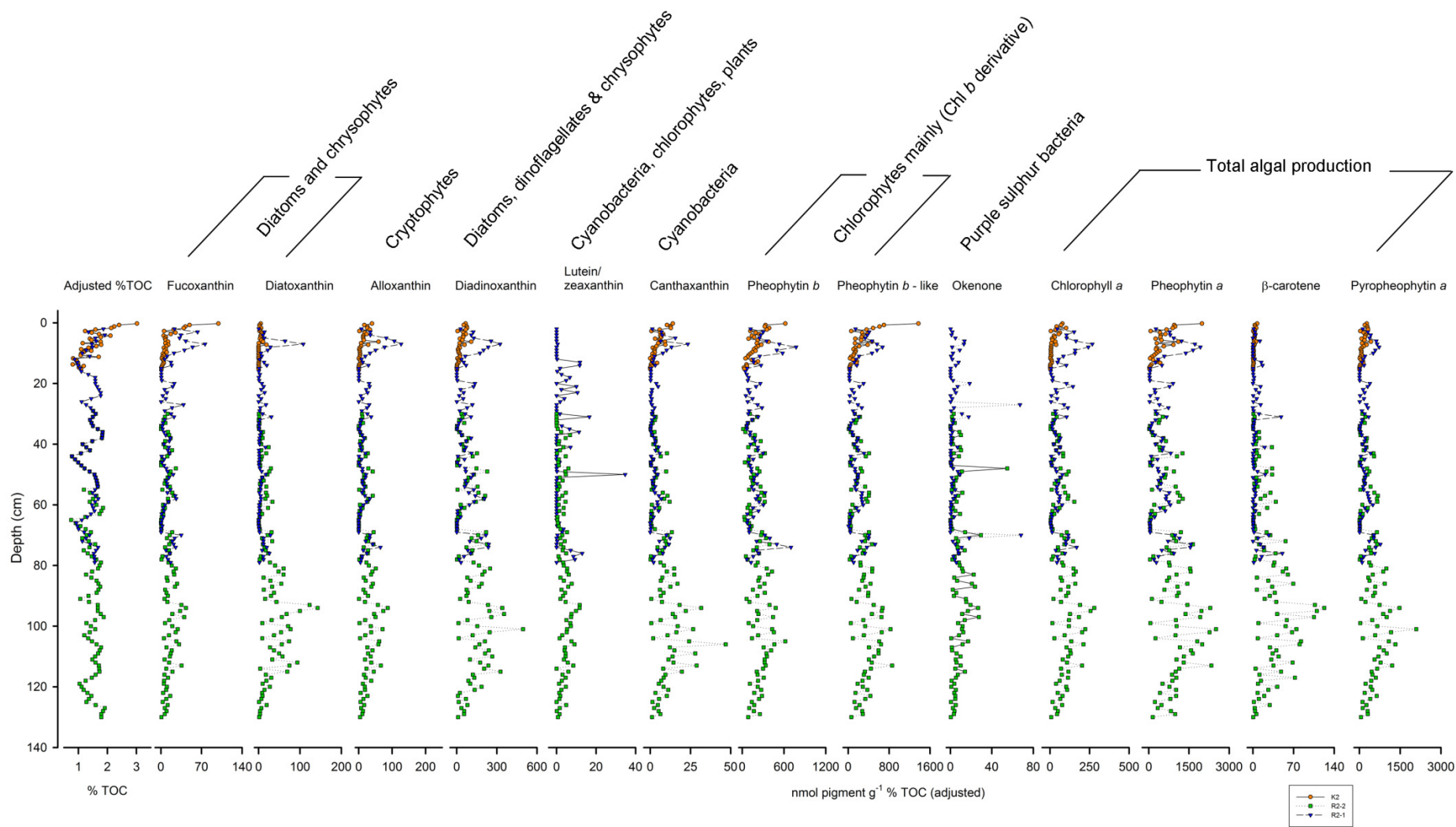


Figure E.2: Stratigraphic pigment diagram corrected by TOC for HON-Kajak K2 (orange circles), Russian overlapping sequences R2-1 (blue triangles) and R2-2 (green squares) cores from lake Disko 4. Pigments fucoxanthin, diatoxanthin, alloxanthin, diadinoxanthin, canthaxanthin, pheophytin *b*, pheophytin *b* - like, okenone, chlorophyll *a*, pheophytin *a*, β-carotene and pyropheophytin *a* are presented with concentrations expressed relative to adjusted TOC.

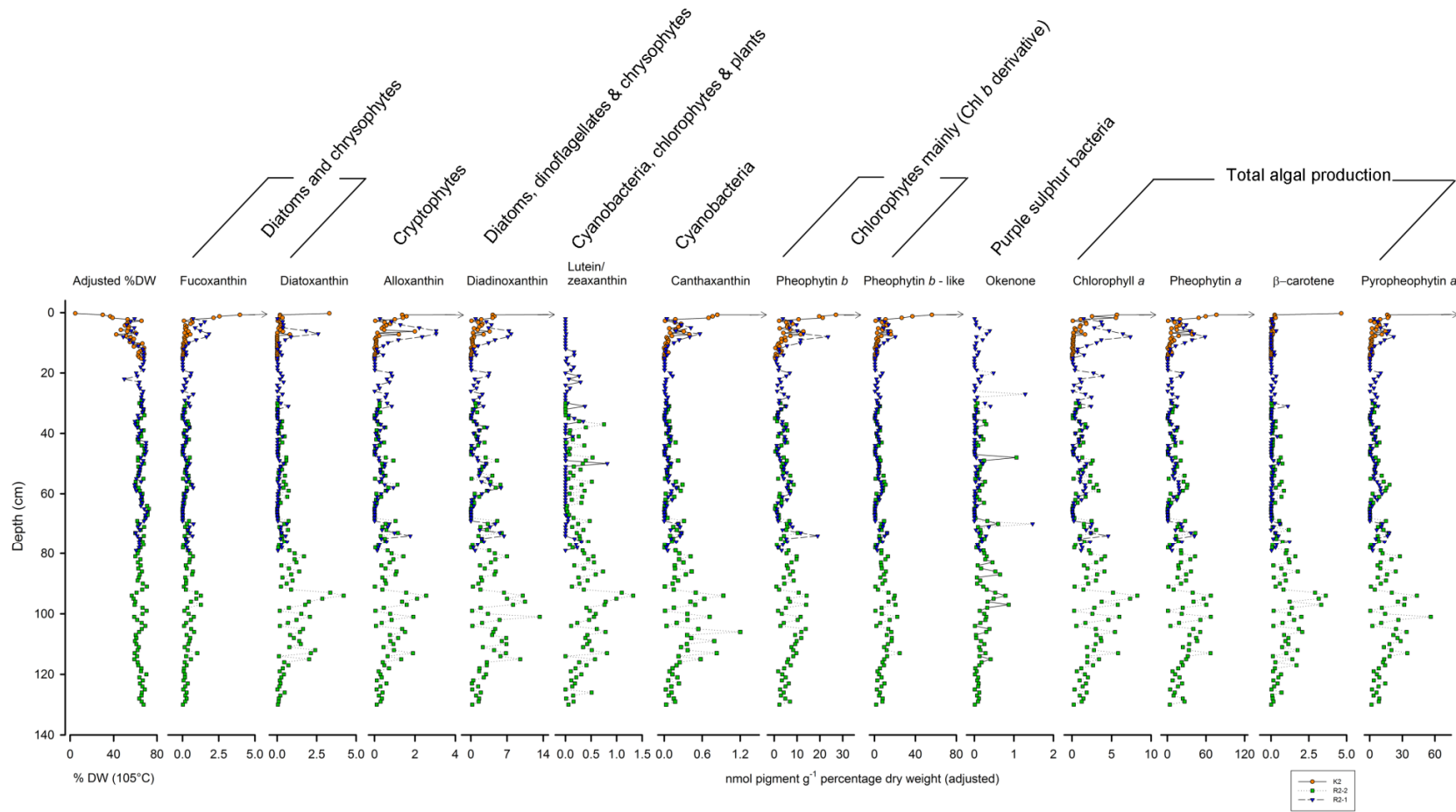


Figure E.3: Stratigraphic pigment diagram corrected by DW for HON-Kajak K2 (orange circles), Russian overlapping sequences R2-1 (blue triangles) and R2-2 (green squares) cores from lake Disko 4. Pigments fucoxanthin, diatoxanthin, alloxanthin, diadinoxanthin, canthaxanthin, pheophytin *b*, pheophytin *b* – like, okenone, chlorophyll *a*, pheophytin *a*, β -carotene and pyropheophytin *a* are presented with concentrations expressed relative to adjusted DW. Arrow indicates top sample is off the scale.